Introduction to

Mineral Processing Design and Operation

PREFACE

In nature minerals of interest exist physically and chemically combined with the host rock. Removal of the unwanted gangue to increase the concentration of mineral in an economically viable manner is the basis of mineral processing operations. This book treats the strategy of beneficiation as a combination of unit operations. Each unit process and its operation is therefore treated separately. Integration of these units leading to the development of viable flow sheets that meets the final objective, is then indicated.

The greatest challenge to a mineral processor is to produce high grade concentrates consistently at maximum recovery from the ore body. To quantify recovery a reasonable idea of the initial concentration of mineral in a lode is required. Proper sampling representing the ore body is therefore essential. The book therefore commences with the techniques of sampling of ore followed by the design and operation of unit processes of comminution that help to release the mineral from the associated rocks. Separation and concentration processes using techniques involving screening, classification, solid-liquid separations, gravity separation and flotation then follow. In the book some early methods of operation have been included and the modern methods highlighted.

The design and operation of each unit process is a study by itself. Over the years, improvements in the understanding of the complexities of these processes have resulted in increased efficiency, sustained higher productivity and grades. Mathematical modeling has helped in this direction and hence its use is emphasized. However, the models at best serve as guides to most processes operations that invariably involve complex interdependent variables which are not always easily assessed or manipulated. To solve the dilemma, plants are increasingly being equipped with instruments and gadgets that respond to changes much faster than humans can detect. Dynamic mathematical models are the basis of operations of these gadgets which are usually well developed, sophisticated, electronic equipment. In this book therefore, the basics of instrumental process control is introduced the details of which belong to the province of instrument engineers.

This book is written after several years on plant operation and teaching. The book is biased towards practical aspects of mineral processing. It is expected to be of use to plant metallurgist, mineral processors, chemical engineers and electronics engineers who are engaged in the beneficiation of minerals. It is pitched at a level that serves as an introduction to the subject to graduate students taking a course in mineral processing and extractive metallurgy. For a better understanding of the subject solved examples are cited and typical problems are set. Most problems may be solved by hand-held calculators. However most plants are now equipped with reasonable numbers of computers hence solution to problems are relatively simple with the help of spreadsheets.

The authors are grateful for the help received from numerous friends active in the field of mineral processing who have discussed the book from time to time. Particular thanks are due

to Dr Lutz Elber and Dr H. Eren who painfully went through the chapter on process control. Authors are also grateful for permission received from various publishers who own material that we have used and acknowledged in the text. And lastly and more importantly to our respective families who have helped in various ways and being patient and co-operative.

A.Gupta and D.S.Yan

Perth, Australia, January 2006

Symbols and Units

A general convention used in this text is to use a subscript to describe the state of the quantity, e.g. S for solid, L for liquid, A for air, SL or P for slurry or pulp, M for mass and V for volume. A subscript in brackets generally refers to the stream, e.g. (O) for overflow, (U) for underflow, (F) for feed, (C) for concentrate and (T) for tailing. There are a number of additions to this convention which are listed below.

a	a constant	-
a	amplitude	m
a_P	particle acceleration	m/s^2
A	a constant	-
A	aperture	microns
A	area	m^2
A_C	cross-sectional area	m^2
A_i	abrasion index	-
A_{ij}	assay of particles in the ith. size and jth. density fractions	-
A_E	effective area	m^2
A_{EFF}	areal efficiency factor	-
A_O	open area	%
A_{OE}	effective open area	%
A_M	assay of mineral	%, g/t, ppm
A_U	underflow area	m^2
b	a constant	-
b	Rosin-Rammler distribution parameter	-
B_{ij}	breakage distribution function	-
c	a constant	-
C	a constant	-
C	circulation ratio or load	-
C	concentration, (mass solid/volume of slurry)	kg/m^3
C_A	concentration of air	kg/m^3
C_C	average concentration of solids in the compression zone	kg/m^3
C_D	drag coefficient	-
C_i	concentration of species i	kg/m^3
C_O	initial concentration (mass of solid/volume of slurry)	kg/m^3
C_{MAX}	maximum concentration (mass of solid/volume of slurry)	kg/m^3
C_t	concentration at time t (mass of solid/volume of slurry)	kg/m^3
$C_{S(C)}$	concentration of solid (C = concentrate, F = feed, T = tail f = froth, P = pulp)	-
C_U, C_F	concentrations of the underflow and feed respectively, (mass of solid/volume of slurry)	kg/m^3
C_{CRIT}	critical concentration	kg/m^3
C_F	correction factor	-
CI	confidence interval	-
CR	confidence range	-
$C_{S(U)}$	solids concentration in the underflow (O = overflow,F = feed)	%
$C_{MS(F)}$	concentration by mass of solids in the feed	%

$C_{VS(F)}$	concentration by volume of solids in the feed	%
CC	concentration criterion	-
CV	coefficient of variation	-
C_∞	concentration at infinite time	kg/m^3
d	a constant	-
d	particle size, diameter	m
d_{32}	Sauter mean diameter	m
d_N	nominal diameter	m
d_{50}, d_{50C}	cut or separation size, corrected cut size	microns
d_B	ball diameter	cm, m
d_F	63.2% passing size in the feed	m
d_L	liberation size	m
d_{MAX}	largest dimension	m
d_{MIN}	smallest dimension	m
d_{MID}	mid-range dimension	m
d_{cutter}	cutter opening	m
d_C	cylpeb diameter	mm
d_w	wire diameter	m
D	discharge mass ratio (liquid/solid)	-
D	displacement, distance, diameter	m
D^*	dimensionless parameter	-
D_C	cyclone diameter	m
D_I	inlet diameter	m
D_O	overflow diameter	m
D_U	underflow diameter	m
e	a constant	-
E_i	partition coefficient of size i = recovery of size i in the U/F	-
E_C	corrected partition coefficient	-
E	energy	kWh
E_C	corrected partition coefficient	-
E_B	energy of rebound	Wh
E_G	specific grinding energy	kWh/t
E_O	efficiency based on oversize	-
E_p	Ecart probability, probable error of separation	-
E_U	efficiency based on undersize	-
E_T	total energy	kW
f	a constant	-
$f(r)$	ball wear rate	kg/h
$f(J_B)$	ball load-power function	-
$f(s)$	suspensoid factor	-
f_P, f_F	function relating to the order of kinetics for pulp and froth	-
f_i	mass fraction of size i in the circuit feed	-
F	feed size	cm, microns
F	floats at SG	-
F	froth stability factor	-
F	feed mass ratio (liquid/solid)	-
F_i	settling factor	-

F_{80}	80% passing size of feed	microns
F_B	Rowland ball size factor	-
F_B	buoyancy force	N
F_C	Bond mill factor	-
F_C	centrifugal force	N
F_D	drag force	N
F_g	gravitational force	N
F_G	correction factor for extra fineness of grind	-
F_{OS}	correction factor for oversized feed	-
F_R	correction factor for low reduction ratio	-
F_S	mass flow rate	kg/s, t/h
F_S	Bond slurry or slump factor	-
g	gravitational constant (9.81)	m/s^2
G	grade (assay)	%, g/t, ppm
G, G_{bp}	net grams of undersize per revolution	g/rev
G'	grinding parameter of circulating load	-
ΔG	free energy	J
h	parameter = x/σ	-
h_1, h_1^*	diatances within the conical section of a mill	m
H	hindrance factor	-
H	height	m, cm
H_t	height at time t	m
H_B	height of rebound pendulum	m
H_B	height of bed	m
H_C	height of ball charge	m
H_C	height of the start of the critical zone in sedimentation	m
H_{OF}	height of the clarification zone (overflow)	m
H_R	height of rest	m
H_S	hindered settling factor	-
H_U	mudline height at the underflow concentration	m
H_∞	height after infinite time	m
I	impact crushing strength	kg.m/mm
I	imperfection	-
J_B	fraction of mill volume occupied by bulk ball charge	-
J_C	fraction of mill volume in cylindrical section occupied by balls and coarse ore	-
J_G	superficial gas velocity	m/s
J_R	fraction of mill volume occupied by bulk rock charge	-
J_P	fraction of mill volume filled by the pulp/slurry	-
k	constant	-
k_A, k_A'	rate constant for air removal via froth and tailings respectively	-
k_F, k_S	rate constant for fast and slow component respectively	min^{-1}
k_i	comminution coefficient of fraction coarser that i^{th} screen	
k_C, k_{C50}	screening rate constant, crowded condition, normal and half size	$t/h/m^2$
k_S, k_{S50}	screening rate constant, separated condition, normal and half size	m^{-1}
K	constant	-
K_{D0}	material constant	-
KE	kinetic energy	kW

L	length	m
L_A	aperture size	m
L_{AE}	effective aperture	m
L_{EFF}	effective grinding length	m
L_C	length of cyclone	m
L_{CYL}, L_{CONE}	length of cylindrical and cone sections	m
L_F	Nordberg loading factor	-
L_{MIN}, L_{MAX}	minimum and maximum crusher set	m
L_T	crusher throw	m
L_V	length of vortex finder	m
L_{VF}	length from end of vortex finder to apex of a cyclone	m
m	moisture (wet mass/dry mass)	-
m	mineralogical factor	kg/m³
$m_{U(F)}$	mass fraction of undersize in the feed	
m_k	mass fraction of makeup balls of size k	-
$m_{U(O)}$	mass fraction of undersize in the oversize	-
$m(r)$	cumulative mass fraction of balls less than size r	-
m_T	mass rate of ball replacement per unit mass of balls	kg/h.t
$m_{U(U)}$	mass fraction of undersize in the undersize	-
$m_{i(U)}$	mass of size i in the underflow (F = feed)	kg
m	mass	g
M	mass	kg, t
M_i	mass/mass fraction of ith increment	kg, t
M_{oi}	cumulative mass fraction retained on ith screen at zero time	-
M_{ij}	mass percent of the ith size fraction and jth density fraction	%
M_B	mass of block	kg
M_B	mass of balls	kg
M_C	mill capacity	t/h
M_C	mass of crushing weight	kg
M_F	mass of feed	t
M_F	mass of fluid	kg
M_{FT}	mass of floats	kg, t
M_F	Nordberg mill factor	-
M_{MIN}	minimum mass of sample required	kg, t
M_R	mass of rock	kg
M_R	mass fraction of rock to total charge (rock + water)	-
M_r	cumulative mass fraction of balls of size r in the charge	-
M_S	mass of striking pendulum	kg
M_S	mass of solid	kg, t
$M_{S(F), S(C), S(T)}$	mass of solid feed, concentrate and tailing respectively	kg, t
$M_{S(f)}$	mass of solid in froth	-
M_{SK}	mass of sinks	kg, t
$M_{S(P)}$	mass of solid in the pulp	kg, t
$\Delta M(t)$	mass of top size particle	kg, t
M_1	mass of new feed	g
M_W	mass of water	kg, t
n	number of revolutions/min	min^{-1}
n	number of increments, measurements	-

n	order of rate equation	-
n(r)	cumulative number fraction of balls of size less than r	-
n_S	number of sub-lots	-
N	number of mill revolutions	-
N	number of strokes/min	min^{-1}
N	number	-
N_L	number of presentations per unit length	m^{-1}
N'	number of particles/gram	g^{-1}
o_i	mass fraction of size i in the overflow	-
p	binomial probability of being selected in a sample	-
p_i	mass fraction of size i in the new feed	-
P	product size	microns
P_{80}	80% passing size of product	microns
P	proportion of particles	-
P	pressure	Pa
P	Powers roundness factor	-
P	Jig power	W
P	JKSimFloat ore floatability parameter	-
P	probability	-
P_A, P_C, P_E, P_F	probability of adherence, collision, emergence, froth recovery	-
P_{CON}	power of the conical part of a mill	kW
P_{CYL}	power for the cylindrical part of a mill	kW
P_D	particle distribution factor	-
P_G	proportion of gangue particles	-
P_{ij}	proportion of particles in the ith. size and j^{th}. density fractions	-
P_L	liberation factor	-
P_M	proportion of mineral particles	-
P_M	mill power	kW
P_{NET}	net mill power draw	kW
P_{NL}	no load power	kW
P_{OS}	period of oscillation	s
P_R	relative mill power	-
P_S	particle shape factor	-
P_S	power at the mill shaft	kW
PE	potential energy	kW
ΔP	pressure drop	kPa
q	alternate binomial probability = 1 − p	-
Q	capacity	t/h
Q_B	makeup ball addition rate	kg/day
Q_B	basic feed rate (capacity)	t/h/m
Q_O	tonnage of oversize material	t/h
Q_U	capacity of the underflow	t/h
$Q_{MS(O)}$	flowrate of solids by mass in the overflow (U = U/F, F = feed)	t/h
$Q_{MS(C)}$	mass flow of solid in concentrate	t/h
$Q_{M(F)}$	capacity, of feed slurry by mass	t/h
$Q_{V(C), (T), (F)}$	flowrate by volume in concentrate, tailing and feed respectively	m^3/h
$Q_{VL(O)}$	capacity (flowrate) of liquid by volume in the overflow (U=underflow, F=feed)	m^3/h

$Q_{VOP(U)}$	flowrate by volume of entrained overflow pulp in the U/F	m^3/h
$Q_{VOL(U)}$	flowrate by volume of entrained overflow liquid in the U/F	m^3/h
$Q_{VOS(U)}$	flowrate by volume of entrained overflow solids in the U/F	m^3/h
$Q_{VS(O)}$	flowrate by volume of solids in the overflow (U = U/F, F = feed)	m^3/h
$Q_{V(f)}$	flowrate by volume in the froth	m^3/h
$Q_{V(O)}$	flowrate by volume of overflow (pulp) (U = underflow)	m^3/h
Q_W	ball wear rate	mm/h
r_o	fraction of test screen oversize	-
r	ball radius	m
r	ratio of rate constants $= k_A'/(k_A + k_A')$	-
r_1, r_2	radius within the conical section of a mill	m
R	radius	m
R	recovery	%
R	reduction ratio	-
R_1, R_2, R_3	Dietrich coefficients	-
$\bar{R}$	the mean radial position of the active part of the charge	m
R'	fractional recovery, with respect to the feed to the first cell	-
R'	mass of test screen oversize after grinding	g
R_C	radius of cone at a distance L_i from cylindrical section	m
Re_A, Re_C	Reynolds number in the apex and cone section respectively	-
Re_P	particle Reynolds number	-
R_F	froth recovery factor	-
R_i	radial distance to the inner surface of the active charge	m
R_o	mass of test screen oversize before grinding	g
R_P	radial distance of particle from the centre of a mill	m
R_{RO}	optimum reduction ratio	-
R_T	radius at the mill trunnion	m
R_V	recovery of feed volume to the underflow	-
R_∞	recovery at infinite time	-
S	speed	m/s
S	sinks at SG	-
S	surface area	m^2
S_B	surface area of ball	m^2
S_B	bubble surface area flux	s^{-1}
S_i	breakage rate function	min^{-1}
S_F	Nordberg speed factor	-
S	spacing, distance	m
S^*	dimensionless parameter	-
SG, SG_S	specific gravity, specific gravity of solid	-
T	period of pulsation	s
T_N	mass percent passing 1/N of the original size	%
t	time	h, min, s
t_D	detention or residence time	h
t_R	effective residence time	s
t_U	time for all solids to settle past a layer of concentration C	h
t_{10}	size that is one tenth the size of original particle	mm
$\bar{t}_A$	mean time taken for active part or charge to travel from the toe to the shoulder	s

$\bar{t}_F$	mean time for free fall from the shoulder to the toe	s
u_i	mass fraction of size i in the underflow	-
U	fraction of void space between balls at rest, filled by rock	-
U_p	fraction of the interstitial voids between the balls and rock charge in a SAG mill occupied by slurry of smaller particles	-
$V_{S(O)}$	volume fraction of solids in the overflow, (U=underflow, F=feed)	-
V_d	volume fraction of solids finer than the d_{50} in the feed ($V_{d50}/V_{S(F)}$)	-
V	volume	m^3
V^*	dimensionless parameter	-
V_C	volume of the mill charge	m^3
V_C	volume of the compression zone	m^3
V_{CONE}	volume of conical section of mill	m^3
V_{d50}	volume of solids finer than the d_{50} in the feed	
V_B	percent of mill volume occupied by balls	%
V_F	volume dilution in the feed = $V_{L(F)}/V_{S(F)}$	-
$V_{L(F)}$	volume of liquid in the feed, (U=underflow, F=feed)	m^3
V_M	volume of mill	m^3
V_O	volume dilution in the overflow = $V_{L(O)}/V_{S(O)}$ or $Q_{VL(O)}/Q_{VS(O)}$	-
V_R	percent of mill volume occupied by rock	%
$V_{S(F)}$	volume of solids in the feed, (U = underflow, O = overflow)	m^3
V_T	terminal velocity	m/s
v	unknown true value	-
v_B^o	velocity of block pendulum before impact	m/s
v_B^1	velocity of block pendulum after impact	m/s
v_S^o	velocity of striking pendulum before impact	m/s
v_S^1	velocity of striking pendulum after impact	m/s
var(d)	distribution variance	-
var(c)	composition variance	-
var(pa)	preparation and analysis variance	-
var(t)	total variance	-
var(x)	variance	-
w	thickness of slurry	m
w	fraction of feed water in the underflow	-
W	width	m
W^*	dimensionless parameter	-
W_E	effective width	m
W_i	Bond Work Index	kWh/t
$W_{i\,Test}$	Bond Work Index, laboratory test	kWh/t
W_{Oi}	operating work index	kWh/t
W_{OiC}	corrected operating work index	kWh/t
W_S	water split = $Q_{ML(O)}/Q_{ML(F)}$	-
x	deviation from the true assay	-
x_{GM}	geometric mean of size interval	microns
x^1	Rosin-Rammler size parameter	microns
$\bar{x}$	Sample mean	-
x_i	i^{th} measurement	-
X	deviation from standard unit	-

α	fractional average mineral content	-
α	Lynch efficiency parameter	-
α, α^0	angle	radians
α_T, α_S	toe and shoulder angles of the charge	radians
α_{TS}	the slurry toe angle	radians
γ	function of charge position and mill speed	-
γ	volume fraction of active part of the charge to the total charge	-
$\gamma_{SA}, \gamma_{SL}, \gamma_{LA}$	surface energy, surface tension, interfacial tension	N/m
ε	coefficient of restitution	-
ε	void fraction	-
Δ	a ball wear parameter	-
κ	a ball wear parameter, wear distance per unit time	-
φ	porosity of a ball bed	-
ϕ	ratio of experimental critical speed to theoretical critical speed	-
ϕ	fraction with the slow rate constant	-
ϕ_C	fraction of critical speed	-
ψ, ψ_S	settling or sedimentation flux	$kg/m^2/s$
ψ_W	withdrawal flux	$kg/m^2/s$
ψ_{CRIT}	critical flux	$kg/m^2/s$
μ	coefficient of friction	-
ρ	specific gravity (dimensionless) or density	$kg/m^3, t/m^3$
ρ_b	density or SG of balls	$kg/m^3, -$
ρ_C	bulk density of the total charge, rock + balls + water	t/m^3
ρ_B	bulk density	kg/m^3
ρ_F	density of fluid	kg/m^3
ρ_O	density of ore	kg/m^3
ρ_L	density of liquid	kg/m^3
ρ_R	density of rock	kg/m^3
ρ_S	density of solid	kg/m^3
ρ_{SL}	density of slurry	kg/m^3
ρ_W	density of water	kg/m^3
ρ_M, ρ_G	density of the mineral and the gangue respectively	$kg/m^3, t/m^3$
σ	standard deviation (where $\sigma^2 = var(x)$)	-
σ_A	statistical error in assay	-
σ_L	standard deviation of a primary increment	-
σ_M	standard deviation on a mass basis	-
σ_P	standard deviation of the proportion of particles in a sample	-
σ_{PA}	standard deviation of preparation and assay	-
σ_S	statistical error during sampling	-
σ_T	total error	-
λ	nominal residence time	s
θ	angle	radians, degree
μ	viscosity	mNm, Pa.s
ν	velocity	m/s
ν_C	critical speed	rpm

v_F	velocity across a screen	m/min
v_N	normalised tangential velocity = v_R/v_T	rpm
v_O	overflow rate	m/s
$v_{O(i)}$	ideal overflow rate	m/s
v_R	tangential velocity at distance R_P	rpm
v_R	rise velocity	m/s
v_S	settling velocity	m/s
v_{So}	initial settling velocity	m/s
v_{St}	settling velocity at time t	m/s
v_T	tangential velocity at the inside liner surface	rpm
v_T	terminal velocity	m/s
ω	rotational speed, angular velocity	s^{-1}, rpm, Hz
$\underline{\omega}$	mean rotational speed	rpm
ω_P	rotational speed of a particle at distance R_P	s^{-1}, rpm
ζ	a milling parameter = function of volumetric filling of mill	-
%S	percent solids	%

Chapter 1. Mineral Sampling

1. INTRODUCTION

A processing plant costs many millions of dollars to build and operate. The success of this expenditure relies on the assays of a few small samples. Decisions affecting millions of dollars are made on the basis of a small fraction of the bulk of the ore body. It is therefore very important that this small fraction is as representative as possible of the bulk material. Special care needs to be taken in any sampling regime and a considerable effort in statistical analysis and sampling theory has gone into quantifying the procedures and precautions to be taken.

The final sampling regime adopted however is a compromise between what theory tells us should be done and the cost and difficulty of achieving this in practice.

1.1. Statistical Terminology

A measurement is considered to be accurate if the difference between the measured value and the true value falls within an acceptable margin. In most cases however the true value of the assay is unknown so the confidence we have in the accuracy of the measured value is also unknown. We have to rely on statistical theory to minimise the systematic errors to increase our confidence in the measured value.

Checks can be put in place to differentiate between random variations and systematic errors as the cause of potential differences. A *random error* (or variation) on average, over a period of time, tend to zero whereas integrated *systematic errors* result in a net positive or negative value (see Fig. 1.1).

The *bias* is the difference between the true value and the average of a number of experimental values and hence is the same as the systematic error. The variance between repeated samples is a measure of precision or reproducibility. The difference between the mean of a series of repeat samples and the true value is a measure of accuracy (Fig. 1.2).

A series of measurements can be precise but may not adequately represent the true value. Calibration procedures and check programs determine accuracy and repeat or replicate/duplicate measurements determine precision. If there is no bias in the sampling regime, the precision will be the same as the accuracy. Normal test results show that assays differ from sample to sample. For unbiased sampling procedures, these assay differences are not due to any procedural errors. Rather, the term "random variations" more suitably describes the variability between primary sample increments within each sampling campaign.

Random variations are an intrinsic characteristic of a random process whereas a systematic error or bias is a statistically significant difference between a measurement, or the mean of a series of measurements, and the unknown true value (Fig. 1.1). Applied statistics plays an important role in defining the difference between random variations and systematic errors and in quantifying both.
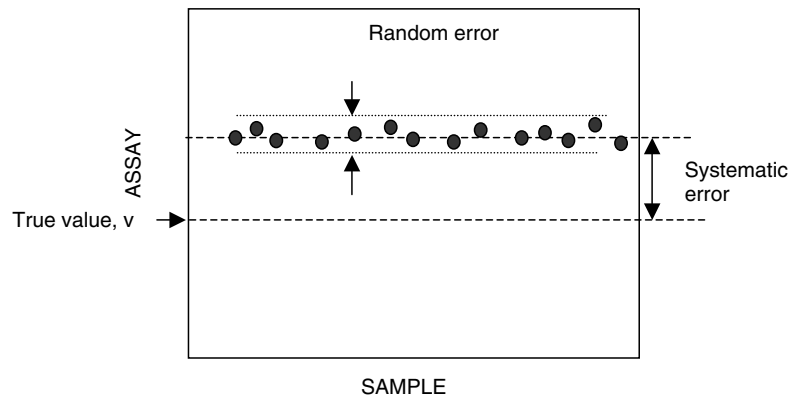
Fig.1.1. Representation of a random and systematic error.

1.1.1. Mean
The most important parameter for a population is its average value. In sampling and weighing the *arithmetic mean* and the *weighted mean* are most often used. Other measures for the average value of a series of measurements are the *harmonic mean*, and the *geometric mean.* *Mode* and *median* are measures of the central value of a distribution. The *mode* forms the peak of the frequency distribution, while the *median* divides the total number of measurements into two equal sets of data. If the frequency distribution is symmetrical, then its mean, mode and median coincide as shown in Figs. 1.3 and 1.4.
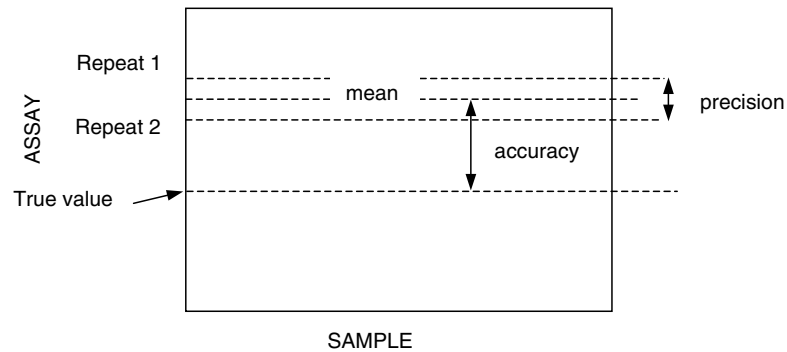
Fig. 1.2. Difference between precision and accuracy.
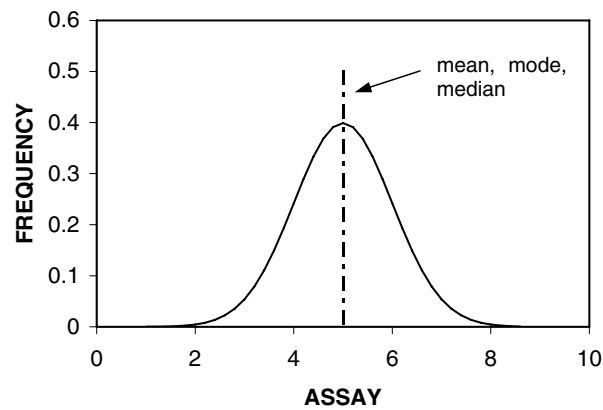
Fig. 1.3. Normal distribution.

For a binomial sampling unit of mixed particles the average percentage of mineral A is calculated by adding up all measurements, and by dividing their sum by the number of measurements in each series.

$$\bar{x} = \frac{\sum x_i}{n}$$ (1.1)

where $\bar{x}$ = sample mean (arithmetic)
        x_i = i^{th} measurement
        n = number of increments
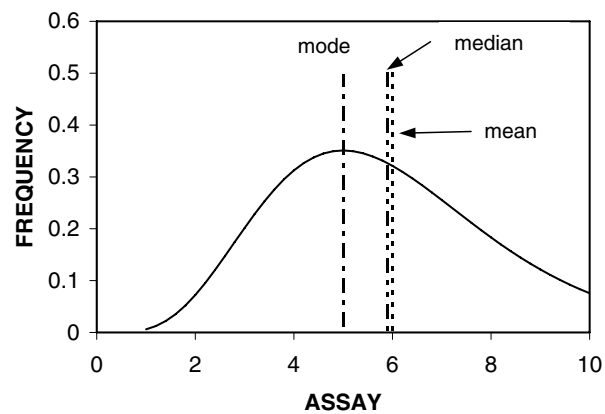
Fig. 1.4. Asymmetrical distribution.

The weighted percentage is calculated, either from the total number of particles in each series, or by multiplying each incremental percentage with the mass in each corresponding increment, and by dividing the sum of all products by the total mass for each series. However, the small error that is introduced by calculating the arithmetic mean rather than the weighted average, is well within the precision of this sampling regime. The following formula is used to calculate the weighted average for a sample that consists of n primary increments:

$$\bar{x} = \frac{\sum (\Delta M_i . x_i)}{M} \qquad\qquad (1.2)$$

where $\quad \Delta M_i \;=\;$ mass of ith increment

$\qquad\qquad M \quad=\;$ mass of gross sample

Due to random variations in the mass of each primary increment the weighted average is a better estimate of v, the unknown true value, than the arithmetic mean.

1.1.2. Variance

The variance, and its derived parameters such as the *standard deviation* and the *coefficient of variation*, are the most important measures for variability between test results.

The term *range* may be used as a measure of variability.

Example 1.1

Consider a binary mixture of quartz and hematite particles with approximately 10% hematite. Samples are taken and the number of hematite particles are counted to obtain the percentage of hematite in the sample. Table 1.1 gives the result of ten samples. For a binomial sampling unit the *range* is (maximum value – minimum value) = 12.6 – 5.7 = 6.9%.

Table 1.1
Sampling with a Binomial Population (Quartz and Hematite).

Number	Sample			
	Quartz	Hematite	Total	% Hematite
1	105	11	116	9.5
2	132	19	151	12.6
3	99	10	109	9.2
4	98	7	105	6.7
5	83	5	88	5.7
6	87	11	98	11.2
7	91	12	103	11.7
8	86	8	94	8.5
9	98	12	110	10.9
10	113	14	127	11.0

SAMPLE
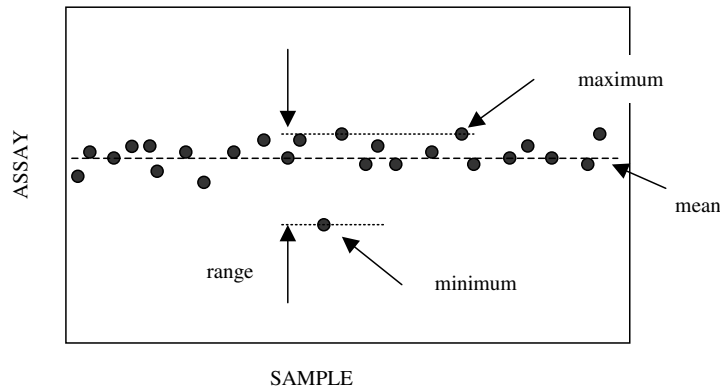
Fig. 1.5. Range of experimental values.

If each series of measurements is placed in ascending order, then the *range* is numerically equal to $x_n - x_1$ so that the range does not include information in increments x_2, x_3,..., x_{n-1}. For a series of three or more measurements the *range* becomes progressively less efficient as a measure for variability as indicated in Fig. 1.5.

For two samples, the *range* is the only measure for precision but this is not sufficient to estimate the precision of a measurement process. The precision of a measurement process requires the mean of absolute values of a set of *ranges* calculated from a series of four or more simultaneous duplicates. This is the variance.

The classical formula for the calculation of the variance is:

$$\text{var}(x) = \frac{\sum (\bar{x} - x_i)^2}{n-1} \approx \frac{\sum x_i^2 - \frac{\left(\sum x_i\right)^2}{n}}{n-1}$$

(1.3)

where   n   = number of measurements
          n-1   = degrees of freedom

The standard deviation, σ, is the square root of the variance. The coefficient of variation (CV), is a measure of precision and is numerically equal to:

$$\text{CV}(\%) = \frac{100 \, \sigma}{\bar{x}}$$

(1.4)

Example 1.2

Variance values from a sampling procedure with a binary mixture of mineral particles is given in Table 1.2.

Table 1.2
Variance values from the sampling example with a mixture of quartz and hematite

Number	Small increment				Large increment			
	Quartz	Hematite	Total	% Hematite	Quartz	Hematite	Total	%Hematite
1	105	11	116	9.48	504	53	557	9.52
2	132	19	151	12.58	350	45	395	11.39
3	99	10	109	9.17	597	56	653	8.58
4	98	7	105	6.67	394	52	446	11.66
5	83	5	88	5.68	428	43	471	9.13
6	87	11	98	11.22	438	52	490	10.61
7	91	12	103	11.65	508	55	563	9.77
8	86	8	94	8.51	533	56	589	9.51
9	98	12	110	10.91	438	50	488	10.25
10	113	14	127	11.02	490	49	539	9.09
			SUM	96.89			SUM	99.51
	Arithmetic mean			9.69	Arithmetic mean			9.95
	Variance			5.0141	Variance			1.1264
	Standard deviation			2.2392	Standard deviation			1.0613
	Coeff. of variation			23.1	Coeff. of variation			10.7

The physical appearance of a sample that consists of fifty primary increments of 5 kg each is similar to that of a sample containing five increments of 50 kg, or to that of 250 kg of a bulk solid. However, the difference in intrinsic precision (as indicated by the variance) may be dramatic, particularly if the variability within the sampling unit is high.

In practical applications of sampling bulk solids we compromise by collecting and measuring unknown parameters on gross samples, and by reporting $\overline{x}$, the sample mean as the best estimate for v, the unknown true value. If all increments are contained in a single gross sample, we have no information to estimate the precision of this sampling regime. If we want to know more about the precision of samples, systems and procedures, it is essential that duplicate or replicate measurements be made, from time to time, to determine the coefficient of variation for each step in the chain of measurement procedures.

1.1.3. Confidence Intervals

Other convenient measures for precision are confidence intervals (CI) and confidence ranges (CR). 95 % confidence intervals and 95 % confidence ranges may be used, although if concern over sampling precision is high, then 99% or 99.9% confidence limits must be considered.

That is, if we repeat a particular experiment 100 times, then 95 times out of 100 the results would fall within a certain bound about the mean and this bound is the 95 % confidence interval. Similarly, confidence limits of 99 % and 99.9 % mean that 99 times out of 100, or 999 times out of 1000 measurements would fall within a specified or known range.

In the draft Australian Standard, DR00223, for estimating the sampling precision in sampling of particulate materials, a confidence interval of 68% is chosen [1].

Fortunately, we don't need to repeat a measurement one-hundred times if we want to determine its 95% confidence interval, either for individual measurements or for their mean. Applied statistics provides techniques for the calculation of confidence intervals from a

limited number of experiments. The variance between increments, or between measurements, is the essential parameter.

The most reliable estimate of σ^2 is var(x), the variance of the sample. The reliability of this estimate for σ^2 can be improved by collecting, preparing and measuring more primary increments, or by repeating a series of limited experiments on the same sampling unit.

The 95 % confidence interval for a normal distribution is equal to ± 1.96 σ from the distribution mean. In practice, we often use the factor 2 instead of 1.96, to simplify calculations and precision statements. The 68 % confidence interval is equal to ± 0.99 σ, for infinite degrees of freedom and if the number of replicate results exceeds 8 then a factor of 1.0 is an acceptable approximation.

1.2. Mineral particles differing in size – Gy's method

Representing large bodies of minerals truly and accurately by a small sample that can be handled in a laboratory is a difficult task. The difficulties arise chiefly in ascertaining a proper sample size and in determining the degree of accuracy with which the sample represents the bulk sample.

In each case the accuracy of the final sample would depend on the mathematical probability with which the sample represents the bulk material. The probability of true representation increases when incremental samples are taken while collecting from a stream, like a conveyor belt for solids and off pipes for liquids or slurries.

Several methods have been put forward to increase the probability of adequately representing the bulk minerals [2-5]. One such method involving both the size and accuracy of a sample taken for assay has been developed by Gy and is widely used [6, 7]. Gy introduced a model based on equiprobable sample spaces and proposed that if:

d_{MAX} =   dimension of the largest particle

M_{MIN} =   minimum mass of sample required

σ^2 =   variance of allowable sampling error in an assay   (in the case of a normal distribution this equals the standard deviation)

then:

$$M_{MIN} = \frac{Kd_{MAX}^3}{\sigma^2} \tag{1.5}$$

K is usually referred to as the sampling constant (kg/m^3)

In mineralogical sampling the dimension of the largest piece (d_{MAX}) can be taken as the screen aperture through which 90-95 % of the material passes. As $\pm$ 2σ represents the probability of events when 95 out of 100 assays would be within the true assay value, 2σ is the acceptable probability value of the sample. The sampling constant K is considered to be a function of the material characteristics and is expressed by:

$$K \quad = \quad P_S \, P_D \, P_L \, . \, m \tag{1.6}$$

where P_S =   particle shape factor (usually taken as 0.5 for spherical particles, 0.2 for gold ores)

P_D = particle distribution factor (usually in the range 0.20 – 0.75 with higher values for narrower size distributions, usually taken as 0.25 and 0.50 when the material is closely sized)

P_L = liberation factor (0 for homogeneous (unliberated) materials, 1 for heterogeneous (liberated) and see Table 1.3 for intermediate material)

m = mineralogical factor

The mineralogical factor, m, has been defined as:

$$m = \left[\frac{(1-\alpha)}{\alpha} \right] [(1-\alpha)\rho_M + \alpha\rho_G] \qquad (1.7)$$

where α is the fractional average mineral content and

ρ_M and ρ_G the specific gravity of the mineral and the gangue respectively

The liberation factor, P_L, is related to the top size, d_{MAX} and to the liberation size, d_L of the mineral in the sample space. It can be determined using Table 1.3. In practice, P_L is seldom less than 0.1 and if the liberation size is unknown then it is safe to take P_L as 1.0.

Table 1.3
Liberation factor as a function of liberation size [9].

Top Size/Liberation Size, (d_{MAX}/d_L)	<1	1-4	4-10	10-40	40-100	100-400	>400
Lib. Factor (P_L)	1.0	0.8	0.4	0.2	0.1	0.05	0.02

When a large amount of sample has been collected it has to be split by a suitable method such as riffling. At each stage of subdivision, samples have to be collected, assayed and statistical errors determined. In such cases the statistical error for the total sample will be the sum of the statistical errors during sampling (σ_S) and the statistical error in assay (σ_A), so that the total variance (σ_T^2) will be:

$$\sigma_T^2 = \sigma_S^2 + \sigma_A^2 \qquad (1.8)$$

When the sample is almost an infinite lot and where the proportion of mineral particles has been mixed with gangue and the particles are large enough to be counted, it may be easier to adopt the following procedure for determining σ_P.

Let P_M = proportion of mineral particles
       P_G = proportion of gangue particles
       N = number of particles

Then the standard deviation of the proportion of mineral particles in the sample, σ_P, will be:

$$\sigma_P = \sqrt{\frac{P_M\, P_G}{N}} \tag{1.9}$$

The standard deviation on a mass basis (σ_M) can be written in terms of the percent mineral in the whole sample provided the densities (ρ) are known. Thus if ρ_M and ρ_G are the densities of the mineral and gangue, then the mass percent of mineral in the entire sample, consisting of mineral and gangue (the assay), will be:

$$A_M = \frac{100\, P_M\, \rho_M}{P_M\, \rho_M + P_G\, \rho_G} \tag{1.10}$$

assuming the particles of mineral and gangue have the same shape and size.

The standard deviation of the entire sample is given by $\sigma_T = \dfrac{dA_M}{dP} \cdot \sigma_P$ or

$$\sigma_T = \left(\frac{(100 - A_M)\,\rho_M + A_M\,\rho_G}{100\sqrt{\rho_M\,\rho_G}} \right) \cdot \sqrt{\frac{A_M\,(100 - A_M)}{N}} \tag{1.11}$$

Example 1.3

Regular samples were required of the feed to a copper processing plant, having a copper content of about 9%. The confidence level of estimation was required to be 0.1 % Cu at 2σ standard deviation. The liberation size of the Cu mineral (chalcocite) in the ore was determined to be 75 μm. The top size of the ore from the sampler was 2.5 cm. Determine the minimum mass of sample required to represent the ore. Given; the density of chalcocite is 5600 kg/m^3 and the density of the gangue is 2500 kg/m^3.

Solution

From the data, d_{MAX} = 2.5 cm

Since the confidence interval required is equal to $\pm$ 0.1 % of a 9% assay,

2σ = 0.1/ 9   or σ = 0.011/2 = 0.00555

Again from the data d_{MAX}/d_L = 25 / 0.075 = 333.33, hence from Table 1.3, P_L = 0.05.

As the ore contains chalcocite (Cu_2S) assaying about 9% Cu, it can be considered to contain [159.2/(63.56 x 2)] x 9 = 11.3% of Cu_2 S. Thus α = 0.113.

i.e. The copper content of Cu_2S is given by the ratio of atomic masses;

$\dfrac{(63.56 \times 2) \times 100}{(63.56 \times 2) + 32.1}$ = $\dfrac{127.1 \times 100}{159.2}$ = 79.8% Cu   (atomic mass; Cu = 63.56, S = 32.1)

The chalcocite content of the ore is then given by:

$$\frac{9 \times 100}{79.8} = 11.3 \%$$

The mineralogical composition factor, m, can now be calculated from Eq. (1.7),

$$m = \left[\frac{(1-\alpha)}{\alpha}\right] \left[(1-\alpha)\rho_M + \alpha\rho_G\right]$$

$$m = \left[\frac{(1-0.113)}{0.113}\right] \left[(1-0.113)\,5600 + (0.113 \times 2500)\right] = 41207.8 \ kg/m^3$$

then from Eq. (1.6),

$$K = 0.5 \times 0.25 \times 0.05 \times 41207.8 = 257.5 \ kg/m^3 \quad and$$

$$M_{MIN} = [257.5 \times (0.025)^3] / (0.00555)^2 = 130.6 \ kg$$

Thus the minimum sample size should be 131 kg.

Note the importance of not rounding off the numbers until the final result. If σ is rounded to 0.0055 then $M_{MIN} = 133$ kg and if σ is rounded to 0.0056 then $M_{MIN} = 128$ kg.

Example 1.4

A composite sample of galena and quartz was to be sampled such that the assay would be within 0.20% of the true assay, of say 5.5 %, with a probability of 0.99, ie. the sample assay would be 5.5 % ± 0.20 %, 99 times out of 100 . Given that the densities of galena and quartz were 7400 kg/m³ and 2600 kg/m³ respectively and the average particle size was 12.5 mm with a mass of 3.07g, determine the size of the sample that would represent the composite.

Solution

Step 1
Determine σ_T in terms of N from Eq. (1.11).

$$\sigma_T = \left(\frac{(100-5.5)\,7400 + 5.5 \times 2600}{100\sqrt{7400 \times 2600}}\right) \sqrt{\frac{5.5\,(100-5.5)}{N}}$$

$$= \frac{37.089}{\sqrt{N}} \qquad\qquad (1.12)$$

To determine N it is necessary to find σ_T

Step 2
To determine the value of σ_T to satisfy the deviation limits so that the area under the curve between the limits will be 99% of the total area, use Table 1.4 below.
From the table, corresponding to a probability of 0.99, the value of the deviation from the standard unit is 2.576.

i.e. $\quad X = \dfrac{x}{\sigma_T} \quad$ or $\quad \sigma_T = \dfrac{x}{X} = \dfrac{0.20}{2.576} = 0.07764$

Substituting in Eq. (1.12), $\quad N = (37.089/0.07764)^2 = 228{,}201.9$

Table 1.4
Probability P vs deviation X, relative to unit standard deviation [9].

Probability p	Deviation from Standard Unit, X $X = x/\sigma_T$	Probability p	Deviation from Standard Unit, X $X = x/\sigma_T$
0.90	1.645	0.97	2.170
0.91	1.705	0.98	2.326
0.92	1.750	0.99	2.576
0.93	1.812	0.999	3.291
0.94	1.881	0.9999	3.890
0.95	1.960	0.99999	4.417
0.96	2.054	0.999999	4.892

Hence the mass of sample necessary to give an assay within the range 5.5 ± 0.20 %, 99 times out of 100 would be $= 228{,}201.9 \times 3.07 = 700{,}579$ g ≈ 701 kg.

1.3. Mineral particles of different density

Where variations in density of individual particles and their composition occur, the following considerations may be adopted to provide the sample size [9]:

1. Divide the material into n density fractions, ρ_1, ρ_2, ρ_3, .. ρ_n varying from purely one mineral to the other, e.g. copper and quartz in a copper ore, and consider n size fractions, d_1, d_2, d_3 ... d_n
2. Consider the mass percent of the ith size fraction and j^{th} density fraction as M_{ij} and
3. Consider A_{ij} and P_{ij} as the assay and the proportion of particles in the ith size and j^{th} density fractions

For sampling a mixture of two components (mineral and gangue) the proportion of particles in the ij fraction would be;

$$P_{ij} = \frac{M_{ij}/d_i^3\, \rho_j}{\sum\left(M_{ij}/d_i^3\, \rho_j\right)} \tag{1.13}$$

And the assay of the mixture, A_{ij} will be approximately equal to:

$$A_{ij} = \frac{\left[\rho_M\left(\rho_{ij}-\rho_G\right)100\right]}{\rho_{ij}\left(\rho_M-\rho_G\right)} \tag{1.14}$$

where ρ_M = density of the mineral and ρ_G the density of the gangue and the standard deviation of the ij^{th} fraction will be:

$$\sigma^2 = \frac{P_{ij}\left(1-P_{ij}\right)}{N} \tag{1.15}$$

For a multi-component system the principles developed in the above Eqs. 1.13 to 1.15 may be extended. Their solution can be achieved easily by a computer. The general equation for overall sample assay is:

$$A_{ij} = \frac{\sum_{ij} d_i^3 P_{ij}\rho_j A_{ij}}{\sum_{ij} d_i^3 P_{ij}\rho_j} \tag{1.16}$$

Example 1.5

A nickel sulphide ore mineral (pentlandite) has an average particle size of 1mm. It is separated into three fractions and the properties of each fraction are:

Fraction	Mass %	Assay, % pentlandite	Density
1 (Concentrate)	2.4	100.0	4.8
2 (Middlings)	81.0	58.9	3.6
3 (Tail)	16.6	0.0	2.65

The lot has to be sampled so that it would assay ± 0.15 % of the true assay having 5% with a probability of 99%

Solution

Step 1.
As the stipulated probability is 0.99 Table 1.4 may be used.

Here $X = \dfrac{0.15}{\sigma} = 2.576$ or $\sigma = 0.058$

Step 2.

Estimate P_{ij} from Eq. (1.13) in the following manner (Table 1.5):

Table 1.5
Calculation of the proportion of particles in the ij^{th} fraction

Fraction		Mass	Assay	SG	Av. Dia	d_i^3	$d_i^3 \times \rho$	Mass % $d_i^3 \rho$	Proportion by No.
i	j	%			d_i		$(7)\times(5)$	$(3)/(8)$	$(9)/\Sigma 9$
(1)	(2)	(3)	(4)	(5)	(6)	(7)	(8)	(9)	(10)
1	1	2.4	100.0	4.8	1	1	4.8	0.5	0.017
1	2	81.0	58.9	3.6	1	1	3.6	22.7	0.776
1	3	16.6	0.0	2.65	1	1	2.65	6.03	0.207
	Σ	100.0						29.23	1.0

Step 3.

With known P and σ, N can be estimated using the equation $\sigma^2 = \dfrac{P_i(1 - P_i)}{N}$

Now follow Example 1.4 to determine the sample size.

1.4. Incremental Sampling

Theoretically, unbiased gross samples can be obtained by collecting a sufficiently large number of single particles from a sampling unit. If each particle has a finite chance of being selected for a gross sample, and if this probability is only a function of its size, then this collection of particles will constitute an unbiased probability sample.

In the practice of sampling bulk solids, such a sample collection scheme is highly impractical. Therefore, we collect groups of particles for primary increments.

Sampling experiments that are based on the collection of a series of small and large increments from a large set of particles, demonstrates that the precision of a single increment sampling regime is a function of the number of particles in a primary increment. As a matter of fact, the formula for the variance of a binomial sampling unit, $\text{var}(x) = N.p.q$, shows the fundamental relationship between probabilities (p, q), the total number of particles in an increment (N), and thus its mass, and the precision for the parameter of interest. Hence, the precision of a single increment is essentially determined by its mass.

The binomial sampling experiment in which $p = 0.095$, and $q = 0.905$ (q = alternate binomial probability $= 1 - p$), can be used to set up a table in which the precision of a primary increment is given as a function of the average number of particles in an increment. In Table 1.6, the 95 % confidence ranges (CR) that are calculated from corresponding 95 % confidence intervals (CI) for the expected number of value particles in each increment, together with their coefficients of variation, are listed.

Since these ranges are based on properties of the binomial distribution, their values are obviously independent of particle size. For a bulk solid with a certain density, its top size determines the mass of a primary increment. Top size is defined as the 95% passing sieve size.

14

Table 1.6
95 % Confidence Intervals and Ranges [10].

Number	Low	High	CV in %
10	0	29.0	98.0
10^2	4.0	15.0	31.0
10^3	7.6	11.4	9.8
10^4	9.2	9.8	3.1
10^5	9.4	9.6	1.0
10^6	9.47	9.53	0.3

The mass of an increment must be such that it is large enough to include the large particles and particles present in the sample should be in the same proportions as in the lot being sampled. The minimum mass of the increment is therefore dependent on the size of the particles being sampled.

The top size of a bulk solid is a measure of length. The mass of a particle is a function of its volume and specific gravity and ultimately a function of its mean diameter or length. The mass of a primary increment then can be defined in terms of the number and mass of particles from the top size range. If no other information is available, then an acceptable rule of thumb is to collect primary increments with a mass equal to 1,000 times the mass of a top size particle.

$$\Delta M = 1,000 \cdot \Delta M(t) \qquad (1.17)$$

where ΔM = mass of primary increment in kg
$\Delta M(t)$ = mass of top size particle in kg.

Experience and theory are embodied in a number of national and international standards on sampling of particulate materials where the sampling regimes are defined in terms of the total number of increments, and the average mass of a primary increment.

It is generally accepted that a primary increment should contain no less than one-thousand (1,000) particles.

In the standard on sampling of iron ore (ISO TC102), the minimum mass for primary increments is specified in relation to the top size, and in Table 1.7 these recommendations are tabulated and compared to calculations for hard coal.

The minimum mass for a primary increment should preferably be defined in terms of the volume of a particle from the top size range.

Once the mass for a primary increment is selected either in accordance with applicable standards or on the basis of the previous guidelines, or determined by the critical design parameters of a mechanical sampling system, the required number of primary increments remains to be defined. Too few increments will result in too low a precision while too many would unnecessarily increase the costs for sampling and preparation.

Most standards for bulk solids contain simple formulae to calculate the required number of increments for a consignment from a given number for the unit quantity (usually 1,000 t), or

from tables that list the minimum numbers of primary increments as a function of the mass of a consignment. ISO TC 102 for iron ore specifies this number on the basis of the three levels of variability which presupposes some knowledge of the expected variability.

Table 1.7
Minimum mass for iron ore & coal primary increments [10].

Top size in mm	ISO TC 102 Iron Ore Mass in kg	ISO 1988 Hard Coal Mass in kg
10	0.3	0.6
20	0.8	0.8
50	4	3
100	12	6
150	20	9
250	40	15

Table 1.8 is extracted from ISO 1988 on sampling of hard coal, and lists the number of primary increments for a 1,000 t unit quantity.

Table 1.8
Number of increments to attain a precision of ±0.1 of the true ash [11].

Condition of Coal	Conveyors Falling Streams	Wagons Barges	Seagoing Vessels	Stock Piles
Cleaned	16	24	32	32
Uncleaned	32	48	64	64

Table 1.9 gives the mass and numbers of primary increments for hard coal, as specified in ASTM D 2234, for consignments of up to 1,000 t, and for an estimated precision of ±10% of the ash content.

For consignments larger than this unit mass of 1,000 tonnes, ASTM D 2234 and ISO 1988 use the same formula to calculate the required number of primary increments:

$$n = n(t) \cdot \sqrt{\frac{\sum M}{1000}}$$ (1.18)

where n = required number of increments
$\sum M$ = mass of consignment in tonnes
n(t) = tabulated number of increments

Table 1.9
ASTM D 2234 Number and Mass of Increments (American Society for Testing and Materials).

Top Size in mm	Cleaned		Uncleaned	
	Mass in kg	Number	Mass in kg	Number
16	1	15	1	35
50	3	15	3	35
150	7	15	7	35

The overall standard deviation of sampling, sample preparation and assay is a function of the variability of the particulate material, the number and mass of the increments and the random errors associated with sample preparation and assay. It can be expressed as:

$$\sigma_T^2 = \frac{\sigma_L^2}{n} + \sigma_{PA}^2 \tag{1.19}$$

where σ_L = standard deviation of a primary increment (from Eq. (1.3))

σ_{PA} = standard deviation of preparation and assay.

In a well-balanced sampling regime the variance of sampling and the variance of preparation should be of the same order of magnitude.

Dividing a consignment of bulk solids into lots, collecting, preparing and assaying samples from each lot, and reporting composite assays for the consignment, impacts significantly on the precision of the final result. The variance of preparation and analysis may easily become a limiting factor for the precision of a sampling regime.

If we solve n, the number of primary increments, from the simplified formula for a sampling regime of only one gross sample per consignment and a single measurement in the final analysis sample, it follows that [10]:

$$n = \frac{\text{var}(d) + \text{var}(c)/\Delta M}{\text{var}(t) - \text{var}(pa)} \tag{1.20}$$

where var(c) = composition variance

var(d) = distribution variance

var(pa) = preparation and analysis variance

var(t) = total variance

The denominator of this formula may easily become a limiting factor for the total precision of sampling regimes since it shows that:

$$n \rightarrow \infty \quad \text{for var(pa)} \rightarrow \text{var(t)}$$

Logically, the total variance cannot be smaller than the variance of preparation and analysis.

Example 1.6

Suppose that we have a consignment of 1,000 t of iron ore with an assay of 65.0% Fe, and that we want to determine the assay with a precision of ±10%.

A precision of ±10% of 65.0% Fe is equivalent to ±6.5% of this iron content, and results in a standard deviation of, $6.5/2 = 3.25$ for a total variance of $3.25^2 = 10.56$. Substitution of this total variance of 10.56, composition and distribution variances of say 1.66 and 0.71, and an average mass of 2 kg for primary increments, in the formula for n, Eq. (1.20), results in:

$$n = \frac{0.71 + 1.66/2}{10.56 - 0.0455} = 0.146 \sim 1$$

In this case, a sampling regime of 1 primary increment of 2 kg would result in the required precision of ±6.5% of the iron content.

For a precision of ±1.0 % instead of ±6.5 %, how many increments must we collect to attain this precision?

For an iron assay precision of ±1.0 % the standard deviation becomes, $1/2 = 0.5$, for a total variance of $0.5^2 = 0.25$. Substitution in Eq. (1.20) would result in a number of 7.5 (or rounded to 8) increments.

If a greater iron assay precision of ±0.25 % is required then the denominator in the above equation becomes negative and it is not possible to obtain that degree of precision sampling from a single lot. The consignment must be divided into sub-lots in order to determine the assay with this precision. Table 1.10 shows a number of possible combinations.

Table 1.10
Precision of Sampling Regimes and the Number of Increments Required [10].

Precision	var(t)	Lots	Increments
±1.0	0.2599	1	8
±0.5	0.0625	1	90
±0.25	0.0156	4	360
±0.25	0.0156	8	155
±0.10	0.0025	32	1430
±0.10	0.0025	64	860

These results show that the assay of this particular type of ore cannot be determined with a precision of ±0.25% at affordable costs because the variance of preparation and analysis rapidly becomes a limiting factor for the total precision.

18

In terms of standard deviations, the number of increments may be calculated from [1]:

$$n = \frac{\sigma_L^2}{\sigma_T^2 - \sigma_{PA}^2} \qquad (1.21)$$

When it is impossible to achieve the desired precision by testing a single gross sample from a lot (eg. The number of increments is impossibly large) then it is necessary to divide the lot into a number of sub-lots, n_S. Then:

$$n = \frac{\sigma_L^2}{n_S \sigma_T^2 - \sigma_{PA}^2} \qquad (1.22)$$

The total number of primary increments for the whole lot then becomes n_S x n.

Example 1.7

Calculate the number of increments required in the sampling of silica in iron ore for a desired overall precision of 0.1, if increment standard deviation is 1.5 and the preparation and assay standard deviation is 0.095.

$$n = \frac{1.5^2}{0.1^2 - 0.095^2} = 2308$$

If the lot is divided into say 8 sub-lots, then:

$$n = \frac{1.5^2}{8(0.1)^2 - 0.095^2} = 32$$

Therefore 32 primary increments are required per sub-lot for a total of 8 x 32 = 256 primary increments in total.

When small amounts of sample are removed from a lot at random and combined to form a composite sample, the problem is to ascertain the incremental amounts and number of increments which would represent the bulk within specified limits. Each individual sample will have an assay equal to, more or less, the true value. Assuming that a normal Gaussian distribution will be obtained if the assays were plotted against frequency, the probability that the assay will be within permissible limits will be given by:

$$P = \sqrt{\frac{2}{\pi}} \int_0^{x_1} e^{-\frac{x^2}{2\sigma^2}} d\left(\frac{x}{\sigma}\right) \qquad (1.23)$$

where   x = deviation from the true assay.

Now if A is the average assay and $A_1, A_2, A_3 \ldots A_N$, are the individual assays of the n sample increments then:

$$A = \frac{1}{n}\left(A_1 + A_2 + A_3 \ldots + A_n\right)$$ (1.24)

and the standard deviation of each increment sample will be:

$$\sigma_L = \sqrt{\sum_n \frac{(A_i - A)^2}{n}}$$ (1.25)

The standard deviation of the entire sample, σ, is related to σ_L by the relation

$$\sigma = \frac{\sigma_L}{\sqrt{n}}$$ (1.26)

Substituting the values of σ and σ_L in Eq. (1.23) and simplifying gives:

$$P = \sqrt{\frac{2}{\pi}} \int_0^{h_1} e^{-\frac{h^2}{2}} dh$$ (1.27)

where $h = \frac{K A \sqrt{n}}{\sigma_L}$, $K = \frac{x}{A}$,   then $h \equiv \frac{x}{\sigma}$ (1.28)

The application of this method of estimating n is illustrated in Example 1.8.

Example 1.8

10 samples were taken from a heap of copper ore each weighing 2 kg. The assays for copper show the following distribution:

Sample No	1	2	3	4	5	6	7	8	9	10
Assay	3.0	2.5	2.2	3.2	2.5	2.5	2.3	2.9	3.3	2.1

The final sample should assay within ± 5% of the true value with a confidence of 99%. Estimate the number of increments.

Solution

Step 1

Average assay $= (A_1 + A_2 + A_3 + \ldots + A_{10})/10 = 2.65$

Standard Deviation, $\sigma_L = 0.400$, from Eq. (1.25).

Step 2

For the probability $P = 0.99$ (given) and using Table 1.4 to simplify the solution of Eq. (1.23),

$h = 2.576$

Step 3

Calculate the value of h in terms of n where, $K = 0.05$, $A = 2.65$ and $\sigma_L = 0.40$, from Eq. (1.28)

i.e. $h = \dfrac{KA\sqrt{n}}{\sigma_L} = \dfrac{0.05 \times 2.65 \sqrt{n}}{0.40}$

Step 4

$$n = \left(\frac{h\,\sigma_L}{KA}\right)^2 = \left(\frac{2.576 \times 0.40}{0.05 \times 2.65}\right)^2 = 60.5$$

Hence 61 increments have to be taken whose weight would be $61 \times 2 = 122$ kg

---

1.5. Continuous Sampling of Streams

When mechanical samplers are employed, the samplers are designed to cut into and withdraw from a stream of travelling material at a predetermined frequency and speed. Cutters could operate linearly or rotate within the stream to be sampled.

1.5.1. Linear Cutters

A schematic design of a linear cutter is illustrated in Fig. 1.6. Linear cutters traverse across the stream to be sampled.

Its operation depends on:

- Cutter opening
- Stroke length
- Cutter speed

The rule of thumb for cutter openings is:

Normal Opening	$\cong$	3 x largest particle size (dry stream)
Minimum Opening	$\cong$	70 mm for fine particles
	$\cong$	60 mm for fine slurry
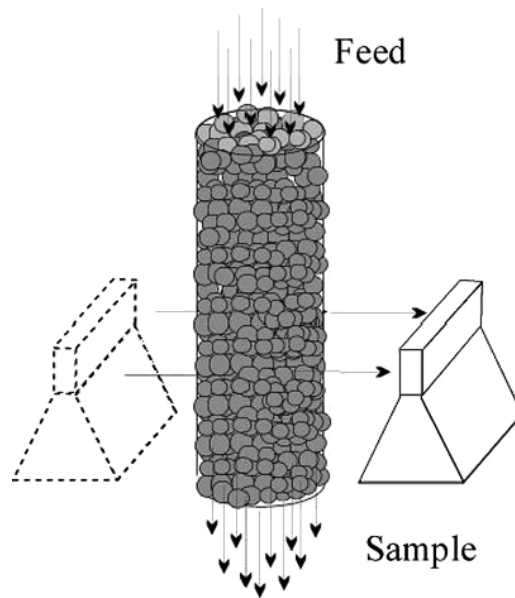
Fig. 1.6. Linear traversing sampler.

It is expected that the opening sizes indicated here would prevent the formation of bridges across the openings in samplers. Also, the wider the cutter opening the greater could be the speed of traversing the cutter.

The stroke length is adjusted to cover the width of the conveyer belt where the stream consists of dry solids, or the width of the stream where liquids or slurries have to be sampled. The amount of sample (M) cut from any stream by a linear cutter is given by:

$$M = \frac{\text{(Feed rate of stream) (Cutter opening)}}{\text{(Cutter speed)}} \qquad (1.29)$$

For a feed rate expressed as kg/s, a cutter speed in m/s and a cutter opening in m, the mass M, is in kilograms. Eq. (1.29) can be expressed in terms of volume and can be written as:

$$V = \frac{(\text{Vol. rate of flow})(\text{Cutter opening})}{(\text{Cutter speed})} \qquad (1.30)$$

where the units for volume rate of flow is m^3/s, cutter opening, m and cutter speed, m/s.

1.5.2. Rotary Arc Cutter

The rotary type of cutters (Fig. 1.7) allows samples to be collected or passed through as indicated in the segments. For unbiased sampling, the edge of the cutters equals the radius of the circle forming the arc. The effective radius, R, swept out by the cutter at any point, in terms of the distance d from the centre of rotation of the cutter to the stream to be sampled along the centreline is given by:

$$R = \frac{d}{\cos\theta}$$
(1.31)

where θ is the angle between the radius of the cutter and the centreline of the solids stream. The cutter opening changes as the cutter moves through the stream, then by simple geometry, the effective cutter opening, d_{cutter}, at any point is approximately given by:

$$\text{Cutter opening, } d_{cutter} \cong \frac{d \tan\alpha}{\cos\theta}$$
(1.32)

If ω is the rotational speed (rpm) of the cutter then the cutter speed, S_{cutter}, parallel to the solid stream, can be given by:

$$S_{cutter} = 2\pi d\,\omega \cos\theta$$
(1.33)

When the leading edge of the cutter reaches the centreline of the discharging conveyor or stream, $\cos\theta = 1$, therefore conditions for d_{cutter} and S_{cutter} reduces to:

$$d_{cutter} = d \tan\alpha \qquad \text{and} \qquad S_{cutter} = 2\pi d\,\omega$$
(1.34)

To determine the quantity of sample taken by the arc cutters, it is necessary to know the cutter angle, α. This may be supplied by the manufacturer for a predetermined position of the cutter or it can be calculated from the following relation:

$$\text{Cutter Angle, } \alpha = \frac{\text{Cutter Arc length}}{2\pi r} \times 360$$
(1.35)

The mass of sample of solids, M, recovered per rotation can be computed from a known flow rate of mineral, M_F, by the expression:

$$M = \frac{\alpha M_F}{360\,\omega}$$
(1.36)

M_F is expressed in kg/s, and ω as rpm.
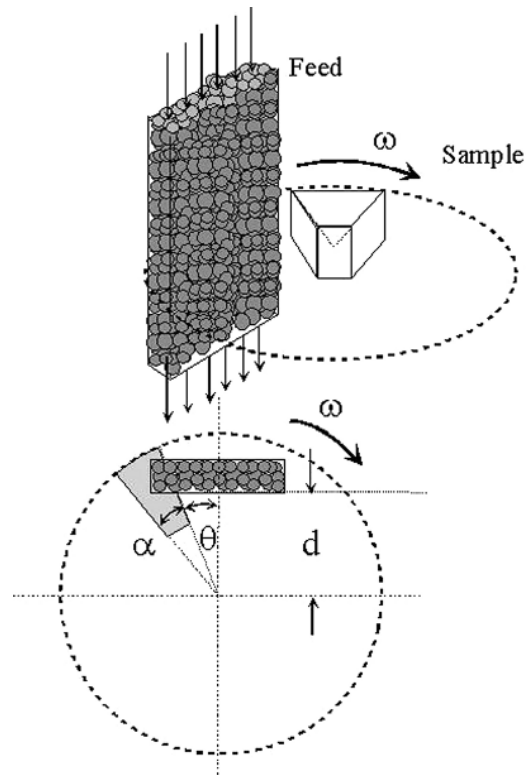
Fig. 1.7. Continuous rotary arc sampler.

The volume, V, of liquid or slurry sampled can similarly be written as:

$$V = \frac{\alpha \; V_S}{360 \; \omega} \qquad\qquad (1.37)$$

V_S is expressed as m^3/s

NOTE: Usually $d = 2/3$ radius R, of the cutter

Example 1.9

Dolomite was carried to the bunkers of a blast furnace at the rate of 200 t/h using a 75 cm wide rubber conveyor belt. The rate of travel of the belt was 61 m/min. The size analysis of dolomite indicated 95 % smaller than 7 cm. The dolomite was sampled as it entered the bunkers using a linear traversing sampler capable of traversing at the rate of 60 cm/s and making 20 cuts per hour. Estimate the mass of sample collected in 10 minutes.

Solution

Step 1
Using rule of thumb, the normal cutter opening $= 3 \times 0.07 = 0.21$ m

Step 2
Using Eq. (1.29):

Sample mass per cut $= \dfrac{200 \times 0.21}{60 \times 60 \times 60} = 0.000194$ t $= 0.194$ kg

Step 3
Mass of sample cut in 10 mins $= 0.194 \times 20 / 6 = 0.647$ kg

---

1.6. Sampling Ores of Precious Metals

Precious metal deposits sometimes contain very low concentrations of discrete metallic particles as in the case of gold deposits. Extra care is therefore needed to collect a representative sample. If it is assumed that the ore comprises of free particles of uniform size then, N, the number of particles required is given by :

$$N = 0.45 \left(\frac{G}{\sigma_S^2} \right) \tag{1.38}$$

where   G   =   grade of the ore , expressed as volume fraction, and

       σ_S =   probable error in sampling, expressed as volume fraction

The number of particles per gram, N', is related to the material density (ρ_S) and particle size by an empirical relation as [12]:

$$N' = \left(\frac{6}{\rho_S d^3} \right) \tag{1.39}$$

where   d   =   limiting screen aperture. This empirical equation covers a range of particle sizes and shapes.

The mass of sample, M to be taken can be given as:

$$M = \frac{N}{N'} = 0.075 \left(\frac{G \rho_S d^3}{\sigma_S^2} \right) \tag{1.40}$$

Gy's method of sampling and determining the minimum mass of sample is also applicable in this case.

Based on Gy's method, Eames [13] indicated that the minimum sample required of gold ores of different particles sizes can be selected from the following table for normal work:

Table 1.11
Minimum Sample Mass for different particle size of gold [13].

Particle Size, mm	Au in Mineral, g/t				
	0.01	0.1	1.0	10	30
50	1.45 mt	143 kt	14.3 kt	1.43 kt	477 t
10	11.4 kt	1.14 kt	114 t	11.4 t	3.81 t
5	1.43 kt	143 t	14.3 t	1.43 t	477 kg
1	11.43 t	1.14 t	114 kg	11.4 kg	3.81 kg
0.5	1.42 t	143 kg	14.3 kg	1.43 kg	477 g
0.1	11.4 kg	1.14 kg	114 g	11.4 g	3.81 g
0.05	1.43 kg	143 g	14.3 g	1.43 g	0.48 g
0.01	11.4 kg	1.14 g	0.11 g	0.01 g	3.81 mg

In developing the table, a 90% confidence level and a relative 15% error has been assumed.

NOTE: A usual practice is to crush 3.5 kg ore to 95% passing 75 micron sieve size and then taking a 200 gram sample for assay.

1.7. Sampling Nomographs

When sampling to determine the grade of a large body of material, the sample of 94 kg (for example) must be reduced to a few grams for chemical analysis. To do this and still maintain the sampling accuracy, Eq. (1.5) suggests that the size of the particles should be reduced to allow a reduction in the sample mass. To optimise a sampling regime, a sampling nomograph is useful.

A nomograph may be drawn up from theory by rearranging Eq. (1.5) to give the variance (σ^2) for a given particle size, d $_{Max}$ as;

$$\sigma^2 = \frac{Kd_{MAX}^3}{M_{MIN}} = \frac{constant}{M_{MIN}} \tag{1.41}$$

Taking the logs of both sides of Eq. (1.41) gives:

$$\log \sigma^2 = constant - \log M_{MIN} \tag{1.42}$$

therefore, a nomograph plotted on a log-log scale will have a slope of -1, as shown in Fig. 1.8.

The use of the figure is illustrated in the following example. A sample of 94 kg (94000g) is crushed to minus 5 mm and a 30 g sub sample is split out for gold assay, using a riffle. The line on Fig. 1.8 shows that as the sample mass is reduced, the error associated with a particle size of 5 mm increases until it exceeds the minimum error specified for this sampling regime for any sample mass below about 200g.

To stay within the specified sampling accuracy, a sampling regime similar to Fig. 1.9 should be followed.
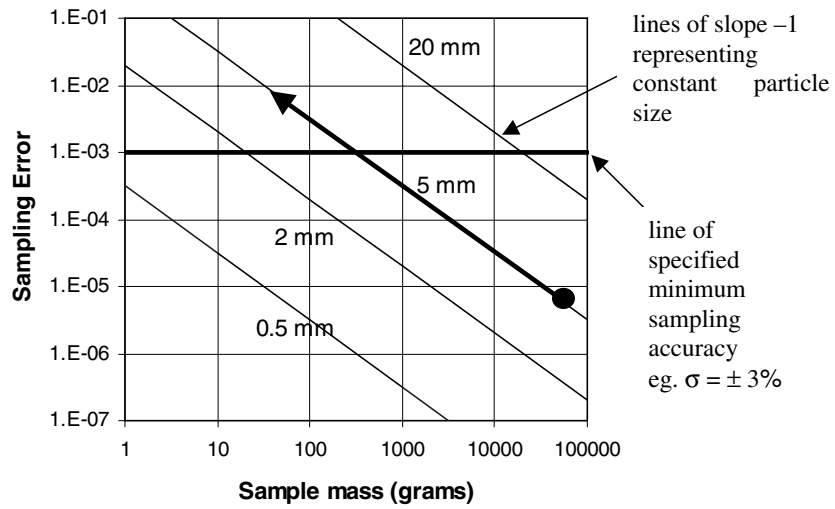
Fig. 1.8. σ^2 vs. sample mass an inappropriate sampling regime (basic sampling nomograph).
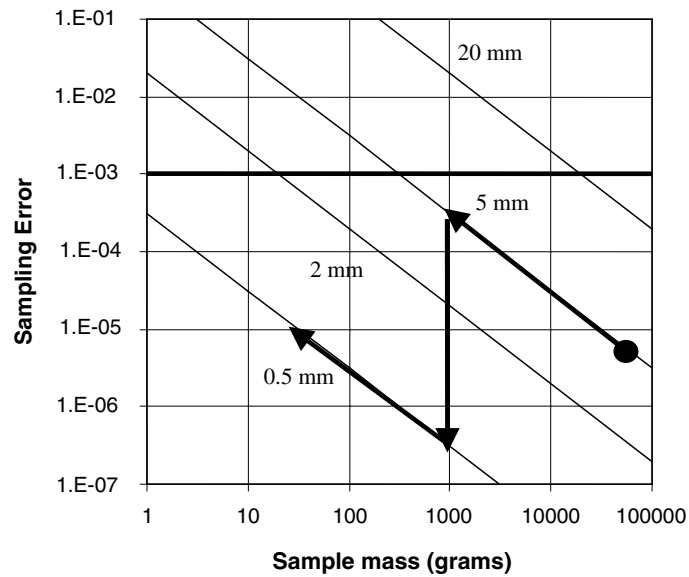
Fig. 1.9. A more appropriate sampling regime.

The 94 kg of minus 5 mm material is sub divided to a sub sample mass of 1000g in the first stage. This 1 kg of sample is then pulverised to minus 0.5 mm and divided again to the required sample mass of 30 g. Following this sampling regime will maintain the sampling procedure below the required sampling error.

To derive a sampling nomograph, Eq. (1.5) is used by calculating the sampling constant K from known data.

An alternative graphical method is to plot sample mass (M) vs top particle size (d_{MAX}) showing the alternation of size and mass reductions required to maintain an acceptable sampling variance, governed by the Gy formula (Fig. 1.10).

This can be achieved in the following manner:

$$\text{From Gy's formula;} \quad M_{MIN} = \frac{K d_{MAX}^3}{\sigma^2}$$

$$\text{and} \quad \log M_{MIN} = (\log K - 2 \log \sigma) + 3 \log d_{MAX} \tag{1.43}$$

Thus for a given value of K and sampling accuracy, this relationship will yield a straight line of slope 3 when plotted on log-log graph paper (Fig. 1.10). All points on this line, (line BDF, Fig. 1.10), have a constant fundamental variance, σ^2. The line represents a "safety line" and splits the graph into two areas.
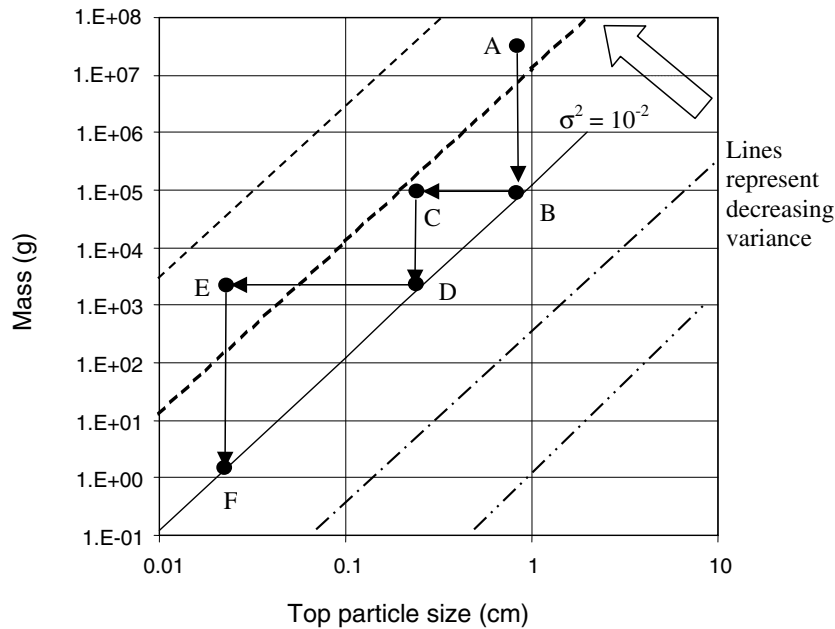
Fig. 1.10. Alternative graphical sample regimes.

To the left of this line, the sample mass is greater than the minimum required, M_{MIN}, and the fundamental sampling variance is less than σ^2.

To the right of the line, the sample mass is less than the minimum and the sampling variance is high and unacceptable. To rectify the situation, either the mass has to be increased or the particle size, d, has to be decreased to bring the sampling regime back to the left of the safety line.

A family of lines of equal variance can be constructed, each parallel to one another (Fig. 1.10). From Fig. 1.10, for a sample mass of 50 tonnes at a particle size of 9 mm, and a desired variance of 10^{-2} or better, the sample can be reduced in mass to 100 kg (A to B) and still maintain acceptable accuracy (to the left of the safety line). To reduce the mass further, the sample must first be reduced in particle size, eg. to 3 mm (B to C). The sample mass can then be reduced to 1 g through a sequence of mass reduction and size reduction (C to D to E to F).

1.8. Problems

1.1

Iron ore was sampled before stock piling with a stacker. One hundred samples taken from the stacker-conveyor showed a standard deviation in the iron assay of $\pm$ 0.5 %. The ore assayed, on average, 59 % Fe. Sieve analysis of the samples showed that the largest size was less than 5 mm and the liberation of Fe was maximum in the size range, -400 + 300 μm. Given that the specific gravity of the ore was 5.3 and the specific gravity of the gangue was 2.6, estimate the minimum mass of sample required representing the stack.

1.2

Run-of-Mine iron ore was conveyed on a conveyor belt and sampled at regular intervals. The sieve analyses and Fe distribution obtained at different sampling frequencies gave the following results:

Size Range, mm	-6 +5	-5+4	-4+3	-3
Mass Fraction %	10	30	50	10
Fe,%	61.2	62.0	64.5	62.0

Frequency	20	26	30	40	45	35	8
Fe %	54.2	54.0	62.2	64.8	65.5	66.0	67.0

The specific gravity of the ore was 5.5 and that of the gangue material was 2.55.
Determine the minimum mass of sample required to represent the Run-of-Mine ore.

1.3

A pile of gold tailings was augered to sample the dump. A 5 cm diameter drill bit was used and samples recovered from different depths. The recovered samples were collected and after mixing thoroughly, the composite was crushed, screened between 125 μm and 75 μm and analysed for gold. The average of 10 gold analyses indicated a value of 200 $\pm$10 ppm gold. The liberation size of the gold was determined as -43 μm. The specific gravity of the gold

bearing minerals was 4.5 and the associated gangue minerals were 2.68. Estimate the minimum size of the sample

1.4

In a metallurgical test, the quality of feed was monitored. Four operators and three similar test equipment were employed. Material lost in the feed after each operation in each test was:

Equipment No	Operator			
	1	2	3	4
1	12.5	13.8	12.2	11.5
	12.8	12.5	12.8	13.1
	12.0	13.4	12.1	12.84
2	12.4	12.8	13.5	13.2
	11.8	13.0	13.0	12.5
	13.2	13.9	12.2	12.8
3	12.6	12.9	13.2	12.6
	12.2	12.07	13.0	12.2
	13.0	12.7	2.8	13.2

Estimate the variance due to operator and experimental error.

1.5

A mechanical sampler was used to sample a stream of iron ore conveyed on a 1.5 m wide travelling conveyor at a rate of 90 m/min. and loaded to carry 12 mt/h of ore. The sample cutter opening was 20 cm square and was operated at a frequency of 5 cuts per minute. The recovered sample was first crushed to –10 mm and then to –2.5 mm and analysed for Fe content. The liberation size of Fe was –65 μm and the standard deviation of the Fe content was ± 0.15 after the first crushing and the same after the second crushing. If the average analysis was 59% Fe, estimate;

1.   The mass of sample cut per minute
2.   The minimum mass of sample required to represent the Fe level of the ore.

1.6

The average assay of a gold sample was 200 ppm Au that varied within 0.5 % of the true assay.95% of the assays had a probability of 0.99 of the true assay. Specific gravity of the gold ore was 5.6 and the gangue was 2.54. Determine the size of a crushed gold ore sample that was taken.

1.7

The mass fractions and distributions of a mixture of sphalerite, chert and middle fractions were determined and the results tabulated below. Compute the size of sample that should be taken such that its assay may be within 0.2% of the true assay, say 5% with a probability of 0.99.

	Sphalerite	Middle fraction	Chert
Mass %	0.15	70.85	29.0
Average Specific Gravity (ρ)	4.00	2.71	2.65
Average Diameter, cm	2.54	2.54	2.54

source: Taggart [9]

1.8

A gold ore was crushed in a jaw crusher down to 3 mm and to 1 mm in a cone crusher and finally in a rod mill to minus 75 µm and sampled at each stage. The standard deviation at the first stage was ± 10 ppm, ± 1 ppm at the second stage and ± 0.1 at the third stage. The confidence level in assaying was 3.0 ± 0.1 %. Estimate the minimum mass of sample to be taken at each stage.

1.9

Three stages of crushing and one stage of riffling were required to get a bauxite ore to the laboratory for testing. The first stage of crushing produced 100 % minus 5 mm, all products from the second stage passed 2 mm and the product from the third stage of grinding passed 125 µm. After each stage, the products were sampled and analysed for alumina. The standard deviations of the alumina determinations were 0.2, 0.1, and 0.05 in the three stages respectively. The ore assayed 2.1 ± 0.2 % of Al_2O_3.

Estimate the minimum mass of the sample that should be taken to represent the ore after each stage.

1.10

10 samples were randomly taken from a 5000 lot of pyrolusite (MnO_2) ore. The composition and distribution of Mn in each lot was determined. The sampler was designed to take 5kg sample at a time. For an assay with a precision of ±1%, estimate the number of increments required.
Data:

No.	1	2	3	4	5	6	7	8	9	10
Mn,%	51.8	50.4	49.8	49.0	52.0	53.0	50.0	51.0	50.8	49.9
Wt%	78.0	76.8	75.5	77.2	79.0	77.5	76.3	78.3	76.9	79.5

The total standard variance was 0.39

1.11
A rotary arc cutter sampler was used to cut samples of a mineral conveyed by a conveyor belt. The sample cutter was placed 75 cm below the conveyor, which travelled at a speed of 90 m/min and carried 50 t of the mineral per min. The maximum cutter opening was 7cm. Estimate:

1. The cutter angle required

2. The quantity of sample taken per cut

REFERENCES

[1]   Draft Australian Standard, DR 00223 2000, Guide to the Sampling of Particulate Materials: Part 3:Estimating sampling precision, Standards Australia, (2000).
[2]   T. Allen, Particle Size Measurement, 2nd edn., Chapman and Hall. (1975).
[3]   H. Heywood, Trans. Institute of Chemical Engineers, 25, (1947), 14.
[4]   R.R. Irani and C.F. Callis, Particulate Size measurement, Interpretation and Application, John Wiley, New York, (1963).
[5]   B. Lister, Mining Magazine, Sept., (1980), 221.
[6]   P.M. Guy, International Journal of Mineral Processing, 3, (1976), 289.
[7]   P.M. Guy, Sampling of Particulate Material: Theory and Practice, Elsevier Scientific Publishing Co., Amsterdam. (1979).
[9]   B.A. Wills, Mineral Processing Technology, 4th edn., Pergamon Press, Oxford, (1989).
[9]   A.F. Taggart, Handbook of Mineral Dressing, John Wiley and Sons, London, (1953).
[10] J.W. Merks, Sampling and Weighing of Bulk Solids, Trans Tech Publications, Clausthal-Zellerfeld, (1985).
[11] AS 1676-1975, Methods for the Sampling of Hard Coal, Standards Association of Australia, (1975).
[12] Quest and Newell 2002, private communication.
[13] J. Eames, Joint Seminar by MICA,AIG,Aus.I.M.M. Sydney, 26th July, (1999), 81.

Chapter 2. Particle Size Estimation and Distributions

2. INTRODUCTION

The term *mineral particle* is loosely used in mineral processing. Particles in a mineral processing plant are never a single size but consist of many different sizes. The particles are also many different shapes which makes characterisation of the quantity, *size*, very difficult.

Unless a particle is spherical or cubic its size determination is never an absolute process. Particles such as (a) and (b) in Fig. 2.1 can uniquely be described by the diameter of a sphere, d_S or the length of the side of a cube, d_C. However, the dimension of particle (c) is difficult to characterise as either the maximum, d_{MAX} or the minimum d_{MIN} or some dimension in between could be used to represent the particle size.
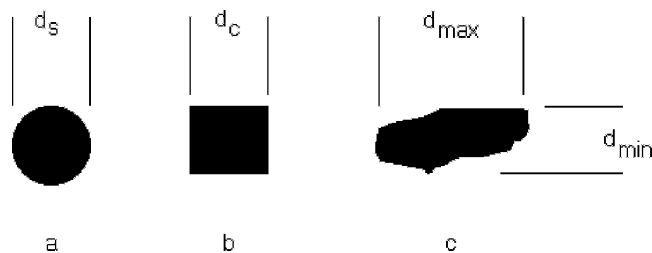
Fig. 2.1. Characterisation of particle size.

2.1. Methods of size estimation

There are many ways the size of an irregular particle could be characterised, with none being absolutely right. For instance, the particle size can be characterized by determining the size of hole or aperture the particle will just pass through (sieve size), or the time the particle takes to settle in a fluid such as water and express the particle size as the size of a sphere that has the same settling rate (Stokes diameter). Particle size could also be expressed as the diameter of a circle that has the same cross sectional area or projected area as the particle, when placed either on its most stable position or randomly oriented positions. In three dimensions, the equivalent volume or surface area of a sphere have also been used to describe a particle size. Visual examination under the optical microscope or electron microscope or the diffraction of a laser beam have been used to derive statistical dimensions of particles. All of these methods do not necessarily give the same measure of size for the same sample of particles. Hence it is necessary to mention the measurement method when quoting particle size.

The particle dimensions measured by optical methods are limited to sizes greater than 100 µm. With an electron microscope, particle sizes down to 0.001 µm can be measured. For gravity sedimentation methods, the particle size should be greater than 1 micron.

Where individual measurements are not required approximate size ranges can be obtained by sieving. The closer the successive sieve sizes are, the closer is the approximation to the real size of the particles held between successive sieves. This information is usually sufficient for most metallurgists and sieving is the most common method of determining size.

2.1.1. Microscopic Method

The use of a microscope to measure the size of irregularly shaped mineral particles can be a tedious and difficult process. A video camera linked to a computer can speed up the process of size recognition by the projected outline of a particle. Video systems are used to size large lumps of rock on conveyor belts and even on the back of dump trucks as the load is tipped into crusher feed bins. The obvious technique is to measure the average distance between two extremities of the particle and the arithmetic or geometric mean of a number of measurements taken. The extremities of the distance to be measured is standardised [1] and taken as the mean cord length of the projected outline as defined by Martin's or Feret's diameter (Fig. 2.2). Martin's diameter is the length of the line bisecting the image of the particle. The bisecting line is taken parallel to a fixed direction, irrespective of the orientation of the particle (Fig. 2.2). Feret's diameter is the mean distance between two tangents on the opposite sides of the apparent outline of the particle. The tangents are perpendicular to an arbitrarily fixed direction, irrespective of the orientation of the particle.

The relative size of particles may also be indicated by reference circles having an equal projected area or perimeter, (Fig. 2.2). The diameter of the reference circle is the arithmetic or geometric mean value of the distances by Martin's or Feret's method. The arithmetic mean diameter measured by either method may be approximated as:

$$d_{AM} = \frac{d_{MAX} + d_{MIN}}{2} \qquad (2.1)$$

where d_{MAX} and d_{MIN} are the averages of several measurements of Martin's or Feret's diameters and d_{AM} is the arithmetic mean diameter. The geometric mean diameter likewise is given by:

Martin's diameter
(divides profile into 2 equal areas)

equivalent area diameter

equivalent perimeter diameter

Feret's diameter

Fixed direction
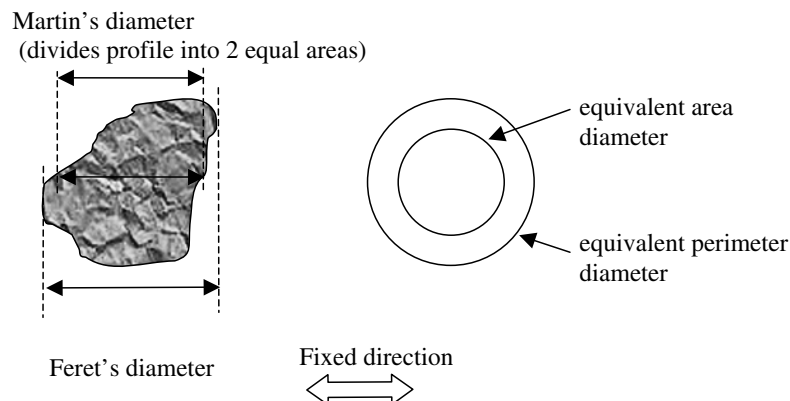
Fig. 2.2. Particle size equivalents.

$$d_{GM} = (d_1\, d_2\, d_3\, d_4\, ...\, d_N)^{1/N} \tag{2.2}$$

$$\text{or} \quad \log d_{GM} = \frac{\Sigma(\log d_N)}{N} \tag{2.3}$$

where N is the number of particles measured.

In some cases the average estimations of diameters is expressed as the Mellor's mean diameter (d_{ML}) which is given by the expression:

$$d_{ML} = 0.632\, [\, (d_{MAX} + d_{MIN})(d_{MAX}{}^2 + d_{MIN}{}^2)]^{0.33} \tag{2.4}$$

This method gives a slightly higher average than the arithmetic mean size of a particle. Therefore when reporting particle size it is necessary to quote the method used.

2.1.2 Particle Size in terms of Volume and Surface Area

Due to the difficulty in measuring length, sometimes the particle size is described in terms of its volume or surface area, as a volume mean diameter or a surface mean diameter. In a sample consisting of several particles, this concept can only be used if it is assumed that all the particles have the same shape. Thus if d is the dimension of the particle and ρ_P the density, then the mass would be proportional to $d^3\rho_P$.

In a mass of sample, M_P, containing N number of particles of characteristic size d_P :

$$M_P = k\, N\, d_P^3\, \rho_S \tag{2.5}$$

where k is a constant, a function of the shape factor, and ρ_S the density of the solid particles.

Eq. (1.48) may be re-written as:

$$d_P^3 = \frac{M_P}{k\, N\, \rho_S} \tag{2.6}$$

If all the particles are assumed to have equal dimensions, which is expressed as the mean volume diameter, d_V, then the sum of the volumes of all the particles of size d_V is equal to the volume of particles in the sample mix. Then;

$$k\, d_V^3 \sum N = \sum k\, N\, d_P^3 \tag{2.7}$$

$$\text{Hence} \quad d_V^3 = \frac{\sum N\, d_P^3}{\sum N} \tag{2.8}$$

Using Eq. (2.6), N may be eliminated from Eq. (2.8). Then on simplifying, the volume mean diameter may be written as:

$$\bar{d}_V^{\,3} = \frac{\sum M_P}{\sum \dfrac{M_P}{d_P^3}} = \frac{1}{\sum \dfrac{M_P}{d_P^3}} \qquad\qquad (2.9)$$

Similarly, the surface mean diameter, $\bar{d}_S$, has been derived by Coulson and Richardson [2] as:

$$\bar{d}_S^{\,2} = \frac{\sum \dfrac{M_P}{d_P}}{\sum \dfrac{M_P}{d_P^3}} \qquad\qquad (2.10)$$

Example 2.1.

Gold nuggets were examined under a microscope and the following frequency distribution was obtained:

Interval	1	2	3	4	5	6
Size, mm	0-1	1-2	2-4	4-8	8-16	16-32
Number	3250	1800	400	120	12	4

Assuming the nuggets are of similar shape, determine the size distribution on a mass fraction basis.

Data: density of gold nugget $= 17580 \text{ kg/m}^3$
Solution

Step 1
Let M_P equal the mass fraction of particles of size d_n and specific gravity ρ_S and let N_n equal the corresponding number of particles in each fraction.

n is the number of size intervals, equal to 6, then:

$$M_P = k \, N_n \, d_n^3 \, \rho_S \quad \text{for } n = 1\text{-}6$$

k is a constant equivalent to the shape factor. In this example, k is taken as 1

Therefore, the mass fraction for each size interval would be:

$$M_P = \frac{N_n \, d_n^3 \, \rho_S}{\sum N_n \, d_n^3 \, \rho_S}$$

The calculations can now be made as follows to estimate M_P values for different values of n:

n	d_n, mm	N	d_n^3	$d_n^3 N$	ρ_S	$d_n^3 N \rho_S$	M_P
1	0.5	3250	0.125	406.25	17580	7.14×10^6	0.0013
2	1.5	1800	3.375	6075	17580	1.07×10^8	0.0199
3	3.0	400	27	10800	17580	1.90×10^8	0.0353
4	6.0	120	216	25920	17580	4.56×10^8	0.0847
5	12.0	120	1728	207360	17580	3.65×10^9	0.6779
6	24.0	4	13824	55296	17580	9.72×10^8	0.1808

2.1.3. Sedimentation Method - Gravity Sedimentation

In metallurgical practice where sedimentation or classification of particles is required, the Stokes diameter is often used to indicate the size of the particle. Stokes' diameter is computed by observing the rate of fall of particles through a stationary fluid medium. The terminal velocity (V_T) of the particle is given by the relation:

$$V_T = \frac{d^2 g (\rho_S - \rho_F)}{18\mu} \quad \text{m/s} \tag{2.11}$$

where d = diameter of a spherical particle, m
$\quad g$ = acceleration due to gravity, m/s^2
$\quad \rho_S, \rho_F$ = density of solid particle and fluid respectively, kg/m^3
$\quad \mu$ = viscosity of the fluid, Ns/m^2 or Pa s (For water, $\mu = 0.001$ Pa s)
$\quad V_T$ = terminal velocity, m/s

Eq. (2.11) is strictly applicable for spherical particles falling through a perfectly still medium and not being "hindered" by other particles or reacting with the medium. To prevent hindrance by other particles, the concentration of the suspension should preferably contain less than 1 % solids. Any hindrance by the walls of the vessel is generally neglected especially when the diameter of the vessel is about 100 times greater than the diameter of the particle being measured.

The expression is not applicable for very small particles or conditions that lead to Brownian movement of particles.

When applying Eq. (2.11) to non-spherical particles the ratio of the maximum to minimum diameter of the particles should be equal to or less than 4. For irregular particles, therefore, the relation does not give the true diameter of a particle, but describes the equivalent spherical diameter or the mean projected diameter d_P of the particle. The mean projected area would be $\pi d_p^2/4$ and the mean volume expressed as, $v = k \, d_p^3$. The constant k is a function of the shape of the particle.

For Spherical particles, $k = \pi/6$
$\quad$ Angular particles, $k = 0.4$ (approximately)
$\quad$ Mineral particles, $k = 0.2$–0.5

Note: Stokes diameter x 0.94 = sieve size (approximately).

Eq. (2.11) can therefore be used to determine the size of individual particles less than 50 μm and preferably greater than 1 μm.

In practice, difficulty arises in determining the terminal velocity (V_T) as the free fall of particles in a medium depends on it's friction against the fluid and buoyancy. The frictional force and the buoyancy acting upwards opposes the downward forces on the falling particle. The combined opposing force known as the "drag" has to be determined to estimate the true value of V_T. For a spherical particle under streamline conditions (also known as laminar or Newtonian conditions), Stokes has determined the drag force, F_D, as:

$$F_D = 6 \pi r \mu V_T \tag{2.12}$$

where   r = radius of spherical particle.

The expression Eq. (2.12) is known as Stokes' Law for laminar flow.

It has been found that F_D varies with the particle diameter, density, velocity of particle and also the viscosity of the medium. The ratio of (d ρ_F V/μ) is a dimensionless number known as the Reynolds number (Re). When the character of fluid flowing past the particle is streamline, then the value of Re is less than 2100. When the flow is turbulent, Re is greater than 4000. Between a Re of 2100 and 4000 is the intermediate or transition stage.

The relation between the drag force and Reynolds number for streamline flow conditions is:

$$F_D = \frac{24}{Re} \tag{2.13}$$

For turbulent conditions, Newton derived the forces due to drag as:

$$F_{DN} = 0.055 \; \pi d^2 V_T^2 \rho_F \tag{2.14}$$

During the settling of a particle under streamline conditions, the force acting on the particle due to gravitational acceleration is given by:

$$mg = \frac{4}{3}\pi r^3 (\rho_s - \rho_F)g \tag{2.15}$$

where   m   = effective particle mass, and
        r   = particle radius

This would be equal to the force at the terminal velocity of the particle, given by Eq. (2.12), i.e.

$$\frac{4}{3}\pi r^3 (\rho_s - \rho_F)g = 6\pi r \mu V_T \quad \text{or}$$

$$V_T = \frac{2}{9\mu} r^2 (\rho_s - \rho_F)g \tag{2.16}$$

This equation is Stokes' equation as given in Eq. (2.11). Under turbulent conditions, similarly:

$$\frac{4}{3}\pi r^3 (\rho_S - \rho_F)g = 0.22\pi r^2 \rho_F V_{TT}^2 \tag{2.17}$$

where V_{TT} is the terminal velocity under turbulent conditions, or

$$V_{TT} = \left[\frac{6rg(\rho_S - \rho_F)}{\rho_F}\right]^{0.5} \tag{2.18}$$

Even though the terminal velocities can be calculated from Eqs. (2.16) and (2.18), in practice it is difficult to ascertain whether the flow past a falling particle is streamline or turbulent. To solve this predicament, F_D is recalculated by considering the dimensionless quantity $[(F_D/\rho_F A V_T^2) \, Re^2]$ to yield an expression which does not include V_T. Now if we consider the drag force/unit projected area, A, of a particle falling freely as F_D', then $F_D' = F_D/A$. We can now write:

$$F_D'.\pi r^2 = \frac{4}{3}\pi r^3 (\rho_S - \rho_F)g \quad \text{or}$$

$$F_D' = \frac{4}{3}r(\rho_S - \rho_F)g \tag{2.19}$$

By multiplying both sides of Eq. (2.19) by the dimensionless factor, $[(F_D'/\rho_F V_T^2) \, Re^2]$ we have:

$$\frac{F_D'}{\rho_F V_T^2}\left[\frac{d\rho_F V_T}{\mu}\right]^2 = \frac{2dg(\rho_S - \rho_F)}{3\rho_F V_T^2}\left[\frac{d\rho_F V_T}{\mu}\right]^2 \quad \text{or}$$

$$\frac{F_D'}{\rho_F V_T^2}[Re]^2 = \frac{2d^3 \rho_F g(\rho_S - \rho_F)}{3\mu^2} \tag{2.20}$$

Similarly we can arrive at an expression, which is independent of d by using the dimensionless factor $[(F_D'/\rho_F V_T^2) \, Re^{-1}]$;

$$\frac{F_D'}{\rho_F V_T^2}Re^{-1} = \frac{2\mu g(\rho_S - \rho_F)}{3\rho_F^2 V_T^3} \tag{2.21}$$

The right hand side of Eq. (2.20) deals with the fluid properties only and therefore can be easily evaluated. The diameter d of the particle falling under any condition can now be computed by equating this value to the left side of Eq. (2.20).
Similarly, the terminal velocity of the particle can be computed from knowledge of the left hand side of Eq. (2.21).

Tables and charts are available, plotting log $[(F_D/\rho_F A V_T{}^2)Re^2]$ against log [Re] and log $[(F_D/\rho_F A V_T{}^2) Re^{-1}]$ against Re. Tables 2.1 and 2.2 give the relationship over a limited range for spherical particles [3]. This data is also presented in graphical form in Fig. 2.3, which can be derived from the empirical correlation [4]:

$$\frac{F_D^{'}}{\rho_F V_T^2} = \left[1.84\,Re^{-0.31} + 0.293\,Re^{0.06}\right]^{3.45} \tag{2.22}$$

As the tables are applicable for spherical particles, Heywood [3] introduced a correction factor for non-spherical particles. To use the correction factor Heywood considered the diameter of the projected area, d_P (of a particle sitting on its most stable position). He calculated the corresponding volume as $k.d_P^3$, where k was a constant and a function of shape and the factor $(F_D/\rho_F A V^2)\,Re^2$.

Other shape factors have been proposed, such as the sphericity factor, S, defined mathematically as [5, 6]:

$$S = \frac{No\min al\ volume\ diameter}{No\min al\ surface\ diameter} = \frac{d_v{}^2}{d_s{}^2} \tag{2.23}$$

where d_V = diameter of a sphere of equal volume
         d_S = diameter of a sphere of equal surface area

The values of log $[(F_D/\rho_F A V^2)\,Re^{-1}]$ and log $[(F_D/\rho_F A V_T{}^2)Re^2]$ corresponding to different values of shape factor, k, are given in Table 2.3. To use this table, log $[(F_D/\rho_F A V^2)\,Re^{-1}]$ is calculated from a measured settling velocity, V_T, using Eq. (2.21) for a spherical particle and the equivalent Re value found from Table 2.2. The correction value from Table 2.3 is then applied to the log Re value to account for the non-spherical shape of the particle. The particle size can be calculated from this corrected value of Re. A similar procedure follows for values of log $[(F_D/\rho_F A V_T{}^2)Re^2]$ calculated from values of particle size d.

Example 2.2

Specular haematite particles from Labrador were sampled to determine the size of individual particles. The average terminal velocity of the particles was determined to be 15 mm/s by allowing single particles to fall through a tall cylinder of water. The density of the ore particles was 5400 kg/m³ and the water at a temperature of 25 ⁰ C. Estimate the approximate size of the particles.

Data: μ (H_2O) at 25 ⁰ C = 0.8904 mPa.s

40
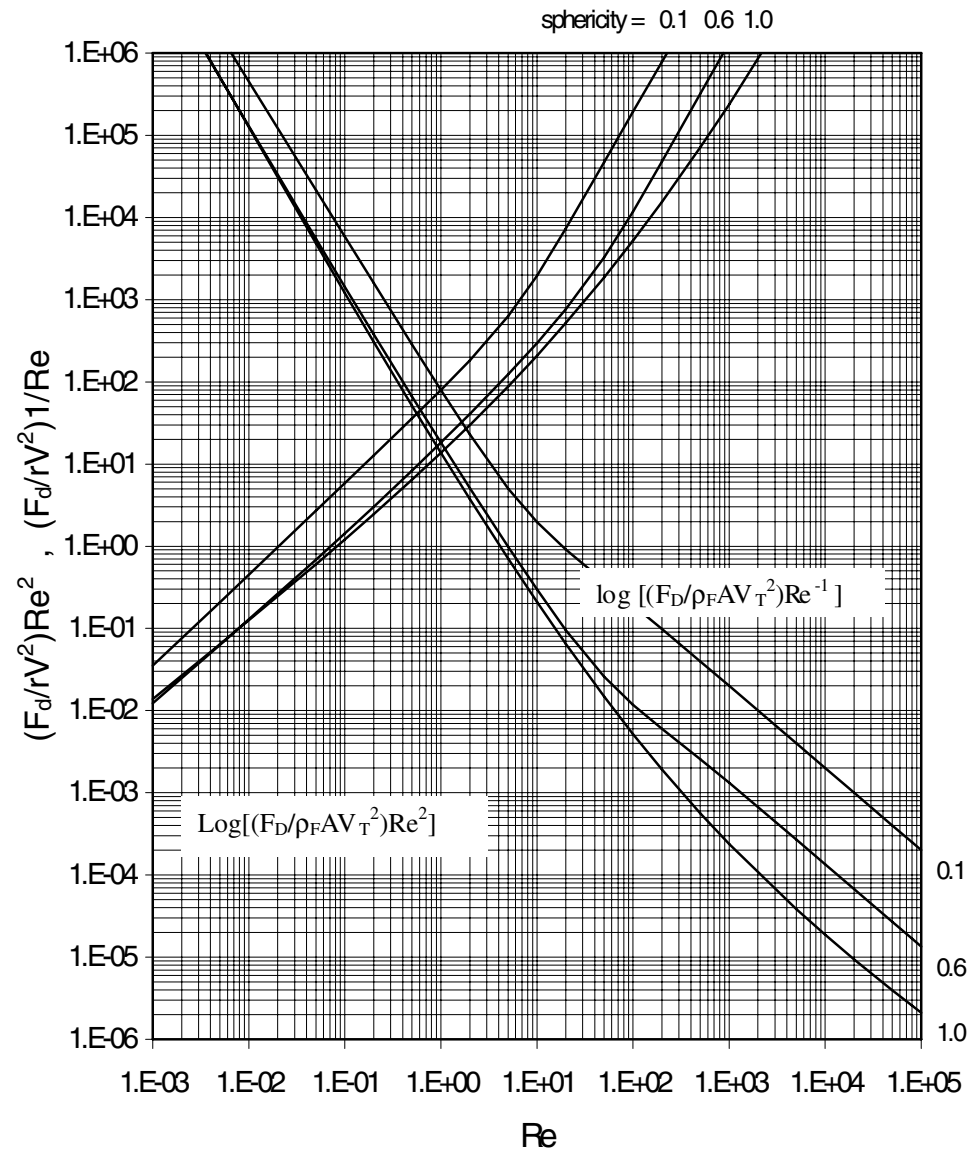
Fig. 2.3. Relationship between $\log[(F_D/\rho_F A V_T^2)Re^2]$ and $\log Re$ and $\log[(F_D/\rho_F A V_T^2)Re^{-1}]$ and $\log Re$ for different particle shape factors, S.

Table 2.1

Relation between log $[(F_D/\rho_F AV_T{}^2)Re^2]$ and log Re [2].

$f(Re^2)$	0.0	0.1	0.2	0.3	0.4	0.5	0.6	0.7	0.8	0.9
$\overline{1}$	$\overline{3}.919$	$\overline{2}.018$	$\overline{2}.117$	$\overline{2}.216$	$\overline{2}.315$	$\overline{2}.414$	$\overline{2}.513$	$\overline{2}.612$	$\overline{2}.711$	$\overline{2}.810$
0	$\overline{2}.908$	$\overline{1}.007$	$\overline{1}.105$	$\overline{1}.203$	$\overline{1}.301$	$\overline{1}.398$	$\overline{1}.495$	$\overline{1}.591$	$\overline{1}.686$	$\overline{1}.781$
1	$\overline{1}.874$	$\overline{1}.967$	0.008	0.148	0.236	0.324	0.410	0.495	0.577	0.569
2	0.738	0.817	0.895	0.972	1.048	1.124	1.199	1.273	1.346	1.419
3	1.491	1.562	1.632	1.702	1.771	1.839	1.907	1.974	2.040	2.106
4	2.171	2.236	2.300	2.363	2.425	2.487	2.548	2.608	2.667	2.725
5	2.783	2.841	2.899	2.956	3.013	3.070	3.127	3.183	3.239	3.295

Where $f(Re^2) = \mathrm{Log}[(F_D/\rho AV_T{}^2)]Re^2$

Table 2.2

Relation between log $[(F_D/\rho_F AV_T{}^2) Re^{-1}]$ and log Re [2].

$f(Re^{-1})$	0.0	0.1	0.2	0.3	0.4	0.5	0.6	0.7	0.8	0.9
$\overline{4}$	3.316	3.231	3.148	3.065	2.984	2.903	2.824	2.745	2.668	2.591
$\overline{3}$	2.517	2.443	2.372	2.300	2.231	2.162	2.095	2.027	1.961	1.894
$\overline{2}$	1.829	1.763	1.699	1.634	1.571	1.508	1.496	1.383	1.322	1.260
$\overline{1}$	1.200	1.140	1.081	1.022	0.963	0.904	0.846	0.788	0.730	0.672
0	0.616	0.560	0.505	0.449	0.394	0.339	0.286	0.232	0.178	0.125
1	0.072	0.019	$\overline{1}.969$	$\overline{1}.919$	$\overline{1}.865$	$\overline{1}.811$	$\overline{1}.760$	$\overline{1}.708$	$\overline{1}.656$	$\overline{1}.605$
2	$\overline{1}.554$	$\overline{1}.503$	$\overline{1}.452$	$\overline{1}.401$	$\overline{1}.350$	$\overline{1}.299$	$\overline{1}.249$	$\overline{1}.198$	$\overline{1}.148$	$\overline{1}.097$
3	$\overline{1}.047$	$\overline{2}.996$	$\overline{2}.946$	$\overline{2}.895$	$\overline{2}.845$	$\overline{2}.794$	$\overline{2}.744$	$\overline{2}.694$	$\overline{2}.644$	$\overline{2}.594$
4	$\overline{2}.544$	$\overline{2}.493$	$\overline{2}.443$	$\overline{2}.393$	$\overline{2}.343$	$\overline{2}.292$				

Where $f(Re^{-1}) = \log[(F_D/\rho AV_T{}^2)Re^{-1}$

Table 2.3

Correction for shape,factor k,and log $[(F_D/\rho_F AV^2) Re^{-1}]$ and log $[(F_D/\rho_F AV_T{}^2)Re^2]$ [2].

log $[(F_D/\rho_F AV^2) Re^{-1}]$	k=0.2	k=0.3	k=0.4	log $[(F_D/\rho_F AV_T{}^2)Re^2]$	k=0.2	k=0.3	k=0.4
$\overline{4}.0$	+0.289	+0.217	+0.185	$\overline{2}$	+0.032	-0.002	-0.022
$\overline{4}.5$	+0.231	+0.175	+0.149	$\overline{1}$	+0.030	-0.003	-0.023
$\overline{3}.0$	+0.173	+0.133	+0.114	0	+0.026	-0.005	-0.025
$\overline{3}.5$	+0.119	+0.095	+0.082	1	+0.021	-0.010	-0.027
$\overline{2}.0$	+0.072	+0.061	+0.056	2	+0.012	-0.016	-0.031
$\overline{2}.5$	+0.033	+0.034	+0.038	2.5	0.000	-0.020	-0.033
$\overline{1}.0$	+0.007	+0.018	+0.028	3	-0.022	-0.032	-0.038
$\overline{1}.5$	-0.003	+0.013	+0.024	3.5	-0.056	-0.052	-0.051
0.0	-0.007	+0.011	+0.022	4	-0.089	-0.074	-0.068
1.0	-0.008	+0.009	+0.019	4.5	-0.114	-0.093	-0.083
2.0	-0.010	+0.007	+0.017	5	-0.135	-0.110	-0.097
3.0	-0.012	+0.005	+0.015	5.5	-0.154	-0.125	-0.109
4.0	-0.013	+0.003	+0.013	6	-0.172	-0.134	-0.120
5.0	-0.014	+0.002	+0.012				

Solution

For simplicity we may assume that the iron ore particles are spherical in shape, therefore Eq. (2.11) may be considered applicable.

From the data: $\rho_S = 5400 \text{ kg/m}^3$
                    $\rho_L = 1000 \text{ kg/m}^3$
                    $\mu \text{ (H}_2\text{0) at } 25 \,^0\text{C} = 0.0008904 \text{ Pa.s}$

Substituting in Eq. (2.11):

$$0.015 = \frac{9.81\,(5400-1000)\,d^2}{18\,(0.0008904)}$$

hence $d = 0.0000746 \text{ m or } 0.0745 \text{ mm.}$

Example 2.3

An irregular shaped mineral particle (shape factor, k = 0.3) had a projected area of 2.16 x $10^{-6}\,\text{m}^2$. It was allowed to settle freely in water held at 20^0C. The mean specific gravity of the particle was 2.65. Estimate the settling velocity of the particle of density, 1120 kg/m^3.

Solution
Step 1
Projected area of particle $= \pi\,r^2 = 2.16 \text{ x } 10^{-6}\,\text{m}^2$

then $r = 0.000829 \text{ m}, d = 0.00166 \text{ m}$

From Appendix D-1 $\rho_L \text{ H}_2\text{O at } 20\,^0\text{C} = 998 \text{ kg/m}^3$
And from Appendix D-2 $\mu \text{ H}_2\text{O at } 20\,^0\text{C} = 1.002 \text{ x } 10^{-3} \text{ Ns/ m}^2$

Step 2
Let the projected diameter of particle be d_P and r_P the radius

The total drag force F_D on particle $= F_D' \; \dfrac{\pi\,d_P{}^2}{4} = (\rho_S - \rho_L)\, g\, k\, d_P{}^3$

Next dividing both sides of the equation by the term $\rho_F V^2$ and multiplying by Re^2

$$\frac{F_D\,Re^2}{\rho_F V^2} = \frac{4\,d_P\,g\,k\,(\rho_S - \rho_F)\,Re^2}{\pi\,\rho_F V^2}$$

substituting $Re = d_p\,V\rho_F/\mu$ and simplifying:

$$\frac{F_D Re^2}{\rho_F V^2} = \frac{4 \, d_P^3 \, k \, g \, (\rho_S - \rho_F) \, \rho_F}{\pi \mu^2}$$

Substituting the data gives:

$$\frac{F_D Re^2}{\rho_F V^2} = \frac{4 \times 0.00166^3 \times 0.3 \times 9.81 \times (1120 - 998) \times 998}{3.14 \times (1.002 \times 10^{-3})^2} = 2078.64$$

$$\log \frac{F_D Re^2}{\rho_F V^2} = \log 2078.64 = 3.3178$$

Then from Table 2.1,

log Re = 1.7143 or Re = 51.79

From Table 2.3 the correction value for log Re corresponding to a shape factor of 0.3 equals - 0.0447.

That is, the corrected value of log Re for the non-spherical particle = 1.7143 − 0.0447 = 1.6696

and Re = 46.73

Now $\qquad$ Re $= d_P V \rho_L / \mu = 46.73$

then $\qquad$ $V = \dfrac{46.73 \times (1.002 \times 10^{-3})}{0.00166 \times 1120} = 0.025$ m/s

---

Usually gravity segregation methods are used to determine particle sizes down to 0.02 microns.

2.1.4. Sedimentation Method - Centrifugal Sedimentation

Eq. (2.11) indicates that the terminal velocity of a particle can be increased and the settling period reduced by increasing the value of the acceleration on the particle. This can easily be achieved both in the laboratory and in industry by the use of centrifuges (Fig. 2.4), where g can be replaced by $r \omega^2$, where r is the radius of the centrifuge and ω is the angular velocity. For a spherical particle, obeying Stokes' Law, the motion of the particle in the centrifuge can be expressed by the equation, for Re < 0.2;

$$\frac{d^2 r}{dt^2} \left(\frac{\pi \, d_P^3 \, \rho_S}{6} \right) + 3 \pi \mu \, d_P \frac{dr}{dt} - \frac{\pi}{6} d_P^3 (\rho_S - \rho_L) \, r \omega^2 = 0 \qquad (2.24)$$

where d_P = particle diameter.
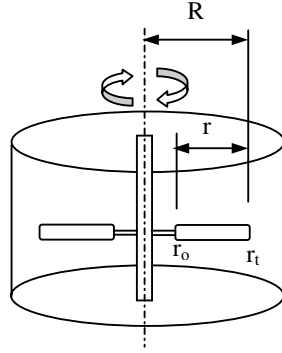
Fig. 2.4.   Laboratory centrifuge.

Neglecting acceleration, Eq. (2.24) may be rewritten as:

$$3\pi\mu d_P \frac{dr}{dt} = \frac{\pi}{6} d_P^3 \left(\frac{\rho_S - \rho_L}{\rho_S}\right) r\omega^2 \qquad \text{or} \qquad (2.25)$$

$$\frac{dr}{r} = \frac{d_P^2}{18\mu} \left(\frac{\rho_S - \rho_L}{\rho_S}\right) \omega^2 \; dt \qquad (2.26)$$

Assuming that the initial position of the particle in the centrifuge was r_o and the final position was r_t, after time t, integration of Eq. (2.26) would give:

$$\ln\frac{r_t}{r_o} = \frac{d_P^2 (\rho_S - \rho_L)}{18\mu \, \rho_S} \omega^2 \; t \quad \text{or}$$

$$d_P = \left[\frac{18\,\mu\,\rho_S}{(\rho_S - \rho_L)\omega^2 t} \ln\frac{r_t}{r_o}\right]^{0.5} \qquad (2.27)$$

Thus from a knowledge of r_o and r_t the diameter d, of a particle, can be estimated. Where turbulent conditions exist, the diameter of a particle can similarly be derived as:

$$\frac{\rho_S}{3 d_P \omega^2 (\rho_S - \rho_L)} = \left[\frac{t}{2\left(\sqrt{r_t} - \sqrt{r_o}\right)}\right]^2 \quad \text{or}$$

$$d_P = \frac{\rho_S}{3\omega^2 (\rho_S - \rho_L)} \left[\frac{2\left(\sqrt{r_t} - \sqrt{r_o}\right)}{t}\right]^2 \qquad (2.28)$$

In commercial centrifuges, the positions of a particle, r_t, at times t_1, t_2, t_3 ... t_n is observed by a light source thus getting a profile of movement of particles when more than one particle is added for centrifuging.

2.2. Particle size distribution

2.2.1. Sieve analysis

Whichever method of measuring particle size is used, the characterisation of a sample according to size is referred to as a size analysis. A size analysis in mineral processing is primarily used to obtain quantitative data about the individual size and size distribution of particles in the process stream. This is important in assessing the quality of grinding, optimum size of feed to a process for maximum efficiency etc.

In most mineral processing applications an approximate size of particles is all that is required. Sieving through standard sieves of known apertures and determining the sieve size on which all the particles are retained can conveniently give the limiting size of a group of particles subjected to the operation. The closer the size of successive sieves the closer would be the estimation to the true size.

Instead of individual measurements of sizes of particles, the mean size of a particle passing through and retained on sieves gives a good approximation of particle size within the sieve ranges.

The sieve size analysis of a mineral sample giving the mass fraction of mineral retained between successive sieve sizes is usually recorded as in Table 2.4. Points to note from the table are:

1. There are no particles larger than 3350 μm, (i.e. the fraction of particles retained on the 3350 μm screen is zero).
2. The mass of material on the 1680 μm sieve equals 24.7 % of the total mass.
3. The mass fraction retained on the 850 μm screen and passing through the 1680 μm screen equals 26.2 %. Similarly, the mass of material between sieve fraction 420 μm and 210 μm equals 9.7 % by mass.
4. The total material retained on the 420 μm sieve equals 0 + 24.7 + 26.2 + 15.2 = 66.1 % by mass.

   Similarly, the mass of mineral retained on the 210 μm sieve = 24.7 + 26.3 + 15.2 + 9.7 = 75.8 %, and so on as seen in column 3 of Table 2.4.

Even though the subsequent sieve openings are related by a factor of $1/\sqrt{2}$ (Tyler's series), a plot of size against mass percent in most cases is far from a straight line. To obtain a specific screen size that passes or retains a given mass, usually some interpolation of the tabled data is required. For example, in Table 2.4, to obtain the 70 % passing size, interpolation between the 1680 and 850 micron screen size is required. This is best done when a linear relationship exists between the size analysis data. A number of empirical relationships have been formulated to linearise the data to make interpolation and extrapolation of the data more accurate. One such method is to rewrite the screen analysis by calculating the cumulative amount retained or passing through a particular sieve as illustrated in Table 2.5 and Fig. 2.5.

Table 2.4.
Sieve analysis results

Size fraction, microns (1)	Mass, % (2)	Cum. Mass, % retained (3)
-3350+1680	28.5	28.5
-1680+850	22.8	51.4
-850+420	13.2	64.6
-420+210	8.4	73.0
-210+105	5.0	78.0
-105+75	2.4	80.4
-75	19.6	100.0
Total	100.0	

Table 2.5.
Size analysis with cumulative masses

Cum. % Passing, (100-Retained)	Sieves, μm	Cum. Mass % retained
100	3350	0.0
71.5	1680	28.5
48.6	850	51.4
35.4	420	64.6
27.0	210	73.0
22.0	105	78.0
19.6	75	80.4
0	Pan	100.0

Plotting the data in this form (Fig. 2.5) does not always result in a linear relationship.

2.2.2. Log-normal distribution

The distribution of sizes in a sample do not often follow a normal distribution, as in Fig. 1.3, but are skewed to the right. It may however match a log-normal distribution. That is, it will take the shape of a normal distribution if the x-axis is a log scale. Then plotting the cumulative percent passing on a probability scale (y-axis) against the sieve sizes on a log scale (x-axis), should produce a straight line. The probability scale is an inverse normal distribution, so plotting a normal distribution on this scale will give a straight line. Such a log-normal or log-probability plot is shown in Fig. 2.6 for the data in Table 2.5.

If this plot is linear (the size distribution is log-normal) then an approximation of the mean of the distribution is obtained from the d_{50}, the 50% passing size. The geometric standard deviation of the distribution is obtained from the 84% passing size since at this point, the particle size is approximately equal to the mean size plus the standard deviation. That is:

Standard deviation $= d_{84} - d_{50}$ (2.29)

In some cases, curvature of the plot is observed in the coarse sizes because the maximum particle size is not equal to infinity.
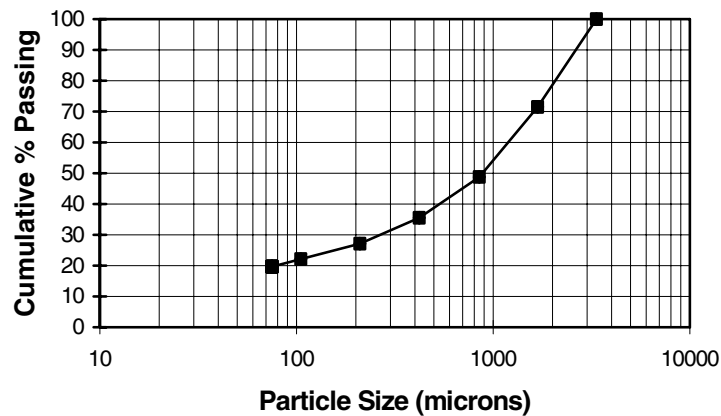
Fig. 2.5. Log-linear plot of cumulative % passing vs size.

2.2.3. Gaudin-Schuhmann Distribution

In some cases where the distribution is skewed, a linear plot can be obtained by plotting the log of the cumulative undersize against the log of the screen aperture, preferably on log-log paper (Fig. 2.7). Such plots are known as Gaudin–Schuhmann plots. In most cases this would yield a straight line. The advantage of such plots is that a limited number of sieves may be used to measure the size of particles lying between any two sieve sizes. It also indicates the distribution of sizes of particles that exist in a sample.

It is not necessary to plot both the cumulative oversize and undersize as each is the mirror image of the other as seen in Fig. 2.8.

The Gaudin-Schuhmann distribution is given as:

$$y = 100 \left(\frac{x}{k}\right)^{a}$$ (2.30)

where y = cumulative mass % passing size x
       x = screen aperture size
       k = size parameter
       a = distribution parameter

Taking the logs of both sides of this equation and rearranging it, then:

$\log y = \log 100 + a \log x - a \log k$ or
$\log y = a \log x + \text{CONSTANT}$ (2.31)

This is the equation of a straight line if x and y are plotted on a log-log scale. The slope of the straight line will be the distribution parameter, a, and the intercept of the straight line, when y = 100 %, will be the size parameter, k. These two parameters characterise the size of the sample. The distribution parameter is a measure of the range of different sizes in the sample and the size parameter is a measure of the top size.
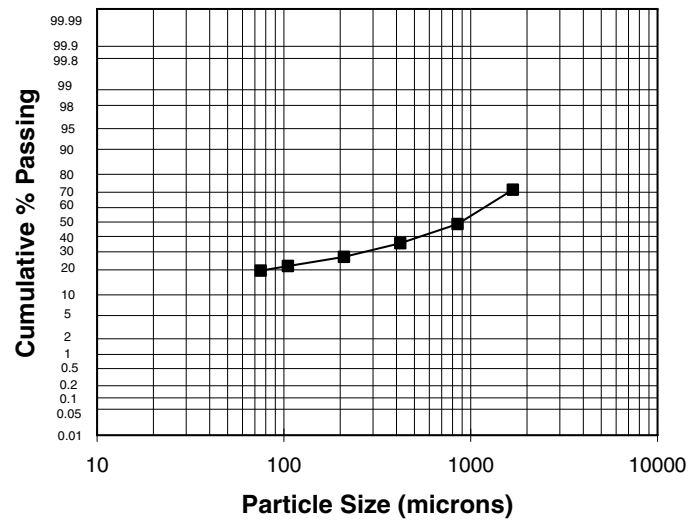
Fig. 2.6. Log-normal plot of size distribution in Table 2.5.
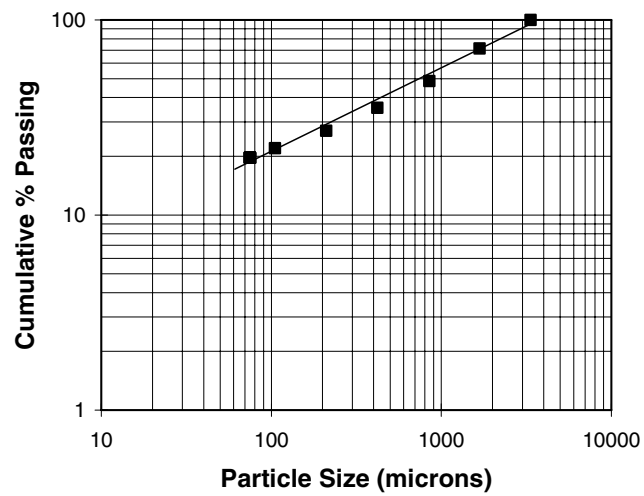
Fig. 2.7. Log-log plot of cumulative % passing (undersize) vs size, (Gaudin-Schuhman plot).
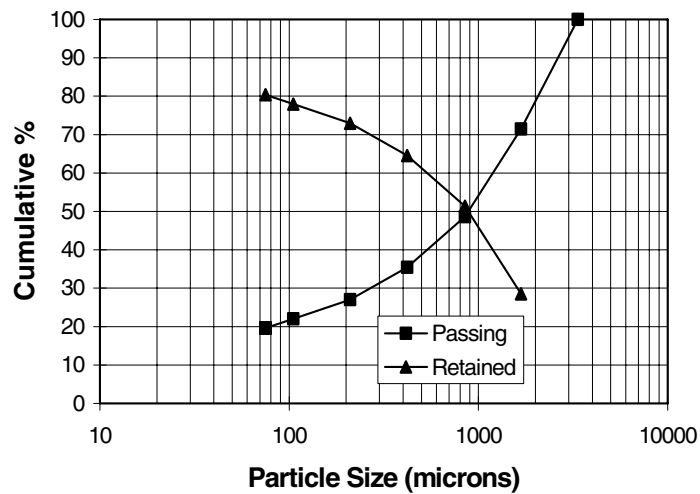
Fig. 2.8. Plot of cumulative % undersize (passing) and oversize (retained).

Calculation of the Slope of a Log-Log Plot

The slope of a graph is taken as the ratio (Y1-Y2)/(X1-X2) where (X1,Y1) and (X2,Y2) are two points on the graph (Fig. 2.9). On a log scale the points are plotted as (X,Y) but are in reality the log of these values. That is, the points correspond to (log X, log Y).
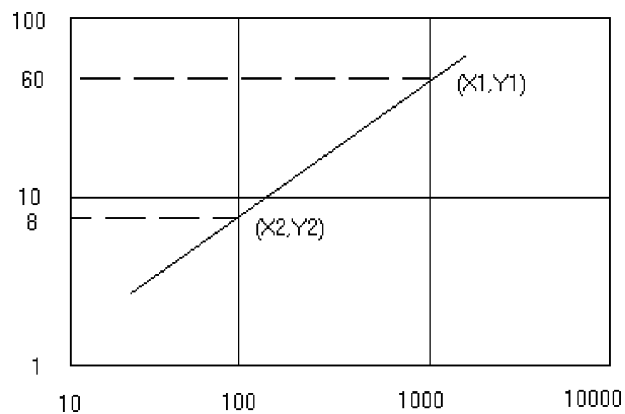
Fig. 2.9. Log-log plot through the points (X1,Y1) and (X2,Y2).

In Fig. 2.9:

Slope $\neq$ $\dfrac{(60-8)}{(1000-100)}$ but

Slope $=$ $\dfrac{(\log 60 - \log 8)}{(\log 1000 - \log 100)}$

Alternatively, if the distance in mm between one log cycle on the Y-axis (say 10-100) is the same distance as one log cycle on the X-axis (10-100) then using a ruler, the slope can also be determined by;

Slope $=$ $\dfrac{(\text{distance from Y2 to Y1 in mm})}{(\text{distance from X2 to X1 in mm})}$

2.2.4 Rosin-Rammler Distribution

An alternative plot, especially suitable for finely ground particles, like that produced in tumbling mills, is to plot log [log 100/(100-y)], or log [log 100/R], against the log of sieve size, where y is the cumulative % passing and R is the cumulative % retained. Such plots are known as Rosin-Rammler plots, (Fig. 2.10). The double log scale expands the fine and coarse ends of the size range (<25 % and > 75 %) and compresses the mid range (30-60 %). Under operating plant conditions approximations in particle size computation and estimation are sufficient for most purposes.

The Rosin-Rammler (or Weibull) distribution is expressed as:

$$R = 100 \exp\left[-\left(\frac{x}{x^1}\right)^b\right] \tag{2.32}$$

where   R   =   cumulative mass % retained on size x
        x^1 =   size parameter, and
        b   =   distribution parameter

Rearranging and taking the logarithm of both sides of Eq. (2.32) gives:

$$\log\left(\frac{100}{R}\right) = \left(\frac{x}{x^1}\right)^b \log e \tag{2.33}$$

Taking logarithms a second time to remove the exponent gives:

$$\log\log\left(\frac{100}{R}\right) = b\log x - b\log x^1 + \log\log e \quad \text{or}$$

$$\log\log\left(\frac{100}{R}\right) = b\log x + \text{CONSTANT} \tag{2.34}$$

A plot of log log (100/R) versus log x should give a straight line. The parameters of the Rosin-Rammler distribution, b and x^1 are obtained from the slope of the straight line and the intercept at the horizontal line at R = 36.79, respectively. Together they completely describe the size distribution. To simplify the calculation of the double log, special graph paper is available (Rosin-Rammler/Weibull paper) where values of cumulative % retained (or cumulative % passing) can be plotted directly on the Y-axis. A line on the graph paper at a cumulative % retained value of 36.79 is included to allow estimation of the parameter x^1. The method of computing for a Rosin-Rammler plot is illustrated in Example 2.4.

Example 2.4

A sieve analysis showed the following results (Table 2.6). Plot the data according to Gaudin-Schuhmann and Rosin-Rammler and determine the mass of the size fraction retained on 200 μm.

Fig. 2.11 is a plot of the cumulative % passing column in Table 2.6 versus size. The Gaudin-Schuhmann plot is a reasonable straight line that shows the fraction of material passing a 200 μm sieve was expected to be 10.1% by mass.

Rosin-Rammler plots can similarly be made either by calculations or using special log paper known as Weibull graph paper that save labourious calculations.

Typical calculations using the data in Table 2.6 is illustrated in Table 2.7.

This can now be plotted on normal graph paper (Fig. 2.12A) or on special Rosin-Rammler paper (Fig. 2.12B). The plot is nearly a straight line, which indicates that the mass fraction retained on 200 microns is about 90.6 % by mass or 9.4 % passing.
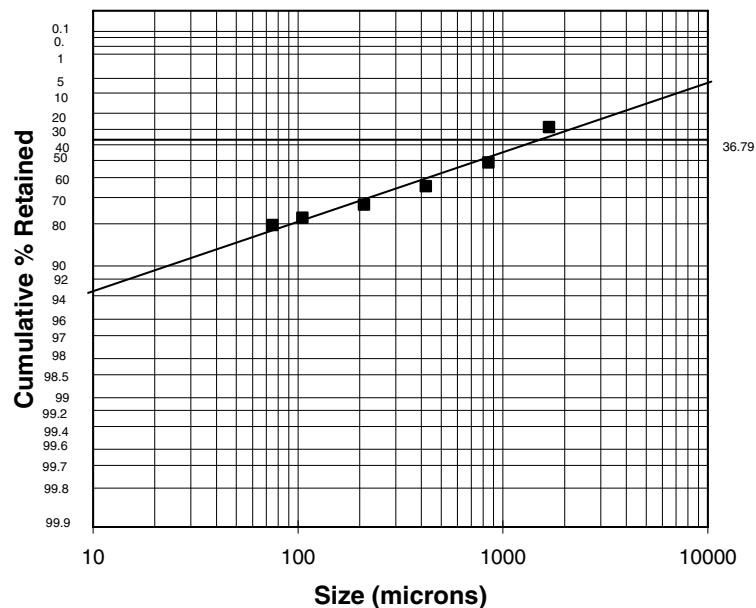
Fig. 2.10. Rosin Rammler plot of data from Table 2.4.

Table 2.6
Sieve analysis, Example 2.4.

Aperture, mm	Mass %	Cum. mass % retained	Cum. mass % passing	Log Cum. mass % retained	Log aperture
13300	0	0	100.0	-	4.12
4750	20.9	20.9	79.1	1.32	3.68
2360	21.1	42.0	58.0	1.62	3.37
1180	20.9	62.9	37.1	1.80	3.07
600	10.3	73.2	26.8	1.86	2.78
300	15.7	88.9	11.1	1.69	2.48
150	4.3	93.2	6.8	1.97	2.18
75	2.3	95.5	4.5	1.98	1.88
-75	4.5	100	0	2.00	-
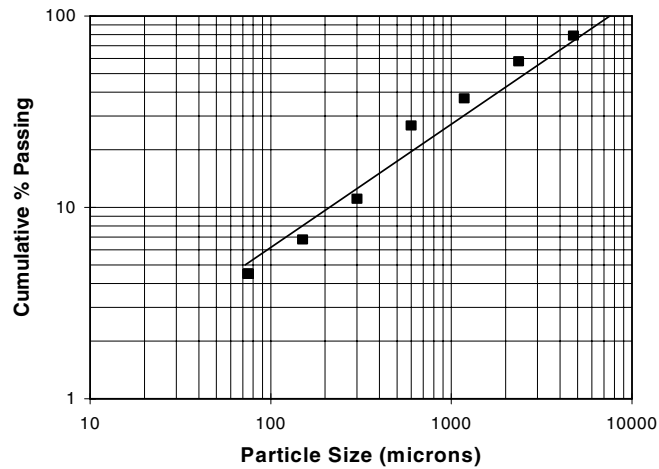
Fig. 2.11. Gaudin-Schuhman plot, Example 2.4.

Table 2.7.
Data for Rosin Rammler plot, Example 2.4.

log Aperture	Cum. mass % Retained, R	1/R	100/R	log100/R	Log[log100/R]
4.12	0				
3.68	20.9	0.0478	4.78	0.680	-0.168
3.37	42.0	0.0238	2.38	0.377	-0.424
3.07	62.9	0.0159	1.59	0.201	-0.696
2.78	73.2	0.0137	1.37	0.136	-0.868
2.48	88.9	0.0112	1.12	0.051	-1.292
2.18	93.2	0.0107	1.07	0.031	-1.515
1.88	95.5	0.0105	1.05	0.020	-1.699
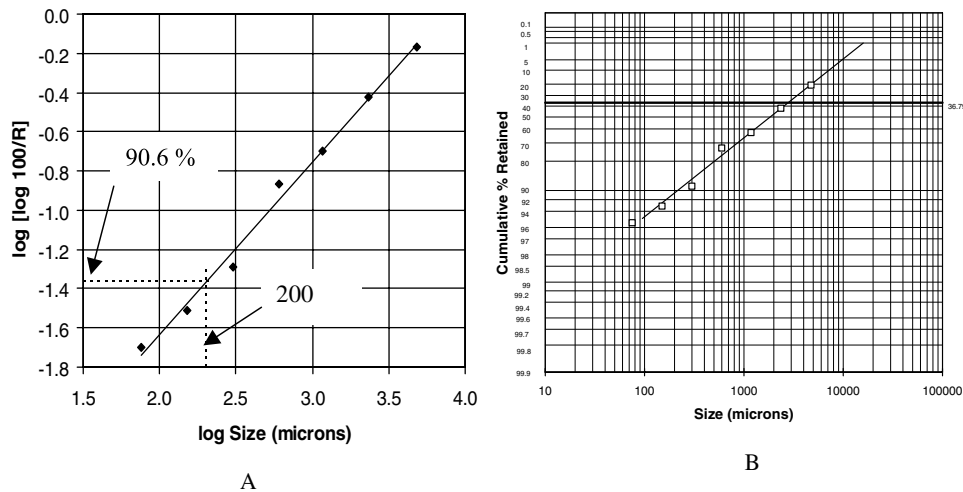
Fig. 2.12. Rosin Rammler plot on: A   normal graph paper according to Table 2.7.

                                         B   plot on special Rosin Rammler paper from Table 2.6.

2.3. Combining size distributions

Since sizing by different methods, (sieving, cyclosizer, laser sizing) covers different size ranges, size distributions from different methods may need to be combined to give a complete size distribution.

Sizing of the same sample by different methods will generally produce different results because of the difference in measurement principle. The difference is related to particle shape. For spherical particles, the Stokes diameter calculated from the settling velocity is exact and the projected area of a sphere is that of a circle of the same diameter. Thus the closer particle shape is to a sphere, the closer the measured sizes will be. For elongated or flat particles the settling velocity will be lower than for spherical particles due to an increase in specific surface area leading to a greater drag force and hence lower terminal velocity. Thus, the Stokes diameter will be lower for elongated particles. On the other hand, these particles will be more stable when resting flatter on a viewing surface and hence will have a larger projected area and hence a larger projected area diameter. In general, the Stokes diameter is smaller or equal to the same particle's sieve diameter.

Table 2.8 shows the results from a size analysis of a fine quartz sample sized by sieving, cyclosizing and with a laser sizer. The -212 micron quartz was dry screened at 75 microns and the -75 micron fraction sized by screening and cyclosizing. The fraction from the last cone of the cyclosizer was collected and allowed to settle before decanting the water and drying the solids. This minus cone 5 material was laser sized for comparison.

For the screening samples, the +38 micron screen fractions were obtained using standard 200 mm diameter BSS screens and the -38 micron fraction wet screened on a 10 micron nylon mesh screen. For comparison, a separate -212 micron sample was completely wet screened on all the above screens and also laser sized.

54
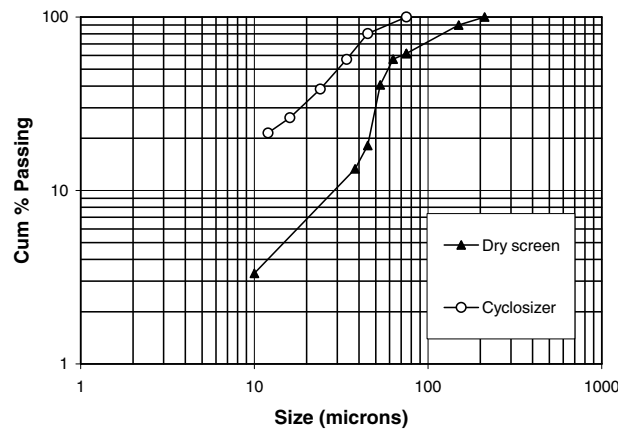
Fig. 2.13. Screening and cyclosizing of –75 micron fraction of –212 micron quartz.

Each sizing method covered some of the same size range to make comparison possible. Fig. 2.13 shows the results of the dry screening and the cyclosizer.

Since the sample that was cyclosized (-75 microns) represents only a portion of the whole sample (61.6%), the results have to be adjusted by multiplying the mass % in the cyclosizer fractions by the -75 micron proportion. ie. for the -45 +34 micron fraction, the scaled cumulative % passing is 0.802 x 61.6 = 49.4 %.

The same applies to the combination of the +75 micron screened results with the -75 micron screened results.

When re-plotted, the data points line up with the +75 micron screen data as seen in Fig. 2.14. The -75 micron dry screened data however deviates from the cyclosizer trend. When the wet screened results are plotted, as shown in Fig. 2.15, the results are aligned very well with the cyclosizer results. This highlights the difference between wet screening and dry screening, particularly for fine material, in this case the -75 micron size range.

The dry screening results show a smaller percentage of material passing each screen below 75 microns compared to the wet screening data. This results because the fine particles tend to stick to the coarser particles and do not pass the screens. The only way to get an accurate sizing by screening in these fine fractions is to use water to flush the fines through the screens. This is a more tedious process but as can be seen from the diagram, is the only way to get accurate results for the fine fractions. In the coarser fractions, fine particles attached to coarse fractions represent a smaller percentage of the mass in that fraction and hence wet screening is less critical. An acceptable procedure would be to wet screen the sample at 75 microns and dry screen the +75 micron fraction while wet screening the -75 micron fraction.

The laser sizer results of the cyclosizer minus cone 5 fraction, normalised to the total sample mass using the procedure described above, is plotted in Fig. 2.16 and fits well with the trend of the cyclosizer fractions and the wet screened results. The laser sized -212 micron sample results are plotted in Fig. 2.17 and are seen to overlap the cyclosizer and wet screening data. This represents a good result for this sample in that the different sizing methods give

Table 2.8
Sizing data for a –212 micron ground quartz sample.

DRY SCREEN

Size passing (μm)	retained (μm)	Mass (g)	Mass %	Cum Mass % Passing	Combined mass %	Cum Mass% Passing
212	150	53	10.1	100	10.1	100
150	75	148.7	28.3	89.9	28.3	89.9
75	0	323.3	61.6	61.6		
		525	100.0			
75	63	13.1	7.2	100.0	4.45	61.6
63	53	48.7	26.9	92.8	16.55	57.1
53	45	65.9	36.4	65.9	22.40	40.6
45	38	14.3	7.9	29.5	4.86	18.2
38	10	29.4	16.2	21.6	9.99	13.3

WET SCREEN

Size passing (μm)	retained (μm)	Mass (g)	Mass %	Cum Mass % Passing	Combined mass %	Cum Mass% Passing
10	0	9.8	5.4	5.4	3.33	3.3
		181.2	100.0		100.0	

CYCLOSIZER (-75μm)

Size passing (μm)	retained (μm)	Mass (g)	Mass %	Cum Mass % Passing	Scaled to whole sample
75	45	10.7	19.8	100.0	61.6
45	34	12.6	23.3	80.2	49.4
34	24	10	18.5	56.9	35.1
24	16	6.6	12.2	38.4	23.7
16	12	2.6	4.8	26.2	16.2
12	0	11.6	21.4	21.4	13.2
		54.1	100		

WET SCREEN

Size passing (μm)	retained (μm)	Mass (g)	Mass %	Cum Mass% Passing
212	150	24.3	11.9	100.0
150	75	51.1	25.0	88.1
75	53	28.8	14.1	63.1
53	45	19.6	9.6	49.1
45	38	13.5	6.6	39.5
38	10	42.9	21.0	32.9
10	0	24.4	11.9	11.9
		204.6	100	

LASER SIZER (-212 μm)

Size passing (μm)	retained (μm)	Mass % Average
600	404	100.0
404	273	99.3
273	203	97.1
203	137	93.5
137	102	84.9
102	75.6	75.6
75.6	50.9	64.7
50.9	41.8	48.3
41.8	28.2	40.3
28.2	19.0	27.1
19.0	11.6	18.4
11.6	7.08	12.0
7.08	3.92	7.9
3.92	2.39	4.4
2.39	1.32	2.3
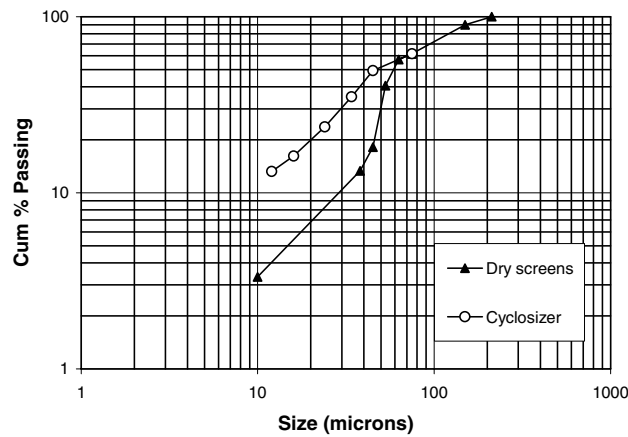
Fig. 2.14. Adjustment of the −75 micron cyclosizer fraction to the total mass of the sample.

comparable results. This has been observed elsewhere for quartz and is an indication that the particles of quartz are close to spherical [7].

As there is no absolute measure of size for irregular shaped particles, different methods of size measurement will give different size distributions. Generally, it is expected that irregular shaped particles will yield different sizing results when measured by different techniques. The differences can be quantified in terms of a shape factor. For example, a conversion shape factor could be defined as:

$$D = d_1/d_2 \qquad\qquad (2.29)$$
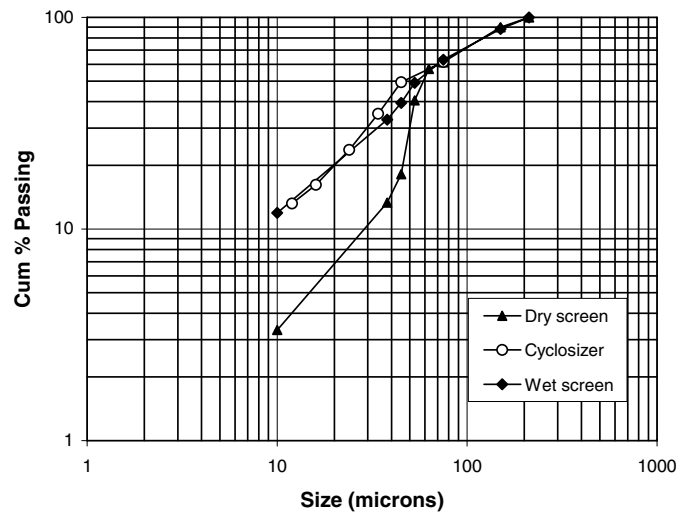
Fig. 2.15. Wet screen data for the −212 micron quartz sample.
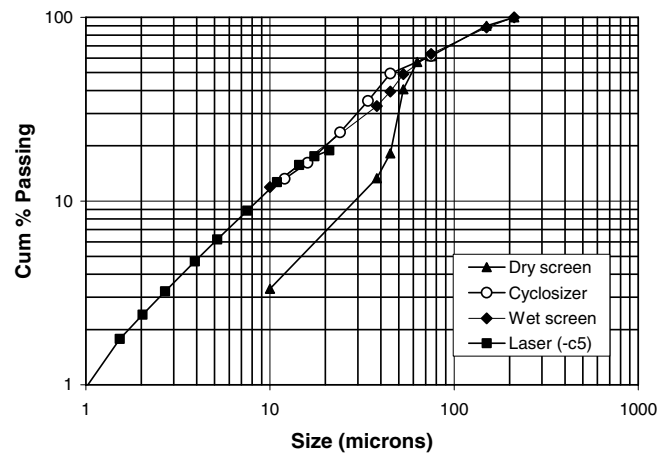
Fig. 2.16. Laser sizing of –cone 5 from cyclosizer.

where d_1 is the size assigned to particles in a narrow size interval and d_2 is the size measured by a second technique for the same interval.

This factor is generally determined experimentally by selecting a number of cumulative % passing values and obtaining the ratio of d_1 and d_2 for each value and taking the average. For example, Fig. 2.18 shows a size distribution obtained by cyclosizer and screening where the distributions don't match. The two plots are roughly parallel and where they overlap, taking the cumulative % passing value of 75% and drawing a horizontal line gives the values of d_1
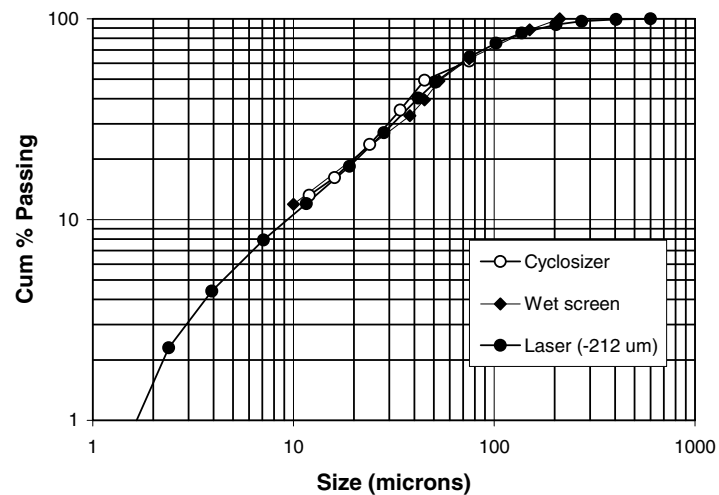
Fig. 2.17. Laser sizing of –212 micron quartz sample.

58
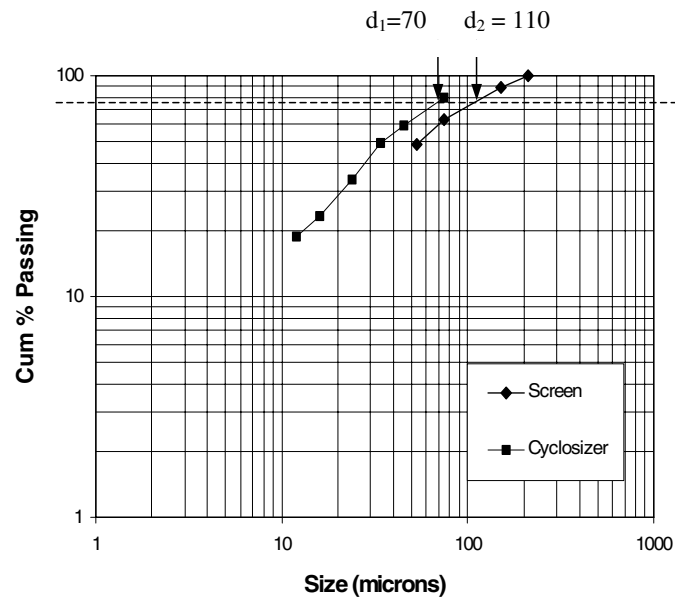
Fig. 2.18. Cyclosizer and screen results from irregular shaped particles

and d_2 as 70 and 110 microns respectively. The conversion shape factor is then calculated as $D = 70/110 = 0.636$ for conversion of data from technique 2 to technique 1. To convert the data from technique 1 to 2, each size point in distribution 1 is divided by the conversion shape factor as shown in Table 2.9 and Fig. 2.19.
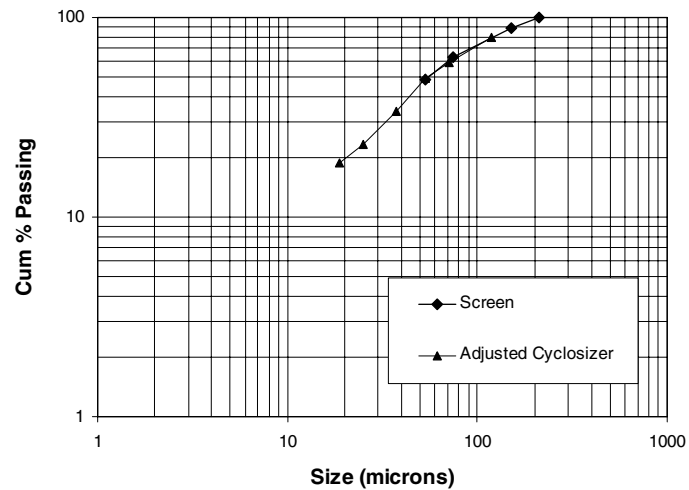
Fig. 2.19. Adjustment of cyclosizer data to form smooth equivalent screen sizings using the conversion shape factor D = 0.636.

Table 2.9
Conversion of cyclosizer data to equivalent screen data using the shape factor, D = 0.636

Size		Cum % Passing	Converted Size, (microns)
Passing (microns)	Retained (microns)		
75	45	79.0	117.9
45	34	59.6	70.7
34	24	49.9	53.4
24	16	33.7	37.7
16	12	23.0	25.1
12	0	18.8	18.9

2.4. Problems

2.1
Data obtained on analysing a tumbling mill product is given below. Plot the data using the Gaudin-Schumann and Rosin-Rammler methods. From the plots estimate the mass fractions retained on 200 μm and 34 μm screens.

Size, μm	1200	600	300	150	75	-75	Total
Feed, mass % retained	1.5	4.0	10.0	22.0	33.0	29.5	100.0

2.2
Using the following data, plot a Rosin-Rammler distribution curve and determine its equation.

Size, μm	2000	1200	850	600	500	350	250	-250	Total
Product, mass % retained	4.0	9.5	12.5	15.5	19.0	16.0	13.0	10.5	100.0

2.3
Samples of the feed to a ball mill and the product after 15 mins of operation were analysed and the results are as follows:

Size, μm	1200	600	300	150	75	-75	Total
Feed, mass % retained	5.0	1.0	15.0	20.0	30.0	29.0	100.0
Product, mass % retained	0.5	2.0	3.0	20.5	34.8	39.2	100.0

Estimate the rate of reduction of the 1000 μm feed size during the mill operation.

2.4
The product from a grinding mill was sampled every 30 minutes for the first hour, then hourly for 4 hours. The samples were screened and analysed yielding the following average size distribution:

Screen Size μm	Mass % Retained				
	Feed	Product after ½ h	Product after 1 h	Product after 2 h	Product after 4 h
800	3.0	1.8	0.6	0.0	0.0
400	8.8	3.0	2.0	0.5	0.2
250	25.6	26.0	22.4	20.2	13.0
125	33.2	25.0	35.0	38.0	32.0
68	24.4	26.0	27.3	27.0	31.2
35	3.3	5.0	8.1	10.3	12.2
-35	1.7	3.2	4.6	4.0	6.4
Total	100.0	100.0	100.0	100.0	100.0

Estimate the rate at which the 100 μm feed size is reduced and its mass fraction after 2 hours of operation

2.5
Two sets of size analysis results are available for a given material. From a Gaudin-Schuhmann plot determine the relations between size and mass distribution in these two cases. Using the equation for case B determine the fines fraction at −53 microns

Size, μm	Case A, mass %	Case B, mass %
+9510	0.0	0.0
-9510+6650	55.5	0.0
-6650+1680	25.0	14.0
-1680+850	10.5	24.0
-850+420	5.0	20.0
-420+210	2.4	14.0
-210+105	1.6	9.0
-105+75	0.0	4.8
-75	0.0	14.2
Total	100.0	100.0

2.6
Gold nuggets were examined under a microscope and the following results were obtained.

Nugget size, mm	0-1	1-2	2-4	4-8	8.16	16-32
number	4500	2900	1100	200	120	4

Determine: 1. the size distribution on a mass basis
2. the size distribution on a surface area basis.

Data: density of gold nugget = 18500 kg/m^3

2.7

A pond contains particles from a process tail stream. If the pond is 500 mm deep, calculate the size of particles still suspended after 30 minutes from entering the pond. The particle density is 2650 kg/m^3.

2.8

The diameter of 6 lots of particles from a sample were measured under an optical microscope and a sedimentation method. The number of particles of each lot were counted and tabulated as:

Lot number	1	2	3	4	5	6
Size, mm	-4 + 2	-2 + 1	-1 + 0.5	-0.5 + 0.25	-0.25 + 0.15	-0.15 + 0.075
Number of particles	38	75	105	153	321	500

The particles were all of similar shape, having a shape factor of 0.3. Estimate:

1.   the size of particles having the same specific surface as the mixture
2.   the surface area per unit volume of particles.

2.9

A cylindrical glass tube of diameter 20 mm and capacity 22 cm^3, is filled with a 12% water suspension of mineral of specific gravity 2.4 and placed in a centrifuge. The centrifuge was then rotated at 3000 rpm for 2 seconds. Estimate:

1.   The diameter of particles that would settle if the movement of particles was under streamline conditions.
2.   The diameter of particles that would settle under turbulent conditions when the rotational speed was increased to 4280 rpm.

Data: Temperature of water = 20°C
        Viscosity of water at 20°C = 1.008 mPas

2.10

A 1% suspension of hematite particles in methanol (1% solution in water) was filled in a cylindrical centrifuge tube 3 cm long x 1.9 cm diameter and rotated at 5000 rpm. Estimate:

1.   the size of particles that would settle every second for 5 seconds at the bottom of the tube.
2.   If the number of particles settling every second were: 200, 120, 80, 60, 20, determine the mean specific surface of the hematite particles.

Data: Relative viscosity of methanol solution at 20°C = 1.3332
        Specific gravity of methanol at 20°C = 0.9964

REFERENCES
[1] B.H. Kay, Chemical Engineering, 73 (1966) 239.
[2] J.M. Coulson and J.F. Richardson, with J.R. Backhurst and J.H. Harker, Chemical Engineering, Vol. 2, Particle Technology and Separation Processes, 4th edn, Butterworth – Heinemann, (1999).
[3] H. Heywood, Journal of Imperial College Chemical Engineering Society, 4 (1948) 17.
[4] A.R. Khan and J.F. Richardson, Chemical Engineering Communications, 62 (1987) 135.
[5] H. Wadell, Journal of Geology, 41 (1993) 310.
[6] H. Heywood, Proceedings 3rd EFCE Symposium Interaction between Fluids and Particles, Institute Chemical Engineers, London, (1962), pp. A1-8.
[7] N.L. Weiss (ed.), SME Mineral Processing Handbook, AIME, New York (1985).

Chapter 3. Size Reduction and Energy Requirement

3. INTRODUCTION

In nature, minerals exist in physical and chemical combinations with each other. To separate minerals of commercial interest from the host rock both physical and chemical methods are employed. Most minerals are mined in the form of large rocks. Others like the ilmenite, rutile, zircon, leucoxene, heavy minerals or alluvial placer deposits of gold are found decimated amongst sand in beaches or in riverbeds. To access the minerals in the host rocks, they have to be crushed and even ground. When a maximum amount of the mineral of interest is separated by comminution from the parent rock, that size is usually known as the liberation size. The aim of comminution is to maximise the liberation of the mineral from the host rock. Usually the concentration of useful minerals in host rocks are low, therefore large tonnages of host rocks have to be mined to recover sufficient quantities of the useful mineral to make the operation commercially viable. The first step in the recovery process of minerals from the host rocks therefore is to reduce the size of rock by crushing and grinding. The equipment used and their operation are discussed in subsequent chapters.

3.1. Design of Size Reduction Processes

The process of size reduction is normally designed to take place in single stage open circuit, single stage closed circuit or multiple stage open or closed circuit In some cases a combination of these methods are adopted. In a single stage, single pass, open circuit size reduction operation, the product consists of a range of particle sizes which seldom achieves the desired degree of liberation. Hence second or even third stages of size reduction are often necessary to progressively reduce the remaining particle size to liberate mineral particles to an acceptable degree (Fig. 3.1).

In closed circuit, the product from the stage of size reduction is separated into relatively fine and coarse fractions. The coarser fraction is then collected and recrushed in the same unit as seen in Fig. 3.2. In so doing the load on the equipment for size reduction is increased and a circulating load is established, but the total number of units required for obtaining the same degree of size reductio is less.

Several options in design exist in closed circuit grinding set-ups. The two most commonly used devices for size reduction are the crushers and grinding mills. The crushers are normally fed with rocks, up to about 1 meter in size, while the grinders are usually fed with rocks crushed down to a maximum size of about 50 mm. Larger rocks produced at the mines are initially separated by grizzlies, broken by hammers and then fed to the crushers

The mechanisms of size reduction during crushing and grinding are different. The chief difference being that in crushing operations the size reduction is more by compression and impact and less by attrition while in grinding, the forces of attrition are much greater. The grinding operation is rather complex and its complexity can roughly be illustrated by Fig. 3.3.

Spherical balls or cylindrical rods are mostly used as the grinding media. These media cascade within a mill and impinge on the ore thus providing a crushing action. As the balls and rods tumble within tubular mills, they provide a grinding action and forces of attrition, all
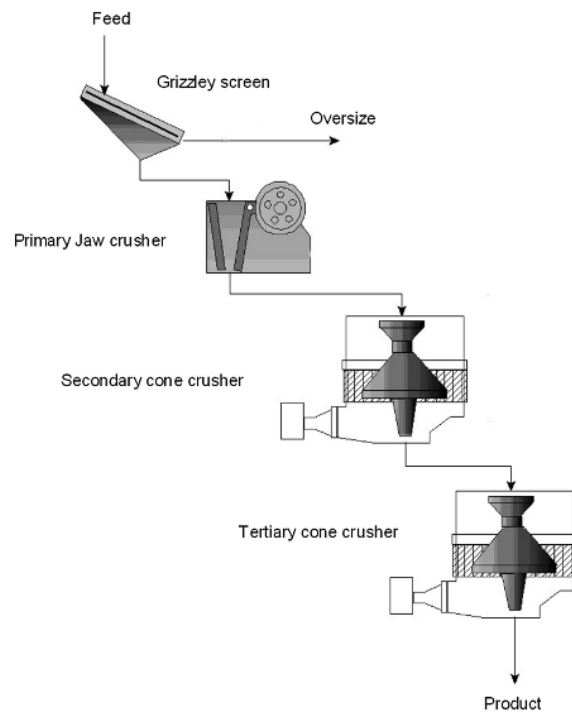
Fig. 3.1. Open circuit crushing
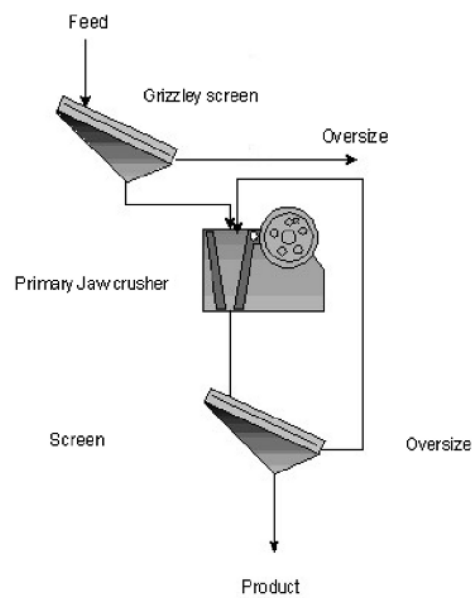
Fig. 3.2.   Closed circuit crushing
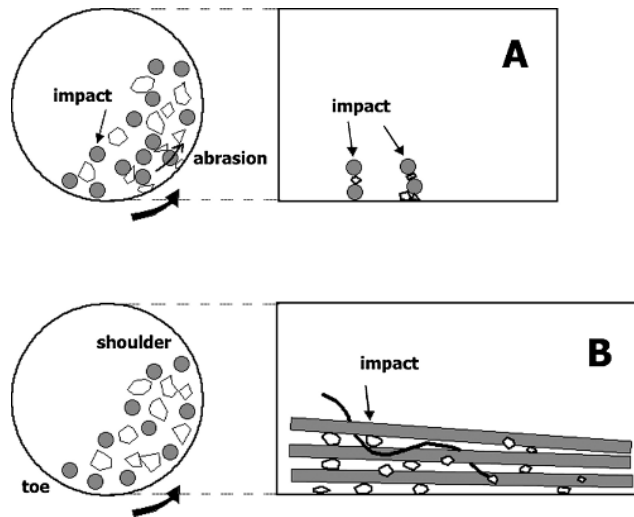
Fig. 3.3. A   Ball Mill; abrasion; impact breakage;
            B   Rod Mill; rods preferentially grind the coarse particles

of which result in further reduction of the size of the rock particles. Impact breakage occurs as balls or rods drop into the toe of the charge and abrasion or attrition occurs as the layer of balls or rods slides over each other or against the mill liner.

In designing a plant for size reduction the two main features of interest are:

1.   The power required for size reduction
2.   The choice of crushers and grinders

The power or energy required is the sum of the work required to crush or grind the rock as well as rotate the mill. The power required depends on the hardness of the rock, the initial size and the final product size required to achieve reasonable liberation of the mineral of interest, from the host rock.

3.2. Energy for Size Reduction - Work Index

Over the years several workers [1–12] have attempted to determine the energy required for crushing rocks. For a metallurgist this study is of interest where it is necessary to liberate the mineral embedded in the rock. It had been generally observed that in the process of size reduction, as the size of the particles diminishes the surface area of the particles increases. So a measure of size or surface area before and after size reduction would indicate the extent of energy expended in the comminution process. Hence if E was the energy used for a desired size reduction, which resulted in a change in surface area S, it has been found that [13–17]:

$$dE = k [S^n dS]$$ (3.1)

where k is a constant and a function of the crushing strength of the rock. Different workers have determined the value of the exponent n, as:

n = − 2   (Rittinger)
n = − 1   (Kick)
n = −1.5   (Bond)

It has been found that Rittinger's expression, n = − 2, is more applicable for coarse size reduction while that of Kick, n = − 1, is more appropriate for finer size reductions in the region where large surface areas of particles are exposed as in the case of grinding operations. Bond's intermediate value of 1.5 covers almost the entire range of particles.

Substituting n = − 1.5 in equation 3.1 and integrating between feed particle size, F, and product particle size, P, yields Bond's general expression for the energy required in size reduction as:

$$ E = 2k \left[\frac{1}{\sqrt{P}} - \frac{1}{\sqrt{F}} \right] $$

(3.2)

where k is a constant and a function of ore characteristics. For size reduction of ore in a closed circuit reduction process Bond derived the specific energy for grinding as:

$$ E_G = 10\, W_i \left[\frac{1}{\sqrt{P}} - \frac{1}{\sqrt{F}} \right] \ \ kWh/t $$

(3.3)

Eq. (3.3) is the result of fundamental work by Bond. It has now been accepted universally. In practice instead of a specific size of feed, a spread of particle sizes is generated at the mines, as a result of blasting, and is charged to the size reduction process. As a result of the crushing operation, a spread of smaller product size is obtained and fed to the grinding mill. To use Eq. (3.3) therefore, Bond considered the work as the energy required for the reduction of feed particles that passed 80% of a particular sieve to a product particle size that passed 80% of a sieve opening.

The final form of Bond's equation for size reduction of a mass of feed, M_F, in closed circuit grinding is now written as:

$$ E_G = 10\, W_i \left[\frac{1}{\sqrt{P}} - \frac{1}{\sqrt{F}} \right] M_F \ \ kWh $$

(3.4)

where   F = 80% passing size of the feed in microns, (written as F_{80})
          P = 80% passing size of the product in microns (written as P_{80})
          W_i = A constant for the ore

W_i is known as the Bond Work Index and represents the work required to reduce the ore from an infinite size to 100 μm.

The value of W_i can be considered to be independent of any classifier placed in the circuit. The terms F and P are usually written as F_{80} and P_{80}, the subscripts denoting the sieve size of feed and product respectively through which 80% of the feed and product passes. The terms $\dfrac{10}{\sqrt{P}}$ and $\dfrac{10}{\sqrt{F}}$ are dimensionless, as the number 10 represents $\sqrt{100}$ microns.

By definition the specific grinding energy is the energy required per unit mass of the rock. The specific grinding energy of a particular mineral is written as:

$$E_G = 10\ W_i \left[\frac{1}{\sqrt{P_{80}}} - \frac{1}{\sqrt{F_{80}}} \right] \quad \text{kWh/t} \tag{3.5}$$

NOTE: 1. kWh/t x 3600 = Joules/t
2. While 80% passing a particular sieve is accepted as standard for determining the Work Index, as recommended by Bond, some use 75% instead.

In Bond's equation, (Eq. (3.3)), the grinding energy, E_G, required for size reduction of rocks in industrial tumbling mills was based on mill shaft power, P_M, and on mill capacity (Q). The relationship between these parameters is:

$$E_G = \frac{\text{Mill Power}}{\text{Mill capacity}} = \frac{P_M}{Q} \tag{3.6}$$

For any rock therefore the energy required for comminution may be determined, provided the Work index W_i is known.

During manual crushing and disintegration of a rock with a hammer, or during mechanical crushing operations, the size reduction of large sized rocks and ores is mostly by sharp impact action, and less so by the impact and attrition experienced in tumbling mills. The equation used by Bond is inappropriate to determine the energy required for crushing. To cover this discrepancy Oka and Majima [9] found that in such cases the exponent of n (1.5) in equation 3.1 should be replaced by (1+[6/B]). This equation reverts to the Bond equation (equation 3.3) by taking the value of B as 12 and integrating, thus;

$$E = k \left[\frac{1}{P^{6/12}} - \frac{1}{F^{6/12}} \right] \tag{3.7}$$

which in effect is the Bond equation.

Bond's original work on establishing the energy for size reduction was established in a 2.44 m (8 foot) internal diameter wet grinding overflow type ball mill. Doubt is now expressed whether the derived empirical equation is applicable to high pressure roller crushers where one stage open circuit takes place. According to Klymowsky and Lin [18] indications are that the Rittinger expression, $E = K\ (1/P - 1/F)$, is more applicable for size reduction by high pressure rolls.

3.3. Estimation of Work Index for crushers and grinding mills

The standard laboratory procedures for estimating work index can be divided into two categories. The first category involves tests on individual particles of rock and the second category deals with bulk rock material. A number of tests are required to get an idea of the rock strength. The standard laboratory procedures adopted in industry are:

- Bond Pendulum test
- Narayanan and Whitens rebound pendulum test
- JKMRC drop test
- Bond ball mill grinding test
- Bond rod mill grinding test

3.3.1 Bond Pendulum Test

In this test the energy required to crush a dry ore particle by the impact of two swinging hammers is determined. The standard method adopted by Bond is as follows [5]:

Two equal hammers, 13.6 kg each, (Fig. 3.4), about 0.7 m in length and the striking face 50 x 50 mm are suspended from two (bicycle) wheel rims. The hammers are raised to a known height and when released strike simultaneous blows on opposite sides of a dry test piece (-7.6 cm + 5.0 cm). The test piece is suspended or supported with its smallest dimension between the hammers. The hammers are initially raised to make an angle of 10° with the vertical then released. After the impact the test piece is examined for fracture and the number of pieces broken is recorded. If the piece is not completely broken, the hammers are raised a further 5° and the process repeated till the piece is completely shattered. The heights of the hammers are recorded each time. At least 10 rock samples should be used per test but 20 is preferred.
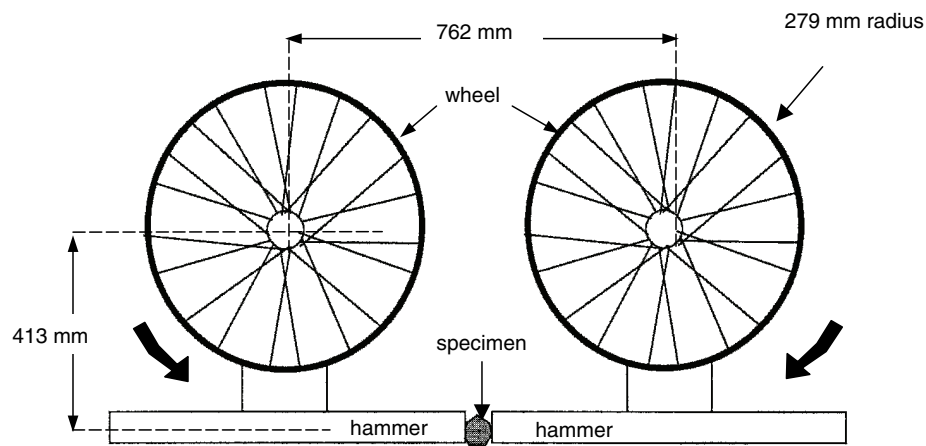
Fig. 3.4.   Bond's Impact Test at the point of impact with the specimen

The impact crushing strength (I) is calculated after each operation from the expression:

$$I = \frac{2 \times \text{Mass of one hammer} \times \text{Final height of hammer}}{d} \quad \text{kg.m/mm} \qquad (3.8)$$

where d = thickness of sample in mm

The value of I is usually averaged over the ten to twenty tests. The impact crushing strength of rocks so determined is used to calculate the Bond crushing work index using the expression:

$$W_i = \frac{C \times I}{\text{Relative Density of sample}} \quad \text{kWh/t} \qquad (3.9)$$

where   C is a constant which converts the impact crushing strength, numerically and dimensionally to the work index,
C = 2.59 in the original Bond equation where I is in ft-lb/in and W_i in kWh/short ton; C = 53.49 for I in Joules/mm and W_i in kWh/t (metric tonne).

The Bond impact test is considered to be inaccurate in that it consistently underestimates the actual operating crushabilities of most materials studied [19].

In a slightly modified apparatus by Metso, the bicycle wheels are replaced by slotted arcs in a fixed circle where notches are calibrated to indicate the energy released by hammers from pre-determined heights or notches. Results from this apparatus require careful evaluation before acceptance.

It should be noted that Bond's Grinding Work Index and Bond's Crushing Index are not the same though in the literature both are referred to as W_i.

3.3.2 Narayanan and Whiten's Rebound Pendulum Test
A slightly different test for measuring the crushing strengths of rocks was developed by Narayanan and Whiten [20]. In this test, the specimen is shattered against a suspended pendulum by an impact pendulum (Fig. 3.5). On impact, part of the energy is absorbed in the shatter of the sample, and part transmitted to the anvil block, which is displaced by the force of impact and commences oscillating. The remaining energy is dissipated as sound, heat etc.

Two sizes of anvil-blocks are used depending on the size of the sample and the size of the impact pendulum. The pendulum characteristics both types are summarised in Table 3.1.

Table 3.1
Alternative rebound pendulum masses

Sample Size, microns	Mass of rebound pendulum (anvil – block)	Mass of striking pendulum
-3150 + 1120	40.35 kg	19.86 kg
-1120 + 475	6.364 kg	4.441 kg

The swing of the pendulum is recorded by a computer, which receives signals from a laser beam impinging on fins fixed to the rebound pendulum. From simple geometry it can be seen

that the displacement, D, of the input pendulum from the rest position is given by:

$$D = L \sin \alpha \qquad (3.10)$$

where L is the length of cord of suspension and α the angle subtended with the vertical from the position of rest. Similarly, the horizontal displacement of the rebound pendulum after impact is given by $L \sin \theta$, where θ is the angle subtended from the vertical from the position of rest of the rebound pendulum. The angle θ is determined from the period of oscillation, P_{OS}, of the pendulum from the swing using the expression:

$$P_{OS} = A + B \, \theta^2 \qquad (3.11)$$

To determine the value of θ, the value of the constants A and B have to be determined. This is carried out by raising the pendulum to at least three heights and the P_{OS} for the first swing of the pendulum determined. The height, H, to which the pendulum is raised, is given by the relation:

$$H = L \, (1 - \cos \alpha) \qquad (3.12)$$

The velocity, v_S^o, of the striking pendulum at the point of impact before collision is:

$$v_S^o \quad = (2 \, g \, H)^{0.5} \quad = \quad 2 \, g \, L \, (1\text{-}\cos \alpha)]^{0.5} \qquad (3.13)$$
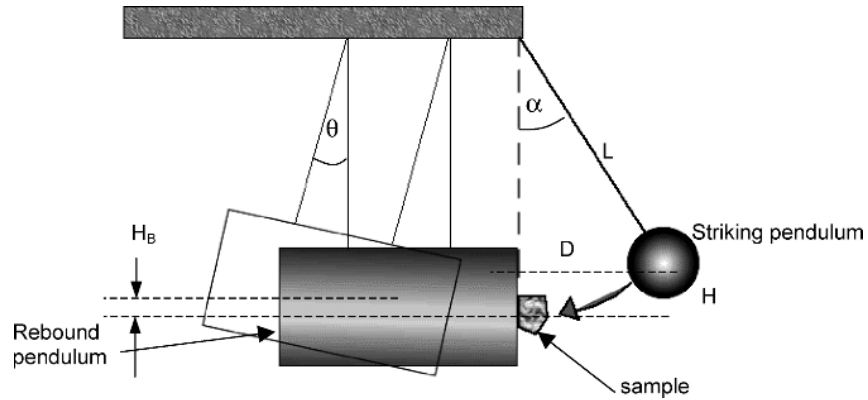
Fig. 3.5. Rebound pendulum device

and the energy of the striking pendulum from the point of release to the point of impact is:

$$E_S \quad = \quad M_S \, H \quad = \quad M_S \, L \, (1\text{-}\cos \alpha) \qquad (3.14)$$

where M_S is the mass of the striking pendulum.

After the strike by the striking or input pendulum, when the block or anvil or rebound pendulum swings away from its position of rest, the velocity of the rebound pendulum would be:

$$v_B^1 = (2 \, g \, H_B)^{0.5}$$ (3.15)

where H_B = the vertical height attained by the block pendulum and
v_B^1 = the velocity of the block or rebound pendulum after impact.
and the corresponding energy of rebound will be:

$$E_B = M_B \, H_B$$ (3.16)

where M_B = the mass of the block or rebound pendulum.

After the impact, the velocity of the striking pendulum decreases, and v_S^o now will be given by:

$$v_S^o - v_B^o = -\frac{\left(v_S^1 - v_B^1\right)}{\varepsilon}$$ (3.17)

where ε = the coefficient of restitution
v_B^o = the velocity of the block before impact
v_S^1 = the velocity of the striking pendulum after impact

As the initial velocity of the rebound block pendulum is zero, applying Newton's Law of conservation of energy, the coefficient of restitution will be:

$$\varepsilon = \frac{(v_B^1 - v_S^1)}{v_S^o}$$ (3.18)

The energy for crushing, E, is the difference between the energy of the input pendulum and the energy of the rebound pendulum and is computed from the following expression:

$$E = E_S \left(1 - \varepsilon^2\right)\left(\frac{M_B}{M_B + M_S}\right)$$ (3.19)

Units: Energy terms (E) = kWh/t = 3600 kJ/t
Mass = kg
The value of ε = 0 – 0.2

The results obtained with the larger anvil block have been found to agree well with the energy consumed in Autogenous and Semi-Autogenous Grinding (SAG) mills, while results from the smaller anvil agree more with ball and rod mill comminution systems. The estimation of energy for crushing by this method could be lengthy and tedious.

3.3.3 JKMRC-Drop Weight Crushing Test

Attempts at a much simpler and direct method of estimating the energy required for crushing rocks have been attempted by several workers like Gross [16], Piret [21], Hoffler and Herbst [22]. The method developed by Brown [23] is now accepted.

Fig. 3.6 is a schematic diagram of the apparatus developed by Brown. Rock is placed on a rigid heavy base-plate and crushed by weights falling from predetermined heights. The fall is channelled by guide rails. Conditions of the test include:

- Weights   range vary from 20 kg to 50 kg
- Drop height   vary from 0.5 to 1.0 m

Specific gravity of rocks should lie between 2800 kg/m^3 and 4000 kg/m^3. The energy of crushing ranges from to 0.01 to 50 kWh/t on a 10 to 50 mm particle size.

The rock sample is usually screened between close size ranges and the average mass of particles determined. The height from which the weight is released to affect breakage is measured.

The energy of breakage per unit mass is calculated from the expression:

$$E = H \frac{0.0272 M_c}{\overline{M}} \quad kWh/t \qquad (3.20)$$

$$= 97.9 \, H \frac{M_c}{\overline{M}} \quad Joules/t$$
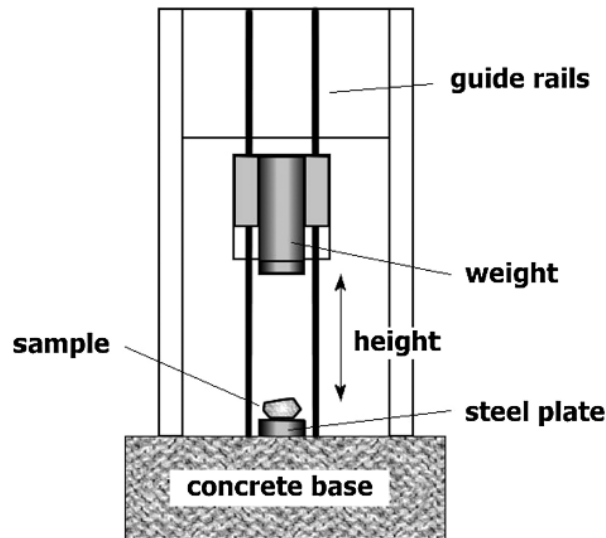
Fig. 3.6. Drop weight test

where E = Input energy per tonne, Joules/t,
       H = Height, cm,
      $\underline{M}_C$ = Mass of crushing weight, kg,
      $\overline{M}$ = Mean mass of sample.

After the crushing operation, the weight comes to rest on the broken particles. Thus the actual distance travelled by the weight is therefore less than the measured height, A correction in the actual distance travelled by the crushing weight has to be made by replacing H by (H–H_R) where H_R is the initial distance from the base plate to the position of rest of the lead weight after crushing. The rebound energy after impact, if present, has been claimed to be very small with respect to the input energy and is therefore neglected [24].

The usual practice is to use a 20 kg block for crushing. The number of particles ranges between 20-50 per size/energy combination totalling 500 to 1300 with a corresponding mass of 50 – 100 kg. If the mass is insufficient, it is increased. The energy of breakage is regulated by the ratio of the mass of the block and the height from which it is dropped. The breakage energy determined by this method agree well with the energy required by commercial crushers and AG/SAG mills. It is used as a useful guide for designing crushers and plant flowsheets.

3.3.4 Bond Ball Mill Standard Test

The method for determining the energy consumptions for tumbling mill conditions has more or less been standardised by laboratory tests and adopted after Bond.

The conditions of the tests are:

Mill Size = 305 mm (internal diameter) x 305 mm (internal length)

Material Dry mineral
         Size – reduced to 100 % < 3350 μm (6 mesh) and about 80% ≤ 2000 μm
         Quantity – 700 cm^3 (tapped down to give a reproducible bulk density)

Mill Charge-Steel Balls – Total mass = 20.125 kg
                               Total No = 285
                               Ball diameters made up as:
                                      43 x 3.7 cm, 9.094 kg
                                      67 x 3.0 cm, 7.444 kg
                                      10 x 2.5 cm, 0.694 kg
                                      71 x 1.9 cm, 2.078 kg
                                      94 x 1.55 cm, 0.815 kg

Mill Rotation – 70 rev/min

Procedure:

Step 1 Ball plus ore charge is ground for 100 revolutions.
Step 2 Ground charge is screened (classified) at the desired test mesh size (D), which is usually 106 μm (150 mesh).
Step 3 Under size is removed and replaced by an equivalent mass of original feed forming a new mill feed.
Step 4. The new mix is ground again as above by the number of revolutions calculated to produce a circulating load of 250%. That is, 28.6% (1/3.5 of total charge) will

pass the required chosen screen at the end of the cycle.

Step 5   The process is continued till the net mass of the undersize produced per revolution is constant. When this is achieved, then the mass, in grams, of the undersize produced per revolution is equivalent to a 250% circulating load.

Step 6   A size analysis is performed on the screen undersize and the original mill feed.

The average of the last three constant net mass of undersize per revolution in grams (G) is the measure of the ball mill grindability.

The ball mill work index, $W_{i\,Test}$, is calculated from the expression:

$$W_{i\,Test} = \frac{48.95}{D^{0.23}\,G^{0.82}\,10\left(\dfrac{1}{\sqrt{P_{80}}} - \dfrac{1}{\sqrt{F_{80}}}\right)} \quad \text{kWh/t} \tag{3.21}$$

where F_{80} =   Feed size (microns) through which 80% of the feed will pass,
        P_{80} =   Product size (microns) through which 80% of the product will pass.
        D =   Aperture (microns) of the classifying screen and
        G =   net mass (grams) of undersize product per unit revolution of the mill.

Note: Bond had used short tons to determine work index. To convert to metric tons the factor 1.1 has been used here, (44.5 x 1.1 = 48.95).

Due to its extensive use, details of the procedure is given in appendix.B-2, B-3.

Instead of 80% passing a certain selected screen size some workers in Australia use 75 % passing. It is therefore imperative that the screen size be mentioned when work index is reported.

The $W_{i\,Test}$ value measured corresponds to the motor output power Bond correlated to an average overflow discharge ball mill of 2.44 m internal diameter, wet grinding in closed circuit with a 250% circulating load.

Eqs. (3.21) and (3.5) are used extensively to calculate the work index and energy for comminution from data collected in operating plants. To distinguish the work index value determined under laboratory conditions from that required at the plant the concept of the plant operating work index (W_{Oi}) was developed by Rowland [25] and described by Rowland and Kjos [10], in terms of the energy requirements in the test mill and the commercial mill. According to Rowland, the ratio of the work indices equals the ratio of energies required in the test and the plant mills. That is:

$$\frac{W_{Oi}}{W_i} = \frac{\text{Energy required at Plant Mill}}{\text{Energy at Test Mill}} \tag{3.22}$$

To calculate the operating work index the work input is obtained from the mill power which, if obtained from the motor power, has to be the power at the mill pinion shaft. That is, if adjustments were coupled directly to the pinion shaft, then motor output power is the mill pinion shaft power. Work input is then obtained from the mill power (kW) by dividing it by the circuit throughput (t/h).

$$W_{Oi} = \frac{mill\,power}{tonnage\left(10\left[\dfrac{1}{\sqrt{P}} - \dfrac{1}{\sqrt{F}}\right]\right)}$$

(3.23)

In the Bond equation, the feed F is the feed to the grinding circuit and the product P, is the product from the grinding circuit. In an open circuit this is straightforward but in a closed circuit mill, where a classifier is installed to return the course fraction to the mill, the work index is based on the work done in reducing the size of the "new feed", that is, the original feed plus the coarse fraction from the product separated at the classifier and returned to the mill feed.

The operating work index is used for:

1. Recording mill performance on a regular basis (hourly, daily etc.)
2. Comparing current performance with historical data
3. Comparing circuits in multi-circuit plants

Since the operating work index includes motor, drive and grinding inefficiencies, it is not directly comparable to the work index obtained from laboratory grindability tests. If motor and drive losses are taken into account, then the operating index divided by the laboratory grindability work index test can be used as a measure of grinding efficiency in the plant.

$$\text{Grinding efficiency} = 100\,\frac{W_{OiC}}{W_{i\,TEST}}$$

(3.24)

where W_{OiC} = operating work index, corrected for non-standard conditions and non-optimum feed,

$W_{i\,TEST}$ = laboratory grindability work index.

3.3.5 Bond Rod Mill Standard Test

Standard conditions for determining the work index of rod mills under laboratory conditions are:

Mill Size = 305 mm (internal diameter) x 610 mm (internal length) with wave type lining

Material Dry mineral
        Size – reduced to 100 % < 13200 μm
        Quantity – 1250 cm^3 (tapped down to give a reproducible bulk density)

Mill Charge-Steel Rods – 6 x 38.1 mm dia x 0.53 m long steel rods plus
                         2 x 44.5 mm dia x 0.53 m long steel rods
                         total mass = 33.38 kg

Mill Rotation – 46 rev/min, 100 % circulating load.

Procedure: (a detailed procedure is given in the appendix)

Step 1   To equalize the charge segregation at the ends of the mill, the mill is rotated in the level position for 8 revolutions then tilted up 5° for 1 revolution, tilted down 5° for 1 revolution then returned to the level position for 8 revolutions and the cycle repeated throughout the test.

Step 2   At the completion of the grind, the mill is tilted at 45° for 30 revolutions to discharge the contents.

Step 3   Ground charge is screened at the desired test mesh size (D).
          Under size is removed and replaced by an equivalent mass of original feed forming a new mill feed.

Step 4   The new mix is ground again as above by the number of revolutions calculated to produce a circulating load equal to the new feed (1250 cm^3), i.e. 100% circulating load.

Step 5   The process is continued till the net mass of the undersize produced per revolution is constant.

Step 6   A size analysis is performed on the screen undersize and the original mill feed.

The average of the last three constant net mass of undersize per revolution in grams (G) is the measure of the rod mill grindability.
The work index is given by:

$$W_{i\,Test} = \frac{68.2}{D^{0.23}\;G^{0.625}\;10\left(\dfrac{1}{\sqrt{P_{80}}} - \dfrac{1}{\sqrt{F_{80}}}\right)}\quad kWh/t \qquad (3.25)$$

Note: 1.   Bond had used short tons to determine work index. To convert to metric tons the factor 1.1 has been used here, (62 x 1.1 = 68.2).
        2. W_i conforms to the motor output on an average overflow rod mill of 2.44 m internal diameter, wet grinding in open circuit.

3.3.6 Factors affecting the Work Index
The $W_{i\,TEST}$ values calculated from Eqs. (3.21) and (3.25) are based on Bond's work using a laboratory size tube mill. It is claimed that the W_i values obtained from a 2.44 m internal diameter tube mill, operating under closed circuit wet grinding conditions agree well with the laboratory sized test mill. However, the Bond Work Index (TEST) so determined has to be corrected for conditions encountered in industry that differ from the above conditions. Bond defined eight correction factors.

1. Correction factor: F1   For conversion of W_i obtained under wet grinding conditions to dry grinding:

$$W_i(Dry) = 1.3 \times W_i(Wet) \qquad (3.26)$$

2. Correction factor: F2   For conversion to wet open circuit grinding index from wet closed circuit grinding:

For open circuit grinding, the correction factor depends on the degree of control required on the product. Table 3.2 gives the multiplying factors against different sieve sizes used for controlling product size in closed circuit grinding.

W_i (wet open Circuit) = W_i (wet closed circuit) x Multiplying factor

For example if Bond's work index W_i = 12.40 for wet closed circuit grinding where an 80% passing control screen was used, then the corresponding value for wet open circuit grinding according to Table 3.2 would be:

W_i open (wet) grinding = W_i x 1.2 (closed) at 80% passing a size control
                         = 12.4 x 1.2 = 14.8

For convenience of calculation, Table 3.2 is plotted in Fig. 3.7.

Table 3.2
Multiplying factor for converting wet closed circuit Work Index to wet open circuit Work Index [26].

Product size control % passing	Multiplying factor	Product size control % passing	Multiplying factor
50	1.035	90	1.40
60	1.05	92	1.46
70	1.10	95	1.57
80	1.20	98	1.70
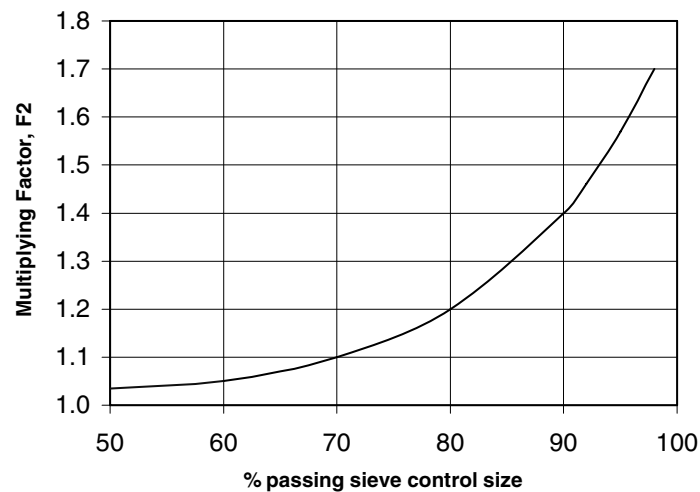
Fig. 3.7. Bond Work Index correction factor F2.

Feed size $> 4000 \, [1.10 \times 13/W_{i \, Test}]^{0.5}$ microns (ball mill) $\qquad$ (3.27)

$\qquad > 16000 \, [1.10 \times 13/W_{i \, Test}]^{0.5}$ microns (rod mill)

That is, greater than $1.5/(\sqrt{W_{i \, Test}})$ cm for a ball mill. In this situation the correction factor F_{OS} is given by Eq. (3.28):

$$F_{OS} = 1 + \frac{P_{80}}{F_{80}} \left(\frac{W_{i \, Test}}{1.10} - 7 \right) \left[\frac{F_{80}}{4000 \sqrt{(1.10 \times 13)/W_{i \, Test}}} - 1 \right] \qquad (3.28)$$

4. Correction factor: F4   For extra fineness of grind: F_G

When the required product size is less than 75 microns and greater than 15 microns, it implies that the product size has to be ground to an extra fine size. In such cases, the work index will depend on the product size. The work index correction required is given by Eq. (3.29):

$$F_G = \frac{P_{80} + 10.3}{1.145 \, P_{80}} \qquad (3.29)$$

5. Correction factor: F5   For low reduction ratio R, for ball mills: F_R

This correction is applicable when the reduction ration, i.e., ratio of feed size to product size is less than 6.

The multiplying factor for different values of F_{80}/P_{80} is determined from the expression:

$$F_R = \frac{2(R - 1.35) + 0.26}{2(R - 1.35)} \quad \text{or}$$

$$F_R = \frac{(F_{80} - 1.22 P_{80})}{F_{80} - 1.35 P_{80}} \qquad (3.30)$$

6. Correction factor: F6   High or Low Reduction Ratio, Rod Milling:

There is an optimum ratio of reduction for each rod mill due to the natural preference to grind the coarser sizes by a rod charge. For higher throughputs leading to a coarser grind due to lower residence times in the mill, the coarser particles spread the rods apart, disrupting the normal grinding action. If the feed to the mill is reduced to attempt a finer grind, the reduction ratio increases, trying to produce a product finer than the rod mill should be capable of producing. For both cases of abnormal reduction ratios, a correction factor, F6, is applied to the Bond Work Index, where:

$$F6 = 1 + \frac{(R - R_{RO})^2}{150} \qquad (3.31)$$

where R_{RO} = optimum reduction ratio for the mill size = $8 + 5 \dfrac{L}{D}$

$\qquad$ L = Rod length
$\qquad$ D = Mill diameter (internal).

This efficiency factor is only used when R is outside the range $R_{RO} \pm 2$.

7. Correction factor: F7   Mill Diameter:

The grinding efficiency changes with mill diameter. The change arises from the change in power drawn by the mill and the change is mill capacity with diameter. The correction factor is given as:

$$F7 = \left(\frac{2.44}{D}\right)^{0.2} \quad \text{for} \quad D < 3.81 \text{ m}$$
$$F7 = 0.914 \quad \text{for} \quad D \geq 3.81 \text{ m} \tag{3.32}$$

where the mill diameter, D, is in meters. It has been shown by Bond that for mills larger than 3.81 m, the reduction in grinding energy resulting from mill diameter ceases and the correction factor is constant at the 3.81 m value of 0.914.

8. Correction factor: F8   Rod Milling:

The correction factor for rod milling is complex and depends on the feed preparation. Bond suggests two conditions:

1. For a rod mill only application, use an efficiency factor of 1.4 when the feed is produced by open circuit crushing, and use a factor of 1.2 when the mill feed is produced by closed circuit crushing.
2. For a rod mill-ball mill circuit, do not apply a mill diameter correction for the ball mill. If the rod mill feed is produced by open circuit crushing, use a factor of 1.2 for the rod mill stage only. If the rod mill feed is 80% passing 12 mm or less (e.g. from a closed circuit crusher) do not apply a rod mill efficiency factor. Other correction factors such as mill diameter and reduction ratio however do apply.

The uncertainty in this correction factor means that it has little value in calculating, W_{iOC} and the efficiency of plant rod mill performance. Thus the test work index value multiplied by the product of the correction factors will provide an estimate of the true (plant) work index value.

$$W_i = W_{i \text{ TEST}} \text{ x F1 x F2 x ... x F7 x F8} \tag{3.33}$$

Factors for condition not applicable should be taken as 1.

The Bond Work Index value changes with the sieve size chosen during a particular test. For example, instead of choosing the screen size through which 80% of the ore passes, the screen size through which 75% of the ore passed may be chosen to suit a particular condition of mill operation. Bond's original expression for the work index is based on 80% of the material passing a screen size. This has now been adopted as the standard. Any deviation from this standard would require the determination of a corresponding equivalence. The method of determining the equivalence may be explained by the following example.

Example 3.1

A gold ore was crushed and screened so that 99% passed 9.5 mm size screen. Laboratory measurement showed that the product size of gold was 75% minus 63 microns. A standard ball-mill Bond test indicated that the grindability was 2.28 grams per revolution at a test screen size of 106 microns. The ore was ground in a wet closed circuit ball mill at a throughput rate of 150 t/h. Estimate the work index for a mill of I.D. 2.0 m.

Solution

Step 1.
Establish the F_{80} by referring to Table 3.3.
Feed size (F_{80}) equivalent from Table 3.3 = 6000 μm

Step 2.
Next establish the P_{80} from a Gaudin-Schuhmann plot of the sieve analysis, if available. If the sieve analysis was not available then use the relation:

$$Size\,2 = \left(\frac{Percent\ Pas\,sin\,g\ Size\,2}{Percent\ pas\,sin\,g\ Size\,1} \right)^2 x\ Size\,1 \qquad (3.34)$$

Table 3.3
Feed size and approximate 80 % passing sizes (in mm)

Material Size 99 % passing	80% passing equivalent	Material Size 99 % passing	80% passing equivalent
38.1	25.0	1.18	0.800
25.4	18.0	0.85	0.550
19.1	12.0	0.60	0.400
12.7	8.5	0.425	0.270
9.50	6.0	0.30	0.150
6.70	4.2	0.212	0.105
4.75	3.0	0.150	0.072
3.35	2.1	0.106	0.055
2.36	1.5	0.075	0.036
1.70	1.0	0.045	0.020

For Size 1 = 63 μm,

$P_{80} = (80/75)^2 x\ 63 = 71.7$ μm,

According to Eq. (3.21):

$$W_i = \frac{48.95}{D^{0.23}\ G^{0.82}\ 10\left(\frac{1}{\sqrt{P_{80}}} - \frac{1}{\sqrt{F_{80}}} \right)} \qquad kWh/t$$

Substituting the values from the data supplied:

$$W_i = \frac{48.95}{106^{0.23} \, 2.28^{0.82} \, 10 \left(\dfrac{1}{\sqrt{71.7}} - \dfrac{1}{\sqrt{6000}} \right)}$$

$W_{i\,Test} = 8.10\ kWh/t$

Step 3. Apply correction factors.
Correction factors F1 and F2 = 1

Optimum feed top size = $1.5/(\sqrt{W_{i\,Test}})$ = $1.5/\sqrt{8.10}$ = 0.53 cm = 5300 microns. The feed size is greater than this hence a coarse feed correction factor needs to be applied.

$$F3 = F_{OS} = 1 + \frac{63}{6000}\left(\frac{8.10}{1.10} - 7\right)\left[\frac{6000}{4000\sqrt{(1.10 \times 13)/8.10}} - 1\right] = 1.0005$$

Since the product size is less than 75 microns:

$$F4 = F_G = \frac{63 + 10.3}{1.145 \times 63} = 1.016$$

The reduction ration = 6000/63 = 95.2, hence F5 = 1

F6 and F8 = 1 and F7 = $(2.44/2.0)^{0.2}$ = 1.041

Thus the overall correction factor, F = 1.0005 x 1.016 x 1.041 = 1.058 and the corrected work index is given by:

$W_i = W_{i\,Test} \times F = 8.10 \times 1.058 = 8.57\ kWh/t$

3.3.7 Effect of the Test Screen Size on the Work Index
The Bond Work Index is not solely a material constant but is influenced by the grinding conditions. For example, the finer the grind size desired, the higher is the kWh/t required to grind to that size. Magdalinovic [27] measured the Bond Work Index of three ore types using different test screen sizes. He produced a correlation between the mass of test screen undersize per revolution, G, and the square root of the test screen size, D:

$$G = K_1 \sqrt{D} \tag{3.35}$$

The constant K_1 is dependent on the ore type. Magdalinovic also produced a relationship between the test screen size and the 80% passing size of the test screen undersize where:

$$D = K_2 P_{80} \qquad\qquad (3.36)$$

The constant K_2 is also dependent on ore type and ranged from 1.4 to 1.5. A regression of Magdalinovic's data including the feed 80% passing size gives an average value of 1.485 for K_2. If we extend this relationship to any sample of screened material then this gives an approximate estimate of the 80% passing size as 67.3% of the top size. This compares with a value of 66.7% of the 99% passing size obtained from data in Table 3.3.

Using Magdalinovic's method, from the results of a Bond Work index test at a single test screen size, the constants K_1 and K_2 can be calculated and from these values, the Work Index at any test screen size can be estimated.

3.3.8 Approximation methods for Work Index

The Bond method of measurement of the grindability of ores in rod mills and ball mills is long and tedious and requires a standard set of grinding conditions; mill size, ball charge etc. A number of approximate methods have been reported that shorten or approximate the work index estimation.

1. Magdalinovic Method:

The method proposed by Magdalinovic [27] reduces the number of grinds required from approximately five to two. The first grind is to determine the grinding rate of screen undersize. This grinding rate is then used to adjust the number of mill revolutions in the second grind to give 250% circulating load.

The method uses the standard Bond Mill (305 mm diameter x 305 mm length) and the Bond ball charge. A summary of the procedure is as follows:

1. The ore is crushed to the same size (-3.35 mm) as in the Bond method and a sub sample taken to determine the size analysis of the new feed (include a screen equal to the test screen in the size analysis to make later calculations easier). From the size analysis, the 80% passing size of the feed, F_{80}, is determined.

2. A mass, M, of 700 mL of the crushed ore is measured which represents the mill charge mass.

3. The "new feed" material is riffle split into two equal portions of mass (M/3.5).

4. Approximately 4 kg of the ore is screened on the test screen (the separating size of the closed circuit screen/classifier) and the undersize is discarded.

5. The oversize is riffle split into two masses equal to (2.5M/3.5). This mass, M_C, represents the circulating mass at 250 % circulating load.

6. One portion of (2.5M/3.5) from step 5 is combined with one portion of (M/3.5) from step 3 to give a combined mass of M, the charge to the first grind.

7. The two remaining portions are combined to give a second mass of M, the charge to the second grind. Thus the feed to each of the two grinds should be identical in terms of mass and size.

8. The first sample is placed into the ball mill and ground for 100 revolutions at a mill speed of 70% of the critical speed.

9. After the grind, the entire sample is screened at the test screen size and the mass of the

oversize is recorded. This mass M_{OS} should be equal to the mass M_C at a circulating load of 250%.

10. The oversize grinding rate constant, k, is calculated using the equation:

$$k = \frac{n(\ln M_o - \ln M_{OS})}{N} \qquad (3.37)$$

where n = number of mill revolutions per minute
       N = number of mill revolutions in the first test
       M_{OS} = mass of test screen oversize after grinding
       M_o = mass of test screen oversize at the beginning of the grinding test

11. The total number of mill revolutions for the second grinding test (N_2) is calculated from the equation:

$$N_2 = \frac{n \, ln(1 + 0.4m_o)}{k} \qquad (3.38)$$

where m_o = fraction of test screen oversize in the new feed (obtained from step 1).

12. The mill is loaded with the second charge and grind for N_2 revolutions.
13. After grinding, the entire mill charge is screened on the test screen and the oversize and undersize weighed. The oversize should be approximately equal to (2.5M/3.5) and the mass of the undersize, M_{US}, should be approximately equal to M/3.5.
14. The size analysis of the test screen undersize is determine and the 80% passing size (P_{80}) of the product calculated.
15. The new undersize per mill revolution, G, in the second grind is then determined using the equation:

$$G = \frac{M_{US} - \frac{1}{3.5} M(1 - m_o)}{N_2} \qquad (3.39)$$

16. The ore Work Index is then calculated using the Bond formula (Eq. 3.21).

This method reduces the time of measurement and where the ore is homogeneous, gives work index values within 7% of the Bond method. However, where the ore contains soft and hard components, a true Bond test will have a recirculating load which is composed predominantly of the harder component and hence will give a higher Work Index value consistent with closed circuit grinding. Since the Magdalinovic method uses the same feed to each grinding step, this harder material in the circulating load is not simulated and hence the method will give a lower Work Index value.

2. Methods using a non-standard mill and charge

If a standard Bond mill is not available then an approximate Work Index value can be obtained if a sample of ore of known Work Index is available [28]. The non-standard mill can

be "calibrated" using the ore of known Work Index as follows:

1. A sample of known mass of the unknown ore is ground for a known period of time to produce the desired grind. Berry and Bruce use 2 kg of –1.7 mm (10 mesh) feed ground wet.

2. The same mass of the ore of known Work Index is ground in the same mill under the same conditions of feed size, mill and charge size and grind time.

3. The size analysis of the feed and products is determined from each grind, and hence the F_{80} and P_{80} values are evaluated.

Since the mill conditions in both grinds are the same, the energy used to grind the unknown ore should be approximately the same as the energy used to grind the reference ore of known Bond Work Index. This can be calculated using Bond's Eq. (3.5). The Bond Work Index of the unknown ore can then be estimated from the equality given in Eq. (3.40).

$$W_{iU} \left(\frac{1}{\sqrt{P_U}} - \frac{1}{\sqrt{F_U}} \right) \approx W_{iREF} \left(\frac{1}{\sqrt{P_{REF}}} - \frac{1}{\sqrt{F_{REF}}} \right) \qquad (3.40)$$

where W_{iU} = Bond Work Index of the unknown ore,
$W_{i\,REF}$ = Bond Work Index of the reference ore,
F_U, P_U = F_{80} and P_{80} of the unknown ore,
F_{REF}, P_{REF} = F_{80} and P_{80} of the reference ore.

Horst and Bassarear [29] used a similar –1.7 mm (10 mesh) feed in a non-Bond laboratory mill according to the following procedure:
1. The size distribution of the reference ore feed is measured.
2. A 1 kg sample of a reference ore (known Bond Work Index) is ground for a period of time to achieve the desired grind.
3. Three samples of the unknown ore under the same grinding conditions are ground for different periods of time that include times shorter and longer than in step 2.
4. The size analysis results from products from the three grinds from step 3 are fitted to a simple first order rate equation:

$$\ln m_i = \ln m_{oi} - k_i t \qquad (3.41)$$

where m_i = cumulative mass fraction retained on the ith sieve,
m_{oi} = cumulative mass fraction retained on the ith sieve at zero time,
k_i = comminution coefficient of the fraction coarser that the ith sieve,
t = time.

5. From the values of k_i, the product size distribution of the unknown ore is calculated from the same feed size distribution as the reference ore, which has been ground for the same time and using Eq. (3.41).
6. From step 5, the 80% passing size of the grind product for the unknown ore is estimated.
7. The Work Index of the unknown ore is then determined from Eq. (3.40).

This method has been shown to be more accurate that the method of Berry and Bruce however the procedure is just as lengthy as the standard Bond test and not all ores follow the simple first order breakage of Eq. (3.41).

3. Simulation methods

An algorithm for the simulation of the Bond grindability, G, was developed by Kapur [30]. The mass of the test screen oversize, M_{OS}, after the first grind of the Bond Test is given by:

$$M_{OS} = M_o \, M f(t) \tag{3.42}$$

where M_o = mass of test screen oversize at the beginning of the grind ,
M = mass of mill charge,
$f(t)$ = a function of grind time, t.

Kapur showed that it was possible to estimate the grindability and the Work Index from the first two cycles of the Bond test. He obtained the following empirical expression for the grindability:

$$G_{bp} = -M_o \, M_1 \, G \, K \tag{3.43}$$

where G_{bp} = mass of the undersize per mill revolution (g/rev),
M_1 = mass of new feed in the first grind,
G = batch grinding parameter, related to the grinding rate of the fresh feed,
$K = \dfrac{2.5}{3.5} \left[\dfrac{G'}{R_o G'} - 1 \right] + 1$, and
G' = grinding parameter of the circulating load.

In practice, K is assumed to be equal to unity. The work index is calculated by an empirical equation:

$$W_i = 2.648 \, P_1^{0.406} \, (-G_2)^{-0.810} \, (R_o M_1)^{-0.853} \, (1-R_o)^{-0.099} \tag{3.44}$$

where G_2 = grinding parameter from the second grind,
P_1 = 80% passing size of the product from the first grind.

The calculated values of G (g/rev), using Kapur's method, were higher than the measured values for softer ores and lower than the measured values for harder ores.

Austin et al. [26] has shown that batch grinding can be simulated by using the size-mass balance grinding equations. It should be possible then to simulate the Bond test by computer simulation, provided that the breakage distribution function, B_{ij}, and the breakage rate function, S_i, are known. Lewis et al. [31] back calculated these breakage functions from the first cycle of a Bond grinding test. Yan and Eaton [32] went further and measured the breakage parameters for two ore types (one hard and one soft) and simulated the Bond test. Their results gave work index values of 13.1 and 5.6 kWh/t compared to measured values of 14.0 and 6.6 kWh/t respectively. The test work involved in determination of the breakage

parameters can be even longer that that required for a Bond test. However potentially much more information can be obtained from the data and further computer simulations.

Subasinghe and Kanau [33] evaluated the breakage distribution function and the rate function of a 1 kg charge of a single size interval (-3.35 + 2.36 mm). The breakage rate and breakage distribution functions were used to simulate the Bond batch grinds using the approach of Lewis et al [31], however, the simulated grindabilities deviated considerably from the measured results.

Subasinghe and Kanau found that the zero order fines production rates, corresponding to (B_{ij} S_j), for the 150 and 106 micron sizes correlated well with the Bond grindabilities. The Bond grindabilities corresponding to the observed gradients evaluated from the regression lines showed a superior correlation compared to those obtained from Kapur's method.

4. Work Index from Rock Mechanics

Everell [34] believed that the mechanism of breakage of particles in a grinding mill was analogous to the slow compression loading of irregular particles and that the specific rate of breakage for a particular size of fragment is an inverse function of the average failure load of the particles. Everell et al [35] developed a model to describe the relationship between the grinding selection function (breakage rate) and the physio-mechanical properties of the rocks. The advantage in such a relationship lies in the wealth of rock strength data determined on drill core during mine development being available to predict energy demands in the comminution circuits.

Briggs [36] measured the tensile strength, using the Brazil tensile test, and the point load compressive strength of four rock types of different grindabilities. These results were compared to the Bond Work Index of the ores as measured by the Magdalinovic method [27]. The results in Fig. 3.8 show that there is a good correlation between the Bond Work Index and the tensile strength and the Equivalent Uniaxial Compressive Strength (EUCS). Some of the scatter in the graphs are due to the structure of the rock. For example one rock type was a banded iron, heavily mineralised with sulphides with numerous planes of weakness on a macro scale. This affected the mechanical properties when tested on large specimens. However when the grinding tests were carried out at relatively small particle sizes, the planes of weakness were no longer present and the ore became more competent.
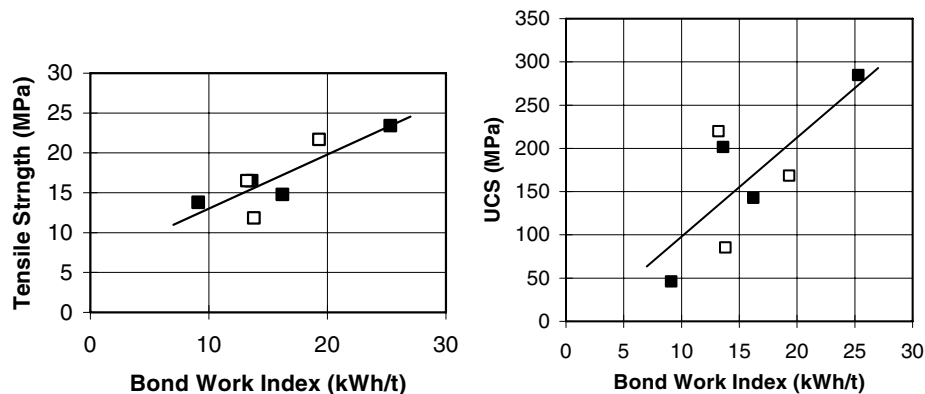
Fig. 3.8.   Bond Work Index vs tensile strength and the EUCS; ■ Briggs [36] □ Yan [37].

The correlation between Bond Work Index and tensile strength is an indication that the grinding mechanism in the work index test favours abrasion type breakage given that tensile strength is a fair indication of the abrasiveness of a rock.

Briggs also measured the breakage rate and breakage distribution function of the ores and compared the breakage rate and Bond Work Index. There was a good correlation between the rock strength data and the breakage rate with higher strength rocks having a lower breakage rate. However the data set for these tests was small and further work needs to be done to confirm the relationship.

Bearman et al [38] measured a wide range of rock strength properties and correlated these to the JKMRC drop weight test data. Conclusions were that this technique will enable the data required for comminution plant design to be obtained from mechanical tests on drill core samples.

5. Chakrabarti's Statistical Method

Chakrabarti [39] has advanced a simple statistical correlation method of estimating work index using the Rosin-Rammler and Gaudin-Schuhmann size distribution parameters. Chakrabarti considered the Rosin-Rammler and Gates-Gaudin-Schuhmann functions of 35 data sets covering work indices between 5.36 and 23.93. The best correlation was found with the Rosin-Rammler parameters.

According to Chakrabarti, the work index of an unknown rock material can be obtained by firstly crushing the rock to less than 3327 microns, avoiding over crushing by using low energy impact or compression and by closing the circuit with a 3327 micron screen. The crushed product is sized using a Tyler standard sieve nest set between 3350 and 75 microns and the Rosin-Rammler distribution parameters determined. The work index is then calculated from the statistical power relation:

$$W_i = a + bx_1 + cx_2 + dx_1^2 + ex_2^2 + fx_1 x_2 \qquad (3.45)$$

where x_1 is the size parameter, x^1, of the Rosin-Rammler equation of 3327 micron feed and x_2 is the distribution parameter, b, of the Rosin-Rammler distribution of the same feed material (see Chapter 2.2).

Chakrabarti suggests that a modified form of the Rosin-Rammler equation gives a better fit to the experimental size distributions. The constants a, b, c, d, e and f were found to have the values of:

$a = 7.581733618, b = 0.003845, c = -14.83865521, d = -6.165619037 \times 10^{-7},$
$e = 15.15586454, f = 0.000789264$

The correlation between experimental and calculated work indices is shown in Fig. 3.9 based on the unmodified and modified Rosin-Rammler function.

Whilst Fig. 3.9 shows that there is a trend, the equation requires further refinement from larger data sets before it can be adopted.

3.3.9 Work Index of Ore Blends

The blending of different ore types is common practice to provide a consistent feed to a process in terms of uniform hardness or assay. When several different ore deposits of varying

88
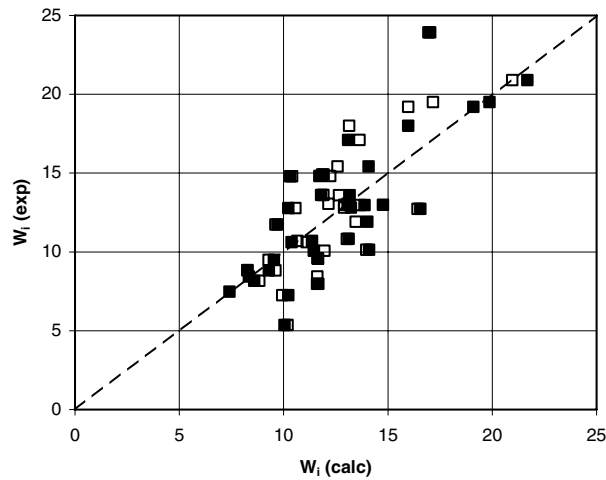
Fig. 3.9. Comparison between calculated and experimental Bond work index values of a range of ore types based on Chakrabarti's correlation (■ modified; □ unmodified Rosin-Rammler equation)

grindabilities are blended prior to closed circuit grinding, the work index of the ore is not an average or even a weighted average of the work indices of the components. The reason for this is that the circulating load will consist predominantly of the harder component and if the circulating load is high then the mill charge will also consist of mostly the harder components. Thus the work index of the blend will be weighted towards the harder components [32]. Fig. 3.10 shows the Bond Work Index of a blend of hard and soft ores as a function of the volume fraction of the softer ore in the blend. The dotted line between the two extremes indicates the weighted average work index based on volume fraction. The work index values of the Magdalinovic method agrees with this average Bond Work Index because the method doesn't simulate the recycling of harder components into the mill charge. On the other hand, the Work Index obtained using the standard Bond test shows the weighting of the Work Index towards the harder component as a result of the circulating load.

Yan and Eaton [32] also measured the breakage rates and breakage distribution functions of the different ore blends in order to predict the Work Index of the blend by simulation of the Bond batch grinding test. Qualitative analysis of the breakage properties suggests that there is an interaction between the components of the blend that affect their individual breakage rates. The breakage properties of the harder material appears to have a greater influence on the overall breakage properties and the Bond Work Index of the blend than the softer material.

Table 3.4
Experimental and simulated Work Indices of ore blends [32].

Ore type	Bond Work Index (kWh/t)	
	Measured	Simulated
Hard	14.0	13.1
50:50 blend	12.0	11.1
Soft	6.6	5.6
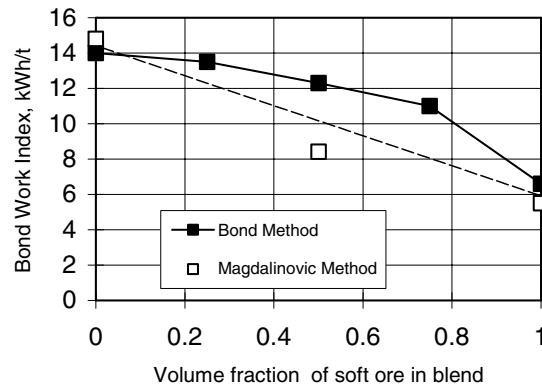
Fig. 3.10. Bond Work Index of a blend of hard and soft ore [32].

Table 3.4 shows the simulated Work Index of the blend of hard and soft ore types. The computer simulation under estimated the value of the Work Index by approximately 1 kWh/t.

3.3.10 Work Index and Abrasion

Size reduction in a tubular mill is also caused by abrasion and attrition. The forces of abrasion act between:

1.   the grinding media and the mineral particles,
2.   the mineral particles themselves, and
3.   between the grinding media themselves.

Separate evaluation of these parameters is difficult. Bond [13] while measuring the wear of the grinding media in tubular mills attempted to measure the attrition between the media and the charge and arbitrarily defined an Abrasion Index by the loss of mass of a standard spindle rotating in a drum on which standard sized minerals are continuously impinging for a set time. Bond's method is now generally accepted as the attrition of metals by minerals.

Bond's Abrasion Test (also known as Allis Chalmers Abrasion Test)

Bond's abrasion test consists of an hardened Cr-Ni-Mo alloy steel paddle (hardness 500 Brinell), 7.62 cm x 2.54 cm x 2.54 cm with 2.54 cm of its length sitting inside a rotor, 11.43 cm diameter. The rotor is covered by a concentric steel drum 11.43 cm in length and 30.54 cm in diameter. Both the rotor and the outside drum are mounted on an horizontal shaft. The rotor rotates at 632 rpm while the drum is rotates in the same direction at 70 rpm. The initial charge mass is 400 grams of −19.0 mm + 12.7 mm size material. The rotors are run simultaneously for 15 minutes. Next, the charge is removed and the process repeated four times. That is, the spindle is exposed to abrasion for 1 hour. The charge recovered each time is collected, mixed, sieved dry and the P_{80} determined. The spindle is also weighed. The loss in mass (in grams) of the spindle gives the attrition index, A_i. The total power used in rotation is noted. The Attrition Index thus determined is included in Table 3.5 for selected minerals. Mathematical correlation with the Work Index has not been reliably established.

Table 3.5
Average Abrasion and Work Index of selected minerals [41].

Mineral	Work Index (W_i)	P_{80}	Abrasion Index (A_i)
Dolomite			0.016
Limestone	11.7	-	0.082
Magnesite	0	-	0.079
Copper Ore	11.7	12,700	0.147
Hematite	8.5	13,450	0.165
Magnetite	13.0	-	0.222
Granite	16.6	14,680	0.388
Taconite	16.3	-	0.775
Quartzite	17.4	-	0.775
Alumina	17.5	15,800	0.891

JKMRC Abrasion Test

JKMRC has developed a slightly different method of estimating abrasion. Their method is similar to the standard laboratory Trommel Test applied for testing the abrasion of iron ore pellets and coke. In this test 3 kg of dry ore, size –55 mm + 38 mm is charged into a horizontal cylindrical steel drum ID 0.30 m x 0.30 m with lifter bars 2.54 cm in height The drum is rotated for 10 minutes at 53 rpm. The sample is then removed and screened to –38 µm. The cumulative mass percent passing each screen size is plotted. The mass percent passing 1/10th (T_{10}) of the original size is taken as the "abrasion parameter".

The concept and use of the factor, T_{10}, has been promoted by Weedon et al, [40] to develop a relation between crushing strength and specific comminution energy. T_{10} is defined as the percent ore passing 1/10th of the original particle size. The meaning of the subscripts can be extended as:

T_2 = % passing 1/2 of the original particle size
T_4 = % passing 1/4 of the original particle size

.

T_{10} = % passing 1/10 of the original particle size

.

.

T_N = % passing 1/N of the original particle size

T_N is the cumulative mass % passing a size d_{GM}, where d_{GM} is the geometric mean of the size interval between sieves. A plot of particle size against T_N where N = 1.2.... N yields the value of T_{10}. The relation between T_{10} and specific breakage energy due to crushing has been established as [24]:

$$T_{10} = A(1 - e^{-B \, E_G})$$

(3.46)

where A and B are ore specific constants and E_G is the specific comminution energy. The parameter A represents the theoretical limiting value of T_{10} (see Fig. 3.11). For hard ores the value of A approximates 50. The value of A.B (the impact parameter) is the slope of the T_{10}–E curve at zero input energy.

The T_{10}–mass distribution curve is useful as it is a description of the product size distribution and the T_{10} can be considered an index of the degree of breakage. The harder the ore, the lower the T_{10} value for a given input energy. Knowing the T_{10} value resulting from a given input energy, the complete product size distribution can be calculated. According to Napier-Munn et al [24]:

For crushing – T_{10} is usually between 10-20% and
For grinding – T_{10} ranges between 20-50%.
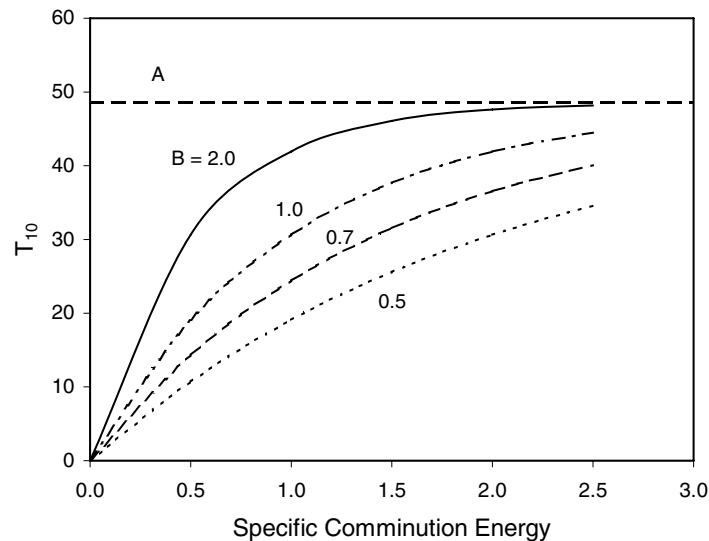
Fig. 3.11.   Relationship between T_{10} and specific comminution energy (Eq. (3.46))

Napier-Munn et al [24] indicate a possible correlation between the impact parameter (A.B) and the Bond ball mill work index given by the equation:

$$A.B = -3.5\ W_i + 117 \tag{3.47}$$

The determination of the T_{10} value and its use in determining the specific breakage energy is illustrated in the following Example 3.2.

Example 3.2

Sample size = 1000 kg, Particle size = −26.5 mm + 25.0mm (geometric mean = Y = 25.7 mm) . The sieve analysis after crushing is given by:

Size analysis of crushed sample

Size, passing mm	(X) Size, retained mm	Mass retained	% mass retained	Cum. mass % passing	1/N = X/Y
25.0	12.5	102.0	10.2	89.8	1.0
12.5	6.3	124.0	12.4	77.4	0.69
6.3	3.3	216.0	21.6	55.8	0.34
3.3	1.4	280.0	28.0	27.8	0.18
1.4	1.0	180.0	18.0	9.8	0.08
1.0	0	98.0	9.8	0	
		1000.0	100		

From a plot of geometric mean size against cumulative mass percent passing shown below, we find that the T_{10} equals 47 and A can be taken as 50 and the value of B as 2.2. Substituting these values into equation 3.46, the energy of crushing is calculated to be 1.28 kWh/t (4604 kJ/t).
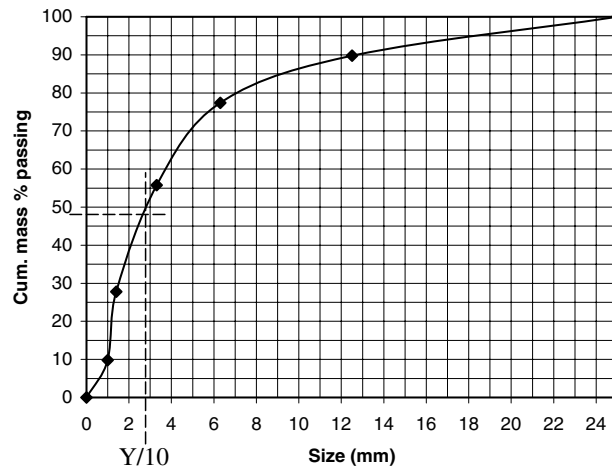
Product size distribution – plot of the size vs. cumulative % passing the lower screen size.
NOTE: the value of T_{10} in this case is high. Usually the value is less than 20.

3.4. Problems

3.1
Dry samples of quartz, galena and limestone ores were ground separately in a standard laboratory size ball mill 305 x 305 mm with a total ball load of 20.1 kg. After 100 revolutions

they were screened through a 150 micron sieve. The amount retained was returned to the mill together with equal amount of fresh ore. The process was repeated till the net mass of the samples were: Quartz = 169.4 grams, Galena = 481.2 grams, Limestone = 192.10 grams. The average feed size, F_{80}, (2000 micron) was the same for each mineral and the final product sizes were Quartz: 75 % passing 93.2 microns, Galena: 75 % passing 72.9 microns and Limestone: 75 % passing 84.4 microns.

Estimate and compare the Work Indices taking that of limestone as the standard.

3.2

The feed size (F_{80}) of a sample of limestone was 3200 μm. The Work Index of the sample was determined in two laboratories and was found to be 11.61 kWh/t (41.8 MJ/t) and 15.0 kWh/t (54 MJ/t) respectively. The product size (P_{80}) was found to be 140 and 219 microns respectively.

Estimate:
1. The size of screen used in each case if the grindabilities (g/rev) were the same in both cases,
2. The constant masses of the samples obtained in each case (g/rev) if the same test sieve size of 350 μm was used.

3.3

Bond's pendulum method was used to determine the crushing strength of a dry sample of gypsum 76 mm x 24 mm x 24 mm. The mass of each hammer was 13.6 kg each. They were released simultaneously from a position making 15^0 with the vertical. The relative density of gypsum is 2.32.

Estimate:
1. Crushing Strength of the gypsum sample,
2. Bond's crushing work index of gypsum,

3.4

A sample of granite passing a 7.5 cm square opening screen was suspended in a Bond's pendulum test. The length of the pendulum was 413 mm and the mass of hammers 13.6 kg each. The sample was completely crushed when the initial position of the pendulums made an angle of 30° with the vertical. The specific gravity of granite is 2.70.

Estimate:
1. The total energy required and energy consumed per cm to crush the sample,
2. The work index.

3.5

A standard Bond laboratory ball mill test was commissioned to estimate the grinding power requirements in the design of an alumina refinery. The size analysis of the R.O.M. ore after preliminary screening was:

Size, mm	-20 +10	-10 +5	-5+2.5	-2.5+1.0	-1.0+0.420	0.42+0.210	-0.210
% by mass	25	40	15	12	5	2	1

The required product size specification was 80% passing 75 μm. Tests were conducted under dry conditions but the commercial mill was expected to operate under dry conditions. The mass of screen undersize per revolution was found to be 1.25 g/rev.

Estimate:
1. The work index using a 106 μm sieve,
2. The work index of the commercial mill,
3. The power required by the commercial mill per tonne of dry bauxite.

3.6

A dry nickel ore was crushed and screened when 99 % of the ore passed 12.5 mm screen .A complete screen analysis showed that the liberation size was 75 μm. Bond's grindability standard rod mill test showed a constant 12.6 grams per revolution. The ore had to be ground in wet rod mills at the rate of 2400 t/day.

Estimate the work index if the :
1. Internal diameter of rod mill was 2 m,
2. Internal diameter of rod mill was 6 m,
3. If a wet rod mill of 2 m I.D. was used instead, what would be the difference, if any, in the power required?

3.7

Bond's work index of a manganese ore (SG. 3.7) was estimated at 12.31 kWh/t when an unknown screen size was used. The ore was charged and ground in a standard ball mill. The feed and product size (80% passing sizes) in the test was 300 microns and 90 microns respectively.
The grindability test was then repeated using a test screen size 20% of that used in the first test.

Estimate:

1. The change in grindability in the second test
2. The test screen sizes at which the work indices were determined in the two tests.

Data: Work index in the second test = 11.26 kWh/t
       Grindability in the second test = 3.03 g/rev.

3.8

To estimate the work index of a quartzite sample, two tests were performed. The first used Bond's pendulum method, the second Narayanan and Whiten's method. In both cases, the mean particle size of feed was 12.5 mm. Indicate the height to which the pendulum has to be raised in order to give the same work index.

Data: Feed size = 11.2 mm, Product size = 1200 μm, S.G. of ore = 2.65
       Coeff. of restitution, ε = 0.20

3.9

The average size analysis of an iron ore after preliminary crushing showed a P_{80} value of 1173 microns This was fed to a wet rod mill which produced a product 80 % of which passed 150 microns. This was then charged continuously to a ball mill, which was required to produce a product of –34 microns for the purpose of pelletising the ore.

The flowsheet considered was dry open circuit crushing and wet rod and closed circuit grinding ball mill grinding.

The internal diameters of both rod and ball mills were 2.5 m and a throughput of 100 t/h was initially expected. Estimate the total energy and power required for grinding by the rod and ball mills. The standard laboratory work index of the ore was 12.5 kWh/t.
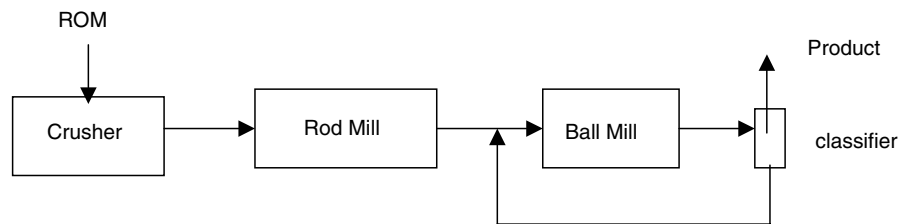
3.10

A representative sample of ore (-37.5+31.5 mm) was crushed in an impact test and the product screened. The screen analysis is given below:

Geom Mean particle size mm	Cum. mass % passing
25.7	99.2
17.6	84.6
8.9	55.1
4.6	28.0
1.1	16

Estimate:
1. The values of T_{10}, T_{25}, T_{50} and T_{75},
2. The specific comminution energy for the ore if A equals 35 and B is 2.

3.11

An ore sample weighing 1.2 kg and particle size –35.5 mm +31.5 mm was crushed in a laboratory impact crusher. The result was noted and is given below. The work index of the ore was 13.2 kWh/t and the limiting value of the impact breakage parameter A was equal to 50 and B is 1.85. Estimate the T_{10} value and determine the energy required in the comminution process.
[Hint: Assume Napier-Munn's Eq. (3.46) is applicable.]

Sieve Size, mm	Mean Particle size (GM), mm	Cum.mass % passing
-26.5+22.5	24.4	100
-22.5+11.2	15.8	87.0
-11.2+5.6	7.92	53.0
-5.6+2.8	3.96	29.0
-2.8+1.4	1.98	10.9
-1.4+0.710	1.00	10.4
-0.710 + 0.355	0.50	10.1
-0.355 + 0.180	0.25	10.0
-0.180 + 0.090	0.13	9.0

3.12

The masses of four different ores and their initial sizes are given in the table below. Also given are their breakage characteristics as obtained from an impact crusher. The work index of ores were 11.8, 13.2, 12.2 and 12.8 kWh/t. Assuming that the impact breakage parameters were the same and the limiting value of the breakage parameter, A , was equal to 50 and B equals 2. Determine:

1. the specific comminution energy in each case,
2. the energy required to crush the entire amounts of each ore sample.

Initial sample size of four ore types

Ore Type	Mass of sample, kg	Initial size of sample, mm
1	1000	-37.5+26.5
2	1250	-25.0+22.4
3	1500	-45.0+37.5
4	1300	-37.5+26.5

Product sizes after breakage of four ore types

Sieve Size, mm	Mean Particle size (GM), mm	Cum. mass % passing Ore 1	Cum. mass % passing Ore 2	Cum. mass % passing Ore 3	Cum. mass % passing Ore 4
-26.5+22.5	24.3	100.0	98.0	100.0	100.0
-22.5+11.2	15.8	88.0	87.0	87.0	80.0
-11.2+5.6	7.9	53.0	76.0	51.0	42.0
-5.6+2.8	4.0	28.0	53.0	22.0	20.0
-2.8+1.4	2.0	12.0	27.0	11.1	8.0
-1.4+0.710	1.0	5.8	13.0	8.0	3.0
-0.710 + 0.355	0.50	2.0	9.0	5.0	2.0
-0.355 + 0.180	0.25	1.0	5.0	2.0	1.0

3.13

In the Nayayanan/Whiten test, the T_{10} (%) values of the product and the corresponding specific comminution energies (E) were determined for an ore. The results are given in the following table.

T_{10} (%)	5	10	15	20	30	35	40
E, Wh/t	0.12	0.20	0.27	0.50	0.75	1.4	1.9

Determine:
1. The impact parameters A and B
2. The work index (W_i) of the ore
3. If the cost of crushing 1000 t of ore if power cost is $ 2.50/GJ

REFERENCES
[1] F. Kick, Dinglers Polytechnisches Journal, 247 (1883) 1.
[2] F. Kick, Dinglers Polytechnisches Journal, 250 (1883) 151.
[3] R.P. von Rittinger, Text Book of Mineral Dressing, Ernst and Korn, Berlin. 1867.
[4] F.C. Bond, Transactions AIME, 169 (1947) 58.
[5] F.C. Bond, Transactions AIME/SME, 193 (1952) 484.
[6] F.C. Bond, The Canadian Mining and Metallurgical Transactions, LVII (1954) 286.
[7] F.C. Bond, British Chem. Eng., 6 (1960) 378 & 543.
[9] R.J. Mitchell, Rock Products Mining and Processing, 67, (1964).
[9] Y. Oka and W. Majima, Canadian Metallurgical Quarterly, 9 (1970) 429.
[10] C.A. Rowland and D.M. Kjos, in Mineral Processing Plant Design, A.L.Mular and R.B.Bhappu, (eds), AIME New York, 1980, pp. 239-278.
[11] A.J. Lynch, Mineral Crushing and Grinding Circuits, Elsevier Scientific, Amsterdam-Oxford-New York, 1977.
[12] L.G. Austin, Powder Technology, 7 (1973) 315.
[13] F.C. Bond, AIChE Annual Meeting, 54, (1963).
[14] R.J. Charles, Transactions AIME, 208 (1957) 80.
[15] A.M. Gaudin, Transactions AIME, 73 (1926) 253.
[16] U.S. Gross, Bureau of Mines Bull, 402 (1938) 1.
[17] R.T Hukki, Transactions AIME/SME, 220, (1961) 402.
[18] I.B. Klymowsky and J. Liu, Comminution Practices, S. K. Kawatra (ed), SME, Littleton, 1997, pp. 99-105.
[19] D.C. Moore, Design and Installation of Comminution circuits, Fall Meeting, SME/AIME. 1982.
[20] S.S. Narayanan and W. Whiten, Transactions Inst. of Mining and Met, 97 (1988) C115.
[21] E.L. Piret, Chem. Eng. Prog., 49 (1953) 56.
[22] J.A. Hoffler and J. Herbst, The European Symposium on Comminution, Ljubljana, Yugoslavia, 1990, pp. 381-397.
[23] D. Brown, JKMRC Internal Reports, 1992.
[24] T.J. Napier-Munn, S. Morrell, R.D. Morrison and T. Kojovic, Mineral Comminution Circuits: Their Operation and Optimisation, JRMC/University of Queensland, 1999.
[25] C.A. Rowland, Proceedings of the tenth IMPC, M.J. Jones (ed),. Institute of Mining and Metallurgy, London, 1973, pp.47-61.

[26] L.G. Austin, R.R. Klimpel and P.T. Luckie, Process Engineering of Size Reduction: Ball Milling, SME-AIME, New York, 1984.

[27] N. Magdalinovic, International J. Mineral Processing, 27 (1989) 125.

[28] T.F. Berry and R.W. Bruce, Canadian Mining Journal, 87 (1966) 63.

[29] W.E. Horst and J.H. Bassarear, Trans. SME-AIME, 260 (1976) 348.

[30] P.C. Kapur, Trans. IMM, 79 (1970) C103.

[31] K.A. Lewis, M. Pearl and P. Tucker, Minerals Engineering, 3 No.1-2 (1990) 199.

[32] D. Yan and R. Eaton, Minerals Engineering, 7 No. 2/3 (1994) 185.

[33] G.K.N.S. Subasinghe and J.L. Kanau, Proceedings Seventh Mill Operators Conference, Kalgoorlie, Western Australia, AusIMM, 2000, pp.69-74.

[34] M.D. Everell, D.E. Gill and L.L. Sirois, Proceedings 6th Canadian Rock Mechanics Symposium, Montreal, 1970, pp.177-193.

[35] M.D. Everell, Trans. SME-AIME, 252 (1972) 300.

[36] N. Briggs, Final Year Thesis, WA School of Mines, Curtin University 1991.

[37] D. Yan, Private communication, 1993.

[38] R.A. Bearman, C.A. Briggs and T. Kojovic, Minerals Engineering, 10 No.3 (1997) 255.

[39] D.M. Chakrabarti, Trans. IMM, 109 (2000) C83.

[40] D.M. Weedon, T.J. Napier-Munn and C.L. Evans, Sulphide Deposits their Origin and Processing, I.M.M. (London), 1990, pp.135-154.

[41] V.C. Marshall, Comminution, Institute of Chemical Engineers, London, 1975.

Chapter 4. Jaw Crusher

4. INTRODUCTION

The first stage of size reduction of hard and large lumps of run-of-mine (ROM) ore is to crush and reduce their size. Softer ores, like placer deposits of tin, gold, mineral sands etc. do not require such treatment. Large scale crushing operations are generally performed by mechanically operated equipment like jaw crushers, gyratory crusher and roll crushers.

For very large ore pieces that are too big for receiving hoppers of mechanically driven crushers, percussion rock breakers or similar tools are used to break them down to size.

The mechanism of crushing is either by applying impact force, pressure or a combination of both. The jaw crusher is primarily an compression crusher while the others operate primarily by the application of impact..

4.1. Design of Jaw Crushers

Jaw crushers are designed to impart an impact on a rock particle placed between a fixed and a moving plate (jaw). The faces of the plates are made of hardened steel. Both plates could be flat or the fixed plate flat and the moving plate convex. The surfaces of both plates could be plain or corrugated. The moving plate applies the force of impact on the particles held against the stationary plate. Both plates are bolted on to a heavy block. The moving plate is pivoted at the top end (Blake crusher) or at the bottom end (Dodge–type crusher) and connected to an eccentric shaft. In universal crushers the plates are pivoted in the middle so that both the top and the bottom ends can move.

The Blake crushers are single or double toggle drives. The function of the toggle(s) is to move the pivoted jaw. The retrieving action of the jaw from its furthest end of travel is by springs for small crushers or by a pitman for larger crushers. As the reciprocating action removes the moving jaw away from the fixed jaw the broken rock particles slip down, but are again caught at the next movement of the swinging jaw and crushed. This process is repeated until the particle sizes are smaller than the smallest opening between the crusher plates at the bottom of the crusher (the closed set). For a smooth reciprocating action of the moving jaws, heavy flywheels are used in both types of crushers.

Fig. 4.1 shows a sketch of a Blake Crusher operated by double toggles and controlled by a pitman. These are commonly used as primary crushers in the mineral industry. The size of the feed opening is referred to as the *gape*. The opening at the discharge end of the jaws is referred to as the *set*.

Fig. 4.2 is a sketch of a Dodge type of crusher. They are comparatively lower in capacity than the Blake crushers and are more commonly used in laboratories.

The factors of importance in designing the size of primary crushers, like a jaw crushers, are:

Vertical height of crusher $\approx$ 2 x Gape (4.1)
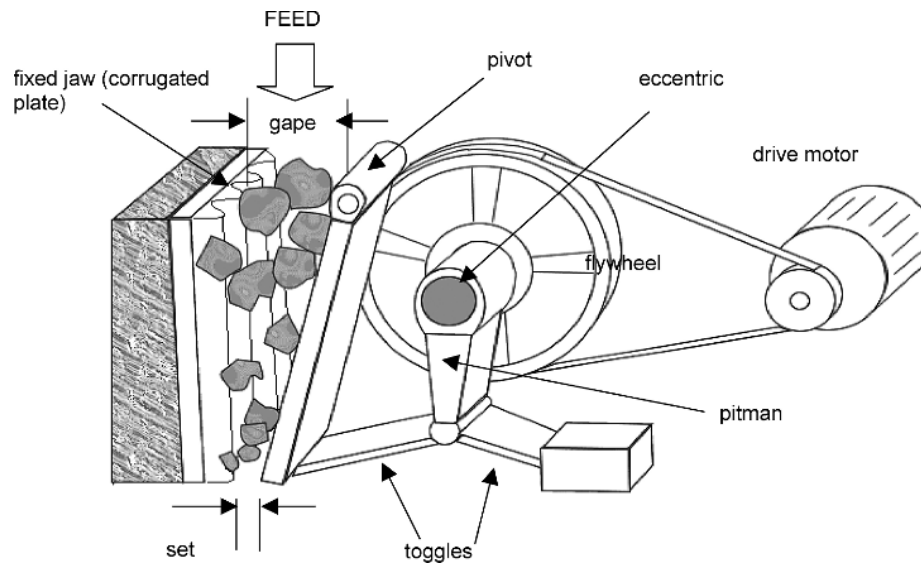
Fig. 4.1. Double-toggle jaw crusher

Width of jaw	> 1.3 x Gape	
	< 3.0 x Gape	(4.2)
Throw	= 0.0502 (Gape)$^{0.85}$	(4.3)

where the crusher gape is in meters.

These dimensions vary as individual manufacturers have their own specifications and their catalogues are a good guide to the geometry and design of individual makes.

4.1.1 Crusher Sizes and Power Ratings

The size of a jaw crusher is usually described by the gape and the width, expressed as gape x width. The common crusher types, sizes and their performance is summarised in Table 4.1. Currently, the dimension of the largest Blake-type jaw crusher in use is 1600 mm x 2514 mm with motor ratings of 250-300 kW. Crushers of this size are manufactured by Locomo, Nordberg (Metso) and others. The Metso crusher is the C 200 series having dimensions 1600 x 2000 mm. driven by 400 kW motors.

For sizing a crusher and ancillaries for open circuit operations, Eqs. (4.1) and (4.3) are helpful as a first approximation. From the equations it can be seen that once the gape has an assigned value the rest of the dimensions follow. To size the gape the largest particle to be charged is considered and the following relation applied:

Largest particle size = 0.9 x Gape   (4.4)
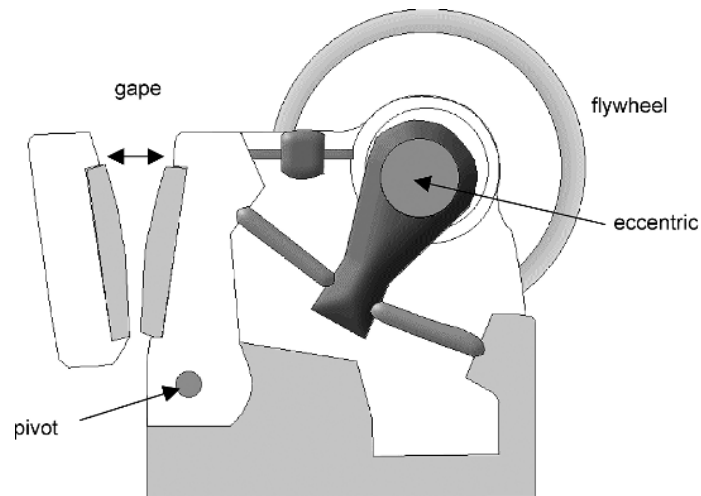
Fig. 4.2.   Dodge jaw crusher

Table 4.1
Jaw crusher performance [1].

Crusher Type	Size, mm				Reduction Ratio		Power, kw		Toggle Speed, rpm	
	Gape,mm		Width,mm		Range	Average	Min	Max	Min	Max
	Min	Max	Min	Max						
Blake, double toggle	125	1600	150	2100	4:1 / 9:1	7:1	2.25	225	100	300
single toggle	125	1600	150	2100	4:1 / 9:1	7:1	2.25	400	120	300
Dodge	100	280	150	28	4:1 / 9:1	7:1	2.25	11	250	300

The largest particle size is generally ascertained by the blast pattern in the pit or the size of shovels and dump-cars used to transport the ore from the mines. Thus, as a general rule, the size of the gape would be 1.1 times the largest size of the lump ores that is to be charged for crushing.

These relations are in turn helpful to size the opening of the scalping screens that are placed in the ore stream before the crusher. The purpose of scalping screens, also called grizzly screens, is to reject lumps of ore greater than the size of the gape. Placement of scalping screens result in smooth and uninterrupted operation of the circuit and also prevent any damage to the crusher by extra large lumps.

4.1.2 Jaw crusher circuits

Primary jaw crushers typically operate in open circuit under dry conditions. Depending on the size reduction required, the primary jaw crushers are followed by secondary and tertiary crushing. The last crusher in the line of operation operates in closed circuit. That is, the crushed product is screened and the oversize returned to the crusher for further size reduction while the undersize is accepted as the product. Flow sheets showing two such set-ups are shown in Figs. 3.1 and 3.2.

Jaw crushers are installed underground in mines as well as on the surface. When used underground, jaw crushers are commonly used in open circuit. This is followed by further size reduction in crushers located on the surface.

When the run of mine product is conveyed directly from the mine to the crusher, the feed to the primary crusher passes under a magnet to remove tramp steel collected during the mining operation. A grizzly screen is placed between the magnet and the receiving hopper of the crusher to scalp (remove) boulders larger than the size of the gape. Some mines deliver product direct to storage bins or stockpiles, which then feed the crushers mechanically by apron feeders, Ross feeders or similar devices to regulate the feed rate to the crusher. Alternately haulage trucks, front-end loaders, bottom discharge railroad cars or tipping wagons are used. In such cases, the feed rate to the crusher is intermittent which is a situation generally avoided. In such cases of intermittent feed, storage areas are installed and the feed rate regulated by bulldozers, front loaders or bin or stockpile hoppers and feeders. It is necessary that the feed to jaw crushers be carefully designed to balance with the throughput rate of the crusher. When the feed rate is regulated to keep the receiving hopper of the crusher full at all times so that the volume rate of rock entering any point in the crusher is greater than the rate of rock leaving, it is referred to as choke feeding. During choke feeding the crushing action takes place between the jaw plates and particles as well as by inter-particle compression. Choke feeding necessarily produces more fines and requires careful feed control. For mineral liberation, choked feeding is desirable.

When installed above ground, the object of the crushing circuit is to crush the ore to achieve the required size for down stream use. In some industries, for example, iron ore or coal, where a specific product size is required (iron ore –30+6 mm), careful choice of jaw settings and screen sizes are required to produce the minimum amount of fines (i.e. – 6 mm) and maximum the amount of lump ore within the specified size range. For hard mineral bearing rocks like gold or nickel ores where liberation of minerals from the host rock is the main objective, further stages of size reduction are required.

4.2. Jaw Crusher Operation

4.2.1 Operating Functions

The ore or rock is fed to the crusher where the jaws are furtherest apart, i.e. at the maximum opening or gape. When the jaws come together the ore is crushed into smaller sizes and slip down the cavity. In the return stroke, further reduction of size is experienced and the ore moves down further. The process is repeated till particles having size less than the bottom opening or set pass through as product.

The rule of thumb applicable for operating a jaw crusher with respect to its design characteristics can be summarised as follows:

Feed size $= 0.8 - 0.9 \times$ gape

Reduction ratio, R   =   1:4 to 1:7
Throw, L_T =   1–7 cm
Speed   =   100 to 359 rpm
Frequency of stroke, v =   100 –300 cycles per min
Length of stroke   = $0.0502 \times gape^{0.85}$

In practice, the operator has to decide on the spacing of the set at the discharge end. This setting has to include the maximum and the minimum positions that the bottom has to open during the oscillation of the bottom end of the jaws. The manufacturer of jaw crushers provides all the controls to adjust these settings. The actual distances are best measured by taking a soft metal, like lead or a ball of aluminium foil, and squeezing it between the jaws at the desired width forming a kind of template. This piece of lead metal is used to check the change of setting during operation.

During the operation of a crusher the bulk density of the material increases and the particle size decreases. With time, wear on the plate surfaces develops resulting in a change to the crusher surface profile. This could alter the throughput and size of the crusher product.

The operation of jaw crushers has been best described mathematically by Whiten [2]. According to Whiten, if a certain particle size, d, in the size distribution curve of a mineral (Fig. 4.3), is less than K_1 then it would pass through uncrushed, being smaller than the opening of the set. But all particle sizes greater than K_2 were smaller than the largest opening between the jaws of the jaw crusher and therefore will always be crushed. The probability P of a particle being crushed or not may be written as:

$P(d)$ = 0   for $d < K_1$
$P(d)$ = 1   for $d > K_2$

$$P(d) \;=\; 1 - \left[\frac{K_2 - d}{K_2 - K_1}\right]^2 \qquad\qquad K_1 < d < K_2 \qquad\qquad (4.5)$$

The values of K_1 and K_2 are primarily functions of the crusher set but also depend on throughput, feed size and liner length and are determined statistically by regression analysis of operating data. Such relationships were initially determined by Lynch [3] and later revised by Anderson [4] as:

$$K_1 \;=\; a_o + a_1\, L_{MIN} - a_2\, Q + a_3\, F_{80} + a_4\, L_{LINER}$$
$$K_2 \;=\; b_o \pm b_1\, L_{MIN} + b_2\, Q + b_3\, F_{80} - b_4\, t_{LINER} + b_5\, L_T \qquad\qquad (4.6)$$

where t_{LINER} is the age of the liner in hours and L_{LINER} is the liner length.

or

$$K_1 \;=\; 0.67\, L_{MIN} \pm 1.956 \text{ mm}$$
$$K_2 \;=\; 1.131\, L_{MIN} + 58.67\, q + 25.4\, T(t) \pm 1.8 \text{ mm} \qquad\qquad (4.7)$$

where q   =   the fraction > 25.4 mm in the feed and
       $T(t)$ =   an interpolating spline function of tonnage.

For a single feed, K_1 and K_2 can be obtained by size analysis. From a large number of data, the value of the exponent of Eq. (4.5) was found to be closer to 2.3 [5]. This mathematical concept of jaw crusher operation has been developed for modelling and subsequent throughput prediction from jaw crushers (see Chapter 10).
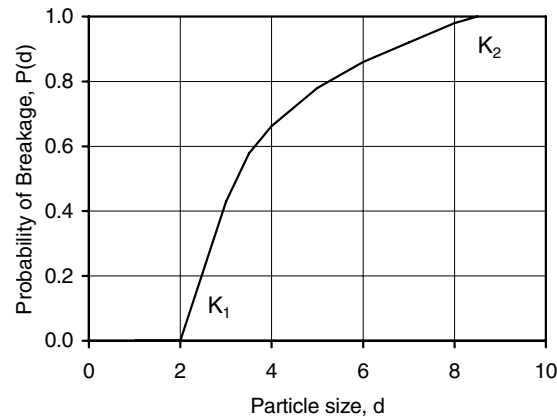
Fig. 4.3. Particle Size vs Probability of crushing particles in a Jaw Crusher (from Eq. (4.5))

4.3. Jaw Crusher Capacity

The capacity of jaw crushers is a measure of the mass or volume of crushed material produced in unit time of operation. The capacity is primarily a function of:

1. Crusher design characteristics like, width and depth of the crushing chamber,
2. Open and closed side settings,
3. Options on feeding method, e.g intermittent feeding, (manual or direct by haulage trucks) and continuous by conveyor belt,
4. Operating characteristics like the length of stroke, the number of strokes per minute, the nip angle.

Mathematically the capacity can be expressed by the general formula:

$$Q = f\ (w, L, L_{MAX}, L_{MIN}, L_T, n, \theta, K) \qquad (4.8)$$

where
Q	=	capacity
w	=	width,
L	=	height (or depth of jaws)
L_{MAX}	=	set maximum (Open Set)
L_{MIN}	=	set minimum (Closed Set)
L_T	=	length of Stroke or Throw
n	=	frequency (Revolutions rpm = cycles per unit time)
K	=	constant related to machine characteristics
θ	=	jaw angle

The mechanism of movement of rocks down the crusher chamber determines the capacity of jaw crushers. The movement can be visualised as a succession of wedges (jaw angles) that reduce the size of particles progressively by compression until the smaller particles pass through the crusher in a continuous procession. The capacity of a jaw crusher per unit time will therefore depend on the time taken for a particle to be crushed and dropped through each successive wedge until they are discharged through the bottom. The frequency of opening and closing of the jaws therefore exert a significant action on capacity.

Following the above concepts several workers, like Hersam [6]. Gaudin [7], Taggart [8], Rose and English [9], Lynch [3], Broman [10], have attempted to establish mathematical models determining the capacity.

Hersam's empirical expression given in Eq. (4.9) does not provide a true value of the capacity, especially of hard rocks.

$$Q = 59.8 \left[\frac{L_T \left(2L_{MIN} + L_T \right) w\ G\ v\ \rho_s\ K}{\left(G - L_{MIN} \right)} \right] \qquad (4.9)$$

where G   = gape, m
       ρ_s = solid density
       K   = ~0.75 for laboratory crushers

Although it is not truly applicable to hard rocks, for soft rocks it is reasonably acceptable [1]. This expression therefore is of limited use. The expressions derived by others are more appropriate and therefore are discussed and summarised here.

4.3.1. Rose and English

Rose and English [9] determined the capacity of a jaw crusher by considering the time taken and the distance travelled by the particles between the two plates after being subjected to repeat crushing forces between the jaws. Therefore dry particles wedged between level A and level B (Fig. 4.4.) would leave the crusher at the next reverse movement of the jaw. The maximum size of particle dropping out of the crusher (d_{MAX}) will be determined by the maximum distance set at the bottom between the two plates (L_{MAX}). The rate at which the crushed particles pass between the jaws would depend on the frequency of reversal of the moving jaw.

The distance, h, between A and B is equal to the distance the particle would fall during half a cycle of the crusher eccentric provided the cycle frequency allows sufficient time for the particle to do so. If v is the number of cycles/min, then the time for one complete cycle is [60/v] seconds and the time for half a cycle is [60/2v]. Thus h, the greatest distance through which the fragments would fall freely during this period, will be:

h = ½ g (30/v)² =   4414.50/v² , m   where g = 9.81 m/s²

Thus   v = 66.4/h$^{0.5}$ (4.10)

Then for a fragmented particle to fall a distance h in the crusher, the frequency must be less than that given by Eq. (4.10). The distance h can be expressed in terms of L_{MIN} and L_{MAX} provided the angle between the jaws, θ, is known. From Fig. 4.4 it can be seen that:
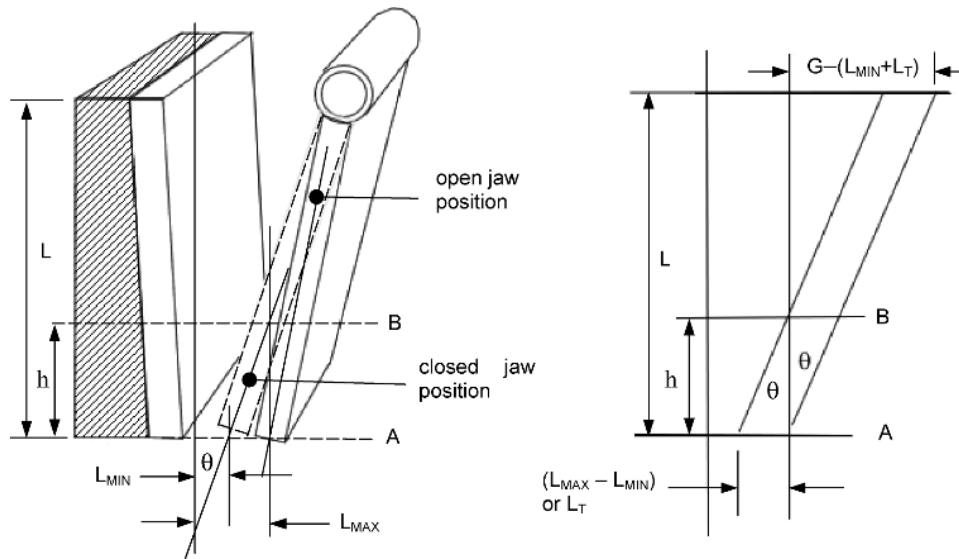
Fig. 4.4. Jaw crusher operating geometry. The motion of the jaw is approximately parallel [9].

$$\tan \theta = \frac{(L_{MAX} - L_{MIN})}{h}$$

(4.11)

$$\text{or} \quad h = \frac{(L_{MAX} - L_{MIN})}{\tan \theta}$$

It follows that h can be decreased by narrowing the difference between the maximum and minimum openings of the set and also by increasing the angle θ between the jaws.

Rose and English [9] observed that with increasing frequency of the toggle movement the production increased up to a certain value but decreased with a further increase in frequency. During comparatively slower jaw movements and frequency, Rose and English derived the capacity, Q_S, as:

$$Q_S = 60 L_T \, v \, W \left(2 L_{MIN} + L_T\right) \left(\frac{R}{R-1}\right)$$

(4.12)

where L_T = throw,
         v = frequency (cycle/min),
         W = width of jaw plates (m),
         L_{MIN} = closed set,
         R = machine reduction ratio (gape/set) and
         Q_S = capacity (slow frequency) in terms of volume of material product per hour.

Eq. (4.12) indicates that the capacity, Q_S, is directly proportional to frequency. At faster movement of the jaws where the particle cannot fall the complete distance, h, during the half cycle, Q_F was found to be inversely proportional to frequency and could be expressed by the relation:

$$Q_F = 132\,435 \; W \; (2L_{MIN} + L_T) \left(\frac{1}{v}\right) \tag{4.13}$$

where Q_F =   Capacity (fast frequency) in terms of volume of material product per hour.

The relationship between the frequency of operation and capacity of the jaw crusher can be seen in Fig. 4.5. This figure is plotted for values of $L_T = 0.228$ m, $W = 1.2$ m, $L_{MIN} = 0.10$ m, $R = 10$, $G = 1$ and the value of v varied between 50 and 300 rpm.

Fig. 4.5 indicates that under the conditions of operation, 93 cycles/min is about the critical frequency beyond which the productivity decreases. The critical crusher frequency, v_C, is given as:

$$v_C = 47 \; \frac{1}{(L_T)^{0.5}} \left(\frac{R-1}{R}\right)^{0.5} \tag{4.14}$$

At this critical frequency the maximum capacity is given by:
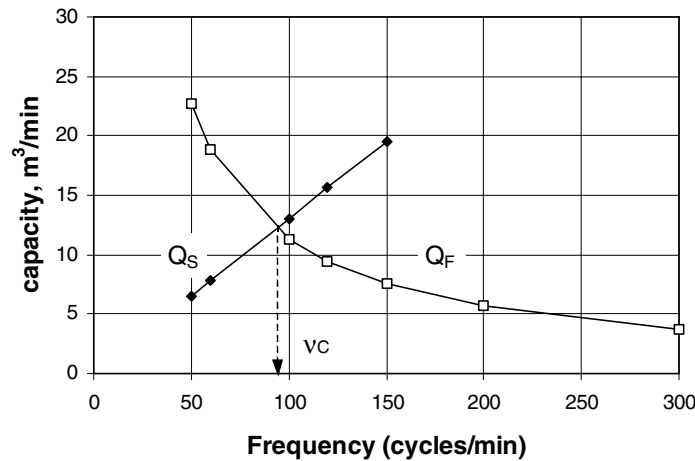
Fig. 4.5. Change of capacity with frequency of the Jaw plate according to Eqs. (4.12) and (4.13). $L_T = 0.228$ m, $W = 1.2$ m, $L_{MIN} = 0.10$ m, $R = 10$, $G = 1$m.

$$Q_M = 60\,W\,L_T\,(2L_{MIN} + L_T)\left(\frac{R}{R-1}\right)\,47\,\frac{1}{(L_T)^{0.5}}\left(\frac{R-1}{R}\right)^{0.5}$$

$$\text{(4.15)}$$

$$Q_M = 2820\,W\,L_T^{0.5}\,(2L_{MIN} + L_T)\left(\frac{R}{R-1}\right)^{0.5}$$

It should be noted that while considering the volume rates, no consideration was made to the change of bulk density of the material or the fractional voidage. However, during the crushing operation the bulk density of the ore changes as it passes down the crusher. The extent of the change depends on:

1. The size distribution of the feed,
2. The break down characteristics which could be different for hard, brittle and friable ores,
3. The packing characteristics,
4. The initial density of the ore,
5. Surface characteristics of the particles.

Rose and English defined the packing characteristics, P_K, as the ratio of the difference of the maximum (d_{MAX}) and minimum sizes (d_{MIN}) of the feed to the mean feed size, (d_{MEAN}):

$$P_K = \left(\frac{d_{MAX} - d_{MIN}}{d_{MEAN}}\right)$$

$$\text{(4.16)}$$

P_K is considered a size distribution function and is related to capacity by some function $f(P_K)$. As the particles decrease in size, while being repeatedly crushed between the jaws, the amount of material discharged for a given set increases. Rose and English related this to the set opening and the mean size of the particles that were discharged. Defining this relation as β it can be written as:

$$\beta = \frac{Set}{mean\ feed\ size}$$

$$\text{(4.17)}$$

The capacity is then dependant on some function which may be written as $f(\beta)$. Eqs. (4.16) and (4.17) must therefore be incorporated into the capacity equation. Expressing capacity as mass of crusher product produced per unit time, capacity can be written as:

$$\text{Capacity} = \text{(Vol. Output per unit time)}\ \rho_S\ f(P_K)\ f(\beta)\ S_C \qquad \text{(4.18)}$$

where S_C denotes a parameter related to the surface characteristics and ρ_S is the density of the ore. Combining Eq. (4.15) with Eq. (4.18), the maximum capacity, Q_M, of the crusher will be:

$$Q_M = 2820\,L_T^{0.5}\,W\,(2L_{MIN} + L_T)\left(\frac{R}{R-1}\right)^{0.5}\,\rho_S\ f(P_K)\ f(\beta)\ S_C\ ,\quad t/h \qquad \text{(4.19)}$$
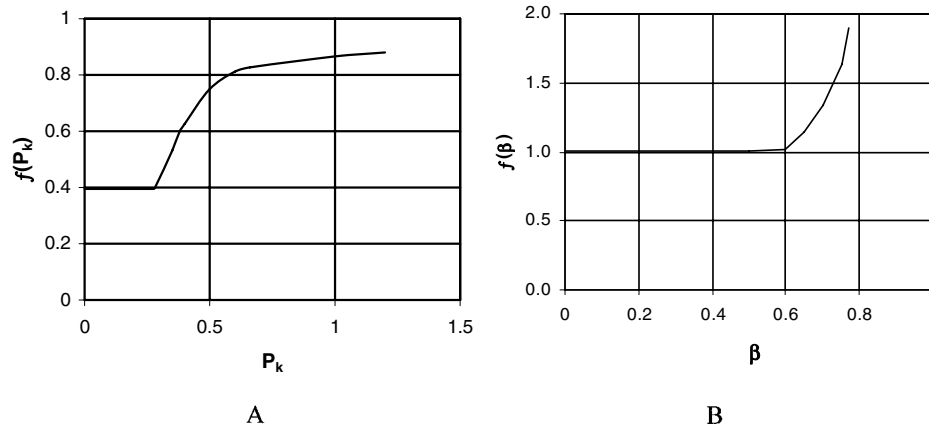
Fig. 4.6. Relation between P_K, $f(P_K)$, β and $f(\beta)$ [9].

The bulk density of the packing will depend on the particle size distribution. The relation between P_K and $f(P_K)$ and β and $f(\beta)$ is shown in Fig. 4.6. It is based on a maximum possible bulk density of 40%.

As the closed set size must be less than the feed size, $f(\beta)$ may be taken as equal to 1 for all practical purposes. The maximum capacity of production can be theoretically achieved at the critical speed of oscillation of the moving jaw. The method of determining the critical speed and maximum capacity is described in section 4.2.3

For actual crusher speeds, the actual crusher capacity is given by;

$$Q_A = Q_M \frac{v}{v_C} \qquad \text{for } v < v_C \quad \text{and}$$

$$Q_A = Q_M \frac{v_C}{v} \qquad \text{for } v > v_C \tag{4.20}$$

4.3.2. Taggart

The capacity of a jaw crusher is given by the amount of crushed material passing the discharge opening per unit time. This is dependent on the area of the discharge opening, the properties of the rock, moisture, crusher throw, speed, nip angle, method of feeding and the amount of size reduction.

In order to calculate the capacity of crushers, Taggart [8] considered the size reduction, R_{80}, as the reduction ratio of the 80% passing size of the feed, F_{80}, and product, P_{80}. This may be written as:

Reduction Ratio, $R_{80} = F_{80}/P_{80}$ (4.21)

The 80% passing size is chosen as data has shown that this is a convenient point where the distorting effect of coarse slabby material on the shape of the size distribution has been removed.

Hersam [6] showed that at a fixed set and throw, a decrease in feed size reduced the reduction ratio and increased the tonnage capacity. A fraction of the crusher feed is usually smaller than the minimum crusher opening at the discharge end (undersize) and therefore passes through the crusher without any size reduction. Thus as the feed size decreases, the amount actually crushed becomes significantly less than the total feed. The crusher feed rate can increase to maintain the same crushing rate. Taggart expressed the relationship between crusher capacity and reduction ratio in terms of a *reduction ton or tonne*, Q_R defined as:

$$Q_R = Q_T . R_{80} \tag{4.22}$$

where Q_T is the capacity in terms of actual tonnage crushed per hour. The quantity of feed actually crushed is determined by subtracting the feed undersize from the total quantity of feed.

The *reduction tonnage* term is dependant on the properties of the material crushed so that for a given reduction ratio, the crusher capacity will vary for different materials. Taggart attempted to compensate for this by introducing the *comparative reduction tonne*, Q_{RC}, which is related to the reduction tonne by the expression:

$$Q_R = K \ Q_{RC} \tag{4.23}$$

The comparative reduction tonne is a standard for comparison and applies for the crushing conditions of uniform full capacity feeding of dry thick bedded medium-hard limestone where $K = 1$. The factor K is determined for different conditions and is a function of the material crushability (k_C), moisture content (k_M) and crusher feeding conditions (k_F). K is expressed as:

$$K = k_C \ k_M \ k_F \tag{4.24}$$

To evaluate K, the relative crushability factor, k_C, of common rocks was considered and is given in Table 4.7. In the table, the crushability of limestone is considered standard and taken as equal to 1.

Table 4.7
Crushability factor of selected rocks (extract from [8])

Rock	Crushability Factor (k_C)	Rock	Crushability Factor (k_C)
Limestone	1.00	Gabbro	0.80
Dolomite	1.00	Quartz	0.80
Slate	0.90	Granite, fine grain	0.80
Granite, Coarse Grain	0.90	Diorite	0.80
Chert	0.80	Basalt	0.75

The moisture factor, k_M, has little effect on primary crushing capacities in jaw crushers and could be neglected. However when clay is present or the moisture content is high (up to 6%)

sticking of fine ores on the operating faces of the jaws is promoted and will reduce the production rate. The moisture effect is more marked during secondary crushing, where a higher proportion of fines are present in the feed.

The feed factor k_F applies to the manner in which the crusher is fed. For example, manually fed intermittently or continuously by a conveyor belt system. In the latter case the rate of feeding is more uniform. The following values for factor k_F are generally accepted:

- For continuous manual feeding, $k_F = 1$
- For continuous mechanical feeding, $k_F = 0.75 - 0.85$

Taggart used the comparative reduction ton (tonne) to estimate the size of the Blake type crusher required for a given duty and its productivity. The procedure is summarised below:

The reduction ratio of the operation is estimated from screen analysis of the feed and product. Where a screen analysis is not available, a rough estimate can be obtained if the relation between the cumulative mass percent passing (or retained) for different size fractions is assumed to be linear (Fig. 4.7).

Fig. 4.7 is a linear plot of the scalped and unscalped ores. The superimposed data points of a crusher product indicates the fair assumption of a linear representation. In the figure, a is the cumulative size distribution of the unscalped feed ore (assumed linear) and b is the cumulative size distribution of the scalped ore. x_S is the aperture of the scalping screen and d_1 and d_2 the corresponding sizes of the scalped and unscalped feed at "x" cumulative mass percentage. Taking x equal to 20% (as we are required to estimate 80% that is passing through) it can be seen by simple geometry that the ratio of the 80% passing size of the scalped feed to the 80% passing size of the unscalped feed is given by:

$$\frac{(d_2 - d_1)}{x_S} = \frac{20}{100} \quad \text{or} \quad (d_2 - d_1) = 0.2 \ x_S$$
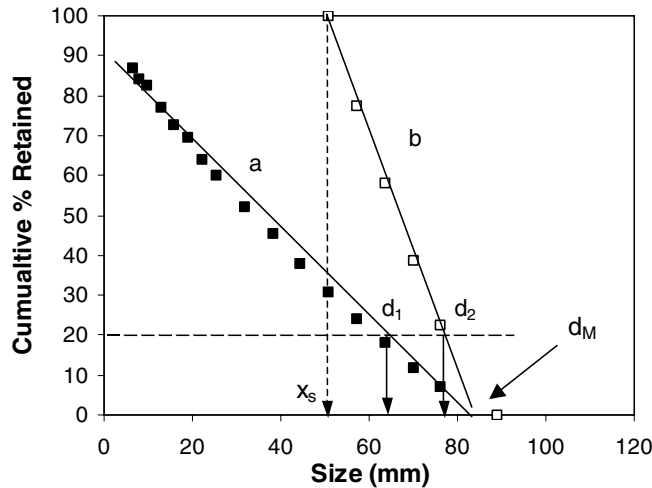
Fig. 4.7. Linear representation of scalped (b) and unscalped (a) crusher feed

i.e $d_2 = d_1 + 0.2\, x_S$ (4.25)

That is, the size of ore passing 80 percent of unscalped ore equals the size of the same cumulative percent of scalped ore plus 0.2 times the aperture of the scalping screen, x_S. That is:

F_{80} (scalped) $= F_{80}$ (unscalped feed) $+ 0.2\, x_S$ (4.26)

The 80% passing size of the feed may be approximated by:

F_{80} (feed) $= 0.8\, S_F$ top size (d_M)   (4.27)

where S_F = Shape factor
                 = the ratio of the intermediate to minimum particle dimension
                 (ranges from ~1.7 for cubic shapes to ~3.3 for slabby rock)

Thus F_{80} (un scalped) $= 0.8\, S_F\, d_M + 0.2\, x_S$ (4.28)

Eq. (4.28) can now be used to calculate R_{80}.

The method is illustrated by example 4.1.

Example 4.1

Run of Mine granite is passed through a grizzly (45.7 cm) prior to crushing. The ore is to be broken down in a jaw crusher to pass through a 11.5 cm screen. The undersize is scalped before feeding to the jaw crusher. Assuming the maximum feed rate is maintained at 30 t/h and the shapes of feed and product are the same and the crusher set is 10 cm, estimate the size of jaw crusher required and the production rate.

Solution

The first exercise is to determine Q_{RC} from equation; $Q_{RC} = Q_R/K$

Step 1
According to the data, the undersized would be = (11.5/45.7) x 100 = 24.2 %

Hence the actual amount to be crushed would be   (100 − 24.2) x 30 = 22.74 t/h = Q_T

Step 2
Determine K, from Eq. (4.24) where $K = k_C\, k_M\, k_F$

From Table 4.7, for granite k_C = 0.85. The moisture factor k_M, may be taken as equal to 1 for granite. The feed factor, k_F, for conveyor belt loading is about 0.75.

Thus the value for K = 0.85 x 1.0 x 0.75 = 0.64

Since adequate screen analysis data are not available we shall use Fig. 4.7.

In this case:

Say x = 20 %, then

$$\frac{(d_2 - d_1)}{x_S} = \frac{20}{100}$$

that is: F_{80} (scalped) $= F_{80}$ (unscalped) $+ 0.2\ x_S$

Again F_{80} (scalped) $= 0.8\ S_F\ d_M\ + 0.2\ x_S$

Substituting values, assuming cubic shaped particles where the shape factor = 1.7, we have:

$$F_{80} = [(0.8 \times 1.7 \times 45.7) + (0.2 \times 10)] = 64.15 \quad cm$$

and

$$P_{80} = 0.8 \times 1.7 \times 11.5 = 15.64 \quad cm$$

$$\therefore R_{80} = \frac{64.15}{15.64} = 4.10$$

Hence: $Q_{RC} = \dfrac{22.74 \times 4.10}{0.64} = 145.4\ tph$

Since the comparative reduction capacity of the jaw crusher is given, the crusher dimensions may now be determined.

For a jaw crusher the thickness of the largest particle should not normally exceed 80 to 85% of the gape. Assuming in this case the largest particle to be crushed is 85% of the gape, then the gape of the crusher should be = 45.7/0.85 = 53.6 cm and for a shape factor of 1.7, the width should be = 45.7 x 1.7 = 78 cm.

From the data given by Taggart (Fig. 4.8), a crusher of gape 53.6 cm would have a comparative reduction tonnage of 436 tph. The corresponding crushing capacity would be:

$$Q_T = \frac{436 \times 0.64}{4.10} = 68.1\ tph$$

and is thus capable of handling the desired capacity of 22.74 tph.

To choose the appropriate jaw crusher therefore, the nearest size commercially available crusher will be used to meet the performance required.
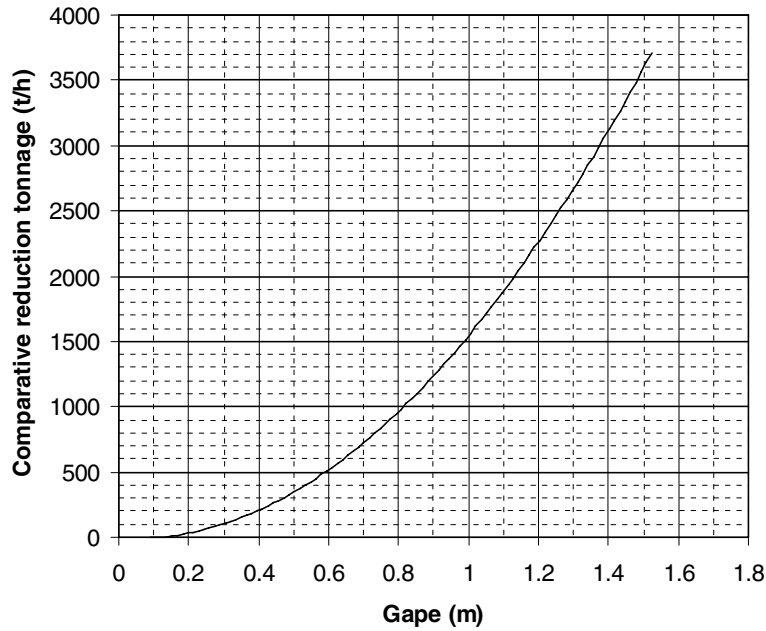
Fig. 4.8. Comparative Reduction Tonne of a Jaw crusher (adapted from [8])

4.3.3. Broman

To determine the capacity of jaw and gyratory crushers, Broman [10] divided the crusher chamber into different sections and determined the volume of each section in terms of the angle that the moving jaw subtended with the vertical. Broman suggested that the capacity per stroke crushed in each section would be a function of the top surface and the height of the section. Referring to Fig. 4.9, if α is the angle of nip between the crusher jaws and L_T and L_{MAX} are the throw and open side setting respectively then:

$$\tan\alpha = \frac{L_T}{h} \quad \text{or} \quad h = \frac{L_T}{\tan\alpha} \tag{4.29}$$

and the area, $\quad A = \left(L_{MAX} - \frac{L_T}{2}\right)\frac{L_T}{\tan\alpha} \tag{4.30}$

where A $\quad = \quad$ area between successive downward movement of the charge in each crushing cycle, such that area A_1 is equal to area A.

This area is defined by the conditions at the discharge end.

Broman neglected the $L_T/2$ term in Eq. (4.30) so that:

$$A = \frac{L_{MAX} L_T}{\tan \alpha} \qquad (4.31)$$

Extending the concept to the entire chamber, Broman deduced the capacity of the crusher, Q, as

$$Q = \frac{W L_{MAX} L_T k 60 v}{\tan \alpha} \qquad m^3/h \qquad (4.32)$$

where W = width of the crushing cavity, m
      v = Speed, rpm
      k = constant, dependent on the properties of the feed material and ranges from 1.5 to 2.5

In Eq. (4.32), v should be less than the critical value above which the capacity decreases. Broman gives this critical speed as a function of crusher throw and nip angle as:

$$v_C = \frac{66.6}{\sqrt{\dfrac{L_T}{\tan \alpha}}} \qquad (4.33)$$
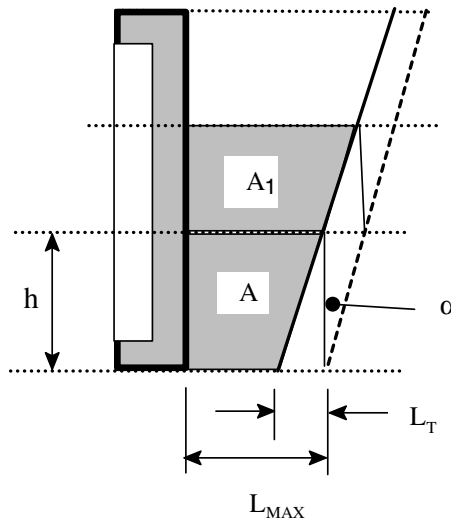
Fig. 4.9. Step by step downward flow of material through a jaw crusher [10].

4.3.4. Michaelson

Michaelson [8] expressed the jaw crusher capacity in terms of the gravity flow of a theoretical ribbon of rock through the open set of the crusher times a constant, k. For a rock of SG 2.65, Michaelson's equation is given as;

$$Q = \frac{7.037 \times 10^5 \, W \, k'(L_{MIN} + L_T)}{\nu} \quad t/h \tag{4.34}$$

for dimensions in meters and k' = 0.18 − 0.30 for straight jaws and 0.32 − 0.45 for curved plates with screened feeds.

Taggart [8] quotes a simple empirical relationship between the capacity and the maximum area of the discharge opening. This *Flow* formula is given as:

$$Q = 930 \, W \, L_{MAX} \quad t/h \tag{4.35}$$

All dimensions are in meters.

4.3.5. Comparison of Methods

For a set of crusher sizes and set openings, the calculations obtained from the work of Rose and English and others can be compared with data from equipment manufacturers. Fig. 4.10 shows a plot of the results. Assuming a value of S_C of 1.0, the calculations show an over-estimation of the capacity recommended by the manufacturers. As Rose and English points out, the calculation of throughput is very dependent on the value of S_C for the ore being crushed. The diagram also indicates that the calculations drop to within the installed plant data for values of S_C below 1.0. Most other calculation methods tend to estimate higher throughputs than the manufacturers recommend hence the crusher manufacturers should always be consulted.

It can be seen that Broman's method yields a higher capacity than the other methods and deviates considerably from the nominal operating capacity.

4.4. Critical Operating Speed

The theoretical analysis by Hersham [6] indicated that the volume rate of output per hour was directly proportional to the frequency of operation of the moving plate. Also at speeds in excess of a critical value the throughput decreases as shown in Fig. 4.5.

To estimate the critical speed of operation it is required to determine the time and distance travelled at the speed of operation of the toggle corresponding to the maximum production rate. Referring to Fig. 4.4 and assuming that particles will fall freely in the crushing chamber during the time the toggle recedes from the crushing position and commences its return to the crushing cycle, we can determine both the time and the distance taken to travel during the maximum frequency of operation.

To determine this distance assume the particles travelled freely due to gravity during the time taken for the toggle to make half a cycle between successive compactions. Let us assume it travels through a distance h and the crusher is set at L_{MIN} with gape G and angle θ between the jaws, then from Fig. 4.4:
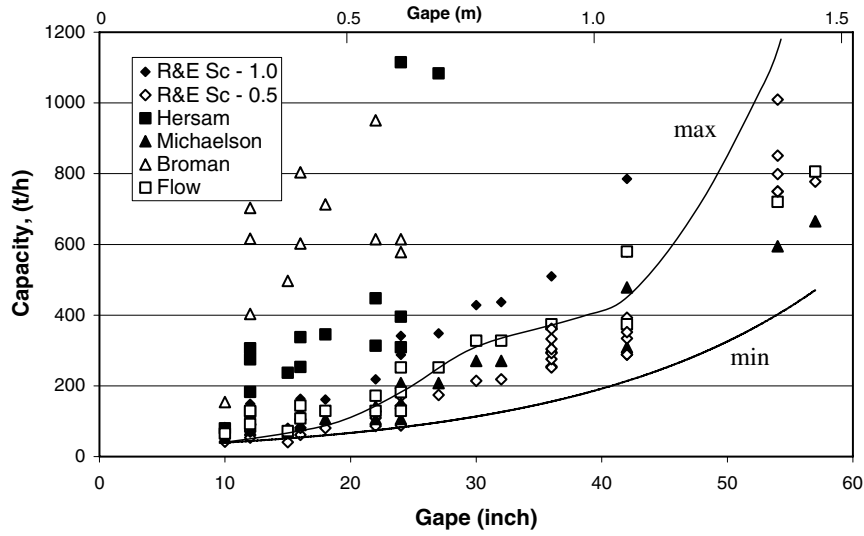
Fig. 4.10. Comparison of crusher throughput as calculated by the Rose and English, Hersam, Michaelson, Flow and Broman equations and manufacturers nominal throughput range (minimum and maximum). The values used in the calculation were 2.6 SG, $f(P_K) = 0.65$, $f(\beta) = 1.0$ and $S_C = 0.5 - 1.0$ (R&E); k = 0.4 (Hersam); k' = 0.3 (Michaelson); k = 1.5 (Broman) and ν = 275 rpm. The max and min lines represent the crushers nominal operating capacity range.

$$\tan \theta = \left[\frac{G - (L_{MIN} + L_T)}{L} \right] \tag{4.36}$$

also: $\quad \tan \theta = \dfrac{L_T}{h} \tag{4.37}$

Hence $\quad \dfrac{L_T}{h} = \left[\dfrac{G - (L_{MIN} + L_T)}{2\,G} \right] \tag{4.38}$

where $\quad L \approx 2\,G$ from Eq. (4.1)

or $\quad h = \left[\dfrac{2\,G}{G - (L_{MIN} + L_T)} \right] L_T \tag{4.39}$

From the laws of dynamics, the distance h travelled by the particles by gravity from a position of rest in time t is given by:

$$h = \frac{1}{2} g t^2 \tag{4.40}$$

Also the time t taken to travel distance h is equal to the time taken to travel half a cycle, and

$$t = 30 / v \tag{4.41}$$

Hence,

$$h = \frac{1}{2} g t^2 = \frac{1}{2} g \left(\frac{30}{v}\right)^2 = \frac{0.5 \times 9.81 \times 900}{v^2} = \frac{4414.5}{v^2} \tag{4.42}$$

Equating Eq. (4.39) and (4.42) and replacing v by the critical frequency v_C we have:

$$\frac{4414.5}{v_C^2} = \left[\frac{2G}{G - (L_{MIN} + L_T)}\right] L_T \tag{4.43}$$

Replacing G as equal to R . L_{MIN} and simplifying Eq. (4.43):

$$v_C^2 = 4414.5 \left[\frac{R L_{MIN} - L_{MIN} - L_T}{2 R L_{MIN}}\right] \frac{1}{L_T} \tag{4.44}$$

According to Eq. (4.2), $L_T = 0.0502\, G^{0.85}$. Substituting this value of L_T into Eq. (4.44) and neglecting the square term:

$$v_C = 47\, L_T^{-0.5} \left(\frac{R-1}{R}\right)^{0.5} \tag{4.45}$$

Eq. (4.45) shows:

1. At a constant reduction ratio, an increase in throw decreases the critical speed,
2. With an increase in reduction ratio, the crusher could be run at higher speeds

Fig. 4.11 illustrates the effect of increasing the throw between 0.01 m and 0.06 m on the critical speed. The graph covers the range of throw normally used in practice. Fig. 4.12 illustrates that at higher reduction ratios, changes in critical speed may not be very significant during the operation of a crusher.

The critical speed calculated by use of Eq. (4.45) has been found to yield slightly lower values when the gape is too small or too large. Rose and English [9] and Kelly and Spottiswood [1], state that the manufacturers recommend that the crushers should be operated at optimum speeds given by the relation:
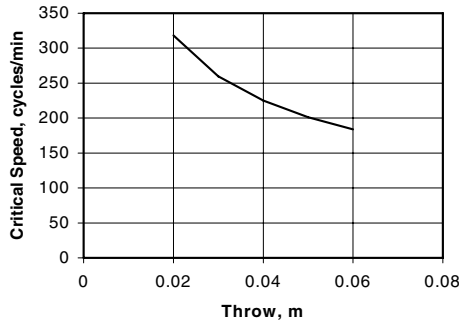
Fig. 4.11. Relation between throw and critical speed (R = 12)
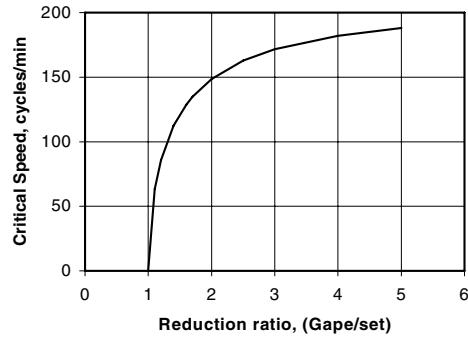
Fig. 4.12. Relation between reduction ratio and critical speed (L_T = 0.05m)

$$v_{OPT} = 280 \exp(- 0.212 \, G^3) \quad \pm 20\% \tag{4.46}$$

4.5. Power Consumption

A number of workers [3], [4], [9], have tried to develop theoretical expressions to estimate the power consumption of a jaw crusher. In most cases these derived values are at best, approximations. The methods most commonly used and found to yield satisfactory results are described.

4.5.1. Rose and English

The expression for computing the power consumption (P) derived theoretically by Rose and English [9] involved the knowledge of Bond's Work index (W_i). To evaluate the work index they considered the maximum size in the feed and also the maximum size of particles in the discharge from the crusher. To determine the size through which 80 % of the feed passed, they considered a large database relating the maximum particle size and the undersize. From the relation it was concluded that F_{80} was approximately equal to 0.7 times the largest size of particle. Taking the largest size of the particle that should be charged to a jaw crusher as 0.9 times the gape, F_{80} was written as:

$$F_{80} = 0.9 \times G \times 0.7 \times 10^6 = 6.3 \times 10^5 \, G \quad \text{microns} \tag{4.47}$$

where the gape, G is in meters.

Also, to establish the P_{80} from the largest product size, Rose and English considered that the largest particle size discharged from the bottom of the crusher would occur at the maximum open set position and hence:

$$P_{80} = 0.7 \, (L_{MIN} + L_T) \, 10^6 = 7.0 \times 10^5 \, (L_{MIN} + L_T) \quad \text{microns} \tag{4.48}$$

where both L_{MIN} and L_T are in meters.

Having estimated F_{80} and P_{80}, the power required was expressed in terms of the Bond work index as:

$$\text{Power} = W_i \, Q \, 10 \left[\frac{1}{\sqrt{P_{80}}} - \frac{1}{\sqrt{F_{80}}} \right] \quad \text{kW} \tag{4.49}$$

where Q = the capacity in t/h,
$\quad\quad$ W_i = is the work index in kWh/t and
$\quad\quad$ P_{80} and F_{80} are in microns.

Eqs. (4.47) and (4.48) can be used to replace P_{80} and F_{80} in Eq. (4.49) to give the power drawn in terms of the crusher dimensions of gape, closed set and throw:

$$\text{Power} = W_i \, Q \, 10 \left[\frac{1}{\sqrt{700,000 \, (L_{MIN} + L_T)}} - \frac{1}{\sqrt{630,000 \, G}} \right] \tag{4.50}$$

Simplifying Eq. (4.50), the power required for a jaw crusher would be:

$$P = 0.01195 \, W_i \, Q \left[\frac{\sqrt{G} - 1.054 \sqrt{(L_{MIN} + L_T)}}{\sqrt{G} \, \sqrt{(L_{MIN} + L_T)}} \right] \quad \text{kWh/t} \tag{4.51}$$

For operating a jaw crusher it is necessary to know the maximum power required consistent with the reduction ratio and the gape and closed side settings. The maximum power drawn in a system will occur at the critical speed. Thus for maximum power, Q in Eq. (4.51) is replaced with Q_M from Eq. (4.19) to give:

$$P_{MAX} = 67.4 \, w \, W_i \, L_T^{0.5} \, (L_{MIN} + \frac{L_T}{2}) \left(\frac{R}{R-1} \right)^{0.5} \rho_S \left[\frac{\sqrt{G} - 1.054 \sqrt{(L_{MIN} + L_T)}}{\sqrt{G} \, \sqrt{(L_{MIN} - L_T)}} \right] f(P_K) \, f(\beta) \, S_C \tag{4.52}$$

Example 4.2

The largest size of ore pieces mined measured 560 mm (average) and the smallest sizes averaged 160 mm. The density of the ore was 2.8 t/m³. The ore had to be crushed in a C-63 type jaw crusher 630 x 440. At a reduction ratio of 4, 18 % of the ore was below the maximum size required. Determine:

1. The maximum operating capacity of the crusher
2. The optimum speed at which it should be operated.

Solution

Step 1.
Assume that the largest size of ore = 0.9 x gape
That is 0.560 = 0.9 x Gape,
Hence Gape = 0.560 / 0.9 = 0.62 m.

Length of Throw, $L_T = 0.0502 \times G^{0.85} = 0.0502 (0.62)^{0.85} = 0.0502 \times 0.666 = 0.033$ m

Width: (assume) = 1.3 x Gape = 1.3 x 0.62 = 0.81.

Set: by definition Gape/Set = Reduction Ratio, and assuming the set = L_{MIN}
        Hence $L_{MIN} = 0.62/4 = 0.16$ m

Step 2.
Determine $f(P_K)$ and $f(\beta)$: from Eqs. (4.16) and (4.17).

From Eq. (4.16): $P_K = \dfrac{0.56 - 0.16}{0.36} = 1.11$

and from Fig. 4.6A therefore $f(P_K) = 0.84$

Also from Eq. (4.17): $\beta = 0.16/0.36 = 0.44$ and from Fig. 4.6 B, $f(\beta) = 1.0$

Step 3.
Neglecting S_C and substituting values in Eq. (4.19).

Max Capacity, $Q = 2820 \times (0.033)^{0.5} \times 0.81 \times (2 \times 0.16 + 0.033) \times \left(\dfrac{4}{3}\right)^{0.5} \times 2.8 \times 0.84 \times 1.0$

            $= 398$ t/h

Step 4.
Optimum Speed:

$v_{OPT} = 280 \times \exp(-0.212\, G^3) = 280 \times \exp(-0.212 \times 0.62^3) = 266$ rpm

---

4.5.2. Lynch

Lynch [3] considered a certain fraction K_2 that was crushed and fragmented in the crusher while a fraction K_1 remained unbroken and passed through the crusher without drawing extra power. Therefore power is required to crush only a limited size fraction of the feed. Lynch defined a size parameter C, given by:

$$C = 25.4 \sum_{i=1}^{n} \frac{t_i}{(S_i + S_{i+1})} \qquad (4.53)$$

where t_i = is the ith element of a size distribution given by $F(x)$ and

S_i and S_{i+1} = the lower limit and upper limits of the ith fraction respectively.

Lynch correlated this size parameter with the current draw I, for crushers at the Mt Isa mine (Australia) operating in closed circuit, by the relation:

$$I = 14.2 + 0.0822\ C + 0.00305\ C^2 \pm 1.8\ amp \qquad (4.54)$$

This expression has been applied with success. Application of this expression in practice is illustrated by Example 4.3.

Example 4.3

The size distribution of an ore to be crushed in a closed circuit jaw crusher was logged as the following table:

Interval	Size	Mass % retained, feed, f(d)	Mass % retained, product, p(d)
1	-229 +50 mm	69.0	0
2	-50 + 38 mm	3.0	2.0
3	-38 + 32 mm	6.0	12.0
4	-32 + 25.4 mm	3.5	13.0
5	-25.4 6.4 mm	12.2	50.0
6	-6.4 + 0 mm	6.3	23.0

If the crusher set is 25.4 mm, estimate the power required to crush the ore.

Solution

Step 1.

For a single set of feed and product size distributions, the values of K_1 and K_2 can be estimated by taking K_1 equal to the closed set of the crusher (25 mm) and K_2 as the top size of the crusher product (50 mm). Then by Eq. (4.5), the mass of material actually crushed is given by:

For interval 2:

$$P(d) = 1 - \left[\frac{50 - 38}{50 - 25} \right]^{2.3} = 0.815\ \text{and}$$

$$t_2 = f(d) \cdot P(d) = 3.0 \times 0.815 = 2.45$$

Similarly, for the other intervals:

Interval	P(d)	t_i	S_{i+1}	S_i	$S_i + S_{i+1}$	t_i / S_{i+1}
1	1	69.0	229	50.0	279.0	0.248
2	0.82	2.45	50.0	38.0	88.0	0.028
3	0.53	3.18	38.0	32.0	70.0	0.045
4	0.04	0.13	32.0	25.4	57.4	0.002
5	0	0	25.4	6.4	31.8	0
6	0	0	6.4	0	6.4	0
					Σ	0.32

Step 2.
From Eq. (4.53): $C = 25.4 \times 0.32 = 8.21$

Hence by substituting in Eq. (4.54) the current, I, will be:

$I = 14.2 + 0.0822 \times 8.21 + 0.00305 \times (8.21)^2$
$= 15.1 \pm 1.8$ Amp

Step 3:
Assuming the voltage = 415 V, Power consumption $= 15.1 \times 415 = 6.3$ kW

4.5.3. Andersen and Napier Munn

The models for determining the power required for operating jaw crushers have mostly been derived using Bond's work index. While these gave satisfactory estimations of power it must be remembered that Bond's expression was derived using a tumbling mill where the forces of comminution are not quite the same as that in jaw crushers. Andersen et al [4] therefore attempted to correlate the energy of crushing as determined by a standard laboratory Pendulum test (see Sec 3.2.3) with that required by a jaw crusher.

Morrell, Napier-Munn, and Andersen [11] recognised that the total energy required by a jaw crusher was a function of the energy required to operate a crusher under load and no load conditions. Again, the power required on load would be different for different particle sizes in the feed. That is, the power will be dependant on the particle size distribution of the feed. Thus if j represented the number of intervals in the distribution of particles of size i, then the mass flow rate of particle size i could be taken as M_i t/h. If P_i represents the probability of breakage of particles of size i and the energy of crushing of size i is Ecs at T_{10} percent, then the calculated pendulum power (P_C) for size i breakage would be:

$$P_C = \sum_{i=1}^{j} Ecs_{T(10)} \, P_i \, M_i \quad \text{in kW} \tag{4.55}$$

If the observed power actually drawn by the crusher under load was P_a then:

$$P_a = S_f \, P_C + P_N \tag{4.56}$$

where P_N is the crusher power drawn under no load, taken as the idling power and S_f the scaling factor for a particular crusher. Substituting the value of P_C from Eq. (4.55) in Eq. (4.56), the actual power of crushing can be determined as:

$$P_a = S_f \sum_{i=1}^{j} Ecs_{T(10)} \ P_i \ M_i + P_N \qquad (4.57)$$

Eq. (4.57) is easily evaluated knowing the value of P_N. To obtain P_a, the $Ecs_{T\ (10)}$ values have to be determined for all the j particle size ranges in the sieve analysis of the feed. S_f is determined by linear regression of sets of crusher data using the following expression:

$$S_f = \left[\frac{(P_a - P_N)}{P_C} \right] \qquad (4.58)$$

The concept of this method has been tested for cone and gyratory crushers and found to be satisfactory with values of S_f ranging from $1.2 - 1.55$. Its application is discussed in Chapter 5 and in Chapter 11 where the prediction of power requirements is considered.

4.6. Problems

4.1
Air-dried limestone was crushed continuously in a laboratory single-toggle Blake jaw crusher designed to provide a throw of 228 mm. The lower opening close set was 102 mm and the maximum bottom opening was 330 mm. The gape was 813 mm and the width of hopper 1067 mm. 90 % of the ore commenced crushing 200 mm from the bottom of the crusher. The Bond Index was estimated as 15 kWh / t. Assuming that the density of the limestone was 2.6 t/ m³ , determine:

1. the optimum RPM of the toggle
2. the maximum annual capacity of crusher with 99% availability
3. Power consumption at the optimum speed

4.2
A single toggle Blake jaw crusher with 22.8 cm x 47.7 cm receiving hopper crushed gold ore at the rate of 85 t/h with closed setting at 2.54 cm and maximum opening of 3.8 cm. The work index of the ore was 13.5 kWh/t.
    Assuming the SG of the ore was 5.4, calculate;

1. Optimum frequency of the toggle cycle
2. Maximum frequency of the toggle cycle
3. The power required.

4.3
The feed to a jaw crusher was –60 mm + 40 mm and the product analysed:

Screen Size, mm	Product, % retained	Screen size, mm	Product '% retained
-8	10.0	+0.35	10.1
+4	21.8	+0.25	5.5
+2	16.3	+0.125	6.2
+0.75	20.1	-0.125	10.0

The compressive strength of the mineral was 20 MN/m². The crusher was next used to crush a second mineral of compressive strength 55 MN/m² at 5 kg/s. The feed size of the second mineral was –55 + 40 mm and yielded a product whose average size was 0.4 mm. Estimate the change in power required during the second operation.

HINT: Rittinger's Law may be written in the form:

$$E = K_R \, f_C \left(\frac{1}{P_{80} - F_{80}} \right) \text{ kWh/t}$$

where   E   = crushing energy,
        K_R = Rittinger's constant
        F_C = crushing strength of the material

4.4
A Blake jaw crusher had the following dimensions: Gape=160 cm, open set = 24.4 cm, close set = 5.0 cm. The width of the hopper was 1.5 times the gape. The ore contained 20% material minus 4.0 cm. The bulk density of the rock was 1.75 t/m³ and the nip angle 22.8⁰.
Determine:

1.   Capacity of crusher
2.   Power consumption if the work index of the material is 12.5 kWh/t
3.   Operating speed
4.   Minimum level at which the feed should be maintained in the feed-hopper.

4.5
A cement manufacturer needed to produce lime at the rate of 140,000 t/year in a rotary kiln operating 360 days in the year. Limestone for the purpose contained 30% CaO. The S.G. of limestone was 2.7. The mined material had a top size of 40 x 100 cm after screening through a grizzly. The kiln accepted top size of 10 cm. A single toggle Blake jaw crusher was available for crushing. Assume the shape factor of the feed and the product was the same.
Determine:

1.   The rate of the toggle movement that would meet the target production.
2.   If the toggle rate was reduced by 25 % indicate the production rate of lime.

4.6

A jaw crusher was used to crush a chert ore. The top size of the ore was 25 cm and the moisture content less than 3 %. It was required to produce a product 100% of which would be less than 4 cm. The shape factor of feed and product was 1.7. Assume that the cumulative weight-size curve was a straight line, determine:

1. Crusher size
2. Rate of crushing, (Q_T)

4.7

A jaw crusher had a gape of 685 mm. It was charged continuously by a conveyor belt to keep a charge level constant at 46 cm from the bottom of the jaws. A reduction ratio of 7.5 was desired. If the maximum opening between the jaws at the discharge end was fixed at 20 cm for a material of density 2.8, compute:

1. The angle between the crusher faces (assume flat)
2. Operating speed and critical speed of operation
3. The rate of crushing when the angle between plates are increased by 2 degrees

4.8

The angle between the straight faces of a Blake jaw crusher was progressively altered from 22^0 to 28^0 in steps of 2^0. 1200 kg of a material of bulk density 1460 kg/m^3 was crushed each time. Indicate:

1. The adjustments to the set that would be necessary each time to maintain same production rate
2. The mathematical relation between the angle of nip and the set.

4.9

Iron ore was crushed in a jaw crusher. The average sizes of the feed (F_{80}) and product (P_{80}) were 50 mm and 10 mm respectively. The energy consumed during crushing was found to be 5 kWh/t. The top size of the material was then altered to an average size (F_{80}) of 75 mm when the product size (P_{80}) of 5 mm was required. Estimate the energy to crush in the altered condition.

HINT:
In the simplified form Kick's equation for energy required to break a particle may be used in this case:

i.e. $E = K \ln (F/P)$

4.10

A single toggle jaw crusher crushed limestone having an average size of 75 mm. The size analysis of the product was:

Size, mm	Mass % retained	Size, mm	Mass % retained
12.5	0.20	1.5	15.0
7.5	8.0	0.75	5.2
5.0	51.0	0.40	2.1
2.5	13.0	0.20	5.5

The power required to crush the limestone was 8 kW. Estimate the power required (Kick's Law) to crush the same limestone having a mean size of 2 mm. Assume all material charged had to be crushed.

4.11

The closed set of an operating jaw crusher was 125 mm. A continuous stream of ore was fed at the rate of 30 t/h. On an average 10% of the ore was less than the set. The F_{80} was 410 mm in size. The crusher was initially operated at 200 rpm at a reduction ratio of 1:4 but the toggle speed was to be increased. Calculate:

1. The maximum speed, v_C, at which it can be operated,
2. The maximum capacity at the maximum operating speed of the toggle.

Data: S.G. of the ore = 2.9

REFERENCES
[1]   E.G. Kelly and D.J. Spottiswood, Introduction to Mineral Processing, Mineral Engineering Services, 1989.
[2]   W.J. Whiten, Journal S. A. Inst. Min. Metall., 72 (1972) 257.
[3]   A.J. Lynch, Mineral Crushing and Grinding Circuits, Elsevier Sc. Publishing, 1977.
[4]   J.S. Andersen and T.J. Napier-Munn, 3rd Mill Operators Conference, Cobar, Australia, (1988).
[5]   T.J. Napier-Munn, S. Morrell, R. Morrison and T. Kojovic, Mineral Comminution Circuits Their Operation and Optimisation, JKMRC, 1996.
[6]   E.A. Hersam, Trans.AIME, 68 (1923) 463.
[7]   A.M. Gaudin, Principles of Mineral Dressing, McGraw-Hill, New-York, 1939.
[8]   A.J. Taggart, Handbook of Mineral Dressing, John Wiley, 1945.
[9]   H.E. Rose and J.E. English, Trans. IMM., 76 (1967) C32.
[10] J. Broman, Engineering and Mining Journal, June (1984) 69.
[11] S. Morrell, T.J. Napier-Munn and J. Andersen, in Communition Theory and Practice, S.K. Kawatra (ed), AIME, 1992.

Chapter 5. Gyratory and Cone Crusher

5.   INTRODUCTION

Gyratory crushers were invented by Charles Brown in 1877 and developed by Gates around 1881 and was referred to as a Gates Crusher [1]. The smaller form is described as a cone crusher. The larger crushers are normally known as primary crushers as they are designed to receive run-on-mine (ROM) rocks directly from the mines. The gyratory crushers crush to reduce the size by a maximum of about one-tenth its size. Usually metallurgical operations require greater size reduction, hence the products from the primary crushers are conveyed to secondary or cone crushers where further reduction in size takes place. Here the maximum reduction ratio is about 8:1. In some cases installation of a tertiary crusher is required where the maximum reduction is about 10:1. The secondary crushers are also designed on the principle of gyratory crushing but the construction details vary.

Similar to jaw crushers, the mechanism of size reduction in gyratory crushers is primarily by the compressive action of two pieces of steel against the rock. As the distance between the two plates decrease continuous size reduction take place. Gyratory crushers tolerate a variety of shapes of feed particles, including slabby rock, which are not readily accepted in jaw crushers because of the shape of the feed opening.

5.1. Design of Gyratory Crushers

5.1.1   Primary crusher

Primary crushers are solidly built to receive large lumps of rock directly from the mines and designed for large tonnage throughputs. Basically gyratory crushers consists of a fixed solid conical shell or bowl (also called concaves) and a solid cone within the bowl called a breaking head (Fig. 5.1). The breaking head is fixed to a central spindle, which is hydraulically suspended or mechanically held from a spider. The bottom end of the spindle usually rests on a hydraulically supported piston. The bottom end of the spindle is connected to a bevel and pinion arrangement with straight or spiral teeth which on rotating by a journal moves the bottom of the shaft eccentrically. In some models, the spindle is fixed at the top and bottom and is made to move side-ways to impart the crushing action. The entire assembly can be visualised as a circular jaw crusher.

Fig.5.1 is a typical sketch of a large gyratory crusher used as a primary crusher to reduce the size of large pieces of rocks produced during blasting in mines. Variations in the design of the breaking head and the mantle have been adopted by different manufacturers. Such variations are adopted from studies on stress distributions of component parts endured during the crushing operation. Effort is also made to improve the efficiency of the mechanical movements of the eccentric shaft. Such details are best described in manufacturer's literature.

The rule of thumb for describing the dimensions of primary gyratory crushers may be summarised as:

1. For sizes < 66 cm, the circumference along the opening = 8 – 10 x gape (measured along the outer perimeter),
2. For sizes > 66 cm, the circumference along the opening = 6.5 – 7.5 x gape (measured along the outer perimeter)
3. The ratio of mantle diameter to grape = 1.3 – 1.7:10
4. The feed size = 0.9 x gape (up to 2 m in diameter)
5. The reduction ratio ranges from 3:1 to 10:1.

The angle of nip for large crushers varies between 21° and 24° (average about 22°) but for curved surfaces it is about 27° to 30° [2]. The distance of openings between the concave and the breaking head at the top and the bottom ends are usually used to describe the size of the gyratory crusher. The other modes frequently adopted are:

1. Bowl diameter at the discharge end x gape
2. Bowl diameter at the feed end x gape
3. Bowl circumference at the feed end x gape
4. Maximum diameter at the head x gape

The designs of the breaking faces differ with different manufacturers.. In so doing the crusher products have different size distributions. The movement of the mantle or conical head that performs the crushing action can be visualised in Fig. 5.2 where it can be seen that as the feed drops down, the mantle squeezes it against the concave and fractures the rock.
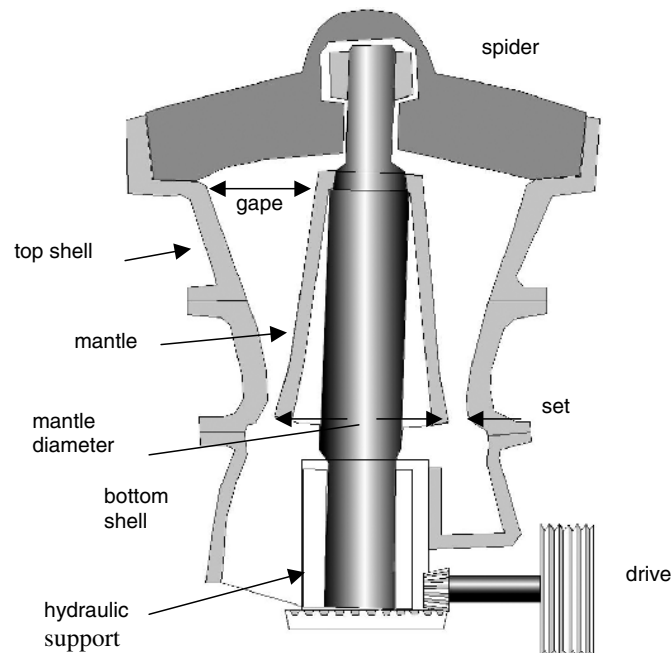
Fig. 5.1. Sketch of a Gyratory Crusher (Crusher size is designated by the gape and mantle diameter).
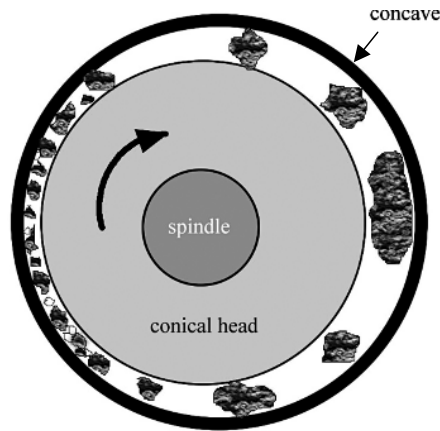
Fig. 5.2. Section of Gyratory Crusher.

When the mantle moves away during its cycle of gyration, the crushed rock slips down to be caught again between the mantle and the concave on the next cycle, resulting in further size reduction. The process is repeated until the sizes of the broken rock are less than the open set at the bottom of the crusher.

The sizes of commercially available gyratory crushers vary considerably. The sizes are usually designated as gape x diameter of mantle (breaking head) or referred to by gape only. For a particular requirement it is advisable to consult manufacturer's literature. As a rough guide Tables 5.1-5.2 summarises the designs and other general characteristics of gyratory crushers manufactured by different manufacturers and distinguished by the lengths of their shafts. The fixed spindle gyratory crusher characteristics are included in Table 5.3.

Table 5.1 Design Characteristics of Long Shaft primary Gyratory Crushers [3].

Characteristics	Small	Large
Size	63.5 - 711 mm	1829 - 2294 mm
Useful height*	0.48 m	10.5 m
Set range	25.4 - 44.5 mm	228 - 305 mm
Rev./minute	700	175
Power, kW	2.2	298

* Denotes distance travelled by particles down the crusher

Table 5.2 Design Characteristics of Short Shaft primary Gyratory Crushers [3].

Characteristics	Small	Large
Size	762 - 1524 mm	2133 - 2794 mm
Set range	50.8 -152 mm	178 -305 mm
Rev./minute	425	275
Motor rating	149	750

Table 5.3 Design Characteristics of Fixed Spindle Gyratory Crushers [3].

Characteristics	Small	Large
Size of receiver opening	203.2 - 813 mm	635 - 5538 mm
Set range	31.7 mm	-
Rev./minutes	750	480
Motor rating , kW	16.8	83.9

According to Weiss [4] long shaft crushers are presently not in use but are being replaced by Short Shaft models.

5.1.2. Secondary and Tertiary cone crushers

Cone crushers were originally designed and developed by Symons around 1920 and therefore are often described as Symons cone crushers. As the mechanism of crushing in these crushers are similar to gyratory crushers their designs are similar, but in this case the spindle is supported at the bottom of the gyrating cone instead of being suspended as in larger gyratory crushers. Fig. 5.3 is a schematic diagram of a cone crusher. The breaking head gyrates inside an inverted truncated cone. These crushers are designed so that the head to depth ratio is larger than the standard gyratory crusher and the cone angles are much flatter and the slope of the mantle and the concaves are parallel to each other. The flatter cone angles helps to retain the particles longer between the crushing surfaces and therefore produce much finer particles. To prevent damage to the crushing surfaces, the concave or shell of the crushers are held in place by strong springs or hydraulics which yield to permit uncrushable tramp material to pass through.

The secondary crushers are designated as *Standard* cone crushers having stepped liners and tertiary *Short Head* cone crushers, which have smoother crushing faces and steeper cone angles of the breaking head. The approximate distance of the annular space at the discharge end designates the size of the cone crushers. A brief summary of the design characteristics is given in Table 5.4 for crusher operation in open circuit and closed circuit situations.
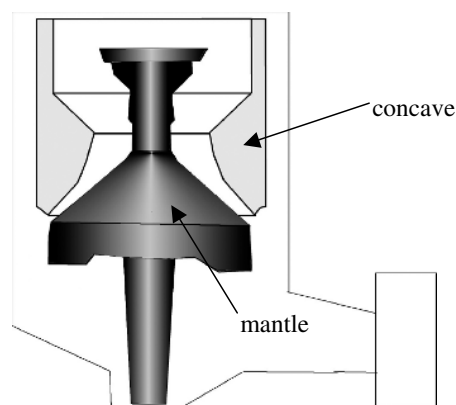
Fig. 5.3. Sketch of a secondary cone crusher.

Table 5.4 Design characteristics of Standard Symons cone crushers [4].

Design Characteristics	Open Circuit		Closed Circuit	
	Maximum	Minimum	Maximum	Minimum
Size, mm	3050	600	3050	600
Crusher chamber size range, mm *	76-432	25-76	76-178	25-51
Discharge setting (closed side)	22-38.1	6.4-15.8	6.4-19	3.2
Power kW	300-500	25-30	300-500	25-30

* Chamber sizes vary between 3-6 numbers within a particular designated crusher size
  to produce fine, medium or coarse sized product.

The Standard cone crushers are for normal use. The Short Head cone crushers are designed for tertiary or quaternary crushing where finer product is required. These crushers are invariably operated in closed circuit. The final product sizes are fine, medium or coarse depending on the closed set spacing, the configuration of the crushing chamber and classifier performance, which is always installed in parallel.

For finer product sizes, i.e. less than 6 mm, special cone crushers known as Gyradisc crushers are available. The operation is similar to the standard cone crushers except that the size reduction is caused more by attrition than by impact, [5]. The reduction ratio is around 8:1 and as the product size is relatively small the feed size is limited to less than 50 mm with a nip angle between 25° and 30°. The Gyradisc crushers have head diameters from around 900-2100 mm. These crushers are always operated in choke feed conditions. The feed size is less than 50mm and therefore the product size is usually less than 6-9 mm.

5.2. Gyratory Crusher Circuit Design

In practice, large primary gyratory crushers are seldom installed underground. They are invariably installed at the surface. The charge is preferably fed directly off trucks, tip-wagons, side dump rail cars, and conveyor belts on to a receiving hopper, which feed the crusher through a chute. Usually a grizzly is placed prior to the feed entering the crusher to remove extra large pieces, which tend to jam the operation. Gyratory Crushers are invariable operated in open circuit.

When a choice has to be made to include a gyratory or a jaw crusher in a circuit, a general rule of thumb is to examine the desired production rate. Where the production rate required is in excess of 900 t/h, gyratory crushers are always the preferred option.

The primary gyratory crushers operate in open circuit while the last stages, either the secondary or tertiary crushers are invariably configured to operate in closed circuits in series with the primary crusher.

The need for the secondary crusher is dictated by the size of the product required. The product size from a primary crusher is limited by the possible reduction ratio, which normally is around 10:1. The feed size to a primary crusher from the mines could be 1 to 1.5 m thus the maximum product size possible is 10 to 15 cm which is normally too large for down stream processing for mineral liberation. Hence secondary and possibly tertiary crusher stages form part of the crushing circuit design.

The final product size from the circuit depends on the close set of the secondary crusher and on the screen apertures. The same logic is used where the final product size requires the installation of tertiary crushers.

To develop a crushing circuit it is useful to remember that the ranges of reduction ratios of crushers are:

- Primary crusher   3:1 to 10: 1
- Secondary crusher   6:1 to 8:1
- Tertiary crusher $\cong$ 10:1

Thus if a project requires a final product size of say 3 mm, then maximum feed size to tertiary crusher should be 30 mm. As this would be the discharge size from the secondary crusher, the maximum feed size of the secondary crusher should be about 240 mm. Similarly the feed size to the primary crusher should not exceed (about) 2400 mm. Once the feed sizes for different stages of crushing are determined the sizes of the crushers can be estimated using the rule of thumb that the gape of crusher is usually 1.1 times the feed size. This rule of thumb for sizing the gape of primary jaw crushers is applicable to crushers up to 2 meters in diameter. Once the gape is determined, the size of the primary crusher can be ascertained from relations given in Table 1. Such considerations are very rough indicators on the possible sizes of crushers that would meet the desired criteria in a crushing circuit. Considerable experience is required to make the final choice of equipment. Mathematical modelling of an operation can make prediction of product sizes easier. This aspect is dealt with in Chapter 11.

5.3. Gyratory Crusher Operation

Most crushing operations are performed in dry conditions. Water is only used occasionally as a lubricant to wash or flush the fines and sticking material on crusher surfaces. Gyratory crushers can accept 8-10% moisture in operation, but the fine content should be preferably less than 10%. The crushing action in gyratory crushers is regarded as rings or "helics" (spirals) of feed down through the crusher of which a single section may be regarded as similar to the jaw crusher. Therefore computations leading to the performance of gyratory crushers may be considered very similar to jaw crushers. Thus, as in jaw crushers, the performance of gyratory crushers will be affected by:

1. Fines content (fine should preferably be less than10%)
2. Inherent and total moisture content in the ore/rock
3. Feed distribution in the crushing area and the bulk density of the feed.
4. Hardness of ore (Work Index).
5. Recirculating load in the case of closed circuit crushing.

The operation of crushers depends on the gyrating speed and the open and closed set positions. For a uniform size of the product it is necessary to charge uniformly and distribute the feed evenly around the spindle keeping a constant level of feed in the crushing chamber. Idling should normally be avoided as the idling load power consumption is about 0.3 times the full load power consumption.

The operation of gyratory crushers is subject to the gape size, diameter of the mantle, the open set, throw and speed of gyration. It also depends on the ore characteristics including the work index of the ore. Manufacturers generally supply the operational characteristics of individual types of gyratory crushers in the form of characteristic curves. Limestone is the usual mineral used for comparative purposes. The performance of selected sizes of gyratory crushers (Table 5.5) operating with ores of various work indices indicate a wide range of performance with different operational settings. For details manufacturer's literature should be consulted.

134

Table 5.5
Gyratory crusher operation [3].

Size Gape x Dia. of mantle, mm	L_{MAX} (Open Set) mm	L_T (Throw) mm	Gyration /min	Capacity (Production) t/h	Work Index of Ore kWh/t
1219 x 1879	200	34	135	2200	-
1371 x 1879	137-223	44	135	3100	-
1828 x 2311	194	44	111	2750	13
1524 x 2268	200-275	37	113	3200	6
1524 x 2268	238-275	37	92	3180	12
1219 x 2057	175-188	37	93	1330	10
1524 x 2591	225	34	134	2290	-

5.3.1. Gyrating Speed of Head
One of the important factors in the operation of a gyratory crusher is to determine the speed of gyration to attain a specific product size at a specific rate. In general, the speed of crushing is inversely proportional to the size of the feed. If the feed size is increased, the speed of gyration has to be decreased. There is some evidence [6, 7] that the speed of rotation required to produce particles less than size d should not be less than that given by the following expression [8]:

$$v \geq \frac{665(\sin\theta - \mu\cos\theta)}{\sqrt{d}} \quad \text{cycles per min} \qquad (5.1)$$

where θ = inclination of the cone to the horizontal
μ = coefficient of friction of the material
d = size of crusher product, cm.

For example, if $\theta = 75°$, d = 10.2 cm and $\mu = 0.2$, then the gyrating speed, v, is given by:

$$v \geq \frac{[66.5\,(0.966 - 0.2 \times 0.259)]}{\sqrt{0.102}} = 190 \text{ cycles per min.}$$

Eq. (5.1) gives a rough guide to the gyration speed of a gyratory crusher of known geometry. However, manufacturers should be consulted regarding details of crusher operation and recommendations based on data on individual models.

5.4. Capacity

5.4.1. Gyratory crushers
The mechanism of crushing is considered similar to that of a jaw crusher. The difference is that instead of wedges, the elements of material in the process of being crushed can be regarded as rings or spirals of which a single section may be regarded as similar to that of a jaw crusher which is inclined at an angle θ to the horizontal. The operation of a gyratory

crusher involves only one-half of its surfaces while in jaw crushers the entire crushing surface is involved.

Using this concept early workers [6,7,9] derived expressions for estimating the capacities of gyratory crushers. Hersam's approach [9] has been described in chapter 4, but its use does not often tally with actual performance. The variation is probably due to the uncertainty in the value of K. Gauldie [6,7] theoretically derived an expression for capacity by considering the angle of inclination of the breaking head and the distance travelled by ore particles during a single cycle of breakage. Gauldie's expression for optimum capacity is:

$$Q = 0.35 \ \pi \sin \theta \ (L_{MAX} + L_{MIN}) \ g \ H \ (\sin \theta - \mu \cos \theta)^{0.5} \tag{5.2}$$

where L_{MAX} = Maximum distance between gyrating head and concave
L_{MIN} = Minimum distance between gyrating head and concave
θ = Inclination of cone to the horizontal
g = Acceleration due to gravity
H = Vertical height of the chamber

Gauldie's expression is difficult to apply in practice as the angle of inclination is difficult to measure. An easier method to estimate capacity is to apply the method advocated by Rose and English for jaw crushers.

5.4.2. Broman

Broman [10] developed an expression for the capacity of gyratory crushers based on the same logic used for jaw crushers. For deriving the expression, Broman considered a cross-section of a surface of material in a crusher and determined the time taken and distance travelled during one cycle of the head. The optimum volumetric capacity of a gyratory crusher is given by the expression:

$$Q_V = \frac{(D_M - L_{MIN}) \pi L_{MIN} L_T \ 60 \ N \ K}{\tan \alpha} \qquad m^3/h \tag{5.3}$$

where Q_V = volumetric capacity of the gyratory crusher, m^3/h
D_M = mantle head outer diameter at the discharge point, m
L_{MIN} = closed set, m
L_T = length of throw, (Stroke length), m
N = number of gyrations per minute,
K = material constant having a value between 2 – 3,
α = angle of nip.

Broman suggests that the frequency should not exceed a critical value as it would result in a decrease in production and has shown that capacities calculated using Eq. (5.3) agree with practice.

5.4.3. Rose and English

The theoretical work of Rose and English [11] to determine the capacity of jaw crushers is also applicable to gyratory crushers. According to Rose and English, Eq. (5.4) can be used to determine the capacity, Q of gyratory crushers:

$$Q = \frac{W_i \, D \, \rho_s \sqrt{L_{MAX} - L_{MIN}} \; (L_{MAX} + L_{MIN}) \, K}{2 \sqrt{\dfrac{R}{R-1}}} \quad \text{tph} \tag{5.4}$$

where W_i = Bond's work index
 D = Diameter of bowl at a given cross-section,
 L_{MAX} = Maximum distance between bowl and lower edge of mantle,
 L_{MIN} = Minimum distance between bowl and lower edge (closed set)
 R = Reduction ratio
 K = Statistical factor

For soft materials, like coal and coke, $K = 0.5$
For harder materials, like quartz and granite, $K = 1$

Capacities of gyratory crushers of different sizes and operation variables are published by various manufacturers. The suppliers have their own specifications which should be consulted. As a typical example gyratory crusher capacities of some crushers are shown in Tables 5.5 and 5.6.

Table 5.6
Gyratory crusher capacity for a feed of bulk density 1600 kg/m^3 at maximum throw [12].

Model	Feed opening (G), mm	L_{MAX} mm	Capacity t/h
42-65	1065	140-175	1635-2320
50-65	1270	150-175	2245-2760
54-75	1370	150-200	2555-3385
62-75	1575	150-200	2575-3720
60-89	1525	165-230	4100-5550
60-110	1525	175-250	5575-7605

5.4.4 Cone Crushers

The methods applicable for estimating the capacities of primary gyratory crushers are also applicable to cone crushers. To select a cone crusher of a definite size, the maximum product size from the primary crusher is first checked. The gape of the secondary crusher should be 1.1 times larger than the largest particle in the feed and the feed should have 80% less than 70% of the feed opening of the crusher. Reference to manufacturer's data on performance of cone crusher sizes is useful. Table 5.7 indicates the performance of cone crushers operating in open circuit. The product is defined as fine, medium and coarse which will depend on the crusher set.

5.5. Power Consumption

To compute the power consumption of gyratory crushers, knowledge of the ore work index and crusher capacity is necessary. In its simplest form, the power consumption is given by:

$$P = W_i \ Q \left[\frac{\sqrt{F_{80}} - \sqrt{P_{80}}}{\sqrt{F_{80}}} \right] \sqrt{\frac{100}{P_{80}}}$$

(5.5)

where
P	=	Power, kW
W_i	=	Work Index, kWh/t
Q	=	Capacity, t/h
F_{80}	=	Size through which 80% of the mineral feed passes
P_{80}	=	Size through which 80% of the product passes

Table 5.7
Typical Capacities of Standard and Short Head Cone Crushers in Open Circuit [12].

Crusher	Type	Feed opening (open), mm	L_{MIN}, mm	Capacity, t/h
HP800	Fine	267	25	495-730
Standard	Medium	297	32	545-800
	Coarse	353	32	545-800
HP800	Fine	33	5	-
Short Head	Medium	92	10	260-335
	Coarse	155	13	325-425
MP1000	Fine	300	25	915-1210
Standard	Medium	390	32	-
2392 mm	Coarse	414	38	1375-1750

This expression has been used by Rose and English [11] to calculate the power required for jaw crushers. The expression is claimed to be applicable for gyratory crushers as well. Eq. (5.5) indicates that once the comminution parameters, F_{80} and P_{80}, are established, the power consumption is directly proportional to the capacity. Thus substituting the value of Q from Eq. (5.4) into Eq. (5.5), the power can be calculated.

Motz [5] suggested that when the work index is not known, a rough guide could be obtained from the expression:

$$\text{Work Index} = \frac{0.0485 \ (\text{Average Impact Strength})}{\rho_s}$$

(5.6)

where the average impact strength is in J/m.

Motz [5] expressed the power requirements of gyratory crushers by the expression:

$$P = \frac{10 \ W_i \ \left(\sqrt{F_{80}} - \sqrt{P_{80}} \right)}{\sqrt{F_{80} \ P_{80}}} \ \text{kW}$$

(5.7)

When a range of particle sizes are charged for crushing, as is usual from run of mine ores, the power required has to be considered for only those particles that are larger than the closed set. The particles smaller than the closed set will gravitate down the crusher chamber and discharged without crushing for which no extra power is required. In actual practice it has been found that for primary crushers, the following rule of thumb applies;

$$\text{Total kW} = \text{Crushing capacity} \times \text{kWh/t} \times K \tag{5.8}$$

For primary crushers, K= 0.75 and for secondary crushers, K = 1

The calculated power described often differs from that observed by manufacturer's ratings hence a material balance method advocated by Whiten [13,14] and subsequently developed and applied by Andersen and Napier-Munn [15,16] is now accepted. This method is described in Chapter 11.

5.6. Problems

5.1
A primary gyratory crusher was required to crush iron ore at the rate of 3000 t/h. The largest size of the Run-of-Mine ore was 1000 mm. The required product size was less than 162 mm. Manufacturer's data indicated that the nearest size of gyratory crusher would be 1370 mm x 1880 mm with a cone angle of 18°. The work index of the ore was 14 kWh/t, the S.G. 4.5 and the coefficient of friction, 0.43.

Calculate:

1. The closed set required to produce the desired product
2. The frequency of gyration.

5.2
A conveyor belt fed a Run-of-Mine iron ore to a gyratory crusher, which had a gape of 356 cm. The maximum opening at the discharge end was 15.0 cm and the close set 4.5 cm. 80 % of the feed and product was less than 15.0 cm and 2.4 cm respectively. The size distribution of feed and product was as follows:

Feed		Product	
Size, cm	Wt,% retained	Size, cm	Wt. % retained
+360	1.0	+4.5	20.2
+180	32.0	+2.4	35.4
+90	38.2	+1.2	13.8
+45	12.3	+0.6	11.8
+25	6.5	+0.3	8.4
-25	10.0	-0.3	10.4
	Σ100.0		Σ100.0

The gyration was 15° to the horizontal. Estimate:

1. The optimum throughput of the crusher,
2. Power required for material having a Bond Work Index of 13.4 kWh/t,
3. Minimum frequency of gyration.

5.3

Limestone having a mean particle size of 50 mm is crushed in a cone crusher the product size analysed.

Size, mm	Mass % retained	Size, mm	Mass % retained
12.0	0.3	1.50	10.0
8.0	8.0	0.75	12.0
6.0	42.0	0.40	5.0
3.0	18.0	-0.4	4.7
			$\sum 100.0$

The power consumed for the operation was 8.0 W/kg. The feed size was then altered to an average size of 20 mm. A product of 0.5 mm (mean size) was required. Estimate the power consumption after the change in feed size.

5.4

A gyratory crusher was installed in a gold mine where it was expected to crush the ore at a rate of 660 t/h. The crusher was arranged to gyrate at 140 cycles/min at an angle of 30° to the horizon. Estimate:

1. Radius of the cone,
2. Change in throughput when the crusher was switched to dolomite (S.G. = 2.8),
3. The change required in the set to maintain the same throughput as the gold ore.

5.5

A cone crusher of height 2.1 m, open side feed opening 30.4 cm and a closed set at 5.1 cm gyrated at 480 rpm to crush quarry limestone scalped at 20.3 cm opening screen. The crusher was expected to crush at the rate of 1000 t/h. Calculate:

1. The level at which the charge has to be maintained
2. Angle of the crusher head

5.6

A gyratory crusher size 33-55 was designed to accept feed of size 68 cm x 178 cm. The open side setting of the discharge opening was 10.2 cm. The rate of gyration was 175 per minute. Calculate:

1. The capacity of crusher for an eccentric throw of 1.6 cm,
2. What would the eccentric throw be if the crusher capacity had to be increased to 600 t/h at the same setting,
3. If the open side setting of the discharge opening was altered to a setting of 12.7 cm what will be the per cent increase in production.

5.7

A gyratory crusher, 122 cm x 304.6 cm, required 300 HP to operate at a gyration of 135 cycles/min. When the eccentric throw was 2.5 cm and open side setting 12.7 cm, it produced 1023 t/h of crushed ore. The open side setting was gradually increased in steps of 1.3 cm to 20.3 cm and tested for productivity during comminution of magnetite ore (S.G. of 5.3). All other variables being the same, establish a relation between productivity and the set at the discharge opening.

5.8

A secondary crusher (size 16-50) with approximate feed opening of 41 cm x 40 cm had an eccentric throw of 1.9 cm. Gyrating at 225 rpm it crushed limestone with an open setting of 3.8 cm. Calculate the per cent change of power required when the open setting was altered to 9.0 cm.

5.9

Dry limestone was crushed at a rate of 100 t/h. 80% of the feed passed a square screen having an opening of 25.4 mm and 80% of the product passed a 3.2 mm square screen. The S.G. of limestone was 2.66 and the Bond Work Index 12.74 kWh/t.
Estimate: The HP required to crush (1 kW = 1.34 HP).

5.10

The feed size to a gyratory crusher is 2.54 cm and nearly uniform. The product analysis is given in column (2) in the table below. The power required to crush the feed was 500 kW. The clearance between the crusher head and cone was then reduced yielding a product whose size distribution was given in column (3) of the same table. Estimate:

1. The power required in the second operation
2. The change in reduction ratio if the power was reduced by 10%.

Size microns	Product analysis	
	After 1st crush	After 2nd Crush
-4750+3350	2.0	
-3350+2360	10.0	2.7
-2360+1700	18.0	10.0
-1700+1180	20.0	13.2
-1180+850	15.0	20.1
-850+600	12.0	20.2
-600+425	10.5	14.2
-425+300	7.6	8.0
-300+212	4.4	7.0
-212+100	0.5	4.0
-100+150		0.4
-150+106	0.1	0.1
-106		0.1
		Σ100.0

5.11
A gyratory crusher received iron ore from the mines at 1.5 m top size. The work index of the ore was determined as 12.5 kWh/t. The height of the bowl was 9.75 m and it was required to produce 300 t/h of crushed material at 175 rpm. Calculate the required crusher set to satisfy the crusher throughput.

5.12
A long shaft suspended spindle gyratory crusher 12.7 cm x 127 cm was commissioned to crush limestone with a work index of 13.2 kWh/t. The crusher was adjusted to a throw of 0.7 cm and the set at 2.54 cm. The average size distribution was:

Size	10.2 cm	7.6cm	5.1cm	2.54 cm	1.27cm
mass%	40.2	23.8	16.1	19.0	0.9

It was operated initially at 500 rpm and then at 600 rpm. Assuming a shape factor equal to 1, estimate:

1   The production at each speed of gyration,
2. The difference in power required between the two speeds of gyration,
3. The critical speed of gyration.

REFERENCES
[1]   S.J. Truscott, A Textbook of Ore Dressing, Macmillan and Co., London, 1923.
[2]   A.F. Taggart, Handbook of Mineral Dressing, John Wiley, 1954, pp. 4-14, 4-29.
[3]   S.C. Westerfield, in Mineral Processing Handbook, N.L. Wiess (ed), SME/AIMME, (1985) 1.
[4]   N.L. Weiss, Mineral Processing Handbook, AIMME, 1985.
[5]   J.C. Motz, in Mineral Processing and Plant Design, A.L.Mular and R.B.Bhappu (eds), SME/AIMME, New York, 1980, pp. 203-238.
[6]   K. Gauldie, Engineering, London, Oct 9, (1953) 456.
[7]   K. Gauldie, Engineering, London, April 30 (1954) 557.
[8]   S.K. Mishra, Private communication (1980).
[9]   E.A. Hersam, Trans. AIME, 68 (1923) 463.
[10] J. Broman, Engineering and Mining Journal, June (1984) 69.
[11] H.E. Rose and J.E. English, Trans. Inst of Mining and Metallurgy, 76 (1967) C32.
[12] Metso Minerals, Retrieved: on 18 January 2006 from http://metsominerals.com; http://www.ckit.co.za/Secure/Brochures/Metso/Nordberg%20HP%20Cone%20crusher/Nordberg%20HP%20cone%20crusher.htm
[13] W.J. Whiten, 10th International Symposium on Application of Computer Methods in Min. Ind., Johannesburg, (1972) 317.
[14] W.J. Whiten, Control '84, J. Herbst (ed), SME, 1984, pp. 217-224.
[15] J.S. Andersen and T.J. Napier-Mann, 3rd Mill Operators Conference, Cobar, NSW, May (1988) 103.
[16] J.S. Andersen and T.J. Napier-Mann, Mining Engineering, 3 (1/2) (1990) 105.

Chapter 6. Roll Crushers

6. INTRODUCTION

Roll crushers consist of two or more adjacent rolls placed parallel to each other and rotated in opposite directions. Single roll crushers are also available which rotate a single roll against a fixed breaker plate. Mineral or rock particles placed between the rolls are nipped and then crushed as they pass between the rolls. Rolls are held against each other by springs. Radical changes to the design of roll crushers have been introduced by Schonert, [1,2] as a result of fundamental work on breakage mechanisms. These roll crushers have large forces of compression and are called High Pressure Grinding Rolls (HPGR). The present tendency is to replace secondary cone crushers by HPGR. The work at Polysius [3] and described by Friedrich and Baum [4], and Otte [5] indicate considerable metallurgical advantage in the extraction of minerals like gold and copper by the use of high pressure grinding rolls. In this chapter these two types of roll crushers are described.

6.1. Design of Roll Crushers

Two types of roll crushers are generally designed. In the first type both rolls are rigidly fixed to a frame with provision for adjusting the lateral position of one of the rolls to control the gap between them. Once set these rolls are locked into place. One roll is attached to the driving mechanism while the other rotates by friction. Single roll crushers are also available which rotate a single roll against a fixed breaker plate. In the second type, at least one roll is spring mounted which forms the driving roll, the other roll rotates by friction (Fig. 6.1). The nest of springs helps to provide uniform pressure along the length of the rolls. The springs are helical and pressure varies with the size of crusher and could be as high as 6 t/meter (about 8300 kPa). In some roll crushers the rolls are individually driven. The drive is either by gears or belt. Both rolls usually rotate at the same speed but some crushers are designed such that one roll could rotate faster than the other. For fine grinding both rolls are rigidly fixed to the base and therefore they do not permit any movement of the rolls during operation. The surfaces of the rolls are either smooth, corrugated or ribbed. Heavy duty toothed rollers are sometimes used as primary crushers but the use of such rollers in the metallurgical industry is very limited.

Some rollers are toothed. The shape of the teeth is generally pyramidal. The roll surfaces play an important part in the process of nipping a particle and then dragging it between the rolls. The corrugated and ribbed surfaces offer better friction and nip than smooth surfaced rolls. The toothed surfaces offer additional complex penetrating and compressive forces that help to shatter and disintegrate hard rock pieces.

The distance between the rolls is adjusted by nuts at the end of one of the rolls. The nip angle is affected by the distance between the rolls. The nip angle is defined as the angle that is tangent to the roll surface at the points of contact between the rolls and the particle. It depends on the surface characteristics of the rolls. Usually the nip angle is between 20° and 30° but in some large roll crushers it is up to 40°.
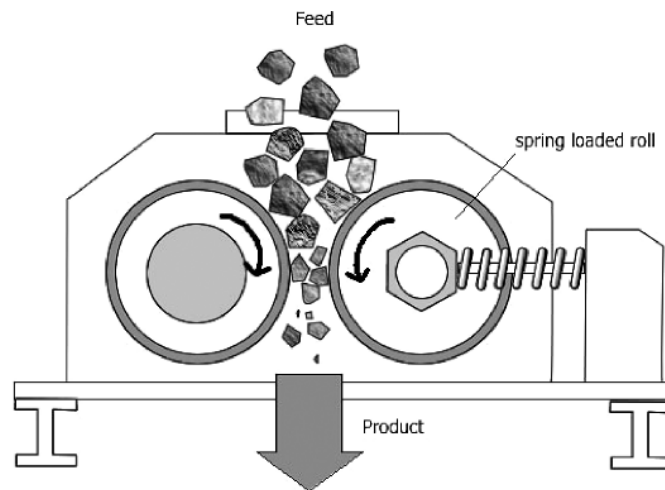
Fig. 6.1. Schematic Diagram of Roll Crusher

6.1.1. Roll Crusher Sizes and Design

The usual crusher sizes and power ratings for different types of roll faces as described by various manufacturers' literatures are summarised in Table 6.1.

Table 6.1
Roll Crusher sizes.

Crusher Surface	Size, mm			
	Width		Diameter	
	Min	Max	Min	Max
Plain Rolls	750	860	350	2100
Toothed Rolls	750	860	1500	1720
Studded Rolls	-	1400	-	2400

Roll crushers are arbitrarily divided into light and heavy duty crushers. The diameters of the light duty crushers vary between 228 mm and 760 mm with face lengths between 250 mm and 460 mm. The spring pressure for light duty rolls varies between 1.1.kg/m and 5.6 kg/m. The heavy duty crusher diameters range between 900 mm and 1000 mm with face length between 300 mm to 610 mm. In general the spring pressures of the heavy duty rolls ranges between 7 kg/m to 60 kg/m. The light duty rolls are designed to operate at faster speeds compared to heavy duty rolls that are designed to operate at lower speeds.

6.1.2. Roll Design

For a particular operation where the ore size is known, it is necessary to estimate the diameter of rolls required for a specific degree of size reduction. To estimate the roll diameter it is convenient to assume that the particle to be crushed is spherical and roll surfaces are smooth. Fig. 6.2 shows a spherical particle about to enter the crushing zone of a roll crusher and is about to be nipped. For rolls that have equal radius and length, tangents drawn at the point of contact of the particle and the two rolls meet to form the nip angle (2θ). From simple geometry it can be seen that for a particle of size d, nipped between two rolls of radius R:

$$\cos\theta = \frac{\left(R + \dfrac{L}{2}\right)}{\left(R + \dfrac{d}{2}\right)} \tag{6.1}$$

where R is the roll radius and L the distance between the rolls.

Simplifying Eq. (6.1), the radius of the roll is given by:

$$R = \frac{L - d\,\cos\theta}{2(\cos\theta - 1)} \tag{6.2}$$

Eq. (6.2) indicates that to estimate the radius R of the roll, the nip angle is required. The nip angle on its part will depend on the coefficient of friction, μ, between the roll surface and the
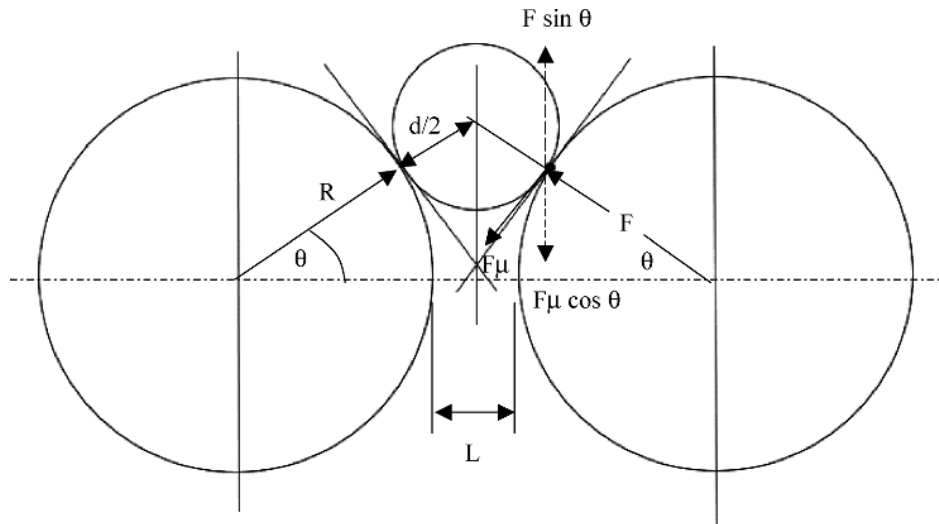
Fig. 6.2. Roll crusher geometry.

particle surface. To estimate μ consider a compressive force, F, exerted by the rolls on the particle just prior to crushing, operating normal to the roll surface, at the point of contact, and the frictional force between the roll and particle acting along a tangent to the roll surface at the point of contact. The frictional force is a function of the compressive force F and is given by the expression, Fμ. If we consider the vertical components of these forces, and neglect the force due to gravity, then it can be seen that at the point of contact (Fig. 6.2) for the particle to be just nipped by the rolls, the equilibrium conditions apply where:

$$F \sin \theta = F \mu \cos \theta \quad \text{or}$$

$$\mu = \tan \theta \quad \text{or} \quad \theta = \tan^{-1} \mu \qquad (6.3)$$

As the friction coefficient is roughly between 0.20 and 0.30 the nip angle has a value of about 11°-17°. However, when the rolls are in motion the friction characteristics between the ore particle will depend on the speed of the rolls. According to Wills [6] the speed v, is related to the kinetic coefficient of friction of the revolving rolls, μ_K, by the relation:

$$\mu_K = \left[\frac{(1 + 1.12 \, v)}{(1 + 6 \, v)} \mu \right] \qquad (6.4)$$

Eq. (6.4) shows that the μ_K values decreases slightly with increasing speed. For speed changes between 150 and 200 rpm and μ ranging from 0.2 to 0.3, the value of μ_K changes between 0.037 and 0.056. Eq. (6.2) can be used to select the size of roll crushers for specific requirements. For nip angles between 11° and 17°, Fig. 6.3 indicates the roll sizes calculated for different maximum feed sizes for a set of 12.5 mm.
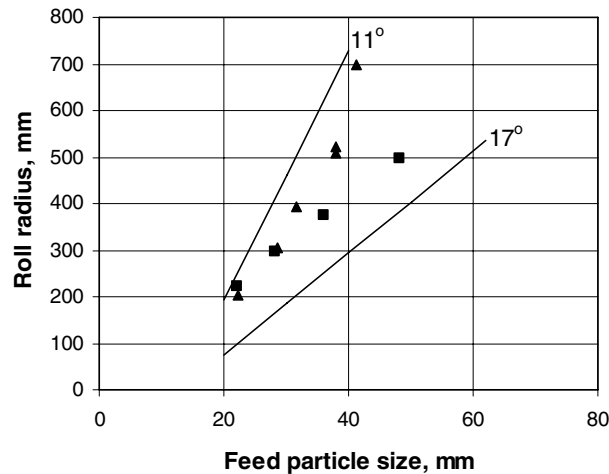
Fig. 6.3. Roll radius for different maximum feed sizes, calculated from a set of 12.5 mm at nip angles of 11 and 17 degrees (solid lines). The points correspond to industrial roll crusher data.

The use of the above expressions to determine the size of rolls to be used for a particular operation is illustrated in Example 6.1.

Example 6.1

The maximum particle size of a limestone sample received from a cone crusher was 2.5 cm. It was required to further crush it down to 0.5 cm in a roll crusher with smooth rolls. The friction coefficient between steel and particles was 0.25, if the rolls were set at 6.3 mm and both revolved to crush, estimate the diameter of the rolls.

Solution
Step 1
Estimate the nip angle using Eq. (6.3)

Substituting friction coefficient $\mu = 0.25$, $\tan \theta = 0.25$ or $\theta = 14.03°$

Step 2
Substituting in Eq. (6.2)

$$R = \frac{(6.3 - 25 \times 0.97)}{2 \times (0.97 - 1)}$$

$$= 300 \text{ mm}$$

and hence the roll diameter $= 600$ mm

It is generally observed that rolls can accept particles sizes larger than the calculated diameters and larger nip angles when the rate of entry of feed in crushing zone is comparable with the speed of rotation of the rolls.

6.1.3. Roll Crusher Circuit Design
Roll crushers are generally not used as primary crushers for hard ores. Even for softer ores, like chalcocite and chalcopyrite they have been used as secondary crushers. Choke feeding is not advisable as it tends to produce particles of irregular size. Both open and closed circuit crushing are employed. For close circuit the product is screened with a mesh size much less than the set.

Fig. 6.4 is a typical set up where ore crushed in primary and secondary crushers are further reduced in size by a rough roll crusher in open circuit followed by finer size reduction in a closed circuit by roll crusher. Such circuits are chosen as the feed size to standard roll crushers normally do not exceed 50 mm.
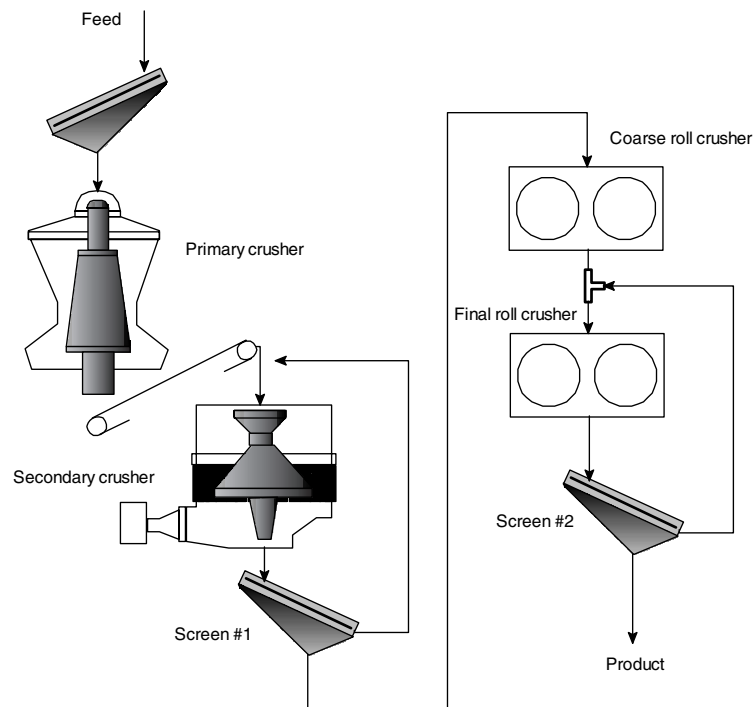
Fig. 6.4. Roll Crusher Design Circuit.

6.2. Operation of Roll Crushers

The feed to roll crushers is usually dry. Moisture tends to clog the crusher and could result in the formation of hard crust, which impairs operation. Hence dry crushing is preferred. Sometimes, water is added between the rolls, which help to prevent formation of the crust and also to remove the hard cake that tends to form on the roll surface. Wet grinding is usually carried out when fine grinding is required.

Rock particles are usually fed through a chute designed to distribute the charge evenly along the width (length) of the roll. About two-thirds of a roll–width is active. As in any crusher, particle sizes less than the distance between the rolls tend to pass through uncrushed. Particles that are larger than the opening is nipped and crushed. The maximum size of particle that is nipped without slippage depends on friction, distance between rolls and roll size.

The size of the product depends on the crusher set, the distance between the rolls. Due to single pass operation it is evident that no middlings or over-size is produced.

The normal speed of operation of commercial light duty rolls is 130-300 rpm compared to heavy duty rolls whose operating speeds are in the region of 80-100 rpm. Regulated slow rate of feeding spread over evenly across the width of rolls is preferred when closed circuit operation is adopted for finer product size.

6.3. Capacity of Roll Crushers

The capacity Q, of roll crushers is directly proportional to its width, W, diameter, D and speed of revolution of rolls [6]. Under continuous and steady feeding conditions the capacity is given by:

$$Q = \pi \, 60 \, D \, W \, \omega \, L \, \rho_B$$

$$= 188.5 \, D \, W \, \omega \, L \, \rho_B \quad t/h \tag{6.5}$$

where D = diameter of roll, m,
         W = width of roll, m,
         ω = speed, rpm,
         L = set or distance between rolls, m,
         ρ_B = bulk SG of the mineral, t/m^3.

In deriving the expression it is assumed that the particles are continuously fed from a height and that the rolls are kept full all the time, that is the rolls are choke fed. Further it is assumed that the product is in the form of a continuous ribbon having the width of the roll and thickness equal to the set. This would give the theoretical production. The actual production will depend on the "ribbon factor, R_F" given by the expression:

$$R_F = 0.0095 \frac{Q}{v_P \, L \, W} \tag{6.6}$$

where Q = Feed rate, t/h,
         v_P = peripheral speed of the roll, m/s.

The ribbon factor is defined as the ratio of the actual tonnage passing through the crusher to the tonnage of the theoretical solid-rock ribbon [7]. In practice, the actual capacity can be as little as 25 % of this calculated capacity, Q. This correction is required due to voids between particles and the increase in bulk density of the particles as it passes through the crushing chamber. When the feed rate is irregular, the capacity would decrease [8].

Eq. (6.5) has been modified by Otte [5] by introducing an efficiency factor, ε and expressing capacity as:

$$Q = 3600 \, \varepsilon \, W \, v_P \, \rho_B \, L \tag{6.7}$$

where ρ_B = bulk density of the feed material, t/m^3,
         ε = efficiency factor which has a value between 0.15 and 0.30, depending on the roll gap or product size.

The product of ($\varepsilon \, \rho_B$) has been termed by Otte as the *operational density*, that is, the density of the product, which is in the form of a continuous ribbon or cake. Otte observed that the operational density of roll crushers are low (0.25 to 0.6 t/m^3).

6.4. Power Consumption of Roll Crushers

Within the same reduction ratio the power consumption of roll crushers vary widely. The power required could be expressed by the general equation:

$$P = \text{Capacity x Reduction Ratio x work index} \qquad (6.8)$$

In industry the low pressure smooth surfaced rolls are designed to draw 8-50 kW of power under dry conditions. The heavy duty rolls draw between 40 and 550 kW depending on size and low moisture conditions. Sufficient data are not available for toothed rolls where crushing forces are complex and crushers often are operated under wet conditions.

6.5. High Pressure Grinding Rolls (HPGR)

In a roll crusher comminution primarily involves individual particles nipped between converging roller surfaces. The forces of compression and friction between the rolls and particles are responsible for size reduction provided the combined forces exceed the compressive strength of the particle. When a large quantity of rock is held between the rolls and subjected to high pressure then comminution could take place by compressive forces as well as by *interparticle* breakage, provided again that the total applied pressure was greater than the crushing strength of the rock pieces. The product again is a continuous "ribbon" of crushed material in the form of a compacted cake.

While studying the specific energy of breakage due to impact and by compressive forces, Schoenert [9,10] observed that the utilisation of the specific energy of breakage as a result of impact was much less than with compressive forces. Thus during high pressure grinding where large compressive forces were applied to a bed of ore, the total energy required would be relatively less compared to comminution systems where impact forces predominate. Schoenert also observed that with decreasing particle size the energy utilisation increased. Several workers [5,11-13] have confirmed Schonert's observations. These observations were developed and finally resulted in the high pressure grinding roll (HPGR) by Krupp-Polysius[14] in conjunction with Schonert. The HPGR are being used with considerable success in the cement, iron ore and diamond industries [4,5,15] and increasingly in the general mineral industry.

Fig. 6.5 illustrates the manner of comminution in HPGR. This figure shows that during the initial stages when the feed size is greater than the gap between the rolls, breakage of particles is due to conventional forces applicable to roll crushers. In such a case, the edge effects of the rolls are significant. As the feed descends, some of the particles that are larger than the gap, experience high compressive forces and therefore reduced in size.; these particles occupy the void spaces between large particles. Interparticle contact therefore increases resulting in transference of more interparticle compressive forces that further crushes the particles. Due to high compressive forces the crushed particles compact forming a continuous product resembling a cake or ribbon. Some plastic deformation also takes place the extent of which depend on the characteristics of the ores and rocks. The compacted particles are subsequently dispersed by a second operation in a grinding mill. It is found [5] that the total energy requirement for the combined operation of HPGR and ball mill is less than the conventional comminution processes.

To perform the operation, pressure is applied hydraulically through four cylinders to the roll that is designed to move laterally. The second roll is immovable. A crushing pressure of the order of 200 MPa is applied. The dimensions of the rolls used in the mineral industry are [5] 0.7– 2.8 m diameter with a Length/Diameter ratio between 0.2 – 0.6. The roll speeds are 85–105 m/min. The roll faces are either studded or have Ni-hard liners. The studs are made of tungsten carbide to combat heavy abrasion but softer studs have better life as they are less brittle.
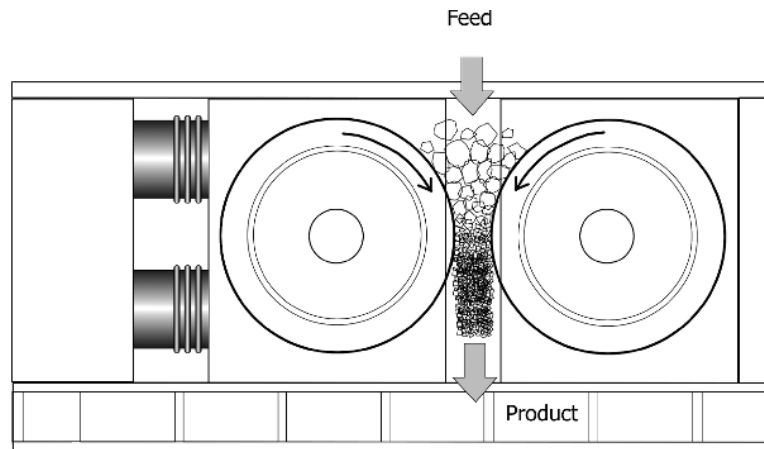
Fig. 6.5. Schematic diagram of a High Pressure Grinding Roll (HPGR).

Both dry and wet crushing and grinding is possible. Crushing rates up to 450 t/h in South African diamond mines and about 400 t/h for hard taconite ores in the USA have been reported by Krupp-Polysius [14]. Design capacities up to 757 t/h are available.

Due to the fact that fine product sizes can be obtained, the HPGR has been used both for crushing and grinding. In a crushing circuit it can replace secondary or tertiary crushers like cone crushers. In grinding circuits it can replace tertiary crushing and installed before a ball mill. In some cases it is installed after the ball mill, as in Kudramukh in India in an iron ore circuit, where the product from the HPGR is fed directly to a pelletising plant [16].

6.5.1. Circuit Design and HPGR

As the product size from HPGR is fine, the present tendency is to replace the conventional secondary and tertiary crushers with a single HPGR unit. Thus liberation size is more economically achieved and the product acceptable for down stream operations such as flotation. In some flow sheets HPGR is placed before the roll crusher in order to induce cracks and fissures in the ore particles. In such cases ball mill grinding is facilitated. Several alternate circuits have been suggested by Baum et al [17] and Patzelt et al, [11,15]. A typical flow sheet for coarse grinding is illustrated in Fig. 6.6. Allers and Blasczyk [18] claims great energy savings when HPGR is used in closed circuit as combined pre-grinder and finishing grinding mill.

6.6. Operation of HPGR

For the operation of High Pressure Grinding Rolls it is necessary to determine the chief operating parameters. That is:
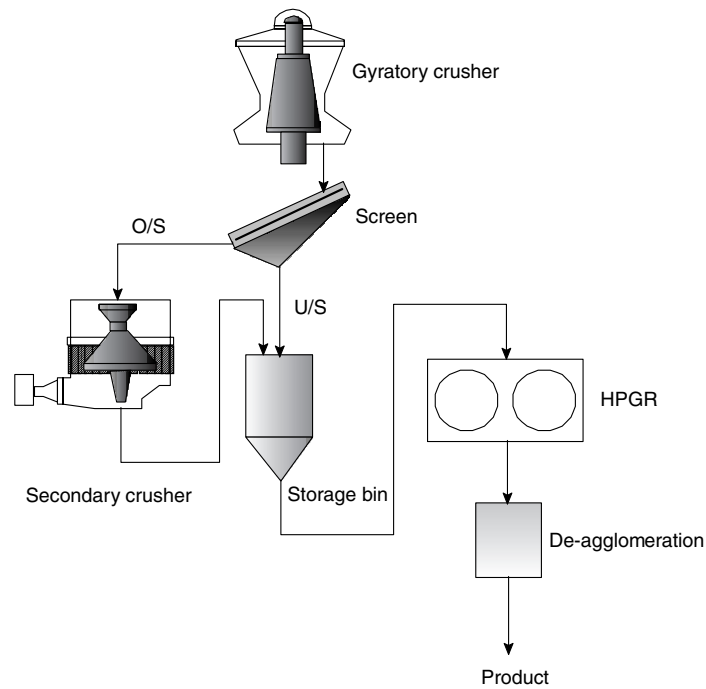
Fig. 6.6. High Pressure Grinding Roll flowsheet.

1. operating pressure,
2. nip angle,
3. gap,
4. roll speed and
5. ore size.

6.6.1. Estimation of Operating Pressure

To operate the HPGR Polycom grinding mill the pressure required is applied hydraulically through four cylinders to the roll that is designed to move laterally. The second roll is immovable. The crushing pressure applied is generally of the order of 200 MPa. but for hard ores, higher pressures are required. For example, in Cyprus Sierrita, a pressure of 340 MPa is used.

The pressure required for crushing should be in excess of 50 MPa [19]. Battersby, Kellerwessell and Oberheuser [20] states that the force required was in the range of 100 kN per linear meter of roll width. Schonert [2] has estimated theoretically the specific comminution pressure on mineral particles trapped between the rolls as:

$$P = F \, (L \, D)^{-1} \, N/m^2 \tag{6.9}$$

where F = Grinding force, kN,
L = Length (width) of roll,
D = Diameter of roll, m.

The maximum pressure on particles is inversely proportional to the interparticle angle of nip and is expressed as:

$$P_{MAX} = F (K D L \theta_{IP})^{-1} \quad MPa \qquad (6.10)$$

K is a material constant with values between 0.18-0.23 and θ_{IP} is the angle of nip for interparticle comminution, defined in Eq. (6.12). It is difficult to use Eq. (6.10) due to the difficulty in determining K. Klymowsky, et al [21] therefore uses average pressure on the particles which is described as:

$$P_{AVE} = F (1000 L R \theta_{IP})^{-1} \qquad (6.11)$$

where R is the radius of the rolls and θ_{IP} the angle of nip of the interparticle particles defined by Eq. (6.13).

6.6.2. Estimation of Nip Angle

The mechanism of breakage in HPGR has been recognised by Klymowsky et al [21] who concludes that in the high pressure region comminution is due to:

1. Interparticle forces acting between particles that are less than the gap,
2. Combination of interparticle plus single particle breakage when the single particles are larger than the gap and being nipped directly by the rolls and crushed before entering the compression zone.

The larger particles are broken prior to entering the compression zone. In the compaction zone the bulk density of the ore is reduced to the bulk density of the cake. These concepts can be visualised in Fig. 6.7.

The angle of nip for the two situations involving single particle breakage was derived as [21]:

$$\theta_{SP} = \arccos \left[1 - \left(\frac{d_{max}}{L_T} - 1 \right) \frac{L_T}{1000 D} \right] \qquad (6.12)$$

and for interparticle breakage, the nip angle θ_{IP}, is:

$$\theta_{IP} = \arccos \left[1 - \left(\frac{\rho_C}{\rho_{B(F)}} - 1 \right) \frac{L_T}{1000 D} \right] \qquad (6.13)$$

where d_{MAX} = maximum size of particle, mm,
L_T = thickness of cake, mm,
D = diameter of roll, m,
ρ_C = density of compacted cake, t/m^3,
$\rho_{B(F)}$ = bulk density of feed,
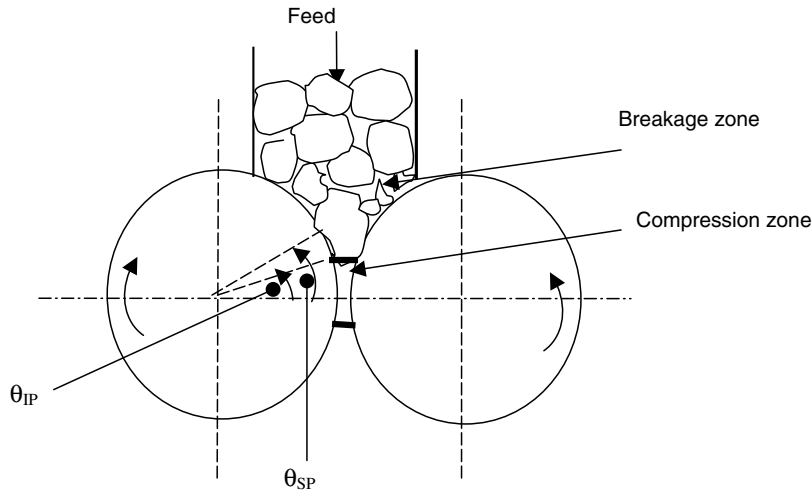
Fig. 6.7. Mechanism of crushing in HPGR [21].

6.6.3. Estimation of the Roll Gap

As the gap determines the product size distribution, it is helpful to predict the gap opening of HPGR. Morrell et al [22] expressed the dimensionless *working gap* as the ratio of the working gap, L_G, to roll diameter, D. This ratio varies linearly with the logarithm of the specific grinding force and can be expressed by Eq. (6.14) as:

$$\frac{L_G}{D} = \left(k_1 v_P^2 \left(\frac{2}{gD} \right) + k_2 v_P \sqrt{\frac{2}{gD}} + k_3 \right) (1 + k_4 \log F_S)$$ (6.14)

where L_G = working gap,
  v_P = peripheral speed of rolls, m/s (normalised),
  g = acceleration due to gravity (9.81 m/s^2)
  D = diameter of rolls, m,
  F_S = specific grinding force, N/mm^2
  k_1- k_4 = material constants.

Eq. (6.14) shows that as the log (F_S) increases L_G/D ratio decreases. The working gap will be affected by the surface characteristics of the roll, moisture content in the ore and the largest size of ore pieces. To evaluate Eq. (6.14), the material constants are determined by laboratory test work.

6.6.4. Roll Speed

The choice of roll speed affects the production rate. However, the choice is between faster and narrower rolls which are easier to operate or slower and wider rolls where control of the

gap across the width could be a problem. Excessive speed is to be avoided as the rolls tend to deflect particles away from the crushing zone reducing the throughput.

Roll speeds are related to the diameter of the rolls. Klymowsky [21] suggests the following peripheral speed for different roll diameters:

1.   For roll diameters < 2 m, peripheral speed $v_P \leq 1.35 \sqrt{D}$
2.   For roll diameters > 2 m, peripheral speed $v_P \leq D$

6.6.5. Feed and Product Size

The feed size and the working gap should be compatible as neither too large nor too small pieces are acceptable. However the hardness of the rock and the type of roll surface also affect the feed size. The recommended feed size therefore depends on the ratio of feed size/working gap. Expressing this ratio as γ the recommendations of Klymowsky [21] is summarised in Table 6.2.

Table 6.2
HPGR feed sizes for different ore types [21].

Rock type	Compressive strength	Feed size/working gap
Soft Ores	< 100 MPa	up to 1.5
Hard rock	> 250 MPa	≤ 1

For hard faced rolls with a smooth surface profile, the feed size can be up to 3 times the working gap. For rolls with studded surface the feed size should be less than or equal to the working gap.

The feed size to the HPGR in some Brazilian mines is 90 % passing 1 mm [3] but the use of coarser feed sizes (16–50 mm) has been reported by Patzelt et al. [15]. At Argyle diamonds, (Australia), Maxton [23] reports charging feed size of 80% passing 75 mm with lumps up to 750 mm.

Product Size

The product size from HPGR can be much finer than the corresponding ball or rod mill products. As an example, the results by Morsky et al [12] is given in Fig. 6.8 where, for the same net input energy (4 kWh/t) the product sizes obtained from HPGR, ball and rod mills are plotted. It can be seen that the fraction below 100 microns is much greater from HPGR compared to that produced by the rod mill operation. Other workers have observed similar results [12,15].

6.7. Capacity of HPGR

The production capacity of HPGR can be taken as the volume of material passing through the gap between two rolls. It therefore depends on the width of the rolls, the working gap and the velocity of material through the gap. The mass flow rate through the gap will therefore be:

Q = Roll width x working gap x velocity of material x density of solids in the gap, or

$$Q = 3.6 \, W \, L_G \, v \, \rho_S \quad t/h \qquad (6.15)$$

where the roll width is in m, L_G is in mm and v is in m/s.
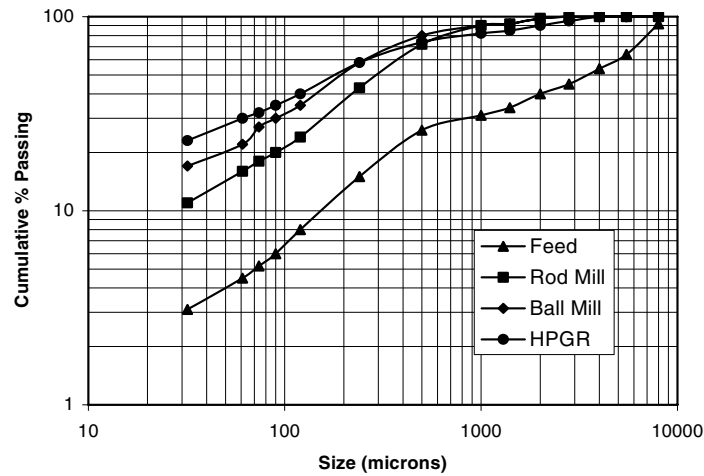
Fig. 6.8. Particle size of product from ball mill and HPGR [12].

A popular way to describe capacity is to express it in terms of specific throughput rate. Seebach and Knobloch [24] and later Morrell [22] have expressed it in dimensionless form as:

$$Q = Q_S \ D \ W \ v_P \ \rho_S \qquad t/h \qquad (6.16)$$

where Q_S =   specific throughput rate,
        D   =   diameter of roll, m,
        W   =   width of roll, m and
        ρ_S =   material density.

Otte (1988) expressed the capacity of HPGR, in terms of the distance between the rolls and the operational density of the ore, as:

$$Q = W \ L_G \ v_P \ \rho_{OP} \qquad t/h \qquad (6.17)$$

where ρ_{OP} =   operational density, t/m^3, (discharge cake density)

From laboratory experiments Morrell indicates that the specific throughput was related to the specific grinding force, F_S, by a linear function of the form;

$$Q_S = k \ (\ 1 + C \ \log F_S) \qquad (6.18)$$

where F_S =   specific grinding force,
        k   =   a factor dependant on roll speed
        C   =   a material constant

The factor for roll speed, k, was evaluated experimentally and is a function of roll speed, v_P, according to the polynomial equation:

$$k = C_1 v_P^2 + C_2 v_P + C_3 \qquad (6.19)$$

where Cr_1-C_3 are material constants. Eq. (6.19) is evaluated experimentally.

The specific throughput rate can then be computed by combining Eqs. (6.18) and (6.19). Thus:

$$Q_S = (1 + C \log F_S)(C_1 v_P^2 + C_2 v_P + C_3) \qquad (6.20)$$

This relation needs to be fully tested.

Lubjuhn and Schonert [25], working with a laboratory model HPGR (diameter 200 mm x length 100 mm) using limestone feed sizes, 0.25-1.0 mm and 1.6 - 6.3 mm, concluded that:

1.   When milling forces varied between 1-6 N/m^2, little effect on throughput was observed,,
2.   When the specific forces of breakage was constant, speed has low significance on breakage,
3.   Corrugated roll surface has greater throughput.

6.8. Power Consumption of HPGR

As a general rule, motor power is the product of capacity and energy input. For HPGR we have seen that the energy input is defined as the specific energy input. In conventional work, Bond's work index is usually accepted as the measure of the net specific energy required for comminution. Klymowsky and Liu [13] found that Bond's work index was not quite applicable in the case of the HPGR as it was determined using a tumbling mill where repeated impact and grinding forces were responsible for size reduction. Further in a tumbling mill cascading particles dropped on a bed of particles, which cushioned the impact and therefore affected the specific energy of size reduction. Klymowsky[14] et al. indicated that the Bond work index was not exactly a constant factor for a given ore. Otte [5] reported an increase of W_i from 13.9 kWh/t to 15.6 kWh/t for a copper ore and 9.4 kWh/t to 15.6 kWh/t for a gold ore. Similar observations were made by Patzelt et al. [11]. Klymowsky et al. advocate that in the case of the HPGR, Rittinger's law (see Chapter 2) was more appropriate than Bond's work index.

To determine the power draw, Morrell et al [21] applied the basic laws of physics. They considered the angular velocity of the roll initiated by a given torque of the roller shaft. According to basic principles of dynamics, the power required at the roll shaft will be:

$$P = \frac{2 \text{ Torque x Angular velocity}}{\text{Diameter of roll}} = \frac{2 \text{ T}\omega}{D} \qquad (6.21)$$

where   T   = Torque (Nm), and
           ω = Angular velocity, (rad/s)

The torque is generated by the angular displacement β of the horizontal force F between the materials, that is:

$$T = \beta \, F \, D \qquad (6.22)$$

or

$$D = \frac{T}{F \, \beta} \qquad (6.23)$$

Note that F is the horizontal component of the grinding force applied by the movable roll and transmitted to the material between the two rolls. F is equal to the specific grinding force times the roll diameter times the roll length. Substituting the value of the diameter D from Eq. (6.23) in Eq. (6.21) gives:

$$P = \frac{2 \, T \, \omega \, F \, \beta}{T} = 2\omega F \beta \qquad (6.24)$$

The angular velocity, ω, will be affected by the specific grinding forces. Morrell et al [22] found experimentally that the angular displacement β, was related to the specific grinding energy by the relation,

$$\beta = (a \, v_P^2 + b \, v_P + c) \, (1 + k \, F_S) \qquad (6.25)$$

where a, b, c and k are constants.

Substituting the value of β in Eq. (6.24) the power required to operate a high-pressure roll will be:

$$P = 2 \, \omega \, F \, (a \, v_P^2 + b \, v_P + c) \, (1 + k \, F_S) \qquad (6.26)$$

Quantitative analysis by Morrell et al [22] verified the validity of this equation.

6.9. Problems

6.1
A smooth surfaced roll crusher had a roll diameter of 910 mm. Its suitability to crush an ore at 10.0 t/h was being examined. Preliminary examination showed that the kinetic friction factor was 0.36 when the speed of revolution was 33 rpm. The average diameter of particles fed to the crusher was 200 mm and the S.G. of the ore was 2.8.

Estimate:

1. the distance between the rolls,
2. the angle of nip,
3. the width of the rolls.

158

6.2

Establish a relation between the diameter of roll and maximum size of ore when the reduction ratios were 2.0, 3.0 and 4.0 and nip angle was held at 15°.

6.3

A roll crusher was installed as a primary crusher to crush rocks of 7.0 cm maximum size. The distance between the rolls was set at 1.5 cm, the diameter of the rolls was 110 cm and the width 100 cm. The particle size distribution of the feed was:

Size , mm	Wt. % retained	Size, mm	Wt. % retained
+7.0	0.0	+0.8	5.3
+3.5	80.0	+0.4	3.2
+1.7	10.6	-0.4	0.9
			Σ 100.0

If the S.G. of the rock was 2.8, and the bulk density was 1.68 t/m^3, determine:

1. the relation between the capacity and the peripheral speed velocity when it varied from 6 m/min to 22 m/min in steps of 4 m/min,
2. the change in the ratio of the coefficient of kinetic friction to static friction between the roll and the particles and the peripheral speed,
3. the ratio of tangential force at the points of contact to the radial forces at the same point of contact between the roll and the nipped particle.

6.4

The roll size of a roll crusher was 30.5 cm x 90.1 cm. Gypsum rock (S.G.= 2.7, bulk density = 1.7 t/m^3) is to be crushed.

Determine:

1. the set in order to crush at the rate of 12 t/h and 10 rpm speed of the rolls.
2. the ratio between capacity and peripheral speed if the set was 2.5 cm,
3. the nip angle when the crusher feed size is 10 cm,
4. the coefficient of friction between roll and gypsum particles.

6.5

At a nip angle of 30°, an approximate relation between peripheral speed v_P (m/min), diameter of rolls D (cm) and sieve size, d (cm) through which 80 % of ore passes is given by the relation:

$$v_P = 1.8D - 40d + 128$$

Establish the relation when the nip angle is changed to 35 and then to 40 degrees. Draw a nomogram relating these variables of a roll crusher.

6.6
A set of rolls was required to crush limestone delivered from a secondary cone crusher at the rate of 52 t/h. The product size from the cone crusher was less than 24 mm. The product size from rolls was expected to be less than 8 mm. The shape factor of the feed was determined to be 1.5. Using the data given below, estimate:

1.   the diameter of rolls,
2.   the width of the rolls.

Data: The bulk density of limestone = 1.6 t/m^3
        Speed of rotation = 75 rpm,
        Nip angle = 25°

REFERENCES

[1]   K. Schonert, in Advances in Mineral Processing, P. Somasundaran (ed), SME/AIME, Chapter 1, 1986, pp. 19-31.
[2]   K. Schonert, 4th Tewksbury Symposium, Melbourne, 1979, p. 3.1.
[3]   Polysius, Engineering Made by Polysius, Report 2001
[4]   J.H. Friedrich and W. Baum, Proceedings of Hidden Wealth Conference, Johannesburg, South African Institute of Mining and Metallurgy, 1996, pp. 125 – 130.
[5]   O. Otte, Proceedings of the Third Mill Operators Conference, Australasian Institute of Mining and Metallurgy, Cobar, May, 1988, pp. 131-136.
[6]   B.A. Wills, Mineral Processing Technology, 2nd ed. Pergamon Press, 1989.
[7]   R.H. Perry and C.H. Chilton, Chemical Engineering Handbook, 5th edition, McGraw-Hill, 1973, pp. 8-22.
[8]   A.F. Taggart, Handbook of Mineral Dressing, John Wiley and Sons, 1953.
[9]   K. Schönert and O R, Knoblock, Zement-Kalk-Gipps II, 1984, p 563.
[10] K. Schönert, in Advances in Mineral Processing, SME/AIME, Chapter 1, P. Somasundaran (ed), 1986, pp. 19-31.
[11] N. Patzelt, J. Knecht and W. Baum, Mining Engineering, June (1995) 524.
[12] P. Mörsky, M. Klemetti and T. Knuutinen, Proceedings of the International Mineral Processing Congress, Chapter 8, 1995, pp. 55 – 58.
[13] I.B. Klymowsky and J. Liu, in Comminution Practice, S. K. Kawatra, (ed), SME/AIME Littleton, Chapter 14, 1997, pp. 99-105.
[14] Krupp Polysius, Experience with High Pressure Grinding Rolls in the Iron Ore Industry, pp. 1-7.
[15] N. Patzelt, J. Knecht, E. Burchardt and K. Klymowsky, Proceedings of the Seventh Mill Operators' Conference, Australasian Institute of Mining and Metallurgy, Kalgoorlie, 2000, pp. 47-55.
[16] J.C. Trembley, Skillings Mining Review, March (2000) 1.
[17] W. Baum, N. Patzelt and J. Kneecht, in Comminution Practice, S.K. Kawatra, (ed), SME Littleton, Chapter 16, 1997, pp. 111-116.
[18] T. Aller and G. Blasczyk, Method and Apparatus for Two Stage Crushing (Hybrid grinding), Patent applied, Section 837946 (DE PS 35 20069.3).
[19] K. Beisner, L. Gemmer, H. Kellerwessel and Zisselmar, European Patent 0 084 373. 1983.

160

[20] M. Battersby, H. Kellerwessell and G. Oberheuser, International Conference in Extractive Metallurgy of Gold and Base Metals, Aus.I.M.M., Kalgoorlie, 26-28 October, 1992, pp 159-165.

[21] R. Klymowsky, N. Patzelt, J. Knecht and E. Burchardt, Proceedings of Mineral Processing Plant Design Practice and Control, SME Conference, Vancouver, 1, 2002, pp 636-668.

[22] S. Morrell, W. Lim, F. Shi and L. Tonda, in Comminution Practices, S.K. Kawatra, (ed), SME/AIME, Littleton, 1997, pp. 117-120.

[23] D. Maxton, Mineral Processing, AMIM, July, 2003, pp 113-117.

[24] M. Seebach and O.R. Knobloch, SME Annual Meeting, Denver, Feb. 1987.

[25] U. Lubjuhn and K. Schonert, Proceedings of XVIII International Mineral Processing Congress, Sydney, 1993, pp. 161–168.

Chapter 7. Tubular Ball Mills

7. INTRODUCTION

The usual objective of reducing the size of run-of mine ore pieces is to separate the mineral of interest contained in the ore body from associated gangue minerals. As crushing only does not generally liberate a mineral, further size reduction is usually required. This is achieved by grinding the crushed ore in tubular mills or devices like pan mills or roller-grinder mills. In tubular mills, a grinding media such as steel balls, rods or hard pebbles, impart the forces required for size reduction. On rotating a mill charged with rocks and grinding media, the entire charge rises against the perimeter of the mill in the direction of motion. On reaching a certain height, part of the charge cascades and falls to the bottom of the mill, the other part tends to slips down but soon travels in the direction of motion of the mill. During this process, the media drops repeatedly on to the rock breaking down its size. Some size reduction also takes place due to abrasive forces. As a result of the combined action of repeated impact and abrasion over time, size reduction takes place and given sufficient time the mineral of interest is liberated.

Some tubular mills are specially shaped mills, like the Hardinge Mill, where only the central portion is cylindrical and the ends are shaped like the frustum of a cone. Straight cylindrical mills however are the more common. The grinding medium generally used is in the form of balls, rods or cylindrical media called cylpebs. Both steel and ceramic balls are in use depending on the hardness of the rock. For soft ores, pebbles are added or simply autogenously ground with no medium. Both wet and dry grinding is common. Fig. 7.1 illustrates the grinding action inside a tubular mill.
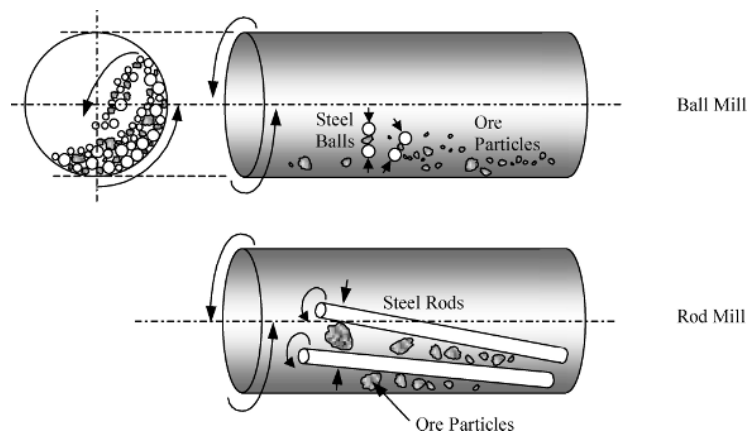
Fig. 7.1. Mechanism of crushing in tubular mills

The media used in the charge generally describes a tubular mill. Thus the medium could be steel or cast iron balls when the mill is designated as a *ball mill*, or it could be steel rods where the mill is known as a *rod mill*. When no grinding medium is charged it is known as an autogenous mill.

In this chapter we initially discuss the design and operation of tubular mills followed by ball mills. The rod mill and autogenous or semi-autogenous mills are described in subsequent chapters.

7.1. Design of tubular mills

Rough outlines of three common types of tubular mills are illustrated in Fig. 7.2. Fig. 7.2 A. shows that the discharge from the mill is by overflow of the contents. It is best suited to fine grinding to 75 – 106 microns.

Fig. 7.2 B indicates a mill where a diaphragm or grate is placed before the exit end so that particles greater than the openings of the diaphragm are not discharged but held back for further grinding. Grate discharge mills give less excessive grinding compared to overflow mills and are best suited to grinds to 150 – 250 microns. In Fig. 7.2 C the discharge opening is at the centre of the mill, while the feed is from both ends of the mill. The mills are therefore designated as a *Centre Periphery Discharge mill*.

The diameter of the feed trunnion is slightly smaller than the discharge trunnion opening to facilitate flow of slurry through the mill and to prevent the slurry from trying to discharge through the feed trunnion. The basic design parameters of the tubular mills include:

1. Size Rated as diameter x length
2. Feed system　　One hopper feed, diameter 40-100 cm at $30°$ to $60°$ entry angle and top of feed hopper at least 1.5 m above the centre line of the mill for ease of entry of feed
3. 　　Feeder　　Single or double helical scoop feeder or a Spout feeder
4. 　　Discharge system　　One exit unit, about 5-110 cm lower than the centre line for overflow mills.

The double helical scoop feeders are generally used in mills designed to operate in closed circuit with classifiers like rake or spiral classifiers, while the spout feeders are preferred for mills operating in closed circuit with a hydrocyclone as classifier. As a general rule hydrocyclone classifiers are located above the tumbling mills so that the classified course fraction from the hydrocyclones can be fed by gravity into the spout of the mills.

The common sizes of mills, the initial size of feed and the reduction ratio of the feed to product sizes achievable in these mills during the comminution process are indicated in Table 7.1.

Table 7.1
Tumbling mill characteristics. *Multicompartment mills: length/diameter ≈ 5.

Parameter	Rod Mill	Ball Mill	Autogenous Mill
Length/diameter Ratio*	1.4 to 1.8	0.5 to 3.5	0.25 to 0.5:1
Feed Size	2.5 cm max	-1.9 cm	Course ore
		-1.25 cm to 0.9 cm	Normal ore
Reduction Ratio	15:1 to 20:1	20: 1 to 200:1	

A - Overflow discharge mill

B - Diaphram or Grate discharge mill

C - Centre-periphery discharge mill
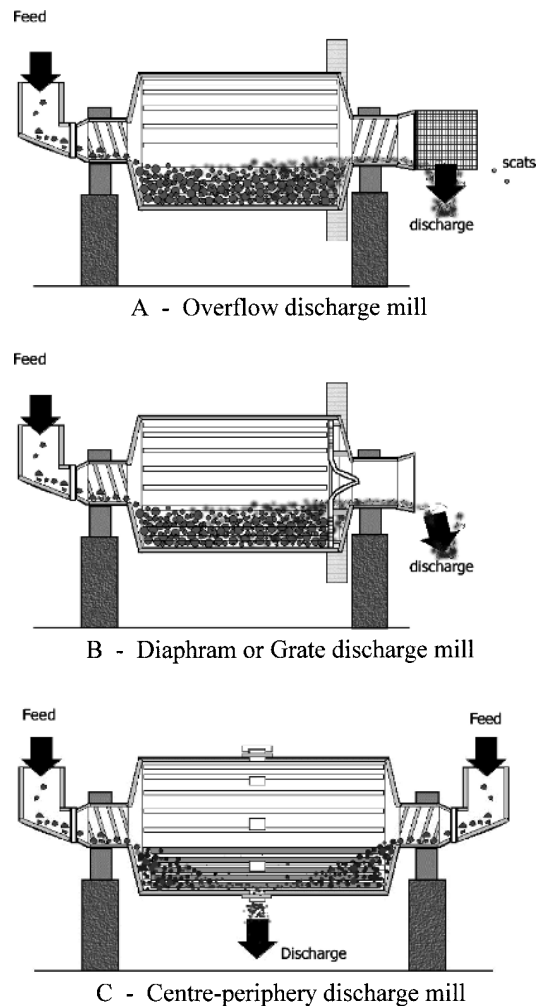
Fig. 7.2. Tubular mill types.

A survey of 40 industrial mills in Australia found that the maximum ball mill diameter in use was 5.34 meters and length 8.84 meters [1]. Autogenous mills range up to 12 meters in diameter.

The length to diameter ratio indicated in Table 7.1 for ball mills are for normal use, but for primary grinding the ratio could vary between 1:1 and 1.8:1. For fine regrinding under open circuit conditions the length to diameter ratio is restricted to the range 1.5:1 to 1.3:1.

Some mills have compartments separated by grates that permit particles having sizes less than the size of the grate to pass through but hold back larger sized particles from entering the next downstream compartment so that further size reduction could take place. In some instances, the different compartments have different sizes of grinding balls, for more efficient grinding.

Several variations of this method of segregating coarser from finer particles within a mill are employed. A mill of this type is the Hardinge mill, where the discharge end of the mill shell is conical in shape. This permits the finer particles to preferentially move into the cone section resulting in some segregation of both fine particles and fine balls within the mill. In the conical section of the mill where the cone narrows down, the drop distance of the charge (and balls) is reduced considerably resulting in lower impact and restricted breakage of the ore. These mills are not very common in the metallurgical industry and are of small tonnage.

Several devices are used to promote a crushing operation within a conventional tumbling mill, such as providing lifters that help to raise the rocks to greater heights before they drop and cascade down. In some cases, the lifters are designed to spiral inside the mill, which promotes faster and possibly more even flow within the mill. The number of such lifters fixed along the perimeter is generally guided by the rule:

Number of lifters $\approx 3.3 \pi$ D (for the mill diameter, D in m) for double wave liners
≈ 6.6 D (for D in m) for single wave liners [2].

The function of the lifters are incorporated into the mill liners, which are designed with different profiles. They serve the dual purpose of saving wear of the steel body of the mill and help to lift the charge to different heights before they cascade or cataract to impinge at the toe of the mill charge. While determining the performance of these mills the influence of the number of lifters is usually neglected. The mills liners could be manganese steel or NI-Hard or high carbon steel either as grid or solid liners. Hard rubber or hard synthetic liners, 65 – 75 mm thick are common. Liner surfaces can be smooth, ribbed or waved. The waves are usually 65 – 90 mm above the liner thickness, for double wave liners and 60 – 75 mm for single wave liners [2]. The rule of thumb is that the wave height is 1.5 – 2.0 times the thickness of the liner. The liner wear is roughly proportional to the speed of rotation of the mill.

Double wave liners are more suited for mills using top ball sizes less than 60 mm. Single wave liners are generally used for mills with ball sizes greater than 60 mm [2]. The bulk density of steel media normally used for grinding reasonably hard ores are:

Balls   4650 kg/m^3
Cylpebs   4700 kg/m^3
Rods   6247 kg/m^3
Cubes   5500 kg/m^3

For softer ores, ceramic balls (90% Al_2O_3) may be used. Their bulk density is around 2200 kg/m^3.

7.2. Operation of Tubular Ball Mills

Tubular ball mills ride on steel tyres or are supported at both ends by trunnions. Girth gears bolted to the shell drive the mill through a pinion shaft from a prime mover drive. The prime movers are usually synchronous motors that operate through an air clutch or gear system. The girth gear is usually located at one end of the mill but depending on the manufacturer, could be located at other places. During rotation, a portion of the charge, (the ore plus the grinding media) is lifted along the perimeter of the shell and after exceeding the angle of repose, part of it slides down while part cascades down and drops to the toe of the shell thus imparting the

grinding and crushing actions (Fig. 7.1). According to Morrell [3], the size reduction is proportional to the ball mass and surface area and that:

Impact breakage $\quad \propto \quad M_B{}^3$
Attrition breakage $\quad \propto \quad 1/S_B$

where M_B is the ball mass and S_B is the ball surface area.

The energy of impact by the steel balls on the rock particles will depend on the height through which they fall and the angle at which impact occurs. The size reduction that follows will depend on:

1. The charge characteristics (mass, volume, hardness, density, size distribution),
2. The characteristics of the grinding media (mass, density, number, ball size distribution)
3. Speed of rotation of the mill
4. Slurry density when wet grinding is adopted

Quantitative estimations of these variables are considered in the following sections with respect to ball mills.

7.2.1. Charge Volume

It is important that the mill should not be overfilled or under filled with the charge. Over loading tends to accumulate fines at the toe of the mill, which results in a cushioning effect thus absorbing the impact, which causes breakage. When the loading of rock is low, excessive ball-to-ball contact again retards the rate of breakage. The operator therefore has to compute the optimum quantity of each constituent to obtain the required product size and to maintain the predetermined output rate while maximising energy efficiency.

The percent of mill volume occupied by the charged material is a function of the bulk volume of the rock and balls. The percent of the mill volume occupied by rock, V_R, will be:

$$V_R = \frac{(\text{Mass of ore} / \text{density of ore})}{\text{Mill volume}} \times 100 \tag{7.1}$$

$$= \frac{\text{Volume of ore}}{\text{Mill volume}} \times 100$$

and the percent mill volume occupied by the grinding media (balls), V_B, will similarly be:

$$V_B = \frac{(\text{Mass of grinding balls} / \text{density of ball material})}{\text{Mill volume}} \times 100 \tag{7.2}$$

$$= \frac{\text{Volume of grinding balls}}{\text{Mill volume}} \times 100$$

Thus if the porosity of the bed containing crushed rock and crushing medium (balls) is φ then:

$$J_R = \frac{\text{Mass of rock/density of rock}}{\text{Mill volume}} \times \frac{1}{1-\varphi} \qquad (7.3)$$

and the fraction of mill volume occupied by the ball charge is:

$$J_B = \frac{\text{Mass of balls/density of balls}}{\text{Mill volume}} \times \frac{1}{1-\varphi} \qquad (7.4)$$

where J_R =   the fraction of the mill volume occupied by the bulk rock charge and

        J_B =   the fraction of the mill volume occupied by the bulk ball charge.

If the masses of the rocks and balls were M_R and M_B respectively and V_M the internal volume of the mill, then the fractional volume of mill occupied by the bulk rock and grinding media will be:

$$J_R = \frac{M_R / \rho_S}{V_M} \times \frac{1}{1-\varphi} \qquad (7.5)$$

$$J_B = \frac{M_B / \rho_B}{V_M} \times \frac{1}{1-\varphi} \qquad (7.6)$$

The maximum possible porosity of the bed is approximately 40% (corresponding to a bulk density of 4.65 for steel balls), but 30 – 40% bed porosity is common. For a closely packed eqi-sized ball charge, the minimum bed porosity would be 26%. In practice, the preferred ratio of $J_R/J_B \approx 0.4$ and the volume fraction of voids between balls at rest, occupied by rock, ranges between 0.6 to 1.1 [4]. The fraction of void space between the balls in the ball charge filled by rock, when the mill is at rest, is given by the ratio of $J_R/(J_B \varphi) = U$ [5].

Normally the bulk rock occupies 20-25% of the mill volume and the balls in a ball mill occupy the remaining charge volume during dry grinding. During wet grinding the slurry occupies the remaining volume after the balls have been charged.

7.2.2. Charge Height

Measurement of the charge height within a mill is a convenient method to estimate the charge volume. As a general rule:

1.   For over-flow ball mills the charge should not exceed 45% of the mill volume,
2.   For grate discharge mills the charge should occupy about 50% of the mill volume.

Fig. 7.3 illustrates a ball mill at rest charged with rocks and grinding balls. Bond [6] has measured the height, H_C, for a number of fillings and obtained a statistical relationship:

$$\text{Charge \%} = 113 - (63 \, H_C/R) \qquad (7.7)$$

where H_C =   vertical charge height from the ball level to the inside liner at the mill centre

            and R the inside radius of the mill (Fig. 7.3).

However, Morrell [7] demonstrated that large errors could be encountered with Eq. (7.7) for small ball charges, less than about 20%.

While the charge height and therefore the volume occupied can easily be measured as shown in Fig. 7.3, it can be convenient in some cases to measure the charge height from dimensions shown in Fig. 7.4.

In this case the bed height, H_B, is taken from the bottom of the mill. This height will be given by:

$$H_B = R(1 - \cos\theta) \tag{7.8}$$

$$\text{and } W = 2R\sin\theta \tag{7.9}$$

As it is difficult to measure the angle θ in practice, it is more convenient to eliminate it from Eqs. (7.8) and (7.9). The bed height can then be written in terms of radius R and width, W, of the charge in the mill as:
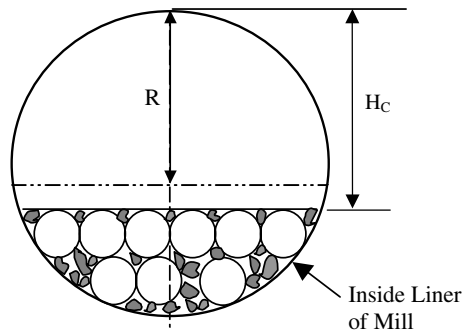
Fig. 7.3. Ball and charge height.
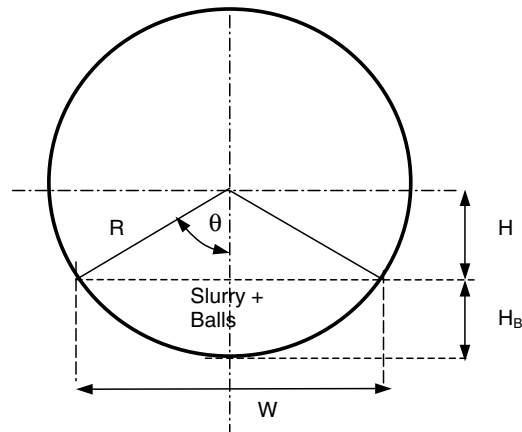
Fig. 7.4. Measurement of bed depth

$$R = 0.5\,H_B + 0.125\,W^2/H_B \tag{7.10}$$

The fraction of mill volume occupied by the charge can also be calculated from the cross-sectional areas of the charge and the mill. An approximation of the cross sectional area of the mill charge, A_C, (segment of a circle) will be [8]:

$$A_C \approx \frac{H_B}{6\,W}\left(3\,H_B{}^2 + 4\,W^2\right) \tag{7.11}$$

Since the cross sectional area of the mill is $\pi\,R^2$, the volume fraction filled by the charge would be:

$$\begin{aligned} J_B &= \frac{A_C}{\pi\,R^2} \\ &= \frac{H_B}{6\,W}\left(3\,H_B{}^2 + 4\,W^2\right)\cdot\frac{1}{\pi\,R^2} \end{aligned} \tag{7.12}$$

From simple geometry, the segment of a circle is also given by the equation:

$$A_C = R^2 \cos^{-1}\!\left(\frac{H}{R}\right) - H\sqrt{R^2 - H^2} \tag{7.13}$$

and from the simple relationships from Figs. (7.3) and (7.4):

$$H_C = R + H = D - H_B$$

$$H = R - H_B \text{ and}$$

$$W = 2\sqrt{R^2 - H^2} \tag{7.14}$$

The ball mill filling can be estimated from the geometry of the ball charge at rest. However, in terms of the angle θ, ball filling (J_B) may also be computed as indicated by Austin et al [5]. These relationships are illustrated in Fig. 7.5. The charge centre of gravity may also be located in a similar graphical way as shown in Fig. 7.6. H_{cog} is the distance from the centre of the mill to the charge centre of gravity.

7.2.3. Ball size at Initial Ball Charge

Ball sizes commercially available for charging in grinding mills range from 10 – 150 mm. The number, size and mass of each ball size used depend on the mill load and whether the balls are being charged for the first time to commence an operation or as replacements for worn out balls.

In determining the size of balls to be charged to commence a milling process, Coghill and De Vaney [10] indicated that the initial ball size was related to the maximum size of the feed. Empirically they related the ball size with feed size by the equation:
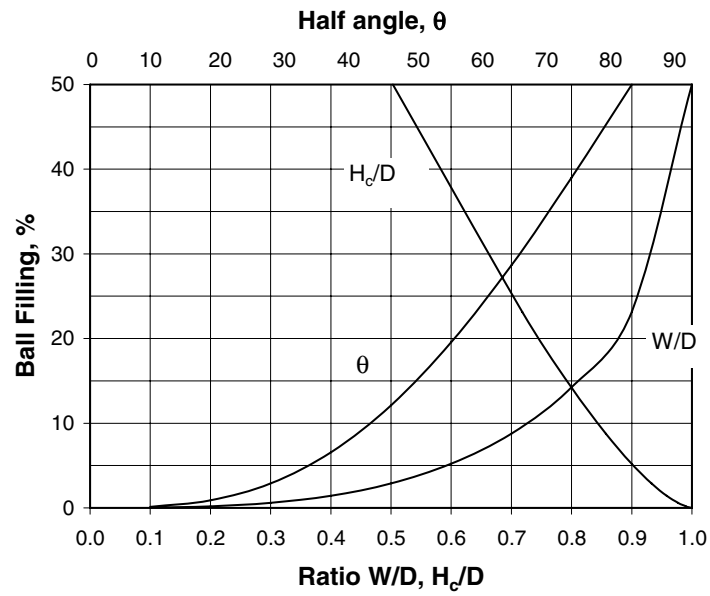
Fig. 7.5. Relation between ball filling (%) and mill charge dimensions [5].
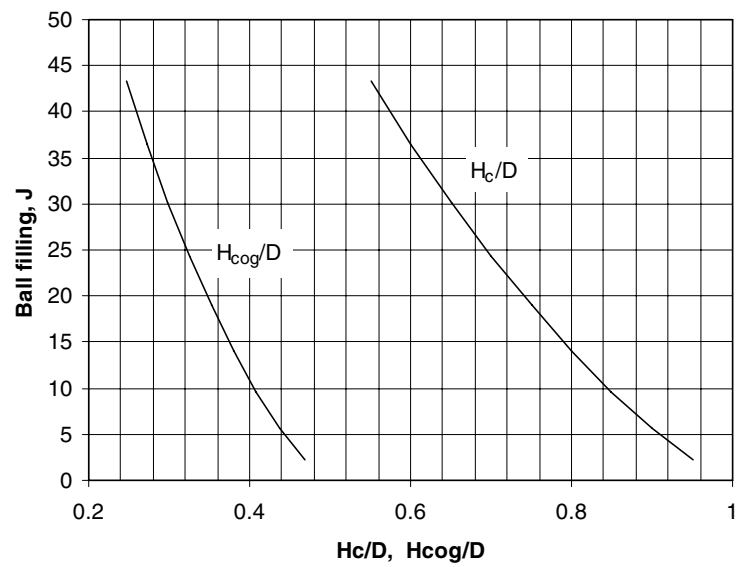
Fig. 7.6. Estimation of the centre of gravity of the charge for a given ball charge, J, [9].

$$d_B = 0.4\,K\,\sqrt{F} \qquad\qquad\qquad (7.15)$$

where   F   = the feed size, cm,
　　　　 d_B = the ball diameter, cm and
　　　　 K   = a proportionality constant described as the grindability factor.

For hard ores the value of K was 37.4 and 29.8 for soft ores. Lawrison [11] gave a value of 55 for chert and 35 for dolomite. The grindability factor, K, incorporates important operating variables. These operating variables were identified for the feed as:

1.   Work index
2.   Largest particle size and size distribution
3.   S.G. of the solids and slurry density

and for the mill:

1.   Mill diameter
2.   Speed of rotation (fraction of the Critical Speed)

Rowland and Kjos [2] considered these variables for determining the largest ball size that should be used to commence grinding. Thus if d_B is the ball diameter (mm), W_i, the work index of the material (kWh/t), F_{80} the feed size (80% passing size in microns) and ϕ_C the fraction of the critical speed of the mill, then the largest size of the ball may be estimated by [12]:

$$d_B = 25.4 \left[\left(\frac{F_{80}}{k}\right)^{0.5} \left(\frac{\rho_S\,W_i}{100\,\phi_C\,(3.281D)^{0.5}}\right)^{0.33} \right] \text{ in mm} \qquad (7.16)$$

where   D   = the inside diameter of the mill (m) and
　　　　 k   = a constant designated as the mill factor.

For steel or cast iron balls the value of the constant k is dependant on the mill type and the grinding circuit. The values of k as determined by Rowlands and Kjos [2] for Allis Chalmers mills are given in Table 7.2.

Table 7.2
Ball Mill k factor [2].

Mill Type	Wet/Dry Grinding	Circuit	k
Over flow	Wet	Open	350
Over flow	Wet	Closed	350
Diaphragm	Wet	Open	330
Diaphragm	Wet	Closed	330
Diaphragm	Dry	Open	335
Diaphragm	Dry	Closed	335

For calculation of the diameter of cylpebs, d_C, to use as a replacement for balls, Doering International [13] provides a modified Bond formula:

$$d_C = 18.15 \left[\left(\frac{F_{80}}{k} \right)^{0.5} \left(\frac{\rho_s \, W_i}{100 \, \phi_C \, (D)^{0.5}} \right)^{0.33} \right] \text{ in mm} \qquad (7.17)$$

The use of Eq. (7.16) and (7.17) is illustrated in Example 7.1.

If the media size formulae estimate a ball size less than 25 mm or a cylpeb size less than 22 x 22 mm then it is recommended that the size be increased by 20-30% [13].

Example 7.1

The size analysis of a gold bearing ore crushed in a jaw crusher indicated that 80 % passed through a 2000 micron sieve. Further size reduction was completed in a 1.0 x 1.5 m wet ball mill rotating at 78 % of the critical speed to liberate the gold. Determine the maximum size of the balls at the commencement of grinding.

Data: S.G. of the ore = 3.86.

Solution

Step 1
In this case as the work index and ball mill conditions are unknown we refer to the Appendix and find that the work index of a gold ore is typically 14.83 kWh/t.

Step 2
To determine the maximum ball size to be charged to grind the ore Eq. (7.16) may be applied, as all the relevant parameters are now known. Therefore substituting in Eq. (7.16) the largest diameter of grinding balls that should be added under wet open circuit condition of grinding is:

$$d_B = 25.4 \left(\frac{2000}{350} \right)^{0.5} \left[\frac{3.86 \times 14.8}{78 \times (3.281 \times 1.0)^{0.5}} \right]^{0.33}$$

$$= 25.4 \times 2.39 \times 0.739$$

$$= 45 \text{ mm}$$

The nearest commercial ball size available is 51.8 mm (or 2.0") and would be used.
If Coghill and de Vaney's equation is used, assuming a moderately soft ore with a value of K = 35, then:

$$d_B = 0.4 \, K \sqrt{F} = 0.4 \times 35 \times (0.2)^{0.5} = 63 \text{ mm}$$

For cylpebs as a replacement for balls, using Eq. (7.17):

$$d_C = 18.15 \left(\frac{2000}{350} \right)^{0.5} \left[\frac{3.86 \times 14.8}{78 \times 1^{0.5}} \right]^{0.33} = 39 \text{ mm}$$

A 40 x 40 mm cylpeb would be selected.

7.2.4. Ball Size as Replacement

During mill operation, grinding balls wear and are reduced in size. In so doing the grinding characteristics change. The extent of wear would depend on the characteristics of the rock present, such as surface hardness, density and composition. The abrasive action on the surface of the balls increases with time. Ball wear and its effect on grinding have been studied extensively over the years [14-18]. The study has been conducted by:

1. Measuring the change in dimension, (i.e. diameter) of the ball and
2. Measuring the change in ball mass.

As a general rule, the wear on balls is directly proportional to the surface area/unit mass and hence inversely proportional to the ball diameter.

The extent of wear on the grinding balls depends mainly on the abrasive nature of the rock and also by mutual attrition. Other factors affecting abrasion of the grinding media are:

1. Speed of mill rotation
2. Mill diameter
3. S.G. of the mineral
4. Work Index of the mineral

Bond [14] measured the wear on the grinding media in terms of the mass loss per unit of energy input to the grinding mill. According to Bond, the average mass losses for wet and dry mills are:

Wet Ball Mill   kg/kWh   = $0.16 \, (A_i - 0.015)^{0.33}$ (7.18)

Dry Ball Mill   kg/kWh   = $0.023 \, A_i^{0.5}$ (7.19)

where A_i =   Abrasion Index.

Rowland and Kjos [2] use a constant of 0.175 in Eq. (7.18) instead of 0.16. The abrasion index of selected minerals is given in the Appendix (Table A-2).

To maintain the grind, the worn balls have to be replaced. The rule of thumb is to add the largest size of ball charged initially at the commencement of operations. Bond [6] and Rowland and Kjos [2] considered the factors affecting abrasion and suggested that the diameter of the replacement ball can be expressed by Eq. (7.16).

Rowland and Kjos [2] recommend Eq. (7.16) for calculating the size of replacement balls as well as for the initial charge.

Azzaroni [19] and Dunn [20] reported that the size of the make up balls could be more conveniently expressed by the simple equation:

$$d_B = \frac{6.3 \, (F_{80})^{0.29} \, (W_i)^{0.4}}{(v \, D)^{0.25}} \quad \text{in mm} \tag{7.20}$$

Eqs. (7.16) and (7.20) provide more or less similar results. This is illustrated in Example 7.2.

Example 7.2

A mineral of S.G. 2.4 was crushed and the average product size of the largest fraction was 6.25 mm. It was fed to a wet overflow ball mill of I.D. 1.5 m and ground in closed circuit at 75% of the critical speed. The work index of the mineral was 12.8 kWh/t. Estimate the largest size of make up ball that should be used.

Solution

To estimate the largest size of replacement balls we shall compare results produced by Bond with that of Azzaroni.

Step 1
The critical speed is given by Eq. (7.38):

$$v_C = \frac{42.3}{\sqrt{D-d}} \quad \text{rpm}$$

where D = the inner diameter of the mill (in meters) and
       d = the size of the grinding balls in meters.

As d is very small compared to the diameter of the mill we shall ignore d and determine v_C thus:

$$v_C = \frac{42.3}{\sqrt{1.5}} = 34.5 \text{ rpm}$$

Step 2
Since the grinding was carried out in a wet overflow mill in closed circuit, the value of k should be taken as 350 (Table 7.2). Substituting data in Eq. (7.16) we get the replacement size of grinding balls as:

$$d_B = 25.4 \left[\frac{6250}{350}\right]^{0.5} \left[\frac{2.4 \times 12.8}{75 \, (3.281 \times 1.5)^{0.5}}\right]^{0.33} = 61 \text{ mm}$$

Step 3
According to Azzaroni's Eq. (7.20), the replacement diameter of ball would be:

$$d_B = \frac{6.3 \ (6250)^{0.29} \ (12.8)^{0.4}}{\left(\dfrac{34.5 \times 75}{100} \times 1.5\right)^{0.25}} = 88 \text{ mm}$$

The closest sizes of commercial balls made are 90 mm and 76 mm. The operator will probably choose the larger size ball.

7.2.5. Ball Wear

During a mill operation, lowering of the power requirement is an indication that ball wear is affecting product quality. The phenomenon of ball wear is complicated as it is affected not only by mill speed, mill diameter, S.G. of the ore and work index, but also by liner type, ball hardness, the forces acting within the mills and the pH of the slurry when wet grinding takes place. The extent of wear could be of the order of 400 to 1200 grams per tonne or more of material milled [21]. A general observation is that for every 1 % change in mill speed the change in ball consumption is about 2 %.

During the grinding process, as the particle sizes diminish, the specific surface area of the particles increases and the diameter of the ball diminishes with ball mass. The ball wear laws can therefore be stated as:

Ball wear $\propto$ Ball surface area [14],
Ball wear $\propto$ Ball Volume [22].

Austin and Klimpel [17] extended the empirical relations of Bond [6,14] and Rowland [23] by giving a theoretical basis to the relation between the cumulative mass fractions of balls charged with their wear. To derive the expression they assumed:

1.   Ball wear was equal to the loss in ball mass,
2.   Ball wear was a function of ball size,
3.   Fresh balls replacing the worn balls had the same characteristics.

Using this concept they determined the change in the entire size distribution of balls charged in a grinding system. According to Austin et al [5], the change in the cumulative mass fraction of balls in the charge due to wear is:

$$\frac{dM_r}{dr} = m_T \, K \, 4\pi \rho_b \frac{[1-n(r)] r^5}{f(r)} \tag{7.21}$$

where M_r = Cumulative mass fraction of balls of size r in the charge,
        m_T = Mass rate of replacement balls per unit mass of balls,
        $n(r)$ = Cumulative number size distribution of ball size, radius r,
        $f(r)$ = ball wear rate, a function of ball radius,

$$\rho_b \quad = \text{S.G. of the balls.}$$

To evaluate Eq. (7.21), the following method was adopted:

1. The term K was defined as: $\quad K = \displaystyle\int_{r_{MIN}}^{r_{MAX}} \frac{1}{r^3} \, dm(r)$ (7.22)

where $\quad m(r) = $ the cumulative mass fraction of balls less than size r in the make up charge

2. The make up balls sizes were considered such that the size $r_{MAX} = r_1 > r_2 > ... > r_k > ... > r_m \geq r_{MIN}$, and

$$K = \sum_k \frac{m_k}{r_k^3}$$ (7.23)

where $\quad m_k = $ mass fraction of makeup balls of size r_k

3. For the make up ball numbers, $n_1 > n_2 > ... > n_k$, so that the number distribution of balls of size r_k is:

$$n_k = \left(\frac{m_k}{r_k^3} \frac{1}{K} \right)$$ (7.24)

4. $f(r)$, was considered a power function of $r^{(2+\Delta)}$, that is:

$$f(r) = \kappa \, 4 \pi \rho_b \, r^{(2+\Delta)}$$ (7.25)

where Δ could have either a positive or negative value, and κ was equal to the wear distance per unit time. Eq. (7.25) can be re-written as:

$$f(r) = [4 \pi \rho_b \, r^2] \, \kappa \, r^{\Delta}$$ (7.26)

The wear rate could also be written as:

$$f(r) = -\frac{dr}{dt}\left[\frac{4}{3} \pi \, \rho_b \, r^3 \right]$$

hence: $\quad f(r) = -\left(\dfrac{4 \pi \rho_b}{3} \right) \dfrac{dr^3}{dt} = \kappa \, 4 \pi \rho_b \, r^{(2+\Delta)}$

or, $\quad f(r) = -\left(4 \pi r^2 \rho_b\right)\dfrac{dr}{dt}$ (7.27)

and $\quad -\left(\dfrac{dr}{dt} \right) = \kappa \, r^{\Delta}$ (7.28)

Substituting Eqs. (7.25), (7.27) and (7.28) in Eq. (7.21) the final equation relating to the cumulative mass fraction of balls in the charge was derived as:

$$M_r = \left(\frac{m_T \ K}{\kappa}\right) \int_{r_{MIN}}^{r_{MAX}} [1 - n(r)] r^{3-\Delta} \ dr \qquad (7.29)$$

To solve the equation, the value of Δ was obtained by trial and error. Eq. (7.29) can be applied when only one ball size is charged. The usual practice is to replace the largest size only. In such a case the ball size distribution considered in Eq. (7.29) is absent, so that the value of $n(r) = 0$ at $r < r_{MAX}$. Eq. (7.29) then simplifies to:

$$M_r = \frac{m_T \ K}{(4-\Delta)\kappa} \left[r_{MAX}^{4-\Delta} - r_{MIN}^{4-\Delta} \right] \qquad (7.30)$$

The value of Δ has been found to range from $0 - 2$ depending on the mill. Substituting the appropriate value of Δ (determined by trial and error) for a particular mill condition, the cumulative mass fraction of ball to be initially charged may be computed.

Eq. (7.30) may be used to estimate the mass rate of make up balls per unit time when one size of ball of maximum size is replaced. In this case; $M_r = 1$. Also, for the same condition, Eq. (7.22) may be integrated to give:

$$K = \frac{1}{r_{MAX}^3} \qquad (7.31)$$

Substituting the value of K in Eq. (7.30) and simplifying:

$$1 = \frac{m_T}{r_{MAX}^3} \ \frac{1}{(4-\Delta)\kappa} \left[r_{MAX}^{4-\Delta} - r_{MIN}^{4-\Delta} \right] \qquad (7.32)$$

The mass rate of make-up per unit mass of balls can now be written as:

$$m_T = \frac{r_{MAX}^3 \ (4-\Delta)\kappa}{\left(r_{MAX}^{4-\Delta} - r_{MIN}^{4-\Delta} \right)} \qquad (7.33)$$

Using the value of Δ and the initial size of the ball (r_0), the size of ball after a time was derived by integrating Eq. (7.27):

$$\left[\frac{r}{r_0} \right]^{1-\Delta} = 1 - \frac{(1-\Delta) \ \kappa \ t}{r_0^{1-\Delta}} \qquad (7.34)$$

Austin has indicated that this concept can successfully be applied in industrial practice.

7.2.6. Ball Bulk Density

To grind and reduce the size of brittle and soft minerals a grinding media of low density can be used while for hard ores like that of gold or taconite, hard steel balls are required. The greater the density and hardness difference between the grinding media and the rock the more efficient would be the grinding operation. It is therefore necessary to use the appropriate density of grinding media for a particular ore type.

Rose and Sullivan [24] suggested that the bulk density (ρ_B) of the balls that are used as a grinding medium could be determined by the relation:

$$\rho_B = (0.016\,\rho_M{}^2 + 20\,\rho_M)^{0.5} - 0.4\,\rho_M \tag{7.35}$$

where ρ_M = bulk density of material whose size reduction is required.

For example if the bulk density of the ore was 1.41 t/m^3, then :

$$\rho_B = (0.016 \times 1.988 + 20 \times 1.41)^{0.5} - 0.4 \times 1.41 = 4.75 \ \text{t/m}^3$$

That is, the bulk density of the grinding medium should be 4.75 t/m^3.

Cast iron and steel balls are normally used in the mineral industry for relatively hard ores. For softer ores, pebbles can be used and for soft and friable ores no grinding medium may be required at all as in Autogenous grinding.

The bulk S.G. of cast iron and steel balls are:

Cast iron   =   4.3 – 4.8 t/m^3
Forged Steel =   4.6 – 4.8 t/m^3

For durability and less wear, tungsten-carbide (94% WC + 6% Co) balls have been used for very hard and abrasive ores. These balls have a S.G. value of about 14.9 t/m^3. For softer ores, ceramic balls made of 90 % Al$_2$O$_3$ and S.G. 3.6 t/m^3 are preferred.

7.2.7. Ball Size Distribution

In practice, at mill startup, instead of charging a single size of ball, usually a range of ball sizes is initially added. In so doing the space between the balls is filled with smaller sized balls, which promotes grinding efficiency. Options of ball size distributions are to some extent determined by experience.

During the grinding operation, the object is to hold an equilibrium charge where the rate of addition of the number and mass of balls equals the rate at which the number of balls are eroded and expelled from the mill plus the rate of loss in mass of balls due to abrasion and wear. That is, the grinding conditions remain constant. The initial charge should therefore be as near as possible to the equilibrium charge. Bond [12] determined the equilibrium charge for different ball sizes commercially available by assuming that the rate of wear and loss in mass of all balls were the same. Bond then established an equilibrium line with a slope of 3.84 passing through the point representing the 100 % passing size of the make up ball. The mid points between each size of commercially available ball sizes is plotted on the x-axis of log-log graph paper and a vertical line drawn from each mid point to determine the points of intersection with the equilibrium line. The equilibrium charge size is then read off the y-axis against each size range. Bond's results are tabulated in Table 7.3.

Table 7.3
Equilibrium Ball Size at commencement of grinding [23].

Top Ball Size, mm	Distribution % mass							
	114	101	89	76	63.5	51	38	25.4
114	23.0							
101	31.0	23.0						
89	18.0	34.0	24.0					
76	15.0	21.0	38.0	31.0				
63.5	7.0	12.0	20.5	39.0	34.0			
51	3.8	6.5	11.5	19.0	43.0	40.0		
38	1.7	2.5	4.5	8.0	17.0	45.0	51.0	
25.4	0.5	1.0	1.5	3.0	6.0	15.0	49.0	100
	100	100	100	100	100	100	100	100

The table indicates the initial ball charge when make up balls of stipulated sizes have to be charged. Based on the equilibrium charge, the ball sizes can be computed for a particular charge. The steps to be followed are illustrated in Table 7.4. The method followed here is an adaptation of that advocated by Taggart [25], which should be consulted for details.

Assume that a mill is charged with a feed whose size distribution is given by columns (1) and (2) in Table 7.4, then calculate the ball size following the steps indicated in Tables 7.3 and 7.4.

Step 1
If sieve sizes and masses retained between sieves are given then determine the geometric mean of the size intervals and calculate the cumulative percent size retained.

Step 2 for Column (3)
Start with the largest size of the feed, here it is 2%. Take this as factor $= 1.29^0 = 1.0$
Then the factor for the next size $= 1.29^1 = 1.29$
Then the factor for next lower size $= 1.29^2 = 1.66$
Again the factor for the following size $= 1.29^3 = 2.15$
and so on for the last value of 1.29^n where n = the number of sieves used in the sieve analysis $- 1$.
Here n = 14

Step 3 for Column (4) - Optimum charge, % Retained
Multiply Column (2) by Column (3) till the product is equal to or just less than 100.
Here at size 5, the product of column (2) x (3) = 149.5 which is greater than 100 and therefore rejected.

Step 4 for column (5)
The daily feed charge to retain equilibrium is approximately equal to the optimum charge.
Divide the % largest size ball in the optimum charge (column (4)) by the percent of this charge found in the equilibrium charge, which is obtained by the constant feed of the largest charge, given in Table 7.3. In this case: 2/23 = 0.87.

Table 7.4
Computation of Ball Size Distribution [25].

Size, mm	Feed Cum % Retained	Factor F*	Optimum Ball charge Cum. % Retained	Daily Feed Ball Size ,mm		Equilibrium Ball charge, % Cum Retained
(1)	(2)	(3) 1.29^n	(4) (2) x (3)	(5) 114 mm 87.0%	(6) 63.5mm 13.0%	(7) (5)+(6)
8.6	2.00	1	2.0	20.1		20.1
4.2	6.0	1.29	7.7	47.1		47.1
1.7	14.0	1.66	23.3	62.7		62.7
0.35	26.0	2.15	55.8	75.4		75.4
0.19	54.0	2.77	149.5**	81.8	4.42	86.2
0.11	70.0	3.57		85.1	10.0	95.1
4.8	90.0	4.61		86.5	12.2	98.7
3.4	95.0	5.94		87.0	13.0	100.0
2.4	100.0	7.67				
1.7	48.7	9.89				
1.2	51.5	12.76				
0.850	53.7	16.46				
0.600	56.4	21.24				
0.425	80.3	27.39				
0.075	93.1	-				

* The factor F is derived from the ratio of cum % of a given ball size to corresponding cum.% size of feed. For largest size the factor =1. For subsequent sizes multiply by 1.29^n where n equals 1,2,3, ... n
** > 100

Thus 87% will be 114 mm balls and the rest will make up to 13%.
Next multiply column (2), Table 7.3, by 0.87 for each top ball size and accumulating the feed ball size distribution recorded in column 5. That is:

23 x 0.87   = 20.1
(31 x 0.87) + 20.1 = 47.1
(18 x 0.87) + 47.1 = 62.7
and so on.

When the cumulative optimum ball charge is > 100, it has obviously to be rejected.

Step 5   for column (6)
The remainder (13%) of the balls have a maximum size of 63.5 mm.
To compute the feed size distribution of balls having this maximum size the computation indicated in step 4 is repeated with the multiplying factor of 0.13. Thus column (6) is now calculated as:

34 x 0.13   = 4.42
(43 x 0.13) + 4.42   = 10.0

(17 x 0.13) +10.0   =   12.2
(6.6 x 0.13) + 12.2   =   13.0

Step 6   Calculation of equilibrium ball charge, % cumulative retained
The sum of columns (5) and (6) gives the equilibrium ball charge per cent cumulative retained and is given in column (7). This is then translated to the nearest ball sizes commercially available.

7.2.8. Mill Rotation and Critical Speed

Initially when the speed of rotation of mills are increased the grinding action increases and so does the mill throughput. But when the speed is greater than a certain value, the charge together with the grinding media tend to cling to the inner wall when neither cataracting nor cascading takes place and the charge centrifuges. In such as case the grinding action is considerably reduced or completely stopped and the power required to turn the mill drops drastically. The speed at which the maximum power in a mill can be drawn is therefore critical and the speed at which the charge centrifuges is known as the *Critical Speed*. All mills have to be rotated at speeds less than the critical speed, for grinding to take place.

To determine the critical speed (v_C) it is necessary to know the diameter of the mill, D, and the diameter, d, of the largest ball (or rod) present as the grinding medium. Fig. 7.7 shows the equilibrium forces on a ball held at position A against the mill liner during the rotation of the mill.
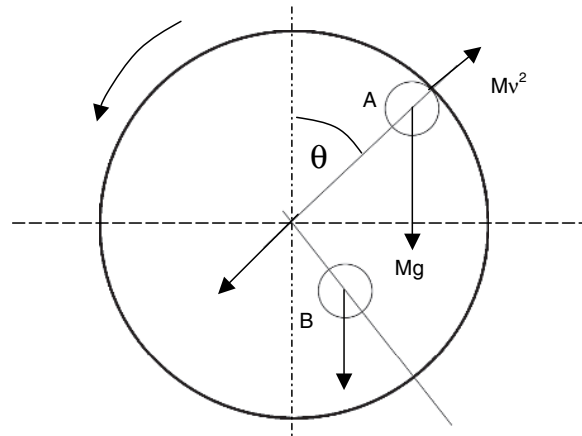
Fig. 7.7. Equilibrium forces on a ball held against the mill liner due to the mill rotation.

At position A the ball is held against the shell wall with a force Mv^2 and it is assumed that no slip takes place between the ball and shell at equilibrium conditions. Position B denotes the centre of gravity of the entire load where the distribution of forces is similar to A but involves several unknown factors like the frictional forces. Due to the complexity of the distribution of forces we shall only consider position A where at equilibrium, the centripetal component of the force due to gravity, $Mg \cos\theta$, equals the opposing centrifugal force $Mv^2/(R - r)$. That is:

$$Mg \cos \theta = \frac{Mv^2}{(R-r)} \quad \text{or}$$

$$\cos \theta = \frac{v^2}{(R-r)g} \tag{7.36}$$

where M = mass of the ball
       g = acceleration due to gravity (m/s^2)
       θ $\doteq$ angle that the ball subtends with the vertical
       v = linear velocity (m/s) of the ball, and
       R, r = radii of the mill and ball respectively.

At the rotational speed ω, $v = 2\pi(R-r)\omega/60$. Substituting this value of v in Eq. (7.36):

$$\cos \theta = \frac{[2\pi(R-r)\omega]^2}{9.81(R-r)60^2} \tag{7.37}$$

At $\theta = 0$, $\cos\theta = 1$, the force of gravity tending to pull the ball off the wall will be at a maximum and the speed required to overcome this force is known as the critical speed. Denoting the critical speed as v_C, we can replace the speed v with v_C and the radius of the path $(R - r)$ may be re-written as $(D - d)/2$. Substituting these values into Eq. (7.37), the critical speed will be given by:

$$v_C = \frac{42.3}{\sqrt{(D-d)}} \quad \text{revs/min} \tag{7.38}$$

for mill and ball diameters in meters.

In practice, friction between balls and the liner does occur. The friction coefficient decreases with:

1.   The smoothness of the liner,
2.   Fineness of the media,
3.   Pulp density and
4.   Abrasiveness of the material to be ground.

The coefficient of friction, μ, may be determined using the relation:

$$\frac{(\text{Rotation of Shell/Unit time})}{\text{Critical Speed}} = \sqrt{\frac{1}{\mu}}$$

That is: $\mu = (v_C/v)^2$ \hfill (7.39)

The rule of thumb to modify the critical speed to suit dry and wet conditions of milling is:

1. For dry grinding, multiply by a factor 0.65
2. For wet grinding, multiply by a factor 0.70

Fig. 7.8 indicates that the above simplified consideration does not cover the entire charge profile (position B in Fig. 7.7) that is in motion within the tumbling mill particularly as the velocity of particles at the periphery and nearer the shell wall will be different from those nearer the centre.
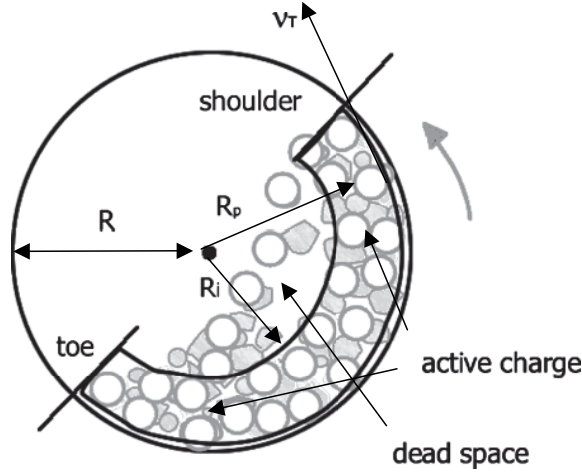
Fig. 7.8. Movement of the charge within a mill.

Napier-Munn et al [26] derived the rotational speed of a particle at a distance R_P from the centre as:

$$\omega_P = \left[\frac{v_N \, R \, (R_P - \zeta \, R_i)}{R_P (R - \zeta \, R_i)} \right] \qquad (7.40)$$

where v_N = the normalised tangential velocity = v_R / v_T,
    v_R, v_T = the tangential velocities at position R_P and the inside liner surface,
       R_P = the radial distance of any particle P located in the active region of the charge,
       R_i = the radial distance to the inner radius of the active charge in the mill.

The term ζ is a function of the volumetric filling of the mill, J_B, and is defined as:

$$\log \zeta = 0.4532 \log (1 - J_B) \qquad (7.41)$$

It can be seen that as J_B approaches 1, ω_P approaches v_N.

Fig. 7.9 is a plot of ζ for different values of J_B. It can be seen that as J_B increases, the value of ζ tends to a negligible value, and ω_P approaches the rotational speed of the mill.
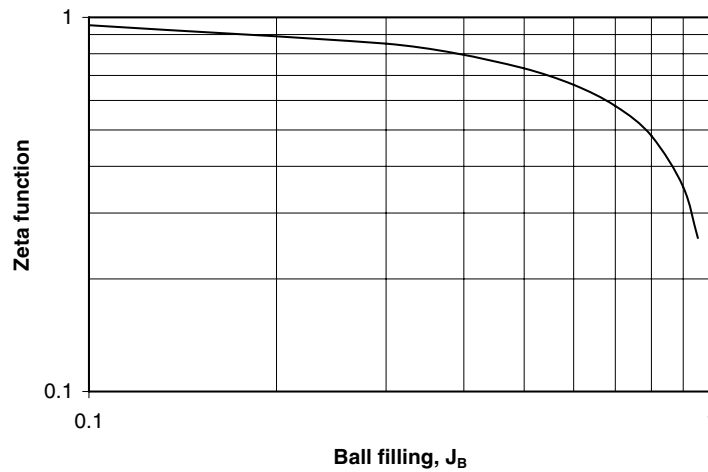
Fig. 7.9. Relation between J_B and ζ from Eq. (7.41).

7.2.9. Mill Conditions and Initial Ball Charge

The grinding actions at various percentages of the critical speed have been empirically and qualitatively described in Table 7.5 where the numbers 1, 2 and 3 indicate the degree of action in ascending order.

Table 7.6 provides a qualitative estimate of conditions inside the mill when different volumes of balls are charged at different speeds of rotation. The numbers 1, 2 and 3 again indicate the degree of action in ascending order.

Table 7.5
Effect of mill speed on grinding action [27]

% Critical Speed	Sliding	Cascading	Centrifuging
10	3	-	-
20	3	-	-
30	3	1	-
40	2	1	
50	2	1	1
60	2	2	1
70	1	3	3
80	1	3	2
90	-	2	3

Tables 7.5 and 7.6 indicate that the optimum conditions of grinding would be between 70-80 % of the critical speed and a ball charge of 35-45% of the mill volume. It is observed from these tables that the position of the charge in a mill depends on the speed of rotation.

184

Table 7.6
Effect of ball charge on grinding action [27].

Ball Charge % Mill Volume	Sliding (all speeds)	Cascading	Centrifuging
5-15	3	-	-
15-25	3	1 (higher speeds)	-
25-35	2	2 (higher speeds)	1(higher speeds)
35-45	1	3 (all speeds)	1(higher speeds)
45-50	1	2 (all speeds)	3 (all speeds)

The higher the speed of rotation, the relatively higher up the mill wall will be the top end (shoulder) and bottom end (toe) of the charge. Morrell [1] related the shoulder and toe positions of the charge with the critical speed. According to Morrell, if ϕ_c is the fraction of the critical speed and α_T and α_S the toe and shoulder angles (in radians) respectively with the horizontal, then the toe angle and shoulder angles can be related to the critical speed by:

$$\alpha_T = \frac{\pi}{2} + 2.5307(1.2769 - J_B)\left[1 - e^{-19.42(\phi - \phi_c)}\right] \quad \text{radians} \tag{7.42}$$

$$\alpha_S = \frac{\pi}{2} - \left(\alpha_T - \frac{\pi}{2}\right)\left((0.3386 + 0.1041\phi_c) + (1.54 - 2.5673\phi_c)J_B\right) \quad \text{radians} \tag{7.43}$$

where ϕ = ratio of experimental critical speed to the theoretical critical speed,

        ϕ_c = fraction of theoretical speed at which the mill is operated,

        J_B = fraction of ball filling of the mill.

For a given mill size, therefore, where the critical speed can be easily determined, by the use of Eq. (7.38), the shoulder and toe angles may be calculated at varying loads and speeds. Fig. 7.10 illustrates such a plot where the toe angle is plotted for different fractional values of the mill speed and the shoulder angle is also plotted against mill speed at corresponding toe angles. For this calculation a constant mill loading of 30 % and a mill size of 1.5 m x 1.5 m was considered under dry conditions of operation. Fig. 7.10 shows that the shoulder angle is likely to be less steep than the toe angle under operating conditions. This figure does not indicate the shoulder and toe angles under wet (slurry) conditions.

7.3. Estimation of Mill Capacity

The capacity of a ball mill depends on its dimensions, the type of mill (overflow or grate discharge), the speed at which the mill rotates, the mill loading, the product size required from a given feed size, the work index, the mill shaft power and specific gravity of the rock. Bond [6] considered these parameters and suggested that the relation between mill capacity and mill shaft power (P_M) was related to the energy required for size reduction, that is, the work index (W_i). Bond expressed the relation by an empirically derived equation:

$$Q = \frac{P_M}{E} \quad \text{t/h} \tag{7.44}$$
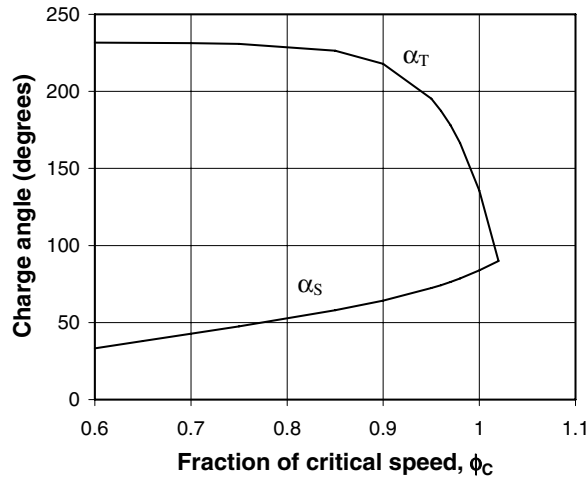
Fig. 7.10. Toe and shoulder angles calculated from Eqs. (7.42) and (7.43).

where P_M = the mill power in kW and
       E = the energy in kWh/t.

In deriving the value of P_M in Eq. (7.44), Bond considered the mill shaft power, the mill load, speed of rotation and the dimensions of the mill in the form:

$$P_M = 7.33 J_B \, \phi_C \left(1 - 0.937 J_B\right)\rho_b \, L D^{2.3} \left(1 - \frac{0.1}{2^{9-10\phi_c}}\right) \tag{7.45}$$

The mill capacity is then derived by dividing Eq. (7.45) with the energy term:

$$E = W_i \left(\frac{10}{\sqrt{P_{80}}} - \frac{10}{\sqrt{F_{80}}}\right) \tag{3.5}$$

In Chapter 3 the work index was described as a function of mineral and mill characteristics such as mineral particle size, moisture content, fineness of grind, reduction ratio, wet or dry operation and the method of charging. The W_i value has to be corrected for these variables to obtain a reasonable value of mill capacity for design purposes.

Austin et al [5] stated that a single expression does not adequately represent the capacity. They considered the capacities of mills greater than and less than 3.81 m in size separately and derived the mill capacities under the two conditions as:

1.   For a mill diameter < 3.81 m

$$Q = \frac{6.13\, D^{3.5}\left(\dfrac{L}{D}\right)\rho_b \left(J_B - 0.937 J_B^2\right)\left(\phi_C - \dfrac{0.1\phi_C}{2^{9-10\phi_C}}\right)}{C_F\, W_{i,TEST}\, 10\left(\dfrac{1}{\sqrt{P}} - \dfrac{1}{\sqrt{F}}\right)} \quad t/h \qquad (7.46)$$

2. For a mill diameter > 3.81 m

$$Q = \frac{8.01\, D^{3.3}\left(\dfrac{L}{D}\right)\rho_b \left(J_B - 0.937 J_B^2\right)\left(\phi_C - \dfrac{0.1\phi_C}{2^{9-10\phi_C}}\right)}{C_F\, W_{i,TEST}\, 10\left(\dfrac{1}{\sqrt{P}} - \dfrac{1}{\sqrt{F}}\right)} \quad t/h \qquad (7.47)$$

where: ρ_b = density of the media (7.9 t/m^3 for steel) and
C_F = a correction factor.

The correction factor, C_F, in Eqs. (7.46) and (7.47), includes all corrections that are required for the determination of W_i including:

1. Wet open circuit and wet closed circuit grinding,
2. Wet and dry grinding,
3. Over size feed and under size fine grinding.

Rowland and Kjos [28] however recommends the factor 6.3 for all ball mill capacities. The use of Eqs. (7.46) and (7.47) is illustrated in Example 7.3.

Example 7.3
A 3 x 3 m wet overflow ball mill in open circuit was charged with 38 tonnes of grinding media in the form of 101 mm diameter balls at a density of 7.9 t/m^3. The mill rotated at 21 rpm. The bed porosity of the material to be ground was 35 % and the work index of the material 13.7 kWh/t (wet grinding). The feed size was 80% passing 2.0 mm and the final product size expected was 80% passing 75 μm. Ignore errors and corrections due to oversize feed and undersize fineness of ground. Estimate:

1. Mill capacity for wet grinding
2. Mill capacity for dry grinding

Solution
Mill Capacity for Wet Grinding
Step 1
Since the mill size is less than 3.8 m, Eq. (7.46) is applicable:

The combined correction factor (C_F) is taken as = 1

Step 2
The critical speed is given by Eq. (7.38) as:

$$\nu_C = \frac{42.3}{\sqrt{3.0 - 0.101}} = 24.8 \text{ rpm}$$

therefore $\phi_C = 21/24.8 = 0.85$

Step 3
Mill capacity can now be computed by substituting data in the Eq. (7.46):

$$Q = \frac{6.13 \times 3.0^{3.5}\left(\frac{3.0}{3.0}\right)7.9\left(0.35 - (0.937 \times 0.35^2)\right)\left(0.85 - \frac{0.1 \times 0.85}{2^{9-(10 \times 0.85)}}\right)}{1 \times 13.7 \times 10\left(\frac{1}{\sqrt{75}} - \frac{1}{\sqrt{20000}}\right)}$$

$$= 28.3 \text{ t /h}$$

Mill Capacity for Dry grinding

To obtain dry grinding Work Index from Wet Grinding Index multiply W_{iWET} by 1.3
In this case therefore, the work index for dry grinding = 13.7 x 1.3 = 17.8 kWh/t
Substituting this value for W_i, in Eq. (7.46):

Q (dry grinding) = 21.8 t/h.

Eqs. (7.46) and (7.47) can help an operator to control mill productivity. For example, consider a mill of diameter 3.5 m and L/D ratio of 1.1. The mill is charged to 35% of its volume with rock, having a $W_{i, TEST}$ value of 12.5 kWh/t. The steel balls used as grinding medium had a S.G. of 7.9 t/m^3. Initially the feed size (F_{80}) was 12,000 microns when the mill produced a product having a P_{80} value of 500 microns. A finer product size was required for down stream operation, but the feed particle sizes changed due to a change in mine operations. Examine the change in mill capacity, all others factors remaining the same.

As the mill size is less than 3.81 meters, Eq. (7.46) can be used to evaluate the mill capacity. If the required product size decreased to 250 microns, then to 125 microns and further to 65 microns, then Fig. 7.11 is drawn using Eq. (7.46) to determine the change in mill capacity with a change in feed size. Fig. 7.12 similarly is drawn to illustrate the effect on capacity due to changing demands of product size while the feed size remained unchanged.

7.4. Mill Power Draw-Mechanical Methods
The motor power required to turn a mill from rest to the operating speed is designed to include the initial starting torque and mechanical arrangements to rotate the mill. Attempts to

188
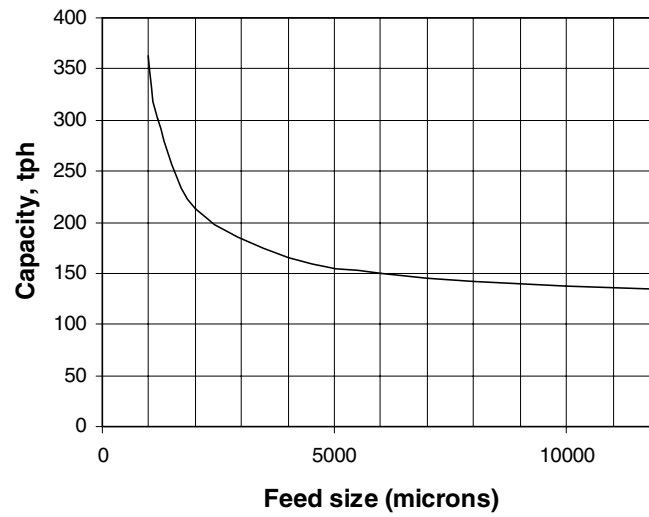
Fig. 7.11. Effect of feed size on ball mill capacity according to Eq. (7.46) for a mill diameter less than 3.81 m.
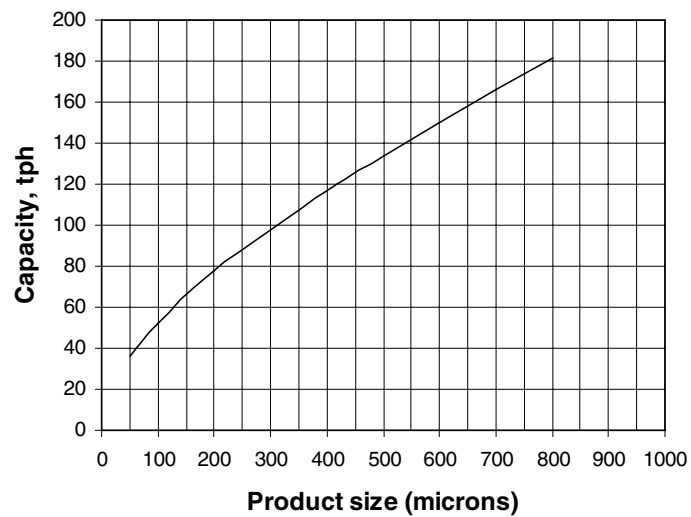
Fig. 7.12. Effect of product size on ball mill capacity according to Eq. (7.46) for a mill diameter less than 3.81 m.

determine the power draw have been either by measuring the energy required to lift the charge till it cascades, or by determining the forces required by the charge to overcome the frictional forces between the charge and the inner surface of the mill and equating it with the forces required to turn the charge round the centre of the mill. Both the approaches are discussed later. However, it is generally accepted from practical experience that the mill power (P_M) is a function of mill capacity and diameter, or more precisely by [5]:

$$P_M = \text{Mill Capacity} \times (\text{Diameter})^n \tag{7.48}$$

where the value of n ranges between 0.3 and 0.5.

It can be easily seen that the energy required for size reduction will be an integral part of the power requirement and therefore mill power can also be written as:

$$P_M = W_i \ \text{Capacity} \tag{7.49}$$

If it is assumed that the mean height through which the balls are lifted and fall are the same for all balls and the length of the mill is considered such that the end effects are negligible, then according to Austin et al [5] for a mill of length L and diameter D loaded with balls of density ρ_b, the mill power could be computed from the expression:

$$P_M = K \ \rho_b \ L \ D^{2.5} \tag{7.50}$$

where K is the proportionality constant. Later workers like Morrell [7], have shown that K is constant only at lower ball loadings.

Power draw during grinding is one of the most important items in the operation of grinding mills. More accurate estimations have been attempted from data observed in the laboratories and also in commercial operations. These attempts are described here as mechanical methods as opposed to theoretical methods involving basics physical laws.

In the following sections some generally accepted mechanical methods for computing mill power are described.

7.4.1. Rose and Sullivan Method

Rose and Sullivan [29] theoretically derived the power required by mills by assuming that the power drawn was proportional to the fraction of critical speed, ϕ_C, and that the rock particles travel in the same manner as the balls. In deriving their expression they also assumed that the porosity of the charge (balls plus crushed rock) was equal to 0.4. The final mill power for dry grinding was derived as:

$$P_M = 1.12 \times 10^{-3} \left(D^{2.5} \ L \rho_b \right) \left(1 + \frac{0.4 \rho_S \ U}{\rho_b} \right) \phi_C \ f(J_B) \tag{7.51}$$

where ρ_S = density of the solid material,
  U = fraction of space between balls at rest that is filled with solid rock,
  P_M = mill power in kW for L and D in meters and ρ_b in kg/m^3
  $f(J_B)$ = a function of ball loading, J_B.

The expression is valid when the mill speed is less than 80% of the critical speed. The function $f(J_B)$ was determined experimentally by Austin et al [5] who found that the power increased up to about 50% loading and then decreased. For the range 0 – 50%, the ball load-power relation could be expressed by a polynomial as:

$$f(J_B) = k_1 \ J_B + k_2 \ J_B^2 - k_3 \ J_B^3 + k_4 \ J_B^4 \qquad \text{for } J_B <0.5 \qquad (7.52)$$

The value of the constants were established as: $k_1 = 3.045$, $k_2 = 4.55$, $k_3 = 20.4$, $k_4 = 12.9$.

7.4.2. Nordberg Method

The Nordberg Group published a practical method for determining the mill size for a given application [9]. In the first instance, the mill power required is calculated using Bond's Eq. (3.5). This is the power that is to be applied at the mill drive to grind a given tonnage from feed to product size. The power input required to maintain a given charge position in the rotating mill, using a torque arm model, was given as:

$$P_M = \frac{M_B \ H_{cog} \sin\alpha \ 2\pi\omega}{13488} \quad \text{in kW} \qquad (7.53)$$

where M_B = mass of the charge, t

H_{cog} = distance from the centre of the mill to the centre of gravity of the charge, m (see Fig. 7.6 and Fig. 7.13)

α = dynamic angle of repose of the charge

ω = speed of the mill, rpm

This equation is a function of the type of mill discharge used, the percent of the critical speed and other grinding conditions and must be correlated against existing installations. This approach does not take into account balls in a cataracting motion.
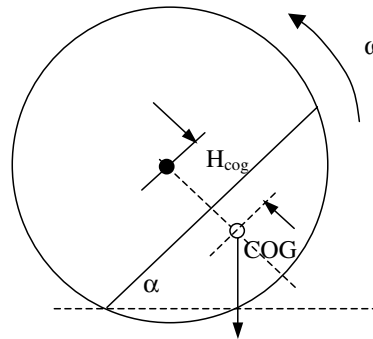
Fig. 7.13. Location of the centre of gravity (COG) of the charge.

The five most significant conditions affecting the mill power are:

1. Mill diameter,
2. Mill length,
3. % charge or ball loading ,
4. Mill speed,
5. Mill type.

An approximate mill power calculation incorporating these factors is given by:

$$P_M = 2.448 \, A \, B \, C \, L \qquad (7.54)$$

where P_M = mill power in kW,
   A = a factor of the mill diameter,
   B = a factor incorporating the % charge loading and the mill type,
   C = a factor incorporating the mill speed, and
   L = the mill length.

Nordberg takes the mill diameter to be the inside liner diameter which can be estimated as the inside shell diameter minus 152 mm (assuming a liner thickness of 76 mm). Nordberg gave the values of the mill factors A, B and C in tabular form but are represented graphically in Figs. 7.14– 7.15.
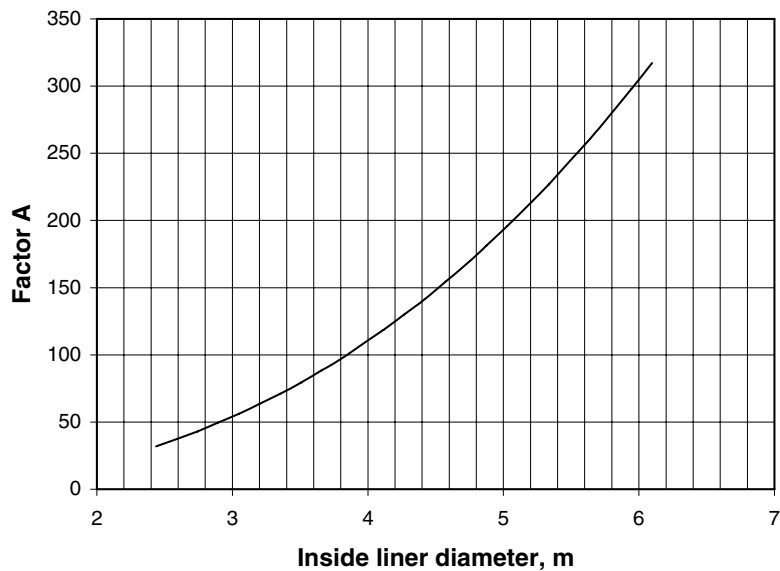
Fig. 7.14. Nordberg factor A as a function of mill diameter [9].
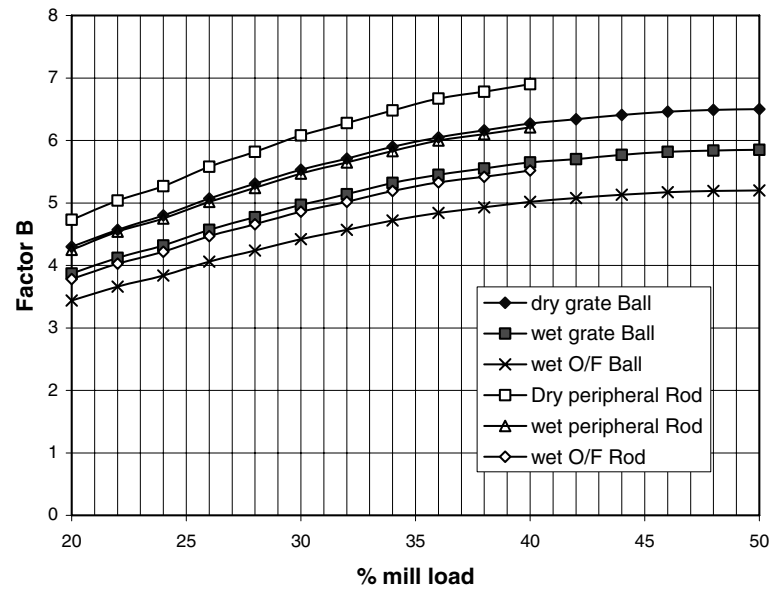
Fig. 7.15. Nordberg factor B as a function of mill type and mill load [9].
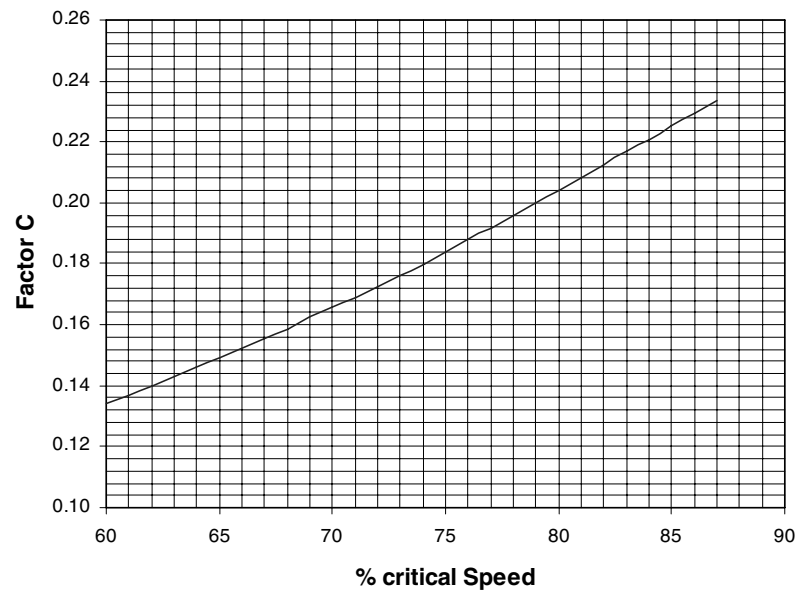
Fig. 7.16. Nordberg factor C as a function of mill speed [9].

The use of expression (7.54) is illustrated by Examples 7.4-7.6.

7.4.3. Blanc Method
Doering International [30] provides an equation for the approximate mill power of a ball mill based on a formula by Blanc, as follows:

$$P_M = \frac{K\,M_B\,\sqrt{D}}{1.3596} \quad \text{in kW} \tag{7.55}$$

where K   = an index related to the mill charge as given in Table 7.7.

Table 7.7
Relationship of factor K to media loading [30].

Grinding media	Media Load fraction				
	0.1	0.2	0.3	0.4	0.5
Steel balls > 60 mm	11.9	11.0	9.9	8.5	7.0
Steel balls < 60 mm	11.5	10.6	9.5	8.2	6.8
Cylpebs	11.1	10.2	9.2	8.0	6.0
Steel media (average)	11.5	10.6	9.53	8.23	6.8

7.4.4. Bond Method
From the results of a large number of observations, Bond [6] established that the power drawn by a mill was:

1.   directly proportional to the length of the mill,
2.   a function of the mill speed,
3.   a function of the total mass of the grinding media plus the rock charged,
4.   a function of the feed characteristics and
5.   a function of the work index of the material.

Bond found that the mill power did not vary linearly with speed but varied linearly with a factor F_C, which in turn was a function of the critical speed, ϕ_C. The relation between the Bond mill factor , F_C, and the critical speed is:

$$F_C = 100\,\phi_C \left[1 - \frac{0.1}{2^{\,9-10\phi_c}}\right] \tag{7.56}$$

Fig. 7.18 illustrates the linear relationship between the mill factor F_C, and the fraction of critical speed. Using this relationship, with a large number of laboratory and industrial mills, Bond proposed the following empirical equation to compute the *shaft power* for mills as:

$$P_S = 7.33\,\phi_C\,J_B\,(1-0.937J_B)\left(1 - \frac{0.1}{2^{\,9-10\phi_c}}\right)\rho_b\,L\,D^{2.3} \tag{7.57}$$

where P_S = Power at the mill shaft in kW for L, D in meters and ρ_b in t/m^3.
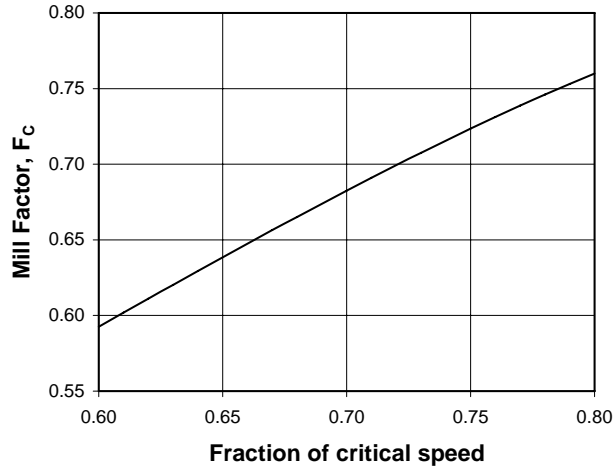
Fig. 7.17. Relation between critical speed and the Bond mill factor, F_C, from Eq. (7.56).

Grinding in wet ball mills is commonly practised in the metallurgical industry. Bond [6] therefore empirically determined the power required for wet grinding and expressed it in terms of unit mass of the grinding media (M_B) as:

$$\frac{P_M}{M_B} = 15.6\ D^{0.3}\ \phi_C\ (1 - 0.937 J_B)\left(1 - \frac{0.1}{2^{(9\ -10\phi c)}}\right) \quad kW/t \qquad (7.58)$$

The mass of balls (the grinding media) is given by:

$$M_B = \frac{\pi D^2}{4} J_B\ L \rho_b\ (1 - \varphi) \qquad (7.59)$$

where φ = the porosity of the bed.

In most cases the bed porosity is around 35 – 40%. Throughout text it has been assumed that the nominal porosity of the bed is 40%. Therefore taking the fractional value of φ as 0.4, the mass of balls can be written as:

$$M_B = \frac{3.14159 D^2}{4} J_B\ L \rho_B\ 0.6 = 0.471 J_B\ L D^2 \rho_b \qquad (7.60)$$

In practice the shaft power for wet overflow mills calculated using Eq. (7.58) appeared to yield higher results than the computed value when :

1.   Maximum ball diameter, $d_{MAX} < 45.7$ mm and

2. Mill ID > 2400 mm.

To correct for this, Bond introduced a factor described as the *slurry or slump factor* and defined it as:

$$F_S = 1.102 \left(\frac{45.72 - d_{MAX}}{50.8} \right) \ kW/t \qquad (7.61)$$

where the ball diameter d_{MAX} is in mm.

To determine the correct mill power the value of F_S is subtracted from Eq. (7.58). Rowland [31] found that Eq. (7.61) had to be modified to suit mills of diameters greater than 3.3 m. The modified *ball size factor* is added to Eq. (7.58) and is given as:

$$F_B = 1.102 \left(\frac{d_{MAX} - 12.5D}{50.8} \right) \ kW/t \qquad (7.62)$$

where D is in meters and d_{MAX} in mm.

Eq. (7.58) appropriately modified by Eqs. (7.61) and (7.62) provide a reasonably good indication of mill power observed in practice. In order to determine the power required by dry grate discharge mills Eq. (7.58) should be multiplied by the factor 1.08 and for wet, low level grate discharge mills, the multiplication factor is 1.16.

When the mill power is computed according to Rose and Sullivan's method and the results compared with that from Bond's equation, it is observed that the fractional filling at which a ball mill draws the maximum power could differ. Rowland and Kjos [2,28,32] have applied Bond's Eq. (7.58) and suggested a slightly modified form of the equation when applied to compute the power required for wet over-flow ball mills. The suggested equation is:

$$\frac{P_M}{M_B} = 4.879 D^{0.3} (3.2 - 3J)\phi_C \left(1 - \frac{0.1}{2^{(9-10\phi_C)}} \right) + F_B \qquad kW/t\text{-balls} \qquad (7.63)$$

Eq. (7.63) is applicable for mill power estimations of wet grinding mills having diameters greater than 3.3 m. Bond's equation for mill power estimation (Chapter 3) was derived from a knowledge of the specific grinding energy, which was related to the work index (W_i) of the material. Rowland and Kjos [2,28] and Austin et al [5] have suggested that the following corrections are necessary when applying Bond's method. These corrections apply both for ball mill and rod mill grinding. Correction factors suggested by Rowland and Kjos [28] that apply for ball mills are given below. Corrections for rod mills are given in Chapter 8.

1. Correction for dry grinding as Bond's work index is carried out under wet conditions,
2. Correction for wet open circuit grinding as extra power is required when compared to wet closed circuit grinding,
3. Correction for over size of feed, i.e. feed size greater than the optimum size. The feed oversize correction factor is defined as:

$$F_{OS} = 4000 \left[\frac{13}{W_i} \right]^{0.5} \qquad\qquad (7.64)$$

The expression for correction is:

$$F_3 = 1 + \frac{1}{R} \left[W_i - 7 \right] \left[\frac{F_{80}}{F_{OS}} - 1 \right] \qquad\qquad (7.65)$$

where   R   = the reduction ratio = F_{80} / P_{80} and
        F_{OS} = optimum feed size given by Eq. (7.64).

4.   Correction when the product size, P_{80}, is less than 75 microns. The correction factor is computed from the expression:

$$F_4 = \left[\frac{P_{80} + 10.3}{1.145 \, P_{80}} \right] \qquad\qquad (7.66)$$

5.   Correction when the reduction ratio is less than 6. The correction factor is:

$$F_5 = 1 + \frac{0.13}{(R - 1.35)} \qquad\qquad (7.67)$$

The total correction factor is the product of the above factors.

The work of Austin et al [5] indicates that Bond's Eq. (7.58) does not adequately describe mill shaft power when the mill diameters were less than 2.4 m. They found that:

$$\frac{P_M}{M_B} \propto \frac{1 - 0.937 J_B}{1 + 5.95 J_B^5} \qquad\qquad (7.68)$$

Therefore they substituted this value into Eq. (7.58) and recommended the use of Eq. (7.69) to calculate the net power for dry batch grinding in mills smaller than 2.4 m diameter:

$$\frac{P_M}{M_B} = \frac{13.0 \, D^{0.5} \, (\phi_C - 0.1) \, (1 - 0.937 J_B)}{(1 + 5.95 J_B^5)(1 + \exp[15.7(\phi_C - 0.94)])} \quad kW/t \qquad\qquad (7.69)$$

where D is in meters and M_B in metric tonnes.

For mill diameters greater or equal to 2.4 m, Bond's Eq. (7.58) should still be used for calculating the mill shaft power. They also suggested that Eq. (7.69) was applicable to various mill conditions when the following multiplying factors are applied to obtain reasonably accurate values of mill power:

1.   From dry batch to wet continuous grinding multiply by 1.07
2.   From net power to pinion shaft power multiply by 1.10

- the total conversion factor is then = 1.07 x 1.10 = 1.18
3.   To convert work index from wet to dry grinding multiply by 1.3

While considering the mill power estimations, the effects of lifters have not been considered by any worker due to the complexity of the situation. The mill power equations indicated above are also applicable to other tumbling mills like AG/SAG mills according to Napier–Munn et al [26]. The use of Bond's method of calculating mill power with modifications indicated above is illustrated in Examples 7.4 and 7.5.

Example 7.4

A 3.5 m x 3.5m wet overflow ball mill was lined with 75 mm rubber lining. 40% of the mill volume was loaded and the mill operated at 17.6 rpm. The diameters of the grinding balls were 70 mm. Calculate:

1.   The critical speed at which the balls will cease to cataract,
2.   The optimum power consumption to operate the mill.

Solution

As the mill was less than 3.81 m in length, Eq. (7.46) could be used to evaluate the mill capacity. Suppose the required product size decreased from 250 microns to 125 microns and then again to 65 microns. Use of Fig. 7.11 and Eq. (7.46) can be made to estimate the change of mill capacity with mill size. Fig. 7.12 could similarly be drawn to illustrate the effect on capacity due to the changing demands of product size while the feed size remains unchanged.

Step 1
Here the internal diameter of the mill is = 3.5 – 2 (0.075) m = 3.35 m.
Substituting in Eq. (7.38) the critical speed of operation would be:

$$v_C = 42.3 / [(3.35 - 0.07)]^{0.5} = 23.4 \text{ rpm}$$

The balls will cease to grind at 23.4 rpm of the mill and at 17.6 rpm, the speed is $\dfrac{17.6}{23.4}$ x 100 = 75% of the critical speed.

Step 2
Rose and Sullivan method
For a dry grind, if we use Eq. (7.52), for a solid density of 2800 kg/m^3, a ball density of 7800 kg/m^3 and assuming a value of U = 1,

$$f(J_B) = 3.045(0.4) + 4.55(0.4^2) - 20.4(0.4^3) + 12.9(0.4^4) = 0.97064$$

From Eq. (7.51):

$$\text{Power} = 1.12 \times 10^{-3} \left(3.35^{2.5} \times 3.5 \times 7800\right)\left(1 + \frac{0.4 \times 2800 \times 1}{7800}\right) 0.75 \times 0.97064 = 523 \text{ kW}$$

Step 3
Bond method
For a bed porosity of 0.4, using Bond's Eq. (7.58):

$$\frac{P_M}{M_B} = 15.6 \times 3.35^{0.3} \times 0.75\left(1-(0.937 \times 0.4)\right)\left(1-\frac{0.1}{2^{(9-(10 \times 0.75))}}\right)$$

$$= 10.14 \text{ kW/t}$$

Since the mill diameter is greater than 2400 mm, but the ball size is greater than 45.7 mm, no slump correction is applied.
From Eq. (7.59), the mass of balls in the charge is estimated as:

$$M_B = \frac{3.14159(3.35^2)}{4} \, 0.4 \times 3.5 \times 7800 \times (1-0.4)$$

$$= 57.75 \text{ t}$$

therefore, Power $= 10.14 \times 57.75 = 585$ kW

Step 4
Rowland and Kjos method
Using the Rowland and Kjos modified Eq. (7.63):

$$\frac{P_M}{M_B} = 4.879 \times 3.35^{0.3}\left(3.2-(3 \times 0.4)\right)0.75\left(1-\frac{0.1}{2^{(9-(10 \times 0.75))}}\right) = 10.15 \text{ kW/t}$$

Since the mill diameter is greater than 3.3 m, the ball size factor, F_B is applied.

$$F_B = 1.102\left(\frac{70-(12.5 \times 3.35)}{50.8}\right) = 0.610 \text{ kW/t}$$

Thus $\dfrac{P_M}{M_B} = 10.15 + 0.610 = 10.76$ kW/t

and Power $= 10.76 \times 57.75 = 621$ kW

Step 5
Nordberg method
From the given data and Figs. 76 – 78, A $=$ 71.1, B $=$ 5.02, C $=$ 0.184.
Thus from Eq. (7.54):
Power $= 2.448 \times 71.1 \times 5.02 \times 0.184 \times 3.5 = 563$ kW

Step 6
Doering (Blanc) method
For steel balls greater than 60 mm and $J_B = 0.4$, K $=$ 8.5

Then from Eq. (7.55):

$$\text{Power} = \frac{8.5 \times 57.75 \sqrt{3.35}}{1.3596} = 661 \text{ kW}$$

Example 7.5

A 2.1 m x 2.1 m dry ball mill was charged with rock and 30 mm diameter balls of density 7.8 t/m^3. At rest the porosity of the bed was 35% and the load was 45% of the mill volume. The mill was operated at 70% of its critical speed and required to grind at the rate of 35 t/h. The ball density is 7800 kg/m^3 and rock density is 2500 kg/m^3. Determine:

1. The mass of the grinding media
2. The net mill power required to operate the mill
3. The power required to grind the same mineral in a wet overflow mill

Solution

Step 1
Mass of grinding media (balls) is given by Eq. (7.59), $M_B = \pi D^2/4 \; J_B \; L \; \rho_b \; (1 - \varphi)$.
Substituting data gives:

$$M_B = (3.14159 \times 2.1^2 / 4) \times 0.45 \times 2.1 \times 7.8 \times (1 - 0.35) = 16.6 \text{ t}$$

Step 2
As the mill diameter is less than 2.4 m, use Austin's Eq. (7.69) to calculate the net mill power. Substituting data values gives:

$$P_M = \frac{13.0 \times 2.1^{0.5} \; (0.70 - 0.1) \; (1 - (0.937 \times 0.45))}{(1 + (5.95 \; (0.45^5))) \; [1 + \exp \; (15.7 \; (0.70 - 0.94))]} \times 16.6 = 95.6 \text{ kW}$$

Step 3
Alternatively, using Rose and Sullivan's Eq. (7.51) for dry grinding gives:

firstly, $f(J_B) = (3.045 \times 0.45) + (4.55 \times 0.45^2) - (20.4 \times 0.45^3) + (12.9 \times 0.45^4) = 0.962$

and $P_M = 1.12 \times 10^{-3} \, (2.1^{2.5} \times 2.1 \times 7800) \left(1 + \frac{0.4 \times 2500 \times 1}{7800}\right) 0.70 \times 0.962 = 89.1 \text{ kW}$

for a value of U = 1.

Step 4
To compute the power required for grinding in a wet overflow mill, Austin's equation is modified by multiplying by the factor 1.07. Thus:

$$P_M = 95.6 \times 1.07 = 102.3 \text{ kW}$$

Step 5

Alternatively, Bond's equation, modified and developed by Rowland and Kjos Eq. (7.63) can be used. Substituting values we have:

$$P_M = 4.879(2.1)^{0.3}(3.2-3(0.45))0.7\left[1-\frac{0.1}{2^{(9-10(0.7))}}\right]16.6 = 127.8 \text{ kW}$$

Step 6

Although the ball diameter is less than 45.7 mm, the mill diameter is less than 2.4 m and hence a slurry factor correction is not necessary.

During a mill operation the I.D. of the liner is subject to wear. As a result, the value of D is affected. To solve this anomaly, add 6% to the calculated value of mill power to obtain the operational power. Rowland and Kjos [2] has suggested that the adjustment required varies between 5-10%.

Taking 6% for adjustment then P_M should be 135 kW.

Example 7.6

A mill is required to grind 250 tph of limestone from an 80% passing size of 10 mm to 100 μm in a closed circuit wet overflow discharge ball mill. Calculate the mill size required to handle the required throughput.

Step 1

From Appendix B.1, the Bond Work index of limestone is 11.25 kWh/t. Using Bond's Eq. (3.5):

$$W = 10 \times 11.25\left(\frac{1}{\sqrt{100}} - \frac{1}{\sqrt{10000}}\right) = 10.125 \text{ kWh/t}$$

and $P_M = 250 \times 10.125 = 2531 \text{ kW}$

Step 2

Since the mill diameter is unknown, choose a range of values of D and use Fig. 7.14 to estimate the factor A:

Mill ID (m)	A
3.2	63.5
3.8	97.5
4.4	141.5
5.0	196.0

Step 3

Assuming a ball loading of 40%, a typical average value for a wet overflow ball mill, then from Fig. 7.15, factor B is 5.0.

Step 4

Choose a range of mill speeds and from Fig. 7.17, factor C is estimated:

Fraction of critical speed	C
0.65	0.149
0.70	0.166
0.75	0.184

Step 5

Using Eq. (7.54) and solving for the mill length for each of the above conditions gives:

Diameter	Length (m)			L/D		
(m)	$\phi_C = 0.65$	$\phi_C = 0.70$	$\phi_C = 0.75$	$\phi_C = 0.65$	$\phi_C = 0.70$	$\phi_C = 0.75$
3.2	21.9	19.6	17.7	6.8	6.1	5.5
3.8	14.2	12.8	11.5	3.7	3.4	3.0
4.4	9.8	8.8	7.9	2.2	2.0	1.8
5.0	7.1	6.4	5.7	1.4	1.3	1.1

Step 6

Choose a suitable diameter to length combination based on the following guide:

1.   Length:diameter ratios for rod mills are normally 1.2:1 to 1.6:1
2.   Length:diameter ratios for ball mills are normally 1:1 to 5:1
3.   The slower the speed the less wear on media and liners
4.   The faster the speed the lower is the capital cost

The highlighted box in the table above indicates suitable mill dimensions.

These calculations are an approximation only and the mill manufacturers should be consulted for final mill selection.

7.4.5. Theoretical Mill Power Draw

The theoretical approach to estimate the mill power draw is based on the concept that in a tumbling mill like the ball mill, repeated forces of impact, compression, abrasion and attrition operate in a complex manner. Due to the application of these complex forces, energy transference take place resulting in stress concentrations within particles. When the forces of stress are greater than the bonding energy the particles disintegrate into two or more particles. Thus the rupture of particles in a tumbling mill is a complicated function of the transference of energy from the grinding media and the mill to the ore particles. Both kinetic and potential energies are transferred to the charge by the rotation of the mill and the falling of the balls (media) from a height. The result is the production of heat and sound energies and the rupture of bond energies between particles. Austin et al [5], Morrell [1,7] and Napier-Munn et al [26]

theoretically assessed the total energy transferred to the charge from mill rotation and related it to the power required to rotate the mill while empty and when fully charged. Austin et al's approach was oversimplified and therefore the approach of Morrell [1] is summarised below:

In deriving the mill power Morrell assumed:

1.   The power drawn was related to the transference of kinetic and potential energies from the rotating mill to the grinding media and charge which was translated to kinetic and potential energies of the charge as it moved within a rotating mill
2.   The energy transferred was recovered by the mill. The heat and sound energy produced was neglected
3.   Power was equal to energy per unit time
4.   During wet grinding in an overflow mill, the movement of the toe of the charge was of importance
5.   In wet grinding the slurry in the centre did not affect the torque of the mill shaft as the load was distributed evenly around the centre
6.   The mass of the slurry influenced the friction between the charge and the mill lining and therefore affected the torque, but its magnitude was small and therefore neglected in the derivation of the power equation.

The total power was considered as the sum of the power required at the cylindrical section plus the power required by the two conical end sections plus the power to rotate an empty mill.

Fig. 7.18 is a schematic diagram of a tubular ball mill of diameter, D and the lengths of the cylindrical and cone sections are L_{CYL} and L_{CONE} respectively. To rotate the mill with no load Morrell [1] empirically determined the no load value of a mill as:

$$\text{No Load Power} = 1.68 \ [D^{2.5} \ \phi_C \ (0.667 \ L_{CONE} + L_{CYL})]^{0.82} \quad kW \qquad (7.70)$$

where D, L_{CONE} and L_{CYL} are in m.

Morrell's derivation for the power required by the cylindrical and the conical sections of grate and overflow type mills are summarised:

***Power required for cylindrical section of Ball mills:* Grate Mill**

Fig. 7.18 illustrates a simplified schematic diagram of the possible position of the slurry (solids + water) and bulk solids plus grinding balls in a stationary wet grinding mill. Fig. 7.19 is a sketch of the cross-section of the mill showing the position of the slurry, the toe and shoulder angles with a certain load in the mill. During rotation, the material at the toe and shoulder ends is displaced in the direction of the rotation. The overall displacement of the materials will be given by the distance moved by the shoulder and toe positions which can be estimated by the change of the toe (α_T) and shoulder (α_S) angles with the horizontal.

To determine the potential and kinetic energies associated at the new positions of the particles in the charge, consider an element of the mill of length, L at radial distance R_i and width dR, The mass flow rate through the element would be:

$$Q_M = v_T \ \rho_C \ L \ dR \qquad (7.71)$$
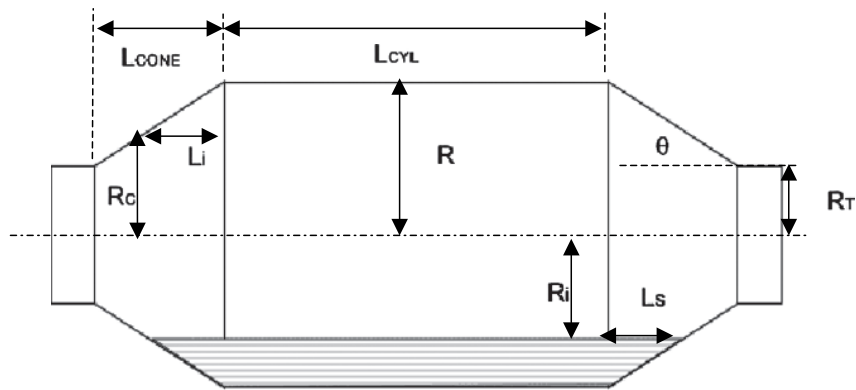
Fig. 7.18. Schematic diagram of a ball mill
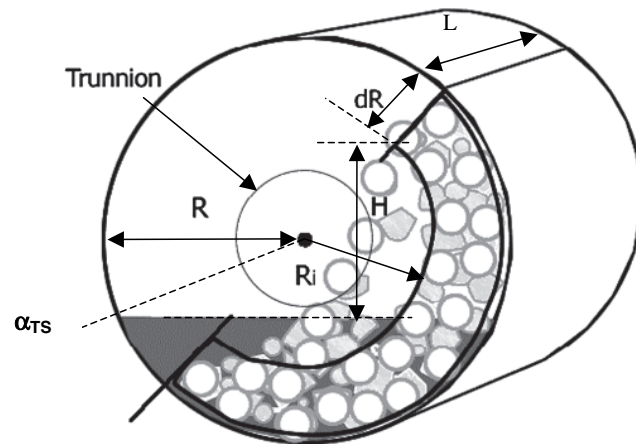
Fig. 7.19. Position of balls, solids and slurry in a wet overflow ball mill.

where v_T = tangential velocity of a particle located at any distance R from the centre, in m/s, and

  ρ_C = density of the total charge, t/m^3.

The rate of potential energy (PE) developed in the particles and balls would depend on the height to which they are raised. If this height is H, then the associated potential energy would be:

$$PE = v_T\,\rho_C\,L\,dR\,g\,H \tag{7.72}$$

where   g   =   the acceleration due to gravity.

From Figs. 7.19 and 7.20 it can be seen that:

$$H = h_1 + h_2 = R_i (\sin \alpha_S - \sin \alpha_T) \tag{7.73}$$

α_S and α_T being the shoulder and toe angles.

The rate of imparting kinetic energy (KE) to the particles would be:

$$KE = \frac{1}{2}(v_T \, \rho_C \, L \, dR)v_T^2 = \frac{v_T^3 \, \rho_C \, L \, dR}{2} \tag{7.74}$$

Hence the rate at which the total energy, E_T, is generated will be the sum of the potential and kinetic energies.

$$E_T = v_T \, \rho_C \, L \, dR \, g \, H + \frac{v_T^3 \, \rho_C \, L \, dR}{2} \tag{7.75}$$

At any radial distance, R_P, in the charge, the tangential velocity is given by:

$$v_T = 2 \pi R_P \omega_P \tag{7.76}$$

where ω_P =   is the rate of rotation of a particle at the radial distance, R_P, in the charge in revolutions/s
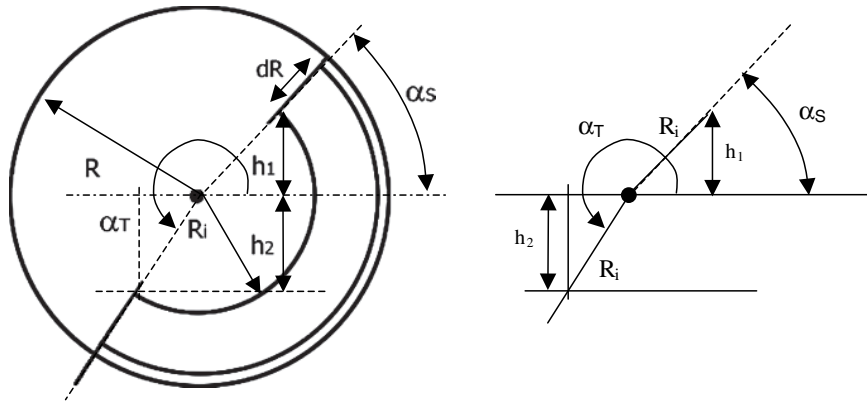
Fig. 7.20. Calculation of the raised ball height, H $(= h_1 + h_2)$

Morrell [1] derived ω_P in terms of the rotational speed of the mill, ω, mill radius R, radial position R_P and R', the theoretical radial position in the active charge where the velocity is zero, as:

$$\omega_P = \left[\frac{\omega\ R\ \left(R_P - R'\right)}{R_P\ (R - R')} \right] \tag{7.77}$$

R' was related to the mill charge volume and written as:

$$R' = R_i\ [1 - J_C]^{0.4532} \tag{7.78}$$

where $\quad J_C = $ fraction of mill volume in the cylindrical section occupied by balls and coarse ore (including voids).

Substituting this value of v_T in terms of ω_P, R' and H in Eq. (7.75) and integrating between the limits R_i and R gives the power, P_{CYL}, for the cylindrical portion of the mill as:

$$P_{CYL} = \frac{\pi\ g\,L\rho_C\,\omega R}{3(R - \zeta R_i)} \left[2\,R^3 - 3\zeta R^2\,R_i + R_i^3\,(3\zeta - 2) \right] \left(\sin\alpha_S - \sin\alpha_T \right) +$$
$$L\rho_C \left[\frac{\omega R\,\pi}{(R - \zeta R_i)} \right]^3 \left[(R - \zeta R_i)^4 - R_i^4\,(\zeta - 1)^4 \right] \tag{7.79}$$

where P_{CYL} is in kW for L, R and R_i in meters, ρ_C in t/m^3, and the fraction of the mill volume filled, ζ, is defined by Eq. (7.41).

Power required for the Cylindrical Section of Ball Mill: Overflow Type

In the case of overflow mills, the slurry reduces frictional forces between the solids and the inside of the mill. Thus the power required for overflow mills would be less than for grate discharge mills. Again as the falling particles impinge on the slurry below and travels down, the slurry provides a buoyancy action. Taking these factors into account Morrell has derived the power required for the overflow mills as:

$$P_{CYL} = \frac{\pi\ g\,L\rho_C\,\omega R}{3(R - \zeta R_i)} \left[2\,R^3 - 3\zeta R^2\,R_i + R_i^3\,(3\zeta - 2) \right]$$
$$\left[\rho_C\left(\sin\alpha_S - \sin\alpha_T \right) + \rho_P\left(\sin\alpha_T - \sin\alpha_{TS} \right) \right] +$$
$$L\rho_C \left[\frac{\omega R\,\pi}{(R - \zeta R_i)} \right]^3 \left[(R - \zeta R_i)^4 - R_i^4\,(\zeta - 1)^4 \right] \tag{7.80}$$

where $\quad \rho_P = $ density of the slurry and
$\qquad \alpha_{TS} = $ the slurry toe angle (Fig. 7.19).

Power for Conical Sections of the Mill

Mills of large dimensions are designed to have a considerable volume at the two conical sections and therefore carry a significant amount of slurry and solids to affect the overall power requirements to rotate it. Morrell [1] determined the power required by the two conical end sections of a mill in the same manner as the cylindrical section. The final form of the equation is:

$$
\begin{aligned}
P_{CON} = {} & \frac{\pi\, g\, L_{CONE}\, \omega}{3(R - R_T)} \left[R^4 - 4 R R_i^3 + 3 R_i^4 \right] \\
& \left[\rho_C \left(\sin\alpha_S - \sin\alpha_T \right) + \rho_P \left(\sin\alpha_T - \sin\alpha_{TS} \right) \right] + \\
& \frac{2\pi^3 \omega^3 L_{CONE}\, \rho_C}{5(R - R_T)} \left(R^5 - 5 R R_i^4 + 4 R_i^5 \right)
\end{aligned}
\tag{7.81}
$$

where R_T = radius at the trunnion,
L_{CONE} = length of cone side,
R_C = radius of cone at a distance L_i from the cylindrical section (see Fig. 7.18)

To evaluate the Eqs. (7.80) and (7.81) the following have to be determined:

1.   the inner radius of the charge (R_i),
2.   the charge and pulp densities.

R_i is estimated by considering the active mass of the charge, the time taken for the charge to travel from the toe to the shoulder position and the time taken for the charge to travel from the shoulder and fall to the toe. From Fig. 7.19, the inner boundary of the active rotating charge is R_i . Thus for a given mass of charge, if the positions of the toe and shoulder are known through the angles α_T and α_S then R_i can be calculated using simple geometry as:

$$
R_i = R \left[1 - \frac{2\pi\gamma J_C}{2\pi + \alpha_S - \alpha_T} \right]^{0.5}
\tag{7.82}
$$

The term γ represents the volume fraction of the active part of the charge to the total charge. The active part can be considered as the fraction of time taken by the charge in the active zone to the total time taken for one complete turn of the charge. That is:

$$
\gamma = \frac{\bar{t}_A}{\bar{t}_F + \bar{t}_A}
\tag{7.83}
$$

where $\bar{t}_A$ = mean time taken for the active part to travel from the toe to the shoulder and
$\bar{t}_F$ = mean time for free fall from the shoulder to the toe.

The mean times in Eq. (7.83) are related to the mean rotational speed, $\bar{\omega}$. That is:

$$\bar{t}_A \approx \frac{2\pi - \alpha_T + \alpha_S}{2\pi\omega} \quad \text{and} \tag{7.84}$$

$$\bar{t}_F \approx \left[\frac{2\bar{R}(\sin\alpha_S - \sin\alpha_T)}{g}\right]^{0.5} \tag{7.85}$$

where $\bar{R}$ is the mean radial position of the active part of the charge and is related to the fraction of the mill volume occupied by the charge. It is given by:

$$\bar{R} = \frac{R}{2}\left[1 + \left(1 - \frac{2\pi J_C}{2\pi + \alpha_S - \alpha_T}\right)^{0.5}\right] \tag{7.86}$$

The fractional ball filling, J_C and J_B, refer to the cylindrical section of the mill. The inner radius of the charge, R_i, can now be determined by substituting the values from Eqs. (7.84) – (7.86) into Eq. (7.82).

To determine the density of the total charge, it is necessary to know the porosity of the charge, the pulp density and the fraction of voidage between balls that is occupied by the slurry. The fractional porosity of the charge has been taken as 0.4. The fractional solids content of the discharge slurry (by volume) can be measured from the discharge of the mill (it was taken as 0.5 by Morrell [1]) and the fraction of the grinding media voidage occupied by ore was taken as 1. With these assumptions the density of the total charge is given by:

$$\rho_C = 0.8\rho_O + \frac{0.6 J_B (\rho_b - \rho_O)}{J_C} + 0.2 \tag{7.87}$$

where ρ_O, ρ_b = the densities of the ore and balls respectively.

This assumes that the pulp density in the mill is the same as the discharge density. Substituting the calculated values of R_i, ρ_C in Eqs. (7.80) and (7.81), the power required by the cylindrical and cone portion is calculated. The total power required by the mill is then:

$$P = [\text{No load power}] + [\text{power determined by Eqs. (7.80) + (7.81)}] \tag{7.88}$$

Morrell [1] indicated that the power determined by this method agreed well with observed values from a survey of 40 mills in Australia with a 95% confidence interval of ± 10.5% relative error.

7.4.6. Electrical Drive of Ball Mills

For driving a ball mill, Rowland and Kjos [2] recommend that the connection to the mill should be either an air-clutch or flexible coupling. The motors should preferably have the following properties:

1.   Torque   Should deliver 130 % starting torque
2.   Motor   Synchronous motors
3.   Speed rating   150-250 rev/min.

Due to the extremely high loads, especially in large commercial mills and for the initial power draw, adequate safety factors must be allowed.

7.5. Problems

7.1
A crushing plant delivered ore to a wet grinding mill for further size reduction. The size of crushed ore (F_{80}) was. 4.0 mm and the S.G. 2.8 t/m^3. The work index of the ore was determined as 12.2 kWh/t. A wet ball mill 1 m x 1 m was chosen to grind the ore down to 200 microns. A 30 % pulp was made and charged to the mill, which was then rotated at 60% of the critical speed. Estimate:

1.   The maximum diameter of the grinding balls required at the commencement of grinding,
2.   The diameter of the replacement ball.

7.2
A 1.0 x 1.5 m ball mill was loaded with a charge that occupied 45% of the mill volume. The diameter of balls was 100 mm. The mill was at first rotated at 25 rpm. After some time the rotation was increased to 30 rpm and finally to 40 rpm. Determine and plot the toe and head angles with the change of speed of rotation.

7.3
A 2.7m x 3.6 m ball mill was filled to 35% of its inner volume. The charge contained 100 mm diameter steel balls. The mill was rotated at 75% of critical speed. The ore size charged was 2.8 mm and the product size (P_{80}) of 75 microns. The work index of the ore was 13.1 kWh/t. Determine the production rate of the mill when operated under wet conditions.
Data : S.G. of ore = 2.8.

7.4
Hematite ore of particle size 4000 microns is to be ground dry to 200 microns (P_{80}). The work index of the ore was determined and found to be equal to15.1 kWh/t. Balls of diameter 110 mm were added as the grinding media. The mill was rotated at 68 % of the critical speed and expected to produce at the rate of 12 t/h. The combined correction factors for W_i equalled 0.9. Calculate:

1.   The volume of the mill occupied by the grinding media.
2.   The mill capacity when the mill load was increased by 10% of its original volume.

Data: ρ_B = 7.9 t/m^3 , Porosity of the bed = 40%

7.5
The feed size of an ore to a 1.7 m x 1.7 m wet ball mill operating in closed circuit was 5000 μm. The work index of the ore was determined under dry open circuit conditions and found to

be 13.5 kWh/t. The mill bed was filled to 30% of its volume with balls of density 7.9 t/m^3. A 20:1 reduction ratio of ore was desired. The mill was operated at 80% of the critical speed. Assuming a bed porosity of 40%, estimate the mill capacity in tonnes per year.

7.6
A ball mill is to produce a grind of 34 micron (P_{80}) product from a feed size of 200 microns at a rate of 1.5 t/h. The grinding media used was 90% Al_2O_3 ceramic ball of S.G. 3.5. The balls occupied 28% of the mill volume. The mill was rotated at 65% of the critical speed. The work index of the ore was 11.3 kWh/t. Estimate the size of the mill required.

7.7
A wet overflow ball mill of dimensions 3.05 m x 3.05 m was charged with nickel ore (pentlandite) of density 4.2 having a F_{80} value of 2.2 mm. The mass of balls charged for grinding was 32 t, which constitutes a ball loading of 35% (by volume). The mill was rotated at 18 rpm. Estimate:

Power required at the mill shaft per tonne of ball,
Power required at the mill shaft when the load (% Vol) was increased to 45%.

7.8
A grate discharge mill of dimensions 4.12 m x 3.96 m was loaded to 40% of its volume with gold ore. The mill drew 10.95 kW power per tonne of balls. To grind the ore to the liberation size the mill was run at 72% of the critical speed when charged with balls 64 mm in size and 7.9 t/m^3 density. Determine:

1   The fraction of the mill filled with balls.
2   The mass of balls charged.

7.9
The feed size to a single stage wet ball mill was 9.5 mm of which 80% passed through a 810 micron sieve. The mill was expected to produce a product of 80% passing 150 microns. The feed rate to the mill was 300 t/h. The ball mill grindability test at 65 mesh showed 12 kWh/t. The internal diameter of the ball mill was 5.03 m and the length to diameter ratio 0.77. The steel balls occupied 18 % of the mill. The total load occupied 45% of the mill volume. If the mill operated at 72% of the critical speed, determine:

The mill power at the shaft during wet grinding,
The mill power at the shaft during dry grinding.

[Hint: For estimating W_i use the applicable correction factors]

7.10
A 5.5 m x 5.5 m ball mill is lined with single wave liners 65 mm thick, which cover the entire inside surface. The centre line length was 4.2 m and the trunnion diameters 1.5 m in diameter. The mill was charged with an ore and 100 mm diameter steel balls as the grinding media so the total filling of the cylindrical section was 40% and the ball fractional filling 0.15 %. The slurry in the mill discharge contained 33% solids (by volume). The mill was expected to

rotate at 12.8 rpm. Estimate the total power required (including the power required for the no load situation).

Data: S.G. of ore = 2.8, S.G. of steel balls = 7.9

REFERENCES

[1] S. Morrell, Trans. Inst. Min. Metall., 105 (1996) C43, C54.
[2] C.A. Rowland and D.M. Kjos, in Mineral Processing Plant Design, L.M. Mular and R.B. Bhappu (eds), SME/AIME, 1980, pp. 239-278.
[3] S. Morrell, in Comminution: Theory and Practice, R.K. Kawatra (ed), 1992, pp. 369-380.
[4] K. Shoji, L.G. Austin, F. Smaila, K. Brame and P.T. Luckie, Powder Technology, 3 (1982) 121.
[5] L.G. Austin, R.R. Klimpel and P.T. Luckie, Process Engineering of Size Reduction: Ball Milling, SME/AIME, New York, 1984.
[6] F.C. Bond, British Chemical Eng., 6 (1961) 378, 543.
[7] S. Morrell, Proceedings of the Fifth Mill Operators Conference, Roxby Downs, AusIMM, 1994, pp. 109-114.
[8] J.W. Harris and H. Stocker, Handbook of mathematics and computational science, Springer-Verlag, New York, 1998.
[9] Anon, Nordberg Reference Manual, Third edition, 1992.
[10] W.H. Coghill and F.D. De Vaney, U.S. Bureau of Mines Tech Bulletin Publication No. 581, 1937.
[11] G.C. Lawrison, Crushing and Grinding, Butterworth, 1974.
[12] F.C. Bond, Mining Engineering, 10 (1958) 592.
[13] Doering International, Retrieved: December 10, 2003, from http://www.cylpebs.com/mahlkoerper/fragebogen/formula.htm.
[14] F.C. Bond, AIChE Annual Meeting, 54 (1963).
[15] P.H. Fahlstrom and T. Andrew, Proceedings 7th, International Mineral Processing Congress, 1964 pp. 515-535.
[16] W.I. Garms and J.L. Stevens, AIME Technical Publication No. 1984, 1946.
[17] L.G. Austin and R.R. Klimpel, Powder Technology, 41 (1985) 279.
[18] T.E. Norman and J.D. Decker, in Mineral Processing Handbook, SME/AIME, 1985, pp. 3C 31-33.
[19] E. Azzaroni, Proceedings of 2nd Asian Symposium on Grinding, Armco-Marsteel Corp., Manila, Philippines. 1981.
[20] D.J. Dunn, Mining Engineering, 41 No. 9 (1989) 951.
[21] E.J. Prior, Mineral Processing, 3rd ed. Applied Science, London. 1974.
[22] E.W. Davis, Trans. AIME, 16 (1919) 250.
[23] C.A. Rowland, in Mineral Processing Handbook, N.L. Weiss (ed), SME/AIME, 1985, pp. 3C 26-56.
[24] H.E. Rose and R.M.E. Sullivan, Vibration Mills and Vibration Milling, Constable, London. 1961.
[25] A.F. Taggart, Handbook of Mineral Dressing, John Wiley, 1954.
[26] T.J. Napier-Munn, S. Morrell, R.D. Morrison and T. Kojovic, Mineral Comminution Circuits Their Operation and Optimisation, JKMRC Monograph Series in Mining and Mineral Processing 2, 1999.

[27] Anon, Nordberg Bulletin 315, Marcy Mill Division and Barber Green Tech Bull. 820-979, 1970, pp 1-17.

[28] C.A. Rowland and D.M. Kjos, in Comminution Practices, R.K. Kawatra (ed), SME/AIME, 1997, pp. 319-338.

[29] H.E. Rose. and R.M.E. Sullivan, Ball, Tube and Rod Mills, Constable, London, 1957.

[30] Doering International, Retrieved: December 10, 2003, from http://www.cylpebs.com/mahlkoerper/fragebogen/critspeed.htm

[31] C.A. Rowland, Proceedings Tenth International Mineral Processing Congress, M.J. Jones (ed), I.M.M. (London), 1974, pp. 47-61.

[32] C.A. Rowland and D.M. Kjos, Principles of Mineral Processing, P. Somasundaram (ed), SME /AIME, 1999.

Chapter 8. Tubular Rod Mills

8. INTRODUCTION

Tubular tumbling mills loaded with rods as the grinding media are used for primary grinding of rocks and minerals. Rods are placed parallel to the length of the mill with their length being about 150 mm shorter than the inside length of mills. The breaking action is almost similar to ball mills but in this case the entire length of a rod is responsible for breakage of particles spread along the length of the mill. The breakage occurs more by a cascading action than by cataracting. The rods fall from a height and roll down the mill so the rods impart an impact force as well as an abrasive action. As the feed enters the mill at one end of the mill there is always a tendency for accumulation at that end, so that the initial size reduction starts more or less at the feed end. With time this action is more spread out along the entire length of the mill. The product size from a rod mill is much more uniform than a ball mill but the overall size is much coarser. Hence a rod mill generally precedes a ball mill in a grinding circuit especially where a fine size product is required.

8.1. Design of Rod Mills

The design characteristics of industrial rod mills are similar to ball mills. Most rod mills used in mineral processing are of the overflow discharge type as illustrated in Fig. 7.2A. Centre peripheral (Fig. 7.2C) and end peripheral discharge mills (Fig. 8.1) are also in use. The feed end is generally fitted with spout feeders, scoop feeders, double scoop feeders or drum feeders.

The spout feeders are designed to have a head of about 1.5 m measured from the bottom of the hopper to the centre line of the feeder to enable smooth passage of the feed into the mill by gravity. The scoop or double scoop feeders are particularly useful where some breaking up of lumps are involved. The drum feeders are fitted with spirals to guide the feed into the mill.

The diameters of the discharge end of the spout feeders are about 100-200 mm larger than the feed end. The mill lengths are more or less guided by the length of rods. The maximum rod length conveniently used is about 6.6 m. The length of the rods are about 100 - 150 mm shorter than the inside mill length.

Data from Rowland [1] indicate that the length to diameter ratio of mills range from 1.2 to 2.3. The largest length mill is around 7 m. The ratio of the length of rod to mill diameter should be greater than 1.25 to avoid the risk of rod tangling. The recommended ratio is 1.4 to 1.6.

The cross-section of the rods is generally circular, but rods having square and hexagonal sections have been used. Rods having cross sections other than round do not have any particular advantage on performance. Rods with round sections are possible easier to handle.

Liners protect the rod mill shell and are made of rubber or steel and are bolted to the shell with or without rubber backing. The liners are 65 to 75 mm thick and 60-90 mm in height. They have different contours and profiles like waves, wedge bar or rectangular which act as lifters for the charge. The liners at the feed and discharge ends are also made of steel but have
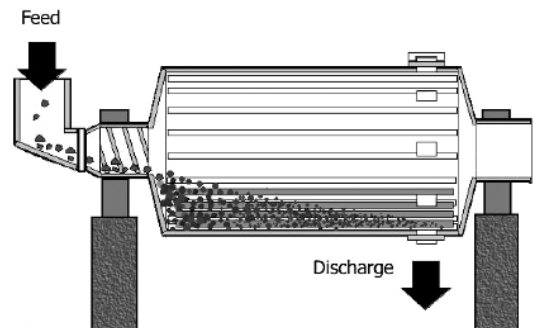
Fig. 8.1. Rod Mill with End Peripheral discharge

smooth surfaces. The headliner and wearing surface could be vertical or inclined as the materials charged into the mill have a tendency to accumulate at the head end and swells. This promotes greater wear to the headliner and also to the rods, which are found to wear down unevenly to almost a fine point in extreme cases. A general observation is that the liner wear in rod mills are much more severe than in ball mills.

The discharge in overflow rod mills falls through a trommel to remove any tramp iron in the material stream.

8.1.1. Design of Rod Mill – Ball Mill Circuits

Due to relatively uniform coarse product size and low slimes, rod mill products have been generally used as feed material for ball mills. The comminution circuits are generally arranged to receive crushed ore from a secondary crusher first to rod mills and then to ball mills. The product from the rod mill is either fed directly to a ball mill or to a classifier. The coarser fraction if then fed to the ball mill. The rod mills are normally operated in open circuit and ball mills normally are operated in closed circuit. Some common circuits are illustrated in Figs. 8.2 – 8.4.

Fig. 8.2 shows a flow sheet where the rod mill is in open circuit and ball mill in closed circuit with a classifier. This is a normal set up as the primary function of a rod mill is to provide a uniform sized feed to the ball mill. Fig. 8.3 shows that the rod mill product is classified and a more uniform feed size is therefore discharged to the ball mill whose primary function is to reduce the size of ore, suitable for down stream use. Such a circuit increases the efficiency of the ball mill grinding. Fig. 8.4 shows both rod and ball mill products are subject to classifier action to bring about a more controlled size of the final product.

In some cases open circuit single stage rod mills are used especially where the product is used directly for gravity concentration or for example in the iron ore industry where the product goes directly to a pelletising plant. Closed circuit rod milling is uncommon but may be used where a coarse grind and a tight tolerance is required on any oversize particles in the product.

214
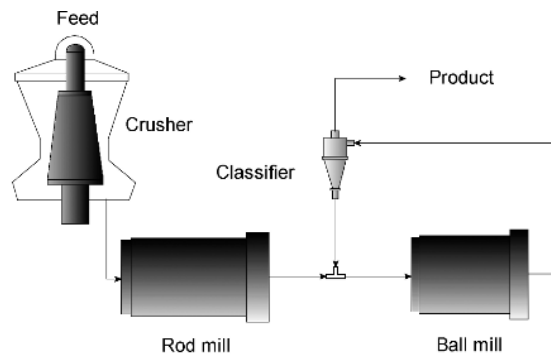
Fig. 8.2. Circuit 1: Rod mill open circuit, ball mill closed circuit.
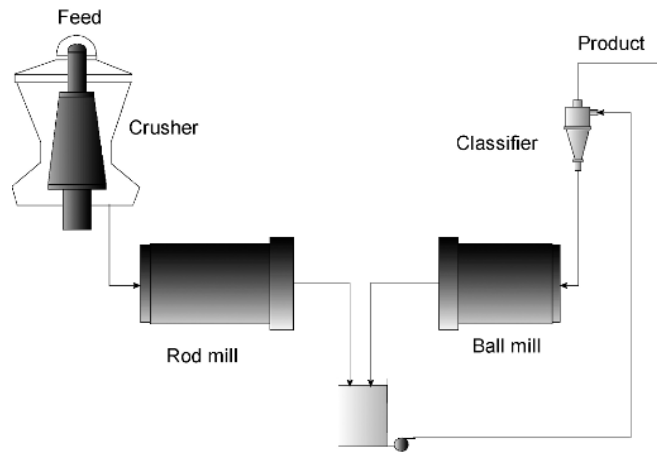
Fig. 8.3. Circuit 2: Rod mill open circuit, ball mill closed circuit with common discharge
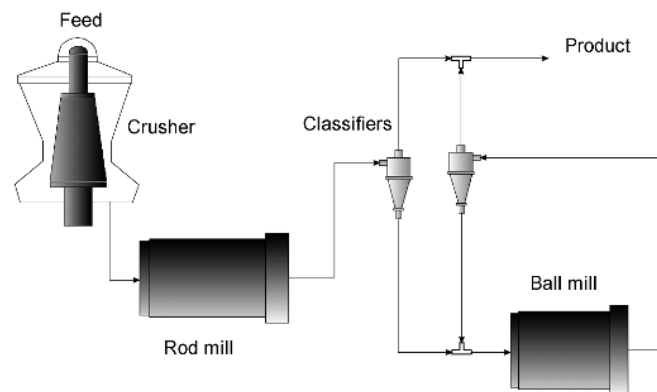
Fig. 8.4. Circuit 3: Rod mill open circuit, ball mill closed circuit with double classification circuit.

8.2. Operation of Rod Mills

8.2.1. Rod Mill Charge

Rod mill charges usually occupy about 45% of the internal volume of the mill. A closely packed charge of single sized rods will have a porosity of 9.3%. With a mixed charge of small and large diameter rods, the porosity of a static load could be reduced even further. However, close packing of the charge rarely occurs and an operating bed porosity of 40% is common. Overcharging results in poor grinding and losses due to abrasion of rods and liners. Undercharging also promotes more abrasion of the rods. The height (or depth) of charge is measured in the same manner as for ball mill. The size of feed particles to a rod mill is coarser than for a ball mill. The usual feed size ranges from 6 - 25 mm.

For the efficient use of rods it is necessary that they operate parallel to the central axis and the body of the mill. This is not always possible as in practice, parallel alignment is usually hampered by the accumulation of ore at the feed end where the charge tends to swell. Abrasion of rods occurs more in this area resulting in rods becoming pointed at one end. With this continuous change in shape of the grinding charge, the grinding characteristics is impaired.

The bulk density of a new rod charge is about 6.25 t/m^3. With time due to wear the bulk density drops. The larger the mill diameter the greater is the lowering of the bulk density. For example, the bulk density of worn rods after a specific time of grinding would be 5.8 t/m^3 for a 0.91 m diameter mill. Under the same conditions of operation the bulk density would be 5.4 t/m^3 for a 4.6 m diameter mill.

During wet grinding, the pulp charged to the mill is usually held between 60 – 75% solids by mass.

8.2.2. Rod Length and Diameter for an Initial Charge

Rod Length

Rod lengths greater than 6 meter are seldom truly straight. Bent rods promote tangling and should be avoided. The rod dimension is also an inverse function of speed, which means that with higher speeds of rotation, smaller rods in larger numbers may be equally effective as a smaller number of larger diameter rods. The reason for this is at higher speed more energy is imparted to the charge to break the ore particles and the number of impacts per unit time will also be higher. The rods should be 152 mm shorter than the inside working length of the mill. Rods have a tendency to break during operation therefore the quality of rod should be carefully chosen.. According to Rowland and Kjos [2] the recommended ratio of rod length to mill working diameter need be between 1.4 and 1.6. to yield acceptable life to the rods with minimum breakages

Rod diameter

Rod diameters have to be carefully chosen since during the grinding process they wear in different manners. For example, at the feed end where the wear is maximum, the rod wears down to a pointed shape. At the middle it wears into an elliptical shape while at the discharge end it becomes conical. This produces uneven stresses along the length as a result the rods break into smaller sizes. The choice of rod diameter is also related to the ore characteristics, chiefly the work index, ore feed size (F_{80}) and the density of the ore. Rowland and Kjos [2] have considered these variables and have established the relation in Eq. (8.1) to calculate the rod diameter:

$$d_R = 25.4 \left[\frac{F_{80}^{0.75}}{160} \left(\frac{W_i \, \rho_S}{100 \, \phi_C \, (3.281 \, D)^{0.5}} \right)^{0.5} \right] \text{ mm} \qquad (8.1)$$

where W_i = rod mill work index, kWh/t,
 ρ_S = SG of the feed ore,
 ϕ_C = fraction of the critical speed,
 D   = diameter of the mill, m,
 d_R = initial diameter of the rod, mm.

However, as in ball mills, a gradation of rod diameters is initially charged to take advantage of the voids between the rods.

8.3.3. Rod Diameter at Replacement

During operation of rod mills, rods have to be replaced occasionally as they are subjected to wear and liable to break. The replacement rate should be equal to the rate at which rod size deterioration occur so that equilibrium is maintained. Bond [3] determined the equilibrium rod sizes in the same manner as for a ball charge. The results are reproduced in Table 8.1.

Table 8.1
Equilibrium charge for maximum rod sizes [2].

Max.Dia of Rod, mm	125	115	100	90	75	65
125	18					
115	22	20				
100	10	23	20			
90	14	20	27	20		
75	11	15	21	33	31	
65	7	10	15	21	39	34
50	9	12	17	26	30	66
Total %	100	100	100	100	100	100

To use the table, determine the largest size of the rod to be charged using Eq. (8.1). Then determine the nearest commercially available size from column 1 of Table 8.1. Then read off the corresponding sizes and percent replacement from the table. For example, if the largest diameter of rod to be charged is computed as 100 mm by using Eq. (8.1), then the size distribution of the rods will be 20% of 100 mm size, 27% of 89 mm size and so on down the column to 17% of 50 mm size. When more than one size of rod is required then follow the procedure shown in Chapter 7 for ball sizes.

8.3.4. Reduction Ratio in Rod Mills

The reduction ratio, R, in rod mills varies from 2 – 20 depending on the characteristics of the ore. The usual reduction ratio is about 8. According to Bond [4], the reduction ratio is a function of length and diameter of the mill. The optimum reduction ratio, R_{RO}, can be written as:

$$R_{RO} = 8 + \frac{5L}{D} \qquad (8.2)$$

where R_{RO} =   Optimum reduction ratio and
          L   =   the internal length of the mill.

Thus if L/D equals 1.5, then R_{RO} equals 15.5. The reduction ratio is affected if the production rate is increased or a coarser product is desired. To account for this, an inefficiency factor was introduced by Bond [4]. The actual reduction ratio is related to the optimum reduction ratio by the *inefficiency factor*, F_I, defined as:

$$F_I = 1 + \frac{(R - R_{RO})^2}{150} \qquad (8.3)$$

If for a certain situation the actual reduction was 20 and R_{RO} was equal to 15.5 for a L/D of 1.5, then the inefficiency factor of 1.138 has to be applied to correct for the computed power required for operating a rod mill. This aspect is discussed later.

8.3. Rod Mill Capacity
The capacity of rod mills will depend on the tonnes of the finished product of required size produced per unit time and thus will be a function of:

1.   Mill Characteristics, i.e., length, diameter, speed of rotation, lifters,
2.   Feed (ore) characteristics i.e., soft, brittle or hard,
3.   Initial and final size of the ore, i.e. the reduction ratio.

The capacity will also depend on the kinetic energy available for transfer from the rods to the feed during its passage through the mill. Under a given load and size requirement, the capacity of a rod mill is therefore proportional to the length and diameter. It is usually considered as:

$$Q = k\,L\,D^{2.5} \qquad (8.4)$$

Austin et al [5] considered the general equation of capacity in the form:

$$Q = k\,L\,D^{2+N} \qquad (8.5)$$

where N was related to the diameter of the mill which decreases with larger mill diameter and k involved the constant $\pi/4$.

The relationship between capacity and mill diameter and length is shown in Fig. 8.5 from data provided by Kurimoto [6]. The trend lines in Fig. 8.5 are calculated from Eq. (8.4) based on the rod mill length and diameters provided by Kurimoto. The figure shows that the effect of an increase in mill diameter on capacity is more significant than an increase in mill length. This is illustrated by Fig. 8.6.

The effect of mill length on capacity as determined by Kurimoto [6] and Marcy [7] for mill length 1.2 m to 4.1 m is plotted in Fig. 8.6. The trend illustrated by both workers is similar.

218
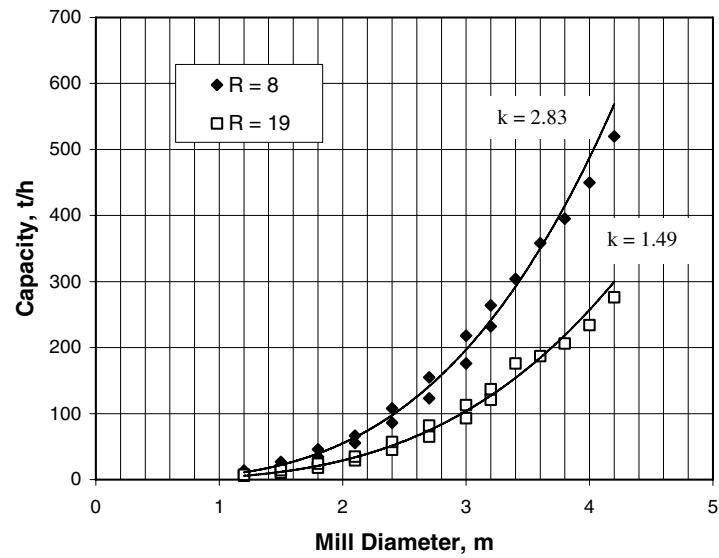
Fig. 8.5. Effect of mill diameter on rod mill capacity for two reduction ratios. The solid lines are calculated from Eq. (8.4) [6].
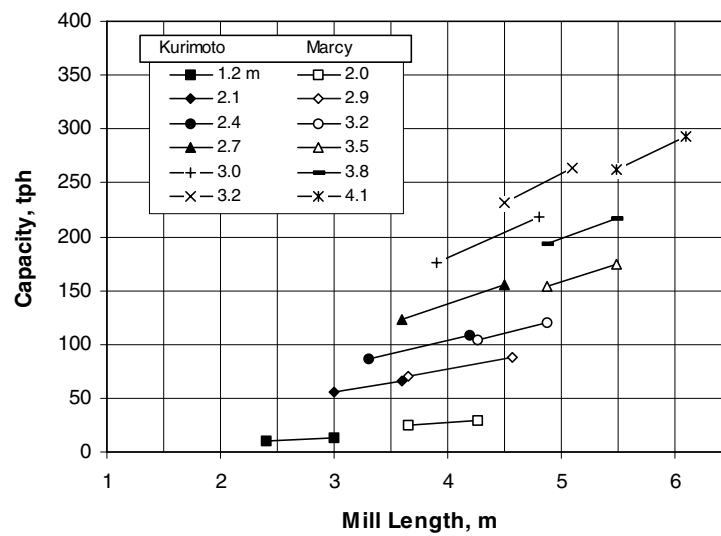
Fig. 8.6. Effect of mill length on the capacity of rod mills for different mill diameters in meters [6,7].
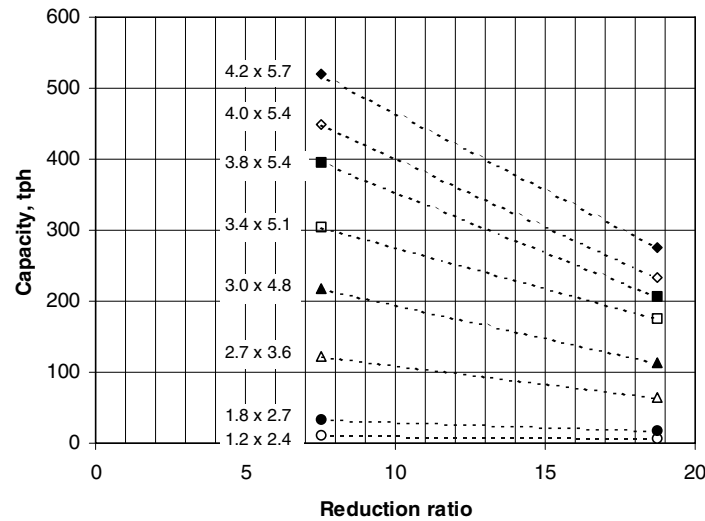
Fig. 8.7. Effect of reduction ratio on the capacity of rod mills for different mill dimensions (diameter x length) in meters [6].

The capacities of larger mills are more sensitive to changes of reduction ratios. Working with eight rod mills of different sizes ranging from 1.2 x 2.4 m to 4.1 x 5.7 m at two levels, Kurimoto [6] confirmed this observation. Fig.. 8.7 shows that rod mill capacities varied inversely as the reduction ratio.

The capacities of rod mills are limited by practical operational problems like:

1. Limitations of steel mills to produce perfectly straight steel rods more than 6 m long
2. Tangling of rods
3. Swelling of the charge, particularly near the feed end
4. Increasing slurry density due to loss of water
5. Faulty liners and lifters

8.4. Rod Mill Power Draft

As in ball mills, the power draft of a rod mill is the product of capacity and work index, which is the energy required to break a mineral of a given size to the required size. The mill power is also increased by increasing the rod charge and the mill speed while the mill power and capacity are both increased with increasing mill length.

Based on these observations and working on wet overflow mills Rowland and Kjos [2] suggested that the power draw at the pinion shaft per unit mass of rods is given by:

$$\frac{P_M}{M_R} = 1.752 D^{0.33} \left(6.3 - 5.4 J_R\right) \phi_C \tag{8.6}$$

where P_M/M_R =   rod mill power per mass of rods, kW/t,

D   = mill inside diameter, m,

J_R = fraction of mill volume occupied by rods,

ϕ_C = fraction of critical speed.

For small ball mills, the power draw under dry batch grinding conditions was derived by Austin et al [5] and the same considerations apply for rod mills. Eq. (8.6) indicates that like any tubular mill the variation of mill power with speed in a rod mill is almost linear. This is true at the initial stages but breaks down when the critical speed is reached. At speeds in excess of the critical speed the power requirements decrease sharply. This is to be expected as rotation in excess of the critical speed results in the charge adhering to the inside liner and do not either cascade or cataract. Typical power requirements for two different mill loadings obtained in a laboratory size mill (0.6 m x 0.31m) with 20 lifters 25 mm high are plotted in Fig. 8.8.

Fig. 8.8 shows that the general characteristics of the change of mill power with mill speed for 17% and 40% mill loadings of a tumbling mill whose critical speed was 101 rpm. It can be seen that at 40% loading the maximum mill power occurred at about 70% of the critical speed while at a lower loading the maximum power drawn was nearly at the critical speed.

Eq. (8.6) indicates that the power required is a function of the critical speed. Some manufacturers recommend an optimum speed of operation of their rod mills. For example Marcy mills suggests that for their mills the peripheral speed should be governed by the relation:

$$\text{Peripheral Speed} = 108.8\,D^{0.3} \qquad\qquad (8.7)$$

where the speed is in m/min for the mill diameter, D, in meters.

The expression is applicable to mill diameters between 1.52 and 4.1 m and the speed of rotation should be chosen accordingly.
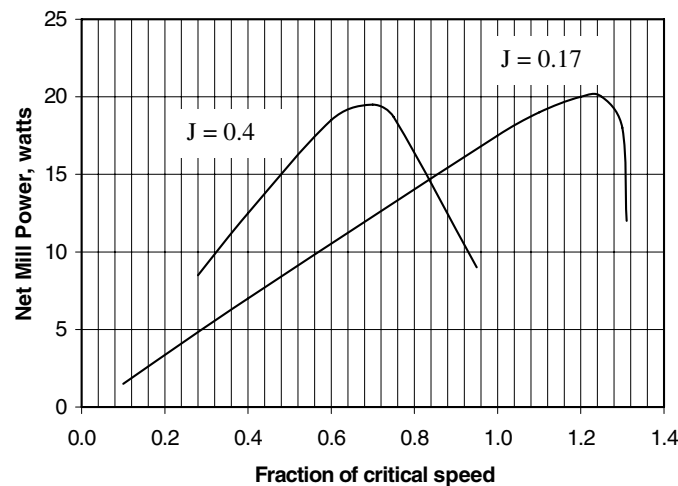
Fig. 8.8. Effect of mill speed on mill power in a 200 mm diameter laboratory mill [5].

Mill Power Corrections

In industrial situations where conditions differ from Bond's set-up [4], Rowland and Kjos has suggested in a series of papers [2,8], that Bond's Eq. (3.25) can be used after correcting for different conditions encountered in industrial practice. Austin et al [5] pointed out similar corrections required to Bond's equation to meet industrial conditions. These corrections are summarised below for specific conditions and are applicable to both rod and ball mills. More than one correction factor may be applicable. All factors are considered separately and the total correction determined.

1. Correction for dry grinding.

Dry grinding power $P_{M(dry)}$ = Wet grinding power $(P_{M(wet)})$ x F_1 (8.8)

F_1 ranges from 1.1 to 2.0 but for most materials is taken as 1.3.

2. Correction for wet open circuit grinding for ball mills.

Power for wet open circuit = F_2 x Power for wet closed circuit   (8.9)

F_2 is known as the inefficiency factor for the wet closed circuit grinding. It is a function of the sieve size used to determine the value of work index, W_i, and the percentage passing this control size. This function has been determined for different percentages passing the controlling sieve size and is shown in Fig. 8.9.

3. Correction for mill diameter (Diameter Efficiency Factor).

To account for the effect of a mill diameter which is different from the 2.44 m mill diameter used by Bond in the determination of W_i, the mill power has to be multiplied by the factor F_3 given below:

$$F_3 = \left(\frac{2.44}{D}\right)^{0.2} \quad \text{for } D < 3.81 \text{ m}$$

$$= 0.914 \quad \text{for } D \geq 3.81 \text{ m} \tag{8.10}$$

where   D   = mill diameter in meters

The solid line in Fig. 8.10 is plotted from Eq. (8.10). For mill diameters greater than 3.81 m, the factor F_3 is constant at 0.914.

4. Correction for oversize feed.

Oversize has been defined by Austin et al [5] when the feed size, F_{80}, exceeds the value given by:

$$F_{80} > 4000 \left(\frac{14.3}{W_{i(test)}}\right)^{0.5} \tag{8.11}$$
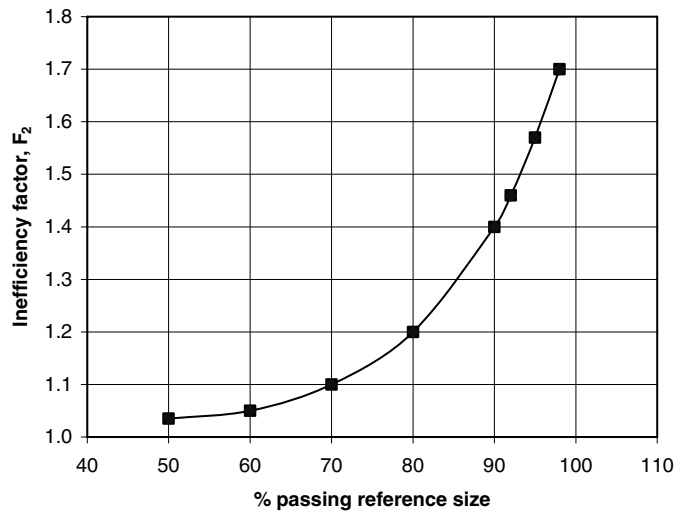
Fig. 8.9. Variation of the inefficiency multiplying factor, F_2, with product size control for ball mill grinding [2].

For the different mill diameters commercially available, the values of F_3 are plotted in Fig. 8.10 from data by Rowland and Kjos [2].
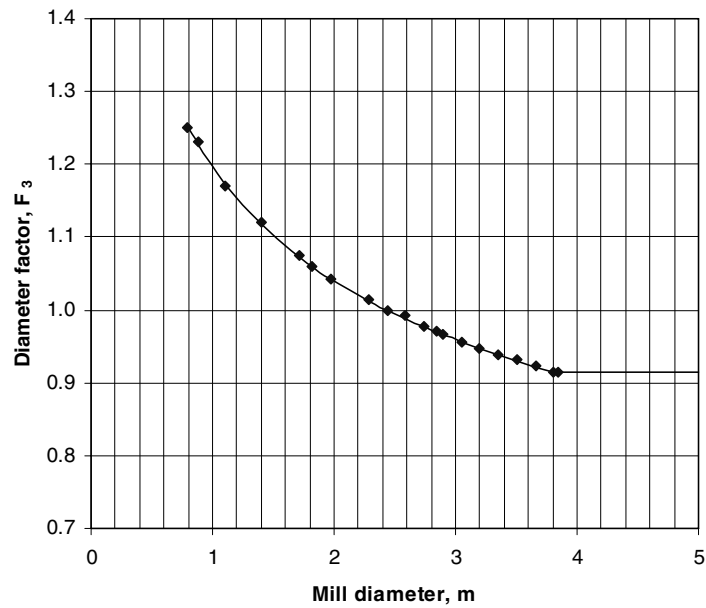
Fig. 8.10. Diameter efficiency factor, F_3 [2] and Eq. (8.10).

The optimum feed size suggested by Rowland and Kjos [2] for a rod mill is:

$$F_{OPT} = 16000 \left(\frac{14.3}{W_i} \right)^{0.5} \tag{8.12}$$

The value of W_i is best taken from an impact test or a rod mill grindability test, which ever is the greater. For a ball mill, the value of the constant in Eq. (8.12) equals 4000 according to Rowland and Kjos, [2].

The correction factor F_4 is given in terms of work index by Rowland and Kjos [2] as:

$$F_4 = 1 + \frac{\left(\dfrac{W_i}{1.1} - 7 \right)\left(\dfrac{F_{80} - F_{OPT}}{F_{OPT}} \right)}{R} \tag{8.13}$$

where R   = the reduction ratio
         F_{OPT} = optimum feed size

This factor is not required for a ball mill fed by a rod mill or if F_4 is less than 1.0.

5. Correction for fineness of grind.

A correction factor for fineness of grind is applicable when greater than 80% of the ground product is less than 75 microns in size.

The correction factor is:

$$F_5 = \frac{P_{80} + 10.3}{1.145 \, P_{80}} \tag{8.14}$$

6. Correction for reduction ratio (low or high).

This correction is mainly for low reduction ratios. The correction factor F_6, need not be applied if:

$$-2 < (R - R^*) < +2 \tag{8.15}$$

where $R^* = 8 + \dfrac{5 L_R}{D}$

         L_R = length of rods, in meters
         D   = inside liner diameter of rod mill, in meters.

Correction factor F_6 is estimated using the equation:

$$F_6 = 1 + 0.0067 \, (R - R^*)^2 \tag{8.16}$$

The correction is not always needed for high reduction ratios but is used if W_i for the rod mill and ball mill is greater than 7.

7. Correction for low reduction ratio in ball milling.

If the ball mill reduction ratio is less than 6 a correction factor, F_7, is applied:

$$F_7 = \frac{2(R - 1.35) + 0.26}{2(R - 1.35)} \qquad (8.17)$$

This correction is particularly applicable for regrind mills.

8. Correction for feed preparation.

For efficient operation of rod mills the feed should preferably be uniform in top size. The manner of feeding either from conveyors or directly from bins and chutes affects the power consumption and mill performance. To correct for feed preparation is difficult. The rule of thumb suggested by Rowland and Kjos [2] is summarised in Table 8.2.

Table 8.2
F_8 feed corrections for rod mill operation [2]

a. For rod mill operation only:

Condition	Correction
Feed prepared by open circuit crushing	use a factor of 1.4
Feed prepared by closed circuit crushing	use a factor of 1.2
Factors F_3, F_4 and F_6 have also to be applied	use F_3, F_4 and F_6

b. For rod mills in a rod mill-ball mill operation:

Condition	Correction
Rod mill feed from open circuit crushing	use a factor of 1.2
Rod mill feed from closed circuit crushing	no factor required
Factors F_3, F_4 and F_6 have also to be applied	use F_3, F_4 and F_6

The total correction F_T, applicable to the rod mill power then is:

$$F_T = F_1 . F_2 . F_3 . F_4 . F_5 . F_6 . F_7 . F_8 \qquad (8.18)$$

For a milling condition when a certain factor is not applicable it should be neglected. The total mill power will then be:

$$P_M = W \times F_T \times \text{Capacity} \qquad (8.19)$$

The above considerations for determining the mill power draw serve as a guide for the selection of mills for a particular job. Examples 8.1 and 8.2 illustrates the method of calculating mill power draw and also to compute the size of mill required for specific purpose.

Example 8.1

A uniform discharge from a closed circuit jaw crusher is 200 t/h. The crusher feeds a wet rod mill such that 80% of the crusher product passes a 16 mm screen. The rod mill feeds a wet ball mill at a feed size of 1.0 mm (1000 microns) and produces a product with 80% passing a 150 micron screen. The rod mill is in an open grinding circuit. Determine:

1. The shaft power of the rod mill
2. The size of the industrial mill

Data: Laboratory Standard Bond Test:
Rod Mill: Grindability Index at 10 mesh = 13.5 kWh/t

Solution

Step 1
From Eq. (3.3) the work is given by:

$$\text{Work} = 10\,W_i \left(\frac{1}{\sqrt{P_{80}}} - \frac{1}{\sqrt{F_{80}}} \right) \qquad \text{kWh/t}$$

(A factor of 1.1 may be required if the work index is in kWh/short ton)

Substituting values:

$$\text{Work} = 10 \times 13.5 \left[\frac{1}{\sqrt{1000}} - \frac{1}{\sqrt{16000}} \right] = 3.20 \text{ kWh/t}$$

Step 2 Evaluate correction factors.
1. Correction factor F_1 is not applicable.
2. Correction factor F_2 does not apply to rod mills.
3. Correction factor F_3 has to be considered after L and D are determined (usually towards the end of the computation). Hence F_3 will be determined later.
4. Since the feed size is 16,000 microns, correction factor F_4 has to be determined.
     Use Eq. (8.12) to determine F_{OPT}, but first determine reduction ratio R.
     Reduction ratio (R) = 16,000/1,000 = 16.0
     Optimum Feed Size (F_{OPT}) = 16,000/(13 x 1.1/W$_i$)$^{0.5}$ = 16,000 x (13 x 1.1/13.5)$^{0.5}$
         = 17,952 microns
Since the feed is less than the optimum, no correction is necessary.
5. Correction factor F_5 is not applicable.
6. Correction factor F_6 is applicable when R is between R* + 2 and R* − 2.
     R* is estimated after mill size determination.
7. Correction factor F_7 is not applicable for rod mills.
8. Correction factor F_8 is not applicable as the circuit is a rod-ball mill circuit and the rod mill is fed from closed circuit crushing.

Step 3
Total Power required for rod mill $= W \times Q = 3.20 \times 200 = 640$ kW

Step 4
Preliminary selection of a commercially available rod mill may now be made from the manufacturer's catalogue. For example, Allis Chalmer's catalogue shows that the nearest mill size would require 655 kW [2]. Such a mill would have the following tentative dimensions:

Mill length   = 4.88 m
Mill diameter = 3.51 m (inside diameter = 3.31 m)
Rod length   = 4.72
Rod load   = 40%
Rod charge   = 90.7 t

Step 5
The diameter efficiency factor, F_3 in step 2 can now be determined using Eq. (8.10) (Fig. 8.10). As the ID of the mill has been provisionally established as 3.31 m, then:

$$F_3 = \left(\frac{2.44}{3.31}\right)^{0.2} = 0.941 \qquad \text{for D} < 3.81 \text{ m}$$

Hence, the corrected power $= 640 \times 0.941 = 602$ kW.

Step 6
Referring again to Allis Chalmer's rod mill performance in Appendix B-4, for a mill power draw of 618 kW, the following mill will be finally suitable:

Mill length   = 4.86 m
Mill diameter = 3.35 m (inside diameter = 3.15 m)
Rod length   = 4.72 m
Rod load   = 45%
Rod mass   = 93.5 t

The factor F_6 is dependant on the reduction ratio and can be calculated once L and D of the mill is established. In this case:

$$R^* = 8 + 5\left(\frac{4.72}{3.15}\right) = 15.5$$

Since $(R - R^*) = (16.0 - 15.5) = 0.5$, the factor F_6 is not applied and the calculated mill power remains the same and so does the final dimensions of the mill.

Example 8.2

Rod Mill –Ball Mill Circuit:
Consider the set-up in example 8.1 along with the following additional data:

Grindability index for the ball mill   = 12.0 kWh/t
Product size from the ball mill   = 150 microns

Determine the size of the ball mill operated in closed circuit.

Solution

Step 1
The discharge from the rod mill is the feed to the ball mill. Therefore in this case the work, W, will be:

$$W = 12.0 \times 10 \left[\frac{1}{\sqrt{150}} - \frac{1}{\sqrt{1000}} \right] \quad kWh/t$$

$$= 6.0 \; kWh/t$$

Step 2   Corrections to the work index value:
Correction factors F_1 and F_2 do not apply
Correction factor F_3 will be calculated after the mill diameter has been determined.
Correction factor F_4:
     Check for oversize using Eq. (8.12).

$$F_{OPT} = 4000 \left(\frac{13 \times 1.1}{12.0} \right)^{0.5} = 4{,}367 \text{ microns}$$

The feed size (1000 microns) is less than this optimum feed size, therefore the correction does not have to be applied.
Correction factor F_5 is not applicable as in this case $P_{80} > 75$ microns.
Correction factor F_6 is determined after mill dimension have been estimated.
Correction factor F_7 is not applied as the reduction ratio is greater than 6 (1000/150 = 6.7)
Correction factor F_8 is not applicable

Step 3
Mill Power required = 6.0 x 200 = 1200 kW

Step 4
To determine the commercially available ball mill that would suit the conditions, refer to the manufacturer's literature, for example, Allis Chalmers' as published by Rowland and Kjos [2]. From the tabulated data, the mill charge and other characteristics corresponding to a power draw of 1273 kW are:

Ball mill length   = 4.57 m
Ball mill diameter   = 4.57 m   (inside liner diameter = 4.39 m)
Ball mill load   = 35%
Ball charge mass   = 113 t
Ball size   = 64 mm

Step 5
The diameter efficiency factor, F_3 in step 2 can now be determined using Eq. (8.10) (Fig. 8.10). As the ID of the mill has been provisionally established as 4.39 m, then:

$F_3 = 0.914$ as $D > 3.81$ m

Hence, the correction factor, $F_3 = 0.914$

Step 6
The factor F_6 is dependant on the reduction ratio and L and D of the mill. In this case:

$$R = \frac{1000}{150} = 6.7$$

$$R^* = 8 + 5\left(\frac{4.57}{4.39}\right) = 13.2$$

Since $(R - R^*) = (6.7 - 13.2) = -6.5$, which exceeds -2, the factor F_6 has to be applied.

Correction factor F_6 is estimated using the Eq. (8.16):

$$F_6 = 1 + 0.0067 (R - R^*)^2 = 1 + 0.0067 (-6.5)^2 = 1.28$$

The corrected mill power then is given by:

Total Power required for the ball mill $= 1200 \times 0.914 \times 1.28 = 1407$ kW

Referring again to Allis Chalmers' ball mill performance table, for a mill power draw of 1412 kW, the same mill dimensions will be suitable if the ball charge is increased to 45% with a charge mass of 144 t.

8.5. Mill Drive

A mill ready to start a grinding operation could be around 150 t in dead weight. Thus the initial torque on the mill shaft is very high and an electric drive motor and drive is designed to cope with it. Fig. 8.11 illustrates a typical change in torque with increasing speed of motor. It can be seen that the running torque of 140% is typical. Indeed provision of 150% of running torque needs to be considered. Depending upon load and size of the mill, the usual torque is between 120% to 140%. Therefore the starting current is high.

To cope with the situation one of the methods practiced is to introduce an air-clutch, which helps to start the motor with no load. When the motor is in full speed the clutch is released to transfer the load smoothly. An alternate arrangement is to use an induction motor or a synchronous motor coupled directly to the pinion shaft of the mill.
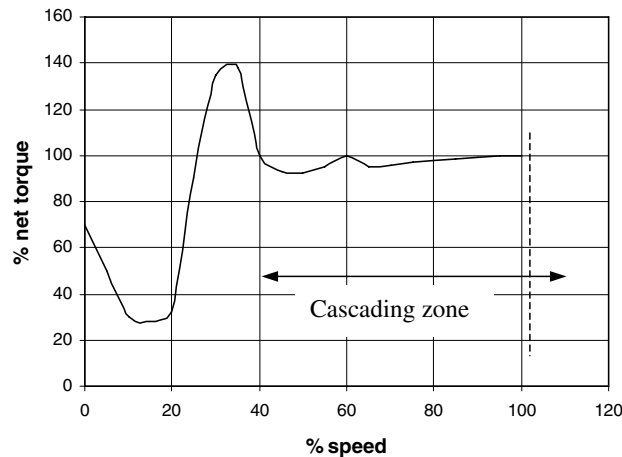
Fig. 8.11. Relation between speed and torque in rod mills [9].

8.6. Problems

As the considerations of rod mills are similar to the ball mills, some of the problems given below require the use of formulae described for ball mill operations in Chapter 7.

8.1.

The inner dimensions of a rod mill were 1.8 x 1.8 m and the largest diameter of rod charged was 76 mm. The mill consumed per tonne of rods was 25 kW/t. Assume the critical speed factor is equal to 0.72. Determine:

1. The limiting speed at which the mill should be permitted to operated,
2. The mill loading.

8.2.

A 3 m x 3 m rod mill was charged with 100 mm diameter steel rods having a bulk density of 5.2 t/m^3. In the stationary state the height of the charge occupied two-thirds of the radius and the porosity of the bed was 35%. Determine:

1. The mill volume occupied by the charge (J)
2. The fraction of the mill volume occupied by the ore if U = 1.1
3. The fraction of mill volume occupied by the rods
4. The mass of rods in the mill.

8.3

A wet rod mill was loaded to 45% of its volume with a charge consisting of a gold ore and steel rods. The rods diameter was 70 mm. The mill had an inner diameter of 1980 mm and

was rotated at 21 rpm with a rod load of 23.8 t. The rock volume was 0.4 times the rod volume after taking into account the porosity of the bed. Estimate:

1. The fraction of the critical speed at which the mill operates
2. The maximum power drawn
3. The difference in power requirements if the mill was filled to the same extent with balls having the same diameter as the rods.

8.4.

The length to inside diameter ratio of a rod mill was 1.5 when the length was 4.72 m. The true density of the grinding media and the ore were 8.0 t/m^3 and 2.35 t/m^3 respectively. 40% of the mill volume was filled with grinding rods. The mill was operated at 60% of its critical speed where 80% of the ground particles passed through the control sieve size. Laboratory tests performed at wet open circuit conditions indicated that the work index of the material to be ground was 13.2 kWh/t. The feed and product sizes were 6000 microns and 250 microns respectively.

Calculate the mill power required for operating at a 100 tph throughput and under conditions of:

1. Wet grinding
2. Dry grinding
3. Power required if the rod mill was a grate discharge type.

8.5

The power consumed by a tumbling mill as measured at the shaft was 152 kW when the mill was loaded with 25.6 t of rods and the load was 45% of the mill volume. The bulk density of the rock charged was 2.6 t/m^3. The mill was operated at 21 rpm, which was 70% of the critical speed. Calculate:

1. The inside dimensions of the mill (assume a L/D = 1.65)
2. The mill power and capacity

Data: Bulk density of rods = 5.6 t/m^3
$W_{i-(test)}$ =   12 kWh/t (corrected)
F_{80} =   12,500 microns
P_{80} =   600 microns

8.6

The internal diameter and length of a dry rod mill measured 2.74 m x 3.6 m respectively. The mill was loaded to 40% of its internal volume with rods weighing 36.1 tonnes. The density of the rod material was 7.8 t/m^3. The work index of the material to be ground was estimated in a laboratory as 12.8 kWh/t. The feed to the mill was from a secondary cone crusher, 80% of which passed a 3500 microns sieve. The 80% passing size of the product was required to be 75 microns at a fraction of critical speed of 0.7. Estimate:

1. The capacity of the mill under dry and wet grinding conditions
2. The power consumption at the pinion shaft under dry and wet conditions
3. The specific grinding energies under dry and wet conditions of grinding.

8.7

The test work index of the feed to a rod mill was 10.1 kWh/t. 80% of the feed passed 2 mm and 80% of the product from the mill passed 40 microns. The mill diameter was 3.9 m and the L/D ratio was 1.4. The formal loading factor initially was 0.35 but later altered to 0.45. Estimate the change in grinding capacity of the mill.

8.8

Gold ore was crushed successively in a primary and then in a secondary crusher. Product from the secondary crusher analysed 80% passing 2000 microns. The object was to further reduce the size by grinding to achieve the liberation size of 45 microns. It was therefore ground in a wet rod mill 2.85 m x 4.27 m using steel rods of 4.11 m in length. The total mass of the rod charge was 63.8 tonnes. The test work index was 13.2 kWh/t. During steady state grinding the mill consumed 6.41 kW/t of rods. Calculate:

1. The percent mill volume occupied by the charge during wet open circuit grinding
2. Optimum operating speed (rpm) of the mill
3. Mill capacity (t/h)

Data: Bulk density of rods = 5.6 t/m^3

      I.D. of the mill = 2.85 m.

8.9

Crushed nickel ore was ground in a wet over-flow rod mill with an inside liner diameter of 4.37 m. 40% of the mill volume was filled with steel rods having a maximum diameter of 70 mm and bulk density 5.6 t/m^3. The mill was operated at 75% of the critical speed to produce a steady product size of 600 microns from a feed size of 1200 microns. Power consumption of the mill was 1,735 kW. Estimate:

1. The rod diameter at commence of crushing
2. The rod length

Data: $\rho_S = 4.5$ t/m^3

8.10

A wet overflow rod mill was operated at 75% of the critical speed and found to draw 8.5 kW/t of rods when the mill was loaded to 35% of its volume. A certain number of rods were then removed and the mill power increased to 8.95 kW/t of rods.

Estimate:

1. Volume of mill occupied by the new charge

2.   The diameter of the mill
3.   Mill capacity after removal of rods.

Data: W_i = 12.8 kWh/t, F_{80} = 10,000 microns, P_{80} = 3,000 microns, ρ_B = 6.27 t/m^3
      L/D = 1.33

8.11
A rod mill was fed from a cone crusher at the rate of 250 t/h with a copper ore. The product size from the cone crusher is 12,000 microns. The rod mill, operating wet and in open circuit, produced a product 80% passing size of 600 microns. The product was then pumped to a ball mill, which was operated wet in closed circuit. The product size (P_{80}) from the ball mill was 75 microns. Both mills were run at 40% load and 70% of the critical speed. Estimate:

1.   The total power required in the operation
2.   The diameter of the mills.

Data: Rod mill W_i = 13.0 kWh/t,
          Ball mill W_i = 11.5 kWh/t.

8.12
A wet rod mill (2.44 m x 3.66 m) was fed from a crusher operating in closed circuit. The feed was delivered by a conveyor at a rate of 50 t/h. The rod mill product was fed to a wet ball mill (2.44 m x 2.44 m). Bulk density of rods = 6.25 t/m^3. The feed and product sizes specified and the laboratory grindability test results were:

Mill	Feed	Product
Rod	F_{80} = 6350 microns	P_{80} = 300 microns
Ball	F_{80} = 300 microns	P_{80} = 63 microns

Grindability Laboratory Test Data:

Mill	Bond work Index W_i, kWh/t
Rod Mill, test at 1400 μm (12 mesh)	13.0
Ball Mill, test at 212 μm (65 mesh)	11.5
Ball mill, test at 150 μm, (100 mesh)	12.2

Between the rod and ball mill an intermediate separator in the form of an hydrocyclone was placed. Determine power at the pinion shaft (including loss due to bearings, friction etc) for:

1.   Wet rod mill grinding
2.   Wet ball mill grinding.

Data: Both mills filled to 35% of their internal volumes,
          Both mills operated at 70% of the critical speed,

REFERENCES

[1] C.A Rowland, in Mineral Processing Handbook, N.L. Weiss (ed), SME/AIME, 1985, pp. 3C 44-56.

[2] C.A. Rowland and D.M. Kjos, in Mineral Processing Plant Design, L.M. Mular and R.B. Bhappu (eds), SME/AIME, 1980 p.264.

[3] F.C. Bond, Mining Engineering, 10 No. 5 (1958) 592.

[4] F.C. Bond, British Chemical Eng., 6 (1961) 378, 543.

[5] L.G. Austin, R.R. Klimpel and P.T. Luckie, Process Engineering of Size reduction: Ball Milling, SME/AIME, 1984.

[6] Kurimoto 2003, Retrieved: December 29, 2003, from http://www.kurimoto.co.jp/english/Products/powdersystem/product/Rodmill.html

[7] Marcy, Bulletin 820-979, Mine and Smelter, Denver, Colorado, 1979.

[8] C.A. Rowland and D.M. Kjos, Principles of Mineral Processing, P. Somasundaram (ed), SME /AIME, 1999.

[9] Marcy, Bulletin 812-280, Mine and Smelter, Denver, Colorado, 1978.

Chapter 9. Autogenous and Semi-Autogenous Mills

9. INTRODUCTION

Disintegration and size reduction of some ores is possible in tumbling mills without the aid of grinding media. Grinding mills in which comminution takes place without grinding aids are known as *Autogenous Grinding* (AG) mills or *Fully Autogenous Grinding* mills (FAG). These mills use large lumps of rock as the grinding media. Mills that use intermediate size rock or pebbles as a grinding medium are also autogenous mills but are known as *pebble mills*. Mills that grind hard ores with fracture characteristics that do not lend themselves to fully autogenous milling are charged with a small amount of steel balls to assist in the size reduction. These are known as *Semi-autogenous Grinding* (SAG) mills. In the mining industry all of these types of mills are in use.

The disintegration and size reduction of ores in AG/SAG mills is brought about by a combination of impact, attrition and abrasion forces during mill rotation. Particles at the toe of the mill charge receive the maximum impact forces from falling rocks and other grinding media. Particles in the body of the mill charge partly slide from different heights and are subjected to attrition and abrasion resulting in size reduction.

The operation of AG/SAG mills therefore involves the use of cheaper grinding media as a replacement for expensive steel balls and rods which greatly affect the wear on liners. They are therefore less expensive to operate. It is necessary that the ore should provide a sufficient amount of lumps that would last for a reasonable time to act as the grinding medium. Such ores have been described as competent ores. Ores that break up easily are referred to as either non-competent or incompetent ore.

In recent times these mills have successfully replaced the conventional rod mill–ball mill configurations. In Australia the number of AG/SAG mills increased from about six in 1984 to more than 40 in the following five-year period [1]. The number of installations world wide by mid 1989 was about 471 and presently the number is growing. One of the main interests in these mills is the possibility of eliminating at least one crushing stage from the conventional size reduction processes. Such replacements lead to savings in capital expenditure in a plant design. The SAG mills have been mostly used for milling hard gold and copper ores with quartz, ultramafic or green stone as host rocks. The Bond Work Index of these ores range between 12 –14 kWh/t. Subsequently SAG mill application has been extended to softer ores, like bauxite and clayey hard-capped gold ores.

This chapter examines the developments in the design and operation of both autogenous and semi-autogenous systems of grinding, for size reduction in metallurgical operations.

9.1. Design of AG/SAG mills

Since the breakage of ore in AG/SAG mills is mostly due to impact on particles and media from a height, these mills generally have a large diameter to length (D/L) ratio. However this ratio varies and mills with large length to diameter ratio are also in use, eg. in South Africa. At present the three types of mills commercially made have the following characteristics:

Mills with large D/L ratio, (High aspect mills)   D/L = 1.5 - 3.0

Mills having equal D and L (Square mills)   D/L = 1
Mills with small D/L ratio or high L/D ratio (Low aspect mills)   D/L = 0.33 - 0.66
                                                                                                      (L/D = 1.5 - 3.0)

Mills are designed with tapered conical ends (Fig. 9.1) or square ends (Fig. 9.2). High aspect mills with conical ends are sometime referred to as *pancake* mills while mills with square ends are called *square* mills. The diameters and lengths of square mills are nearly equal.

Some dry autogenous mills operating in Canada are 8.5 m in diameter and 1.5 m in length. These are known as Aerofall mills. The Cadia Hill (Australia) wet SAG mill is 12.2 m in diameter with a 20 MW motor and in 2004 was the largest diameter mill in operation in the world. Mill sizes up to 13.4 m diameter are considered feasible with current technology [2]. The largest volume mill in the world was constructed for Tarkwa, Ghana in 2004. The mill is 8.23 m diameter by 12.19 m effective grinding length (EGL) or inside liner length. The mill is operated in a single stage grinding circuit.

Most AG and SAG mills have slotted steel and rubber liners and are fitted with lifter bars. The liners are either waved or grid type. The grid liners are being increasingly used due to their longer life brought about by ore and balls being trapped in the grids. The trapped ores and balls build up a hard surface on the liners protecting them somewhat from wear. The present tendency is to use composite liners with lifters at the feed end of a mill to initiate impact crushing followed by wave liners along the rest of the length of the mill. Several combinations are constantly being tried to improve liner and shell life. The basic object of liner design is to promote comminution by impact and attrition instead of abrasion.

The discharge ends are fitted with slotted grates acting as a diaphragm, which holds back the larger particles from discharging into the product stream. The size, spacing and design of the holes in the diaphragm are important as they affect the rate of throughput and product size. Open-ended discharge helps to solve problems arising out of high-speed mill rotation in the region where the speed is in excess of 90% of the critical speed. To improve the efficiency of diaphragms at high speeds of rotation, curved lifters have been used [3]. Three types of discharge ends are used, namely mills with wide peripheral discharge, mills having a scoop after the grate to lift the product and mills having the discharge through a trunnion.
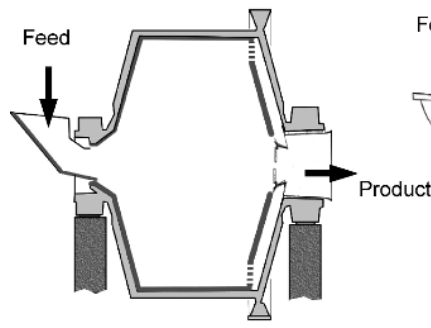
Fig. 9.1. High aspect ratio AG/SAG mill   Fig. 9.2. Square AG/SAG mill with grating.
              with grating and conical ends.

The feeders are either spout or chute type. Low aspect mills are usually seen with spout feeders, while the high-aspect mills are fitted with chutes. As a rule of thumb the chute opening is about 4 times larger than the largest rock size, 100% of which should pass down the chute. The AG/SAG mills generally receive ore directly from the crushing plants with alternative arrangements made to receive ore from a stockpile. In rare cases the feed is directly from the mine.

Schematic diagrams of a typical semi-autogenous mill with large D/L ratio (Fig. 9.1) and a square mill (Fig. 9.2) are illustrated below.

A variety of grates with varying patterns, numbers and sizes are used. Some grates have tapered holes. The main idea is to prevent the build up of middlings inside the mill, which after a period of operation tends to build up and inhibit production rate. The dry autogenous Aerofall mills do not have any gratings. They are swept with an air draft. The draft carries and discharges grounded particles of a size commensurate with the air velocity.

9.1.1. Design of AG/SAG Circuits

In designing a crushing-grinding circuit, the concentration of the mineral in an ore and its down stream treatment is of prime importance. Equally important is the liberation size of the mineral, which determines the ultimate grind. The commonly used circuits for AG/SAG mills are:

1.   open circuit with a trommel or screen as the classifier,
2.   closed circuit with cyclone classifier,
3.   open circuit with closed circuit ball mill, and
4.   open circuit followed by a secondary crusher and then ball milling.

The first two types may be called single stage operation while the last two are two-stage operations. Most AG/SAG mills operate in open circuit (Fig. 9.3) when the product size is usually coarse. Usually provision exists for installing a classifier like a straight screen, a trommel or a curved DSM screen to remove critical sized pebbles (scats). For finer and more uniform product, closed circuit grinding with classifiers, like a hydrocyclone, is usually employed (Fig. 9.4). A two stage close circuit-grinding set-up with hydrocyclone is shown in Fig. 9.5.

The main problem in designing and operating an AG/SAG circuit is the tendency to build-up the 25 –50 mm fraction of the charge which hampers throughput. This specific size fraction that builds up in the mill is referred to as the *critical size*. Therefore pre-treatment of the feed should be such that the presence of this fraction is minimal. If the build up of critical sized pebbles is too great 50 – 90 mm slots are cut into the grate (pebble ports) to allow the scats to discharge from the mill. These scats are crushed before returning to the SAG mill or passing onto a ball mill in an ABC (Autogenous/Ball mill/Crusher) circuit (Fig. 9.3 and 9.6).

Instead of recycling the larger size fraction, the oversize product from AG/SAG mills is sometimes prevented from discharging from the mill by using a reverse spiral at the discharge end and washes back into the mill for further grinding [4].

Otte [5] and Patzelt et al [6] have suggested that High Pressure Grinding Roll (HPGR) mills be included in the grinding circuits of AG/SAG mills. The intention is to take care of the presence of critical size pebbles in the SAG product streams and to produce a finer and more uniform product. It has been claimed that the final product was more amenable to flotation and leaching circuits that follow in some operations. A typical SAG-HPGR-Ball mill circuit
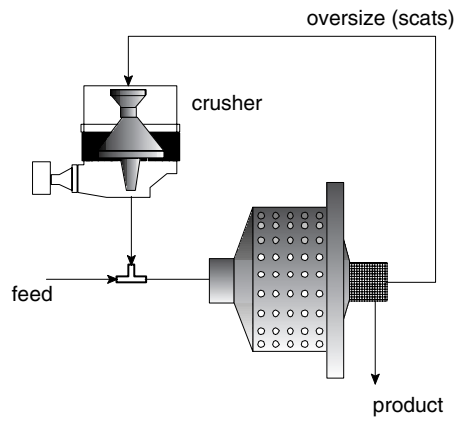
Fig. 9.3.   SAG mill circuit – with provision
            for scats recycle
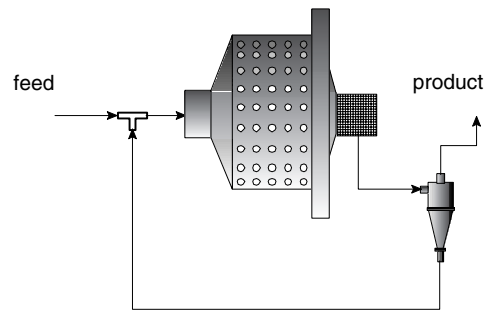
Fig. 9.4. SAG mill in closed circuit
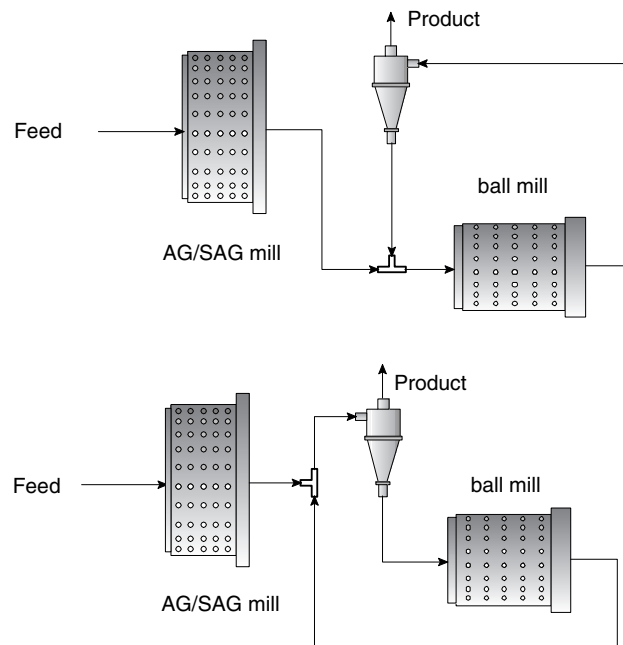
Fig. 9.5. Two stage autogenous – ball mill circuits
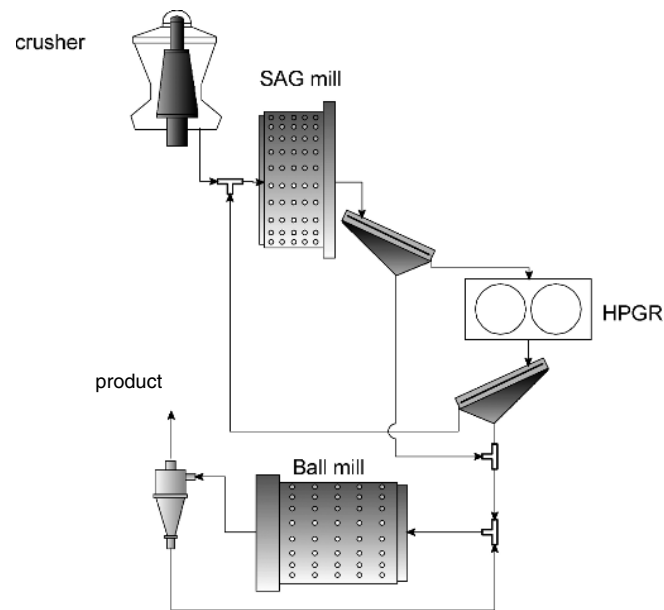
Fig. 9.6. SAG mill, HPGR and ball mill in an ABC closed circuit

suggested by Patzelt et al [6] is shown in Fig. 9.6 where the pebbles from the SAG mill are crushed in the high pressure grinding rolls.

It is a general observation that SAG mills are helpful for grinding where wide variations in the grindability of ores are experienced. Siddall [1] indicates that for weathered ores with a work index of 12-14 kWh/t, both single stage and multi-stage operation can be adopted. However, single stage mills are the preferred option due to its simplicity of operation. For single stage application, square or low-aspect ratio mills are used. This is due to attrition being the preferred force of comminution after breakage by impact and also the circulation load could be less, thus aiding throughput.

In multi-stage circuits the usual options are:

1. open circuit SAG mill,
2. closed circuit ball mill.

The Australian experience of milling lateritic ore is to use a high-aspect ratio mill at the initial stages of operation using a single stage circuit. With time, as the hardness of the ore increases with depth in the mine, a second stage ball mill is added.

While designing a circuit for a particular ore, the problem that often arises is to decide whether to choose a high or low aspect mill. The answer to the problem lies in the total power requirement in the circuit. This aspect is discussed in section 9.4.

Low aspect mills are best suited to low to medium competent ores while high aspect mills are more commonly used for competent ores either as single stage circuits or autogenous-ball mill two stage circuits. The larger diameter and short length provides better impact breakage for the competent ore.

9.2. Operation of AG/SAG Mills

9.2.1. Feed Size

The feed to high aspect AG/SAG mills are usually preferred from gyratory crushers, while the feed to low aspect mills are preferred from jaw crushers. Depending on the set, the maximum size of the particles discharged from gyratory crushers is about 300 mm and from jaw crushers is about 180-100 mm, thus the optimum feed size may be taken to range between 150-300 mm.

According to MacPherson and Turner [7] the optimum feed size consistent with maximum power draw is given by the relation:

$$F_{80} = 53.5 \, D^{0.67} \tag{9.1}$$

where F_{80} = feed 80% passing size in mm,
D = inside diameter of the mill in meters.

The feed in AG and SAG mills contains a fraction that serves as the grinding medium. These larger ore fractions break the smaller particles but also breakdown themselves and exit the mill as product. In due course, the ore feed competency can change as fresher, harder ore is mined at deeper levels. This will alter the balance between the lump grinding media and the softer components of the ore as the harder lumps will breakdown more slowly. Gradually therefore, steel balls will have to be charged to help break the more competent lumps to retain the balance and maintain throughput. In other words, the comminution process is gradually taken over by the steel balls. The number of steel balls and their size depend on the hardness of the ore, the original ore size and the size distribution. Increasing the ball size and decreasing their number would increase the kinetic energy of breakage but the frequency of impact would decrease. On the other hand increasing ball numbers increases the breakage rate and therefore increases the throughput rate. Hence a balance between the number and size of balls is required. Ball sizes used under Australian conditions normally range between 100 mm and 125 mm with a maximum of 175 mm. For ores that easily disintegrate (classed as incompetent), 50 mm size balls may be used, whereas harder ores may require 150-175 mm balls to maintain the required tonnage.

The rate of breakage of particles is found to be dependent on particle size as shown in Fig. 9.7. Austin et al. [8] considered the initial increase in breakage rate to be dominated by attrition. At some larger size, the particle are too big to be successfully nipped and crushed and hence breakage rates decrease. At this point breakage essentially results from abrasion. As the particle size approaches the media size, breakage rates increase again as impact breakage becomes dominant.

9.2.2. Mill Volume

As the first step in working with milling circuits, it is necessary to estimate the mill volume to calculate the charge. Estimation of cylindrical mill volumes is no problem but SAG mills

240
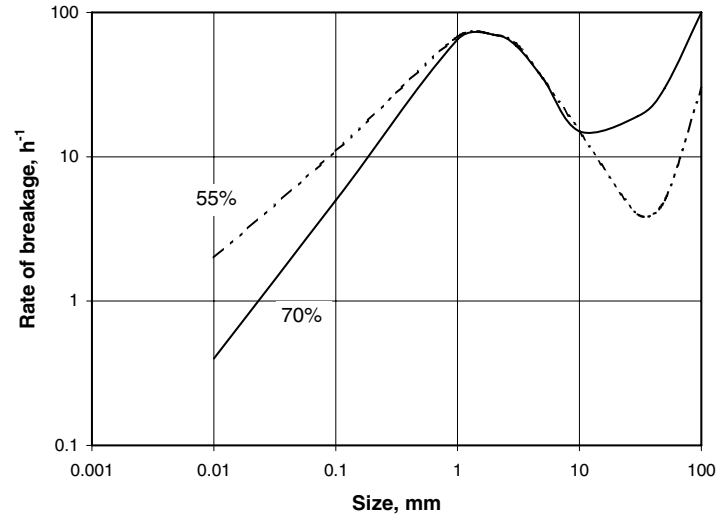
Fig. 9.7. Breakage rate distribution for different size intervals for mill speeds of 55 and 70% of the critical speed [4].

having *pancake* sections with conical bulged ends could be a problem. The cones on either side may or may not be of the same size and could have different cone angles. For estimating the total mill volume the frustum of the two cones have to be added to the cylindrical section of the mill. Fig. 9.8 shows the dimensions of a pancake SAG mill where the dimensions of the cone at one end of the mill is described with subscripts 1 and the corresponding dimensions of the cone at the other end is described using subscripts 2. From simple geometry the cone volumes, V_{CONE}, are in fact the two frustums of the cones and their total volumes will be given by:

$$V_{CONE} = \left(\tfrac{1}{3}\pi\, r_1^2 \left(h_1 + h_1^*\right) - \tfrac{1}{3}\pi \left(\frac{d_1}{2}\right)^2 h_1^* \right) + \left(\tfrac{1}{3}\pi r_2^2 \left(h_2 + h_2^*\right) - \tfrac{1}{3}\pi \left(\frac{d_2}{2}\right)^2 h_2^* \right) \qquad (9.2)$$

It can also be seen that $r_1 = \dfrac{h_1 + h_1^*}{h_1^*}\left(\dfrac{d_1}{2}\right)$, and hence $h_1 + h_1^* = h_1 \left(\dfrac{1}{1 - \dfrac{d_1}{2r_1}} \right)$

Substituting and rearranging according to Austin [9], the total volume of the SAG mill, V_M, is:
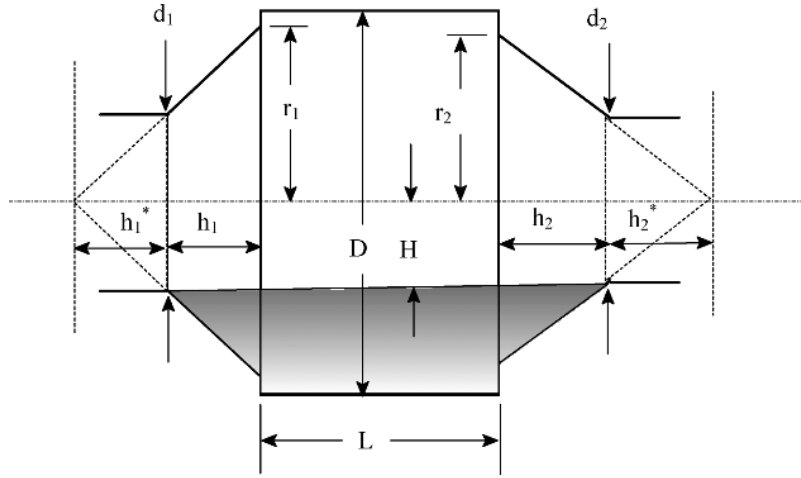
Fig. 9.8. Pancake SAG mill with unequal conical ends

$$V_M = \left(\frac{\pi D^2 L}{4}\right)\left[1+\left(\frac{h_1}{3L}\right)\left(\frac{2r_1}{D}\right)^2\left(\frac{1-\left(\frac{d_1}{2r_1}\right)^3}{1-\left(\frac{d_1}{2r_1}\right)}\right)+\left(\frac{h_2}{3L}\right)\left(\frac{2r_2}{D}\right)^2\left(\frac{1-\left(\frac{d_2}{2r_2}\right)^3}{1-\left(\frac{d_2}{2r_2}\right)}\right)\right] \qquad (9.3)$$

The units for all dimensions shown in Fig. 9.8 are meters, hence the unit of V_M is m^3.

9.2.3. Mill Charge

Usually a SAG mill is charged to 30-35% of its interior volume. The grinding balls occupy 5–15% of the volume [10]. The charge volume can be estimated by measuring the distance between the top level of the charge and the central axis of the mill. It can also be computed from known bulk volumes of ore (slurry densities for wet milling) and bulk density of balls.

The fractional mill volume containing the charge (solids plus balls) is represented by the symbol J_C. For SAG mills, J_C should include the two conical sections. Using the internal volume of the mill from Eq. (9.3), Austin [9] calculated the volume of the mill charge in terms of J_C as:

$$V_c = \left(\frac{\pi D^2 J_c L}{4}\right) + 0.075\,\pi\left[r_1^2\left(\frac{h_1}{1-\frac{d_1}{2r_1}}\right)\left(\frac{H}{r_2}\right)^3\left(\left(\frac{r_1}{H}\right)^{3.25}-1\right)+r_2^2\left(\frac{h_2}{1-\frac{d_2}{2r_2}}\right)\left(\frac{H}{r_2}\right)^3\left(\left(\frac{r_2}{H}\right)^{3.25}-1\right)\right] \qquad (9.4)$$
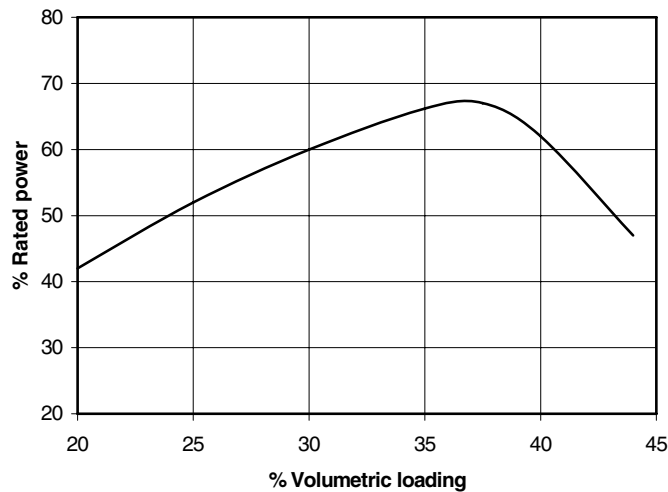
Fig. 9.9. Relation between volumetric loading and SAG mill power for low ball charge and soft ore [11].

The charge volume may also be measured indirectly during operation by the use of predetermined relationships between mill load and power. A typical relation is illustrated in Fig. 9.9.

The mill load is usually measured by load cells or strain gauges. The sensitivity of the power load curve will depend on the method of measurement and the sensitivity of the instrument. Fig. 9.9 shows that overloading of the mill takes place when the mill is loaded in excess of 35%. The mill is then unstable.

Pilot plant work by MacPherson and Turner [7] showed that the ball charge should be about 5% of the mill volume. MacPherson and Turner thus recommend 3 – 8% of the mill volume needs to be steel balls. Reviewing the Australian scene however Siddall [1] observes that the ball load can be up to 15% for the grinding of lateritic ores under Australian conditions in a single stage mill.

Using modelling and simulation of AG/SAG mills, Morrison and Morrell [12] indicated that in most cases, power efficiency increases with mill load.

9.2.4. Mill Speed

During normal operation the mill speed tends to vary with mill charge. According to available literature, the operating speeds of AG mills are much higher than conventional tumbling mills and are in the range of 80–85% of the critical speed. SAG mills of comparable size but containing say 10% ball charge (in addition to the rocks), normally operate between 70 to 75% of the critical speed. Dry Aerofall mills are run at about 85% of the critical speed.

The breakage of particles depends on the speed of rotation. Working with a 7.32 m diameter and 3.66 m long mill Napier-Munn et al [4] observed that the breakage rate for the finer size fractions of ore (say 0.1 mm) at lower speeds (eg. 55% of the critical speed), were

higher than that observed at higher speeds (eg. 70% of the critical speed). For larger sizes of ore, (in excess of 10 mm), the breakage rate was lower for mills rotating at 55% of the critical speed than for mills running at 70% of the critical speed. For a particular intermediate particle size range, indications are that the breakage rate was independent of speed. The breakage rate–size relation at two different speeds is reproduced in Fig. 9.7.

9.2.5. Effective Grinding Length

For conical ended mills, the effective grinding length will be different to the length of the cylindrical section of the mill as the cone ends increase the mill volume and hence the load in the mill. The amount of increased mill load and hence the increased effective grinding length will depend on how far up the cone the mill load extends.

Assuming the cones on each end of the mill are the same size and the feed and discharge trunnions were the same diameter and equal to 25% of the mill diameter, Morrell [13] estimated the effective mill length from:

$$L_{EFF} = L_{CYL}\left(1 + 2.28 J_C \left(1 - J_C\right)\frac{\overline{L}_{CONE}}{L_{CYL}}\right)$$ (9.5)

where $\overline{L}_{CONE}$ = mean cone length = 0.5 (centre line length – cylindrical length).

9.2.6. Ball Wear

In a continuous AG/SAG process the wear of the liners and balls is measured by the change of the total mass of a mill. The wear rate of the grinding balls (expressed in terms of kg/day) is indicative of their replacement rate. The make up rate, Q_B, in kg/day, may be estimated by [9]:

$$Q_B = \frac{\pi D^2 L}{4}\left(0.6 J_B \rho_b\right)\left(\frac{8 Q_W}{d}\right) 24 \times 10^3$$ (9.6)

where Q_W = wear rate of the ball radius, mm/h,
   d   = make up ball size, mm,
   L, D   = the length and diameter of the mill in meters,
   ρ_b = ball density in t/m^3.

9.3. AG/SAG Mill Power

In designing crushing – grinding flow sheets, correct estimations of mill power draw is important as it serves as one of the deciding factors for selecting an option between AG/SAG mills. In most cases the circuit with the least or optimal power consumption is the preferred choice.

The mill power is usually determined in a laboratory scale mill and if possible, followed by a pilot plant trial. The value is then scaled up to the desired commercial size. According to MacPherson and Turner [7] if the dimensions of the proposed commercial or full scale plant and the pilot plant mill (or laboratory mills) are known, then the scale up can be achieved using the following equation:

$$P_M = 1.05\, P_{TEST} \left[\left(\frac{L}{L_{TEST}} \right) \left(\frac{D}{D_{TEST}} \right)^{2.65} \right] \qquad (9.7)$$

where P_M = gross mill power of the full scale mill, kW,
$\quad\quad P_{TEST}$ = mill power for the test mill, kW,
$\quad\quad$ L, D   = length and diameter of the full scale mill, m,
$\quad\quad L_{TEST},\ D_{TEST}$ = length and diameter of the test mill, m.

Eq. (9.7) is applicable for mill loadings between 25% and 30%. The mill capacity can be estimated by dividing 90% of the gross mill power by the net grinding power per tonne from the test mill.

Several workers have attempted to determine the power draw for Autogenous and Semi-autogenous mills [7,9,14,15]. For autogenous mills, like the dry Aerofall mills, MacPherson and Turner [7] established that the power consumption was a function of mill diameter and length. For dry commercial AG mills they derived the power as:

$$P_M = 0.992\ L\ D^{2.8}\ \rho_c \qquad (9.8)$$

where ρ_c = bulk density of the mill charge (rock plus balls and water), t/m^3
$\quad\quad$ L, D are in meters and P_M is in kW.

Morrison and Morrell [12] suggest that the larger diameter mills are more power efficient. Austin [9] has considered both low aspect and high aspect types of autogenous grinding mills and arrived at a general expression for mill power that is applicable to both types. Austin considered the mill power as the sum of the power required by the central cylindrical portion and that required by the two end cones. The mill power for either AG or SAG mill can be computed from the equation:

$$P_M = K\ D^{2.5}\ L \phi_C \left(1 - \frac{0.1}{2^{9-10\phi_c}} \right) \rho_C\ J_C\ (1 - A J_C)(1 + F) \qquad (9.9)$$

where K   = a constant,
$\quad\quad$ J_C = volume fraction of the cylindrical portion of the mill filled by the charge,
$\quad\quad$ A   = constant.
$\quad\quad$ (1+F) = correction for conical ends to a cylindrical mill.

The value of F is given by the following expression for $J_C < 0.45$:

$$F = \frac{0.046}{J_C(1-AJ_C)} \left(\frac{\frac{h_1}{L}}{\left(1-\frac{d_1}{2r_1}\right)} \left[\left(\frac{1.25\frac{r_1}{D}}{0.5-J_C} \right)^{0.1} - \left(\frac{0.5-J_C}{1.25\frac{r_1}{D}} \right)^{4} \right] + \frac{\frac{h_2}{L}}{\left(1-\frac{d_2}{2r_2}\right)} \left[\left(\frac{1.25\frac{r_2}{D}}{0.5-J_C} \right)^{0.1} - \left(\frac{0.5-J_C}{1.25\frac{r_2}{D}} \right)^{4} \right] \right) \qquad (9.10)$$

The symbols refer to Fig. 9.8.

Eq. (9.10) is valid for normal mill loadings of 25% to 30% and can be readily used, provided detailed dimensions of the mill are known.

A theoretical approach to the problem was made by Austin [9], which provided a practical solution to the mill power. The following is a synopsis of his work.

Austin considered the potential and kinetic energies associated with the particles by tracing their movement within the mill. The movement of the mill, which lifts the particles and the grinding media to a certain height, imparts the kinetic energy to the particles. The particles and the grinding media slide down or cataract to the toe of the charge. The potential energy of the paths of the particles was obtained from the earlier works of Vahl and Kingma [16] and Hogg and Fuerstenau [17]. Austin then combined the kinetic and potential energies and developed the mill power expression as:

$$P_M = k \sin \alpha \, \sin^3 \theta \, \rho_c \, \phi_c \, L D^{2.5} \, (1 + \gamma)$$ (9.11)

$$\text{where} \quad \gamma = 0.188 \left[\frac{\phi_c^2}{\sin \alpha} \right] \left[\frac{1 - \cos^4 \theta}{\sin^3 \theta} \right]$$ (9.12)

P_M = mill power in kW,
K = a constant and the angles α and θ are as indicated in Fig. 9.10.

This model does not account for the friction of particles on the surface, but it is assumed that the flow down the surface of the charge is smooth.

Austin recognised that Eq. (9.11) was similar in structure to Bond's mill power equation for cylindrical mills [18]. On this basis, Austin suggested that the power of SAG mills could be given by:

$$P_M = K \, D^{3.5} \, J_c \, (1 - A J_c) \left(\frac{L}{D} \right) \phi_c \left(1 - \frac{0.1}{2^{9 - 10\phi_c}} \right) \rho_c$$ (9.13)
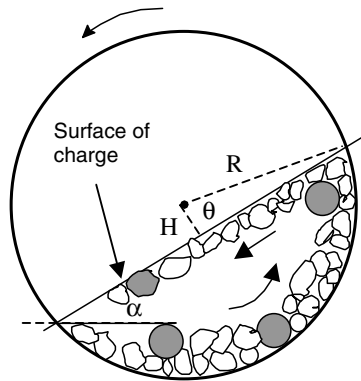
Fig. 9.10. Movement of particles in a tubular mill as modelled by Hogg & Fuerstenau [16] and Austin [9].

Austin used a value of 1.03 for the constant A compared to Bond's recommended value of 0.937, while Gutiérrez and Sepúlveda [19] advocated a value of 1.065. Austin developed the value of ρ_C in terms of the mass fraction of the charge (rock plus balls and water) in SAG mills and the fractional filling of the mills as:

$$\rho_C = \frac{(1-\varphi)\, J_C \left(\dfrac{\rho_R}{M_R}\right) + 0.6 J_B \left(\rho_b - \dfrac{\rho_R}{M_R}\right)}{J_C} \qquad (9.14)$$

where ρ_R = density of the rock (mean), t/m^3,
  ρ_b = density of the balls, t/m^3 (8.0 for steel),
  φ = porosity of the bed,
  J_C = fractional volume of the cylindrical portion of the mill filled with all charge (rock plus balls),
  J_B = fractional volume of the cylindrical portion of the mill filled with balls,
  M_R = mass fraction of rock in the total charge (rock plus water).

The constant 0.6 in Eq. (9.14) is derived from assuming a ball bed porosity of 0.4. Alternative expressions for the charge density is given by Moly-Cop [20]:

$$\rho_C = \frac{\left((1-\varphi)\rho_b\, J_B + (1-\varphi)\rho_R\,(J_C - J_B) + \rho_p\, U_p\, \varphi\, J_C\right)}{J_C} \qquad (9.15)$$

where ρ_p = density of the pulp and
  U_p = fraction of the interstitial voids between the balls and rock charge occupied by the slurry of smaller particles.

and Morrell [20]:

$$\rho_C = \frac{J_C\, \rho_R\,(1-\varphi + \varphi U_p\, \rho_S) + J_B\,(\rho_B - \rho_R)(1-\varphi) + J_C\, \varphi\, U_p\,(1-\rho_S)}{J_C} \qquad (9.16)$$

where ρ_S = solids fraction in the slurry by volume,

  $= \dfrac{\rho_p - \rho_w}{\rho_R - \rho_w}$

Substituting the value of ρ_C from Eq. (9.14) into Eq. (9.13) with K = 10.6 and A = 1.03, Austin obtained the final equation of the mill power as:

$$P_M = 10.6\, D^{2.5}\, L\, (1 - 1.03\, J_C)\left[(1-\varphi)\left(\frac{\rho_R}{M_R}\right) J_C + 0.6 J_B\left(\rho_b - \frac{\rho_R}{M_R}\right)\right]\phi_C\left(1 - \frac{0.1}{2^{9-10\phi_C}}\right) \quad (9.17)$$

Eq. (9.17) may be simplified by making use of the following conventions:

1. Effective porosity of the total charge, $\varphi = 0.3$ (30 %),

2. $J_B = \dfrac{\text{Mass of balls}}{0.6 \, \rho_b \, V}$,

3. $M_R = 0.8$.

Austin suggests that the mill power so obtained is applicable to both AG and SAG mills. Neale and Edwards [11] has used this model to control AG and SAG mills and has indicated that the predicted and measured values agree. However, Neale and Edwards' test work was limited to a few observations only.

As observed before, the mill power draw usually increases with an increase in loading until it reaches a peak and then decreases. Austin [9] has determined the maximum load at which the power draw peaks. This is shown in Eq. (9.18):

$$J_{MAX} = \left[1 - \frac{0.6 \, A \, J_B}{(1-\varphi)}\left(\frac{\rho_b \, M_R}{\rho_R} - 1\right)\right]\left(\frac{1}{2A}\right) \qquad (9.18)$$

Taking the recommended value of A as 1.03, Eq. (9.18) transforms to:

$$J_{MAX} = 0.485\left[1 - \frac{0.618 \, J_B}{(1-\varphi)}\left(\frac{\rho_b \, M_R}{\rho_R} - 1\right)\right] \qquad (9.19)$$

The following general observations can be made on mill power consumption [3]:

1. Since mill power is proportional to $D^{2.5}$, larger diameter mills will draw more power per mill volume than small diameter mills. However, long mills (low aspect) may consume more power than high aspect mills due to a larger charge mass out weighing the effect of mill diameter. Low aspect mills retain fines and overgrind material and hence may be up to 16% less efficient than high aspect mills,
2. Diaphragm mills draw 16% more power than overflow mills with the same effective grinding length,
3. SAG mills greater than 9 m in diameter draw about 10% less power than theoretical,
4. In commercial operations it is usual to install 10-20% extra power to meet variations in load primarily due to change in ore characteristics, charging rate etc.

9.3.1. Normalised (Relative) Mill Power

For design and operating purposes it is often necessary to compare performances between mills. A convenient way for comparison is to use the concept of normalised mill power. Austin derived the expression for normalised power which when substituted in Eq. (9.17) provides the relative mill power, P_R, as [11]:

$$P_R = (1 - 1.03 J_C)\left((1-\varphi)\left(\frac{\rho_R}{M_R}\right)J_C + 0.6 \, J_B\left(\rho_b - \frac{\rho_R}{M_R}\right)\right) \qquad (9.20)$$
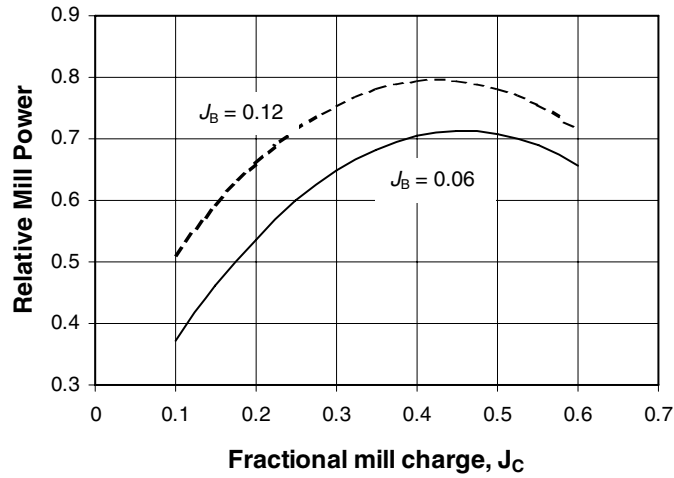
Fig. 9.11. Relation between mill load and relative mill power as expressed in Eq. (9.20) at two ball loadings.

Eq. (9.20) does not contain terms relating to the dimensions of the mill. Therefore P_R is independent of mill size.

The relation between mill load and relative mill power follows the same pattern as the mill load-mill power relation as shown in Fig. 9.9. Fig. 9.11 illustrates this relationship for 6% and 12% ball loads, taking 2.8 as the S.G. of the ore and 8.0 t/m^3 as the density of the balls.

9.3.2. Net Power and No Load Power

The mill power draw has been extensively studied by Morrell [13,21]. His basic assumptions were similar to that of Austin. In addition to computing the power required for a mill Morrell considered the individual power requirements for the cylindrical section and the two conical sections at either end of mill as the *net power*. The gross power was then the sum of the *no load power* and the *net power*. Thus:

$$P_M = P_{NL} + P_{NET} \tag{9.21}$$

The no load power is a measure of some of the power losses in the gears, bearings and electrical components and is the gross power draw of the mill when empty, obtained either during commissioning of the mill or when ground out for a mill reline. Morrell [13] developed an empirical expression for the no load power draw of ball, SAG and AG mills as:

$$P_{NL} = 1.68 \, D^{2.05} \left(\phi_C \left(0.667 L_{CONE} + L_{CYL} \right) \right)^{0.82} \tag{7.70}$$

where P_{NL} = no load power in kW for L and D in meters.

The net power draw, P_{NET}, is given by:

$$P_{NET} = K D^{2.5} L_{EFF} \rho_C J_C \left(\frac{5.97\phi_C - 4.43\phi_C^2 - 0.985 - J_C}{(5.97\phi_C - 4.43\phi_C^2 - 0.985)^2} \right) \phi_C \left(1 - (1 - 0.954 + 0.135 J_C)e^{-19.42(0.954 - 0.135 J_C - \phi_C)}\right)$$

$$(9.22)$$

where K   = a constant (9.1 for grate discharge mills, 7.98 for overflow discharge mills)

  L_{EFF} = effective grinding length

9.3.3. Mill Power, Load and Mill Operation

The operation of AG and SAG mills may be guided by the relation between maximum mill load and mill power as given in Eq. (9.17) and modified later by Morrell (Eq. 9.22). The following general remarks are of interest:

1. While starting a mill, a low power draw suggests the feed rate has to be increased.
2. A high power draw indicates a high mill loading.
3. While operating the mill, a low power draw indicates that the ball or rock charge has to be increased.
4. A high power draw could mean a build up of critical size particles (usually 50 mm to 80 mm).
5. In long mills where the residence time of the ore is longer, if the mineral is not removed soon after liberation, it will be overground and produce more slime that may be harmful for down stream operation, like flotation.
6. In longer mills segregation is more pronounced.
7. Altering the ratio of lifter spacing to height can increase the grinding rate and therefore the power required.

   It is worth noting that in practice the maximum power draw is not constant, but the mill power draw varies with:

1. volumetric load,
2. rock properties (density, hardness, particle size distribution, grindability, competency of ore or otherwise),
3. pulp density and pulp characteristics, and
4. rate of feed.

Every effort is made to keep these values constant during operation.

9.4. Choice of Options between AG and SAG Mills

The selection of a mill for autogenous or semi-autogenous grinding is complicated by the fact that the hard and large particles in the ore itself forms the grinding medium and in turn has to be reduced in size. The selection will therefore depend on:

1. the intrinsic property of the ore, and
2. the total power requirement by the mill and the circuit configuration.

The intrinsic properties of the ore that are most relevant and have to be established are:

1.　the competency of the ore, and
2.　the work index.

An ore like quartzite is very competent and will not break up easily in a SAG mill. Soft and fragile ore like bauxite or specular hematite will break up relatively easily. Again clayey and oxidised ore may be too soft to serve as a grinding medium and therefore are classified as *incompetent* ore. According to Smith [22], an option to install an AG/SAG mill in preference to a normal tubular ball mill may be considered when the unconfined compressive strength of the ore is less than 180 MPa, the Bond crushing work index is less than 20 kWh/t and the Bond rod mill work index is not significantly higher than the Bond ball mill work index and both are not significantly higher than 15 kWh/t.

To determine the competency of ore, a semi quantitative laboratory test has been developed by Rowland and Kjos [23]. In this test, the sample consists of 50 selected rock pieces, 102 to 165 mm in size, with the total mass between 200 and 250 kg. The rock pieces are charged in a cylindrical drum 1.8 m in diameter and the drum rotated at 26 rpm for 500 rotations. The product is analysed for size distribution and the number of rock pieces equal to or larger than 19 mm is determined. The size distribution of the unknown ore is then compared with those of ores known to be suitable for autogenous or semi-autogenous grinding.

For the advanced media competency test, rocks from the Rowland and Kjos competency test, ranging between –75 mm and + 19 mm, are subjected to a Bond impact crushing work index determination. A rod or ball mill work index test is also carried out and the data used to determine the autogenous or semi-autogenous mill required [24].

The JKMRC test developed at the University of Queensland is now almost standard in Australia [4]. The JKMRC distinguish between the breakage at high energy levels and at low energy levels. For the high energy level (impact breakage), the drop weight test is used and for the low energy breakage (abrasion), the tumbler test is recommended. The drop weight test has been described in Chapter 3. The tumbling test is as follows.

Test conditions:

1.　Mill size : 305 x 305 mm with 4 lifter bars 6.38 mm in height,
2.　Ore size　: - 55 mm + 38 mm,
3.　Sample mass : 3 kg,
4.　Speed of rotation : 70 % of the critical speed,
5.　Rotation time : 10 minutes.

The product is analysed for size and from the size distribution curve the T_{10} value is determined. The specific grinding energy, E_G, is then determined from the equation:

$$T_{10} = A(1 - e^{-B\,E_G})$$

$$\text{or } E_G = -\frac{1}{B}\ln\left[1 - \frac{T_{10}}{A}\right] \tag{9.23}$$

The method of determining T_{10} and the constants A and B is explained in Chapter 3. The specific energy of breakage, E_G, is then calculated and used in simulation programs like JKSimMet (Australia,) and BRGM (Europe). These programs provide quantitative and closer estimations of total mill power of different combinations of mill circuits. The basis of these programs is that the power is contributed from a series of physical operations like impact, abrasion and attrition. Hence these have to be determined individually. Determination of these parameters has been described in Chapter 3.

For cases where a large quantity of ore is not available for testing, Morrell [25] has developed a SAG Mill Comminution (SMC) test to generate the A and B values. The SMC test is a small-scale version of the drop weight test that can be used on smaller sized samples cut from drill core. The test estimates a drop weight index (DWI) that is correlated to the A and B values produced by the full sized drop weight test.

Typical results of tests taken from a randomly chosen Temora Gold ore operation in Australia with two different ball loads as reported by McPheat and Morrison [24] is given in Table 9.1.

Table 9.1
Laboratory Test Results on Temora Gold Ore [23].

Operation	Autogenous	Semi-autogenous 1	Semi-autogenous 2
Ball Charge, %	Nil	6	8
Feed Rate, kg/hr	200	790	840
Mill Discharge Solids %	63	67	67
Mill Charge, %	26	20	18
Product Size , P_{80}	750 μm	5330 μm	5790 μm
Net Power, kWh/t	36.7	7.1	7.8

From the table it can be seen that the power required for autogenous grinding was highest. It can therefore be concluded that autogenous grinding was not suitable with this particular gold ore but semi-autogenous operation with about 8% ball charge was the preferred option.

Based on these test results a 6.7 m diameter x 2.1 m length SAG mill and a 3.3 m x 6.1 m ball mill were installed for commercial operation in closed circuit with a hydrocyclone. The SAG mill had a 6-8% ball charge and the power consumption was 8 kWh/t, which agreed well with the expected value.

9.5. Problems

9.1
In a SAG mill the dimensions of the mill were 9.75 m x 3.5 m and the specific gravities of the mineral and that of the balls charged were 4.1 and 7.9 respectively. The mill was rotated at 75% of its critical speed when 8 % of the mill volume was charged with grinding balls. Estimate:

1. The mill power drawn,
2. The maximum mill filling possible.

9.2

An 8 m x 4 m SAG mill was progressively filled through a charging chute 1.0 m in diameter. The charge consisted of mineral plus balls plus water. The total charge volume was increased progressively such that the fractional fillings of the mill volumes after each increase were: 0.1, 0.2, 0.3, 0.4 and 0.5. Assume that the porosity of the bed remained unchanged at 40% and 40% slurry was charged. Estimate:

1. The possible position (H) of the charge below the central axis of the mill,
2. Determine the relation between H, radius R and fraction fillings, and
3. The maximum fractional volume of mill filled by the total charge.

9.3

A 13 m x 6 m meter SAG mill had a cylindrical feed chute 1 meter in diameter. It was charged with 70% slurry of gold ore and steel balls 10.2 cm in diameter, which occupied 8% of the total inner volume of the mill. The entire charge occupied 42 % of the internal volume. If the porosity of the charge is 30%, estimate:

1. Mass of balls charged,
2. Mill power.

Data: Density of steel ball and ore is 8.6 and 3.0 t/m^3 respectively. The mill speed is 70% of the critical speed.

9.4

A high aspect SAG mill had an ID of 6.0 m and the length measured 4.0 m along the central line. The mill was charged with ore having a S.G. of 2.65 and the load was 40% of the mill volume. The grinding media steel balls occupied 12.2 % of the mill volume. The mill was rotated at 75% of its critical speed, which was 12.9 rpm. Estimate:

1. The charge density, ρ_C
2. The toe angle,
3. The shoulder angle.
(Assume the porosity of the charge = 40%).

The end cone dimensions of the mill were:

Variable	Value	Variable	Value
r_1	2.75 m	r_2	2.6 m
d_1	2 m	d_2	2 m
h_1	1.5 m	h_2	1.2 m

9.5

Using data in problem 9.3.4, estimate:

1. The theoretical power required by the cylindrical portion of the mill
2. The no load power
3. The gross power.

9.6

Using data in problem 9.3.4 estimate the error in theoretical power consumption by the mill if the power required by the end cones were neglected.

9.7

A gold plant was expected to treat 1000 t of ore per day. A high aspect SAG mill was contemplated. Tests were carried out in a laboratory mill of length 1.0 m and D/L equalled 2. It was found that the test mill power required was 1.49 kW. Calculate the power that may be required by the commercial mill.

(Assume: The commercial mill maximum load would be 35% and the ball load 8%).

9.8

An autogenous mill of ID 6.7 m and an effective grinding length of 2.1 m was fed with ore of SG 3.8 to 20% of its volume. The mill was operated continuously 24 hours per day at 1200 t per day and 75% of the critical speed. The solids in the mill charge were at 80% solids. Estimate:

1. The power consumption per tonne per day.
2. The cost in power to run the mill if the power cost is $27.78 per GJ.

9.9

A SAG mill of diameter 9.0 m and width 6.0 m was charged to 40% of the mill volume with ore of SG 3.2 when the porosity was 38%. With grinding time the ball load changed from 10% to 5% and the bed porosity to 12%. Estimate the change in power due to the change in mill conditions. The mill was run continuously at 70% of the critical speed. The ball density was 7.8 t/m^3 and the mill contents were at 80% solids.

REFERENCES

[1] G.B. Siddall, Proceedings of SAGSEM '89, SAG Milling Seminar, Australasian Institute of Mining and Metallurgy, Perth, 1989, pp. 8-22.

[2] P. Reese, Proceedings of 2000 New Zealand Minerals and Mining Conference, Australasian Institute of Mining and Metallurgy, Wellington, 2000.

[3] D. Burgess, Proceedings of SAGSEM '89, SAG Milling Seminar, Australasian Institute of Mining and Metallurgy, Perth, 1989, pp. 132-170.

[4] T.J. Napier-Munn, S. Morrell, R. Morrison and T. Kojovic, Mineral Comminution Circuits Their Operation and Optimisation, JKMRC, 1996.

[5] O. Otte, Proceedings of the Third Mill Operators Conference, Australasian Institute of Mining and Metallurgy, Cobar, 1988, pp. 131-136.

[6] N. Patzelt, J. Knecht, E. Burchardt and K. Klymowsky, Proceedings of the Seventh Mill Operators Conference, Australasian Institute of Mining and Metallurgy, Kalgoorlie, 2000, pp. 47-55.

[7] A.R. MacPherson and R.R. Turner, in Mineral Processing Plant Design, A.L. Mular and R.B. Bhappu (eds), SME-AIME, New York, 1980, pp. 279-305.

[8] L.G. Austin, R.R. Klimpel and P.T. Luckie, Process Engineering of Size Reduction: Ball Milling, SME/AIME, New York, 1984.

[9] L.G. Austin, Minerals and Metallurgical Processing, 7 (1990) 57.

254

[10] F. Penna, in Mineral Processing and Hydrometallurgy Plant Design – World's Best Practice, A.M. Norton Jackson, G. Dunlop and P. Cameron, (eds), Australian Mineral Foundation, South Australia, 1999, pp. 43-47.

[11] A.J. Neale.and R.P. Edwards, SME Annual Meeting, Albuquerque, New Mexico. 1994.

[12] R.D. Morrison and S. Morrell, in Comminution Practices, R.K. Kawatra (ed), SME, Colorado, 1997, pp. 139-146.

[13] S. Morrell, Transactions of the Institution of Mining and Metallurgy, 105 (1996) C43, C54.

[14] A.A Dor and J.H. Bassarear, in Design and Installation of Comminution Circuits, A.L.Mular and G.V. Jergenson (eds), AIME, New York, 1982, pp. 439-473.

[15] L.G. Austin, C.A. Barahona and J.M. Menacho, Powder Technology, 46 (1986) 81.

[16] L. Vahl and W.G. Kingma, Chemical Engineering Science, 1 No. 6 (1952) 253.

[17] R. Hogg and D.W. Fuerstenau, Transactions, SME-AIME, 252 (1972) 418.

[18] F.C. Bond, British Chemical Eng., 6 (1961) 378, 543.

[19] L.R. Gutiérrez and J.E. Sepúlveda, Centro Investigaciones de Mineria y Metallurgia, Santiago, Chile, (1983), 380.

[20] Moly-Cop 1999, Moly-Cop Tools, Retrieved: 16 February 2004, from www.puc.cl/sw_educ/simula/excel/ Mill_Power_SAG_Mills.xls.

[21] S. Morrell, Proceedings of the 5th Mill Operators Conference, Roxby Downs, Aust. Inst. Mining and Metall., 1994, pp. 109-114.

[22] R. Smith, AMMTEC, Private communication and Retrieved: 18 February 2004, from http://www.ammtec.com.au/services/comminution.html.

[23] C.A. Rowland and D.M. Kjos, SME-AIME Annual Meeting, Acapulco, Mexico. 1974.

[24] I.W. McPheat and R.D. Morrison, Proceedings of SAGSEM '89, SAG Milling Seminar, Australasian Institute of Mining and Metallurgy, Perth, 1989, pp. 30-45.

[25] MEI On-line 2004, Retrieved: 2 February 2004, from http://www.min-eng.com/commin/44.html.

Chapter 10. Mathematical Modelling in Comminution

10. INTRODUCTION

The process of comminution has been observed and studied over the years. Statistical correlations of variables have been used to develop mathematical models describing unit and integrated operations. The approach has necessarily been mechanistic, [1]. With a better understanding of the processes and application of basic laws of physics, mathematical models have been developed to describe operations more fully. The developed models help to simulate the process. With the aid of computers a range of options can be easily simulated and optimum conditions of operations and circuit designs determined with relative ease and accuracy. This technique provides rapid answers on plant designs and optimum conditions of operation under specific plant conditions.

The basic approach in the modelling of comminution systems is to recognise the fact that all the comminution processes accept ore and imparting energy, disrupt the binding forces between particles constituting the ore. Depending on the process used, either a single impact or multiple impacts are applied till disintegration and size reduction takes place to acceptable values.

In the metallurgical industry, size reduction commences as soon as rocks are mined or quarried. By the very nature of mining and quarrying operations, the material consists of a range of sizes. We have seen in the case of crushers that a fraction of mined material could be too small and pass through a breaking device without further size reduction. The remainder has to be subjected to a comminution process. Each individual particle larger than the size required has to be broken down. The fragments from each particle that appear after first breakage again may consist of a fraction that requires further breakage. The probability of further breakage would depend on the particle size distribution in the breakage product and also would be machine specific.

Comminution is a repetitive process. It is continued till all the particles in a certain size fraction have been broken down to an acceptable size. Thus the design of the equipment used to break particles and the duration the material remains in the breaking zone controls the ultimate size of the product. Standard sieves are used to obtain quantitative estimates of the extent of size reduction. Usually the Tyler standard sieve series, with a ratio of $1/\sqrt{2}$ between each sieve, is used. This nest of sieves has been accepted as the international standard.

In modelling comminution systems, the basic idea is to obtain a mathematical relation between the feed and product size. It is necessary to take into account all the variables involved in the operation including the machine characteristics.

The process of comminution is considered to be represented by two processes:

1. a particle is selected for breakage,
2. a broken particle produces a given distribution of fragment sizes.

The distribution of sizes produced from a single breakage step is known as the *breakage* or *appearance* function. It denotes the relative distribution of each size fraction after breakage.

The breakage function is often found to be independent of the initial size but is not necessarily so. In the matrix form it is written as a lower triangular matrix.

The probability of breakage of certain particle sizes will be greater than others as they pass through the breakage stage. Thus selective breakage action takes place and the resulting proportion of particles broken from a size interval is known as the *selection function* or *probablility of breakage*.

Using these concepts, mathematical relations between feed size and product size, after comminution, have been developed. The development of such relations for specific machines is described in this chapter.

10.1. Basis for Modelling Comminution Systems

All comminution processes impart forces to break and reduce ore size. Provided the total breaking energy imparted is greater than the bonding energy between individual particles, the particles disintegrate producing a distribution of smaller sizes. The breakage usually starts from a point (or area) of stress concentration and propagates within the particle along planes of weakness. The disintegration breakage could be either along cleavage planes or inter-granular. Forces responsible for abrasion and chipping also play an important part as already described for tumbling machines.

An attempt to illustrate the mechanism of breakage is made in Fig. 10.1 where the size analysis of a single breakage event is given in column 3 (this is the breakage function). For single particles present in each size fractions 1, 2, 3, ... N , the application of force is shown by solid arrows and the conceptual stress lines are indicated by the dotted lines. The movement of fragments to the same or lower sizes is indicated by the dotted arrows. Column 1 also shows the size distribution of the feed, with particles of smaller sizes represented in grey. Column 4 shows the product from breakage after n number of size reductions. Rows 1, 2, ..., N show the progenies from the single size fraction of size 1. It can be seen that the mass of size 1, when broken, distributes itself into other size fractions. The distribution becomes more complicated if fragments of breakage from other sizes in the feed are included. At some stage the size fraction in size 1 will disappear, as the particles sizes are distributed to smaller sizes. The process continues to n number of breakages. It should be noted that the total mass remains the same.

To identify the products in different size fractions two conventions have been adopted. Firstly, the mass fraction of particles remaining in size 1, after breakage of particles of size 1 is designated as $b_{1,1}$. Similarly for material broken from size 1 into size 2, the mass fraction is $b_{2,1}$ and so on. Thus $b_{3,1}$, $b_{4,1}$ etc. to $b_{N,1}$ represents those particles present in the 3rd, 4th... , N^{th} sieve size intervals obtained from breakage of particles of size 1. Similarly, the breakage from size 2 of the feed will be recognised as $b_{2,2}$, $b_{3,2}$ ... $b_{N,2}$ and so on. In the general case, when one particle in size j of the feed is broken into the ith size fraction of the product it is designated as $b_{i,j}$.

The second convention advocated by Austin et al. [2] is to record the cumulative amount passing each sieve instead of that retained. This is represented as $B_{i,j}$ where i and j have the same convention

The form of the breakage function is shown in Fig. 10.2 for two types of materials.

10.1.1. Estimation of the Breakage Function

Several workers like Broadbent and Callcott [3], Gaudin and Meloy [4], Kelsall and Reid [5], Klimpel and Austin [6], Lynch [1], Austin et al. [2] have attempted to describe the breakage
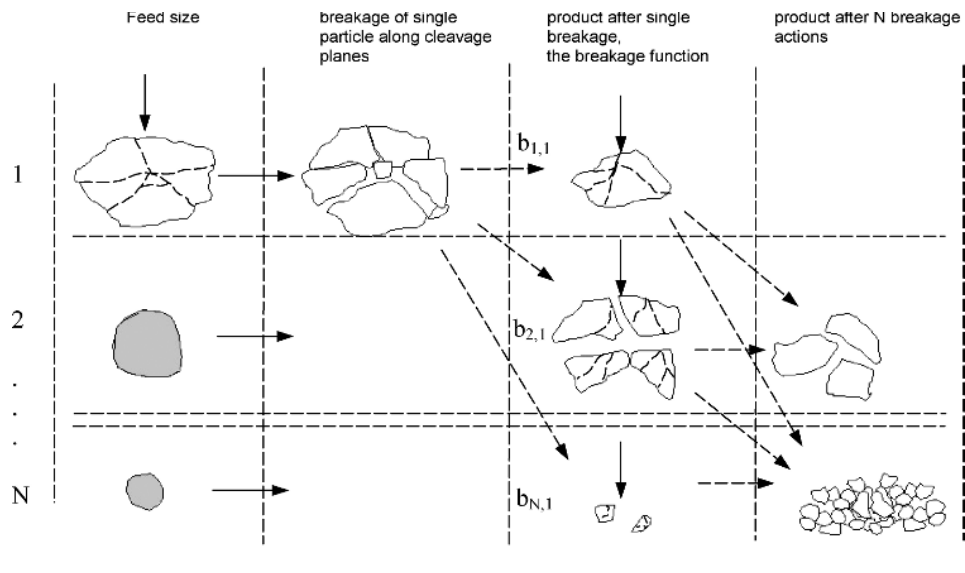
Fig. 10.1. Representation of the distribution of particles after breakage. Solid arrows represent the applied force for breakage and dotted arrows indicate the distribution of fragments of breakage to the same or lower sizes. The fragments shown represent breakage of an original single size particle.
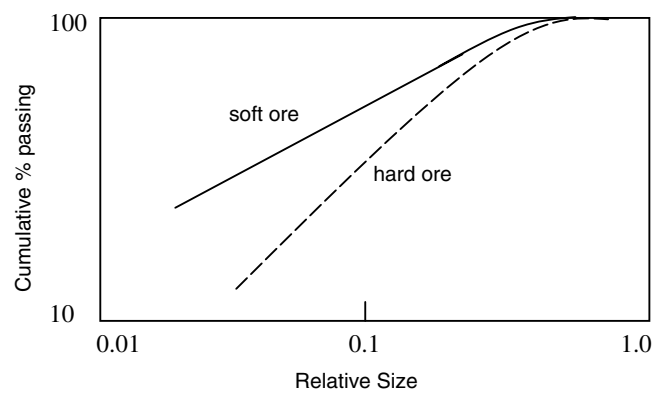
Fig. 10.2. Breakage distribution function of hard and soft ore.

function mathematically. Klimpel and Austin's formula encompasses most of the others and is given below:

$$B(d_i) = 1 - \left[1-\left(\frac{d_i}{d_j}\right)\right]^{n_1} \left[1-\left(\frac{d_i}{d_j}\right)^2\right]^{n_2} \left[1-\left(\frac{d_i}{d_j}\right)^3\right]^{n_3}$$

(10.1)

where d_j = is the original size being broken,
  d_i = size of the progeny fragment of breakage,
  n_1-n_3 = constants depending on the particle shape and flaw density within the particles and
  $B(d_i)$ = the cumulative mass fraction finer than d_i where $d_j > d_i > 0$.

The expression used by Broadbent and Callcott [3] is much easier to use to determine the distribution of particles after breakage. In this case, if d_j is the size of the original particle, which is subjected to size reduction and $B(d_i)$ the fraction of particles less than size d_i then the size distribution of the breakage products is given by the breakage matrix which allows the determination of the individual elements:

$$B(d_i) = \frac{1-e^{-\frac{d_i}{d_j}}}{1-e^{-1}} = 1.58\left(1-e^{-\frac{d_i}{d_j}}\right)$$

(10.2)

This expression is material independent and hence can only be an approximation. In general, a *standard* breakage function of this kind have proved to give reasonable results for rod and ball mills where breakage is primarily due to impact and shatter but is not adequate where attrition is important such as in autogenous mills [7].

In defining the matrix an implicit assumption is that the particles of different sizes are broken in a similar manner (*normalised* breakage) and that no agglomeration takes place. B is an $N \times N$ matrix where the elements of B denotes the proportion of material that occurs in that particular size range after breakage. As no agglomeration is assumed, it is obvious that the elements above the diagonal will be zero. Thus B may be written as a lower triangular matrix:

$$\begin{bmatrix} B_1 & 0 & 0 & \cdots & 0 \\ B_2 & B_1 & 0 & \cdots & 0 \\ B_3 & B_2 & B_1 & \cdots & 0 \\ \vdots & \vdots & \vdots & \ddots & 0 \\ B_N & B_{N-1} & B_{N-2} & \cdots & B_1 \end{bmatrix}$$

(10.3)

If we consider the standard sieves in a $1/\sqrt{2}$ series then the numerical values of the breakage function would be:

0.1004, 0.1906, 0.1661, 0.1361, 0.1069, 0.0814, 0.0607 etc.

Example 10.1 illustrates the use of Eq. (10.2) for estimating the breakage function.

An alternate method of determining the breakage function has been advocated by Napier-Munn et al. [8] and already discussed in Chapter 3. In this method the relative size distribution after breakage is plotted against the cumulative percent passing and the T_{10} index determined. A plot of the breakage index T_{10} (fraction or %) against T_N (fraction or % passing $1/N^{th}$ of the parent size) gives the material breakage function. This relationship is expressed as [9]:

$$T_N = 1-(1-T_{10})^{\left(\frac{10-1}{N-1}\right)^{\alpha}}$$

(10.4)

where α = a material specific parameter.

Another simple method to determine B values in batch grinding is to take an appropriate amount of a sample of ore of one size fraction, grind for a short time and determine its size distribution by sieve analysis. The sample is then returned to the mill and the tumbling action repeated for different lengths of time. After each time interval, samples are taken out of the mill and a size distribution determined. A compromise is made between too short a grind time to provide insufficient mass for accurate sieving and too long a grind time to give excessive re-breakage of fragments. A correction is applied to account for any re-breakage that does occur. For example, the BI or BII methods of Austin and Luckie [10] may be used. B values may be normalisable and reduced to a vector.

In the BII method, re-breakage of primary progeny fragments are compensated for by assuming that the product of the breakage rate function and the breakage distribution function, S_jB_{ij}, is approximately constant. Under these conditions, the breakage distribution function is obtained from:

$$B_{i1} = \frac{\log\left(\frac{1-P_i(0)}{1-P_i(t)}\right)}{\log\left(\frac{1-P_2(0)}{1-P_2(t)}\right)}$$

(10.5)

where $P_i(0)$ = cumulative mass fraction less than size d_i at time 0,
$P_i(t)$ = cumulative mass fraction less than size d_i at time t, and
$B_{i,1}$ = cumulative mass fraction of particles passing the top size of interval i from breakage of particles of size 1.

The recent trend is to use back-calculation methods to obtain the B values. This method of calculations is beyond the scope of this book, the interested reader is directed to the original work by Austin et al. [2].

Example 10.1

This is a numerical example of the methods of calculating the breakage function from a sieve analysis of single particle breakage in a laboratory mill, ground for 2 minutes. For breakage of single size, −2400 + 1200 microns, the sieve analysis is:

Interval	-	1	2	3	4	5	6
Size , µm	2400	1200	600	300	150	75	-75
Feed % retained	-	72.3	16.5	8.5	1.5	0.3	0.9

1. Broadbent and Callcott method

The breakage function is described in Eq. (10.2) as:

$$B(d_i) = \frac{1 - e^{-\frac{d_i}{d_j}}}{1 - e^{-1}}$$

$B(d_i)$ is the proportion of material of initial size d_j that is less than d_i in the product. The size d_i refers to the top size of the interval. That is, d_2 is the top size of the interval $-1200 +600$ µm in this example. The initial size d_1 (i.e. $j = 1$) is the actual average particle size for the top fraction ($-2400 +1200$ µm) and is the geometric mean of the two sizes. That is:

$$d_1 = (2400 \times 1200)^{0.5} = 1697 \ \mu m$$

From Eq. (10.2),

for $i = 1$, $d_i = d_j$, $B(d_1) = 1$

for $i = 2$, $d_2 = 1200$, $d_2/d_1 = 1200/1697 = 0.70713$

$$\text{then} \ \ B(d_2) = \frac{1 - \exp\left(-\frac{d_2}{d_1}\right)}{1 - \exp(-1)} = \frac{1 - \exp\left(-\frac{1200}{1697}\right)}{1 - 0.36788} = 0.80197$$

Similarly for other values of i:

Size interval	d_i	$B(d_i)$
1	1697	1.0
2	1200	0.80197
3	600	0.47113
4	300	0.25633
5	150	0.13383
6	75	0.06839

Since $B(d_i)$ is the proportion less than size d_i, the proportion broken into size d_i is obtained by subtracting $B(d_i)$ from $B(d_{i-1})$ or from 1 in the case of the top size. That is:

$B(1,1) = 1 - 0.80197 = 0.1980$

$B(2,1) = 0.80197 - 0.47113 = 0.3308$

$B(3,1) = 0.47113 - 0.25633 = 0.2148$

$B(4,1) = 0.25633 - 0.13383 = 0.1225$

$B(5,1) = 0.13383 - 0.6839 = 0.0654$

$B(6,1)$ is the material broken into size interval 6, that is, less than 75 microns. This remainder is the 'pan' of the size distribution and is given by $1 - \text{sum}(B(i,1)) = 0.0685$.

Size interval	d_i	$B(d_i)$	$B(i,j)$
1	1697	1.0	0.1980
2	1200	0.80197	0.3308
3	600	0.47113	0.2148
4	300	0.25633	0.1225
5	150	0.13383	0.0654
6	75	0.06839	0.0685

The B matrix can then be written in the following form ('pan' fraction not included):

$$\begin{bmatrix} 0.1980 & 0 & 0 & 0 & 0 \\ 0.3308 & 0.1980 & 0 & 0 & 0 \\ 0.2148 & 0.3308 & 0.1980 & 0 & 0 \\ 0.1225 & 0.2148 & 0.3308 & 0.1980 & 0 \\ 0.0654 & 0.1225 & 0.2148 & 0.3308 & 0.1980 \end{bmatrix}$$

2. JKMRC method

If values of K_1 and K_2 are 45.4 and 1.15 respectively and the specific comminution energy from a drop weight test was 2.8 kWh/t then from Eq. (3.45):

$$T_{10} = 45.4 \left(1 - e^{-1.15\,(2.8)}\right) = 43.6\%$$

From Eq. (10.4) for a value of $\alpha = 0.75$ the following set of T_N values can be calculated from this T_{10} value for $Y = 1.697$ mm:

Size (mm)	N	T_N	$b_{i,j}$	$b_{i,j}$ corrected	Size (mm)	N	T_N	$b_{i,j}$	$b_{i,j}$ corrected
1.20	1.4	0.997	0.003	0	0.150	11.3	0.404	0.205	0.206
0.600	2.8	0.849	0.148	0.148	0.075	22.6	0.257	0.147	0.147
0.300	5.7	0.609	0.240	0.241	0.038	45.3	0.159	0.097	0.098

Column 4, the breakage function $(b_{i,j})$, is obtained by subtracting the cumulative % passing mass fraction (T_N) from the previous row (T_{N-1}). The value of $b_{1,1}$ should be zero as no products of breakage should report to size 1 from the breakage of any size. If this value is not zero (0.003 in this case) then $b_{1,1}$ is made equal to zero and the subsequent values adjusted by dividing each term by $(1-b_{1,1}) = (1-0.003) = 0.997$ (the total mass minus the mass in the first interval).

3. Austin and Luckie method

In this procedure, a single size ball mill feed in ground for a short time (1-3 minutes). The product is sized and provided no more than about 30% of the top size mass is broken, then the breakage distribution function can be estimated from Eq. (10.5) (BII method), as shown in the table below.

Interval	Passing size μm	Retained size μm	Feed % retained	Cumulative % passing	$B_{i,1}$	$b_{i,1}$
1	2400	1200	72.3	100	1	0.000
2	1200	600	16.5	27.7	1	0.622
3	600	300	8.5	11.2	0.378	0.291
4	300	150	1.5	2.7	0.087	0.049
5	150	75	0.3	1.2	0.038	0.010
6	75	0	0.9	0.9	0.029	0.029

For the data in the table above, $P_2(0)$ is the fraction of material in interval 2 before grinding (screening only) and should be small. This is the sieving error and in this example, we'll assume it is equal to 0.01. All other values of $P_i(0)$ should be zero. $P_2(2)$ is the cumulative fraction passing the top size of interval 2 after 2 minutes of grinding and is equal to 0.277 in this example. Similarly for interval 3, $P_3(2)$ is equal to 0.112. The first term $B_{1,1}$ is equal to 1 by definition, since when a particle breaks it is assumed to fall to smaller sizes. Similarly, $B_{2,1}$ is also equal to 1 as particles broken from size interval 1 must be less than the top size of interval 2 (which is the bottom size of interval 1). The first calculation then is for $B_{3,1}$:

$$B_{3,1} = \frac{\log\left(\frac{1-0}{1-0.112}\right)}{\log\left(\frac{1-0.01}{1-0.277}\right)} = 0.378$$

and

$$B_{4,1} = \frac{\log\left(\frac{1-0}{1-0.027}\right)}{\log\left(\frac{1-0.01}{1-0.277}\right)} = 0.087 \quad \text{and so on.}$$

The retained form of the breakage function, $b_{i,j}$ is calculated as before by:

$$b_{i,1} = B_{i,1} - B_{i+1,1}$$

For example: $b_{3,1} = 0.378 - 0.087 = 0.291$

10.1.2. Estimation of the Selection Function

When an ore or rock sample is charged to a breakage system, it contains particles in several size ranges. During breakage, the probability of breaking the larger sizes within a size

fraction is considerably greater compared to the smaller sizes. That is, a certain proportion of particles within each size range is preferentially reduced in size. Thus selective breakage occurs within a size range. The proportion of particles within each size range that is broken is represented by S. Thus S_1, S_2, S_3 ... S_N will be the fraction of material in each size fraction that would be selected for size reduction with the remaining particles passing through without any change in size. This is known as the *selection function* (or the *specific rate of breakage*) which can be mathematically expressed as a diagonal matrix where each element of the matrix represents the proportion of particles that has the probability of breakage.

In a batch grinding process, if the total mass load in the mill is designated as M, the mass fraction of size i in the mill load is m_i and the specific rate of breakage (or the fractional rate of breakage or the mass of size i broken per unit time per unit mass of size i present) is S_i, then for a first order breakage process:

$$\text{Rate of breakage of size i} \propto \text{mass of size i} = m_i(t)\, M \tag{10.6}$$

$$\text{or} \quad -\frac{d[m_i(t)M]}{dt} = -S_i\, m_i(t)\, M \tag{10.7}$$

where S_i = the proportionality constant and
$\quad\quad m_i(t)$ = the mass fraction of size i after a grind time, t.

Since the total mass is constant in a batch mill and if S_i is independent of time, then on integration, Eq. (10.7) becomes:

$$m_i(t) = m_i(0)\, \exp(-S_i\, t) \tag{10.8}$$

or taking logs:

$$\log m_i(t) = \log m_i(0) - \frac{S_i\, t}{2.303} \tag{10.9}$$

A plot of $\log m_i(t)$ against grind time, t, should give a straight line of slope $(-S_i/2.303)$ as shown in Fig. 10.3.

10.2. Mathematical models of comminution processes

The approaches more commonly accepted for the modelling of comminution processes are:

1. The matrix model,
2. The kinetic model,
3. The energy model

The technique adopted for developing a model is to establish a material balance of components and an energy balance of the comminution system. The material balance of a comminution system in operation may be stated as:

$$[\text{Feed in} + \text{Breakage}] = [\text{Total Product out}] \tag{10.10}$$
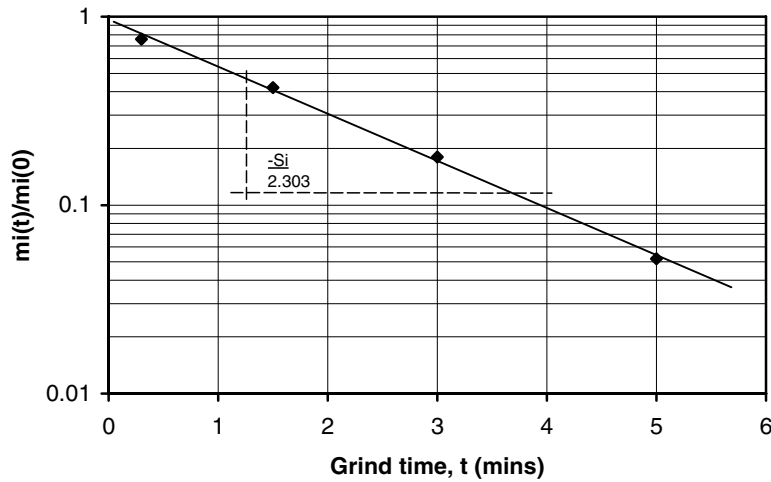
Fig. 10.3. First order plot for breakage rate determination from Eq. (10.9).

and the energy balance as:

$$\begin{bmatrix} \text{Energy input} \\ \text{(for breakage)} \end{bmatrix} = \begin{bmatrix} \text{Energy transmittd to the} \\ \text{particles for breakage} \end{bmatrix} + \begin{bmatrix} \text{Energy transformed as} \\ \text{heat and sound energies} \end{bmatrix} \quad (10.11)$$

The transformation of input energy to produce heat and sound energies are often very small and therefore always neglected in the energy balance equation.

A fundamental assumption in the approach is that the residence time of particles in the mill is the same as if the entire charge is mixed thoroughly and is uniform. Hence the approach is known as the *perfectly mixed model*.

The mass balance and the energy balances give similar results.

10.2.1. Matrix Model

Lynch [1] expressed the relation between the selection function S and feed analysis using a matrix model representing the feed and product size distributions as N size ranges. The matrix was developed by assuming S_i to be the proportion of particles within a sieve fraction, i, that would break preferentially (the others being too small). Representing the feed size distribution by the matrix F, the fraction that would selectively break would be S•F. Thus if F_1, F_2, F_3...F_N are the masses of material in each size fraction and S_1, S_2, S_3...S_N are the proportion of particles that have the probability of breaking in the corresponding size intervals then according to Lynch, the breakage process can be written in the matrix form as:

Size	Feed	Selection function						Mass of particles broken	

$$
\begin{array}{c}
1 \\
2 \\
3 \\
4 \\
\vdots \\
N
\end{array}
\begin{bmatrix}
F_1 \\
F_2 \\
F_3 \\
F_4 \\
\vdots \\
F_N
\end{bmatrix}
\bullet
\begin{bmatrix}
S_1 & 0 & 0 & 0 & \cdots & 0 \\
0 & S_2 & 0 & 0 & \cdots & 0 \\
0 & 0 & S_3 & 0 & \cdots & 0 \\
0 & 0 & 0 & S_4 & \cdots & 0 \\
\vdots & \vdots & \vdots & \vdots & \ddots & \vdots \\
0 & 0 & 0 & 0 & \cdots & S_N
\end{bmatrix}
=
\begin{bmatrix}
F_1 S_1 \\
F_2 S_2 \\
F_3 S_3 \\
F_4 S_4 \\
\vdots \\
F_N S_N
\end{bmatrix}
\qquad (10.12)
$$

Thus we see that the mass of the product from breakage of selected particles will be:

$$\text{Mass of product} = S \bullet F \qquad (10.13)$$

and the mass of unbroken particles will be $(I - S \bullet F)$ where I represents the *identity* matrix.

The total product of breakage will be the sum of the broken and the unbroken particles. The broken particles will have a distribution, B, the breakage function. The breakage function B is for all the particles actually broken, and therefore the product fragments from breakage can be represented by B•S•F. The entire breakage operation being a sum of broken and unbroken particles can now be expressed by the general equation:

$$P = B \bullet S \bullet F + (I - S) \bullet F \qquad (10.14)$$

Eq. (10.14) is the mathematical relation between the feed, breakage and product. It serves as the basis of mathematical models that describes the process of comminution of a particle. This equation gives a relation between the feed and the product from known matrices of breakage and selection functions. In actual breakage operations however, the product is subject to some classification (either internal to the breakage unit or external) and the classifier oversize is combined with the original feed to form a new feed for the next breakage stage. The character and composition of the input feed changes and so does the B and S values. The situation is easily understood by examining Fig. 10.4 where the contribution of the oversize fraction from the classifier to the feed process is clearly illustrated.

The oversize fraction is recycled for further comminution and the undersize forms the product from the breakage unit. If we used the conventional symbols of F and P for feed and product size distributions, q the size distribution to the classifier, B, S and C the breakage, selection and classification functions respectively and all terms are considered as vectors, then for the breakage process the mass balances may be written as:

At the feed end:

$$F_2 = F_1 + Cq \qquad (10.15)$$

where F_2 is the size distribution of the feed plus the oversize from the classifier.

At the product end:

$$P = (I - C) \bullet q \qquad (10.16)$$
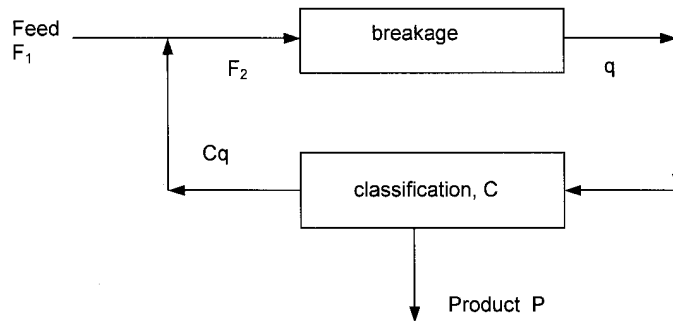
Fig. 10.4. Schematic representation of a breakage-classification sequence of events.

According to Eq. (10.14) breakage is given by:

$$q = (B \cdot S + I - S) \cdot F_2 \tag{10.17}$$

Substituting the values F_2 and q in Eq. (10.16) and simplifying, Lynch [1] derived the matrix model for comminution as:

$$P = (I - C) \cdot (B \cdot S + I - S) \cdot [I - C \cdot (B \cdot S + I - S)]^{-1} \cdot F_1 \tag{10.18}$$

This model is a quantitative relation between feed size distribution and product size distribution in comminution systems. It has been widely accepted.

10.2.2. Kinetic Model

The matrix model considers the size reduction, especially in grinding process, as a number of discrete steps, which consists of a repeated selection-breakage-classification cycle. Researchers like Kelsall and Reid [11], Whiten [12], Lynch [1], Austin et al. [2], have treated size reduction as a continuous process and Gault [13] has elaborated on the time-dependant process characteristics.

Loveday [14] and Austin et al, [2] have found experimentally that in the case of batch grinding the breakage rate obeyed a first order law as in a chemical reaction, though there is no valid reason for it. The breakage rate constant was a function of particle size. The basic assumption was that the entire charge was mixed thoroughly and was therefore uniform during the grinding process. Following their work, the kinetics of the breakage process may be described as:

1. the rate of disappearance of particles in size range j by breakage to any smaller size range, i,
2. the rate of appearance of size i from breakage of particles of size j,
3. the rate of disappearance of size i by breakage to smaller sizes.

Referring to Eq. (10.7) and using the same symbols we can write:

Rate of disappearance of size j $\quad = \quad S_j\, m_i(t)\, M$ $\qquad\qquad\qquad$ (10.19)

Rate of appearance of size i $\qquad = \quad b_{i,j}\, S_j\, m_i(t)\, M$ $\qquad\qquad\qquad$ (10.20)

Rate of disappearance of size i $\quad = \quad S_i\, m_i(t)\, M$ $\qquad\qquad\qquad$ (10.21)

For a constant mass, M, the material size-mass balance would be:

$$\frac{d}{dt}[m_i(t)] = \sum_{\substack{j=1 \\ i>1}}^{i-1} b_{ij}\, S_j\, m_j(t) - S_i m_i(t) \quad \text{for} \quad N \geq i \geq j \geq 1 \qquad (10.22)$$

Eq. (10.22) is the basic *size-mass rate balance* model for batch grinding of rocks and ores. The rate of production of material less than size x_i is the sum of the rates of production of material less than size x_i by breakage of all larger sizes and is given by:

$$\frac{dP(x_i,t)}{dt} = \sum_{\substack{j=1 \\ i>1}}^{i-1} B_{i,j}\, S_j\, m_j(t) \quad N \geq i \geq j \geq 1 \qquad (10.23)$$

and $\qquad = 0 \qquad\qquad\quad i = 1$

where $\quad P(x_i,t) = \sum_{k=N}^{i} m_k(t)$

For the modelling of continuous steady state mills, the breakage equation is combined with the material residence time distribution. The two extremes of residence time distributions are *plug flow* and *fully mixed*. For plug flow, all material have the same residence time and hence the batch grinding equation is applicable when integrated from time zero to the residence time. The solution to this integration was originally proposed by Reid [15] and is known as the *Reid solution*.

The general form of the solution is:

$$m_i(t) = \sum_{j=1}^{i} a_{ij}\, e^{-S_j t} \qquad\qquad \text{for } N \geq i \geq 1 \qquad (10.24)$$

where
$$a_{ij} = \begin{cases} 0 & \text{for } i < j \\[2mm] m_i(0) - \displaystyle\sum_{\substack{k=1 \\ i>1}}^{i-1} a_{ik} & \text{for } i = j \\[4mm] \dfrac{1}{S_i - S_j} \displaystyle\sum_{k=j}^{i-1} S_k\, b_{ik}\, a_{kj} & \text{for } i > j \end{cases} \qquad (10.25)$$

For i = 1 this gives:

$$m_1(t) = m_1(0)e^{-S_1 t}$$ (10.26)

and for i = 2:

$$m_2(t) = \frac{S_1 b_{21}}{S_2 - S_1} m_1(0)e^{-S_1 t} + m_2(0)e^{-S_2 t} - \frac{S_1 b_{21}}{S_2 - S_1} m_1(0)e^{-S_2 t}$$ (10.27)

For i > 2 the number of terms in the expression expand rapidly.

For a fully mixed mill at steady state the equation becomes:

$$P_i = F_i + \tau \sum_{\substack{j=1 \\ i>1}}^{i-1} b_{ij} S_j m_j - S_i m_i \tau \quad \text{for } N \geq i \geq j \geq 1$$ (10.28)

where τ = mean residence time.

To estimate P_i using Eq. (10.28) it is necessary to determine S_i, the breakage rate constant. This is determined experimentally by a log-log plot of the fraction of particle size j remaining after different grind times. From the slope of the plot, the value of S can be obtained.

10.3. Modelling Crushing and Grinding Systems

The general principles and techniques described for mathematical modelling of comminution systems are directly applicable to conventional crushers and grinding mills used in mining and metallurgical operations. Little work has been done on their application to other forms of grinding mills like the Roller Mills, Fluid energy mills, vibratory or attrition mills. These mills are essentially pulverisers. In the mineral industry, pulverisation is seldom required to liberate a mineral from its gangue content. In fact, over grinding is usually not encouraged. Hence in this book the discussions are confined to conventional industrial crushing and grinding systems and not to grinding by pulverisers.

10.3.1. Modelling Jaw and Gyratory Crushers

In Chapter 4 we have already seen the mechanism of crushing in a jaw crusher. Considering it further we can see that when a single particle, marked 1 in Fig. 10.5A, is nipped between the jaws of a jaw crusher the particle breaks producing fragments, marked 2 and 3 in Fig. 10.5B. Particles marked 2 are larger than the open set on the crusher and are retained for crushing on the next cycle. Particles of size 3, smaller than the open set of the crusher, can travel down faster and occupy or pass through the lower portion of the crusher while the jaw swings away. In the next cycle the probability of the larger particles (size 2) breaking is greater than the smaller sized particle 3. In the following cycle therefore, particle size 2 is likely to disappear preferentially and the progeny joins the rest of the smaller size particles indicated as 3 in Fig. 10.5C. In the figure, the position of the crushed particles that do not exist after comminution is shaded white (merely to indicate the positions they had occupied before comminution). Particles that have been crushed and travelled down are shown in grey. The figure clearly illustrates the mechanism of crushing and the classification that takes place within the
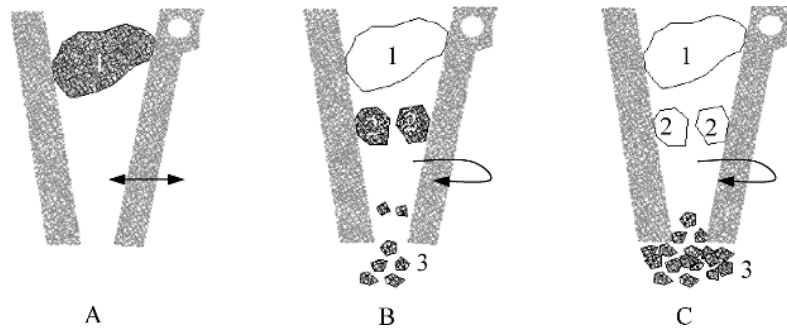
Fig. 10.5 Classification within a jaw crusher.

breaking zone during the process, as also illustrated in Fig. 10.4. This type of breakage process occurs within a jaw crusher, gyratory crusher, roll crusher and rod mills. Eq. (10.18) then is a description of the crusher model.

In practice however, instead of a single particle, the feed consists of a combination of particles present in several size fractions. The probability of breakage of some relatively larger sized particles in preference to smaller particles has already been mentioned. For completeness, the curve for the probability of breakage of different particle sizes is again shown in Fig. 10.6. It can be seen that for particle sizes ranging between $0 - K_1$, the probability of breakage is zero as the particles are too small. Sizes between K_1 and K_2 are assumed to break according a parabolic curve. Particle sizes greater than K_2 would always be broken.
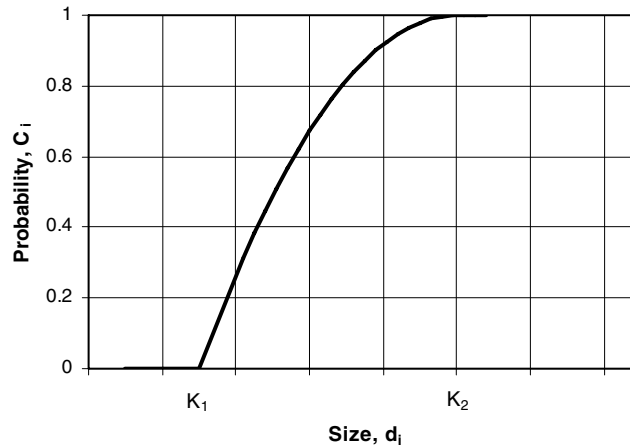
Fig. 10.6 Classification function, C_i, in a crusher [1,16].

According to Whiten [16] this classification function C_i, representing the probability of a particle of size d_i entering the breakage stage of the crusher, may be expressed as:

$$C_i = 0 \qquad \text{for } d_i < K_1$$

$$C_i = 1 - \left[\frac{d_i - K_2}{K_1 - K_2} \right]^2 \qquad \text{for } K_1 < d_i < K_2, \text{ and}$$

$$C_i = 1 \qquad \text{for } d_i > K_2 \qquad (10.29)$$

Where the upper and lower sieve sizes for the ith size interval is known, C_i can be obtained from:

$$C_i = \int_{d_i}^{d_{i+1}} \frac{C_i}{d_{i+1} - d_i} \, dd \qquad (10.30)$$

d_i and d_{i+1} are the upper and lower sieve sizes of the ith size fraction.

For jaw, gyratory and cone crushers, K_1 is the value of the set and K_2 the size above which all particles will be broken. The recommended value of the exponent in Eq. (10.29) is 2.3 [8].

The classification function can be readily expressed as a lower triangular matrix [1,16] where the elements represent the proportion of particles in each size interval that would break. To construct a mathematical model to relate product and feed sizes where the crusher feed contains a proportion of particles which are smaller than the closed set and hence will pass through the crusher with little or no breakage, Whiten [16] advocated a crusher model as shown in Fig. 10.7.

The considerations in Fig. 10.7 are similar to the general model for size reduction illustrated in Fig. 10.4 except in this case the feed is initially directed to a classifier, which eliminates particle sizes less than K_1. The coarse classifier product then enters the crushing zone. Thus only the crushable larger size material enters the crusher zone. The crusher product is combined with the main feed and the process repeated. The undersize from the classifier is the product.
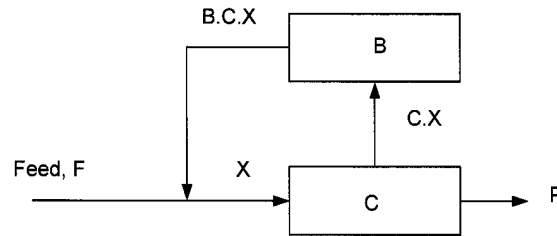
Fig. 10.7. Crusher model [16].

In order to describe the operation mathematically, Whiten [16] and Lynch [1] considered the mass balances at the feed and product ends and derived the relation between crusher feed and product as:

$$P = (I - C) \cdot (I - B \cdot C)^{-1} \cdot F \qquad (10.31)$$

where
  P = vector for product size distribution (mass),
  I = unit diagonal matrix having all elements = 1 (remaining are = 0),
  C = classification function written as a diagonal matrix,
  F = feed size distribution (mass).

Eq. (10.31) is the widely accepted model of crushers that is used to predict the size distribution of products in different types of crushers.

While considering the above aspects of a model of crushers it is important to remember that the size reduction process in commercial operations is continuous over long periods of time. In actual practice therefore the same operation is repeated over long periods so the general expression for product size must take this factor into account. Hence a parameter v is introduced to represent the number of cycles of operation. As all cycles are assumed identical the general model given in Eq. (10.31) should therefore be modified as:

$$P = X^v \cdot F \qquad (10.32)$$

where $X = (I - C) \cdot (I - B \cdot C)^{-1}$

The method of evaluating a crusher model is illustrated in Example 10.2.

Example 10.2

The size distribution of an ore to be fed to a cone crusher was:

Size, mm	-100 +50	-50+25	-25 +12.5	-12.6 +6	-6
Mass %	10	33	32	20	5

The breakage and classification matrices, B and C have been determined as:

$$B = \begin{bmatrix} 0.58 & 0 & 0 & 0 \\ 0.2 & 0.6 & 0 & 0 \\ 0.12 & 0.18 & 0.61 & 0 \\ 0.04 & 0.09 & 0.2 & 0.57 \end{bmatrix} \qquad C = \begin{bmatrix} 1.0 & 0 & 0 & 0 \\ 0 & 0.7 & 0 & 0 \\ 0 & 0 & 0.45 & 0 \\ 0 & 0 & 0 & 0 \end{bmatrix}$$

Estimate the size distribution of the crusher product.

Solution

Using Eq. (10.31):

Step1
Multiple vectors B • C written in matrix form:

$$
B \cdot C = \begin{bmatrix} 0.58 & 0 & 0 & 0 \\ 0.20 & 0.60 & 0 & 0 \\ 0.12 & 0.18 & 0.61 & 0 \\ 0.04 & 0.09 & 0.2 & 0.57 \end{bmatrix} \bullet \begin{bmatrix} 1.0 & 0 & 0 & 0 \\ 0 & 0.7 & 0 & 0 \\ 0 & 0 & 0.45 & 0 \\ 0 & 0 & 0 & 0 \end{bmatrix} =
$$

$$
\begin{bmatrix} 058\text{x}1+0\text{x}0+0\text{x}0+0\text{x}0 & 0.58\text{x}0+0\text{x}0.7+0\text{x}0+0\text{x}0 & 058\text{x}0+0\text{x}0+0\text{x}0.45+0\text{x}0 & 0.58\text{x}0+0\text{x}0+0\text{x}0+0\text{x}0 \\ 0.2\text{x}1+0.6\text{x}0+0\text{x}0+0\text{x}0 & 0.2\text{x}0+0.6\text{x}0.7+0\text{x}0+0\text{x}0 & 0.2\text{x}0+0.6\text{x}0+0\text{x}0.45+0\text{x}0 & 0.2\text{x}0+0.6\text{x}0+0\text{x}0+0\text{x}0 \\ 0.12\text{x}1+0.18\text{x}0+0.61\text{x}0+0\text{x}0 & 0.12\text{x}0+0.18\text{x}0.7+0.61\text{x}0+0\text{x}0 & 0.12\text{x}0+0.18\text{x}0+0.61\text{x}0.45+0\text{x}0 & 0.12\text{x}0+0.18\text{x}0+0.61\text{x}0+0\text{x}0 \\ 0.04\text{x}1+0.09\text{x}0+0.2\text{x}0+0.57\text{x}0 & 0.04\text{x}0+0.09\text{x}0.7+0.2\text{x}0+0.57\text{x}0 & 0.04\text{x}0+0.09\text{x}0+0.2\text{x}0.45+0.57\text{x}0 & 0.04\text{x}0+0.09\text{x}0+0.2\text{x}0+0.57\text{x}0 \end{bmatrix}
$$

$$
= \begin{bmatrix} 0.58 & 0 & 0 & 0 \\ 0.2 & 0.42 & 0 & 0 \\ 0.12 & 0.126 & 0.2745 & 0 \\ 0.04 & 0.063 & 0.09 & 0 \end{bmatrix}
$$

This is more conveniently calculated using a spreadsheet programme that has matrix functions, such as Excel®.

Step 2
Now determine (I – B•C) and (I – C)

$$
(I - B \cdot C) = \begin{bmatrix} 1-0.58 & 0-0 & 0-0 & 0-0 \\ 0-0.2 & 1-0.42 & 0-0 & 0-0 \\ 0-0.12 & 0-0.126 & 1-0.2745 & 0-0 \\ 0-0.04 & 0-0.063 & 0-0.09 & 1-0 \end{bmatrix} = \begin{bmatrix} 0.42 & 0 & 0 & 0 \\ -0.2 & 0.58 & 0 & 0 \\ -0.12 & -0.126 & 0.7255 & 0 \\ -0.04 & -0.063 & -0.09 & 1 \end{bmatrix}
$$

and

$$
(I-C) = \begin{bmatrix} 0 & 0 & 0 & 0 \\ 0 & 0.3 & 0 & 0 \\ 0 & 0 & 0.55 & 0 \\ 0 & 0 & 0 & 1 \end{bmatrix}
$$

Step 3
Inverting the matrix gives:

$$(I-B \cdot C)^{-1} = \begin{bmatrix} 2.3810 & 0 & 0 & 0 \\ 0.8210 & 1.7241 & 0 & 0 \\ 0.5364 & 0.2994 & 1.3784 & 0 \\ 0.1952 & 0.1356 & 0.1241 & 1.0 \end{bmatrix} \text{ and}$$

$$(I-C) \cdot (I-B \cdot C)^{-1} = \begin{bmatrix} 0 & 0 & 0 & 0 \\ 0.2463 & 0.5172 & 0 & 0 \\ 0.2950 & 0.1647 & 0.7581 & 0 \\ 0.1952 & 0.1356 & 0.1241 & 1 \end{bmatrix}$$

Lynch [1] circumvents the task of matrix inversion by letting $X = (I - B \cdot C)^{-1} \cdot F$

Hence $(I - B \cdot C) \cdot X = F$ or

$$\begin{bmatrix} 0.42 & 0 & 0 & 0 \\ -0.2 & 0.58 & 0 & 0 \\ -0.12 & -0.126 & 0.7255 & 0 \\ -0.04 & -0.063 & -0.09 & 1 \end{bmatrix} \bullet \begin{bmatrix} x_1 \\ x_2 \\ x_3 \\ x_4 \end{bmatrix} = \begin{bmatrix} 10 \\ 33 \\ 32 \\ 20 \end{bmatrix}$$

Now find the values of x_1, x_2, x_3 and x_4 as:

$(0.42\ x_1) + (0.x_2) + (0.x_3) + (0.x_4) = 10$, therefore $x_1 = 23.8$

$(-0.2\ x_1) + (0.58\ x_2) + (0.x_3) + (0.x_4) = 33$, therefore $x_2 = 65.1$

$(-0.12\ x_1) + (-0.126\ x_2) + (0.7255.x_3) + (0.x_4) = 32$, therefore $x_3 = 59.4$

$(-0.04\ x_1) + (-0.063\ x_2) + (-0.09\ x_3) + (1.x_4) = 20$, therefore $x_4 = 30.4$

Step 4
From the inverse matrix, the final product then is:

$$P = (I-C) \cdot (I-B \cdot C)^{-1} \cdot F = \begin{bmatrix} 0 & 0 & 0 & 0 \\ 0.2463 & 0.5172 & 0 & 0 \\ 0.2950 & 0.1647 & 0.7581 & 0 \\ 0.1952 & 0.1356 & 0.1241 & 1 \end{bmatrix} \bullet \begin{bmatrix} 10 \\ 33 \\ 32 \\ 20 \end{bmatrix} = \begin{bmatrix} 0 \\ 19.5 \\ 32.6 \\ 30.4 \end{bmatrix}$$

or using the X matrix from the Lynch procedure:

$$P = (I-C) \cdot X = \begin{bmatrix} 0 & 0 & 0 & 0 \\ 0 & 0.3 & 0 & 0 \\ 0 & 0 & 0.55 & 0 \\ 0 & 0 & 0 & 1 \end{bmatrix} \bullet \begin{bmatrix} 23.8 \\ 65.1 \\ 59.4 \\ 30.4 \end{bmatrix} = \begin{bmatrix} 0 \\ 19.5 \\ 32.7 \\ 30.4 \end{bmatrix}$$

This gives the size distribution of the products from the given feed after comminution.

10.3.2. Modelling Ball Mills

Perfect mixing model

In metallurgical operations, ball mills operate continuously and the process is repeated until such time as the required liberation size of the mineral is achieved. Whether the operation is batch or continuous the grinding mill model has been developed on the assumption that the contents are perfectly mixed and the mill can be represented by one perfectly mixed segment or a number of perfectly mixed segments in series [17]. In the steady state operation therefore, a mass balance forms the basis of the model. That is:

| Feed | + | material broken from larger particles | = | material selected for breakage in the mill | + | material discharged. |

These parameters can be evaluated in the following way:

1. Feed rate: Denoted by the matrix F.
2. Removal rate for breakage: R.s where R is a diagonal matrix giving the breakage rate of each component of the mill contents, s, (for any component i, the rate of breakage is R_i . s_i). The mill contents matrix, s, represents the mass of the mill contents retained in each size fraction.
3. Appearance rate: Denoted by A·R·s where A is the appearance matrix (i.e., it is the same as the B matrix and can similarly be obtained experimentally, analytically or approximate values assumed).
4. Discharge rate: Denoted by P = D·s, where D is a triangular matrix giving the fractional rates at which the components of the mill are discharged. For a perfectly mixed mill the product will be the same as the mill contents. However classification within the mill may occur, particularly for grate discharge mills, hence the product from the mill includes D and s.

These factors are combined to obtain the rate of change of mill contents:

$$\frac{\partial s}{\partial t} = A \cdot R \cdot s - R \cdot s + F - P \tag{10.33}$$

$$= (A \cdot R - R - D) \cdot s + F \tag{10.34}$$

At steady state the rate of change of mill contents is zero, or $\dfrac{\partial s}{\partial t} = 0$

Hence Eq. (10.34) would be:

$$(A \cdot R - R - D) \cdot s + F = 0 \tag{10.35}$$

Since $P = D \cdot s$ or $s = D^{-1} \cdot P$, we can substitute for s in Eq. (10.35). Simplifying the resulting equation the mathematical model for ball mills may be written as:

$$P = D \cdot R^{-1} \cdot (D \cdot R^{-1} + I - A)^{-1} \cdot F \tag{10.36}$$

This perfect mixing model has been successfully used to simulate ball mill and rod mill operations. It can be used for steady state and dynamic simulations of milling processes.

It is possible to evaluate Eq. (10.35) providing the model parameters A, R and D are known. The parameters R and D however are interdependent and can only be determined if data on the mill contents are available. This is not always known in industrial mills. This may be overcome by lumping the two together as a combined parameter $D \cdot R^{-1}$.

To evaluate the model parameters, assuming a steady state condition: Rearrange Eq. (10.35) and substituting $s = D^{-1} \cdot P$:

$$0 = F + (A \cdot R - R - D) \cdot s = F + A \cdot R \cdot D^{-1} \cdot P - R \cdot D^{-1} \cdot P - P \tag{10.37}$$

or $\quad F - P = (I - A) \cdot R \cdot D^{-1} \cdot P \tag{10.38}$

or $\quad P = D \cdot R^{-1} \cdot (I - A)^{-1} \cdot (F - P) \tag{10.39}$

From Eq. (10.33):

$$R \cdot s = (I - A)^{-1} \cdot (F - P) \tag{10.40}$$

and hence $\quad P = D \cdot R^{-1} \cdot R \cdot s \tag{10.41}$

Eq. (10.40) can be solved if the inverse of $(1 - A)$ is known, but this is seldom available. However, Eqs. (10.40) and (10.41) are two simultaneous equation in R·s. Both these equations are triangular matrix equations and can be solved using the back substitution technique. To use this technique the equations have to be arranged in the matrix form:

$$\begin{bmatrix} (I - A_{11}) & 0 & 0 & \cdots & 0 \\ -A_{21} & (I - A_{22}) & 0 & \cdots & 0 \\ -A_{31} & -A_{32} & (I - A_{33}) & \cdots & 0 \\ \vdots & \vdots & \vdots & \ddots & 0 \\ -A_{n1} & -A_{n2} & -A_{n3} & \cdots & (I - A_{nn}) \end{bmatrix} \bullet \begin{bmatrix} (R \cdot s)_1 \\ (R \cdot s)_2 \\ (R \cdot s)_3 \\ \vdots \\ (R \cdot s)_n \end{bmatrix} = \begin{bmatrix} (F_1 - P_1) \\ (F_2 - P_2) \\ (F_3 - P_3) \\ \vdots \\ (F_n - P_n) \end{bmatrix} \tag{10.42}$$

Expanding: $\quad (1-A_{11}) \cdot (R \cdot s)_1 = (F_1-P_1)$ $\qquad$ (10.43)

or $\qquad (R \cdot s)_1 = \dfrac{(F_1 - P_1)}{(1 - A_{11})}$ $\qquad$ (10.44)

and $\qquad -A_{21} \cdot (R \cdot s)_1 + (1 - A_{22}) \cdot (R \cdot s)_2 = (F_2 - P_2)$ $\qquad$ (10.45)

from which $\quad (R \cdot s)_2 = \dfrac{(F_2 - P_2) + A_{21} \cdot (R \cdot s)_1}{(1 - A_{22})}$ $\qquad$ (10.46)

The general solution can therefore be written as:

$$(R \cdot s)_i = \dfrac{(F_i - P_i) + \sum\limits_{j=1}^{i=1} A_{ij} \cdot (R \cdot s)_j}{(1 - A_{ii})}$$ $\qquad$ (10.47)

$(R \cdot s)_i$ can then be substituted in Eq. (10.41) to calculate $(D \cdot R^{-1})$. If the size distribution of the mill contents is known then the discharge matrix can be calculated from $P = D \cdot s$ and hence the rate of breakage matrix, R, can be determined from D·R-1.

While considering the mass balance in a breakage system, Lynch and Whiten [18] and later Gault [13] related the discharge rate from the mill with the volumetric feed rate and the dimensions of the mill as:

$$D = \left[\dfrac{4\,V}{D^2\,L} \right] D^*$$ $\qquad$ (10.48)

where $\quad D^*$ = standard discharge rate function,
$\qquad\quad$ V = volume feed rate
$\qquad\quad$ D = the mill diameter
$\qquad\quad$ L = the length of mill.

D^* is a diagonal matrix which is independent of size unless classification at the mill discharge occurs. D^* has diagonal values near unity. The combined parameter $D \cdot R^{-1}$ varies with the feed rate and:

$$D \cdot R^{-1} = f(D \cdot R^{-1})^*$$ $\qquad$ (10.49)

where $\quad f$ = a function of the feed rate to the mill and
$\qquad (D \cdot R^{-1})^*$ = a constant

For example, the breakage rate parameter could be defined as:

$$D \cdot R^{-1} = \dfrac{4V}{D^2 L} (D \cdot R^{-1})^*$$ $\qquad$ (10.50)

Example 10.3 illustrates the use of Eqs. (10.47)–(10.50).

Example 10.3

The feed and product size distribution of a ball mill is given below. The feed rate was 200 t/h. The feed rate was increased to 285 t/h. Estimate the product size distribution at the higher feed rate.

Data: Appearance matrix A has the following values:

0.188, 0.321, 0.208, 0.105, and 0.021

Size, Microns	Feed % Retained	Feed Mass, t/h	Product % Retained	Product Mass, t/h
1200	6.4	12.8	0.3	0.6
600	18.4	36.8	6.5	13.0
300	22.8	45.6	9.5	19.0
150	29.1	58.2	15.4	30.8
75	22.0	44.0	28.9	57.8
-75	1.3	2.6	39.4	78.8
total	100	200	100	200

Solution

Writing a simple spreadsheet can easily solve the problem. But for those using a calculator the following steps for calculations would be useful.

Step 1
A is a lower triangular matrix, therefore the elements in the diagonal, A_{ii} are all 0.188.

That is: $(1-A_{11}) = (1-0.188) = 0.812$

Then:

$$(R \cdot s)_1 = \frac{(F_1 - P_1)}{0.812} = \frac{12.8 - 0.6}{0.812} = 15.02$$

$$(R \cdot s)_2 = \frac{(F_2 - P_2 + (A_{21}(R \cdot s)_1))}{0.812} = \frac{36.8 - 13.0 + (0.321 \times 15.02)}{0.812} = 35.25$$

$$(R \cdot s)_3 = \frac{(F_3 - P_3 + (A_{31}(R \cdot s)_1) + (A_{32}(R \cdot s)_2))}{0.812}$$

$$= \frac{45.6 - 19.0 + (0.208 \times 15.02) + (0.321 \times 35.25)}{0.812} = 50.54$$

$$(R \cdot s)_4 = \frac{\left(F_4 - P_4 + (A_{41}(R \cdot s)_1) + (A_{42}(R \cdot s)_2) + (A_{43}(R \cdot s)_3)\right)}{0.812}$$

$$= \frac{58.2 - 30.8 + (0.105 \times 15.02) + (0.208 \times 35.25) + (0.321 \times 50.54)}{0.812}$$

$$= 64.70$$

$$(R \cdot s)_5 = \frac{\left(F_5 - P_5 + (A_{51}(R \cdot s)_1) + (A_{52}(R \cdot s)_2) + (A_{53}(R \cdot s)_3) + (A_{54}(R \cdot s)_4)\right)}{0.812}$$

$$= \frac{44.0 - 57.8 + (0.021 \times 15.02) + (0.105 \times 35.25) + (0.208 \times 50.54) + (0.321 \times 64.70)}{0.812}$$

$$= 26.47$$

Step 2

Next calculate the $D \cdot R^{-1}$ matrix from Eq. (10.41).

$$\begin{bmatrix} P_1 \\ P_2 \\ P_3 \\ P_4 \\ P_5 \end{bmatrix} = \begin{bmatrix} (D \cdot R^{-1})_{11} & 0 & 0 & 0 & 0 \\ 0 & (D \cdot R^{-1})_{22} & 0 & 0 & 0 \\ 0 & 0 & (D \cdot R^{-1})_{33} & 0 & 0 \\ 0 & 0 & 0 & (D \cdot R^{-1})_{44} & 0 \\ 0 & 0 & 0 & 0 & (D \cdot R^{-1})_{55} \end{bmatrix} \bullet \begin{bmatrix} (R \cdot s)_1 \\ (R \cdot s)_2 \\ (R \cdot s)_3 \\ (R \cdot s)_4 \\ (R \cdot s)_5 \end{bmatrix}$$

Solving for $D \cdot R^{-1}$:

$$P_1 = (D \cdot R^{-1})_{11} \cdot (R \cdot s)_1 \quad \text{or} \quad (D \cdot R^{-1})_{11} = \frac{P_1}{(R \cdot s)_1} = \frac{0.6}{15.02} = 0.0399$$

$$P_2 = (D \cdot R^{-1})_{22} \cdot (R \cdot s)_2 \quad \text{or} \quad (D \cdot R^{-1})_{22} = \frac{P_2}{(R \cdot s)_2} = \frac{13.0}{35.25} = 0.3688$$

and similarly:

$$(D \cdot R^{-1})_{33} = 0.3759$$

$$(D \cdot R^{-1})_{44} = 0.4761$$

$$(D \cdot R^{-1})_{55} = 2.1832$$

Step 3

Assuming the breakage rate is constant over the range of 200 – 285 t/h, then from Eqs. (10.48) and (10.50):

$$(D \cdot R^{-1})_{200 \, t/h} = \left(\frac{4 \, V_{200}}{D^2 \, L}\right)(D \cdot R^{-1})^* \text{, and}$$

$$(D \cdot R^{-1})_{285 \, t/h} = \left(\frac{4 \, V_{285}}{D^2 \, L}\right)(D \cdot R^{-1})^*$$

then $(D \cdot R^{-1})_{285 \, t/h} = \left(\dfrac{V_{285}}{V_{200}}\right)(D \cdot R^{-1})_{200 \, t/h}$

For constant % solids in the mill at the two flow rates, the volume flow rates are proportional to the solid flow rates, hence:

$$(D \cdot R^{-1})_{285 \, t/h} = \left(\frac{285}{200}\right)(D \cdot R^{-1})_{200 \, t/h} \quad \text{and}$$

$(D \cdot R^{-1})_{11} = 1.425 \times 0.03993 = 0.0569$

$(D \cdot R^{-1})_{22} = 1.425 \times 0.3688 = 0.5255$

$(D \cdot R^{-1})_{33} = 1.425 \times 0.3759 = 0.5357$

$(D \cdot R^{-1})_{44} = 1.425 \times 0.4761 = 0.6784$

$(D \cdot R^{-1})_{55} = 1.425 \times 2.1832 = 3.1111$

The mill product is then given by the Eq. (10.36):

$$P = D \cdot R^{-1} \cdot (D \cdot R^{-1} + I - A)^{-1} \cdot F$$

The matrix $(D \cdot R^{-1} + I - A)$ may now be calculated using the normal rules of matrix addition and subtraction:

$(D \cdot R^{-1} + I - A) =$

$$\begin{bmatrix} 0.0569 & 0 & 0 & 0 & 0 \\ 0 & 0.5255 & 0 & 0 & 0 \\ 0 & 0 & 0.5357 & 0 & 0 \\ 0 & 0 & 0 & 0.6784 & 0 \\ 0 & 0 & 0 & 0 & 3.1111 \end{bmatrix} + \begin{bmatrix} 1 & 0 & 0 & 0 & 0 \\ 0 & 1 & 0 & 0 & 0 \\ 0 & 0 & 1 & 0 & 0 \\ 0 & 0 & 0 & 1 & 0 \\ 0 & 0 & 0 & 0 & 1 \end{bmatrix} - \begin{bmatrix} 0.188 & 0 & 0 & 0 & 0 \\ 0.321 & 0.188 & 0 & 0 & 0 \\ 0.208 & 0.321 & 0.188 & 0 & 0 \\ 0.105 & 0.208 & 0.321 & 0.188 & 0 \\ 0.021 & 0.105 & 0.208 & 0.321 & 0.188 \end{bmatrix}$$

$$= \begin{bmatrix} 0.8689 & 0 & 0 & 0 & 0 \\ -0.321 & 1.3375 & 0 & 0 & 0 \\ -0.208 & -0.321 & 1.3477 & 0 & 0 \\ -0.105 & -0.208 & -0.321 & 1.4904 & 0 \\ -0.021 & -0.105 & -0.208 & -0.321 & 3.9231 \end{bmatrix}$$

and taking the inverse:

$$
\left[\left(D \cdot R^{-1}+I-A\right)\right]^{-1}=\begin{bmatrix} 1.1509 & 0 & 0 & 0 & 0 \\ 0.2762 & 0.7476 & 0 & 0 & 0 \\ 0.2434 & 0.1781 & 0.7420 & 0 & 0 \\ 0.1721 & 0.1427 & 0.1598 & 0.6710 & 0 \\ 0.0405 & 0.0411 & 0.0524 & 0.0549 & 0.2549 \end{bmatrix}
$$

By matrix multiplication:

$$
D \cdot R^{-1} \cdot\left[\left(D \cdot R^{-1}+I-A\right)\right]^{-1}=
$$

$$
=\begin{bmatrix} 0.0569 & 0 & 0 & 0 & 0 \\ 0 & 0.5255 & 0 & 0 & 0 \\ 0 & 0 & 0.5357 & 0 & 0 \\ 0 & 0 & 0 & 0.6784 & 0 \\ 0 & 0 & 0 & 0 & 3.1111 \end{bmatrix} \bullet \begin{bmatrix} 1.1509 & 0 & 0 & 0 & 0 \\ 0.2762 & 0.7476 & 0 & 0 & 0 \\ 0.2434 & 0.1781 & 0.7420 & 0 & 0 \\ 0.1721 & 0.1427 & 0.1598 & 0.6710 & 0 \\ 0.0405 & 0.0411 & 0.0524 & 0.0549 & 0.2549 \end{bmatrix}
$$

$$
=\begin{bmatrix} 0.0655 & 0 & 0 & 0 & 0 \\ 0.1452 & 0.3929 & 0 & 0 & 0 \\ 0.1304 & 0.0954 & 0.3975 & 0 & 0 \\ 0.1167 & 0.0968 & 0.1084 & 0.4552 & 0 \\ 0.1261 & 0.1279 & 0.1631 & 0.1708 & 0.7930 \end{bmatrix}
$$

and the product is calculated by:

$$
P=D \cdot R^{-1} \cdot\left[\left(D \cdot R^{-1}+I-A\right)\right]^{-1} \cdot F=\begin{bmatrix} 0.0655 & 0 & 0 & 0 & 0 \\ 0.1452 & 0.3929 & 0 & 0 & 0 \\ 0.1304 & 0.0954 & 0.3975 & 0 & 0 \\ 0.1167 & 0.0968 & 0.1084 & 0.4552 & 0 \\ 0.1261 & 0.1280 & 0.1631 & 0.1708 & 0.7930 \end{bmatrix} \bullet \begin{bmatrix} 18.24 \\ 52.44 \\ 64.98 \\ 82.94 \\ 62.70 \end{bmatrix} = \begin{bmatrix} 1.19 \\ 23.25 \\ 33.21 \\ 52.00 \\ 83.49 \end{bmatrix}
$$

Thus at the feed tonnage of 285 t/h the ball mill product size distribution is tabulated in the table below. For comparison, product size distribution at 200 t/h throughput is also given. The results show that the effect on the product size distribution of increasing the feed rate from 200 t/h to 285 t/h, in this particular example is not great.

Simulated product size distribution

Size, microns	P at 285 t/h	P % at 285 t/h	P % at 200 t/h
1200	1.19	0.4	0.3
600	23.25	8.2	6.5
300	33.21	11.7	9.5
150	52.00	18.2	15.4
75	83.49	29.3	28.9
-75	91.85	32.2	39.4
Total	285	100	100

10.3.3. Modelling Rod mills

A study of the movement of materials in a rod mill indicates that at the feed end the larger particles are first caught between the rods and reduced in size gradually towards the discharge end. Lynch [1] contended that the next lower size would break after the sizes above it had completely broken. He described this as *stage breakage*, the stages being in steps of √2. The size difference between the particles at the two ends of the mill would depend on:

1. mill length,
2. speed of grinding, and
3. feed rate.

The presence of this size difference indicates that a *screening effect* was generated within a rod mill and that the movement of material in the mill was a combination of breakage and screening effects. The breaking process was obviously repetitive and involved breakage function, classification function and selection functions. Therefore for rod mills an extension of the general model for breakage within each stage applies, where the feed to stage (i+1) is the product from stage i. That is, within a single stage i, the general model defined by Eq. (10.18) applies.

$$P = (I-C)\cdot(B\cdot S + I - S)\cdot[I-C\cdot(B\cdot S + I - S)]^{-1}\cdot F = \left[\prod_{j=0}^{j=v}\right]\cdot X_j\cdot F \qquad (10.51)$$

The number of stages, v, is the number of elements taken in the feed vector. A stage of breakage is defined as the interval taken to eliminate the largest sieve fraction from the mill feed or the feed to each stage of breakage. The very fine undersize is not included as a stage.

The breakage function described by Eq. (10.2) could be used. For the classification matrix, which gives the proportion of each size that enters the next stage of breakage, the value of the element in the first stage C_{11} equals 1. That is, all of size fraction 1 is completely reduced to a lower size and all the particles of the classification underflow are the feed to the second stage of breakage and so on. Hence the classification matrix is a descending series. If we take the √2 series, then the classification matrix C can be written as:

$$C = \begin{bmatrix} 1 & 0 & 0 & 0 & 0 & 0 \\ 0 & 0.5 & 0 & 0 & 0 & 0 \\ 0 & 0 & 0.25 & 0 & 0 & 0 \\ 0 & 0 & 0 & 0.125 & 0 & 0 \\ 0 & 0 & 0 & 0 & 0.0625 & 0 \\ 0 & 0 & 0 & 0 & 0 & 0.032 \end{bmatrix}$$ (10.52)

The selection matrix S is machine dependant. It is affected by machine characteristics, such as length (including length of rods) and the speed of operation. Both B and C have to be constant to determine the selection function S within a stage.

In Whiten's model [16] for the probability of breakage against the size of particles, considering a single stage operation, we see that:

1. The region between K_1 and K_2 is almost linear (actually it is a part of a parabola, Fig. 10.6)
2. K_2 decreases with time as the material travels down the mill towards the discharge end
3. $K_1 = S \cdot C$

Thus for each stage a similar matrix can be developed resulting in a step matrix which provides a solution of the rod mill model. Calculations are similar to that shown previously for grinding mill models.

10.3.4. Modelling AG / SAG Mills

While in conventional tumbling mills the size reduction is primarily by impact of grinding media (steel balls or rods) in AG or SAG mills the size reduction is mainly by abrasion and chipping off of particles and less so by impact. The process is complicated by:

1. the grinding medium itself disintegrating with time,
2. the transport of the material through the mill is constrained by the size, shape and apertures in the grate at the discharge end, and
3. the slurry characteristics during wet milling, such as the viscosity and density.

Stanley [19] and Duckworth and Lynch [20] in attempting to describe the process have quantified these variables and derived mathematical models to suit the operation of these mills. Additional considerations were advocated by Leung et al. [21] and later by Morrison et al. [22] who introduced the concept of high and low energy breakage of particles in their models. The high energy was defined as breakage due to crushing and impact and the low energy breakage due to abrasion.

Some evidence of the different kinds of breakage within SAG mills has been reported (Austin et al. [23], Améstica et al. [24], Napier-Munn et al. [8]). Working with experimental SAG mills the breakage rate was plotted against the particle size. The curves showed that at the initial stages the breakage rate increased proportionally with particle size, subsequently the rate decreased but again increased (Fig. 9.7). These inflections in the curve have been attributed to the change in the mechanism of breakage from surface abrasion effects to crushing effect.

In an earlier work, Austin et al. [23] identifies three mechanisms of breakage, namely, normal fracture caused by balls and large pebbles that formed the grinding medium, chipping off of particles rendering them roundish and spherical, and finally abrasion. However, Loveday and Whiten [25] have questioned the interpretations of Austin's data.

To develop a mathematical model of the process, Améstica et al. [24] considered the discharge grate as a classifier. Their conceptual model is illustrated in Fig. 10.8. The dotted lines in the figure indicate the conceptual movement of material in the mill where the grate acting as classifier returned its *underflow* to the main feed stream for further size reduction and its *over flow* formed the final product from the mill. The measured classification function is shown in Fig. 10.9.
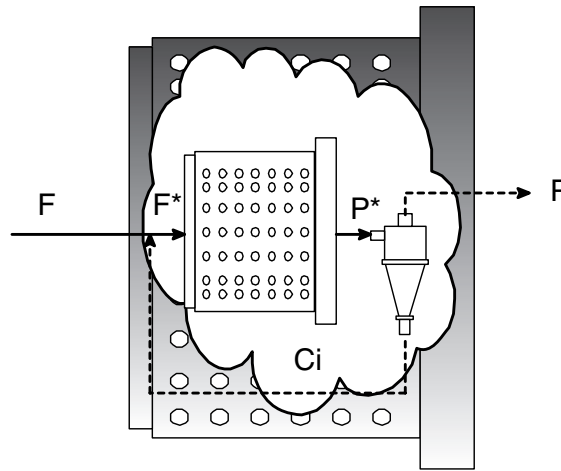
Fig. 10.8. Conceptual diagram of material flow in a SAG mill [23,24]
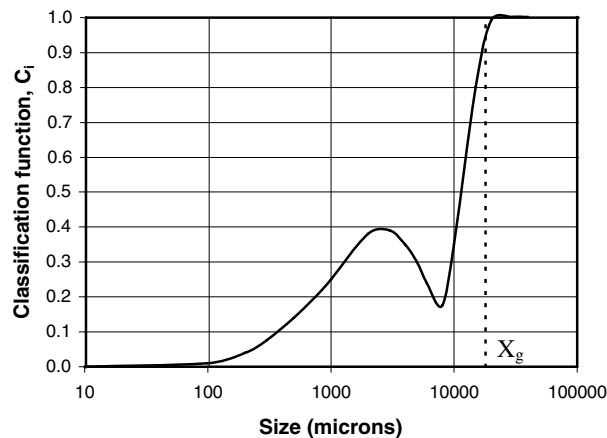
Fig. 10.9. Internal classification in a SAG mill with grate size X_g [24]

In Fig. 10.9, c_i represents the fraction of size i which is returned to the mill. The drop in c_i close to the grate size was observed on a number of occasions. The mill product, P_i was calculated from the expression:

$$P_i = P_i^* (1+C)(1-c_i)$$

(10.53)

where P_i^* = the product from the mill grind (pre-internal classification), and
C = an apparent internal circulation ratio.

The feed to the internal mill is given by:

$$(1+C)F_i^* = F_i + (1+C)P_i^* c_i \quad \text{and}$$

(10.54)

$$(1+C) = \frac{1}{1 - \sum_{i=1}^{N} P_i^* c_i}$$

(10.55)

The relationship between F_i and P_i is given by the size-mass balance or population balance model for a fully mixed mill at steady state:

$$P_i^* = F_i^* + \left(\frac{M_H}{M_F}\right) \sum_{j=1}^{i-1} b_{ij} S_j m_j - \left(\frac{M_H}{M_F}\right) S_i m_i$$

(10.56)

where M_H = hold up mass,
M_F = feed mass,
m_i = mass fraction in the ith size interval,
F_i^*, P_i^* = mass fraction of size i in the internal mill feed and product.

Leung et al. [21], Morrell [26] and Napier-Munn et al. [8] made a similar and simpler approach by considering that the classification at the grate allowed a certain fraction of the mill hold-up to always pass through. This fraction contained particles smaller than a certain size, X_m which in turn is less than the grate aperture and had fluid characteristics similar to water. Further they considered that the solids in the slurry containing particles of size greater than the grate aperture would never pass through. Slurries containing particle sizes in-between would pass depending on the probability of classification function. This concept is somewhat similar to that advocated for the crusher model by Whiten [16]. According to Leung et al [21] the discharge containing only small size solids is considered to behave like water passing through orifices in the grate and can be represented by AB in the log-size-classification curve (Fig. 10.10). The remaining slurry was classified at the grate, the classification followed line BC representing sizes associated with the discharge. Napier-Munn et al. [8] recognised that the characteristics of flow of products, (solids and water) through the grate were different. They assumed that the slurry passing through obeyed the laws of fluid flow through orifices, as propounded by the well-known Bernoulli theorem. Thus the fluid flow through the grate opening was considered as:
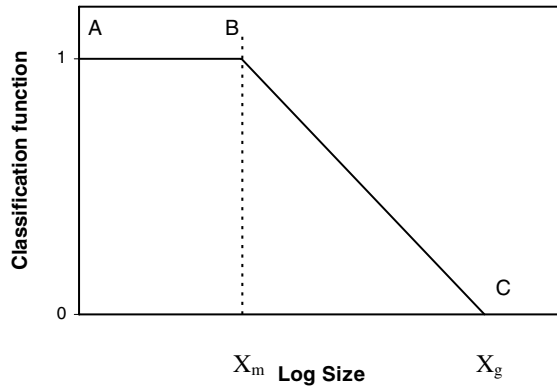
Fig. 10.10. Classification function C, against particle size [8].

$$Q_V = A_G \sqrt{2gH} \qquad\qquad (10.57)$$

where Q_V = the volumetric flow rate through an aperture in the grate,
        A_G = the cross section of the grate aperture,
        H = head of fluid,
        g = acceleration due to gravity.

The problem in Eq. (10.57) was to establish the value of H, the head of fluid, as it would depend on the rate of rotation, the solid-liquid ratio, the porosity of the bed and the inclination of the liquid level inside the mill. Morrell et al. [27] therefore considered an average radial position defined as γ, which was the ratio of the open areas of all apertures at a radial position r_i from the centre to the radius of the mill inside diameter. Symbolically this was written as:

$$\gamma = \frac{\Sigma (r_i A_i)}{R \, \Sigma A_i} \qquad\qquad (10.58)$$

where A_i = total area of apertures at radial position r_i, and
        R = mill radius.

Morrell [26] also considered that the product flow was made up of flow of the fluid through the zone of grinding medium (i.e. between balls and some solids), and flow from the *pool zone* created by separation of excess slurry from the tumbling charge (slurry in excess of the charge volume and the interstices in the charge). The empirical equation representing the flow rate through the grinding media (m³/h) was determined as:

$$Q_M = 6100 J_H^2 \, \gamma^{2.5} A \phi_C^{-1.38} \, D^{0.5} \qquad\qquad J_H \le J_{MAX} \qquad\qquad (10.59)$$

and the equation representing the flow through the pole zone as:

$$Q_t = 935 J_S \gamma^2 A D^{0.5} \qquad\qquad J_S = J_P - J_{MAX}, J_P > J_{MAX} \qquad (10.60)$$

where J_H = net fraction of slurry hold-up within the interstitial spaces of the grinding media,

  J_S = net fractional volume of slurry in the slurry pool,

  J_{MAX} = maximum net fraction of slurry in the grinding zone,

  J_P = net fraction of the mill volume occupied by pulp/slurry,

  γ = mean relative radial position of the grate apertures (as defined by Eq. (10.58)),

  A = total area of all apertures, m^2,

  ϕ_C = fraction of the critical speed of the mill,

  D = mill diameter, m,

  Q_M = volume flow rate through the grinding media zone, m^3/h

  Q_t = volume flow rate of slurry through the pool zone, m^3/h.

If the flow through the mill is assumed to follow the perfect mixing model, then the volumetric flow of material of size i would be:

$$P_i = D_i \bullet s_i \qquad\qquad (10.61)$$

where D_i = discharge rate of particles of size i,

  P_i = the volumetric flow rate of size i in the mill product, and

  s_i = the volume of size i in the mill content.

The discharge rate is thus $D_i = \dfrac{P_i}{s_i}$ (10.62)

Substituting $P_i = Q_M$, in Eq. (10.62), the discharge rate D_i would be:

$$D_i = \left[\frac{6100 J_H^2 \, \gamma^{2.5} A \, \phi_c^{-1.38} \, D^{0.5}}{s_i} \right] \qquad\qquad (10.63)$$

From simple geometry, $s_i = \dfrac{\pi D^2}{4} J_P$

Hence the discharge rate model for AG/SAG mills may be written as:

$$D_i = \left[\frac{6100 J_H^2 \, \gamma^{2.5} A \, \phi_C^{-1.38} \, D^{0.5}}{0.25 \pi D^2 J_P} \right] = \left[\frac{7770 \, J_H^2 \, \gamma^{2.5} A \phi_C^{-1.38}}{D^{1.5} J_P} \right] \qquad (10.64)$$

In addition to the flow rate and discharge considerations within a SAG mill, the high energy required for breakage of larger particles by impact was attributed to the top 20% of the

feed. The size reduction of the remainder was assumed to be due to abrasion requiring low energy of breakage.

The high-energy estimate required for size reduction was attributed to the potential energy (PE) transmitted to particles falling from a height equal to the diameter of the mill. This energy value was determined by the twin-pendulum test and the T_{10} parameter estimated. The energy E was then calculated by using Eq. (3.45).

For low energy breakage determination, a tumbling abrasion test is used to generate the low energy T_{10} parameter. Combining the high and low energy T_{10} parameters, a combined appearance function can be calculated as:

$$A = \frac{(T_{LE} A_{LE}) + (T_{HE} A_{HE})}{(T_{LE} + T_{HE})} \qquad (10.65)$$

where   A   = combined appearance function,

          A_{LE}, A_{HE} = low and high energy appearance functions respectively,

          T_{LE}, T_{HE} = low and high energy T_{10} parameters, respectively.

From the equations describing the combined appearance function, the discharge rate and breakage rate, the material balance of SAG mills for the feed, mill holdup and discharge resulted in the perfect mixing model for AG/SAG mills given by:

$$P_i = F_i + \sum_{\substack{j=1 \\ i>l}}^{i} R_j s_j A_{ij} - R_i s_i \qquad (10.66)$$

and $P_i = D_i \cdot s_i$ (Eq. (10.61))

where P_i = rate of production of particles of size i,

         F_i = mass rate of particles of size i in the feed,

         A_{ij} = appearance function or breakage distribution function of particles of size i from particles of size j,

         R_j = breakage rate of particles of size i,

         s_j = amount of particles of size i in the mill contents and

         D_i = rate of discharge of particles of size i.

10.3.5. High Pressure Grinding Rolls (HPGR)

A satisfactory mathematical model of HPGR has not yet been established [28]. The forces of compression and size reduction are complex and some light on its complexity has been indicated by Schönert and Sander [29] and Lubjuhn and Schönert [30]. Discussion of this topic is beyond the scope of this book. The interested reader is directed to the original papers.

10.3.6. Stirrer Ball Mills

While in a ball mill the body of the mill rotates and the charge made to rotate by the help of lifters (provided by the shape of mill liners), in stirrer mills the body is stationary and the charged moved by stirrers rotating inside the mill. These mills have been introduced over the last two decades for grinding down to very fines sizes that is required to liberate finely disseminated minerals in some host rock. Several types of such mills are now available such

as the vertical stirred mills (Tower mill, Vertimill, Metroprotech mill) and horizontally stirred mills (ISAmill). The difference between them is in the stirring mechanism The Tower Mill uses a helical screw while the ISAmill uses a horizontal shaft with various shapes and sizes of discs. The grinding media used are hardened steel balls, river sand or ceramics.

The feed size (F_{80}) to the mills ranges between 45 and 100 microns and the product size around 3 microns and less.

The mechanism of size reduction is entirely different from the ball mills. In this case the size reduction is mostly by attrition. Morrell et al.[31] examined the applicability of the rate-size mass balance model and the perfect mixing Whiten model to ultra-fine grinding in a Tower Mill. Further work in this direction is in progress.

10.4. Problems

Most problems arising out of this chapter need the use of computer programs. A few that can be solved by hand held calculators are included here.

10.1

In numerical example 10.3, the product from the first stage of breakage was calculated. Continue calculations to determine the products from the second and third stages.

10.2

Using the particle size distribution obtained from a batch grind at short grind time, determine the breakage distribution function using the BII method for an incomplete sieving error of 0.01.

Interval	Size, μm	Feed % retained
1	5600	78.7
2	4000	9.04
3	2800	5.16
4	2000	3.12
5	1400	1.76
6	1000	0.87
7	710	0.41
8	0	0.94

10.3

A ball mill was designed to operate at the rate of 1 million tonnes of iron ore per year working 360 days in the year. The characteristics of the grind are given in the table below.

Size microns	Feed % retained	Product
2000	1.3	0
1000	8.5	1.2
500	16.0	3.4
250	25.0	11.7
125	20.0	18.1
75	18.0	12.2
-75	11.2	53.4

It was desired to increase the plant throughput to 1.2 m t/year. If all other conditions remain the same, estimate the product size expected.

10.4
Ore samples were taken from a grinding mill operating as a batch process. The feed size distribution, breakage functions and size analysis of samples taken at intervals of 10 minutes up to 30 minutes are given. Determine:

1. The breakage rate of the top two feed sizes
2. The % passing 710 µm after 1 hour of operation.

Hint: Assume breakage was constant within a size range. May need to use Solver in Excel (or similar) for part of the calculation.

Data:

Feed Size, micron	Mass %	Breakage function	t=10 min	t=20 min	t=30 min
1400	8.2	0.1980	5.5	3.6	2.4
710	15.6	0.3380	12.2	10.0	7.9
355	22.0	0.2148	18.8	15.3	10.0
180	25.7	0.1224	21.4	17.6	13.0
90	12.5	0.0645	13.2	16.4	22.6
53	8.2	0.0338	10.9	13.5	15.2
-53	7.8	0.0285	17.6	23.6	28.9
	100.0	1.000	100.0	100.0	100.0

10.5
A copper ore was charged in a rod mill for size reduction. Three different ore sources are to be treated. At steady state conditions the following results were obtained:

Size, range	Feed Size (1) mm	Feed Size (2) mm	Feed Size (3) mm	Selection function	Breakage Function	Classification function
1	10.1	3.2	23.0	1.0	0.1980	1.0
2	21.2	5.8	18.0	0.5	0.3308	0
3	25.4	14.3	18.6	0.25	0.2148	0
4	13.4	18.2	12.5	0.125	0.1225	0
5	6.5	21.0	6.5	0.062	0.0654	0
6	4.1	8.2	8.6	0.032	0.0338	0
7	15.3	6.0	4.7	0.016	0.0172	0
8	4.0	21.3	5.1	0.008	0.0087	0

Determine the product sizes after each change of feed size.

10.6
A drop weight test on a single size fraction (-5.6+4.75 mm) at different comminution energies, E_G, gave the following product sizes:

	Test 1, E_G = 5.11 kWh/t		Test 2, E_G = 3.87 kWh/t		Test 3, E_G = 2.80 kWh/t		Test 4, E_G = 2.39 kWh/t	
Size (mm)	Mass %	Cum % passing	Mass %	Cum % passing	Mass %	Cum % passing	Mass %	Cum % passing
4.0	0	100.0	0	100.0	0	100.0	0	100.0
2.0	11.0	89.0	8.1	91.9	9.6	90.4	10.0	90.0
1.0	25.7	63.3	27.5	64.5	30.9	59.5	30.6	59.5
0.5	21.3	42.0	23.5	40.9	21.7	37.8	23.3	26.1
0.25	13.9	28.2	16.0	24.9	13.1	24.7	14.4	21.7
0.125	10.0	18.2	10.0	14.9	8.6	16.1	8.6	13.1
0.063	7.8	10.5	6.7	8.2	6.6	9.4	5.8	7.3
0	10.5		8.2		9.4		7.3	

1. Determine the T_{10} value for each set of test results
2. Determine the relationship between T_{10} and E_G
3. Estimate the value of α in the relationship between T_N and T_{10} (Eq. (10.4))
4. For a comminution energy of 25 kWh/t determine the T_{10} value and hence estimate the appearance function

10.7

In a ball mill experiment, the feed size and classification function is assumed constant. If the breakage function changes, e.g. as a result of a change in ore type, estimate the change in product size from the following data:

Size range	Rate function, DR^{-1}	Feed tonnes	Breakage Function 1	Breakage Function 2	Breakage Function 3
1	0.04	19.9	0.189	0.138	0.033
2	0.369	37.8	0.331	0.248	0.350
3	0.376	44.8	0.215	0.229	0.170
4	0.476	27.1	0.123	0.160	0.084
5	2.18	20.3	0.065	0.090	0.038

10.8

A crusher treats ROM ore at a rate of 100 t/h. From the crusher/ore characteristics given below, estimate the product size distribution.

Size fraction	Classification function	Feed Mass %	Breakage Function
1	1	15	0.195
2	0.5	28	0.27
3	0.1	35	0.18
4	0	22	0.09

REFERENCES

[1] A.J. Lynch, Mineral crushing and grinding circuits, their simulation, optimisation, design and control, Elsevier Scientific Publishing Company, Amsterdam. 1977.

[2] L.G. Austin, R.R. Klimpel and P.T. Luckie, Process Engineering of Size Reduction: Ball Milling, SME/AIME, New York, 1984.

[3] S.R. Broadbent and T.G. Callcott, Philosophical Transactions of the Royal Society of London, A249 (1956) 99.

[4] A.M. Gaudin and T.P. Meloy, Transactions, AIME/SME, 223 (1962) 40.

[5] D.F. Kelsall and K.J. Reid, Proceedings, AIChE/Institute Chem. Engineering Symposium Series, No. 4, 1965, pp. 14 – 20.

[6] R.R. Klimpel and L.G. Austin, Transactions of the Society of Mining Engineers, 232 (1965) 88.

[7] A.J. Lynch and M.J. Lees, in Mineral Processing Handbook, N.L. Weiss (ed), SME/AIME, 1985, pp. 3A 28-55.

[8] T.J. Napier-Munn, S. Morrell, R. Morrison and T. Kojovic, Mineral Comminution Circuits Their Operation and Optimisation, JKMRC, 1996.

[9] R.P. King, Modeling and simulation of mineral processing systems, Butterworth Heinemann, Boston. 2001.

[10] L.G. Austin and P.T. Luckie, Powder Technology, 5 No. 4 (1972) 215.

[11] D.F. Kelsall and K.J. Reid, Symposium on size reduction, Sydney University Chem. Engineering Association, February, 1969.

[12] W.J. Whiten, Proceeding, Symposium on Automatic Control Systems Mineral Processing Plants, AusIMM, Southern Queensland branch, 1971, pp. 129-148.

[13] G.A. Gault, PhD Thesis, University of Queensland, 1975,

[14] B.K. Loveday, Journal of the South African Institute of Mining and Metallurgy, 68 (1967) 111.

[15] K.J. Reid, Chemical Engineering Science, 20 (1965) 953.

[16] W.J. Whiten, Proceedings, 10th International Symposium on the Application of Computer Methods in the Minerals Industry, Johannesburg, 1972, pp. 317-323.

[17] W.J. Whiten, *Chemical Engineering Science*, 29 (1974) 588.

[18] A.J. Lynch and W.J. Whiten, 34th Annual Meeting of American Chemical Society, 1967

[19] G.G. Stanley, Ph.D Thesis, University of Queensland, 1974.

[20] C.A. Duckworth and A.J. Lynch, XIV International Mineral Proceeding Congress, CIM, Toronto, session III, paper 1, 1982.

[21] K. Leung, R.D. Morrison and W.J. Whiten, Copper '87, Santiago, 1987.

[22] R.D. Morrison, T. Kojovic and S. Morrell, Proceedings of SAGSEM '89, SAG Milling Seminar, Australasian Institute of Mining and Metallurgy, Perth, 1989, pp. 254-271.

[23] L.G. Austin, C.A. Barahona and J.M. Menacho, Powder Technology, 51 (1987) 283.

[24] R. Améstica, G.D. González, J. Barría, L. Magne, J. Menacho and O. Castro, Proceedings, XVIII International Mineral Processing Congress, Sydney, 23-28 May, 1993, pp. 117-130.

[25] B.K. Loveday and W.J. Whiten, Transactions of the Institution of Mining and Metallurgy, 111 (2002) C39.

[26] S. Morrell, in Comminution: Theory and Practice, S.K. Kawatra (ed), AIME, Chapter 27, 1992, pp. 369-380.

[27] S. Morrell, W.M. Finch, T. Kojovic and H. Delboni, 8th Euro Symposium on Comminution, Stockholm, 1994, pp. 332-343.

[28] L.G. Austin, K.R. Weller and I.L. Lim, Proceedings, XVIII International Mineral Processing Congress, Sydney, 1993, pp. 87-95.

[29] K. Schönert and U. Sander, Powder Technology, 122 (2002) 130.

[30] U. Lubjuhn and K. Schönert, Proceedings, XVIII International Mineral Processing Congress, Sydney, 1993, pp. 161-168.

[31] S. Morrell, U.J. Steins and K.K. Weller, Proceedings of the XVIII International Mineral Processing Congress, Sydney, Aust. Inst. Mining and Metall., 1993, pp. 61-66.

Chapter 11. Screening

11. INTRODUCTION

Minerals of interest exist in nature in the dispersed state, as a separate entity, for example native gold particles in silica rock, or in the combined form, like nickel sulphide or chalcopyrite in an host rock. Often due to relative differences in the hardness, friability and crushability between the mineral and host rocks, minerals may be "liberated" by repeated crushing and other comminution processes. The particles produced, having different sizes and shapes, can be separated over screens that allow particles that are less than the aperture of the screen to pass through while retaining the others. Such separations of mineral constituents can be an efficient and cheap method to concentrate a mineral and to reject the gangue constituents in some mineral ores.

Separations of dry materials by screens and sieves are generally attempted down to about 75 microns. Finer materials have a tendency to blind the sieve openings. In such cases, screening in the presence of water helps. Separations of even finer sizes are difficult on a sieve. For such fine material other processes have to be adopted like *classification*.

In the metallurgical industry a distinction is made between screening and sieving. The mechanism of size separation by both is the same, but screening generally applies to industrial scale size separations while sieving refers to laboratory scale operations.

In this chapter the design of different types of screens and their operation are described.

11.1. Basic Design features in Screens
The three most important design features of screens are:

1. Surface and aperture,
2. Types of screens,
3. Screen movement.

11.1.1. Surface and Aperture

Coarse Screen Surface – Grizzly
For the metallurgical industry coarse scalping screens are generally fabricated by welding steel rails, rods or bars forming grids of a desired pattern. These are usually known as grizzly screens. The selection of rails varies in size from about 7.4 kg/m to about 225 kg/m. The rails usually run parallel to each other for the entire length of the screening surface. The spacings in between are of the order of 5 – 200 mm. For smooth flow of materials the openings are tapered, the top being wider than the bottom. Heavy-duty grizzly bars are cast from manganese steel having double tapers [1]. These are designed to receive lump ore from railroad wagons, tipper cars and other bulk material handling systems that discharge from considerable heights. They are therefore very robustly built.

The rail grizzlies can be installed to operate in a horizontal flat plane, but they are often inclined to aid transport of ore across the screen. The inclination is of the order of $30 - 40°$. For sticky ores the inclination could be up to $45°$. For very sticky ores, vibrators are employed to facilitate continuous operation.

When rods are used to fabricate grizzlies, they are usually free rotating, or mechanically driven. The rods rest on bearings and rotate in the direction of material flow acting like a conveyor. The space between the rolls is the aperture of the grid.

While designing a grizzly for a specific purpose, the openings between the grizzly bars should be commensurate with the size of the receiving hopper where the product has to be discharged. Usually the maximum distance between the grizzly rails is 0.9 times the maximum hopper opening feeding say, a crusher.

Grizzlies can be designed with more than one deck (usually not more than two). The top deck has a scalping action while the lower deck aims to yield the final size. The two decks produce a coarse, middle and finer fraction. The coarse and middlings have to be recrushed and re-screened to an acceptable size.

Medium Screens and Screen Surfaces

These are used for screening medium size particles that are less than 100 mm but greater than about 2 mm. The screens are fabricated from:

1. Plates mainly by drilling or punching to produce a perforated pattern,
2. Woven wire surfaces to various designs.

Perforated or Punched Plates

Plates made of plain carbon or alloy steels, including stainless steel are used to make perforated screens. Hard plastics such as polyurethane and rubber are also used with reasonable success. Holes are punched, drilled or cast directly during the manufacturing process of the sheets. Shape of the apertures are usually circular, square, or rectangular. The circular holes are equally spaced at the corners of an equilateral triangle or at the four corners of a square or elongated rectangular pattern. Simple patterns of apertures are illustrated in Fig. 11.1. Hole spacings at $60°$ are common. Several variations of patterns are industrially available, like staggered squares, holes or slots or combinations of squares and rectangles. In general the square pattern is most accurate but the throughput could be less than the rectangular patterns which have much more open areas.

a   b   c
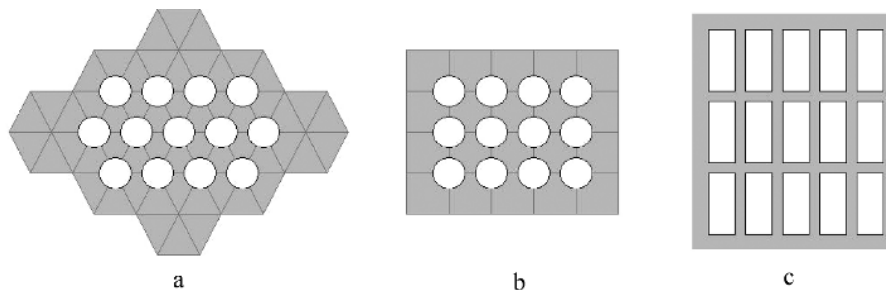
Fig. 11.1. Screen perforation patterns on plates: a – circular apertures on a $60°$ pattern; b – circular apertures on a square pattern; c – rectangular apertures

The percent of open area of plates with circular holes, drilled one-half diameter apart, is about 5% more than those drilled on the corners of a square. When the holes are one diameter apart the difference is less. The amount of open area for diagonal and square spacings can be estimated by simple geometry. Thus if d is the diameter of the hole and s the minimum spacing between them, then the percent of holed area for square and diagonal spacings would be (Fig. 11.2):

For diagonal spacing $\qquad A = \dfrac{\left(\dfrac{\pi}{8} d^2\right)}{\sin 60\left(\dfrac{1}{2}\right)(s+d)^2} = \dfrac{0.907\, d^2}{(s+d)^2}$ $\qquad\qquad$ (11.1)

and for square spacing $\qquad A = \dfrac{\left(\dfrac{\pi}{4} d^2\right)}{(s+d)^2} = \dfrac{0.785\, d^2}{(s+d)^2}$ $\qquad\qquad$ (11.2)

The perforated plates are often rubber clad. The rubber sheets have apertures slightly larger than the base plate. The holes in the rubber conform to the product size. The rubber cladding helps to absorb the force of impact of feed material falling onto the screen. They also retard abrasion of the steel and promote a longer screen life. The elasticity of the rubber helps to reduce blinding of the screens. An added advantage of rubber-clad screens is a considerable reduction of noise level. The rubber sheets are about 7mm – 25 mm thick and held down by a steel frame with bars and bolts.
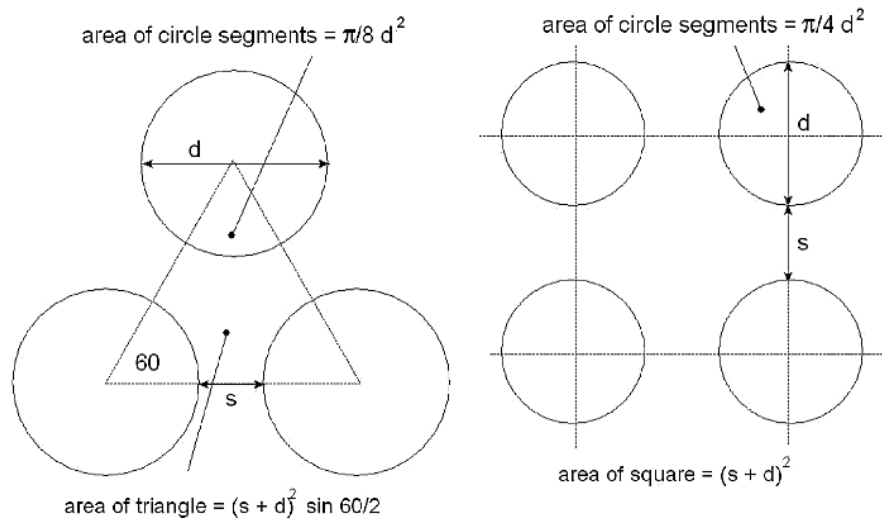
Fig. 11.2. Geometry of open area for diagonal and square placement of circular openings.

Woven Wire Screens

For woven screens, wires of uniform cross section are usually taken for both warp and weft strands. Occasionally the diameter of the warp is greater than the weft.

The wire material used depends on the environmental circumstances. Thus plain carbon steel wires are used for general purposes but for corrosive atmospheres stainless steel wires are used. Other types of metal wires commonly used are brass, bronze, monel metal (Ni-Cu alloys) and different types of aluminium alloys. Wires or threads made of plastics material, especially polyurethane are increasingly being used for areas where strong acidic, caustic or wet environments prevail.

When screens are woven with straight profile wires with circular cross-section, the wires have a tendency to move during the screening operation. Crimped wires help to lock the wires in place. Weaves with double crimped wires are now common. For smoother operation the weave is designed to provide a flat top.

The patterns of weaves are usually square, but rectangular weaves with length to width ratio of 2 or more are also common in the mineral industry. Matthews [2] suggests that for a crimped wire mesh, a rectangular aperture is stable with a slot ratio of 12:1 with large wire and 4:1 with small wire.

Wire screens are mounted on frames and held down tightly by strips of metal (or plastics) and held down firmly using bolts. For large screens appropriate supports are spaced. These support strips occupy space and therefore reduce the effective screening area. Several alternative methods of holding the screens have been devised, like side hooks.

Since the advent of different types of plastics in the form of wires and threads, industrial screens with fabricated plastic are common. The usual plastic wire thickness ranges from 5 – 25 mm. Plastic screen cloths are woven to produce square or rectangular slots that are in line or staggered. The slots are set either parallel to the direction of the flow or across. The open areas of different weaves and patterns depend on the dimensions of the wires. The common types of apertures, their dimensions and the corresponding open areas are given in Table 11.1.

Table 11.1
Screen data for rubber screen fabric [2].

Type of Aperture	Aperture dimension, mm	Open Area, %
Square hole, in line	35 190	49 – 63
Square hole, staggered	8-30	33 – 44
Round hole, staggered	12-190	30 – 48
Slotted hole, staggered (flow parallel to slot)	2 x 25 0.30 x 40	28 – 41
Slotted hole, staggered (flow across slot)	1.5 x 25 0.14 x 25	23 – 42

The available aperture per unit area of screen is the most important criteria of screens. The apertures may be determined if the diameters of the weft and warp wires are known. Fig. 11.3 shows the warp and weft wires of a woven screen cloth with square openings and the rectangular aperture of a typical profile bar screen. It can be seen that the available screening area is the space between the materials forming the aperture. This space is expressed as a percent of the area of the screen. If we assume that the screen wires have round sections of

diameter d_1 and d_2, forming a square aperture, and if A_1 and A_2 were the clear areas, then for the square screen, open area A_1 must be equal to area A_2 or equal to any such area A_N. If we also assume that the distances between them were as shown, and $d_w = d_{w1} = d_{w2}$, then from Fig. 11.3A, the percent clear open area of the screen, A_O, will be:

$$A_O = \left(\frac{L_A}{L_A + d_w} \right)^2 \times 100 \qquad (11.3)$$

where A_O =   open area expressed as percent,
   L_A =   aperture,   and
   d_w =   diameter of wire (or horizontal width of bar or plates, if used).
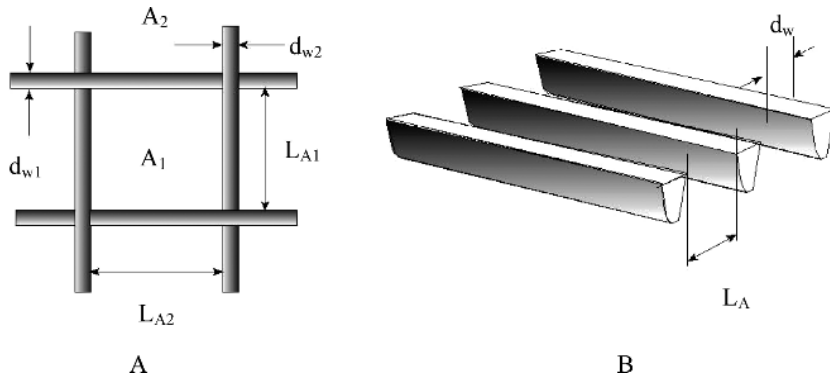
Fig. 11.3.   A – square or rectangular opening between wires, bars or strips; B – parallel openings between wedge wires

For a rectangular opening, the open area will be given by:

$$A_O = \frac{L_{A1} \, L_{A2}}{\left(L_{A1} + d_{w1} \right) \left(L_{A2} + d_{w2} \right)} \times 100 \qquad (11.4)$$

where L_{A1} and L_{A2} are the aperture dimensions and d_{w1} and d_{w2} the wire diameters.

When the screens are set at an angle θ to the horizontal then the effective aperture will be diminished and will be equal to the projection of the actual screen aperture. The available area will then be modified as Area . $\cos \theta$.

For parallel bar screen surface (Fig. 11.3B) the open area is;

$$A_O = \frac{L_A}{L_A + d_w} \times 100 \qquad (11.5)$$

The mesh of a screen is defined by the relation $M = (L_A + d_w)^{-1}$ for measurements in inches or $M = 25.4 (L_A + d_w)^{-1}$ for measurements in millimetres. When M is substituted in Eqs. (11.3) and (11.4), the mesh size may be calculated. For example the mesh number of a square opening of screen will be:

$$\text{Mesh size of square opening,} \quad M = \sqrt{\frac{25.4^2 A_O}{100 L_A^2}} \tag{11.6}$$

The use of these expressions for designing screens is illustrated in Example 11.1.

Example 11.1

A stainless steel woven wire screen with a square aperture had an aperture 3.18 mm square. The diameter of the wire was 1.2 mm. Determine:

1. The percent open area when the screen was operated in an horizontal position,
2. The percent open area when the screen was operated at a slope of 20°,
3. The mesh size of the screen.

Solution

Step 1
As the entire screen is fabricated with wire of diameter of 1.2 mm, Eq. (11.3) is applicable for the horizontal screen.

Thus for an horizontal screen:

$$\text{Percent open area} \quad A_O = \left(\frac{L_A}{L_A + d_w}\right)^2 .100$$

$$= \left(\frac{3.18}{3.18+1.2}\right)^2 .100$$
$$= 52.7\%$$

Step 2
For an inclined screen:

$$\text{Effective percent open area} \quad A_{OE} = A_O \cos 20 \quad = 49.5\%$$

Step 3

$$\text{Square opening in mesh,} \quad M = \sqrt{\frac{25.4^2 A_O}{100 L_A^2}}$$

$$= \sqrt{\frac{25.4^2 \times 52.7}{100 \times 3.18^2}} = 6 \text{ mesh (approximately)}$$

Choosing the screen aperture to pass a specific size of particle depends on the angle of inclination of the screen, the amplitude and frequency of the vibration in a way that is not easily predicted. Fig. 11.4 however shows a first estimate of the size of screen aperture required for a given maximum particle size reported by various sources. The screen aperture guidelines provided by Metso [3] for inclined screens are the particle size + 5-10% for a wire mesh, + 25-30% for rubber screen surfaces and + 15-20% for polyurethane screens. The data from Deks Tyer [4] are for inclined polyurethane screens sizing natural grain material. The data from Taggart [5] are for square mesh screens mounted horizontally and with a steeply sloping surface. Taggart also provides empirical data for round apertures that are 20-30% larger than the equivalent square aperture to pass the same size particle.
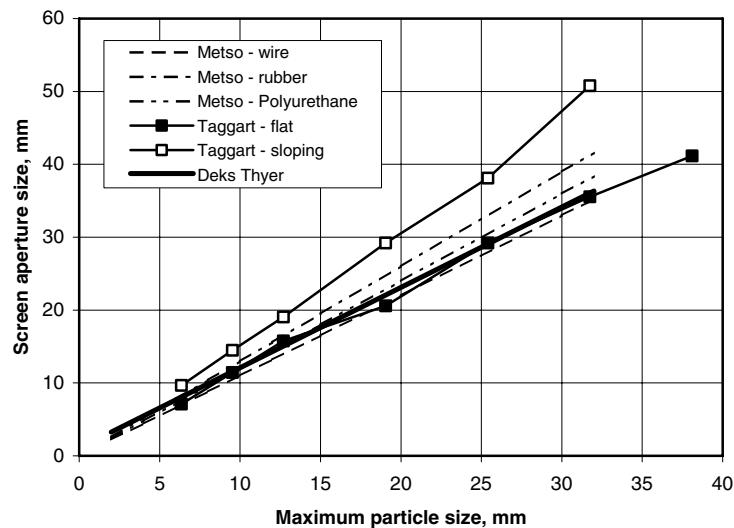
Fig. 11.4. Estimate of the screen aperture required to pass a given particle size [3,4,5].

11.1.2. Types of Screens

The usual industrial screen is either a stationary or dynamic type. They may be described as:

1. Stationary and straight,
2. Stationary and curved,
3. Vibrating straight,
4. Vibrating and curved, or
5. Cylindrical and revolving.

In mineral processing plants, the use of cylindrical screens (*trommels*) is limited to washing of ores for removing clayey material, desliming, oversize (scat) separation at a mill discharge and in dewatering operations. As their use is limited, these screens have not been considered here.

Stationary and Straight Screens Surfaces

Stationary screens are operated either in horizontal or inclined planes. The inclination is to assist material transport and is consistent with the angle of repose of the material. A relatively steep installation is preferred for higher throughputs but the quality of separation is likely to be affected as the effective aperture and open area are decreased. An aperture above the separation size can be selected to overcome this problem.

During the process of screening, particles on the screen deck encounter the apertures where they either fall through or are held back. Obviously particles larger than the aperture opening cannot pass through. A fraction of particles, although smaller than the aperture also do not pass through the first time they encounter an aperture as they fall across the apertures and are held back. In subsequent encounters, the probability of passing through is increased. Particles that are flaky are more likely to have similar problems. Particles that are elongated, but with cross section less than the aperture, will pass through provided they approach the aperture at an appropriate angle. Fig. 11.5 shows the effect of shape and size of particles during screening. Both A and C particles are prevented from passing through, A being larger in size than the aperture while C is elongated with one dimension greater than the size of the opening. Particle C will however pass through in any subsequent encounter if it approaches the screen at a suitable angle as shown in aperture D. Particle size B will always pass through. Thus both shape and size are of importance in a screening operation. Particle sizes that are near to the aperture size are the most difficult to screen. It is a general observation that particles having a size 0.75 to 1.5 times the aperture are the most difficult to screen.

When a screen is overloaded such that the top layer does not come in contact with the screen surface, the top layer will be discharged as oversize while containing fine particles. In
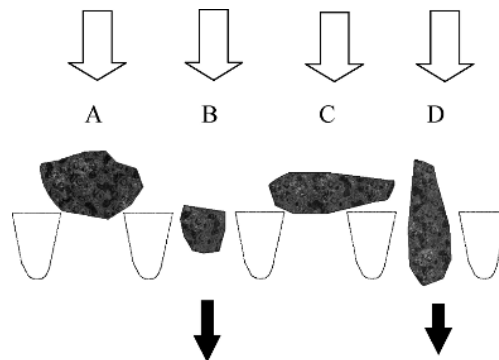
Fig. 11.5. Behaviour of particle size and shape at screen surface. Particle A is too big to pass through in any orientation; particle B will pass in any orientation; elongated particles can pass through only in orientation D but not if it lies flat on the screen in orientation C.

such cases the movement of the bottom layer of particles on the screen, aided by the movement of the screen, will promote the possibility of particles at the top surface approaching the screen surface. Increasing the length of the screen and the screening time will likewise improve the probability of particles in the stratified top layer approaching the screen surface. Thus both time of screening and the movement of particles on the screen surface are important criteria in the designing and operation of screens.

A less common straight screen is the probability screen where the aperture is considered on the basis of the probability of a certain size of material passing the aperture.

Stationary Curved Screens

The commonly used stationary and curved screen is known as the DSM screen or sieve bend. It is named after the Dutch State Mines who first developed and introduced it to the mineral industry. It is used for wet screening and for dewatering slurries.

These screens have screening surfaces made of stainless steel wedge-bars fixed parallel to each other across a frame shown schematically in Fig. 11.6. The stainless steel wires are tapered from about 2mm down to about 1mm. They are bent forming a 40° to 60° concave with a radius of curvature between 900 mm and 2000 mm depending on the length of the screen. The bars spacings are from 0.35 mm to 3.5mm. A uniform flow of slurry is discharged over a weir on to the curved surface. Alternately, multiple nozzles are spread across the width to disperse the slurry uniformly over the screening surface. The commercial sizes range from about 750 mm to about 2500 mm in length and about 50 mm to 2400 mm in width.
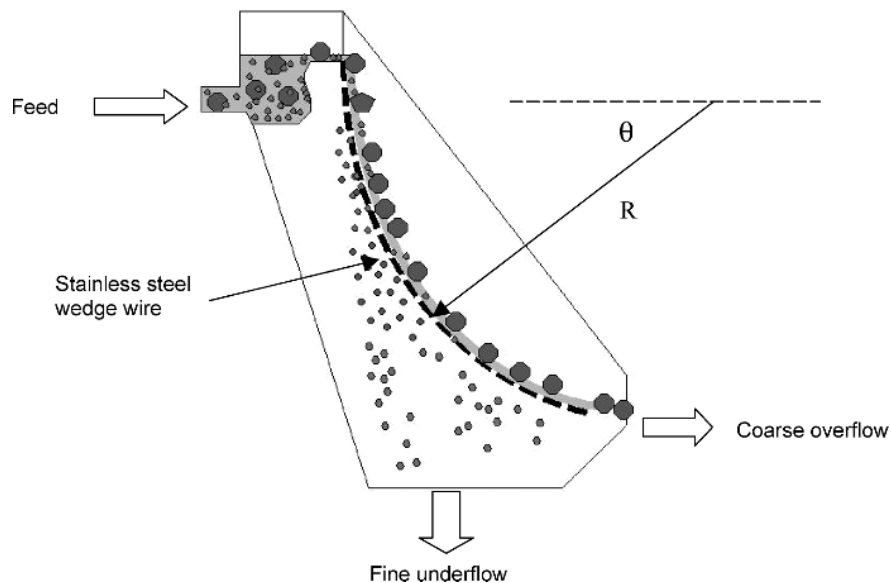
Fig. 11.6. Schematic diagram of a sieve bend

The feed arrangements induce enough potential for gravity forces to act and for the slurry to gravitate down the screen. The curvature of the screen helps the slurry to cling to the surface by centrifugal force. The surface tension of the fluid also contributes to the flow of slurry against the screen surface. The pressure against the screen depends on the stream thickness at any point of the screen, the density of feed and the angle that the centre of the screen makes with the horizontal, θ (see Fig. 11.6). The pressure differential across the screen slit as a result of gravity, at any point x, is given by the relation derived by Fontein [6] as:

$$\Delta P = D \rho_{SL} g \sin\theta \qquad (11.7)$$

where   D   = thickness of slurry at any point x
        ρ_{SL} = density of slurry
        θ   = the angle that the centre of the curvature makes with the horizontal

and the liquid pressure, ΔP_C, against the wedge wire screens (bars) due to centrifugal forces is:

$$\Delta P_C = \frac{D \rho_{SL} v_{SL}^2}{R} \qquad (11.8)$$

where v_{SL} is the slurry feed velocity, and R the radius of curvature of the screen.

In deriving the total pressure Fontein considered the pull due to surface tension of the liquid, thus deriving the total pressure drop across slot per unit slot width as:

$$\Delta P_T = \Delta P_G + \Delta P_C + \Delta P_\gamma \qquad (11.9)$$

where $\Delta P_\gamma = \frac{\gamma \cdot \mu}{W}$ is the pull of the liquid in a radial direction due to surface tension γ across the width of slot, W and μ a coefficient that can be determined experimentally.

According to Stavenger [7], in order to maximise the water split to the screen undersize, the velocity of slurry should be high (12–18 m/s) when the slit width is small (50–150 microns). For larger spacings (350–3000 microns) the velocity may be as low as 3 m/s.

During industrial operations if the particle size in the slurry is less than 200 microns the sieve bends tend to blind rapidly. Feeding at a higher velocity or incorporating a rapped or vibrated screen assembly tends to clear the material between the wedges. According to Fontein [6] however, the blockage can be prevented when the Reynolds number (Dvρ/μ) is 1000 or greater and that blockage is most likely when the Reynolds number is in the region of 300. (D represents the slit width, v the velocity, ρ and μ the density and viscosity of the fluid respectively).

Size separations take place at each encounter of the slurry with the screen bar where the slurry is cut and sliced off, taking with it a fraction of the fines present in the slurry. Each bar therefore encounters classified slurry. The course fraction in the slurry with a size greater than the spacings between the wedge bars continue to travel over the screen surface and collect at the end of the screen. The amount of slurry sliced off at each aperture depends on the distance between the slots and the radius of curvature of the screen. Fontein [6] quantitatively determined the amount sliced off each time, L_{SL} as:

$$L_{SL} = \frac{L_A^2}{2\,R} \qquad\qquad (11.10)$$

where L_A = slot aperture and
 R = the radius of curvature of the screen.

The size of separation is directly related to the wedge bar spacing. A log-log plot of slot spacing and separation size is linear as indicated in Fig. 11.7 [7].

This figure indicates that the separation size of a sieve bend varies from 50–95% of the slot aperture. For separation sizes less than 200 microns the incidence of screen blinding is high. In such cases the velocity of particles over the screen is increased by application of hydraulic pressure on the slurry. Alternatively arrangements are made to tap or vibrate the screens and agitate the surface by a combination of tapping and vibrations.

As a rule of thumb the thickness of the slurry layer passing through the aperture should be less than half the slot opening to avoid clogging of the screen.

In the metallurgical industry, size separations by sieve bends are usually confined to the range of 200–3000 μm though feed sizes can be up to 12 mm. The sieve bends commonly used are gravity fed at a slurry velocity of about 180 m/min and solids in the slurry as high as 50%. Typical bar spacings range between 0.35 to 3.5 mm with angles 45° to 50°. Where pressure is employed, the angles and the length of sieves are about 270° and length about 2300 mm.

During operation, the top edge of the screens wear out thereby affecting the thickness of the slurry layer passing through the screen and hence the size of separation. Industrial curved screens are therefore designed to flip the surface around when the top edge becomes worn in
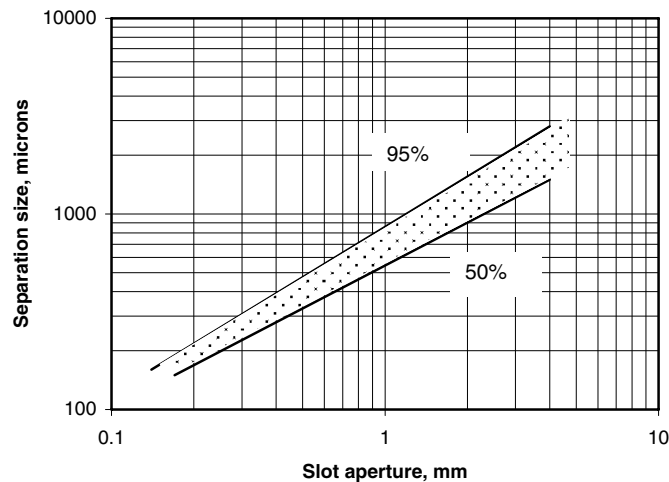
Fig. 11.7. Relation between bar spacing and diameter of separation of particles [7].

order to expose the lower end of the wedge bar to the descending stream of slurry thus increasing the operating life of the screens.

11.1.3. Vibrations and Movement of Straight and Curved Screens

Blinding of screens during operation is one of the most contentious and difficult factors that a screen designer has to face. A partial and probable solution is to use a design that is clad with hard rubber or plastics. In practice however, no screen is really free from blinding. The most effective way to reduce blinding is to impart vibratory or circular motion to the screen.

To impart the motion, the screen surfaces are rigidly fixed on to a frame. The frame in turn is fixed to moving devices that are either mechanically or electrically driven. Several ingenious methods of movement and vibration of screen surface have been devised over the years. These have been classified according to the manner of movement. Some authors like, Colman and Tyler [1], have preferred to classify screens according to the number of bearings which are mechanically responsible for different movements. In Table 11.2 an attempt is made to classify screens according to the manner of motion and also incorporating Colman's concept of bearings. As the movement of the shaft also controls the screen motion this is also included in Table 11.2.

The vibrating devices are mounted either at the feed end, centre of the screen frame or near the discharge end. The vibrations are controlled by large steel springs attached to the bottom of the frames or by suspended hangers and cables. Air cushions are also used. Some novel devices include use of bouncing balls that strikes the screen under surface and help to keep the apertures from blinding. Stretching plain carbon wires, 1.0–1.22 mm in diameter, in grooves about 254 mm apart along the entire length of the screen induces similar action. The wires are taught and vibrate against the screen loosening any accumulation in the apertures.

Camshafts sitting on eccentric bearings, connecting rods or cranks impart reciprocating movements. Slow reciprocation is of the order of 150 rpm with stroke length varying between 75–100 mm. A fast reciprocation is 200–300 rpm at 25–75 mm stroke.

Table 11.2
Design and movement of screens [8].

Screen Motion	Shaft No	Shaft Type	No. of Bearings	Throw	Stroke length, mm	Frequency, rpm
Oscillating, Linear	1	Eccentric	2	Circular	<25 ***	500-2500
Vibratory	1	Eccentric	2	Circular	15-30	25-500
Forward	2	Double Eccentric	4**	Forward, positive	-	-
Reciprocating	2	Reciprocating and Eccentric	4	-	25-75 75-100	200-300 150
Sifter, Circular	4	Eccentric	-	-	-	-
Sifter, Gyratory*	4	-	-	-	-	500-600
Sifter, Circular	4	-	-	-	-	-

* Movement circular at feed end and reciprocating at discharge end.
** Two for bearings and two for shafts
*** Stroke length usually less than 10 mm

The primary objective for imparting vibrations to screens is to aid segregation of fines through the bed to the screen surface, dislodge accumulations at the apertures and to keep the screen active at all times. However, the shape of particles, moisture content and the number of times a particle is able to approach the screening surface complicate the process. The probability, p, of a particle passing through a screen has been shown by Gaudin [9] to be:

$$p = \left(\frac{L_A - d_P}{L_A + d_W}\right)^2 \tag{11.11}$$

where d_P = the particle size of which 50% passed through the screen.

This probability is affected by the amplitude, frequency and direction of vibration. Miwa [10] has estimated the number of presentations (N) of particles on to the screen surface by considering the effective aperture (L_{AE}), the diameter of the wire (d_W) of the screen, the length of screen (L) and taking a particle size, d_{50}, at which 50% of the material of this size passes or is retained on the screen. The expression is given by:

$$N = \frac{1}{L}\left[\frac{0.833\,(L_{AE} + d_W)}{(L_{AE} - d_{50})}\right]^2 \tag{11.12}$$

The value of N includes vibration (amplitude and frequency) and other variables related to screening. Therefore N can be regarded only as an index of vibration and therefore of screening.

It should be noted that:

1. Increasing the amplitude of vibration initially increases the percentage passing through a screen. After reaching a peak, a further increase of vibration decreases the amount passing through.
2. Change in frequency has little effect on the amount passing through the screen.

11.2. Operation of Straight Screens

11.2.1. Basic Considerations

Two criteria are used to assess screen performance, *Capacity* and *Efficiency*. Capacity is simply the quantity of material fed to the screen per unit time per unit area of screen surface. In reality capacity should be quoted along with efficiency. Capacity and efficiency are generally conflicting quantities. Any screen can have its capacity increased, but this is likely to be achieved at the expense of efficiency.

The basic purpose of screening is to separate particles larger or smaller than the aperture of a screen. An ideal screening condition would be to have a monolayer of a mixture of sizes of particles on the screen surface so that the probability of each and every particle passing or not passing can be determined. As illustrated in Fig. 11.5 the passage of each particle will depend on its size, shape and the angle at which it reaches an aperture. To attain the required angle, a particle may require several presentations. If the screen was sufficiently long it could eventually approach the aperture at the appropriate angle and pass through. If the length was

insufficient then in spite of the particle size being smaller than the aperture it may report as oversize. Thus the length of the screen is important. The length of screen provides the screening efficiency and the width indicates the throughput rate. Ultimately the probability of passing will depend on the initial mass of particles in the feed stream that would pass after N approaches to the aperture and the mass fraction remaining that had not passed. This can be written as:

$$\frac{M}{M_i} = (1-p)^{N_L} \qquad (11.13)$$

where
M_i = the initial mass of undersize in the feed stream,
M = the mass of undersize remaining on the screen after N attempts,
N_L = the number of presentations per unit length of screen and
p = the probability of a particle passing through the screen.

Eq. (11.13) implicitly assumes that the probabilities of all particles passing in every attempt are equal. Substituting the value of p from Eq. (11.11) in Eq. (11.13) gives:

$$\frac{M}{M_i} = \left[1 - \left(\frac{L_A - d_P}{L_A + d_W} \right)^2 \right]^{N_L L} \qquad 11.14$$

On simplifying Eq. (11.14) by neglecting the higher powers and replacing d_P by d_{50} as the particle size that is equally split between the overflow and underflow, we get Eq. (11.15) as:

$$d_{50} = L_A - \frac{0.833 \left(L_A + d_W \right)}{L^{0.5} N^{0.5}} \qquad (11.15)$$

Eq. (11.15) indicates that if the d_{50} was experimentally determined along the length of the screen of known wire diameter (d_W), then the aperture and number of attempts could be determined.

The screening process however is complicated by the fact that in practice a layer of particles are charged on to a screen and the probability of particles at the bottom of the layer and against the screen surface passing through the screen will be greater than those at the top of the layer. Also the particle size distribution on the screen surface along the length will be different as illustrated in Fig. 11.8 where it can be seen that screening along the length of screen is not uniform. Two factors are in operation. First, due to uneven stratification of the particle layers on the screen surface, undersize particles may not reach the screen surface due to excessive bed depth. Secondly, the probability of passing when the undersize particles do reach the surface. Thus Eq. (11.15) is not exactly applicable to a real situation. It can however be used as an indicator.

From the above discussions it is seen that absolute separation of different sized particles using a screen is difficult as it involves probabilities of movement of particles at different stages that may be difficult to determine.

A screen is said to behave perfectly if, in a mixture of different sizes of materials, all material of a particular size less that the screen aperture is separated from the mix. In general, a screening operation does not produce a perfect separation therefore it is necessary to express
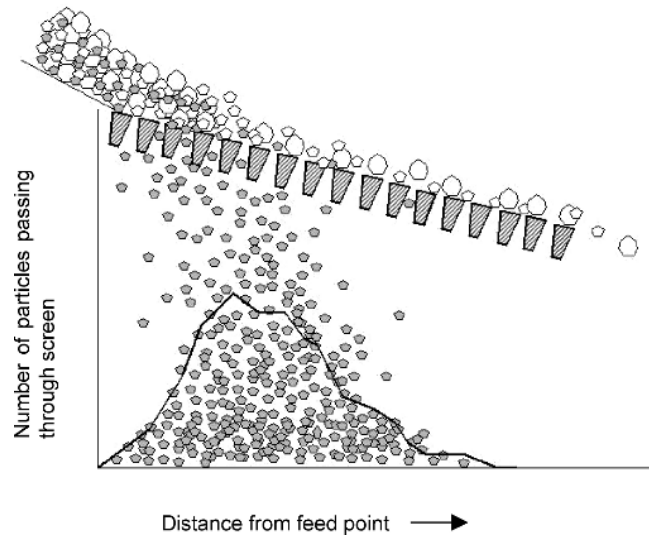
Fig. 11.8. Particle size distribution during a screening operation and the profile of screened undersize.

the efficiency of the process. Depending on whether one is interested in removing oversize or undersize material, screening efficiencies may be defined in a number of ways.

Assuming that in a continuous screening process of a material, the mass flow rate of solid feed is given by $Q_{MS(F)}$ and the distribution of the overflow and underflow rates is:

Mass flow rate of solid in the overflow $Q_{MS(O)}$
Mass flow rate of solid in the underflow $Q_{MS(U)}$
Mass fraction of undersize in the feed $m_{U(F)}$
Mass fraction of undersize in the oversize $m_{U(O)}$
Mass fraction of undersize in the undersize $m_{U(U)}$

Then the screen efficiency, E_o, based on the oversize will be:

$$E_O = \frac{Q_{MS(O)}\ (1 - m_{U(O)})}{Q_{MS(F)}\ (1 - m_{U(F)})} \qquad (11.16)$$

and the screen efficiency, E_U, based on undersize:

$$E_U = \frac{Q_{MS(U)}\ m_{U(U)}}{Q_{MS(F)}\ m_{U(F)}} \qquad (11.17)$$

The overall efficiency, $E = E_O \times E_U$

Substituting values from Eqs. (11.16) and (11.17), the overall efficiency of screens would be:

$$E = \frac{Q_{MS(O)} \; (1 - m_{U(O)})}{Q_{MS(F)} \; (1 - m_{U(F)})} \times \frac{Q_{MS(U)} \; m_{U(U)}}{Q_{MS(F)} \; m_{U(F)}} \tag{11.18}$$

The values of $\left[\dfrac{Q_{MS(O)}}{Q_{MS(F)}}\right]$ and $\left[\dfrac{Q_{MS(U)}}{Q_{MS(F)}}\right]$ can easily be determined from a material balance of the system.

11.2.2. Material Balance of a Screen in Operation

In any screening operation the size analysis of the feed, oversize and undersize indicates the partition of a particular size. Fig. 11.9 shows the cumulative distribution curves where size 1 is the coarsest and size 12 the finest screen size used.

In a dynamic system at steady state, the mass flow rate of feed material charged for screening must be equal to the sum of the mass flow rate of material discharged in the overflow and underflow. Mathematically therefore:

$$Q_{MS(F)} = Q_{MS(O)} + Q_{MS(U)} \tag{11.19}$$

As the screen partitions the total feed material into overflow and underflow streams, we can write, using the above symbols:

$$Q_{MS(F)} \; m_{U(F)} = Q_{MS(O)} \; m_{U(O)} + Q_{MS(U)} \; m_{U(U)} \tag{11.20}$$
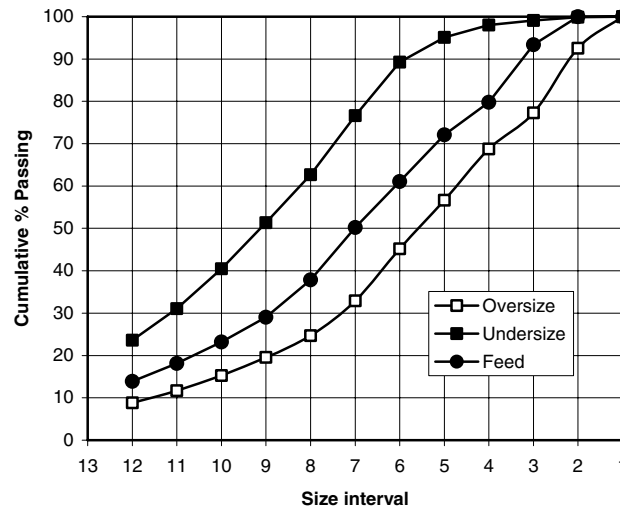
Fig. 11.9. Distribution of particles over a screen.

Substituting the value of $Q_{MS(U)}$ from Eq. (11.19) in Eq. (11.20) and rearranging we have:

$$\left[\frac{Q_{MS(O)}}{Q_{MS(F)}}\right] = \frac{\left(m_{U(F)} - m_{U(U)}\right)}{\left(m_{U(O)} - m_{U(U)}\right)} \tag{11.21}$$

Similarly substituting the value of $Q_{MS(O)}$ from Eq. (11.19) in Eq. (11.20) we get:

$$\left[\frac{Q_{MS(U)}}{Q_{MS(F)}}\right] = \frac{\left(m_{U(O)} - m_{U(F)}\right)}{\left(m_{U(O)} - m_{U(U)}\right)} \tag{11.22}$$

Eqs. (11.21) and (11.22) can now be substituted in Eq. (11.18) to give the efficiency of the screen as:

$$E = \left[\frac{m_{U(F)} - m_{U(U)}}{m_{U(O)} - m_{U(U)}}\right]\left[\frac{m_{U(O)} - m_{U(F)}}{m_{U(O)} - m_{U(U)}}\right]\left[\frac{1 - m_{U(O)}}{1 - m_{U(F)}}\right]\left[\frac{m_{U(U)}}{m_{U(F)}}\right] \tag{11.23}$$

The use of the Eq. (11.23) is illustrated in example 11.2.

Because the efficiency Eqs. (11.16) and (11.17) use laboratory measured data using square mesh sieves, these equations are meant for square mesh industrial screens and are not strictly applicable to rectangular mesh. Using these formulae and square mesh laboratory screening data of rectangular industrial mesh screen products, calculated efficiencies in excess of 100% are possible. To overcome this problem, Leonard [11] defined the efficiency of screens in terms of the amount of total misplaced material (fines in oversize and coarse in undersize). Thus:

$$E = \frac{\text{rate of feed} - \text{rate of undersize in oversize fraction} - \text{rate of oversize in undersize fraction}}{\text{rate of feed}}$$

For a material balance of the undersize product, using Eqs. (11.19) and (11.20), the distribution of the undersize can be expressed as given in Eq. (11.22). Substituting these terms into the Leonard's efficiency equation and simplifying we get:

$$E = \left(1 - m_{U(O)}\right) - \left[\frac{m_{U(F)} - m_{U(O)}}{m_{U(U)} - m_{U(O)}}\right]\left(1 - m_{U(O)} - m_{U(U)}\right) \tag{11.24}$$

Leonard's method is illustrated by example 11.2

Osborne [8] considered the efficiency of a square aperture screen as the ratio of the amount that actually passes through the screen to the amount that should pass through the screen. The screen efficiency then is:

$$E = \frac{100 \ Q_{MS(U)}}{Q_{MS(F)} \ m_{U(F)}} = \frac{100}{m_{U(F)}} \left(\frac{m_{U(F)} - m_{U(O)}}{m_{U(U)} - m_{U(O)}} \right) \qquad (11.25)$$

Example 11.2

A gold ore is screened through a 30 mm screen. The average size distribution of the feed, oversize and undersize were determined and graphed below. Determine the efficiency of the screen.

Solution (Efficiency 1)

From the graph we can see that for a 30 mm separating size, $m_{U(F)} = 46\%$, $m_{U(O)}$ in oversize $= 7.5\%$ and $m_{U(U)}$ in undersize $= 90\%$.

Using Eq. (11.23) and directly substituting the values:

$$E = \left[\frac{(0.46 - 0.90)}{(0.075 - 0.90)} \right] \left[\frac{(0.075 - 0.46)}{(0.075 - 0.90)} \right] \left[\frac{1 - 0.075}{1 - 0.46} \right] \left[\frac{0.90}{0.46} \right] = 0.834$$

The efficiency is 83.4%.

Note: Usual screen efficiencies encountered in industry are of the order of 60% to 85%.
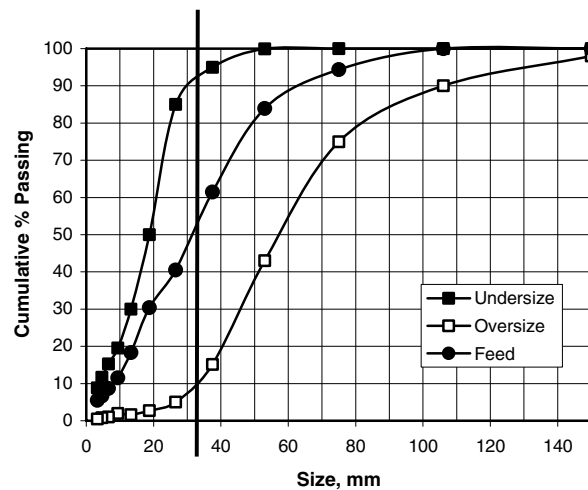
Solution (Efficiency 2)

Substituting values into Leonard's Eq. (11.24):

$$E = (100 - 7.5) - \left[\frac{46 - 7.5}{90 - 7.5}\right](100 - 7.5 - 90) = 91.3\%$$

Solution (Efficiency 3)
Substituting values into Osborne's Eq. (11.25):

$$E = \frac{100}{0.46}\left(\frac{0.46 - 0.075}{0.90 - 0.075}\right) = 101.4\%$$

Example 11.3
From a crushed quartz sample the fraction less than 2 mm had to be removed by screening. The feed sample contained 35% of minus 2 mm material. After screening the oversize fraction contained 10% of minus 2 mm size and the undersize contained 82% of minus 2 mm size.

Determine the efficiency of the screen.

Solution (Efficiency 1)
Substituting the values into Eq. (11.23):

$$E = \left[\frac{(0.35 - 0.82)}{(0.10 - 0.82)}\right]\left[\frac{(0.10 - 0.35)}{(0.10 - 0.82)}\right]\left[\frac{1 - 0.10}{1 - 0.35}\right]\left[\frac{0.82}{0.35}\right]$$

$$E = 73.5\%$$

Solution (Efficiency 2)
Using Eq. (11.24) expressed as percentage, i.e.,

$$E = (100 - 10) - \left[\frac{35 - 10}{82 - 10}\right](100 - 10 - 82)$$

$$E = 87.2\%$$

Solution (Efficiency 3)
Substituting values into Eq. (11.25):

$$E = \frac{100}{0.35}\left(\frac{0.35 - 0.10}{0.82 - 0.10}\right) = 99.2\%$$

11.2.3. Screen Efficiency and the Tromp Curve

Since a feed may contain a whole range of particles of different properties, such as grade or size, then the separation efficiency may be different for different particles. That is, we need to take into account the amount of misplaced material that can occur or the difficulty of separation of some of the particles.

In 1937, Tromp [12] introduced a graphical method of assessing separation efficiency which is universally used and is alternatively referred to as; *Tromp Curve, Partition Curve* or *Performance Curve.*

We can refer to any characteristic in the feed or any other stream, in general terms as characteristic i, where i can refer to a size interval for size separators. The amount of misplaced material to an output stream is referred to as the *partition coefficient* (also called the distribution factor or probability factor). The partition coefficient is then defined as;

$$\text{partition coefficient} = \frac{\text{mass of material of characteristic "i" in a stream}}{\text{mass of material of characteristic "i" in the feed}} = \frac{M_{Ui}}{M_{Fi}} \quad (11.26)$$

It may be expressed as a fraction or a percentage. The partition coefficient is essentially the recovery of a given characteristic (size in this case) to a stream, usually the positive response stream, but not always. To some extent it incorporates a measure of the grade as well since it indicates how much of each particle characteristic is present in the output stream. For example, the partition coefficient tells us how much undersize to oversize particles are there in the stream and if the fine sizes are enriched in the valuable mineral then an indication of the grade follows. However grade is not really a factor in this measure of efficiency or performance, it depends on the particle characteristic the separator is using to generate the output streams. For example, a process separating on particle size can work efficiently if there is no change in grade between the feed and the output streams, e.g. if the feed was all the same mineral.

Having obtained the partition coefficient, this is plotted against the **mean** separating characteristic of the fraction to generate the performance curve, as shown below. The mean values plotted may either be the arithmetic mean or the geometric mean.

A Perfect Separation

Let us consider a screen as our separating unit and the screen aperture is 2 mm. In a perfect separation, any particle that is less than 2 mm should go through the screen and hence the amount remaining on the screen at the completion of the process (the oversize) should be zero. Any particle that is greater than 2mm should remain on the screen and hence the amount of this material in the oversize product should be 100%. That is, the partition coefficient for −2mm material in the oversize product will be zero and the partition coefficient for the +2mm material in the oversize product will be 1.0 or 100%. The performance curve will then have the shape of the solid line in the Fig. 11.10. That is, there will be a sharp jump from 0 to 1.0 (or 100%) at the separation point. This separation point is referred to as the d_{50}.

If the partition coefficient is calculated with respect to the negative response stream instead of the usual positive response stream, the performance curve will have the same shape but will be a mirror image about the d_{50}. The d_{50} point will be the same, either way.

The performance of any separator depends on three factors:

1. the characteristic composition of the feed (eg, the size distribution, the density composition etc.),
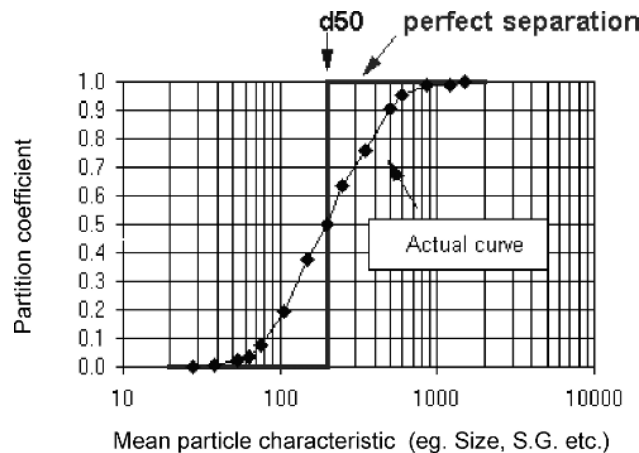
Fig. 11.10. Tromp curve for a screen

2.   the value of the size where separation occurs, and
3.   the sharpness with which the unit separates the feed.

Often the performance criterion required is the ability of the separator to make a sharp separation and to compare different separators this must be free of the influence of feed composition and the size of separation. Only then can the performance of units treating different feeds and separating at different sizes be compared directly.

The performance curve is a convenient way of showing the sharpness of separation, however, as a means of comparison between different separating units, a numerical figure is better for describing the deviation from ideal behaviour. These numerical figures are based on the error between the actual curve and the line of perfect separation, and are termed the *probable error*, *error area* or *ecart probability* (see Fig. 11.11).

One way of quantifying the deviation from the perfect separation is to determining the area between the performance curve and the ideal curve provided the partition coefficient values range from 100 to 0 (that is, there is no by-pass or short circuiting of material). This area is termed the error area. If several performance curves are plotted on the same axes then this area provides a means of comparing the sharpness of separation.

Another method of characterising the performance curve is to determine 50% of the difference between the separating size at a partition coefficient of 0.75 (or 75%) and 0.25 (or 25%). This figure may be referred to as the Ecart probability (E_p), the probable error or the probable deviation.

$$E_p = \frac{d_{75} - d_{25}}{2}$$

(11.27)

If the performance curve is a straight line between the d_{75} and d_{25} points then the probable error is a measure of the slope of this curve, through the d_{50} or 50% point.

314
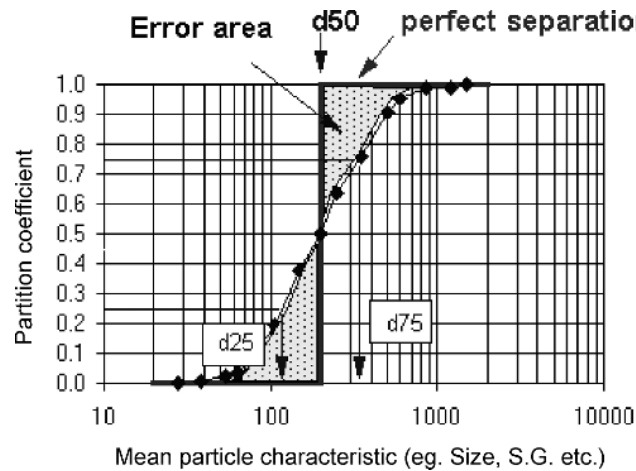
Fig. 11.11. Quantifying the deviation from ideal performance.

That is, $\text{slope} = \dfrac{\Delta Y}{\Delta X} = \dfrac{0.75 - 0.25}{d_{75} - d_{25}}$ (11.28)

and from the definition of E_p above,

$$E_P = \frac{1}{4 \times \text{slope}}$$ (11.29)

or, the probable error is proportional to the reciprocal of the slope.

So as the slope of the performance curve approaches the vertical (infinity), the probable error approaches zero or the smaller the probable error, the greater the sharpness of separation (the closer to a perfect separation the performance of the separator becomes).

The degree of misplacement of material is not symmetrical about the 50% horizontal. For example the misplacement in the fine fraction may be greater than the misplacement in the coarse fraction since the fines have to segregate to the screen surface before it leaves the unit whereas it is more difficult for coarse particles to enter the undersize unless there are worn or broken wires on the screen surface.

In this case of asymmetrical performance curves, we could define;

a 75% partition error = d_{75}/d_{50}, and

a 25% partition error = d_{50}/d_{25} (11.30)

to give a more precise description of the deviation from ideal behaviour, but usually the probable error, E_p, is satisfactory.

When performance curves were first developed, the performance curves, which were drawn for gravity separations, were believed to be independent of the characteristic (density) of separation. With time however it became apparent that the curve tended to steepen as the density of separation decreased. That is, at low densities, the separation tended to be sharper than those at higher separation densities. The French research organization, Cerchar (Centre D'Études et de Recherches de. Charbonnage de France) was the first to recognise the relationship between sharpness of separation and separation density. They consequently coined the term *Imperfection*, designated I, which was defined as:

$$I = \frac{E_P}{d_{50} - 1} \tag{11.31}$$

They believed that the d_{50} increases in proportion to (d_{50} - 1). Since then, it has been suggested by other workers that the formula for Imperfection should be:

$$I = \frac{E_P}{d_{50}} = \frac{d_{75} - d_{25}}{2\,d_{50}} \tag{11.32}$$

The usefulness of the Imperfection as a sharpness of separation criteria, independent of the d_{50}, has been questioned and the reader is refer to the work by Peng et al. [13] for a detailed discussion of these criteria.

The method usually employed to draw the Tromp curve and its interpretation is illustrated in Example 11.4.

Example 11.4

The size fractions of a screen feed, oversize and undersize stream sample are given in the table below. The oversize represented 62.5% of the feed mass flow rate. Draw the Tromp curve for the separation and determine:

1. The separating size,
2. The probable error,
3. The imperfection.

Solution

The solution is best understood by following the calculations shown in Table 11.3.

In the table:
Columns A and C are the analyses of the oversize and undersize streams
Column B = Column A x yield in oversize (0.625 in this example)
Column D = Column C x yield in undersize (0.375 in this example)
Column E = Sum of columns B and D giving the reconstituted feed
Column F = Partition Coefficient = B/(B + D).

Table 11.3
Sizing data for a screen oversize and undersize fraction

Size, microns	Mean Size, microns	Oversize stream		Undersize stream		Calculated Feed	Partition Coefficient
		Mass % A	Mass in sample B	Mass % C	Mass in sample D	E= B+D	F = B/E
16000	17889	37.5	23.44	0.5	0.19	23.63	0.99
8000	11314	32.0	20.00	1.0	0.38	20.38	0.98
4000	5657	13.0	8.13	10.6	3.98	12.10	0.67
2000	2828	7.4	4.63	12.1	4.54	9.163	0.50
1000	1414	3.6	2.25	15.0	5.63	7.875	0.28
500	707	2.5	1.563	18.0	6.75	8.313	0.19
250	354	2.0	1.25	20.0	7.50	8.750	0.14
125	177	1.5	0.94	19.8	7.42	8.363	0.11
-125		0.5	0.31	3.0	1.13	1.438	0.22
		100.0	62.5	100.0	37.5		

The partition coefficient may now be plotted on a semi-log paper as shown in Fig. 11.12.
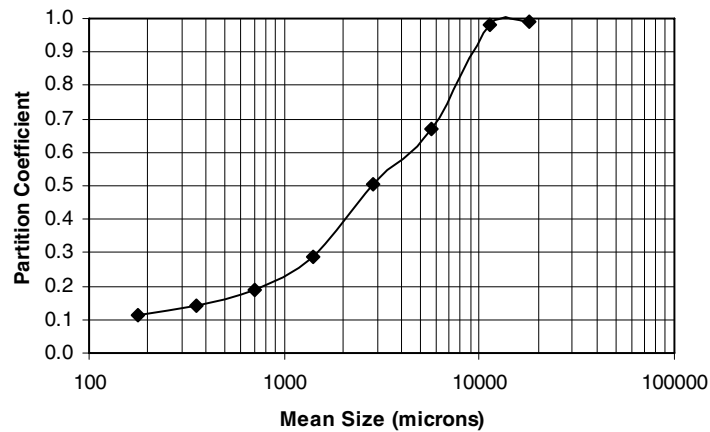
Fig. 11.12. Tromp curve of screen data.

Reading off Fig. 11.12 it can be seen that:

1. The separation size, $d_{50} = 2800$ μm and the d_{25} and $d_{75} = 1200$ and 6600 μm respectively,

2. The efficiency $E_P = \dfrac{(d_{75} - d_{25})}{2} = \dfrac{6600 - 1200}{2} = 2700$

3. Imperfection $I = \dfrac{2700}{2800} = 0.96$

11.2.4. Bed Depth

The bed depth of material on the screen affects the efficiency and the performance of a screen. Fig. 11.8 shows that the profile of a bed of material on the surface of a screen is far from uniform. The feed end of the screen surface is overloaded while the rest of the screen surface is thinly spread with the material. The fraction of particles in the feed stream that is smaller than the sieve openings and occupying upper layers of the feed stream need time and agitation to work their way down to the screen surface. Agitation of the screen surface imparts fluid properties to the bed of particles. The material on the screen expands and the larger particles tend to travel up. The smaller particles tend to gravitate down the voids created by the expansion of the bed. The stratification of the bed has the added advantage that it helps to minimise the agitation of the smaller particles by holding them down on the surface of the screen. Thus the depth of the bed, the rate of feed and the inclination of the screen are of major importance to the screen operation. Too thick a bed will tend to delay stratification, while too thin a bed reduces the efficiency as it allows unconstrained movement of particles on the screen. Hence the bed thickness at the discharge end is more important than the feed end. The bed thickness at the discharge end will in turn depend on the length of the screen. According to Matthews [2] for screens of length from 1.8 m, the bed depth at the discharge end should be a minimum of about 1.5 –2.0 times the average particle size, and for screen lengths of about 7.2 m the thickness of the discharge end should be about 2.5 to 3.0 times the average particle size. Thus if the screen length was 2 m and the average particle size 850 microns, then the minimum bed height at the screen discharge end should be about 1.3 mm.

Manufacturers have charts available relating the capacity (which includes the width of the screen) and the depth of bed. The general relationship relating bed depth, feed rate and width of screen, according to Osborne [8] is:

$$D = \frac{50\,Q_O}{3\,W_E\,v_F\,\rho_B}$$

(11.33)

where D = bed depth, mm,
  Q_O = tonnage of oversize material, t/h,
  v_F = transport rate across the screen, m/min,
  W_E = effective width of the screen, m,
  ρ_B = bulk density, t/m³.

The effective area of the screen (the total area minus the area of clamps and fittings) is given approximately by the equation:

$$A_E = (W - 0.15)L$$

(11.34)

where W and L are the width and length of the screen in meters respectively.

Some authors [14,15] have related the bed thickness with the bulk density of the material to be screened. The general conditions are:

1. For material of bulk density 1.6 t/m³, the bed depth at the feed end should not exceed 4 times the size of the aperture,
2. For material of bulk density 0.8 t/m³, the bed depth should not be greater than 2.5 – 3 times the size of aperture.

The bed depth is also related to the slope of the screen. While a quantitative relation between these parameters has not been established, the following observations can be made [2]:

1. For screen widths of 0.6 – 2.5 m the inclination should not be less than 16° and a maximum of about 26° for capacities 15 – 270 t/h.
2. When the slope is greater than 20° the capacity is markedly reduced as the effective aperture area is reduced by 0.93 times.
3. For longer screens, eg. 4.8 meters, screen manufacturers recommend a further addition of 2° and for screens about 6 meters, 4° should be added.

11.3. Capacity and Screen Selection of Straight Screens

The above discussion indicated that the capacity of a screen is related to the screen characteristics and the material characteristics. The screen characteristics include:

1. available area,
2. aperture (size and type),
3. slope,
4. method of vibration, and
5. number of decks.

The material characteristic include:

1. size and shape of material ,
2. moisture content,
3. rate of throughput, including depth of material layer,
4. dry or wet screening.

The capacity of a screen is referred to either in terms of the oversize or in terms of the undersize product streams. For a square mesh sieve at a slope of 18°, where maximum efficiency is expected, Taggart [5] suggests that the capacity of a screen should be based on that size fraction in the feed that is most difficult to separate. This fraction is described as the percent of critical size and the basic function is described here as F_B.

$$F_B = \frac{73.14 L_A \rho_B}{C} \qquad (11.35)$$

where
F_B = basic feed rate, t/h/m of screen width,
L_A = aperture in mm (square mesh),
ρ_B = mass of material/m^3, and
C = percent of critical size taken as the percent of feed between the *critical* size of 0.75 to 1.5 of the screen aperture.

The actual feed rate, F, in tonnes per hour per meter of screen width, is related to the basic feed rate, F_B, by the relation:

$$F = F_B R \qquad (11.36)$$

The factor R is a function of the screen efficiency and the vibration intensity. The relation between R and the efficiency factor was determined experimentally for screens of different lengths. Typical curves for 1.8 m and 2.4 m length screens are reproduced in Fig. 11.13.

The efficiency factor is the fraction of true undersize in the screen oversize based on the amount of near size particles (*percent of crtitical size*, C). Thus if the feed analysis is known then C can be established and R determined from efficiency and vibration intensity values using Fig. 11.13. From the R values, the actual screen feed rate can be determined using Eq. (11.36).

For example, if the feed size distribution has 32% greater than the screen aperture and 25% of the feed is between 0.75 and 1.5 times the screen aperture and after screening, the oversize contains 10% of undersize material then;

$$\text{Efficiency factor} = \frac{\text{mass of undersize in the oversize}}{\text{mass of critical size}} \qquad (11.37)$$

$$= \frac{(\text{fraction of undersize in the oversize}) \times (\text{mass of oversize in the feed})}{C \times (1 - \text{fraction of undersize in the oversize})}$$

$$= \frac{m_o \, M_o}{C \, (1 - m_o)}$$

$$= \frac{0.10 \, (32)}{25(1 - 0.10)} = 0.14$$
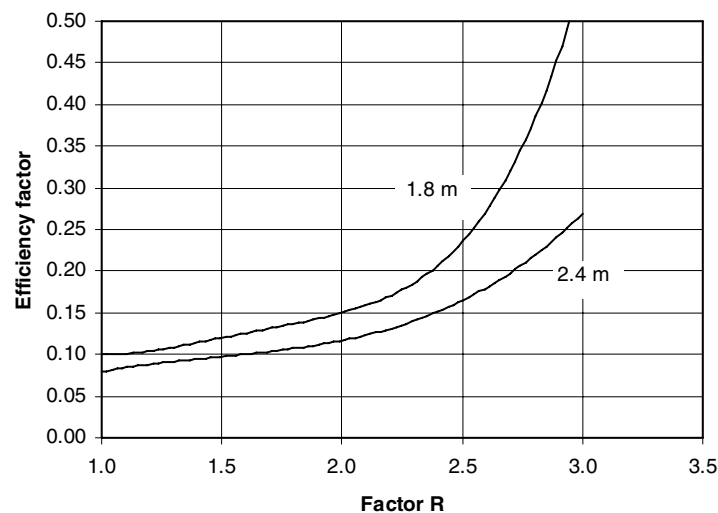
Fig. 11.13. Screen capacity factors [5].

The above considerations are for screens with normal vibration intensity. For vibration intensities above normal, the relation between R and the efficiency factor has to be established. Screen manufacturers normally supply these.

Having estimated the actual feed rate the dimensions (L x W) of the screen can be estimated using the expression [5]:

$$W = \frac{t/h \text{ of total feed}}{\text{Actual feed rate per meter}} = \frac{Q}{F} \tag{11.38}$$

A much simpler method to determine capacity and screen dimensions is to consult empirical screen performance data produced by screen manufacturers like Hewitt-Robins and Nordberg (Metso). The method followed is similar to that advocated by Taggart [5] and modified by Colman and Tyler [1] and Kelly and Spottiswood [14]. Their procedure is summarised as follows:

The basis of the calculations is Eq. (11.36) which is re-written as:

$$Q = A \, F_B \, C_R \tag{11.39}$$

where F_B =   the basic capacity, $t/h/m^2$,
        Q =   mass rate of flow, (t/h), also taken as the t/h of undersize in the feed, or the total feed to the screen deck depending on the data source,
        C_R =   Combined correction factor,
        A =   Area of open surface.

The basic capacity F_B is considered as the unit capacity defined as the capacity per m^2 of screen surface. The data provided by different sources however may define Q and F_B in different ways. For example, Gluck [16] and Cedarapids [17] define Q and F_B as the total feed to the screen deck while Colman [15] and Nordberg (Metso) [18] define these terms as the tonnage passing through the screen or the tonnage of undersize in the screen feed.

The basic production rate is a function of screen aperture. The relation between aperture and basic capacity has been determined empirically and for some screen types is given in Fig. 11.14. Though most metallic ores have similar screening characteristics, other materials may have different screening characteristics so the appropriate specific capacity curve should be used. The difference between the data sets reflects the difference in the definition of base capacity and the different *standard* screening conditions used.

The correction factor C_R takes into account all the variables listed below. These corrections factors have been determined empirically and are based on the conditions assumed for deriving the basic equation. In all, eleven factors are identified. These are designated by various symbols by different screen manufacturers and are numbered C_1–C_{11} in this book. The descriptions of these variables are as follows. The values of the corresponding factors are given in Figs. 11.16-11.23 and Tables 11.3-11.5.

C_1 =   mass factor
C_2 =   open area factor
C_3 =   % oversize material
C_4 =   % undersize (fines) in the feed
C_5 =   screen efficiency factor
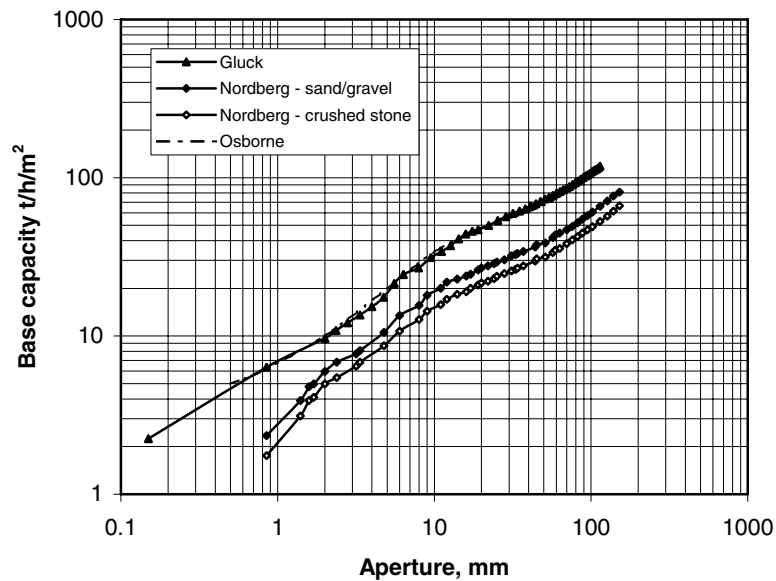
Fig. 11.14. Relation between aperture and Base Unit Capacity expressed as tonnes per hour per square meter for different screen types.

Gluck [16] – using a bulk density of 1.6 t/m³;
Nordberg (Metso) [18]– 50% oversize in feed, 25% half size, slope 20°, 92-95% efficiency; Osborne [8] – 60% open area.

C_6	=	deck factor
C_7	=	screen slope
C_8	=	adjustments to aperture shape
C_9	=	adjustment for particle shape
C_{10}	=	adjustments for wet screening
C_{11}	=	adjustments due to moisture

The correction factor C_R is the product of all the correction factors representing the deviation from the standard conditions and adjustments to the specific conditions. That is:

$$C_R = C_1 C_2 C_3 C_4 C_5 C_6 C_7 C_8 C_9 C_{10} C_{11} \qquad (11.40)$$

The significance of these factors and the method of determination are:

C1: Mass Factor

The correction factors were derived at normal vibrating speeds of screens using a material of bulk S.G. 1.602 t/m³ which was considered as standard. Factors for higher vibrations are available from the manufacturers. Where the bulk density of a specific material is different

from the standard, it has to be corrected by taking the ratio of the specific gravities [8]. That is:

$$\frac{F}{F_B} = \frac{\rho}{1.602} \qquad (11.41)$$

where   F   = capacity at the actual bulk density and
          F_B = capacity at the standard bulk density (1.602 t/m^3)

Hence the correction factor C_1 = $\rho/1.602$

C2: Open Area Factor

While deriving the basic equation, the capacity for different open areas of screens were determined using standard woven wire screens having square apertures. Commercial screens differ from this standard. Correction factors were therefore determined by simple formulae such as:

$$C_2 = \frac{\% \, \text{Open Area of screen}}{A_{OB}} \qquad (11.42)$$

where A_{OB} = the base open area used.
                eg. 50% [16,17], 60% [8], 100% [14], variable [18].

The open area used by Nordberg (Metso) [18] in Eq. (11.42) changes depending on the screen aperture. The relationship between the base open area and screen aperture is shown in Fig. 11.15.

C3: Correction Factor for Oversize

The standard oversize in the feed is mainly taken as 25%. When the oversize percent in the feed is greater than 25%, then stratification of bed layer is incomplete, which leads to a screening error. This error has to be allowed for and a correction is made for different percentages of oversize. The correction factor, C_3, from several sources is reproduced in Fig. 11.16.

C4: Correction Factor for Undersize (Fines)

The fines are defined as the percent less than half the screen aperture. It is a convenient measure of the ease of screening. By convention, 40% fines in the feed is taken as the standard case. This is used to establish the basic unit capacity of screens. The difficulty or otherwise of screening is therefore related to 40% fines content in the feed. This is assigned a factor equal to 1.00. Factors for different fines content have been derived over a range of undersizes. Factors for the percent half size or the percent of feed passing half the aperture size were determined and are plotted as correction factor C_4 in Fig. 11.17.

In a multi-deck screen, the percentage of half size in the feed to the screen is expressed as the percentage of the feed to the deck under consideration. For example, in a double deck screen, if the total screen feed contains 35% passing half the lower deck screen aperture size and 70% passing the upper deck aperture size then the percentage half size for the bottom screen is 35/70 = 50% (see Fig. 11.18).
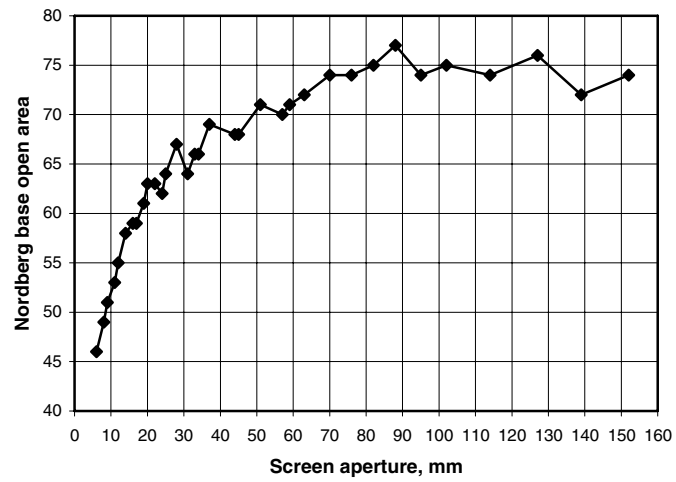
Fig. 11.15. Base open area versus screen aperture [18].
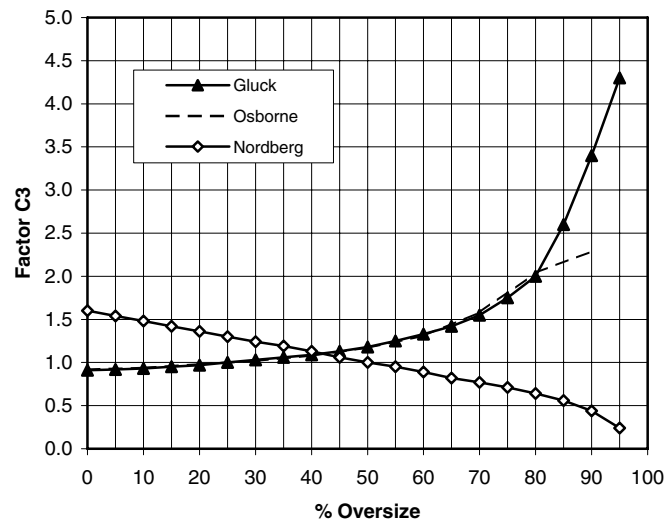
Fig. 11.16. Correction factor C_3 for percent oversize in the feed.
Gluck [16] – 25% oversize in feed, Osborne [8] – 25% oversize in feed
Nordberg (Metso) [18]– 50% oversize in feed.
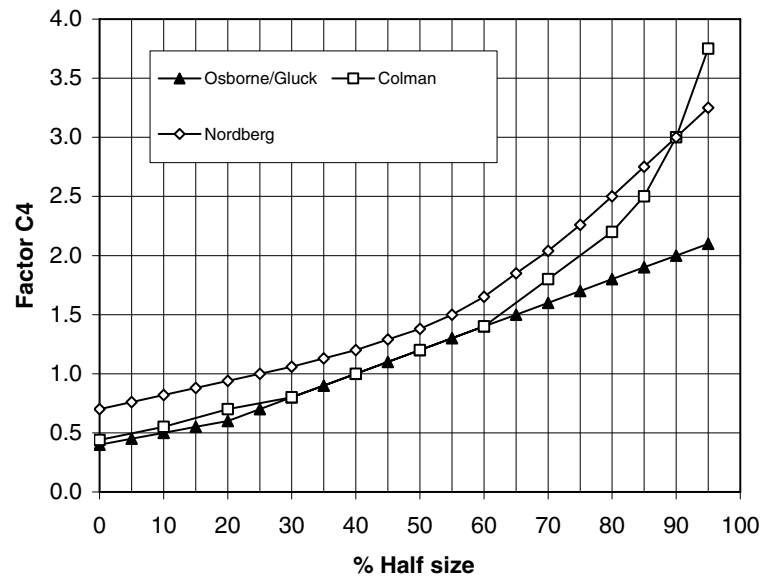
Fig. 11.17. Relation between percent half size and Correction Factor C_4

Gluck [16] – 40% half size, Osborne [8] – 40% half size,
Nordberg (Metso) [18]– 25% half size, Colman [15] – 40% half size.
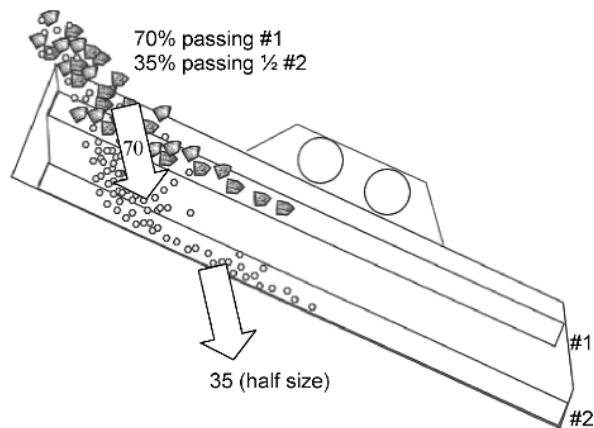
Fig. 11.18. Half size percentage for multi-deck screens

C5: Screen Efficiency Factor

In industrial screening, efficiencies of 100% is not achievable. Hence 90 – 95% efficiency is considered as the maximum for normal wire screens. During scalping operations Colman [15] suggests that the efficiency should be taken as 80 – 85%. For normal wire screens, the correction factors for different efficiencies have been determined and are reproduced in Fig. 11.19.

C6: Deck Factor

Fig. 11.8 shows that the effective screening does not take place immediately at the charging end of the screen as the material has to travel some distance for stratification to take place. When a bottom deck is set up the effective screening takes place further down the screen. Thus the effective screening area is reduced. The reduction of area at the top deck is not significant. Fig. 11.20 indicates the possible manner of the loss in effective screening area in deck 2.

The correction factor for the top deck is therefore considered as unity. For the lower decks, the correction factors are given in Table 11.4 as recommended by Colman [1,15] and Gluck [16].

Table 11.4
Correction for the number of decks (Deck Factor, C_6) [15-18].

Deck position	Correction factor, C_6
top deck, (No.1)	1.0
second deck (No. 2)	0.9
third deck (No. 3)	0.8
fourth deck (No.4)	0.7
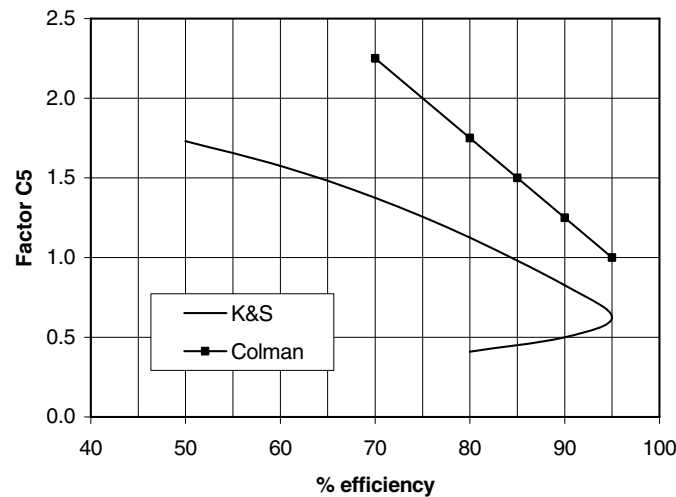
Fig. 11.19. Desired Efficiencies for varying loads, factor C_5.
Colman [15] – 95% efficiency base; Kelly & Spottiswood [14] – 85% efficiency base.
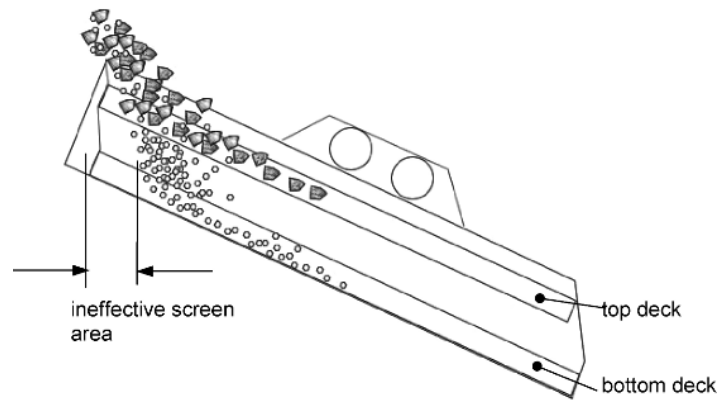
Fig. 11.20. Inactive area on screen due to deck position.
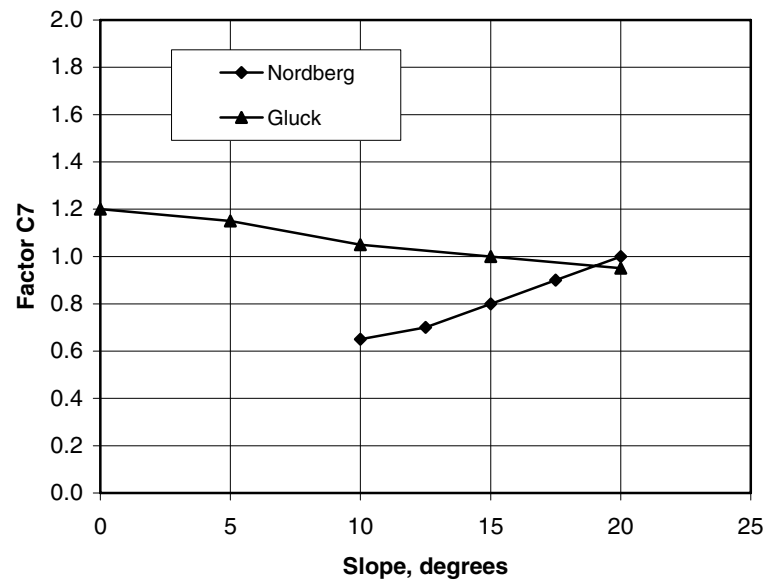
Fig. 11.21. Correction Factor C_7 for the slope of the screen.
Nordberg (Metso) [18] – 20° slope standard, Gluck [16]– 15° slope standard.

C7: Correction due to the Screen Slope

It is usual to set the screen between 18 and 25° in a normal close circuit crushing operation. Increasing slope results in increased speed of movement of material but in so doing could result in a reduced effectiveness of the screen. The correction factor for different screen inclinations are indicate in Fig. 11.21.

C8: Correction for Aperture Slot Shape (Slot Factor)

Fig. 11.1 illustrates some commonly used aperture shapes. The basic flow rate calculations are based on a square aperture. For non square apertures, a correction factor applies. Except for the round apertures all others regular apertures may be described by the aperture length to width ratio (L/W). Some slight differences between the correction factor values have been published and some data are included in Table 11.5.

Table 11.5
Correction factor C_8 for slot shape. Gluck [16], Colman [15].

Aperture shape	Gluck		Colman		Nordberg (Metso)	
	L/W	C_8	L/W	C_8	L/W	C_8
square	1	1	< 2	1	1	1
rectangular	> 6	1.6	> 25	1.4	3 – 4	1.15
rectangular	3 – 6	1.4	4 – 25	1.2	> 4	1.2
rectangular	2 – 3	1.1	2 – 4	1.1		
circular	-	0.8			-	0.8

C9: Correction for Particle Shape

Fig. 11.5 illustrates the effect of particle shape on screening. Shapes of irregular particles are difficult to describe. The divergence from sphericity or cube can be described in terms of the length/width ratio. An elongated particle is defined as a particle having a length to width ratio greater than 3 and a size between 0.5 and 1.5 times the aperture size. Correction factors have been determined as a function of the percentage of elongated particles in the feed and the various data values are plotted in Fig. 11.22.

C10: Correction Factor for Wet Screening

Water is added during industrial screening for purposes, including;

1. as an aid to screening
2. removal of accumulations in the apertures which tend to block screens
3. reducing dust

Too much water however is inadvisable as it could unnecessarily lead to agglomeration. Colman recommends 15 L/min to 25 L/min per cubic meter of feed for efficient wet screening (1 – 2.5 vol. %, Gluck [16]). But this would depend severely on the composition of the gangue content. For example the bentonite and kaolinite content could lead to sticky material. This can be obviated by a different size of screen openings. The assistance given by water in screening is dependant on the screen aperture. It is generally observed that when the feed size is 25 mm or greater, the error due to water is minimal (wet screening is less effective). As the aperture decreases the correction factor varies as indicated in Fig. 11.23.
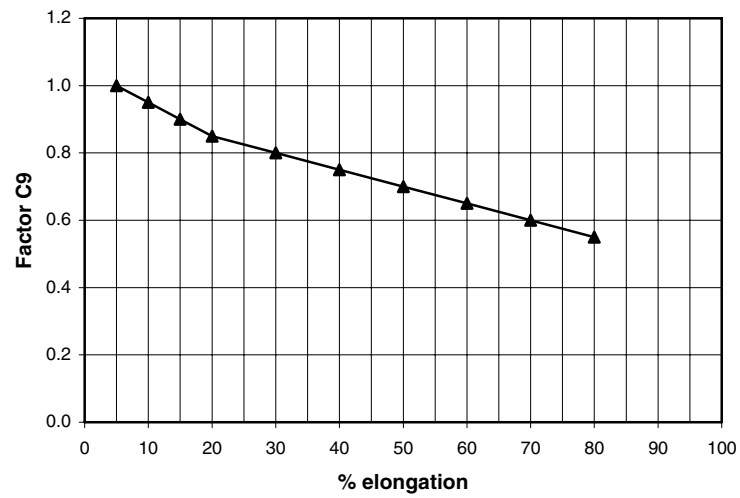
Fig. 11.22. Correction factor for particle shape, C_9; Gluck [16].
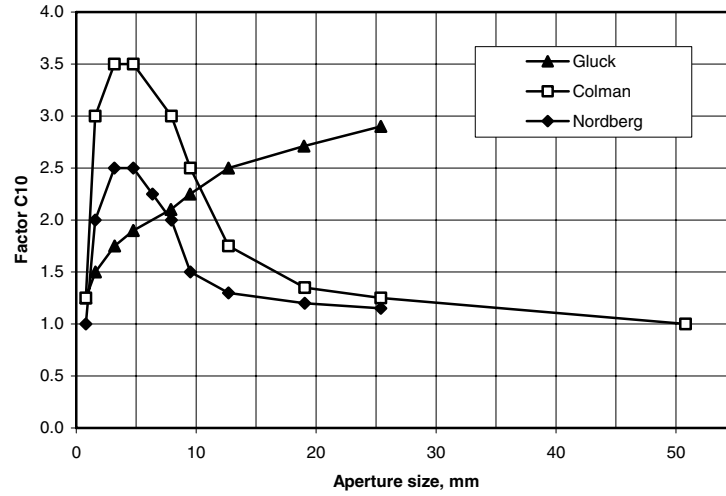
Fig. 11.23. Correction Factor C_{10} for wet screening at different apertures. (Gluck [16], Colman [15], Nordberg (Metso) [18]).

C11: Correction FACTor for Moisture Content

Most ores have inherent and surface moisture. On mining and storage, part of the surface water tends to evaporate. The inherent moisture content is difficult to remove and is only slightly reduced on exposure to air. Most of the inherent water is therefore retained. When the total moisture content is 5% or less, the ore is considered more or less *dry* and generally the screening operation is satisfactory. This condition is considered to have a correction factor of 1. When the moisture is retained the factor is taken as 1.25. When the ore does not contains hygroscopic material, the factor is 0.85 and for sticky, hygroscopic material the factor is taken as 0.75 (Table 11.6)

Table 11.6
Correction factor C_{11} for feed condition [16,17].

Condition	C_{11}
Moist or dirty stone, muddy or sticky	0.75
Moist ore from underground, > 14%(vol) moisture	0.85
Dry quarried rock < 4-10% (vol) moisture	1.0
Dry uncrushed material, dried or hot material	1.25
Wet screening with sprays	1.75

The application of Eq. (11.39) to determine the area of screen for a given flow rate and solid characteristics is illustrated by Example 11.5.

Example 11.5

The size distribution of a dry crushed ore as determined by a standard sieve analysis is given below. The ore was stockpiled and then withdrawn at the rate of 40 t/h for screening on an 850 micron square mesh screen. A screening efficiency of 79 % was desired. The open area of the screen was 70%. The bulk density and moisture content of the mineral was 2.7 t/m^3 and 18% respectively. The screen is inclined at 15 degrees to the horizontal and particle shape is estimated at 10% elongation. Determine the surface area and the screen size to be used.

Size (microns)	% Passing	Size (microns)	% Passing
3350	100	210	24.2
1680	75.3	105	18.4
850	49.1	75	10.6
420	33.9	-75	6.0

Solution *Using the Gluck data*

Step 1: Base capacity
From Fig. 11.14, the basic capacity of a screen at 850 microns = 6.2 t/h/m^2

Step 2: Correction factors
1.   The mass correction factor $C_1 = 2.7/1.602 = 1.685$
2.   The open area factor, $C_2 = 70/50 = 1.4$
3.   From the size distribution of the ore, the percentage of the feed greater than the screen aperture (850 microns) $= 100 - 33.9 = 66.1\%$.
      From Fig. 11.16 the correction due to over-size material in the screen feed, $C_3 = 0.95$
4.   The percentage of the feed less than half the aperture (420 microns) is 24.2%. From Fig. 11.17, $C_4 = 0.7$
5.   For a screen efficiency of 79% and Fig. 11.19, the correction factor for screen efficiency, $C_5 = 1.3$
6.   For a single deck screen the factor $C_6 = 1$
7.   For a screen inclined at 15 degrees, the slope factor from Fig. 11.21, $C_7 = 1.03$
8.   For a square aperture, from Table 11.4, $C_8 = 1$
9.   At an elongation figure of 10%, $C_9 = 0.95$ (Fig. 11.22)
10.   For dry screening, the wet screening factor, $C_{10} = 1$ (Fig. 11.23)
11.   For a moisture of 18%, the correction for feed condition, $C_{11} = 0.85$ (Table 11.5)

The overall correction factor is given by:

$$C_R = 1.685 \times 1.4 \times 0.95 \times 0.7 \times 1.3 \times 1 \times 1.03 \times 1 \times 0.95 \times 1 \times 0.85 = 1.696$$

Step 3. Screen Area

From Eq. (11.39); $A = \dfrac{F}{F_B \, C_R} = \dfrac{40}{6.2 \times 1.696} = 3.8 \text{ m}^2$

Available screen sizes having areas close to the calculated value are (Table 11.7):
3052 x 1219 mm (area 3.72 m^2) and 3659 x 1219 mm (area 4.46 m^2)

These calculations are an indication only. Screen manufacturers should be consulted for data pertaining to specific screening equipment.

Table 11.7
Typical industrial screen sizes [17,18,19].

Width mm	Area m^2	Width mm	Area m^2	Width mm	Area m^2	Width mm	Area m^2
254	0.31	508	1.24	1524	5.57	2134	10.41
305	0.37	610	1.49	1219	5.95	1829	11.15
356	0.43	914	1.67	1524	6.50	2134	11.71
356	0.54	914	2.23	1829	6.69	2438	11.89
610	0.56	1219	2.23	1524	7.43	2134	13.01
406	0.62	914	2.79	1829	7.80	2438	13.38
610	0.74	1219	2.97	1524	8.36	2438	14.86
406	0.74	1219	3.72	1829	8.92	2438	17.84
508	0.93	1219	4.46	2134	9.10		
508	1.08	1524	4.65	1524	9.29		
610	1.11	1219	5.20	1829	10.03		

11.4. Operation of Curved Screens

11.4.1. Capacity of Curved Screens

The capacity of a curved screen surface (sieve bend), like straight screens, is a function of screen open area. In addition, the greater the curvature of the screen surface the greater is the centrifugal force and therefore a greater capacity is expected. The capacity and separation of the oversize and the undersize of curved screens depend on:

1. the feed layer thickness which is related to the feed rate,
2. the radius of curvature. This is significant when less than 760 mm and velocities greater than 3 m/s,
3. the angle θ subtended against the horizontal, see Fig. 11.6,
4. the Reynolds number $\dfrac{(L\, v\, \rho)}{\mu}$ where L is the slot width, v the velocity of slurry through the slot, ρ the density of the slurry and μ the viscosity of the slurry,
5. the kinematic viscosity (μ/ρ),
6. the slot width,
7. the surface tension,
8. the shape of the wedge bars, i.e. triangular of rectangular,
9. the mode of vibration (where employed),
10. the number of slots and the slot spacing.

The influence of the above variables on the overflow and underflow streams has not been quantitatively established satisfactorily. However it is generally observed that relatively smaller radii of curvature result in comparatively higher centrifugal force and therefore more capacity. If we consider the ratio of underflow to feed rate as the measure of capacity then the conditions contributing to maximum capacity will be;

1. the greatest ratio of length of screen opening to thickness of the feed layer,
2. the maximum slot width on the screen,
3. the Reynolds number (Re) is a maximum, that is when the viscosity is a minimum and the product (L ρ v) is a maximum,
4. the maximum thickness of bed that does not promote stratification.

The capacity would be adversely affected by;

1. a small angle θ, and
2. a low feed velocity

At low Reynolds numbers, up to approximately 300, the ratio of the undersize capacity to the feed capacity increases but above 400 the Reynolds number does not have any further significant effect on capacity (Fig. 11.24).

The sieve bends commonly used for metallurgical operations are gravity fed having angles between 45° and 50° and with typical bar spacings between 0.15 to 3.0 mm. The capacity is up to 4.3 m^3/min/m width. They are used for classification of feed sizes ranging from 100 µm to 12,000 µm with feed solid content as high as 45% by volume.
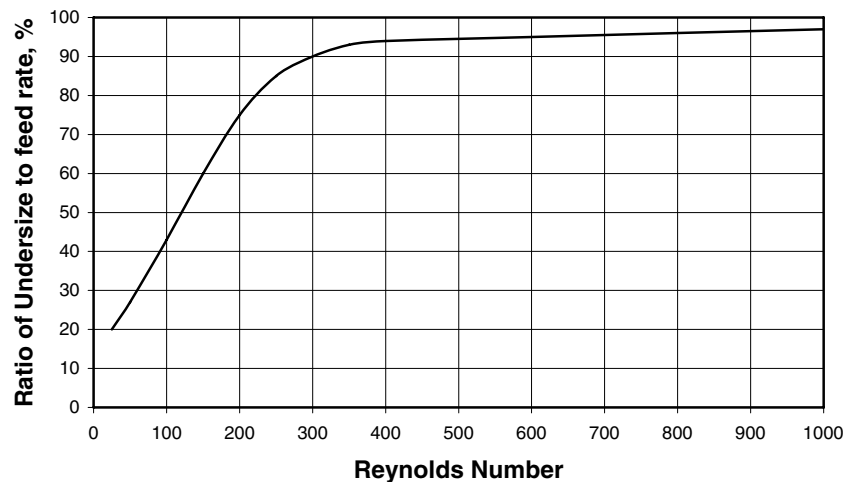
Fig. 11.24. Effect of Reynolds Number on sieve bend capacity [7].

11.4.2. Rapid Method to Determine Sieve Bend Size

Stavenger [7] has recommended a rapid method for estimating the sizes of sieve bends. Like Taggart [5] he has considered the productivity at size ranges less than and more than 300 microns and a minimum feed flow velocity of 3 m/s. The calculations are based on two statistical relations:

1. Bar spacing and diameter of separation (Fig. 11.7) and
2. Bar spacing and capacity (Fig. 11.25)

For example, from Fig. 11.7, considering a separation size which is approximately 50% of the slot width, a separation size of 1000 μm will require a 2.2 mm slot width. Then from Fig. 11.25, for an 800 mm screen length and a slot width of 2.2 mm then screen capacity would be 4.5 m³/min/m of screen width.

11.5. Modelling of the Screening Process

The screening process involves material transport along the screen, the probability of undersize particles passing through the apertures of the screen and stratification of fine particles in the particle bed to the screen surface. Modelling of these processes can be quite complex with the result that predicting screening performance has been based on empirical data of the basic capacity per square meter of screen surface combined with correction factors for deviation from the standard screening conditions. These predictions are only an estimate and give no prediction of particle size distribution or screen efficiency.

Under certain circumstances screening and sieving can be represented as a rate process though in practical situations a number of overlapping processes may occur.
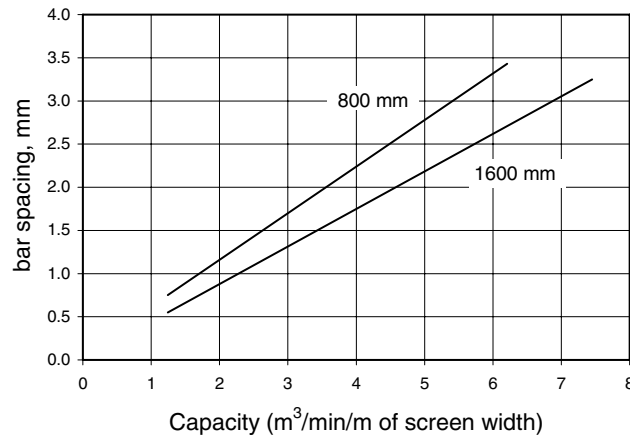
Fig. 11.25. Relation between volumetric capacity and slot width for two screen lengths (800 and 1600 mm) [7].

11.5.1. Two Process Treatment

Ferrara and Preti [20] proposed that during screening, particles are subjected to two distinctly different types of condition, crowded or separated screening depending on their position on the screen deck and the feed and vibration conditions. This leads to two different rate processes.

Crowded Screening

Crowded screening occurs when the flow rate is above a critical value (F_C) such that the material bed is so thick that only particles in the layer immediately in contact with the screen are capable of passing through the screen. The eventual passage of a particle under crowded conditions depends on two distinct statistical phenomena:

1. the probability of a particle reaching the screening surface through stratification and
2. the probability that the particle will pass through the screen.

As long as the upper layers are capable of replenishing the contact layer, that is, probability 1 is higher than probability 2 and particles are hindered by neighbouring particles from passing through the screen, the rate of passage will remain constant and will be given by:

$$-\frac{dF_L}{dL} = k_C \qquad (11.43)$$

where F_L = mass flow rate on the screen per unit width, at a distance L from the feed point, and

k_C = rate constant for the crowded condition.

In practice, a range of particle sizes will be present and a separate equation will apply for each particle size d_i, then:

$$-\frac{d\left(F_L\, m_{iL}\right)}{dL} = k_{Ci}\, m_{iL} \qquad (11.44)$$

where m_{iL} = mass fraction of particles in size interval i in the bed at distance L from the feed point.

Because F_L and m_{iL} are functions of L, this becomes on integration:

$$-\ln\left(1 - E_{iU}\right) = k_{Ci} \int_0^L \frac{dL}{F_L} \qquad (11.45)$$

where E_{iU} = mass of size interval i reporting to the undersize stream as a fraction of the mass of size i in the screen feed (the partition coefficient of the undersize) and

$(1 - E_{iU})$ = E_{iO}, the partition coefficient of the oversize.

A plot of $\ln(1 - E_{iU})$ versus $\int_0^L \frac{dL}{F_L}$ should then give a straight line of slope equal to k_{Ci}.

Eq. (11.45) can be used to calculate the screen performance curve provided the rate constant

and the function $\int_0^L \frac{dL}{F_L}$ is known.

Ferrara et al. [21] introduced a new variable, χ_j defined as:

$$\chi_j = \frac{\ln E_{jO}}{\ln E_{iO}} = \frac{k_{Cj}}{k_{Ci}} \qquad (11.46)$$

where   j   = size fraction of particles on the screen that affects the kinetics of particles of size d_i (mean size of particles in interval i)

and   for $0 \le d_j < L_A$, $k_{Cj} \ne 0$, $\chi_j \ne 0$
              for $d_j \ge L_A$, $k_{Cj} = 0$, $\chi_j = 0$

where d_j = mean size of particles in interval j

The crowded screening equation then becomes:

$$F\left[\int_0^{L_A} m_{jF} \frac{1}{\chi_j}\left(E_{iO}^{\chi_j} - 1\right) d\,d_j + \int_{L_A}^{\infty} m_{jF} \ln E_{iO}\, d\,d_j \right] = -k_{Ci}\, L \quad \text{for } 0 < d_i < L_A \qquad (11.47)$$

for $d_i \geq L_A$ $k_{Ci} = 0$ and $E_{iO} = 1$

Incorporating the Gaudin model of screening probability [9], then χ_j can be expressed as:

$$\chi_j = \left[\frac{L_A - d_j}{L_A - d_i}\right]^\gamma \tag{11.48}$$

where γ = 2 for square mesh and 1 for wedge wire screens.

If $d_i/L_A = 0.5$ then:

$$k_{Ci} = k_{C50}\, 2^\gamma \left(1 - \frac{d_i}{L_A}\right)^\gamma \tag{11.49}$$

where k_{C50} =   the kinetic constant in the crowded condition for particles of size equal to half the aperture size (ie. $d_i/L_A = 0.5$).

Substituting Eq. (11.49) into Eq. (11.47), screening in the crowded condition is then described by the equation:

$$F\left[\int_0^{L_A} m_{jF}\frac{1}{\chi_j}\left(E_{iO}^{\chi_j} - 1\right)\mathrm{d}d_j + \int_{L_A}^{\infty} m_{jF}\ln E_{iO}\,\mathrm{d}d_j\right] = -k_{C50}\,2^\gamma\left(1 - \frac{d_i}{L_A}\right)^\gamma L \tag{11.50}$$

for $d_i < L_A$

Separated Screening

For mass flows across the screen less than F_C, the particles behave as isolated particles and do not interfere with each other. For these conditions, the quantity of particles that pass through the screen, dF, in the small incremental length dL is proportional to dL and the rate F at which particles enter dL. Therefore assuming a first order relationship:

$$-\frac{\mathrm{d}F_L}{\mathrm{d}L} = k_s\, F_L \tag{11.51}$$

For a feed of size interval i:

$$-\frac{\mathrm{d}(F_L\, m_{iL})}{\mathrm{d}L} = k_{Si}\, F_L\, m_{iL} \tag{11.52}$$

Integration of Eq. (11.52) and including the screen oversize partition coefficient gives:

$$E_{iO} = \exp(-k_{Si}\,L) \quad \text{for } 0 < d_i < L_A \tag{11.53}$$

and for $d_i > L_A$, $k_{Si} = 0$ and $E_{iO} = 1$.

Substituting the similar relationship to Eq. (11.49):

$$k_{Si} = k_{S50} \, 2^\gamma \left(1 - \frac{d_i}{L_A}\right)^\gamma \tag{11.54}$$

into Eq. (11.53) gives the approximate separated screening equation:

$$E_{iO} = \exp\left[-k_{S50} \, 2^\gamma \left(1 - \frac{d_i}{L_A}\right)^\gamma L\right] \tag{11.55}$$

Combined Screening

For screening conditions where both crowded and separated screening occur, the overall oversize efficiency is given by:

$$E_{iOL} = E_{iOL(C)} \, E_{iO(L-L(C))} \tag{11.56}$$

where E_{iOL}, $E_{iOL(C)}$, $E_{iO(L-L(C))}$ = oversize efficiency for screen lengths L, L_C and L-L_C,

L_C = the distance from the feed end to the point of transition from crowded to separated screening condition.

Substituting the expressions for the crowded and separated screening efficiencies (Eqs. (11.45) and (11.55) gives:

$$E_{iOL} = \exp\left[-k_{C50} \, n_d \, 2^\gamma \left(1 - \frac{d_i}{L_A}\right)^\gamma\right] \tag{11.57}$$

where $n_d = \int_0^{L_c} \frac{dL}{F_L} + \frac{L - L_c}{C}$, and

$$C = \frac{k_{C50}}{k_{S50}}$$

The variable n_d is not easily determined but is constant under set operating conditions. Ferrara et al. [21] estimate C as F_C, the mass flow rate on the screen per meter width at L_C.

The combined parameter $k_{C50}.n_d$ and γ can be estimated by fitting screening data to Eq. (11.57). This will allow screen efficiencies and product sizes to be modelled. For design work, the separate parameter k_{C50} needs to be evaluated as well as γ.

To determine these parameters, Eq. (11.50) is written in the form:

$$F\left[\sum_{j=1}^n m_{jF} \frac{1}{\chi_j}\left(E_{iO}^{\chi_j} - 1\right) + \ln E_{iO} \sum_{j=n+1}^m m_{jF}\right] = -k_{C50} \, 2^\gamma \left(1 - \frac{d_i}{L_A}\right)^\gamma L \tag{11.58}$$

for $1 \le i \le n < L_A$ and $E_{iO} = 1$ for $L_A < n+1 \le i \le m$

where   m   = the number of size intervals and
        n   = the number of size intervals less than the screen aperture.

To evaluate the parameters, the screening process is simulated using Eq. (11.58) for interval i using guessed values of the parameters and minimising the sum of the squares of the residuals:

$$\Phi = \sum \left(E_{iO} - E_{iO}^*\right)^2 z_i$$

where E_{iO}, E_{iO}^* = experimental and calculated screen oversize efficiency and
        z_i = a weighting factor.

Ferrara et al. [21] likened the significance of the crowded rate constant, k_{C50}, to the basic capacity, F_B, in the empirical approach to screen sizing in that they both depend on the screen aperture, the open area of the screen, the aperture shape, vibration characteristics and screen slope. The parameter γ affects the ratio of probabilities for different particles passing through the screen.

In screen design, it would be necessary to know how k_{C50} and γ varies with screen aperture and the other screening parameters in much the same way as the data exists for the base screen capacity.

Example 11.6

A set of screening data was used to obtain the screening parameters as given below;

k_{C50}	25 t/h/m^2	γ	1.8
Screen length, L	3.5 m	Screen feed/width	60 t/h/m
Screen aperture, L_A	0.004 m		

Calculate the screen performance and the oversize and undersize distributions given the following screen feed: Note, in this case, interval 1 is the smallest size interval.

Interval, i	Screen size, m	Mean size, m	Mass fraction, m_i
7	0.0060	-	0.2
6	0.0040	0.0049	0.3
5	0.0035	0.0037	0.2
4	0.0025	0.0030	0.1
3	0.0015	0.0019	0.08
2	0.0005	0.0009	0.05
1	0	0	0.07

Solution

Substitute the screen parameters into Eq. (11.58) and solve for E_{iO}. This is easily performed using a computer. A spreadsheet solution is shown below.

For the feed size shown, the number of intervals less than the screen aperture, $n = 5$ and the total number of intervals, $m = 7$. A set of initial starting values for E_{iO} are estimated as follows;

size	Eio (guessed)
7	1
6	1
5	0.800
4	0.300
3	0.050
2	0.010
1	0.002

Then, starting with $i = 1$; $j = 1 - 5$

	j	χ_i (equ (11.48))	$m_{jF}(E_{iO}^{\chi_j} -1)/\chi_i$	j	m_{jF}
	1	1	-0.012	6	0.3
$i = 1$	2	0.669	-0.160	7	0.2
	3	0.323	-0.502	$\Sigma =$	0.5
	4	0.093	-0.472		
	5	0.008	-0.562		
		$\Sigma =$	-1.709		

For $i = 1$, the left hand side of Eq. (11.58) is then:

LHS $= 60 \, (-1.709 + (\ln 0.002 \times 0.5) = -289.0$

and the right hand side of Eq. (11.58) is:

RHS $= -25 \times 2^{1.8} \, (1 - (0.00025/0.004))^{1.8} \times 3.5 = -271.3$

Using *Solver* in MS-Excel® to zero the square of the difference between the LHS and RHS values using E_{1O} as the variable gives a fitted value for E_{1O} of 0.0031. Repeating the procedure for other values of i from 2 to 5 gives the following results:

size	Eio (fitted)
7	1
6	1
5	0.957
4	0.586
3	0.155
2	0.021
1	0.0031

From the partition coefficients, the oversize and undersize distributions can be estimated from the feed size distribution. The following graphs show the fitted performance curve and the predicted size distribution of the oversize and undersize.
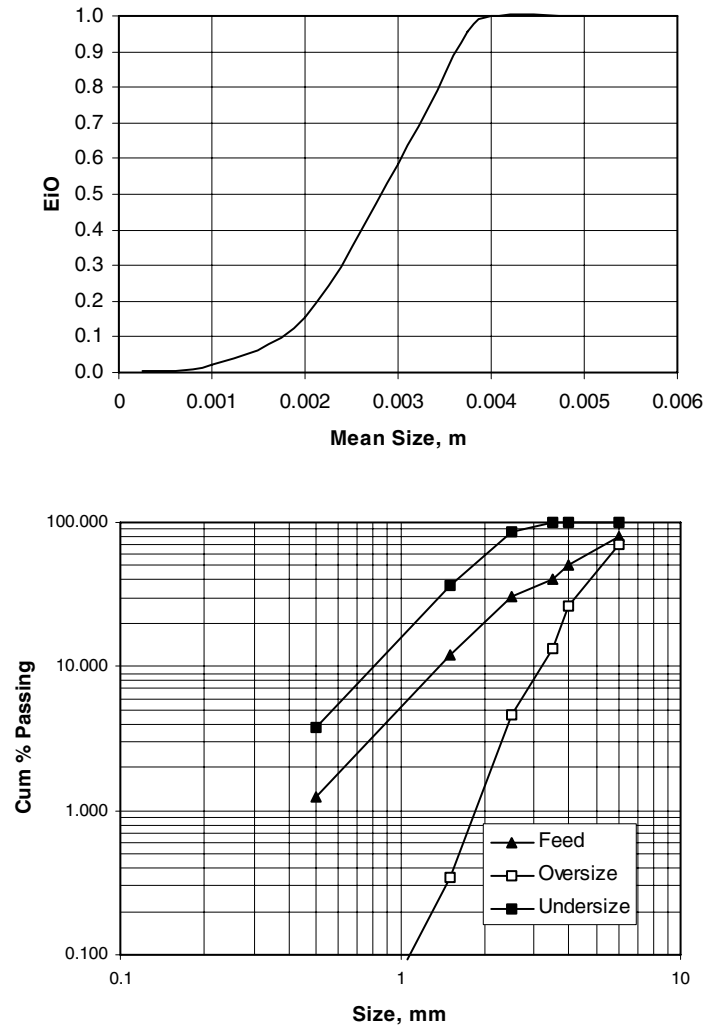
Segregation Treatment

Subasinghe et al. [22] considered screening to be described by two simultaneous first order rate processes; segregation and passage through the screen. Segregation of undersize material through the bed to reach the screen surface depends on the size of the undersize relative to the

surrounding particles, the size distribution in the bed and the screen vibration. Particle passage through the screen was reported first order under conditions giving rise to a constant probability of passage. Combining these two processes, Subasinghe et al. obtained the following equation for the fraction of size i retained on the screen after length L, m_{iL}, as:

$$E_{iO} = \frac{[k_{iG} \exp(-k_{iP} L) - k_{iP} \exp(-k_{iG} L)]}{k_{iG} - k_{iP}} \quad \text{for} \quad 0 \le i \le L_A \qquad (11.59)$$

where k_{iG} = rate constant for size i segregating to the screen surface and
       k_{iP} = rate constant for size i passing through the screen.

Analysis on a set of screening data using Eq. (11.59) to estimate k_{iG} and k_{iP} showed that as the particle size became small relative to the screen aperture, the segregation rate decreases and the passage rate constant increases while if the particle size approaches the aperture size (near size particles), the segregation rate constant increases and the passage rate constant approaches zero. For intermediate values of d_i/L_A, the value of k_{iG} approaches the value of k_{iP} and a dynamic equilibrium exists between the two processes.

The variation of k_{iG} and k_{iP} with particle size for this data set were described by the empirical correlations:

$$\ln k_{iG} = -4.311 + 21.810 \, (d_i/L_A) - 54.876 \, (d_i/L_A)^2 + 40.544 \, (d_i/L_A)^3 \qquad (11.60)$$

$$\ln k_{iP} = 0.8779 - 16.744 \, (d_i/L_A) + 40.120 \, (d_i/L_A)^2 - 37.310 \, (d_i/L_A)^3 \qquad (11.61)$$

Thus from known values of k_{iG} and k_{iP}, the size distribution of the screen undersize can be estimated. However, evaluation of more data sets are required to determine how k_{iG} and k_{iP} vary with equipment and particle characteristics.

Subasinghe et al. [22] observed that plots of the expression in Eq. (11.59) had a similar shape to a 2 parameter survival function of the Weibull distribution function and that in the form of a Rosin-Rammler function was adequate to describe the screen products as:

$$E_{iO} = \exp\left[-\left(\frac{L}{B}\right)^A \right] \qquad (11.62)$$

The constants A and B were fitted to third order polynomials and for the same set of screening data used above:

$$A = 1.196 - 2.803 \, (d_i/L_A) + 15.74 \, (d_i/L_A)^2 - 14.13 \, (d_i/L_A)^3 \qquad (11.63)$$
$$\log B = 1.000 + 0.147 \, (d_i/L_A) - 1.013 \, (d_i/L_A)^2 + 2.570 \, (d_i/L_A)^3 \qquad (11.64)$$

The shape of a performance curves for a vibrating screen is shown in Fig. 11.26. The upturned end of the curve at fine sizes is attributed to the low proportion of fines in the feed and the rate of segregation of fines is low at this size, possibly as a result of the fines adhering to coarser particles.

The JKMRC modelled the screen on the basis of the efficiency curve, described by the equation:
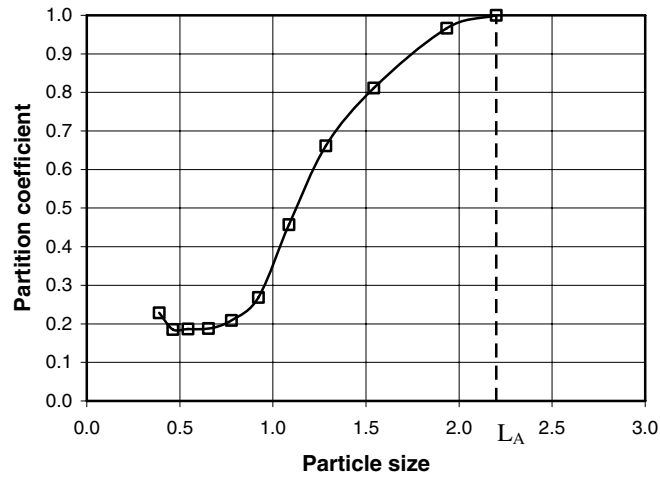
Fig. 11.26. Efficiency curve for a vibrating screen (after Subasinghe et al. [22])

$$E_{iO} = \exp\left[-n\frac{A_o}{100}\left(1-\frac{d_i}{L_A}\right)^{\gamma}\right]$$ (11.65)

where n   = an efficiency parameter which is related to the number of attempts the particle has to pass the screen,
A_o = the percent open area,
d_i = particle size, and
γ = approximately 2

This equation applies for the regular shaped central portion of the curve in Fig. 11.26. The variation of the efficiency factor with respect to the operating conditions is obtained from a set of regression equations of the form [23]:

$Ln\,(n) = K_1 + K_2.F + K_3.P_1 + K_4.P_2$ for $F < F_1$ (11.66)

$Ln\,(n) = K_5 + K_6.F + K_3.P_1 + K_4.P_2$ for $F_1 \leq F \leq F_2$ (11.67)

where $K_5 = K_1 + (K_2-K_6).F_1$

$Ln\,(n) = K_5 + K_6.F_2 + K_3.P_1 + K_4.P_2$ for $F > F_2$ (11.68)

where K_1, K_2, K_3, K_4, K_5 and K_6 are regression constants. K_5 and K_6 are usually set at zero
P_1 = percent of the feed in size interval i
P_2 = percent of the feed less than d_C, a critical size close to L_A

F_1, F_2 = feed rate/screen width corresponding to points of slope change in the relationship between F and n.

The upturned end of the curve is described by a function SF which is determined from experimental data and is related to the percent fines and the fines feed rate:

$$SF = K_7 + K_8.100m_{kF} + K_9.F_k \qquad (11.69)$$

where K_7, K_8, K_9 are regression constants and
  m_{kF} = fraction of the feed that is less than size d_k
  F_k = feed rate of material that is less than size d_k
  d_k = smallest screen.

This fines factor accounts for the fine particles that adhere to larger particles and hence are retained in the oversize fraction. The quantity of this misplaced material is dependant on the surface area of the particles. This is expressed as:

$$A_S \propto \sum_{i=1}^{n} \left[\frac{V_i}{\left(\frac{d_i + d_{i+1}}{2} \right)} \right] \qquad (11.70)$$

where A_S = total surface area,
  V_i = particle volume in interval i, and
  d_i = the top size of the interval i.

The tonnage of fines (particles less than the finest screen eg. 6.3 mm in example 11.6) that are retained within the oversize fraction, is given by;

$$F_{FO} = SF \times A_S \qquad (11.71)$$

The screen length is scaled from the efficiency factor, n.

Example 11.7

Product from a jaw crusher is screened at 63 mm using a single deck vibrating screen. The parameters of the Whiten and White model have been determined from survey data and are given below.

For a feed of 285 tph and a feed size distribution given below, calculate the oversize and undersize size distributions.

Screen feed rate, Q	285 tph	K_1	3.5
Screen open area, A_O	64%	K_2	-0.004
Screen width, W	3.048 m	K_3	0
Screen length, L	10.97 m	K_4	0
Aperture size, L_A	63 mm	K_5	-8.5
Ore SG	3.8	K_6	0
F_1	3000 t/h/m	K_7	0.035
F_2	0	K_8	0.0025
γ	1.86	K_9	-0.0015

Feed size analysis:

Size, mm	% Retrained	Size, mm	% Retrained
152	2	63	9
125	2	45	17
106	7	31.5	6
100	4	19	10
90	12	6.3	10
75	11	0	10

Solution

From the size distribution of the feed the cumulative % passing data is calculated:

Size mm	Mean size mm	Feed %	Feed mass	Feed % passing
152		2	5.70	98
125	138.5	2	5.70	96
106	115.5	7	19.95	89
100	103.0	4	11.40	85
90	95.0	12	34.20	73
75	82.5	11	31.35	62
63	69.0	9	25.65	53
45	54.0	17	48.45	36
31.5	38.3	6	17.10	30
19	25.3	10	28.50	20
6.3	12.7	10	28.50	10
0	3.15	10	28.50	0
		100	285.0 tph	

From this distribution,

F = 285/3.048 = 93.5 t/h/m

d_k = 6.3 mm

m_{kF} = 0.10

F_k = 93.5 x 0.10 = 9.35 t/h/m

Since F < F_1, using Eq. (11.66);

ln (n) = 3.5 + (-0.004 x 93.5) + (0 x P_1) + (0 x P_2) = 3.126

and n = 22.8

Now from Eq. (11.65), the partition coefficient of the oversize, E_{iO}, can be calculated;

Interval "i"	Size, d_i mm	E_{iO}
1	152	1
2	125	1
3	106	1
4	100	1
5	90	1
6	75	1
7	63	1
8	45	0.242
9	31.5	0.018
10	19	0.001
11	6.3	0.00
12	0	0.00

For example, considering size interval 8;

$$E_{iO} = \exp\left[-22.8 \times \frac{64}{100}\left(1 - \frac{45}{63}\right)^{1.86}\right] = 0.242$$

Note, for $d_i > L_A$, $E_{iO} = 1$.

The size distribution of the screen oversize and undersize can then be calculated from the screen feed. The table below shows the results and example calculations for one size interval is given below:

for size interval 8,

$$E_{8O} = \frac{\text{mass of size interval 8 in the O/S}}{\text{mass of size interval 8 in the feed}}$$

mass of size 8 in the O/S = 0.242 x 48.45 = 11.73 tph

and mass of size 8 in the U/S = 48.45 − 11.73 = 36.72 tph

Size, d_i	Mean size	E_{io}	Feed mass	Mass O/S	% O/S	O/S Cum % passing	Mass U/S	% U/S	U/S Cum % passing	A_{iS}
mm	mm		tph	tph			tph			
152	-	1	5.70	5.70	3.9	96.10	0.00	0.0	100.0	
125	138.5	1	5.70	5.70	3.9	92.19	0.00	0.0	100.0	0.01
106	115.5	1	19.95	19.95	13.7	78.53	0.00	0.0	100.0	0.05
100	103.0	1	11.40	11.40	7.8	70.72	0.00	0.0	100.0	0.03
90	95.0	1	34.20	34.20	23.4	47.30	0.00	0.0	100.0	0.09
75	82.5	1	31.35	31.35	21.5	25.82	0.00	0.0	100.0	0.10
63	69.0	1	25.65	25.65	17.6	8.26	0.00	0.0	100.0	0.10
45	54.0	0.242	48.45	11.73	8.03	0.22	36.72	26.4	73.6	0.24
31.5	38.3	0.018	17.10	0.308	0.21	0.01	16.79	12.1	61.5	0.12
19	25.3	0.001	28.50	0.016	0.01	0.00	28.48	20.5	41.0	0.30
6.3	12.7	0.000	28.50	0.000	0.00	0.00	28.50	20.5	20.5	0.59
0	3.15	0.000	28.50	0.000	0.00	0.00	28.50	20.5	0.0	2.38
			285.0	146.0	100		139.0	100		4.00

The surface area for each size interval is given by Eq. (11.70);

For size interval 8, $A_{ss} = \dfrac{\left(\dfrac{48.45}{3.8}\right)}{\left(\dfrac{63+45}{2}\right)} = 0.236$

and the total surface area is given by $A_S = \Sigma A_{iS} = 4.00$

The fines factor in given by Eq. (11.69);

$SF = 0.035 + (0.0025 \times 100 \times 0.1) + (-0.0015 \times 9.35) = 0.046$

and the tonnes of fines in the oversize;

$F_{FO} = 0.046 \times 4.00 = 0.184$ tph

This fines factor should be added to the fines fraction of the screen oversize and subtracted from the screen undersize to give a corrected partition coefficient in the table below.
The efficiency curve and predicted size distributions are shown in the graphs below.
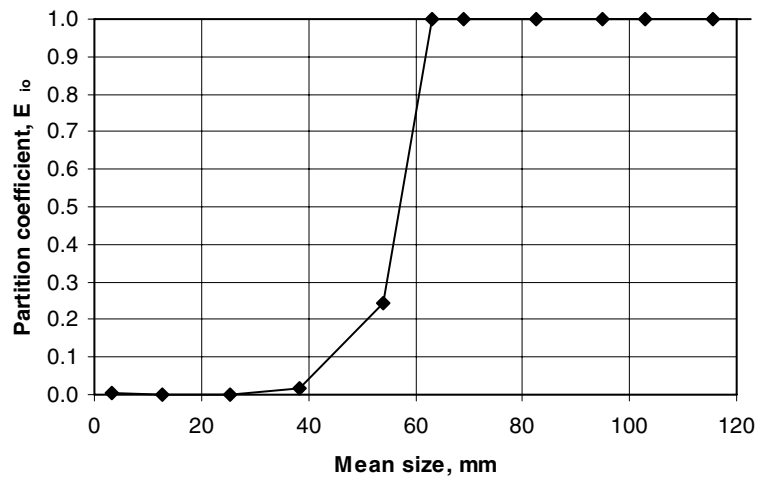
The predicted partition curve for the screen in Example 11.7
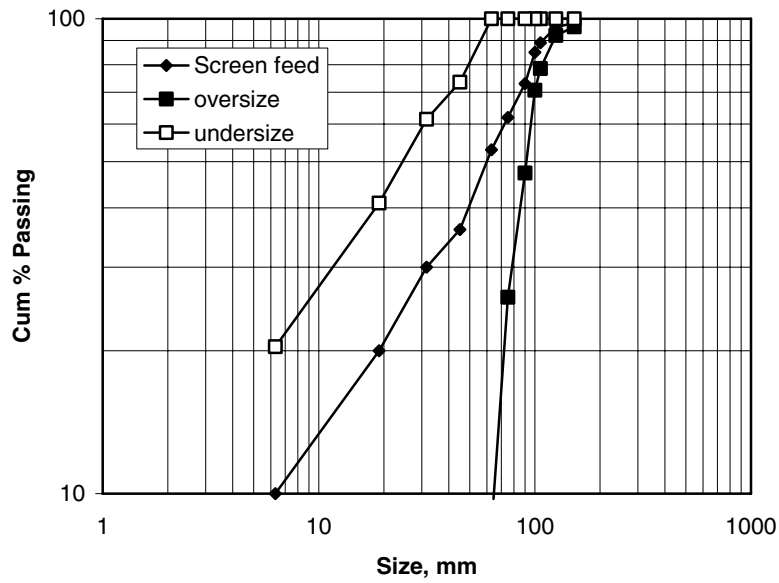
Predicted screen oversize and undersize using Eq. (11.65).

The corrected partition coefficient based on the fines factor

Size, d_i mm	Mean size mm	Mass O/S tph	% O/S	O/S Cum % passing	Mass U/S tph	% U/S	U/S Cum % passing	Adjusted E_{iO}
152	-	5.70	3.90	96.10	0.00	0.0	100.0	
125	138.5	5.70	3.90	92.20	0.00	0.0	100.0	1
106	115.5	19.95	13.65	78.55	0.00	0.0	100.0	1
100	103.0	11.40	7.80	70.76	0.00	0.0	100.0	1
90	95.0	34.20	23.39	47.36	0.00	0.0	100.0	1
75	82.5	31.35	21.45	25.92	0.00	0.0	100.0	1
63	69.0	25.65	17.55	8.37	0.00	0.0	100.0	1
45	54.0	11.73	8.02	0.35	36.72	26.5	73.5	0.242
31.5	38.3	0.31	0.21	0.14	16.79	12.1	61.4	0.018
19	25.3	0.02	0.01	0.13	28.48	20.5	40.9	0.001
6.3	12.7	0.00	0.00	0.13	28.50	20.5	20.4	0.000
0	3.15	0.18	0.13	0.13	28.32	20.4	0.0	0.006

11.5.2. Modelling Sieve Bends

In the sieve bend, separation is considered the result of thin layers of slurry sliced off the slurry stream passing over the screen surface and being diverted to the screen underflow. Fontein [6], considered the main parameters in the sieve bend separation are:

1. the ratio d_{50}/L_A and
2. the fraction of the feed stream reporting to the undersize stream, F_U.

The separation size of the screen should be small compared to the screen aperture (d_{50}/L_A small) to minimise blinding, while F_U is a function of the separating size with high values of F_U yielding large separating sizes. Analysing the factors that contribute to the thickness of the diverted layer Fontein derived the equations:

$$\frac{d_{50}}{L_A} = \frac{K_1 L_A}{R} + \frac{K_2}{f(Re_S)}\left(\frac{L_F}{R} + \frac{L_F\, g\sin\theta}{v^2} + \frac{K_3 \gamma_S}{\rho_P\, v^2 L_A}\right)^{0.5} \quad \text{and}$$

$$F_U = \frac{K_4\, L_A^2\, N}{L_F\, R}\, f(Re_S) + \frac{K_5\, L_A\, N}{L_F}\left(\frac{L_F}{R} + \frac{L_F\, g\sin\theta}{v^2} + \frac{K_3 \gamma_S}{\rho_P\, v^2 L_A}\right)^{0.5} \quad (11.72)$$

where   K   = constants,
        N   = number of slots,
        R   = radius of curvature of the screen surfaces,
        Re_S = Reynolds number of the slot, $L_A v\, \rho_P/\mu$,
        v   = feed velocity,
        L_F = thickness of feed layer,
        θ = angle of arc of the screen surface, and
        γ_s = surface tension.

Fontein showed that at high Reynolds Numbers, the separation size of the DSM screen was around half of the aperture size. This relationship is likely to change however as the screen aperture increases or decreases (Fig. 11.7).

The DSM screen may be modelled on a reduced performance curve. Lynch [24] produced a linear relationship between the corrected d_{50} and the screen design parameters:

$$\log(d_{50C}) = K_1 \log L_A + K_2 Q_W w_U + K_3 M_F + K_4 \tag{11.73}$$

where $\quad d_{50C}$ = corrected separation size
$\qquad Q_W$ = volumetric flowrate of the feed
$\qquad w_U$ = fraction of feed water split to the underflow
$\qquad M_F$ = mass % solids of the feed
$\qquad K$ = constant

Based on laboratory and plant data, Lynch [24] obtained values of the constants K as follows:

$\qquad K_1$ = 1.1718, $\qquad K_2$ = 0.001372
$\qquad K_3$ = 0.0029 $\qquad K_4$ = 2.45

11.6. Screening and Crushing Circuits

When grizzles are used to receive ROM ores they are primarily used as a scalping screen and more often as a single deck operation in open circuit. The capacity of scalping screens is given by the screen dimensions, the depth of bed, the bulk density of material and the speed of travel of material on screen surface. The capacity may be written as:

$$Q_S = 6 \times 10^{-5} \left(D W v \rho_B \right), \quad t/h \tag{11.74}$$

where $\quad$ D $\quad$ = Bed depth at the feed end, mm,
$\qquad$ W $\quad$ = Width of screen, m,
$\qquad$ v $\quad$ = velocity of travel, m/min,
$\qquad$ ρ_B $\quad$ = bulk density, kg/m^3

Most commercial screening is performed in closed circuit, particularly in crushing and grinding operations. Since these are continuous processes the oversize from the screen is returned continuously for re-crushing. In so doing the original character of the feed changes and results in an altered feed size distribution and change in bulk density. Therefore, the screen size to be used has to be reassessed under the new conditions. The methodology of screen selection however remains the same.

11.7. Problems

11.1
A 5 mm square aperture single deck screen woven with 1.0 mm uniform diameter stainless steel wire was used to classify a crushed and dried mineral having the following sieve analysis:

Size mm	mass% retained	Size mm	mass% retained
15	7	2.5	11.3
10	12.8	1	7.5
7.5	16.2	0.5	3.7
5	23.6	0	2.5
3.75	15.4		

The bulk density of the mineral was 1.5 t/m^3 and the feed rate required was 100 t/h. Estimate:

1. The area of screen
2. The size of screen for effective screening
3. If the screen had two decks estimate the area of each.

11.2
Iron ore of bulk density 2080 kg/m^3 containing 5% moisture by volume had the following screen analysis:

Size, mm	Cum mass % Passing
50	100
25	95
12.5	90
6.3	75
3.0	35

The ore had to be screened at the rate of 180 t/h through a 12.5 mm screen. The clamps and strips holding down the screen occupied 12 % of the screen surface. Determine:

1. The effective area of the screen,
2. The bed height to be maintained,
3. The flow rate at 20° inclination of screen.

11.3
A gold ore was crushed in a secondary crusher and screened dry on an 1180 micron square aperture screen. The screen was constructed with 0.12 mm diameter uniform stainless steel wire. The size analysis of the feed, oversize and undersize streams are given in the following table. The gold content in the feed, undersize and oversize streams were; 5 ppm, 1.5 ppm and 7 ppm respectively. Calculate:

1. The mass ratios of the oversize and undersize to the feed,
2. Overall efficiency of the screen,
3. Distribution of gold in the oversize and undersize streams.

Size	Cum mass % Retained		
micron	Undersize	Feed	Oversize
3350	0	0	0
2360	4.0	7.8	20.0
1700	10.0	42.0	68.2
1180	63.4	78.9	86.7
850	84.0	89.4	94.2
600	94.0	99.0	97.2
425	96.0	100	98.0
212	100		100

11.4

Iron ore with a moisture content of 6% was fed to a screen at the rate of 200 t/h. The screen had a square opening of 12.5 mm made of uniform stainless steel wire. The size analysis of the feed was:

Size mm	Cum. Mass % Passing
38	100
25	96
12.5	84
6.3	39
3	16.6

Assume the bulk density of the ore is 1600 kg/m^3 and the screen length equals the width. Determine:

1. the size of the screen,
2. the screening efficiency if the feed rate was increased to 250 t/h,
3. the efficiency of screening when the depth of bed on the screen was increased by 10%.

11.5

A cassiterite ore (SG 7.0) was crushed in a jaw and cone crusher yielding a product whose average size was 25% greater than 16 mesh. The crushed ore was screened on a 16 mesh screen having a clear opening of 1 mm (wire diameter 0.59 mm) inclined at 20° to the horizontal. Calculate:

1. the screen area required for a feed rate of 60 t/h,
2. the change in feed rate if the slope was reduced to a horizontal position, but maintaining the same efficiency,
3. the percent of fine material in the undersize product when the efficiency was 80%.

Assume a bed porosity of 40%.

11.6
The effective length and width of a vibrating screen was 1.5 m and 10 m respectively. The screen was made of wire 10 mm in diameter with an open area of 70 %. The feed size of a mineral to be screened was 48% oversize and 30% less than half the aperture of the screen. The speed of travel of the material over the screen was 15 m/min and the feed rate 50 t/h. The bulk density of the material was 1.8 t/m^3. Estimate:

1. The depth of the material on the screen,
2. Comment on the suitability of the screen if the feed rate was increased to 120 t/h.

11.7
A vertical shaft furnace was designed to operate on a coke size of 60 x 30 mm. Coke from a coke oven, after preliminary crushing in a hammer mill, gave the following size analysis:

Size, mm	Mass % retained
−100 + 85	14
−85 + 42.5	31
−42.5+25	22
−25 + 18	8
−18 + 15	3
−15 + 7.5	8
−7.5	14

The coke was screened over a single-decked screen with circular holes, inclined at an angle of 25 degrees. The moisture content of the coke was 4%. The feed rate to the shaft furnace was 759 t/day. The maximum permissible bed depth on the screen was 100 mm. Assume that the screen length equals 1.2 times the width, screen open area is 40%, the density of coke is 600 kg/m^3, the bed porosity was 40% and the screen efficiency was 40%. Determine:

1. the capacity of the screen,
2. the effective screen area,
3. the travel rate of material over the screen.

11.8
The oversize from a 12.5 mm aperture screen was fed to a crusher. The efficiency of the screen was 80%. The product size from the crusher was 80% minus 12.5 mm at a close set of 12.5 mm and was returned to the screen for sizing. The initial feed to the screen was 120 t/h and the screen undersize was also 120 t/h at steady state. Estimate the recirculating load on the screen

11.9
The feed to a 3 deck screen gave the following analysis:

Feed size, mm	Cum. mass percent passing
75	100
50	90
36	70
24	33
12	15
6	10
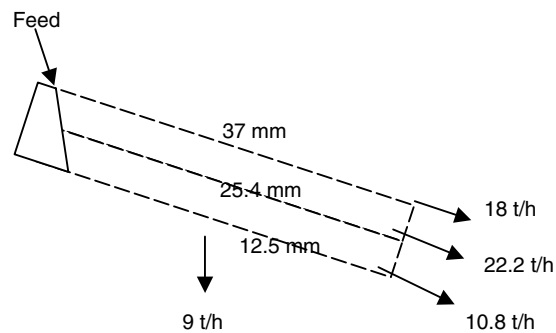
The screen was fed at the rate of 60 t/h. The screen opening and the product rate from each deck is given above.

Determine the minimum area of each screen and a suitable final screen size.

11.10
A sieve analysis of a silicious gravel containing 5% moisture is given below.

The ore was to be screened at 6 mm using a single deck square opening screen having a 42 % open area. The bulk density of the ore was 3.2 t/m^3. Assuming the length/width ratio is 1.5, estimate the area of the screen.

Feed size, mm	Mass % retaiined
25	25
12.5	30
6	32
3	10
0	3

REFERENCES

[1]   K.G. Colman and W.S. Tyler, in Mineral Processing and Plant Design, A.L. Mular and R.B. Bhappu (eds), SME/AIME, 1980, pp. 341-361.

[2]   C.W. Matthews, in SME Mineral Processing Handbook, N.L.Weiss (ed), SME/AIME, 1985, pp. 3E 1-13.

[3]   Metso 2002, Basics in Mineral Processing, 1st Edition, Metso Minerals.

[4]   Deks Thyer, Profit from Deks Thyer Polyurethane Screen Cloths, brochure, Deks Thyer.

[5]   A.F. Taggart, Handbook of Mineral Dressing, John Wiley, New York, 1953.

[6]   F. J. Fontein, American Institute of Chemical Engineers-Institution of Chemical Engineers, London, 1965, pp. 1:123-130.

[7]   P.L. Stavenger, in Mineral Processing Handbook, N.L.Weiss (ed), SME/AIME, 1985, pp. 3E 19-25.

[8]   D.G. Osborne, Solid –Liquid Separations, L. Svarovsky (ed), Butterworths, London, 1977, pp. 149-169.

[9]   A.M. Gaudin, Principles of Mineral Dressing, McGraw-Hill, 1939.

[10] S. Miwa, Chemical Engineering, Japan, 24 (1960) 150.

[11] J.W. Leonard, Determination of Industrial Screen Efficiency, Trans. SME/AIME,. 256 , No. 3, 1974 pp. 185-187.

[12] K. F. Tromp, Collier Guardian, May 21 (1937) 28.

[13] F.F. Peng, A.D. Walters, M.R. Geer and J.W. Leonard, in Coal Preparation, J.W. Leonard, (ed), AIME, 1979. pp. 18- 1-101.

[14] E.G. Kelly and D.J. Spottiswood, Introduction to Mineral Processing, Mineral Engineering Services. 1989.

[15] K.G. Colman, in Mineral Processing Handbook, N.L.Weiss (ed), SME/AIME, 1985 pp. 3E 13-19.

[16] S.E. Gluck, Chemical Engineering, 72 (1965) 179.

[17] Cedarapids, Pocket Reference Book, Cedarapids Inc.

[18] Nordberg, Reference Manual, 3rd Edition, Nordberg Inc. 1992.

[19] Jacques, Retrieved: August 31, 2004, from http://www.terexjaques.com/screens.htm

[20] G. Ferarra, and U. Preti, Proceedings, XI International Mineral Processing Congress, Cagliara, 1975, pp. 183-217.

[21] G. Ferarra, and U. Preti and G.D. Schena, International J. of Mineral Processing, 22 (1988) 193.

[22] G.K.N.S. Subasinghe, W. Schaap and E.G. Kelly, International J. Mineral Processing, 28 (1990) 289.

[23] T.J. Napier-Munn, S. Morrell, R. Morrison and T. Kojovic, Mineral Comminution Circuits Their Operation and Optimisation, JKMRC, 1996.

[24] A.J. Lynch, Mineral crushing and grinding circuits, their simulation, optimisation, design and control, Elsevier Scientific Publishing Company, Amsterdam. 1977.

Chapter 12. Classification

12. INTRODUCTION

After initial liberation of a mineral constituent from its ore by crushing, grinding and screening, separation of minerals by size are normally attempted by a classifying process. In mineral processing operations, classification and separation of mixtures of fine and coarse particles and also of lighter and heavier particles may be performed in a wet or dry state. The majority of separations are carried out in a liquid environment because of an increased efficiency. The basic technique employed is to allow particles to settle under gravity in a liquid medium (usually water). The higher terminal velocity of irregular shaped, coarser, heavier particles allows these particles to reach the bottom of the vessel at a faster rate compared to particles that are smaller and lighter. Removing the settled particles while the others are still settling offers a simple means of a separation. For very small particles, like clay or silt, whose size approaches colloidal dimensions, long times are required to settle and the small difference in settling rates of these fine particles leads to low separation efficiency. To accelerate the settling rate of these fine particles, centrifugal forces are employed such as in cyclones or hydrocyclones.

In this chapter we shall confine ourselves to the design and operation of the common types of classifiers, namely those that depend on gravity forces alone and those that employ a combination of gravity and centrifugal forces.

12.1. Design Features of Mechanical Classifiers

The design of mechanical classifiers includes a settling tank and a mechanism to remove the settled solids from the bottom of the tank. The settled solids are usually conveyed away by some discharge system while the overflow is collected in launders and pumped away. The classifier designs differ mainly in the mode of removing the underflow and the overflow slurries. Immersed spiral or rakes are generally used for underflow slurries and an open launder carries the overflow. Fig. 12.1 is a sketch of a spiral classifier where the spiral conveyor is installed within the bowl. The spiral operates along the sloping sides of the tank and dredges the thick sludge out of the tank Fig. 12.2 shows the spiral conveyor replaced by a rake, which drags the sand up the incline for discharge.

Fig. 12.3 shows a submerged rotating rake inside a conical bowl, which collects the settled sand in a well from which it is conveyed or pumped away. Classifiers are either rectangular or circular in shape with the bottom inclined at an angle. The circular tanks are more common.

12.1.1. Spiral classifiers

The shape of the spiral classifier tanks is usually rectangular (Fig. 12.1). The feed is introduced at a position about halfway along the length of the settling tank. The tank slopes range from $14°$ to $18°$. The slope is adjusted such that the top end is higher than the height of the overflow weir. The spirals impede the downward slurry movement resulting in some build up. The sides are therefore raised. Classifiers with raised sides are generally called high or *H-type* classifiers. In contrast, classifiers with low sides and shallow tanks are known as
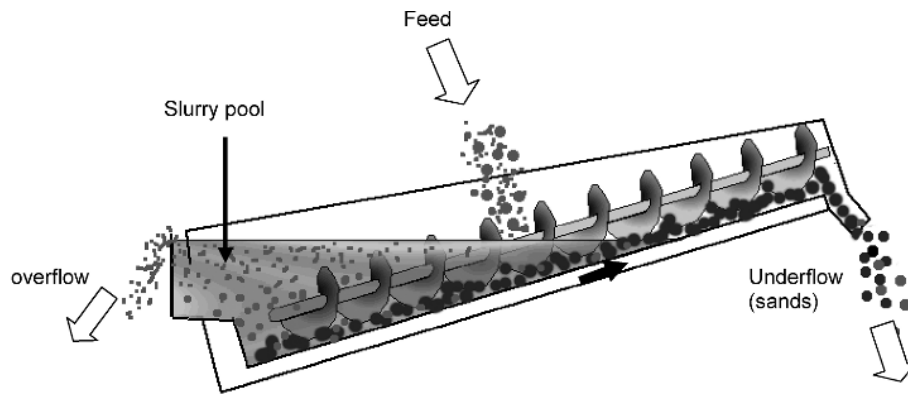
Fig. 12.1. Sketch of a spiral classifier.
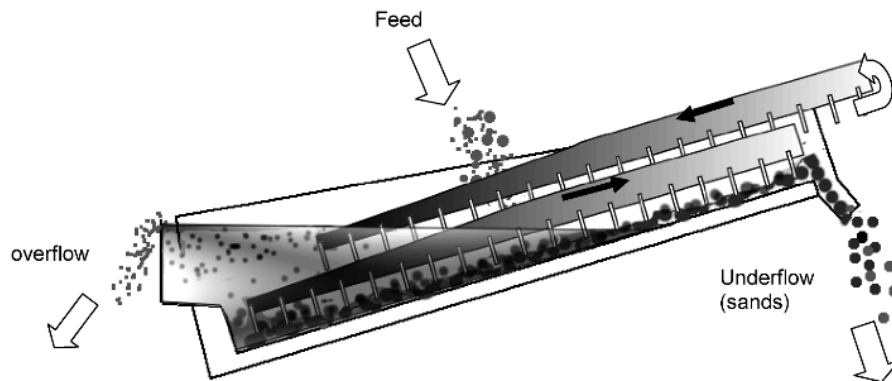
Fig. 12.2. Sketch of a rake classifier.
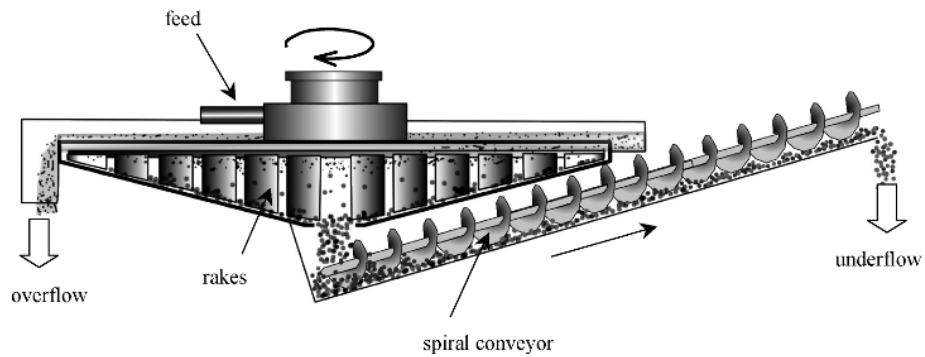
Fig. 12.3. Sketch of a Bowl Classifier with spiral conveyor for collecting sand from the tank and discharging to the launder at the top end of the vessel.

356

S-type classifiers. The S type classifiers have almost gone out of use. The maximum lengths of H type classifiers are about 14 m with widths of 0.5 to 7 m and spirals up to 2400 mm in diameter. The speed of rotation of the spirals varies inversely with size. Thus classifiers with a 300 mm spiral diameter revolve at about 8-20 rpm while the 2000 mm diameter spirals rotate at about 2-5 rpm to give a sand conveying speed of 2-3.5 m/s. The raking capacity of the large classifiers is approximately 200 t/h while smaller classifiers have raking capacities as low as 1.5 t/h. To some extent the capacities depend on the number and design of the helix in the spiral. The helix could be single, double or even triple pitch. The pitch is related to the diameter of the spirals. It is generally of the order of 0.5 to 0.75 times the diameter of the shaft. The number of helix may be single (simplex) or two side by side (duplex) depending on the dimensions of the tank.

Some spiral classifiers have flared sides. This increases the capacity. For example, in a simplex type H classifier, the capacity is increased 1.3 times and for a duplex type H classifier, the capacity may be increased 2-3 times.

The feed size of particles to spiral classifiers is in the region of 150 microns and coarser. The overflow particle size distribution depends both on the height of the weir and a baffle placed before the weir. The baffle is placed within the tank and located at a distance of approximately 38 mm (maximum about 380 mm) from the weir. The flow rate of the overflow stream ranges from 1 t/h to around 40-45 t/h. Increasing the feed flowrate increases the overflow rate, decreases the residence time and increases the fraction of coarse particle sizes in the overflow stream. A slow feed rate, well spread out along the width, is preferred for finer feeds to eliminate or reduce the presence of coarser sizes in the overflow stream.

12.1.2. Rake classifiers
When rakes are used in place of spirals, the classifiers are called Rake classifiers. These are less common than spiral classifiers. The rakes consist of one or more parallel lines of steel plates that hang from a central shaft or shafts. The plates are hinged on to these shafts and have a reciprocating movement. As in spirals, the plates agitate the settling solids and drag the settled particles up the inclined base of the tank. At the end of the stroke the plates rise sharply and then are lowered back into the tank after an eccentric movement to its original position. On repeating the operation the settled matter is conveyed up the inclined slope and finally discharged into the sands launder. The overflow stream passes over a weir at the bottom end of the tank and pumped to the next processing stage.

Typical sizes and stream characteristics of rake classifiers are summarised in Table 12.1 and Table 12.2.

Table 12.1
Rake Classifier summary [1].

Description	Dimensions	
	Min.	Max.
Size	1.2 m	4.8 m
Tank slope	9.4°	11.7°
Rake speed	5 strokes/min	30 strokes/min
Capacity	20 t/day/m-width-stroke	-
Power	7.6 kWh	15.2 kWh

Table 12.2
Stream Characteristics of Classifiers [1].

Streams	% Solids, mass
Feed	65 (max.)
Overflow	1-35
Underflow	75-83

However, the larger industrial sized rake classifier tanks are around 3.7 m to 12 m in length and 4.5 m to 5 m in width.

12.1.3. Cone classifiers

The cone classifier is the simplest of all of the classifiers, however its use in industry is relatively limited. The classifier vessel is conical in shape. The feed enters the vessel (Fig. 12.3) through a centrally located inlet pipe. Initially the bottom spigot is closed. When the slurry reaches a certain height, the spigot is opened. The settled particles then discharge through the spigot. The finer particles travel with the water to the periphery and overflow into a launder.

The mechanism of settling in cone classifiers was described by Kojovic and Whiten [2] as the settling of coarse particles against an upward flowing overflow stream. The mechanics of settling depended on:

1. Particle size, d
2. Velocity of slurry in the cone section, v
3. Overflow volume fraction of solids,
4. Underflow and overflow pulp densities, and
5. Viscosity of the slurry, μ_{SL}

In the ideal case, where the particles are considered as perfect spheres and the medium through which they fall as infinite with no wall effect, Stokes Law describes the terminal velocity of the particles as:

$$v_T = \frac{d^2 \, g(\rho_S - \rho_F)}{18\mu} \tag{12.1}$$

where v_T = terminal velocity
ρ_S, ρ_F = density of solid and fluid (liquid or gas)
g = acceleration due to gravity
d = particle diameter (sphere)
μ = viscosity of the fluid (liquid or gas)

The free fall of the particles depend on the Reynolds number, Re, and the Froude number, Fr. Using these dimensionless numbers, a quantitative estimation of the separation of irregularly shaped particles of different sizes can be obtained. According to Kojovic and Whiten [2] for a cone of vertical height H and apex diameter D_U (Fig. 12.4), the dimensionless groups, Re and Fr, in the cone section and apex sections are:

Reynolds number, Cone section, $\mathrm{Re_C} = \dfrac{2\,\rho_{SL}\,v\,H}{\mu}$ (12.2)

Froude number, Cone section, $\mathrm{Fr_C} = \left[\dfrac{\rho_{SL}}{(\rho_S - \rho_{SL})}\right]\dfrac{v^2}{gH}$ (12.3)

Reynolds number, apex section, $Re_A = 2D_U\sqrt{gH}\,\rho_{SL}$ (12.4)

Using these dimensionless numbers Kojovic and Whiten derived the underflow solids concentration, $C_{S(U)}$, and the 50% size split (d_{50C}) for cone classifiers as:

$$C_{S(U)} = \dfrac{8.56\,\exp(2.38\,V_{S(F)})\,\mathrm{Fr_C}^{0.07}\,\mathrm{Re_A}^{0.17}\left[\dfrac{d_{80}}{H}\right]^{0.10}}{\mathrm{Re_C}^{0.09}\left[\dfrac{A_U}{A_C}\right]^{0.24}} \quad \text{and}$$ (12.5)

$$d_{50C} = \dfrac{\exp(7.02 V_{S(O)})\,\mathrm{Fr_C}^{0.28}\left(\dfrac{d_{80}}{H}\right)^{0.53}}{\exp(7.05(V_{S(F)} - V_{S(O)}))\,\mathrm{Re_C}^{0.33}\left(\dfrac{A_U}{A_C}\right)^{0.48}} \cdot 2H$$ (12.6)
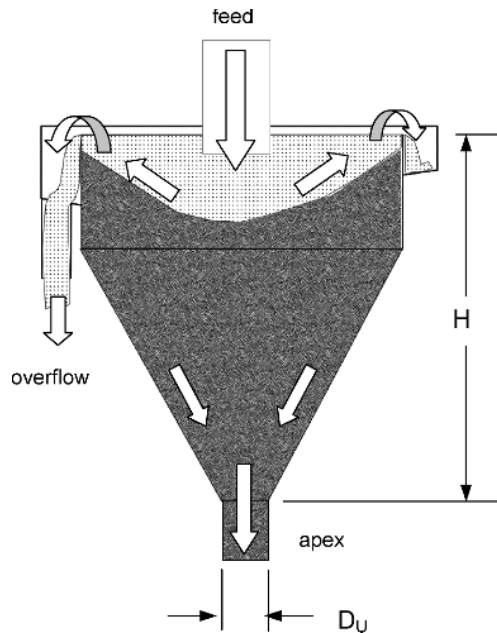
Fig. 12.4. Cone classifier.

where $V_{S(F)}$ = volume fraction of solids in the feed
$V_{S(O)}$ = volume fraction of solids in the overflow
Fr_C = Froude number, cone section
Re_A = Reynolds number, apex section
Re_C = Reynolds number, cone section
A_U = cross sectional area of the apex (underflow)
A_C = cross sectional area of the cone
d_{80} = particle 80% passing size of the feed

Kojovic and Whiten suggest that both Eqs. (12.5) and (12.6) are applicable for industrial cone classifiers having diameters between 0.073 m and 3 m and feed rates of 1.2 to 5000 L/min.

12.1.4. Bowl classifiers

The bowl classifiers are similar to cone classifiers except that a bowl with relatively shallow sides replaces the deep cone. The feed, in the form of slurry, enters the bowl through a centrally located pipe. The slurry in the bowl is gently agitated by rotating immersed rakes. The relatively heavy particles settle to the bottom of the bowl, which slopes towards the centre of the tank. The settled particles are collected by the submerged rakes and guided to the discharge end by a conveyor for dispatching as the underflow fraction.

The maximum diameter of industrial size bowl classifiers is around 7.8 m. and minimum around 1.2 m. In some bowl classifiers vibrating plates operate just under the surface of the slurry to help break up agglomerated particles. The present tendency is to replace the rakes with vibrating plates.

12.2. Designing the Pool Area of Mechanical Classifiers

In practice the effective area of the bowl appears smaller than the actual bowl size. This is also true for spiral and rake classifiers. The ratio of the effective area to the actual area is known as the *areal efficiency*. Fitch and Roberts [3] have determined the areal efficiencies factors of different classifiers as shown in Table 12.3.

Table 12.3
Areal efficiency of pool classifiers [3]

Classifier	Areal efficiency factor	
	Minimum	Maximum
Rake	0.2	0.6
Spiral	0.2	0.6
Bowl	0.4	0.6

The percent areal efficiency is affected by the speed of the rake. For submerged rakes, Hitzrot and Meisel [1] determined the relation between the stroke rate and areal efficiency. Their relation is reproduced in Fig. 12.5 where it can be seen that the areal efficiency decreases with increasing stroke rate and therefore with agitation.

For designing the pool area of a classifier, the concept of areal efficiency is necessary. Also it is necessary to estimate the settling forces, the size of the overflow particles, the
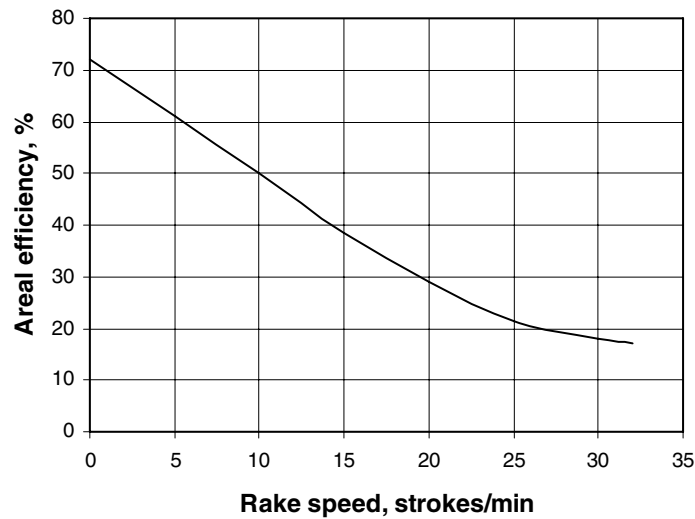
Fig. 12.5. Effect of rake speed on areal efficiency [1].

volume flow rate of the overflow or underflow stream and the settling rate of the heavier particles. The settling rate in turn depends on the shape of the particles and any disturbance in the pool. Roberts and Fitch [4] and Fitch and Roberts [3] considered these factors and stated that the product of these factors determined the settling rate. In the case of spherical particles, the settling rate is given by:

$$\text{Settling rate} = v_S \, H \, P_S \, A_{EF} \tag{12.7}$$

where v_S = the settling rate of spherical particles at infinite dilution (no hinderance)
 H = the hindrance factor
 P_S = the shape factor and
 A_{EF} = the areal efficiency factor included to account for a decrease is settling rate resulting from turbulence or contact with other particles in the pool.

To determine the pool area A, it is assumed that the settling rate was related to the volume of water passing over the weir. The quantity of overflow liquid (water) passing over the weir in unit time will be:

$$Q_{VL(O)} = v_S \, A \, H \, P_S \, A_{EFF}$$

or $$A = \frac{Q_{VL(O)}}{v_S \, H \, P_S \, A_{EFF}} \tag{12.8}$$

To apply Eq. (12.8) to non-spherical particles Fitch and Roberts [3] considered v_S as the settling rate of spheres under ideal conditions, (that is an infinite, undisturbed volume of

water) and the shape factor, P_S, as the deviation of the particle shape from a sphere. The values of each parameter were determined in the following manner:

1.   Estimation of v_S:
Under ideal conditions of settling, the terminal velocity, v_T, is given by:

$$v_T = \left(g\left(\frac{\rho_S - \rho_L}{\rho_L}\right)\left(\frac{\mu}{\rho_L}\right) \right)^{\frac{1}{3}} \quad m/s \qquad (12.9)$$

where ρ_S = density of solids, kg/m^3,
       ρ_l = density of liquid, kg/m^3,
       μ = viscosity of liquid, Pa.s,
       g = acceleration due to gravity, $9.81 m/s^2$.

While the ideal settling velocity is related to the dimensionless Reynolds number, for non-ideal system, Roberts and Fitch considered a reduced Reynolds number, Re_R, defining it as:

$$Re_R = \left(\frac{d_{50}\, v\, \rho_L}{\mu}\right) \qquad (12.10)$$

where d_{50} = the size of separation

For different values of reduced Reynolds number the values of the dimensionless term v_S/v can be determined. Such a plot is reproduced in Fig. 12.6 for Reynolds numbers varying between 1 and 1000. In practice the value of Re_R is estimated and the value of v_S/v determined from Fig. 12.6. Then from a known value of v the value of v_S is determined.

2.   Estimation of the hindrance factor, H:
The estimation of the hindrance factor H for separation size d_{50}, also involves considerations of the ideal state of settling. Further it is assumed that:

1.   all coarse particles have been separate in the pool,
2.   the concentration of the finer particles ($<d_{50}$) remain unchanged, and
3.   a void fraction, ε, exists between the particles in the settling zone.

The void fraction ε was expressed as:

$$\varepsilon = \frac{1}{1 + (V_d / V_F)} \qquad (12.11)$$

where V_F = volume dilution in the feed, $(V_{L(F)}/V_{S(F)})$,
       V_d = volume fraction of solids finer than the d_{50} in the feed, $(V_{d50}/V_{S(F)})$,
       V_{d50} = volume of solids finer than the d_{50} in the feed,
       $V_{S(F)}, V_{L(F)}$ = volume of solids and liquid respectively in the feed.
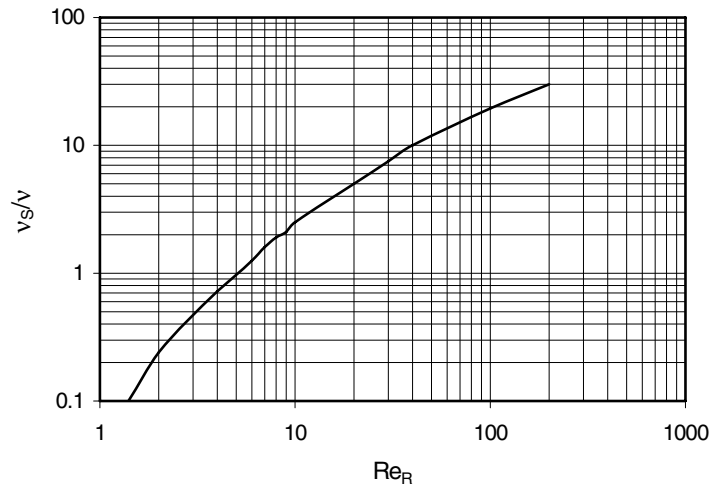
Fig. 12.6. Relation between reduced Reynolds number, Re_R and dimensionless v_S/v [3].

$$\text{or} \qquad \varepsilon = \frac{V_{L(F)}}{V_{L(F)} + V_{d50}} \qquad\qquad (12.12)$$

The hindrance factor is defined by some power function of the void fraction, which in turn is related to Reynolds number and particle shape. Mathematically this is written as:

$$H = \varepsilon^{f(Re, P_s)} \qquad\qquad (12.13)$$

For different values of Reynolds number and shape factors (see Table 12.4), the function $f(Re, P_S)$ can be calculated and plotted. Such a plot is shown in Fig. 12.7 using data from the work of Fitch and Roberts [3]. Thus for different values of ε, obtained from Eq. (12.12), the hindrance factor, H, can be estimated.

3.   Estimation of shape factors:
The shape factors of selected minerals are given in Table 12.4.

Table 12.4
Typical shape factors of selected minerals [3].

Particles	Shape factor
spheres	1.0
cubes	0.93
sand	0.9
crushed galena	0.7
crushed dolomite/pyrite	0.67
crushed quartz	0.5
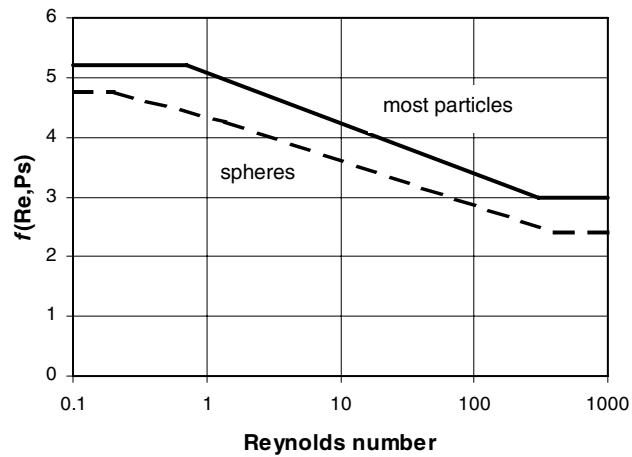
Fig. 12.7. Relation between Reynolds number and the function f(Re,P$_s$) [3].

Eq. (12.8) can be now be used to compute the pool area for a given volume of overflow, $Q_{VL(O)}$. Example 12.1 illustrates the method of sizing pool area of gravity settling classifiers.

Example 12.1

A slurry containing 50% solids (quartz) is to be classified at a rate of 100 tph at a separation size of 250 microns in a rake classifier. The density of the solids is 2650 kg/m^3 and the size analysis given in the table below. The water recovery to the overflow is 95% at an areal efficiency of 0.5. Estimate the pool area.

Particle size, microns	710	355	180	90	45	-45
Cum. Mass % retained	10	25	45	60	75	100

Data: Viscosity of water equals 0.001 Pa.s, density of water, 1000 kg/m^3 and density of solid, 2650 kg/m^3.

Solution

Step 1
To determine the pool area, use Eq. (12.8) and determine each parameter.

The velocity parameter can be determined using Eq. (12.9). Substituting data we have: the velocity parameter v as:

$$v = \left[9.81 \left(\frac{2650 - 1000}{1000} \right) \left(\frac{0.001}{1000} \right) \right]^{1/3} = 0.0253 \ \text{m/s}$$

Step 2

The reduced Reynolds number, Re_R, is obtained by using Eq. (12.10).

$$Re_R = \left[\frac{0.00025 \times 0.0253 \times 1000}{0.001} \right] = 6.325$$

From Fig. 12.6 at a Re_R value of 6.325, the value of $\frac{v_S}{v_T} = 1.4$,

that is, $v_S = 1.4 \, v_T = 1.4 \times 0.0253 = 0.0354$ m/s

Step 3

Feed volume dilution, $V_F = \dfrac{(100 - \% \text{solid in feed}) \rho_S}{(\% \text{solid in feed}) \rho_L} = \dfrac{(100 - 50) \, 2650}{50 \times 1000} = 2.65$

From the data, the feed solid is 65% minus 250 microns. That is, the mass fraction of solids less than the separation size is = 0.65 which is also the volume fraction assuming that all solids have the same density.

Step 4

Next the void fraction, ε, is determined by using Eq. (12.11). Substituting values:

$$\varepsilon = \frac{1}{\left(1 + (0.65/2.65) \right)} = 0.803$$

Step 5

To determine the hindrance factor H, the Reynolds number has to be estimated.

From data: Reynolds number = $Re_R \cdot (v_S/v) = 6.325 \times 1.4 = 8.86$, and from Fig. 12.7 the corresponding exponent $f(Re_R, P_S) = 4.3$.

Substituting these in equation in Eq. (12.11) we have:

$$H = 0.803^{4.3} = 0.389$$

Step 6

As the suspension is quartz, its shape factor can be taken as 0.5 (Table 12.4).

We may now substitute the values of v_S, H, P_S and A_{EFF} in Eq. (12.8) to determine area A if $Q_{VL(O)}$ is known. Otherwise:

$$\frac{Q_{VL(O)}}{A} = v_S \, H \, P_S \, A_{EFF} = 0.0354 \times 0.389 \times 0.5 \times 0.5 = 0.0034 \quad \text{m}^3/\text{s/m}^2$$

Step 7
From the available data,
Water in the feed = 100 x (100 - %solids)/% solids = 100 x (100 – 50)/50 = 100 t/h
Water in the overflow = 100 x 0.95 = 95 t/h = 95,000 kg/h
$(Q_{VL(O)})$ = 95000/1000 = 95 m³/h = 0.0264 m³/s

Thus, the classifier area, A = 0.0264/0.0034 = 7.76 m²/100 t/h feed
= 7.76/100 = 0.077 m²/t/h

Also, the solids in the overflow = 100 x 0.65 = 65 t/h

And hence the % solids in the overflow = 65 x 100/(65 + 95) = 40.6%

12.3. Design Features of Centrifugal Classifiers

12.3.1. Hydrocyclone classifiers

Rapid settling and classification is achieved by increasing the force acting on the particles by replacing the gravitational force by centrifugal forces. Several types of equipment based on this principle are used for the purpose, like the hydrocyclone, Dyna Whirlpool and basket centrifuges. The hydrocyclone is the simplest and is the only one discussed here. The hydrocyclone has no moving parts and is the easiest to operate. Fig. 12.8 is a sketch of a typical hydrocyclone. The feed entry is either tangential to the centre line of entry or forms an involuted entry. The cross-section of the entry pipe is usually circular, oval or rectangular; each of which provide a different velocity profile inside the feed chamber and the cyclone cone. The top of the feed chamber is closed with a plate through which a pipe known as a vortex finder passes. The bottom of the vortex finder protrudes below the feed chamber. Below the feed chamber the body of a cyclone is shaped like an inverted cone, which converges to a smaller cone, which serves as the outlet of the coarser size fractions in the feed. The feed chamber and the cones are lined inside with rubber or synthetic linings due to abrasive nature of most metallurgical slurries. The lining material is hard rubber, neoprene or urethane. In some cases, the protective lining is sprayed inside forming a hard monolithic bond with the base metal. The apex is sometimes fitted with a concentric, hardwearing synthetic rubber inner sleeve, which can be squeezed hydraulically or pneumatically to alter the diameter of the opening.

Hydrocyclones are occasionally provided with nozzles just above the apex for injecting water to compensate for water loss and loss of fines [5]. However constant effort is made to improve on the design, aimed at improvement of the flow dynamics of the slurry inside the cyclone.

Krebs [6] has introduced the *Spintop* hydrocyclones with circular inlet forming a well defined involute feed entrance, parabolic body to provide a smooth transition between the cylindrical and conical sections, bell shaped vortex finder increases rotational acceleration to give a sharper separation and solid centre core in the vortex finder to replace the air core, stablising the rotational flow [7]. For coarse size separation the "Flat bottom cyclones" has been introduced [8]. The fully flat bottom instead of a conical section increases the separation size by a factor of 2. The flat bottom hydrocyclone produces a very clean underflow by
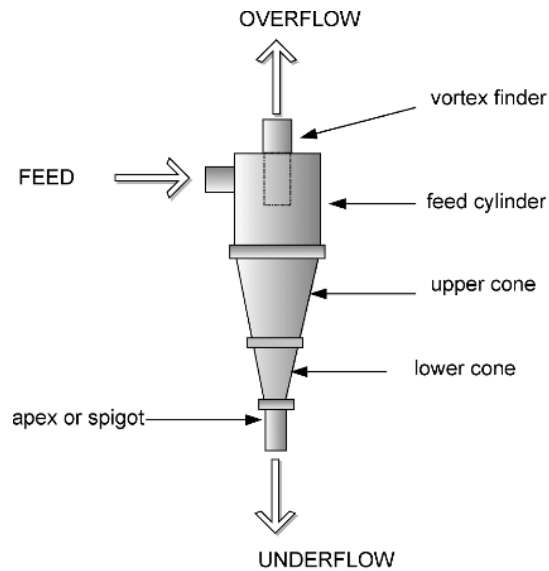
Fig. 12.8. Schematic diagram of an hydrocyclone.
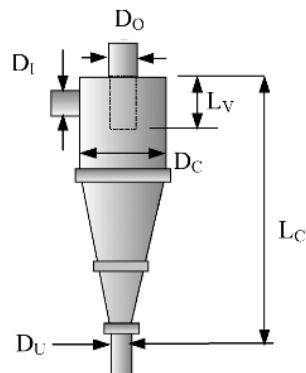
Fig. 12.9. Nomenclature of the hydrocyclone parts.

forcing a large amount of coarse and fine solids to the overflow. Cyclones with 90-degree cone angles are also available.

The actual dimensions of most models for metallurgical operations have been derived from experimental results. Suggested relations between design variables are given in Tables 12.5 and 12.6. Experience has shown that the dimensions of an hydrocyclone acting as a classifier and a dewatering tool are slightly different. These differences are also indicated in Table 12.5.

Popularly used symbols for describing different parts of an hydrocyclone are shown in Fig. 12.9 and used in the tables.

Table 12.5.
Dimensions of Hydrocyclones [9,10].

Hydrocyclone (Dewatering)	Hydrocyclone (Classifier)
Inlet diameter $D_I = D_C/4$	Inlet diameter $D_I = D_C/7$
Vortex finder diameter, $D_O = D_C/3$	Vortex finder diameter, $D_O = D_C/5$
Length or height, $L_C = 5 D_C$	Diameter of underflow $= D_C/15$
Length of vortex finder, $L_V = 0.4 D_C$	Length of vortex finder, $L_V = 0.4 D_C$
	Length of cyclone $= 3 D_C$

Table 12.6
Standard cyclone as defined by different authors.

Cyclone Parameters	Mular and Jull [11]	Arterburn [12]
Cross-sectional area of feed pipe at point of entry	6-8% of the cross-sectional area of the feed chamber	$(0.015-0.02)\,\pi\, D_C^2$
Vortex finder diameter, D_O	35-40% of D_C	$0.35\, D_C$
Cone Angle	$12°$ for $D_C < 250$ mm	$12°$ for $D_C < 250$ mm
	$20°$ for $D_C > 250$ mm	$20°$ for $D_C > 250$ mm
Apex diameter	$> 0.25\, D_O$	$> 0.10\, D_O$

However, as a general rule:

1. the inlet cross sectional area is roughly 70% of the cross sectional area of the feed chamber,
2. the diameter of the vortex finder is about 25-40% of the cyclone diameter, and
3. the diameter of the apex is 25% of the vortex finder.

The apex diameter is selected to discharge the maximum possible density of slurry, avoiding the roping condition of the discharge stream.

Tarr [13] presented graphical relationships between the cyclone dimensions for optimum operating conditions. These relationships are shown in Figs. 12.10 and 12.11.

Presently the largest hydrocyclone in use has a diameter of 2.3 m (90 inch) and the least cone angle about $10.5°$ in contrast to the usual cone angles of $20°$ [14]. The lower cone angle produces a finer separation.

The following general observations can be made for designing:

1. Rectangular sections of the inlet is probably better than other sections.
2. Increased inlet area permits increased input and therefore imparts increased tangential velocity to the slurry inside the cyclone.
3. Larger diameter cyclones are more suitable for coarse size separations as acceleration in the feed chamber is less. (Mular and Jull, [11] suggest that the acceleration of slurries in similar but small diameter cyclone could be 40 times less).

368
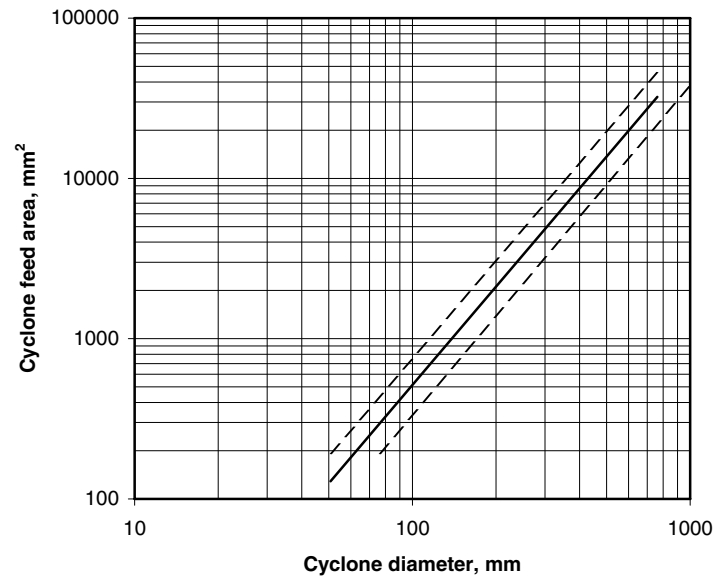
Fig. 12.10. Approximate relationship between cyclone diameter and feed inlet [13].
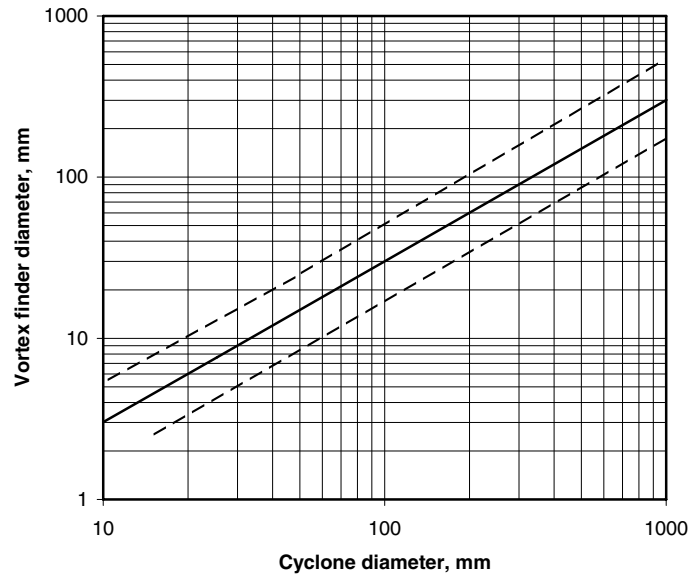
Fig. 12.11. Approximate relationship between cyclone diameter and vortex finder diameter [13].

4. Longer cylindrical sections tend to yield high underflow recoveries.
5. Shorter cylindrical sections yield coarse separations [15].
6. Smaller cone angles are suitable for finer separations.
7. Larger cone angles are suitable for producing sharper and coarser separations.
8. Apex diameter should have the flexibility so that it may be adjusted and be just larger than that at which roping occurs. [*Roping is a condition of discharge through the apex when the discharge slurry appears like rope and is not flared or spread out*].
9. If the pressure drop is greater than 70 kPa the ratio (D_O/D_U) should be less than 3.5-4.0. If greater than this then the air core diameter will be greater than the apex leading to unstable and inefficient operation [13,15].

12.4. Operation of Mechanical Classifiers

The feed to the mechanical classifier with a rectangular cross-section is spread along the width and is usually directed towards the top end. On entry, the solids in the slurry commence to settle, the coarser and denser particles settling at a faster rate than the others. Particles settling to the bottom form a layer (region *5* in Fig. 12.12), which is least disturbed by the blades of the rakes or spirals and possibly serves to protect the base of the tank. Region *4* is the zone of moving sands dragged into the underflow by the raking mechanism. Above the bottom layers is the zone marked *3* in Fig. 12.12 where hindered settling occurs. A continuously changing concentration gradient is set up in this layer, the upper portion being least concentrated and the lower end having the maximum concentration of particles. The mechanical rakes or spirals continuously stir this zone, breaking up agglomerated particles and generally accelerating the separation process. The layer marked zone *2* is where maximum agitation takes place, the lighter and smaller particles are separated here where they join with the overflow stream and are carried over to the overflow launder. The heavier particles settle by gravity to zone *3* forming the thick bottom layer. The surface of the top layer *1* is at the same level as the weir allowing the light particles to flow over to the overflow launder.

Separation of solids in classifiers has been the study of workers like Fitch [16], Stewart and Restarick [17], Reid [18], Schubert and Neesse [19] and Fitch and Roberts [3]. While Stewart and Restarick recognised four zones, others like Schubert and Neesse considered that the slurry was divided into two layers at a particular height and diffusion and sedimentation
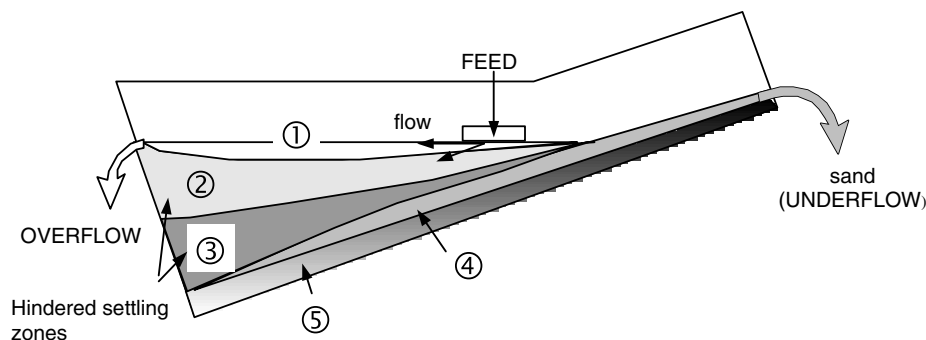
Fig. 12.12. Slurry movement and zones of particle separations in an operating classifier.

velocities were significant at this level. Reid [18] also considered particle movement as two streams that travelled as plug flow with *intense radial mixing*. Reid proposed that the recovery R, of a size d_i was given by the expression:

$$R = 1 - e^{-0.6931 \left(\frac{d_i}{d_{50}} \right)^s}$$

(12.14)

where d_i = the mean of the size interval i in the sieve analysis of the feed.

Plitt [20] examined the equation and stated that the value of s varied from 1 to 3.8. Fitch and Roberts made a much simpler approach. They considered the mass balance of water in a classifier and expressed it as:

volume rate of water, $Q_{VL(F)}$ = volume rate of water, $Q_{VL(U)}$ + volume rate of water, $Q_{VL(O)}$
      in the feed   in the underflow   in the overflow

They also considered that:

1. the fraction of size of particles that travelled to the overflow depended on the settling velocity,
2. the settling rate was affected by turbulence,
3. the ratio of any size, d_i, to the settling rate of the separating particle will remain effectively constant.

Taking $Q_{VL(F)}$ and $Q_{VL(O)}$ as the volume rates of flow of feed and overflow water they derived an expression for the fraction of particles of size, d_i, that was removed and separated into the overflow, E_i, as:

$$E_i = \frac{Q_{VL(O)}}{Q_{VL(F)}} K \left[1 - F_i \right]$$

(12.15)

where F_i = the settling factor described as the ratio of the settling rates of particles of size d_i and d_{50} (the separation size)

       K = a factor taking into account the change in concentration of particles of size, d_i and is represented by the ratio of the volume fraction of size i in the overflow to size i in the feed. K is always greater than unity.

For gravity pool classifiers, Eq. (12.15) can be simplified to:

$$E = \frac{Q_{VL(O)}}{Q_{VL(F)}} \left[1 - F \right]$$

(12.16)

Fitch and Roberts determined the settling factors for different ratios of particle size d_i and d_{50} where d_i was the lower size of size interval i. The results obtained are indicated for four selected sizes in Fig. 12.13 where the x-axis is a root 2 series of numbers.
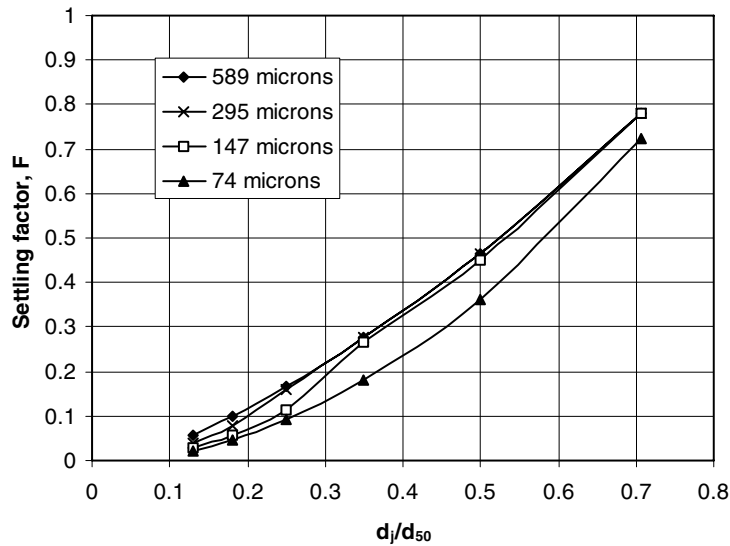
Fig. 12.13. Settling Factors of selected separation sizes (d_{50}) [3].

To determine E_i, it is necessary to know $Q_{VL(O)}$. It was suggested by Fitch and Roberts that $Q_{VL(O)}$ may be eliminated from the equation indirectly by using the water balance in the following manner.

The method is summarised below:

Let $Q_{MS(F)}$ =   the mass flowrate of solids in the feed stream of any size interval i,

   $Q_{MS(U)}$ =   the mass flowrate of solids in the underflow stream.

The mass balance of water may be written as:

$$Q_{VL(O)} = Q_{VL(F)} - Q_{VL(U)} \tag{12.17}$$

Substituting the value of $Q_{VL(O)}$ in Eq. (12.16):

$$E = \left[\frac{Q_{VL(F)} - Q_{VL(U)}}{Q_{VL(F)}} \right] (1 - F) \tag{12.18}$$

But, $E = \dfrac{Q_{MS(F)} - Q_{MS(U)}}{Q_{MS(F)}} = \left[\dfrac{Q_{VL(F)} - Q_{VL(U)}}{Q_{VL(F)}} \right] (1 - F) \tag{12.19}$

By substituting and simplifying, the mass of solids in the size interval in the underflow would be:

$$Q_{MS(U)} = F.Q_{MS(F)} + \frac{Q_{VW(U)}}{Q_{VW(F)}}\left[Q_{MS(F)} - F.Q_{MS(F)}\right] \qquad (12.20)$$

Experience has shown that about 51% of the void space in the underflow is occupied by slurry of the overflow stream consistency. Hence while estimating the characteristics of the underflow stream this factor has to be taken into account.

Examples 12.2 illustrates the method advocated by Fitch and Roberts [3] for computing the performance of a gravity classifier, like a Rake Classifier.

Example 12.2

A quartz slurry, made of 45% solids in water is fed to a rake classifier. The size distribution of the dry quartz is given in the table below. The classifier was commissioned to classify and cut at 500 microns. Estimate the underflow and overflow particle size distribution. The S.G. of quartz is 2.54 and the density of water is 1.0.

Feed size distribution of quartz

Particle Size, microns	Cum. mass % passing
4000	85
200	80
1000	62
600	52
300	45
150	25
75	10

Solution

A log-log plot of the size distribution is seen in the figure below.

To calculate the stream characteristics, consider each stream separately. For convenience, assume a feed rate of 100 mass units (g, kg or t). The procedure to follow is to determine the lower sieve size fraction of each size interval and then to determine the mass of solid in each size fraction of the feed. The calculations are illustrated in tabulated form for ease of understanding.

Step 1
In the table below:
Column 1   A root 2 series of numbers represented by the x-axis, d_i/d_{50}, in Fig. 12.13
Column 2   A root 2 series of screens based on the separation size as the top size (500 μm) obtained by multiplying column (1) by the separation size.
Column 3   Feed size distribution (cumulative % passing), obtained from the table or figure above.
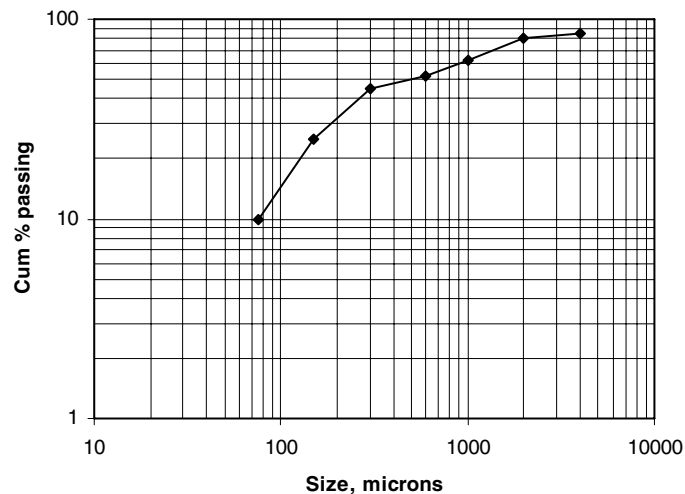
Size distribution of the feed quartz

Size i	$\sqrt{2}$ series	Sieve sizes	ΣP_i	R_i	F **	$M_{S(U)}$	$M_{S(O)}$	$M_{S(O)}$ %	Cum % O/F
	d_i/d_{50}	$(1)x500^*$		$(3)_i-(3)_{i+1}$		$(4)x(5)$	$(4)-(6)$	$\dfrac{(7)}{\Sigma(7)}$	$\Sigma(8)$
	(1)	(2)	(3)	(4)	(5)	(6)	(7)	(8)	(9)
	1	500	50	50	1	49.4	0.6	1.50	98.50
1	0.707	354	48	2.0	0.78	1.56	0.44	1.10	97.40
2	0.50	250	40	8.0	0.465	3.72	4.28	10.71	86.69
3	0.35	175	30	10.0	0.275	2.75	7.25	18.14	68.56
4	0.25	125	20	10.0	0.165	1.65	8.35	20.89	47.67
5	0.18	90	13	7.0	0.098	0.69	6.31	15.79	31.87
6	0.13	65	8.4	4.6	0.056	0.26	4.34	10.86	21.01
	0.00	0	0	8.4	0	0	8.40	21.01	
				$\Sigma100$		$\Sigma60.02$	$\Sigma39.98$	$\Sigma100$	

* lower end of the particle size in a size interval. ** take nearest sizes from Fig. 12.13.
ΣP_i – cumulative % passing; R_i – mass % retained; F – settling factor; $M_{S(U)}$ – mass settled; $M_{S(O)}$ – mass not settled; $M_{S(O)}$% - mass % overflow.

Column 4   The mass % retained (or actual mass, based on the 100 unit feed mass assumed) obtained by subtract the cumulative mass% in size fraction i from size fraction i+1, column (3).

Column 5   Take the settling factor, F, from the nearest size in Fig. 12.13.

Column 6   Multiply column (4) by column (5). This gives the mass distribution of particles that settles. For the separation size interval (top size), an empirical figure of 0.6 is subtracted for rake, spiral classifiers to account for misplaced material.

Step 2
To determine the size distribution in the overflow stream.

Column 7   Subtract the mass of solids that settle from the feed mass in each size fraction
            to give the mass of particles that doesn't settle, column (4) – column (6).

Summing column (7) will give the total mass of solids in the overflow.

Column 8   size distribution of the overflow, column (7) x 100/Σ(7)
Column 9   Cumulative percent in overflow, Σ(8)

Step 3
To determine the cumulative percent underflow product

According to Fitch and Roberts [6], the mass of solids reporting to the overflow, column (7)
in the table above, is accompanied with all of the feed water. A portion of the overflow pulp
is entrained with the underflow solids and this adds fines to the underflow, hence affecting the
underflow size distribution as well as providing the underflow water.
The proportion of overflow solids entrained in the underflow is taken as equal to the water
split to the underflow, $Q_{VL(U)}/Q_{VL(F)}$.

1.   determine the ratio of $Q_{VL(U)}/Q_{VL(F)}$

$Q_{VL(U)}$ can be estimated from the volume of solids in the feed (or the percent solids in the
slurry).

$$\frac{Q_{VL(F)}}{Q_{VS(F)}} = V_F = \frac{(100 - \%\,Solid\,in\,feed)\,.\,\rho_S}{\%\,Solid\,in\,feed\,.\,\rho_W}$$

From the given data:

$$V_F = \frac{(100 - 45)\,2.54}{45 \times 1.0} = 3.104$$

2.   the volume dilution in the overflow, $V_O = Q_{VL(O)}/Q_{VS(O)} = Q_{VL(F)}/Q_{VS(O)}$ assuming that
      all the feed water initially goes to the overflow.

Thus, $V_O = \dfrac{Q_{VL(F)}}{Q_{VS(O)}} = \dfrac{Q_{VL(F)}}{Q_{VS(F)}}\,.\,\dfrac{Q_{VS(F)}}{Q_{VS(O)}} = V_F\,.\,\dfrac{Q_{MS(F)}}{Q_{MS(O)}} = V_F\,.\,\dfrac{100}{Q_{MS(O)}}$ for a 100 mass feed

$V_O = 3.104 \times 100/39.98 = 7.76$

3.   Fitch and Roberts [3] estimate that on average the underflow solids entrain
      approximately 51% of overflow pulp by volume.

That is, $\dfrac{Q_{VOP(U)}}{(Q_{VOP(U)} + Q_{VS(U)})} = 0.51$ and $\dfrac{Q_{VS(U)}}{(Q_{VOP(U)} + Q_{VS(U)})} = 1 - 0.51 = 0.49$

where $Q_{VOP(U)}$ = volume of entrained O/F pulp in the U/F,

$Q_{VS(U)}$ = volume of settled solids in the U/F.

Therefore $\dfrac{Q_{VOP(U)}}{Q_{VS(U)}} = \dfrac{0.51}{0.49} = 1.04$

and $Q_{VOP(U)} = 1.04 Q_{VS(U)} = 1.04 \dfrac{Q_{MS(U)}}{\rho_S} = 1.04 \dfrac{(Q_{MS(F)} - Q_{MS(O)})}{\rho_S} = 1.04 \dfrac{(100 - Q_{MS(O)})}{\rho_S}$

4. Since the volume ratio of water to solid in the entrained pulp in the U/F is the same as in the overflow:

$$V_O = \frac{Q_{VL(O)}}{Q_{VS(O)}} = \frac{Q_{VOL(U)}}{Q_{VOS(U)}}$$

where $Q_{VOL(U)}$, $Q_{VOS(U)}$ = volume of entrained O/F water and solids in the U/F respectively.

Then $(1 + V_O) = \dfrac{Q_{VOL(U)} + Q_{VOS(U)}}{Q_{VOS(U)}} = \dfrac{Q_{VOP(U)}}{Q_{VOS(U)}}$

and $\dfrac{V_O}{(1 + V_O)} = \dfrac{Q_{VOL(U)}}{Q_{VOP(U)}}$

Since the water in the U/F is assumed to be made up entirely of the water entrained from the O/F, $Q_{VOL(U)} = Q_{VL(U)}$ hence:

$$Q_{VL(U)} = \left[\frac{V_O}{(1 + V_O)} \right] \cdot Q_{VOP(U)} = \left[\frac{V_O}{(1 + V_O)} \right] \cdot \frac{1.04(100 - Q_{MS(O)})}{\rho_S} \text{ per 100 units of solid.}$$

Since the volume of water in the feed, $Q_{VL(F)} = \dfrac{100(100 - \% \text{solid in feed})}{\% \text{solids in feed} \times \rho_W}$

then $\dfrac{Q_{VL(U)}}{Q_{VL(F)}} = \dfrac{1.04(100 - Q_{MS(O)})}{\rho_S} \cdot \left[\dfrac{V_O}{1 + V_O} \right] \cdot \dfrac{\% S_F \cdot \rho_W}{100(100 - \% S_F)}$

where $\% S_F$ = % solids in the feed.

Substituting values from the given data:

$$\frac{Q_{VL(U)}}{Q_{VL(F)}} = \frac{1.04(100-39.98)}{2.54} \cdot \left[\frac{7.75}{1+7.75}\right] \cdot \frac{45 \times 1.0}{100(100-45)} = 0.18$$

That is, 18% of each size fraction in the overflow is entrained in the underflow.

Step 4
We can now construct the following table to obtain the underflow particle size distribution. The column numbers follow in sequence from the previous table.

Size interval	O/F entrained (7) x 0.18	Mass of underflow (6)+(10)	Mass % underflow (11)/Σ(11)	Cum. % underflow Σ(12)
	(10)	(11)	(12)	(13)
	0.11	49.51	73.73	26.27
1	0.08	1.64	2.44	23.83
2	0.76	4.48	6.68	17.16
3	1.29	4.04	6.02	11.14
4	1.49	3.14	4.67	6.46
5	1.13	1.81	2.70	3.77
6	0.77	1.03	1.54	2.23
	0.15	1.50	2.23	0
		Σ67.15	Σ100	

Column 10   Column (7) x $(Q_{VL(U)}/Q_{VL(F)})$
Column 11   Mass settled (6) +entrained fines (10)

Thus column (9) and column (13) provide the required particle size distribution in the two streams.

During the operation of the mechanical classifiers, slurry is fed evenly along the width of the classifier and at a distance of about two-thirds of the length of the tank measured from the bottom weir. The feed slurry normally carries 70% – 80% solids. Water is added so that the solids in the slurry can easily settle. Too much dilution or too little water addition, affects the particle size distribution of the overflow stream. Hence an optimum amount of water has to be determined and maintained.

Separations in such mechanical classifiers are achieved for particles of 600 microns down to about 75 microns. The baffle positions and its depth below the surface controls the velocities and particle size of the overflow stream. Lowering the baffle level obviously promotes coarser particles in the overflow.

One of the greatest problems in the operation of mechanical classifiers is the surging of the slurry. To counter this, water additions and maintaining relatively constant slurry characteristics help. Clayey matter promoting slimes and thixotropic slurries could be an added source of trouble in operation.

12.5. Capacity of Mechanical Classifiers

Usually the capacities are recommended in manufacturer's literature. Overflow capacity is normally the limiting design capacity of mechanical classifiers. The overflow volume can be expressed as [21]:

$$Q_{V(O)} = W H v \tag{12.21}$$

where $Q_{V(O)}$ = overflow volume, m^3/s
  W   = weir width, m
  H   = weir height, m
  v = flow velocity from the feed to the overflow, m/s

or $Q_{V(O)} = \frac{1}{2} A v_T$

where A   = pool area
  v_T = terminal velocity, m/s

For spiral classifiers, the overflow solids capacity may be given by [21]:

$$Q_{MS(O)} = n k_2 k_3 (3.92 D^2 + 0.67 D) \text{ for low weir pools} \tag{12.22}$$

and $$Q_{MS(O)} = n k_2 k_3 (3.12 D^2 + 0.42 D) \text{ for high weir pools} \tag{12.23}$$

where $Q_{MS(O)}$ = overflow solids capacity, t/h
  n   = the number of spirals
  k_1 = factor from Table 12.7
  k_2 = solids density correction factor, Table 12.7

In some cases the sand raking capacity is the determining factor in sizing mechanical classifiers. Hill [22] describes an empirical equation for the raking capacity:

$$Q_{MS(U)} = 0.035 W P \rho_B (D - 0.75 W) \tag{12.24}$$

where $Q_{MS(U)}$ = raking capacity, t/h/spiral revolutions/min
  W   = flight width, m
  P   = flight pitch, m
  ρ_B = bulk density of the solids in the underflow, kg/m^3
  D   = diameter of the spiral, m

The effect of spiral diameter on the raking capacity is given by (Hill, 1982):

$$Q_{U2} = Q_{U1} \left(\frac{D_2}{D_1} \right)^3 \tag{12.25}$$

Table 12.7
Factors k_1 and k_2 for spiral classifiers capacity, [21].

Cut size, μm	400	300	200	150	100	74	53	44
Pulp/t of O/F	1.8	2.0	2.33	4.0	4.5	5.7	6	7.5
k_1 (low weir)	1.95	1.7	1.46	1.00	0.66	0.46	-	-
k_1 (high weir)	-	-	2.9	2.2	1.60	1.00	0.57	0.36
SG of solids	2.0	2.5	3.0	3.5	4.0	4.5	5.0	
k_2	0.75	0.92	1.08	1.25	1.42	1.58	1.75	

12.6. Operation of Centrifugal Classifiers

In the minerals industry cyclones are normally operated under wet conditions and seldom as dry classifier. The feed, in the form of a slurry, on entering the feed chamber is divided into two streams as a result of the inlet pressure of the slurry and the swirling action inside the feed chamber and the conical section of the hydrocyclone. The denser particles which settle faster are forced down by the combined gravity and centrifugal forces while the less dense and lighter particles remain near the central axis of the cyclone and exit through the vortex finder. Some lighter particles however are entrapped in the heavier particle stream and are lost through the apex while some heavier particles are similarly lost to the overflow stream.

The hydrocyclone is a classifier with no moving parts and its operation depends on:

1. the characteristics of the feed scream and
2. the geometry of the cyclone.

The characteristics of the feed stream includes:

1. size and size distribution of solids in the feed stream,
2. pulp density (percent solids in the slurry) and pulp viscosity, and
3. inlet pressure (pressure differential between inlet and vortex finder outlet).

The geometry of the cyclone involves:

1. inlet shape and inlet area,
2. cyclone dimensions (length of cylindrical section, total overall length and cone angle),
3. inlet, vortex finder and apex diameters.

The feed size varies from coarse (150 microns and more) down to fines. In open circuit operation the solid content of the slurry is about 30% and in closed circuits, it could be as high as 60% [23]. For most operations the feed pressure ranges between 345 kPa to 700 kPa and in actual practice depends on cyclone diameter. The minimum pressure for a stable air core is around 30–35 kPa [21]. The feed velocity is about 3.7–6.1 m/s [15] and its acceleration in the feed chamber is inversely proportional to the hydrocyclone diameter, [11].

12.6.1. Efficiency of separation in hydrocyclones
By convention the efficiency of operation and separation of hydrocyclones are determined by the sharpness of separation and the d_{50} value. Less conventional but also widely used is the

d_{95} cut point which is the size at which 95% of the particles have the probability of reporting to the underflow.

To determine the efficiency of separation of a sample of known size distribution, pulp density and flow rate, a hydrocyclone of known geometry, including the inlet, overflow and underflow diameters, is operated in closed circuit until a steady state is reached. Simultaneous samples of the feed, overflow and underflow streams are collected dried and analysed for size distribution. The calculations involved to determine the efficiency are best understood by the following example.

Let us assume that a hydrocyclone is fed with slurry and at steady state the operating conditions are:

1.	Feed rate	=	55.0% solids at 206.5 t/h
2.	Overflow rate	=	19.6% solid at 29.4 t/h
3.	Underflow rate	=	78.2% solids at 177.1 t/h

and the size analysis of samples from each stream are given in Table 12.8.

Table 12.8
Partition coefficient calculations

Size μm	Geom. mean size $\sqrt{d_i d_{i+1}}$	Feed mass, t	Overflow mass, t	Underflow mass, t	Calculated feed, t (4)+(5)	Partition coefficient (5)x100/(6)
(1)	(2)	(3)	(4)	(5)	(6)	(7)
-600+425	505.0	120.0	0	121.0	121.0	100.0
-425+300	357.1	26.0	0.6	24.0	24.6	97.6
-300+250	273.9	13.0	2.0	11.0	13.0	84.6
-250+150	193.6	12.0	4.7	8.2	12.9	63.6
-150+106	126.1	9.0	4.6	4.2	8.8	47.7
-106+75	89.2	5.0	3.2	2.2	5.4	40.7
-75	-	21.5	14.3	6.5	20.8	31.3
		Σ 206.5	Σ 29.4	Σ 177.1	Σ 206.5	

The partition coefficient is the recovery of particles in each size fraction to either the underflow or the overflow (see Tromp curve, Chapter 11).

The distribution of water in the different streams may be determined as:

Water in feed	=	100–55.0 = 45.0%
Water in overflow	=	100–19.6 = 80.4%
Water in underflow	=	100–78.2 = 21.8%

Hence:

$$\text{mass of water in feed} = 206.5 \times \frac{45}{55} = 169.0 \text{ t/h}$$

$$\text{mass water in overflow} = 29.4 \times \frac{80.4}{19.6} = 120.6 \text{ t/h}$$
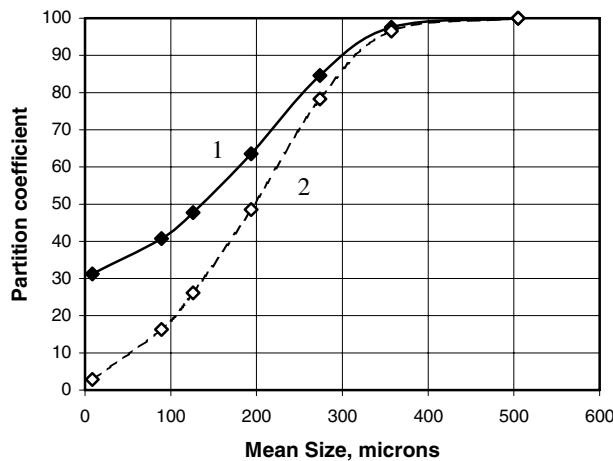
Fig. 12.14. Typical performance curves of a hydrocyclone (1-actual, 2-corrected).

$$\text{mass water in underflow} \quad = \quad 177.1 \times \frac{21.8}{78.2} = 49.4 \ t/h$$

A plot of mean particle size against the partition coefficient (column (2) vs column (7), Table 12.8) yields the partition curve 1 shown in Fig. 12.14.

Fig. 12.14 is a typical distribution curve for a hydrocyclone underflow stream. The curve shows that the cyclone cut size, separation size or d_{50} is 135 microns. A similar curve can be drawn for the overflow stream which in effect will be a mirror image of the underflow curve.

Note that the curve does not pass through the origin. It has been suggested [9,24,25] that this is due to a fraction of the slurry bypassing the cyclone and not being classified. Thus if 5% of the feed slurry bypassed the unit then only 95% of the slurry would be subjected to the classification process. Thus the d_{50} calculated by the above method has to be corrected. Kelsall [5] suggested that the fraction of solids in each size fraction that is bypassed from the feed to the underflow is in the same ratio as the fraction of feed water that reported to the underflow. This is not necessarily true, according to Austin et al [26], however, Kelsall's assumption is simple and widely accepted as it yields a reasonably accurate correction for the true d_{50} value. The usual symbol for the corrected cut size is d_{50C}. Using Kelsall's concept, the manner of evaluating the d_{50C} value is illustrated in Table 12.9 and details of the calculation are shown below:

Mean Size   Corrected partition coefficient, E_C (% recovery to U/F)

505       $\dfrac{121-(0.292 \times 121)}{121-(0.292 \times 121)} \times 100 \ = \ 100$

357       $\dfrac{24-(0.292 \times 24.6)}{24.6-(0.292 \times 24.6)} \times 100 \ = \ 96.6$

$$274 \qquad \frac{11-(0.292\times13)}{13-(0.292\times13)}\times100 \;=\; 78.3$$

$$\vdots \qquad\qquad\qquad\qquad \vdots$$

$$d_i \qquad \frac{m_{iU}-(w\ m_{iF})}{m_{iF}-(w\ m_{iF})}\times100 \quad \text{or} \quad \frac{E-w}{1-w}\times100$$

where d_i = mean size of screen interval i

       m_{iU}, m_{iF} = mass in size interval i in the underflow and feed respectively

          w   = fraction of feed water in the underflow

A plot of the corrected percent recoveries (column (3), Table 12.9) against the mean particle size (column (1), Table 12.9) gives the corrected partition curve (curve 2 in Fig. 12.14). From the curves it can be seen that in this specific case, the d_{50} value is 135 μm and the corrected d_{50C} value is 198 μm.

Table 12.9
Correction of partition coefficient

Geom. Mean size, μm	Partition coefficient	Corrected partition coeff.
(1)	(2)	(3)
505.0	100.0	100.0
357.1	97.6	96.6
273.9	84.6	78.3
193.6	63.6	48.5
126.1	48.9	27.8
89.2	38.5	13.1
8.7	31.3	2.9

It can be easily seen that the corrected curve represents the efficiency of separation of that portion of the slurry that is subjected to classification. The sharpness and separation efficiency values can be quantified by reading the values of d_{25}, d_{75} and d_{50} from the graph and are calculated in the same manner as described for screen classifiers.

	Uncorrected	Corrected
d_{75}	235	263 μm
d_{25}	-	125 μm
d_{50}	135	198 μm
d_{65}	200	237 μm
d_{35}	45	155 μm

Imperfection = $(d_{75}-d_{25})/2d_{50}$	-	0.35
75% partition error = (d_{75}/d_{50})	1.74	1.33
Sharpness Index = d_{25}/d_{75} [21]	-	0.48
= d_{35}/d_{65} (high bypass)	0.23	-

The cyclone Imperfection ranges from 0.2 – 0.6 with an average of around 0.3 [21].

The water split between the feed and the underflow will depend on the diameter of the apex (D_U) and the vortex finder (D_O). From limited experimental data, Lynch [21] observed that the water split bears a linear relation ship with the apex diameter. For all particle sizes data, Lynch derived the equation:

$$W_S = -1.61 + \frac{193\,(D_U - 1.41)}{Q_{ML(F)}} \qquad (12.26)$$

where W_S = Water split, $Q_{ML(O)}/Q_{ML(F)}$,
        D_U = Apex diameter, m,
        $Q_{ML(O)}$ = Mass flow rate of water in the overflow, t/h and,
        $Q_{ML(F)}$ = Mass flow rate of water in the feed, t/h.

The corrected efficiency curve derived after correcting for the water split is specific for the specific slurry and cyclone geometry. To apply the method in a wider context, such as different flow rates, slurry percent solids, diameters of vortex finder and apex, Lynch and Rao [24] normalised the curve by dividing each particle size, d, by d_{50C}. Plotting d/d_{50C} against the fraction to underflow they obtained a series of curves which described the performance of a hydrocyclone independent of operating conditions and hydrocyclone size. Lynch and Rao tested the curves for four cyclone diameters (10.2, 15.2, 24.5 and 28.1 cm) and obtained similar curves. Such plots are illustrated as reduced efficiency curves. Using the above data a typical curve is plotted in Fig. 12.15.

The advantage of plotting in this manner is that the results can be translated to any larger size cyclone.
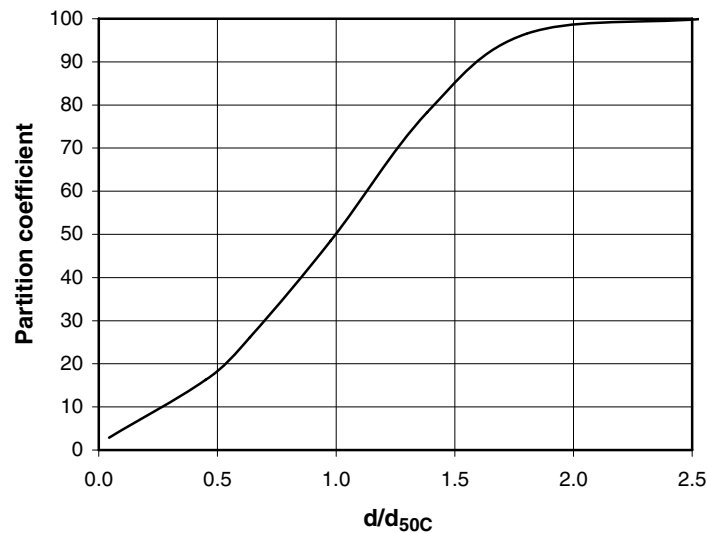
Fig. 12.15. Reduced efficiency curve.

It must be emphasised that the reduced efficiency curves for different minerals of different density and shape are different but as the size d is simply divided by a constant, the nature of the curve remans unaltered.

Attempts have been made to derive the equation of the reduced efficiency curve [18,24,27-29]. The derivation by Lynch [24] is now widely used and is represented by the equation:

$$E_C = \frac{[e^{\alpha(d/d50)} - 1]}{[e^{\alpha(d/d50)} + e^{\alpha} - 2]}$$

(12.27)

where E_C = the corrected partition coefficient and
       α = the efficiency parameter

The value of α is typically 3 – 4 for a single stage cyclone but can be as high as 6. A closed circuit grinding operation can have values around 2.5. Fig. 12.16 illustrates typical efficiency curves drawn for three arbitrarily selected values of α. It can be seen that with increasing values of α, the curves are steeper indicating a greater efficiency of classification and sharpness of split.

As this method of representing classification is independent of cyclone geometry, it is successfully used to scale up laboratory results to full-scale industrial units. It has been found that results accurately predict industrial scale operations.

It is important to note that in practice, the value of α cannot be determined directly from the d/d_{50C} value. It has to be determined by a trial and error method. However, Han and Chen [30] obtained an empirical correlation, based on a similarity principle, for α as:
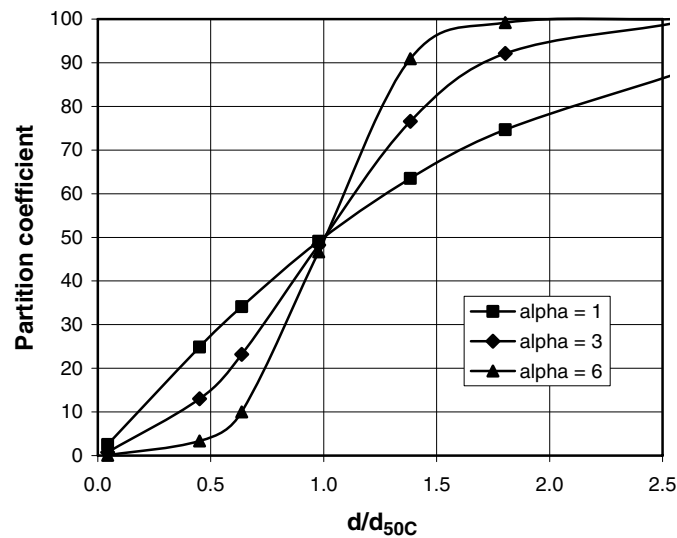
Fig. 12.16. The effect of efficiency parameter, α on the shape of the performance curve.

$$\alpha = 6.11 \left(\frac{10 D_U}{D_O}\right)^{-2.02} \left(\frac{d_F^3 \rho_L (\rho_S - \rho_L) g}{\mu^2}\right)^{0.16} \left(C_{MS(F)}\right)^{1.27} \left(\frac{10000 d_{50C}}{D_C}\right)^{-0.79} \qquad (12.28)$$

where d_F = the 63.2% passing size of the feed.

Each bracketed term is dimensionless so that the units have to be consistent. That is, if d_F is in meters then all other diameters are also in meters, ρ is in kg/m^3, g is m/s^2 and viscosity, μ, is in Pa s (or N/m^2).

12.6.2. Effect of cyclone variables on operation

As the operation of hydrocyclones depend on large number of interdependent variables, attempts have been made by a number of workers to determine the extent of the effect of the individual variables [30,34-36]. A survey of the literature indicates the following general conclusions. These conclusions were drawn by varying a single parameter while keeping others constant.

A. Cyclone geometry:

1. d_{50C} will increase with increasing vortex finder diameter,
2. d_{50C} will increase with decreasing spigot diameter,
3. d_{50C} will increase with increasing inlet diameter,
4   d_{50C} will decrease with increasing length.

B. Slurry characteristics:

1. Finer the feed size the smaller the d_{50C} value,
2. Increased feed rate decreases the d_{50C} value,
3. Increased SG of the feed solids decreases the d_{50C} value.

These general relations were quantified by using regression analysis by several workers starting as early as 1949 and 1954 by Dalhstrom. The relations established later by Lynch and Rao [24], Plitt [28] and Arterburn [12], are now more generally accepted.

In deriving the models it is obvious that only non-roping conditions were applicable. A roping discharge condition can be seen simply by observing the nature of the discharge stream. For instance, Fig. 12.17 shows a normal condition of flow (A) where the stream is flared like a fishtail and a rope discharge (B) where the underflow discharges as a continuous stream resembling a *rope*. The normal spray discharge has a cone angle of 20-30° with a hollow center [12].

To prevent a roping condition, the underflow density must be kept below a limiting value. The roping conditions have been quantified by Laguitton [31] who stated that the limiting underflow and feed conditions for roping is:

$$V_{S(U)} < 0.56 + 0.20 \, (V_{S(F)} - 0.20) \qquad (12.29)$$

and by Mular and Jull [11] as:

$$V_{S(U)} \leq 0.5385\, V_{S(O)} + 0.4911 \tag{12.30}$$

where $V_{S(U)}$ = the volume fraction of the solids in the underflow and
$V_{S(F)}$ = the volume fraction of the solids in the feed stream.

For values of $V_{S(U)}$ greater than the right hand side of Eqs. (12.29) and (12.30), roping is likely to occur. Eq. (12.30) suggests that a higher underflow density can be achieved, without the risk of roping, if the cyclone is operated with a high overflow density. A higher solid density will also allow a higher underflow density before roping occurs. For example, for an overflow of 30% solids and a solid S.G. of 2.7 the underflow will start to rope at approximately 78% solids by mass whereas for a solid S.G. of 3.7, the underflow density can be increased to around 82% solids before roping occurs [11]..

Plitt et al [32] indicate that the particle size of the underflow is the controlling factor for changing from a normal spray to roping discharge but Bustamante [33] asserts that the ratio of the underflow to overflow discharge diameters are the governing factors. Concha et al [34] has quantified this ratio in relation to roping conditions. These authors state that roping will occur if the air core diameter is greater than the spigot diameter. Since the air core diameter depends on the surface tension, viscosity and overflow and underflow diameters, the ratio D_U/D_O will be a determining variable. Table 12.10 gives some limiting values.

Table 12.10
Transition from spray to roping discharge.

	D_U/D_O	Condition
Bustamante [33]	< 0.34	Roping discharge
	0.34 – 0.5	Roping or spray
	> 0.5	Spray discharge
Concha et al [34]	< 0.45	Roping
	0.45 – 0.56	Roping or spray
	> 0.56	Spray discharge
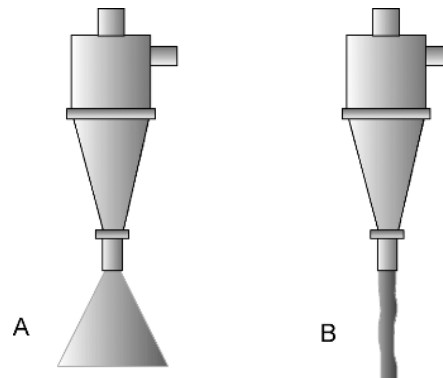
Fig. 12.17.   Hydrocyclone discharge. A - Normal spray discharge, B – rope discharge

For efficient hydrocyclone operation it is necessary to operate as close to roping conditions as possible, so that maximum coarse particles are removed.

12.7. Hydrocyclone Models

The operation of hydrocyclones depends on a number of interdependent variables. Attempts to inter-relate them with performance has been made by several workers [27,35-37]. Most workers used crushed quartz or limestone slurries as the medium in their laboratory studies. Lynch used real sulphide ores (copper, lead) in his investigation.

The model developed by Lynch and Rao [24] was obtained as a product of individual (quantitative) relationships of each variable with the d_{50}. Using a Krebs hydrocyclone, 508 mm in diameter they found that the d_{50} was a function of particle size and cyclone geometry. They determined three different equations corresponding to arbitrarily defined coarse, medium and fine particle sizes. However their final model encompassed this variation and is now written as:

$$\log d_{50C} = \quad 4.18\, D_O - 5.43\, D_U + 3.04\, D_I + 0.0319\, C_{MS(F)} \qquad (12.31)$$
$$- 3.6\, Q_{V(F)} - 0.0042\, (\%{+}420) + 0.0004\, (\%{-}53)$$

where $C_{MS(F)}$ = % solids by mass in the feed,
  $Q_{V(F)}$ = volume flowrate of feed, m^3/s,
  C_{+420} = % + 420 μm in the feed,
  C_{-53} = % – 53 μm in the feed,
  D_O, D_I, D_U = diameters of the overflow, inlet and underflow respectively, m,
  d_{50C} = cut size in microns.

The constants strictly apply for a Krebs cyclone and limestone slurry, but is widely used for most slurries with fair accuracy. For minerals of different densities to limestone, a correction may be applied, such as the one given in Eq. (12.32).

$$\frac{(d_{50C})_1}{(d_{50C})_2} = \sqrt{\frac{(\rho_{S2} - \rho_L)}{(\rho_{S1} - \rho_L)}} \qquad (12.32)$$

Lynch and Rao's model has been subsequently modified by Nageswararao [38] who included the cone angle of the cyclone and hindered settling conditions. The hindered settling factor was taken as the ratio of free settling to hindered settling. H_S, and written as:

$$H_S = \frac{10^{1.82 V_{S(F)}}}{8.05\left[1 - V_{S(F)}\right]^2} \qquad (12.33)$$

where $V_{S(F)}$ = volume fraction of solids in the feed slurry.

The final model translates, with slight modification by JKTech [39], to:

$$\frac{d_{50C}}{D_C} = K_{D0}\left(\frac{D_O}{D_C}\right)^{0.52}\left(\frac{D_U}{D_C}\right)^{-0.47}\left(\frac{P}{\rho_{SL}\, g D_C}\right)^{-0.22}\left(\frac{D_I}{D_C}\right)^{-0.50}\left(\frac{L_{CYL}}{D_C}\right)^{0.15}\theta^{0.15}\, D_C^{-0.65}\, H_S^{0.93} \qquad (12.34)$$

where P = feed Pressure, kPa,
g = acceleration due to gravity,
θ = cone angle, degrees,
H_S = hindered settling factor ,
K_{D0} = material constant depending on the SG and size of particles in the feed,
L_{CYL} = length of the cylindrical section, m,
D_C = diameter of the cylindrical section, m,
ρ_{SL} = feed slurry density, t/m^3,
d_{50C} = cut size in microns.

To evaluate Eq. (12.34), K_{D0} has to be determined for each case. As this is not possible, it is estimated in a laboratory using a laboratory size hydrocyclone and scaled to suit a particular condition. This model has been applied with considerable success.

Using pure silica suspensions, Plitt [28], Plitt et al [40] and later Arterburn [12], developed mathematical models relating the operational variables and the cut point. Both these models were derived empirically from experimental data obtained in laboratory size hydrocyclones. According to Plitt:

$$d_{50C} = \frac{k_1\, 2689.2\, D_C^{0.46}\, D_I^{0.6}\, D_O^{1.21}\, \mu^{0.5}\, \exp(0.063\, C_{VS(F)})}{D_U^{0.71}\, L_{VF}^{0.38}\, Q_{V(F)}^{0.45}\, (\rho_S - \rho_L)^{0.5}}$$

(12.35)

where L_{VF} = free vortex height (distance from end of vortex finder to apex), m
D_C = cylindrical diameter, m
D_U, D_I, D_O = underflow, inlet and overflow diameters, m
$Q_{V(F)}$ = volumetric flowrate of the feed, m^3/s
$C_{VS(F)}$ = % solids by volume in the feed
d_{50C} = corrected cut size, microns
μ = liquid viscosity, mPa.s
ρ_S, ρ_L = density of solid and liquid respectively, kg/m^3, and
k_1 = a calibration factor (taken as 1.0 when no data is available)

Austin et al [26] state that the models advocated by Lynch and Rao and Plitt yield d_{50C} values that depend on the conditions of determination and were more suited for dilute slurries. Despite this, the expressions are extensively used to design and operate industrial size cyclones.

Arterburn [12] derived a simpler relation, which is also used extensively but mostly for the designing of hydrocyclones. According to Arterburn, for a *typical* Krebs hydrocyclone:

$$d_{50C} = \frac{8253.5\, D_C^{0.67}}{\Delta P^{0.28}\, (\rho_S - \rho_L)^{0.5}\, \left[1 - (1.9 V_{S(F)})\right]^{1.43}}$$

(12.36)

where D_C is in meters, ΔP in kPa, ρ_S and ρ_L in kg/m^3 and d_{50C} in microns.

An alternative empirical approach for hydrocyclone models has recently been attempted by Han and Chen [30] using the similarity principle. According to Han and Chen:

$$\frac{d_{50C}}{D_C} \times 10^4 = 9.03 \left(\frac{10 D_U}{D_O} \right)^{-1.26} \left(C_{MS(F)} \right)^{0.54} \qquad (12.37)$$

Han and Chen used a 50 mm diameter cyclone with a cone angle of 12° and a quartz slurry with particle size distributions in coarse, medium and fines ranges between 250 μm and 10 μm. A coefficient of correlation in excess of 0.95 is claimed.

Bradley [9] as early as 1965 and later Klimpel [41] and Austin et al [26] have indicated that the viscosity of the slurry also affects the efficiency curve and therefore the d_{50C} value. As viscosity generally decreases with an increase in temperature, it is likely that the cut point will also depend on temperature. Work in this area has been reported by Gupta and Eren [42].

12.8. Hydrocyclone Capacity

Assessing the capacity of hydrocyclones has been the study of several workers. The generally acceptable relation for capacity, $Q_{V(F)}$, is given by:

$$Q_{V(F)} = k \, \Delta P^{0.5} \qquad (12.38)$$

Empirically, the exponent for pressure drop has been found to range from 0.44 – 0.56. The constant, k, is a function of cyclone dimensions and the pressure and flow characteristics of the slurry entering the feed chamber. According to Dahlstrom, the capacity is also proportional to the square of the cyclone diameter and is given by the relation:

$$Q_{V(F)} = k \times 10^{-3} \, \Delta P^{0.5} \, D_C^2 \qquad (12.39)$$

where $Q_{V(F)}$ = the volumetric flow rate of pulp in the feed, m^3/h,
         ΔP = the feed pressure, kPa,
         D_C = the diameter of the cyclone, m.

Tarr [13] developed a graphical solution relating capacity and diameter of the cyclone. The relation is reproduced in Fig. 12.18 where the mean values of feed capacities are plotted against cyclone diameter.

For more appropriate values of capacities Tarr states that the capacities have to be adjusted according to the percent solids in the slurry and the feed pressure of the slurry. Such adjustments, described as correction factors, are shown in Fig. 12.19 and Fig. 12.20.

A further correction factor was introduced by Tarr to account for the differences in specific gravity of minerals as the original expression was derived using a quartz slurry. This correction factor is given in Eq. (12.40).

$$\text{Correction factor} = \left[\frac{2650 - 1000}{\rho_S - 1000} \right]^{0.5} \qquad (12.40)$$

The derivation of Tarr's method was based on "typical" hydrocyclone dimensions.
An application of the method is given in Example 12.3.
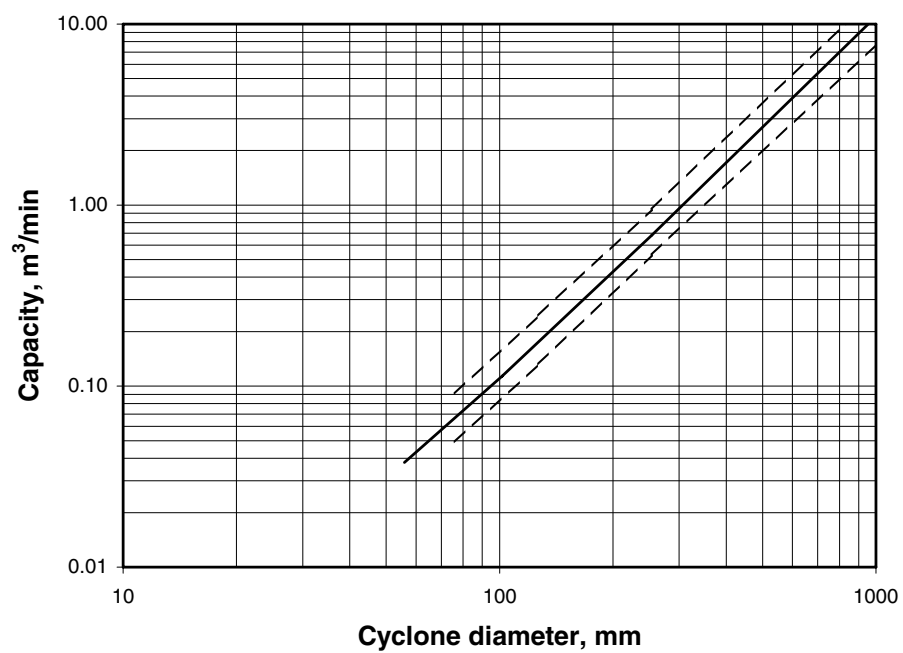
Fig. 12.18. Capacity of typical hydrocyclone of varying diameters [13].

Fig. 12.19. Correction factor for different solids content in the feed [13].
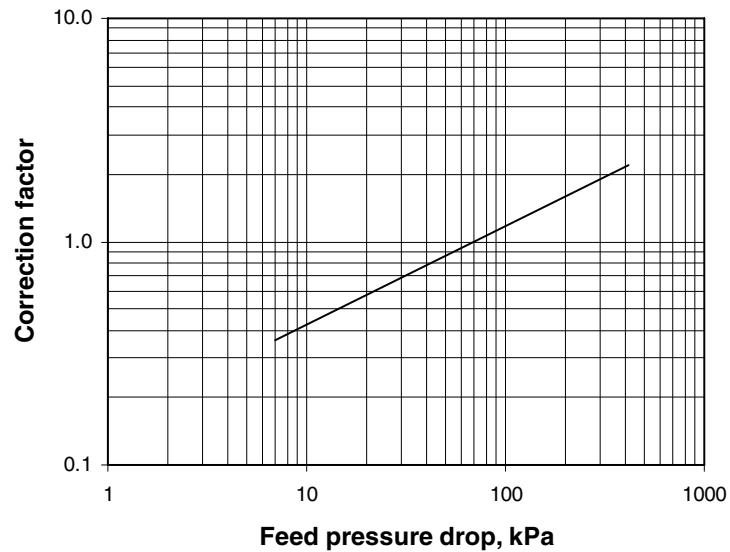
Fig. 12.20. Correction factor for capacity at different input pressure [13].

Example 12.3

A 35% pulp (by volume) had to be classified in a 100 mm diameter hydrocyclone at an inlet pressure of 100 kPa. Determine the cyclone capacity under the following operating conditions:

Specific gravity of solid = 2650 kg/m^3

Solution
From Fig. 12.18 the capacity corresponding to a 100 mm diameter cyclone is 0.1 m^3/min.
Correction factor for 34 % solids in the feed (Fig. 12.19)   = 1.32
Correction factor for pressure (Fig. 12.20)   = 1.2

Hence Capacity = 0.1 x 1.32 x 1.2 = 0.16 m^3/min.

Fitch and Roberts [3] considered the diameter of the vortex finder, D_O, the inlet diameter, D_I, and the input pressure, ΔP, to calculate the capacity of cyclones. The hydrocyclone capacity, $Q_{V(F)}$, is given by:

$$Q_{V(F)} = 10.55 \, D_O^{0.73} \, D_I^{0.86} \, \Delta P^{0.42} \qquad (12.41)$$

The unit of $Q_{V(F)}$ is m^3/min with D_O and D_I in meters and pressure in kPa.

Nageswararao (1995) considered all the variables in a hydrocyclone and derived the relation between the hydrocyclone variables, feed mass flow rate and geometry of the hydrocyclones as:

$$Q_{V(F)} = K_{Q0} \frac{D_C^{1.90}}{\theta^{0.1}} \left[\frac{\Delta P}{\rho_{SL}} \right]^{0.50} \left[\frac{D_O}{D_C} \right]^{0.67} \left[\frac{D_I}{D_C} \right]^{0.45} \left[\frac{L_C}{D_C} \right]^{0.2} \qquad \{12.42\}$$

where K_{Q0} = a constant depending on the feed solids and determined experimentally in a laboratory size cyclone of known parameters and scaled to the size for a commercial cyclone.

The dimensions, D and L, defined in Fig. 12.9, are meters, θ the cone angle, degrees, ΔP in terms of kPa and $Q_{V(F)}$ in m^3/h. Expression 12.42 was determined using limestone and hydrocyclones diameters ranging between 102 and 381 mm. The expression is a revised version of the equation statistically arrived at by Lynch and Rao [24] and later modified by Lynch and Morrell [37].

The throughput through the hydrocyclone can also be measured in terms of flow through the vortex finder, or apex. However, the sensitivity of the split (d_{50}) is largely dependant on the throughput of the underflow.

Plitt [28] developed a series of models to describe the behaviour of a cyclone. These models estimate the d_{50C}, pressure drop, the sharpness of separation and the flow split.

The Plitt equation for the flow split is:

$$S = \frac{Q_{V(U)}}{Q_{V(O)}} = \frac{k_2 \, 3.79 \left(\dfrac{D_U}{D_O} \right)^{3.31} L_{VF}^{0.54} \left(D_U^2 + D_O^2 \right)^{0.36} \exp(0.0054 \, C_{VS(F)})}{H^{0.24} \, D_C^{1.11}} \qquad (12.43)$$

or

$$S = \frac{Q_{V(U)}}{Q_{V(O)}} = \frac{k_2 \, 6.56 \left(\dfrac{D_U}{D_O} \right)^{3.31} \rho_{SL}^{0.24} L_{VF}^{0.54} \left(D_U^2 + D_O^2 \right)^{0.36} \exp(0.0054 \, C_{VS(F)})}{P^{0.24} \, D_C^{1.11}}$$

where H   = pressure head in meters of slurry,
       P   = pressure drop in Pa,
$Q_{V(U)}$, $Q_{V(O)}$ = volume flowrate in underflow and overflow respectively, m^3/h,
       $C_{VS(F)}$ = % solids by volume in the feed,
       D, L = dimensions in meters,
       ρ_{SL} = slurry density in kg/m^3,
       k_2 = a calibration factor (taken as 1.0 when no data is available).

The other Plitt models are:

$$P = \frac{k_3 \; 0.0651 \; Q_{V(F)}^{1.8} \exp(0.0055 \; C_{VS(F)})}{D_C^{0.37} \; D_I^{0.94} \; L_{VF}^{0.28} \; (D_U^2 + D_O^2)^{0.87}} \qquad (12.44)$$

where $Q_{V(F)}$ = the volume flowrate of the feed, m³/h, and

$$m = k_4 \; 10.10 \exp(-1.58 R_V) \left(\frac{D_C^2 L_{VF}}{Q_{V(F)}} \right)^{0.15} \qquad (12.45)$$

where m   = sharpness of separation
       k_3, k_4 = calibration factors (taken as 1.0 when no data is available)
       R_V = recovery of feed volume to the underflow

$$= \left(\frac{S}{1+S} \right)$$

Using the similarity principle, Han and Chen [30] obtained the expression for the throughput for a 50 mm cyclone as:

$$Q_{V(F)} = 0.14 \left(\frac{10 \, D_O}{D_C} \right)^{0.9} \left(\frac{d_{50C} \times 10^4}{D_C} \right)^{0.68} g^{0.5} D_C^{2.5} \qquad (12.46)$$

12.9. Hydrocyclone Circuits

Almost all crushing and grinding circuits include hydrocyclones in close circuit to yield a product of the required size distribution. Hydrocyclones are generally installed at an elevated position above the grinding unit so that the coarse underflow product can flow by gravity back to the grinding unit for further size reduction. The configurations adopted in practice are varied. Three typical set ups are illustrated in Fig. 12.21.

For a better control of the product size, hydrocyclones are connected in series (Fig. 12.22), while for greater throughput cyclones are connected in parallel.

While operating in series, the underflow from the first cyclone forms the feed to the second cyclone. Trawinski [43] suggests that the second cyclone should be operated at as near to roping conditions as possible. Dahlstrom and Wai-Ping Kam [35] suggest that in addition to metallurgical advantages, two stage classification leads to energy savings. It can be easily seen that when one cyclone is in operation a mass balance illustrates the distribution of products between the oversize and undersize. Such a mass balance is illustrated in Fig. 12.23. The distribution of a particular size i in the feed between overflow and underflow can therefore be determined.

Defining the fraction that goes selectively to the coarser stream as selectivity E_i, the selectivity (partition coefficient) can be determined using the expression indicated by Austin et al [26].

$$E_i = \frac{(\text{mass fraction of size i in underflow})(\text{mass of underflow stream})}{(\text{mass fraction of size i in feed})(\text{mass of feed})} \qquad (12.47)$$

oe $\quad E_i = \dfrac{U u_i}{F f_i}$ $\qquad\qquad\qquad\qquad$ (12.48)

where $\quad$ F, O, U $\;=\;$ the flow rates of feed, overflow and underflow and,
$\qquad\qquad$ $f_i, o_i, u_i \;=\;$ the mass fraction of the size i in the respective streams.
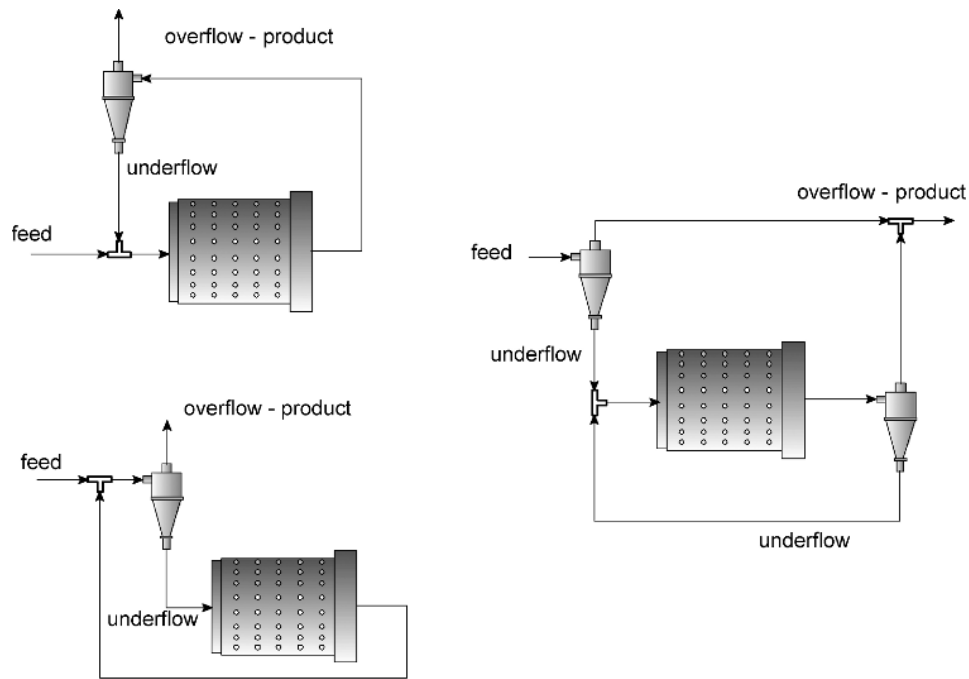
Fig. 12.21. Hydrocyclones in closed circuits with grinding mills.
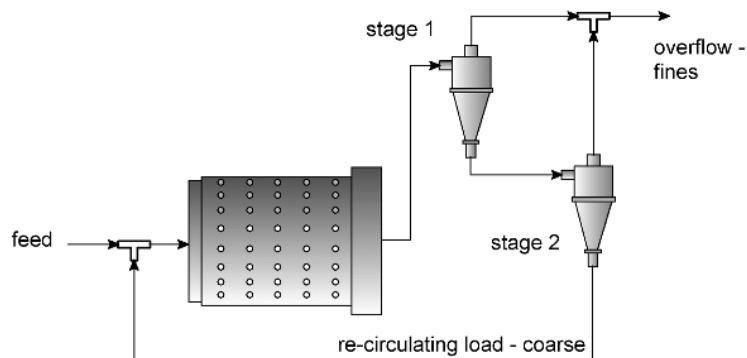
Fig. 12.22. Hydrocyclones connected in series, two stage classification.
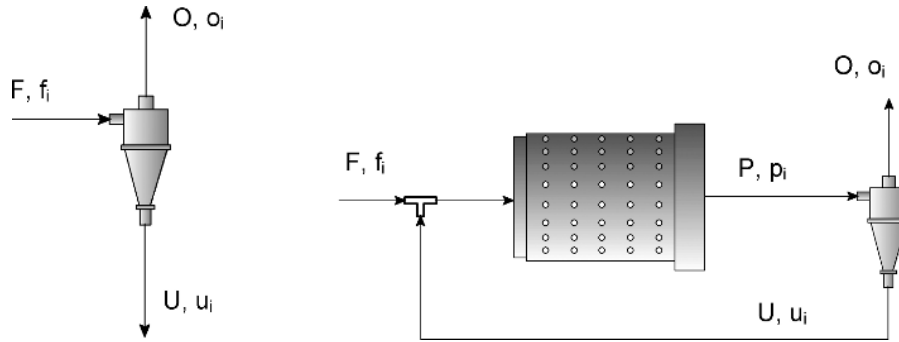
Fig. 12.23. Mass balance in hydrocyclone. F, O, U, C represents the mass flows in the cyclone feed, overflow, underflow and recirculating load

However, since most hydrocyclone circuits operate in closed circuit, the recirculating load or ratio also needs to be included in the Eq. (12.48). Describing each stream symbolically as in Fig. 12.23 the mass balance, at steady state, may be re-written as:

$$E_i = \frac{C\,u_i}{(1+C)\,p_i}$$

(12.49)

where   C   = the circulation ratio = $\dfrac{\text{Mass flow rate of underflow stream}}{\text{Mass flow rate of overflow stream}}$,

p_i = mass fraction of size i in the new cyclone feed.

So when two cyclones are involved, say in series with the second stage retreating the coarse stream (Fig. 12.22), then the overall partition will be a product of each E_i, say E_{i1} and E_{i2} for particle size d_i. Thus the overall partition of size i, E_{iT}, will be:

$$E_{iT} = E_{i1}\,E_{i2}$$

(12.50)

The E_{iT} value will depend on the manner of the hook up of the cyclones. For two cyclones in series with the overflow retreated in the second stage, Luckie and Austin [29] proposed the expression:

$$1 - E_{iT} = (1 - E_{i1})(1 - E_{i2})$$

(12.51)

12.10. Problems

12.1
An alkaline slurry from a bauxite grinding mill was scheduled to be classified using a spiral classifier at the underflow rate of 1100 t/day. The width of the classifier flight was 1.3 m and the outside diameter of the spiral flights was 1.2 m. Estimate the pitch of the spirals if the spiral speed is 5 rev/min and the bulk density of the underflow solids is 2000 kg/m^3.

12.2
A Krebs D-6B (6 inch) hydrocyclone was placed in open circuit to classify a predominantly silicious ore. The dimensions of the hydrocyclone were:

Inlet pipe diameter	40 mm
Overflow pipe diameter	45 mm
Apex diameter	13 mm
Feed density	62% solids
SG of the solids	2.65
SG of the slurry	1.629

Determine:

1. The feed rate to obtain a cut point at 150 microns
2. The cut point if the dilution is halved due to faulty operation

Take $L_V = 3 D_C$ and all pipe dimensions are internal.

12.3
A hydrocyclone had the following dimensions:

Spigot diameter	2.5 cm
Cyclone diameter	12.5 cm
Vortex finder	5.0 cm
Inlet diameter	3.1 cm
Included angle	12°

A pulp slurry of S.G. 1.24, containing solids of S.G. 2.9 was fed at a rate of 200L/min. Trial runs indicated a d_{50} of 100 microns. Determine:

1. The pressure differential,
2. The underflow flow rate.

12.4
The diameter of a typical hydrocyclone was 30.5 cm. The apex was fitted with a rubber sleeve 12 cm in length and 8.0 cm in internal diameter. A quartz suspension at a density of 1.33 was fed to the cyclone at the rate of 1000L/min. The underflow measured 75% solids. The apex diameter was reduced by 10 % twice. Estimate :

1. The change in the cut point after each setting of the apex
2. The roping conditions for the cyclone operation.

12.5

The volume flow rate of pulp fed to a hydrocyclone was 129 L/min. Its solid content was held at 32% by volume. Samples of the feed, under flow and over flow streams were taken simultaneously, dried and a size analysis carried out. The results obtained were:

Underflow rate = 30 L/min
Overflow rate = 99 L/min

Particle size, μm	Feed mass%	Underflow mass%	Overflow mass%
+212	2.6	6.24	0.0
-212+150	8.9	18.77	0.4
-150+106	22.1	42.59	2.8
-106+90	10.8	13.99	6.8
-90+75	7.9	7.26	8.3
-75+63	7.8	4.77	9.4
-63+53	5.8	2.57	6.0
-53+45	4.8	1.22	5.7
-45+34	6.5	0.83	10.4
-34	22.80	1.75	50.23
Total	100.00	100.0	100.0

Draw a partition curve and from it determine:

1. Cut point (d_{50}),
2. Water split,
3. Corrected cut point (d_{50C}),
4. Imperfection.

12.6

An hydrocyclone is to be installed in a closed circuit grinding circuit with a mill discharge containing 30% solids by volume. The solid density is 2800 kg/m^3 and the density of water is 1000 kg/m^3. Given that the maximum pressure deferential between the inlet and overflow was 50 kPa and the throughput from the mill was 800 t/h, estimate:

1. The dimensions of a suitable hydrocyclone if there are two operating in parallel,
2. The cut point.

12.7

A hydrocyclone classifier is fed with quartz slurry at the rate of 20.8 t/h from a grinding mill. The underflow is recirculated. The screen analysis of each stream were determined with the following results:

No.	Size, µm	Feed mass %	Overflow mass %	Underflow mass %
1	+300	25	0	33.2
2	-300+250	15.3	0	20.3
3	-250+150	11.6	0.2	15.4
4	-150+106	12.8	5.4	15.2
5	-106+75	9.6	18.3	6.7
6	-75	25.7	76.1	9.2
Total		100	100	100

Determine:

1. The circulation ratio
2. The efficiency of the cyclone

12.8
The input and output streams of an operating cyclone were sampled simultaneously for the same period of time. The dried samples were analysed for size distribution and the mass per cent retained on each size fraction was determined with the following results:

No.	Size, µm	Feed mass %	Overflow mass %	Underflow mass %
1	+425	1.5	0	2
2	-425+300	3.8	0	6.3
3	-300+212	6.2	0.3	12.9
4	-212+150	10.7	1.8	21.2
5	-150+106	16	15.2	28
6	-106+75	23	26.2	10
7	-75+53	28	38.4	5
8	-53	10.8	18.1	14.6
Total		100	100	100

Data:

% Solids in Feed slurry	=	35%
% Solids in Overflow	=	17.2%
% Solids in Underflow	=	70.2%
Feed capacity (dry solids)	=	25 t/h
Solid density	=	2650 kg/m^3
Inlet pressure	=	35 kPa
Apex diameter	=	6.0 cm
Vortex finder diameter	=	14.2 cm
Mass split to the underflow	=	39.4%

After a steady state operation the solid content of feed slurry was increased by 20% while all other conditions remained the same. Determine the size distribution of each stream under the altered condition.

12.9

If a second cyclone is added in series to the cyclone in problem 12.8, what is the effect of the overall efficiency of the classification. What will be the size distribution of the cyclone U/F of the second stage? The partition coefficient of the second stage cyclone is given as:

No.	Size, μm	E_{i2}
1	+425	1.000
2	-425+300	0.996
3	-300+212	0.887
4	-212+150	0.520
5	-150+106	0.223
6	-106+75	0.077
7	-75+53	0.021
8	-53	0.010

12.10

A rod mill discharge is to be classified in a straight sided, single pitch screw classifier. The classifier feed has the following size distribution:

Particle size, μm	Feed mass%
+710	2.6
-710+425	8.9
-425+250	22.1
-250+125	10.8
-125+75	7.9
-75	7.8
Total	100.00

If the classifier is to separate the feed at 200 microns estimate the classifier area and screw diameter if the feed capacity required is 100 t/h.

Data:

Solid density	=	2740 kg/m^3
Water density	=	1100 kg/m^3
Water viscosity	=	0.001 Pa.s
Classifier feed	=	40% solids (by mass)
Overflow	=	35.1% solids (by mass)
Spiral speed	=	5 rpm
Areal efficiency	=	0.45

Assume pitch is 0.5 x spiral diameter.

REFERENCES

[1] H.W. Hitzrot and G.M. Meisel, in SME Mineral Processing Handbook, N.L. Weiss (Ed), AIME, 1985, pp. 3D 46-59.

[2] T. Kojovic, and W.J. Whiten, XV111 International Mineral Processing Congress, Sydney, 1993, pp. 251-255.

[3] B. Fitch and E.J. Roberts, in SME Mineral Processing Handbook, N.L. Weiss (Ed), AIME, 1985, pp. 3D 1-10.

[4] E.J. Roberts and E.B. Fitch, Trans. AIME, 205 (1956) 1113.

[5] D.J. Kelsall and J.A. Holmes, Hydrocyclones, U.S. Patent No. 3,130,157, April 21, 1964.

[6] Krebs patent no 6,024,874, Bulletin Number 00032701. CDR

[7] Vortex Ventures 2005, Retrieved: January 21, 2005, from, http://www.vortexventures.com/Products/SpintopHydrocyclone/SpintopHydrocyclone.htm

[8] Krebs Engineers Internet publication 2005, Retrieved: January 26, 2005 from http://www.krebs.com/products.php/product/8/D-Series+Super

[9] D. Bradley, The Hydrocyclone, Pergamon Press, London, 1965.

[10] E.G. Kelly and D. J. Spottiswood, Introduction to Mineral Processing, Mineral Engineering Services. 1989.

[11] A.L. Mular and N.A. Jull, in Mineral Processing Plant Design, A.L. Mular and R.B. Bhappu (eds.), SME/AIME, Chapter 17, 1980, pp. 376-403.

[12] R.A. Arterburn, in Design and Installation of Communication Circuits, A.L. Mular and G.V. Jorgensen (eds), AIME, 1982, pp. 592-607.

[13] D.T. Tarr, IADC Conference on Hydrocyclones, Dallas, May, 1976.

[14] Krebs, 2005, Retrieved : January 26, 2005, from http//www.krebs.com/about.php/article/3/Krebs+builds+World's+largest+cyclone

[15] D.T. Tarr, in SME Mineral Processing Handbook, N.L. Weiss (ed), AIME, 1985, pp 3D 10-45.

[16] B. Fitch, Industrial & Eng. Chemistry, 54 No. 10 (1962) 44.

[17] P.S.B. Stewart and C.J. Restarick, Trans. Institute of Mining and Metallurgy, 76 (1967) . C225-230.

[18] K.J. Reid, Canadian Metall. Quarterly, 10 (1971) 253.

[19] H. Schubert and T. Neesse, in Proceedings, 10th International Mineral Processing Congress, IMM, London, 1974, pp. 213-239.

[20] L.R. Plitt, CIM Bull, 64 (1971) 114

[21] K. Heiskanen, Classification Handbook, Larox Oy, 1987.

[22] R.B. Hill, in Design and Installation of Communication Circuits, A.L. Mular and G. Jorgensen (eds), Chapter 33, AIME, New York, 1982, pp. 608-623.

[23] B.A. Wills, Mineral Processing Technology, 6th Edition, Butterworth-Heinemann, 1997,

[24] A.J. Lynch and T.C. Rao, in Proceedings Eleventh International Mineral Processing Congress, Cagliari, Italy, 1975, pp. 2 45-269.

[25] L.G. Austin and R.R. Klimpel, Powder Technology, 29 (1981) 277.

[26] L.G. Austin, R.R. Klimpel and P.T. Luckie, Process Engineering of Size Reduction: ball milling, SME/AIME, 1984.

[27] A.J. Lynch, Mineral Crushing and Grinding Circuits, Elsevier, 1977.

[28] L.R. Plitt, CIM Bull., 69 (1976)114.

[29] P.T. Luckie and L.G. Austin, Trans. Institute of Mining and Metallurgy, 84 (1975) C253.

[30] Y. Han and B. Chen, XVIII International Mineral Processing Congress, Sydney, AusIMM, 1993, pp. 263-265.

[31] D. Laguitton, *SPOC Manual - Unit Models and Fortran Simulators of Ore and Coal Process Equipment: Classification and Coal Processing*, D. Laguitton (ed), Chapter 5.1, Part B, CANMET, 1985.

[32] L.R. Plitt, B.C. Flintoff and T.J. Stuffco, in 3rd International Conference on Hydrocyclones, Elsevier, Oxford, 1987, pp. 21-34.

[33] M.O. Bustamante, Effect of the Hydrocyclone Geometry on Normal Operation Conditions, *MSc. Thesis*, University of Concepción, 1991.

[34] F. Concha, A. Barrientos, J. Montero and R. Sampaio, International Journal of Mineral Processing, 44-45 (1996) 743.

[35] D.A. Dahlstrom and Kam Wai-Ping, International Journal of Mineral Processing, 22 (1988) 239.

[36] K. Rietema, Chemical Engineering Science, 15 (1961) 298.

[37] A.J. Lynch and S. Morrell, in Comminution Theory and Practice, S.K. Kawatra (ed.), AIME, 1992, 405.

[38] K. Nageswararao, Aus.IMM Proceedings, 300 No. 2 (1995) 21.

[39] T.J. Napier-Munn, S. Morrell, R. Morrison and T. Kojovic, Mineral Comminution Circuits Their Operation and Optimisation, JKMRC, 1996.

[40] L.R. Plitt, J.A. Finch and B.C. Flintoff, in Euro. Symposium Particle Tech, Amsterdam, 1980, pp. 790-804.

[41] R.R. Klimpel, Powder Technology, 31 No. 2 (1982) 255.

[42] A. Gupta and H. Eren, Proceedings, AusIMM, 295 No. 2 (1990) 31.

[43] H. Trawinski, Engineering Mining Journal, 177 (1976) 115.

Chapter 13. Solid – Liquid Separation

13. INTRODUCTION

The process of grinding and classification involves the use of large quantities of water. In the gold industry for instance, the rule of thumb is a tonne of water for a tonne of ore. This bulk of water has to be separated or reduced for down stream treatment for recovery of the mineral in the ore. The separation of solids from liquids is usually achieved by gravity sedimentation in thickeners. For fine particles this is a slow process. In general 75-80 % of the water can be separated and removed by thickeners. For further water removal, filters are used where in excess of 90% of the water can be removed. The thickener operation can be a batch or continuous process, with either co-current or counter-current flow of underflow and overflow slurries. The filtering operation may also be batch or continuous.

For rapid solid-liquid separations, centrifugal forces are used and equipment similar to those described under classification are employed. In this chapter, we shall deal mostly with thickeners working under gravitational forces.

13.1. Design Features of Thickeners

Thickeners are essentially clarifiers producing a clearer over flow. The design considerations are based on the settling rates of the slowest settling particles and conditions for minimum disturbance of the medium (water) through which the solid particles are allowed to settle. To achieve these objectives cylindrical tanks with conical or flat bottoms are used and the velocity of the feed slurry entering the settling tank is minimised to reduce turbulence in the settling tank. A schematic diagram of a typical thickener is shown in Fig. 13.1. The feed in the form of slurry is generally guided by a launder, which is laid at a slope just sufficient for the slurry to flow without depositing any solids. The feed launder terminates in a feed well located at the centre of the tank. The feed well is designed to break the fall of the slurry and dissipate the energy.

The feed well is concentric with the rake driving shaft. The rakes are bolted or welded on to this drive shaft and for long and large rakes they have additional support from cables. Usually four rakes are employed of which two may be short and two long. Attached to the rakes and below them are spikes, particularly in situations where the sludge is thick. The spikes help to break up the sludge and render it more suitable for pumping. The rakes are driven by a motor which is mounted on a plate above the well. An alternative is to mount the drive motor on a track running along the rim of the tank. A bridge usually runs from the periphery to the centre of the tank. It is supported by the wall of the feed well and the rim of the tank. The bridge serves as a walkway and also carries an open launder (or pipe), which carries the slurry to the feed well. In some designs the bridge spans the entire length of the tank. As in clarifiers, the bottom of most tanks slope towards the centre where the thickened underflow sludge accumulates. When a flat bottomed tank is designed, the settled sludge builds up to form its own slope depending on the angle of repose of the material thus forming an artificial sloping tank bottom. The sludge collected at the bottom is discharged through an outlet shaped like a cone with steep cone angle. Alternately, the thickened slurry is swept

towards a trench at the bottom of the tank. Usually a scraper is installed for smooth delivery of sludge from the discharging cone or trough. A slush or centrifugal pump subsequently removes the sludge.

The thickener tanks are usually fabricated using steel sheets. But tanks with concrete sides are quite common. Some small tanks (usually < 30 m in diameter) are made of plastics. The whole assembly is installed either above ground sitting on pillars or at ground level with the discharge well below the ground level. In the latter case, an access tunnel is provided where the discharging pump is located. In some installations the discharge pump is located above the tank; in such cases, a suction pipe runs down the centre column to the bottom well. Alternatively, a submerged motor pumps the under flow slurry to the top of the tank discharging its contents to a holding tank.

Several variations are known to exist. For instance the rakes are either supported by cross beams or truss above the tank or supported by the central column and cables. The cables are also connected to torque meters.

Fig. 13.1 is a sketch of a *bridge thickener* where the bridge runs across the thickener tank. The bridge support the rakes and the motor rotating the rakes sit on a platform in the centre of the tank. The rakes are bolted to the central column which is rotated by the motor. The Bridge thickeners have a maximum diameter of about 30 meters.

When the rakes are supported entirely by the central pillar, the access bridge usually runs half way on the tank surface terminating on the central pier. The centre pier thickeners are considerably larger than the Bridge type. The diameter of the tank ranges from about 35 - 180 meters.

A variation is the *tray thickener* where trays or compartments are placed one on top of the other. Each tray acts as a thickener and the assembly operates in parallel with a common pier or shaft where the rakes are fixed. Clarification takes place in series operation, that is, the thickener underflow from the top compartment serves as feed to the lower compartment. Ultimately the underflow from say, a six tray thickener, form the final thickened underflow. Similarly all the overflow from each tray combine forming the final overflow slurry. Fig. 13.2 is a schematic diagram of a 3-compartment clarifier. Up to seven compartments are available.
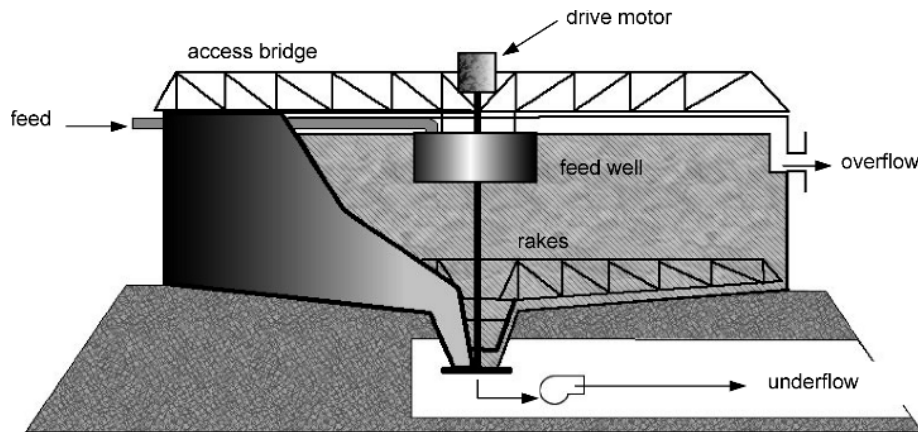
Fig. 13.1. Sketch of a thickener showing the access bridge, feed well, rakes supported by the central column and cables and the underflow discharge.
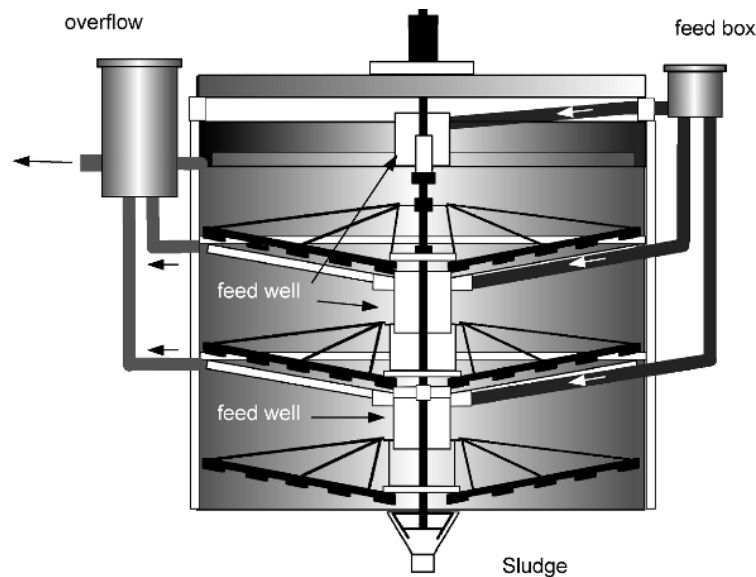
Fig. 13.2 . Schematic diagram of a tray type clarifier, after Dahlstrom and Fitch [1].

The thickening process is accelerated by the addition of flocculants *Hi-Capacity thickeners* allow a mixing arrangement in the feed box where the flocculant is intimately mixed. The other design features of the Hi-Capacity thickeners are similar to the Bridge thickeners.

While installing the feed pipe or launder to thickeners, the slope is held at 1 to 1.5. King [2] suggests that this slope provides minimum turbulence of the settling slurry in the tank. The feed is actually made to enter about a meter below the surface of the tank level thus helping to minimise turbulence.

The feed well diameters are between 1 and 1.2 m with lengths of 1.2 to 5 m. Tank sizes vary according to feed characteristics and the sedimentation time. Manufacturers such as Dorr-Oliver-Eimco, [3] have suggested that the water depth should be between 3.0 and 3.6 m and the feed well size about 25% of the basin area.

The rake-drives in bridge clarifiers are either centre driven (as shown in the Fig. 13.1) where the motor is mounted on a support plate or are peripheral driven. When the sludge is too thick and the rakes struggle to move or in extreme cases cease altogether, the rakes are designed to rise either mechanically of pneumatically. Usually the torque on the rakes is monitored and the rakes rise automatically at a fixed torque level. This precautionary procedure is generally attached to thickeners of diameter greater than 10 meters. The allowable torque is about 5-30 times greater than normal operating torque [1].

A recent innovation is the Dorr-Oliver Eimco E-Cat thickeners which has dispensed with the rakes and introduced *clarifying cylinders* through which the suspension passes to produce the clear over flow (Fig. 13.3). These thickeners are designed for rapid sedimentation by the use of flocculants. The clarified slurry then passes through filters producing a clear overflow.

feed

feed mix

overflow

clarifying
cylinders

cones

dewatering cones

underflow
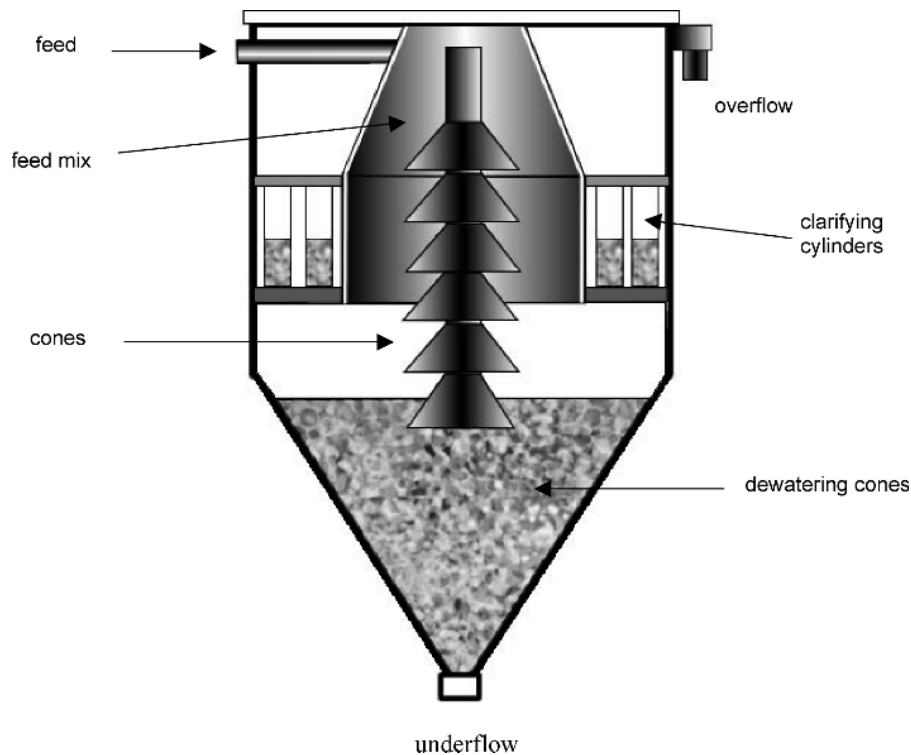
Fig. 13.3. Clarifier/Thickener, Dorr Oliver Eimco [4].

13.2. Thickener Design-Batch Process

Thickeners have been designed using the basic laws of sedimentation. Empirical methods devised by manufacturers are also used for rapid work. For designing , the chief criterion is to determine the relation between the settling velocity and the dimensions of the vessel to be used for each particular slurry. The settling velocity for a particular slurry can be easily determined in the laboratory by using small-scale tests. The tests consist of determining the downward movement of the boundary of the clear liquid and the suspension. It has been found that this rate is initially constant but the rate decreased as the particles slowly settled to the bottom and the interface met the sludge zone. This can easily be visualised from Fig. 13.4 where the progressively increasing concentration with depth is shown. It is obvious that the deeper the vessel and longer the time given for settling, the clearer will be the supernatant liquid and the thicker will be the sludge.

The decrease in the settling rate is due to hindrance by increased crowding of the particles as they settle and collect at the bottom of the vessel. At the sludge-forming layer, the particles pack down by displacing the liquid in between. In so doing, the clear liquid level rises. These considerations apply both to batch and continuous processes, with the difference that in the continuous process a balance between the flow rate of the overflow stream and the removal rate of the sludge has to be maintained.
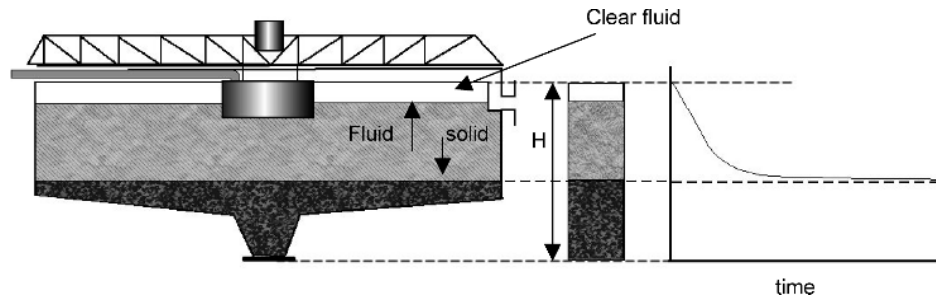
Fig. 13.4. Sedimentation in a thickener.

These considerations originally used by Coe and Clevenger [5] are now in use extensively .The quantitative basis for designing the thickener area assumes that :

1. Settling rate was a function of concentration,
2. The volume rate of discharge of the clear supernatant liquid was equal to the difference of the rate of feed of the slurry minus the rate of removal of the thickened layer.

For determining the thickener area, Coe and Clevenger assumed that the liquid moving upwards is always greater than the movement downwards. The mass of liquid flowing upwards is given by:

$$(F - D) \, Q_{M(F)} \qquad t/h \qquad\qquad\qquad (13.1)$$

where F =   the feed mass ratio (liquid/solids, also known as the feed *dilution*),
D =   discharge mass ratio (liquid/solid) and
$Q_{M(F)}$ =   Feed capacity by mass, t/h

At equilibrium, the upward velocity of liquid equals the downward velocity of the solids. Thus if v_S is the velocity of sedimentation, A the cross-sectional area of the tank, in m^2, and ρ_L the specific gravity of the liquid, then at equilibrium:

$$\left(\frac{F - D}{A \, \rho_L} \right) Q_{M(F)} \;=\; v_S \qquad\qquad\qquad (13.2)$$

hence, $A \;=\; \left(\dfrac{F - D}{v_S \, \rho_L} \right) Q_{M(F)} \qquad\qquad\qquad (13.3)$

In practice, to determine the design value of the thickener area, a number of laboratory sedimentation tests are run using 2 litre cylinders and determining the value of v_S for a range

of F values. The maximum value of A is taken as the design cross-sectional area of the thickener tank.

Dahlstrom and Fitch [2] has analysed each of the settling zones and arrived at a practical expression similar to the expression of Coe and Clevenger for sizing a thickener. Considering that the flow rate in the clear zone should be less than the settling rate of the smallest particle that has to be removed by settling, they derived the velocity of sedimentation as:

$$v_s = \frac{[F-D]}{\rho} Q \tag{13.4}$$

This equation is similar to Eq. (13.2) by Coe and Clevenger. Dahlstrom and Fitch [2] suggested that the actual sedimentation rate must be multiplied by the areal efficiency factor, A_{EF} to obtain a realistic value. The areal factor is a function of the tank dimensions (height and diameter) and ranges between 0.20 and 0.25.

Eqs. (13.3) and (13.4) are extensively used to determine the cross-sectional areas of tanks. The laboratory estimations are performed at different concentrations of F and D and the largest value of A is taken as the designed size of the tank as in the Coe and Clevenger method. For practical purposes they suggest a scale-up factor of 1.25 – 1.5 for thickener units less than 15.2 m in diameter and 1.3 – 1.5 for units greater than 15.2 m in diameter.

13.3. Thickener Design-Continuous Thickeners

For designing continuous thickeners, the three most important parameters that need to be established are:

1. Cross sectional area of the tank
2. Depth of thickened layer
3. Depth of the clarifying zone

Other factors include discharge slurry properties, such as liquid/solid ratio, viscosity and the characteristics of pumping.

13.3.1. Estimation of Cross-Sectional Area of Tank

Coe and Clevenger's equation fails to accurately estimate the cross-sectional area of the tank when the slurry is treated with a flocculating agent. In such cases the mathematical approach of Kynch [6] as applied by Talmage and Fitch [7] is more suitable. A particular advantage is that while several determinations of settling velocities, v_S, are required by Coe and Clevenger's method, a single estimation is sufficient when analysis of the sedimentation curve is made. To apply Kynch's method the following assumptions are made:

1. The concentration of particles in any horizontal plane is uniform,
2. Differential settling due to differences in shape, size   or composition of mineral particles do not take place,
3. The sedimentation velocity is a function of concentration and tends to zero at a concentration equivalent to the sediment layer at the bottom of the container,
4. The wall effect is negligible.

A single laboratory test therefore involves the suspension of a slurry in a 2 litre tall transparent cylinder and measuring the clear fluid interface with the slurry at different times

till the level falls and all particles settle at the bottom as sludge. Where the sedimentation rate is very slow or the supernatant liquid remain turbid and unclear, flocculants are added.

If required, rakes are introduced to break up agglomerated particles. A typical sedimentation curve indicating the height of the interface with time and the structure of the slurry in the cylinder is shown in Fig. 13.5. It can be seen that at the initial stages, the rate of fall of the interface is nearly constant. When the settling rate of the bulk of the slurry diminishes, (as seen in cylinder 4), the clear zone-sludge interface merges and the curve then flattens out. At this stage, further lowering of the clear level interface can take place by the expulsion of water between the particles in the sludge. Fig.13.5 shows that at time $t = 0$, the height of the interface is H_o. As it is assumed that the concentration of slurry is uniform across the cross-section of the tube, at any height, H_1, the concentration of the sludge will be the same across the settling tube.

For a dispersed slurry, the solids start settling at a uniform velocity which is a function of the local solids concentration [5,6]. As the settled solids build up at the bottom of the container, the boundary between the settling solids and slurry of the initial concentration starts to rise in the slurry as indicated in Fig. 13.5. Zones of intermediate concentration between the initial and final concentrations will move upwards from the bottom at a rate related to the concentration of solids in that zone. When the rising and settling zones meet, the settling slows and is controlled by the extraction of retained water from the solids as it goes through compaction.

The rise velocity of the zone of concentration C, from the bottom of the cylinder to the interface of the settling mudline, v_R, given by;

$$v_R = \frac{dH}{dt} = -\frac{d\psi}{dC} \tag{13.5}$$

and is represented by the line OY in Fig. 13.5. ψ is the settling flux, kg/m^2/s.
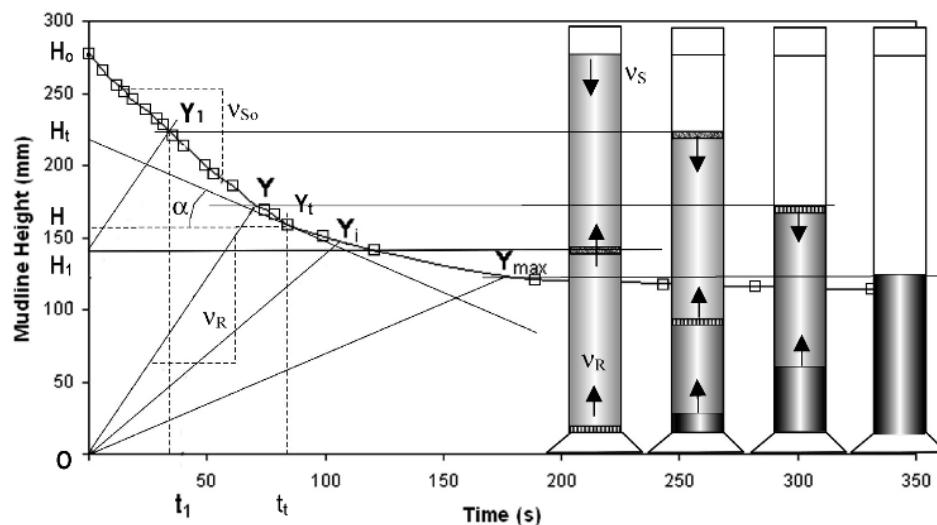
Fig. 13.5. Settling curve – Kynch's interpretation.

If line OY represents the initial uniform concentration C_O then higher concentrations resulting from settling solids at the bottom of the cylinder are represented by lines of lower slope, OY_i (for intermediate concentration) until the maximum concentration of the settled solids is reached and represented by C_{MAX} and line OY_{MAX}. Any line parallel to these will represent the rise velocity of zones of the same concentration, C, so line H_1Y_1 will represent a zone of concentration C_O which originates from height H_1 in the slurry propagating upwards and reaching the mudline interface at Y_1 after time t_1.

Since the sedimentation rate is dependant on concentration only, until the zone of initial concentration from the cylinder bottom reaches the interface, the sedimentation rate of the interface will be constant and hence the rate v_{So} will be represented by a straight line, H_OY.

According to Kynch, if a tangent is drawn to the settling curve at point Y_t, the slope, α, corresponds to the settling velocity,v_{St}, of the layer or zone of concentration C_t just below the settling interface. The intercept of the tangent on the Y-axis, H_t, corresponds to the height of slurry of uniform concentration equal to C_t. Then by a mass balance:

$$H_t C_t = H_O C_O \tag{13.6}$$

for a cylinder of constant cross-sectional area. Consequently, a plot of settling rate versus concentration can be constructed from a single settling curve.

Kynch's theory has been tested experimentally on many occasions and found to hold for the batch settling of equi-sized rigid spheres in water but deviates for flocculated suspensions that form compressive sediments [8].

Yalcin [9] reported the sedimentation curves of a copper-nickel tailings for several initial percent solids. By constructing tangents to the low density pulp curve at different higher percent solids, using the Kynch construction, estimates of the settling rates can be compared to the actual measured sedimentation rates of these slurries. Fig. 13.6 shows such a construction on the settling curve of an unflocculated slurry having an initial concentration of 5% solids. The estimates of the settling rates of the higher % solids are obtained from the tangents to the 5% sedimentation curve, intersecting the Y-axis at the mudline heights corresponding to 15, 25, 35 and 45% solids. Fig. 13.7 shows the measured sedimentation velocities versus the Kynch estimates from the slope of the tangents. The plot for the estimates from the 5% solids curve shows considerable difference from actual measured values being higher than the estimates according to the Kynch theory. If the estimates are constructed from the 15% solids curve for slurries of higher densities, Fig. 13.7 shows a closer correlation between the estimates and real sedimentation velocities. The estimates constructed from the 25% solids curve are similar to that obtained from the 15% solids curve.

Figs. 13.8 and 13.9 show similar constructions for a flocculated gold tailings at 20, 30 and 40% solids. In this case, the Kynch estimates of the settling velocities are in close agreement with the actual measured velocities.

Although the Kynch theory is not considered suitable for all mineral slurries, especially flocculated slurries, nevertheless it can give satisfactory results as indicated in Fig. 13.9. It is still used for thickener design calculations [8].

Talmage and Fitch [7] showed that the settling velocity was related to the concentration. For a point on the settling curve of time t and height H_t, the equation is:

$$C_t = \frac{C_O H_O}{H_t + v_{St} t_t} \tag{13.7}$$
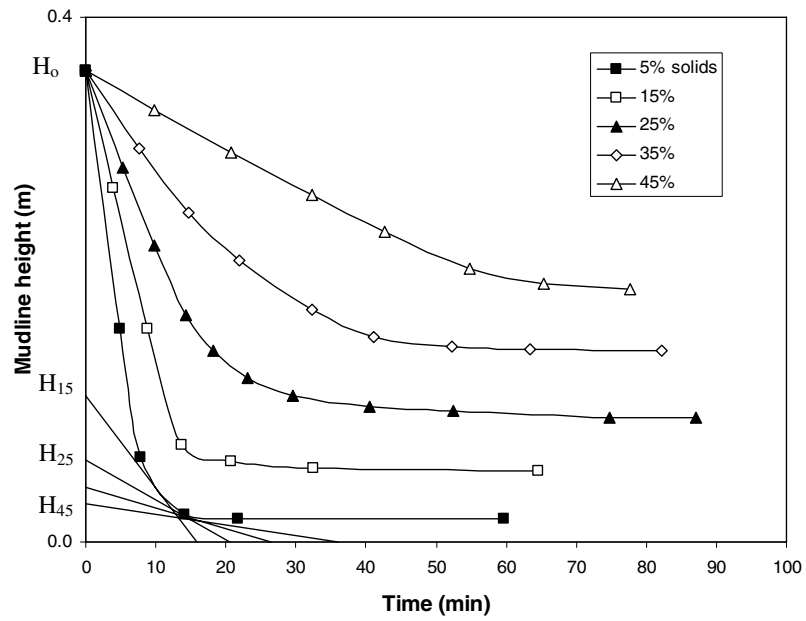
Fig. 13.6. Cu-Ni tailing sedimentation data replotted from Yalcin [9] with Kynch construction on the 5% solids curve.
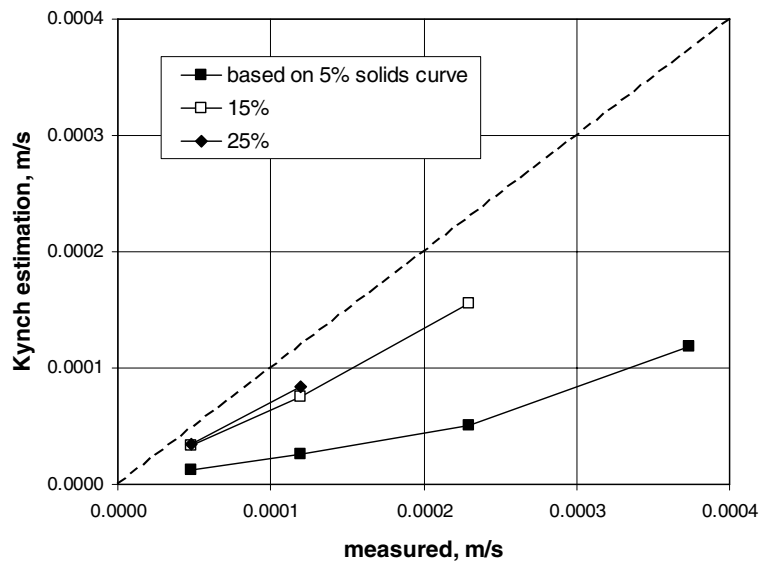
Fig. 13.7. Kynch estimated sedimentation rates compared to measured rates for different % solid slurries, (data from [9]).
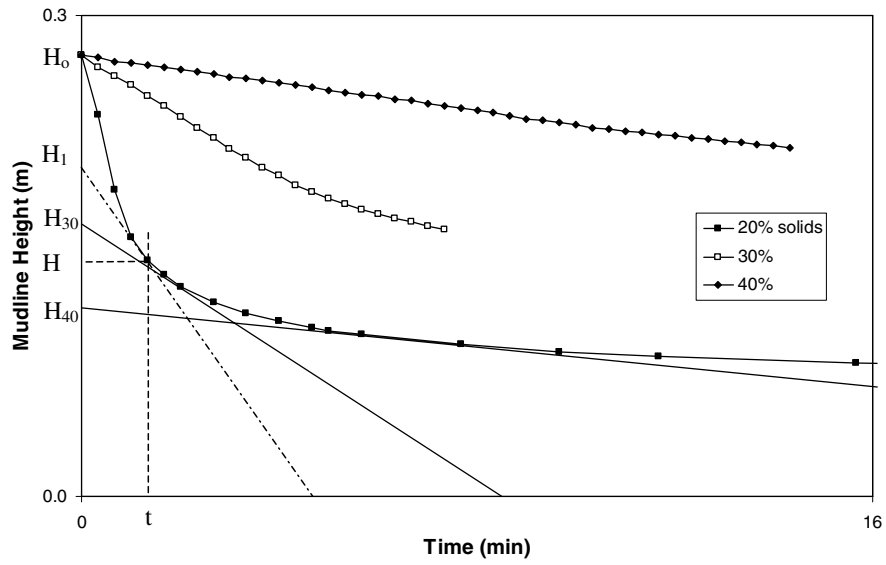
Fig. 13.8. Sedimentation curves of a flocculated gold tailing with Kynch construction on the 20% solids curve.
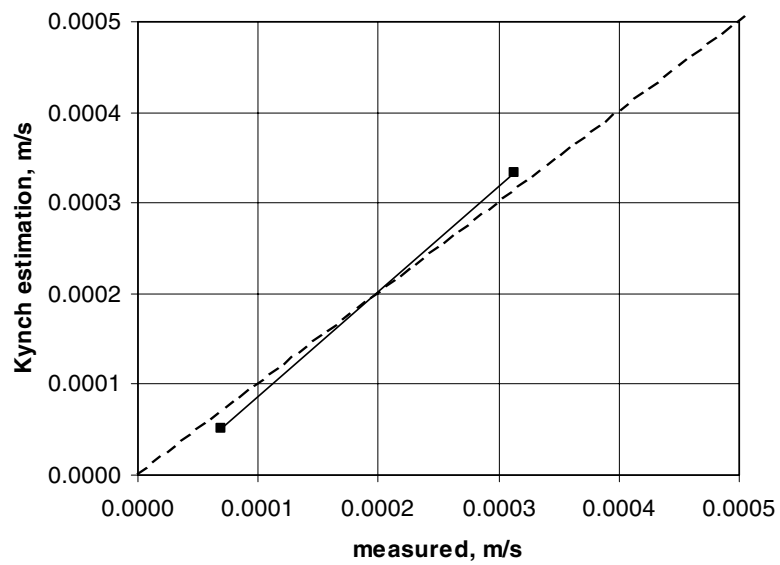
Fig. 13.9. Kynch estimated sedimentation rates compared to measured rates for a flocculated gold tailing.

In a batch settling test, the mass of solids in the test cylinder is given by C_OH_OA. If the time taken for all the solids to settle past a layer of concentration C is t_U then C_OH_OA/t_U represents the quantity of solids that can be brought through the concentration layer per unit time. The area of thickener required to settle 1 tonne of solid per unit time is then given by:

$$A = \frac{t_U}{C_oH_o} \qquad m^2/t/h \qquad\qquad (13.8)$$

The time t_U is obtained by drawing a line from mudline height H, corresponding to the concentration C, at a tangent to the settling curve. The intersection of this tangent with the mudline corresponding to the underflow concentration is the value t_U on the time axis. This is illustrated in Fig. 13.10.

The maximum thickener area requirement will occur when the tangent is drawn through the compression point on the sedimentation curve since this tangent will give the highest value of t_U in the free settling range which, according to Talmage and Fitch [6] is the zone determining the unit area. When the line, corresponding to H_U, intersects the settling curve above the compression point, the value of t_U corresponding to the maximum thickener area will be the point of intersection with the settling curve, shown as $t_{U(1)}$ in Fig. 13.10.

Fig. 13.5 shows that a near steady concentration is reached at about Y_{MAX}. Assuming this to be an equilibrium state, a material balance of solid and liquid can be made. Svarovsky [10] expressed the area of the tank in terms of the overflow rate. From a material balance, the
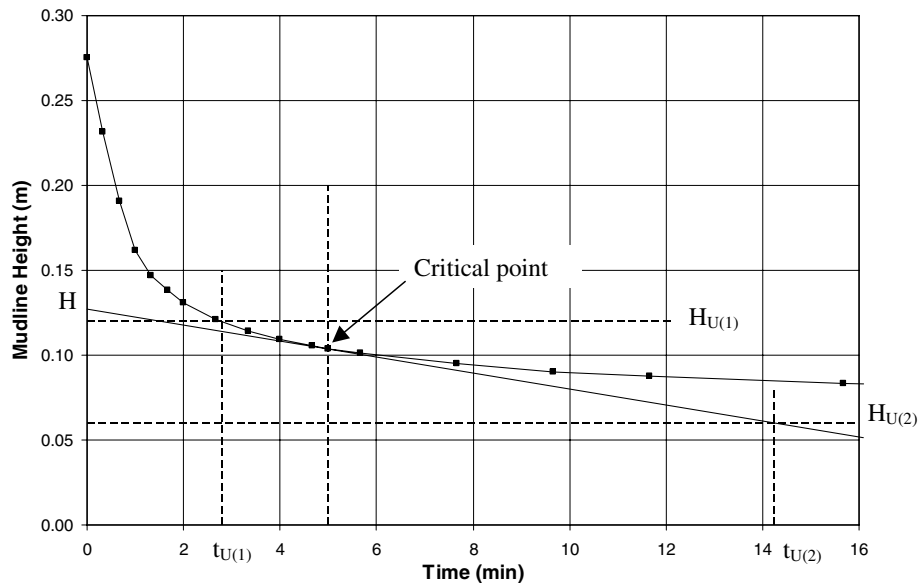
Fig. 13.10. Talmage and Fitch construction for determination of t_U; $t_{U(1)}$ is the value where H_U lies above the critical point and $t_{U(2)}$ is the value where H_U lies below the critical point.

ratio of the overflow rate to feed rate can be determined in terms of feed and underflow concentrations as:

$$\frac{Q_{V(O)}}{Q_{V(F)}} = \frac{C_U - C_F}{C_U}$$

(13.9)

where $Q_{V(O)}, Q_{V(F)}$ = volumetric overflow rate and feed rate, m^3/s,

C_U, C_F = concentrations of the underflow and feed respectively, expressed as the mass of solid/volume of slurry, kg/m^3.

The overflow rate can be easily measured providing the velocity of the underflow is measured and is constant. The overflow rate for the system is related to the liquid rise velocity by the equation:

$$Q_{V(O)} = A\, v_{(O)}$$

(13.10)

where $v_{(O)}$ = liquid rise velocity or overflow velocity.

Substituting this value in Eq. (13.9) and simplifying, the area of the tank may be expressed as:

$$A = \frac{Q_{V(F)}}{v_O} \left[\frac{C_U - C_F}{C_U} \right]$$

(13.11)

Eq. (13.11) gives the area of the cross-section of the tank at a known feed rate, known concentrations of feed and underflow and liquid rise velocity.

13.3.2. Determination of Critical Point

The Talmage and Fitch and other methods of thickener design require the determination of the critical point on the sedimentation curve. As the solids settle they pass from free settling to hindered settling to compression conditions. At each of these transitions there is a discontinuity in the sedimentation curve. In the free settling region, the settling rate is constant and representative of the initial solids concentration. When the solids concentration increases to the point where the near neighbours start to influence the settling rate of the particles, the settling rate slows and is affected by the concentration of nearest neighbours. The slurry is in a hindered settling condition and the decrease in settling rate is referred to as the *first falling rate*. The settling behaviour becomes non-linear, inversely proportional to the solids concentration. When the solid concentration increases to the extent where the solids touch, settling ceases and further consolidation of the solids occurs by compression. This further drop in sedimentation rate is referred to as the *second falling rate* and a second discontinuity in the settling curve will occur (Fig. 13.11). The end of hindered settling and the start of the compression zone is referred to as the *compression* or *critical point*. This discontinuity in the settling curve is not always readily discernable and some procedures have been suggested to try and locate the compression point on the settling curve.

These procedures try to replot the data to accentuate the discontinuity in the settling behaviour, making some assumption as to the shape of the curved sections:

1. replot on log-log axes. The upper and lower sections of the curve generally approximate straight lines which intersect at the critical point.

2. draw tangents to the sedimentation curve at both ends and bisect the angle formed. The line bisecting the angle often intersects the sedimentation curve close to the critical point. This however will change as the scale on the axes changes [11]. See Fig. 13.12.

3. The mudline height at the critical point, H_C, can be obtained from a plot of dH/dt versus time as indicated by Mondal and Majumdar [12], Fig. 13.13. Again, the change in slope at the critical point should be evident. Barnea [13] also plots the differential:

$$\frac{H_{n-1} - H_{n+1}}{t_{n+1} - t_{n-1}} \quad \text{versus} \quad \frac{H_n - H_\infty}{H_0 - H_\infty}$$

where n is one data reading on the sedimentation curve. H_n is defined as the mean of H_{n-1} and H_{n+1}. See Fig. 13.14.

4. Plot the distance log $(H - H_\infty)$ versus time where H_∞ is the final (equilibrium) sedimentation height (at infinite time). If the curved sections of the sedimentation curve are represented by an inverse exponential function, then plotting the log of the height vs. linear time will give a straight line and a change in slope will occur at the sedimentation discontinuity [14]. See Fig. 13.15.

5. Dahlstrom and Fitch [1] assumes the start of the compression of the sediment takes place at a mudline height half way between the initial height and the final height of the sediment; ie. $H_C = H_0 - H_\infty$. For the sedimentation curve in Fig. 13.11, this gives an estimate of the critical point at 56 s. This point appears to be the start of the hindered settling zone rather than the compression zone. This method and the bisected angle method are not recommended.

From the sedimentation curve given in Fig. 13.11, the critical point estimation by the various methods is given in Table 13.1

Table 13.1
Critical point estimates, t_C, from the sedimentation data in Fig. 13.11 by various methods.

Method	Hindered settling, s	Critical point, s
Log-log plot	~58	~410
Bisected angle	-	145
Roberts	60	590
Mondal and Majumdar	80	580
Barnea	40	460
Dahlstrom and Fitch	-	56

The Roberts, Barnea and Mondal methods appear to give similar estimates. The log-log plot gives little deviation from a straight line and the critical point is less easily identified for this data. On the Barnea plot, for this data, it is also difficult to identify the critical point.
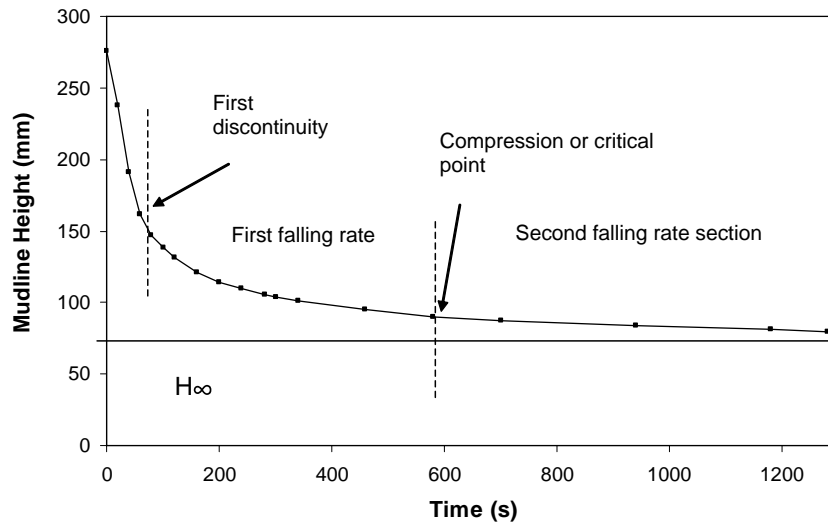
Fig. 13.11 Batch settling tests showing discontinuities at the transition from free settling to hindered settling and to compression.
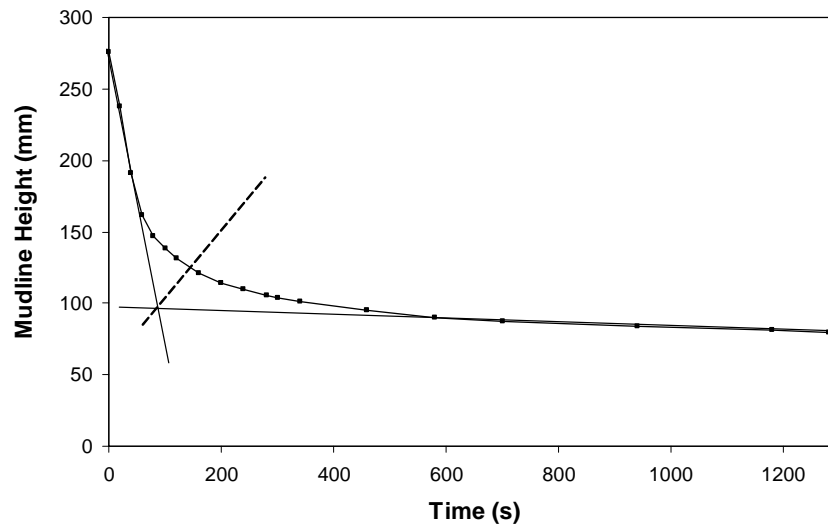
Fig. 13.12. Rough location of the critical point by bisecting the angle formed by two tangents to the extremities of the sedimentation curve [11]. Critical point at 145 s.
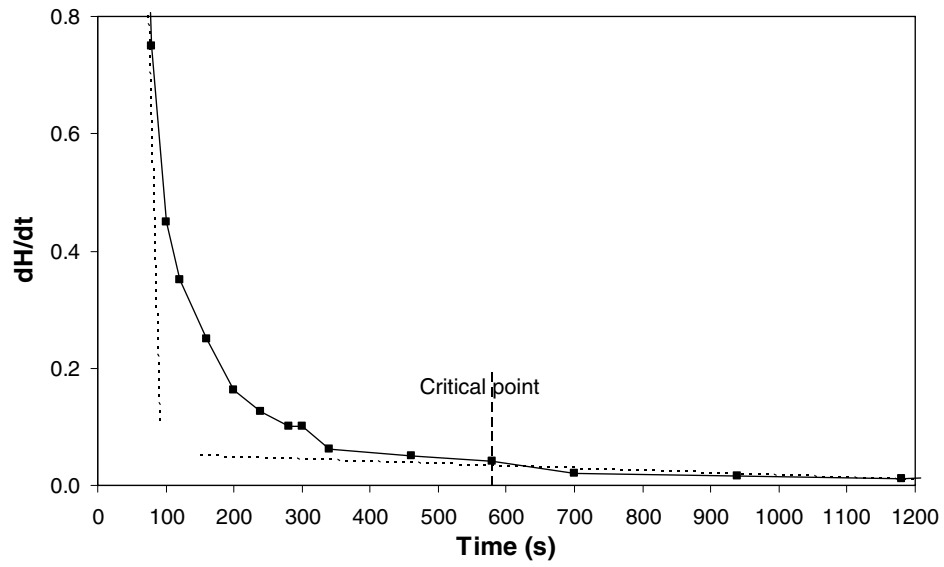
Fig. 13..13. Plot of change in slope versus time [12]. Critical point at 580 s.
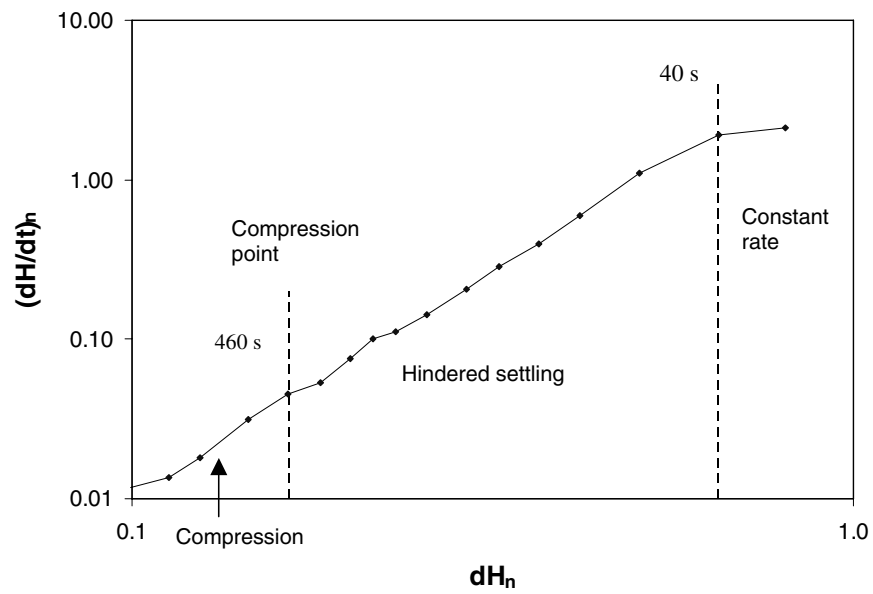
Fig. 13.14. Barnea (1977) plot where $(dH/dt)_n = \dfrac{H_{n-1} - H_{n+1}}{t_{n+1} - t_{n-1}}$ and $dH_n = \dfrac{H_n - H_\infty}{H_O - H_\infty}$.

416
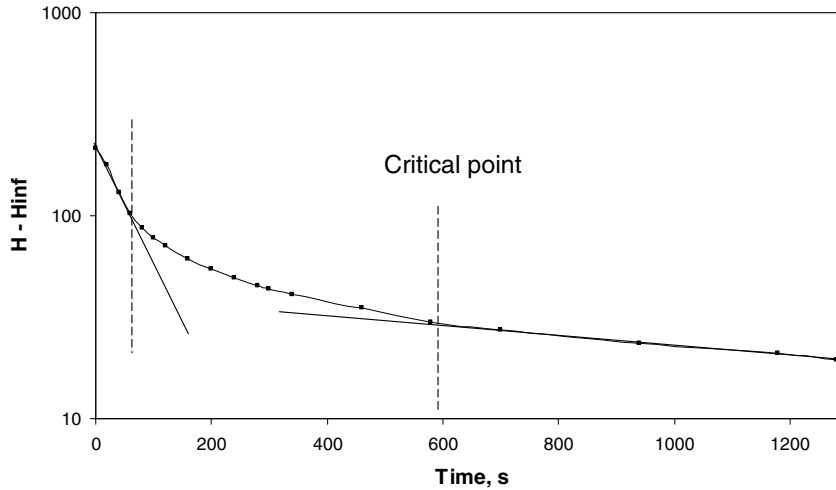
Fig. 13.15.   Plot of log (H − H∞) versus time to accentuate the change in slope at the two
discontinuities in the sedimentation curve [9,14]. Critical point at 590 s.

13.3.3. Determination of Settling Flux

Instead of using the concentrations of streams it is more convenient to express Eq. (13.10) in terms of the mass of sedimentation per unit area, known as the settling flux (ψ) and given by:

$$\psi = C_t v_s \qquad (13.12)$$

Substituting the value of C_t from Eq. (13.6):

$$\psi_t = \frac{C_o H_o}{H_t} . v_{st} \qquad (13.13)$$

Thus on the sedimentation curve, if tangents are drawn at several points, then the slopes and intercept with the H axis gives the corresponding flux–concentration curve as shown in Fig. 13.16.

The settling flux curve can only be reconstructed from the sedimentation curve for the conditions where the gradient to the flux curve is decreasing with increasing concentration. That is, conditions which are found in the normal sedimentation test and are represented by concentrations higher than the point of inflection on the flux curve.

A non-graphical approach was proposed by Yalcin [9] and is dependant on a power law relationship between the slurry % solids and sedimentation time being established.   For the 20% solids slurry in Fig. 13.8 the underflow % solids corresponding to each mudline height is plotted against time in Fig. 13.17.   From Fig. 13.17:

$$\%S = k\, t^n = 31.06\, t^{0.1961} \qquad (13.14)$$
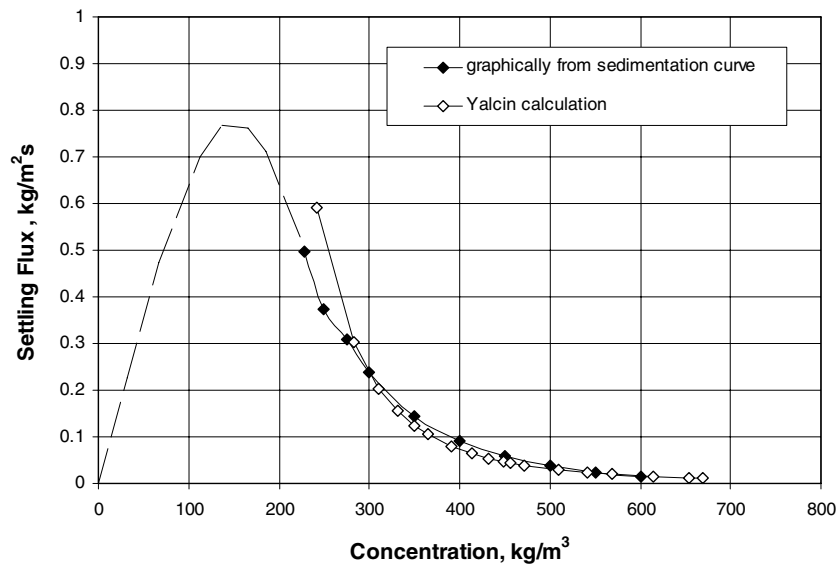
Fig. 13.16. Settling flux calculated from tangents to the 20% solids pulp curve in Fig. 13.8.

$y = 31.06x^{0.1951}$

$R^2 = 0.9643$
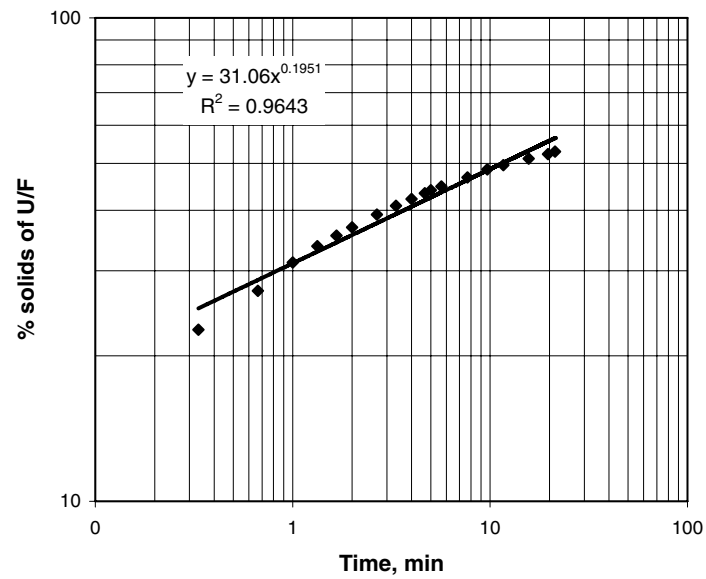
Fig. 13.17. Relationship between underflow % solids and sedimentation time for a gold tailing at 20% solids initial concentration.

At any mudline height, H and time t_t on the sedimentation curve (Fig. 13.5), the % solids (%S) corresponding to the slurry near the interface having a settling rate of v_S is given by the intercept of the tangent to the curve, H_t. The % solids at H_t is given by [9]:

$$\frac{1}{\%S_t} = \frac{1}{\%S_O} - \frac{(H_O - H_t)\rho_w}{100 C_O H_O}$$ (13.15)

where $\%S_t$ = % solids at time t and
$\%S_O$ = initial % solids (at t = 0).

Substituting for %S from Eq. (13.14) into Eq. (13.15) and rearranging gives:

$$H = \frac{100 H_O C_O}{\rho_w k} \cdot t^{-n} + H_O\left(1 - \frac{100 C_O}{\%S_O \rho_w}\right)$$ (13.16)

Then, differentiating Eq. (13.16) with respect to time:

$$\frac{dH}{dt} = v_S = -\frac{100 n H_O C_O}{\rho_w k} \cdot t^{-(n+1)}$$ (13.17)

Thus for any sedimentation time, t_t, the value of H is obtained from Eq. (13.16), v_S from Eq. (13.17) and H_t from Fig. 13.5:

$$H_t = H + v_S t_t$$ (13.18)

The % solids below H_t ($\%S_t$) is then obtained from Eq. (13.15). Thus a series of v_S values can be obtained for different underflow % solids, which are related to the solids concentration by the equation:

$$C = \frac{\%S}{\dfrac{\%S}{\rho_s} + \left(\dfrac{100 - \%S}{\rho_w}\right)} \quad kg/m^3$$ (13.19)

Points on the settling flux curve can thus be evaluated as shown in Fig. 13.16 for a gold tailing sample. Good agreement is found between the calculated flux and the graphically estimated flux values.

A second graphical method was advocated by Jernqvist [15,16] and described by Kelly and Spottiswood [17] and is based on the laboratory determination of batch settling in a tall cylinder. The time axis of the height-time curve is reversed and the following steps taken:

Step 1: The Y-axis is extended to form the Y-axis of the solid flux-concentrate curve.

Step 2: Draw a horizontal line to form the x-axis of the flux curve.

Step 3: Let the initial concentration of the slurry be C_O located on the C axis. Through C_O draw a vertical line.

Step 4: Through H_O draw a horizontal line, indicating concentration (could be the C axis).

Step 5: Draw a tangent to the sedimentation curve, say α_1. Through the origin of the flux curve draw line OF parallel to the tangent α_1.

Step 6: From the intersection of α_1 with the y-axis, draw a horizontal line to cut the vertical line through C_O at H_1. Join origin O' to H_1 and proceed to cut the x-axis at C_1. Draw a vertical line through C_1 to cut the OF line at 1. This point of intersection is a point on the flux-concentration curve.

Step 7: Repeating steps 5 and 6, several points can be obtained which on connecting, provide the ψ - concentrate curve.

The construction of the (ψ-C) is illustrated in Fig. 13.18 and compares well with other techniques. The scale used for the flux axis must be consistent with the dimensions of the other 3 axes. This procedure also assumes that the sediment is not compressible.
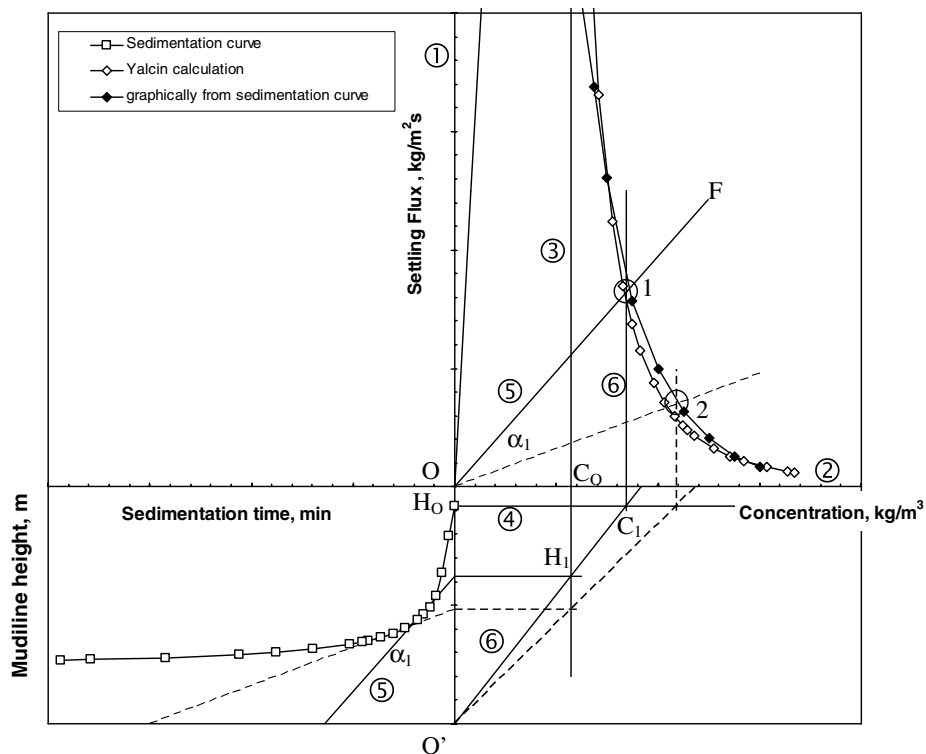
Fig. 13.18. Jernqvist method for construction of the flux curve from a sedimentation curve [15,16].

The thickener area is then obtained from the settling flux value according to the equation:

$$A = \frac{Q_{M(F)}}{\psi} \qquad (13.20)$$

For smooth operation of a thickener and to achieve the required properties of the product streams it is imperative to know:

1. the maximum allowable concentration of the underflow,
2. the optimum conditions of the overflow and the concentration of the feed slurry.

This information is derived from the flux-concentration and flux-time curves.
In continuous sedimentation process two forces are simultaneously in operation:

1. Sedimentation flux (ψ_S),
2. Withdrawal flux (ψ_W).

Thus the total flux is given by:

$$\psi_T = \psi_S + \psi_W \qquad (13.21)$$

The two flux-concentration curves and the total flux curve resulting from the combination of each set of data are shown in Fig. 13.19. The combined flux curve shows a minimum value at some critical concentration, C_{CRIT}. The corresponding minimum flux, ψ_{CRIT}, is the maximum that the thickener can handle. At a concentration less than C_{CRIT}, solids enter the sludge layer faster than can leave via the underflow and hence the concentration, C, increases up to C_{CRIT}. At concentrations greater than C_{CRIT}, solids leave the underflow faster than is entering sludge layer and hence C drops to C_{CRIT}.

Coe and Clevenger [5] suggested that at this critical concentration, the flux of solids to the underflow of a continuous thickener would be a minimum and the critical flux, ψ_{CRIT}, is the maximum flux that can flow through the thickener into the underflow at steady state. This critical flux is rate determining and will determine the thickener area for a given feed rate and underflow density, according to Eq. (13.20).

Yoshioka et al. [18] obtained the critical flux from the settling flux-concentration curve by constructing a tangent to the curve passing through the underflow concentration C_U on the x-axis (Fig. 13.19). The tangent is called the *Operating Line* and the intercept on the flux axis is the critical flux, and the thickener area is:

$$A = \frac{Q_{M(F)}}{\psi_{CRIT}} = \frac{Q_{V(F)} C_0}{\psi_{CRIT}} \qquad (13.22)$$

It should be noted that if $\psi_O > \psi_{CRIT}$ then the thickener is overloaded and corrective action is necessary.

Oltmann [19] suggested a simple empirical approach to the critical flux determination and hence thickener area. In cases where the settling rate at the beginning of the sedimentation test is non-linear due to turbulence resulting from mixing, an extrapolation of the linear settling rate section to the horizontal extension of H_O will give the start time t_a (Fig. 13.20).
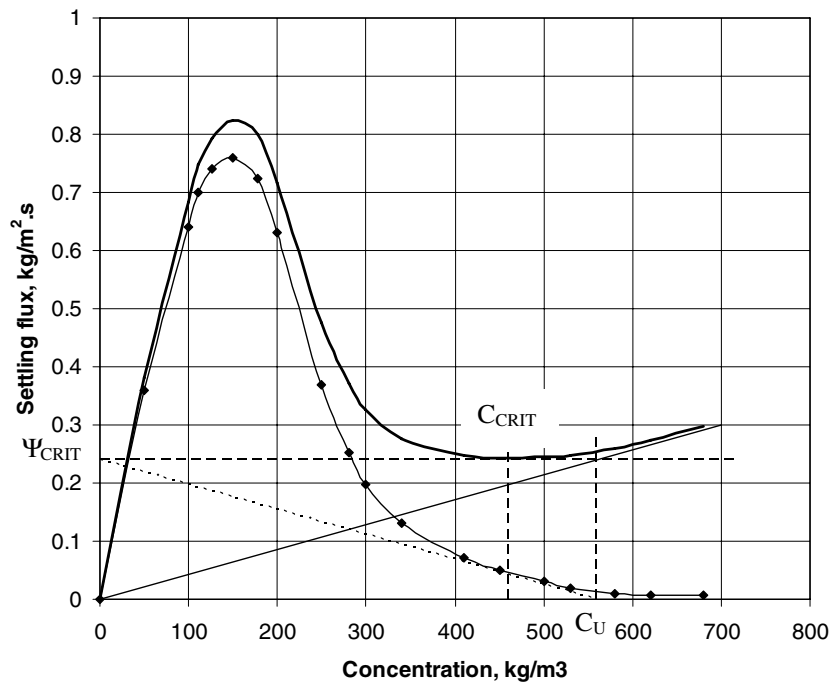
Fig. 13.19. Flux curves for a continuous thickener [17].
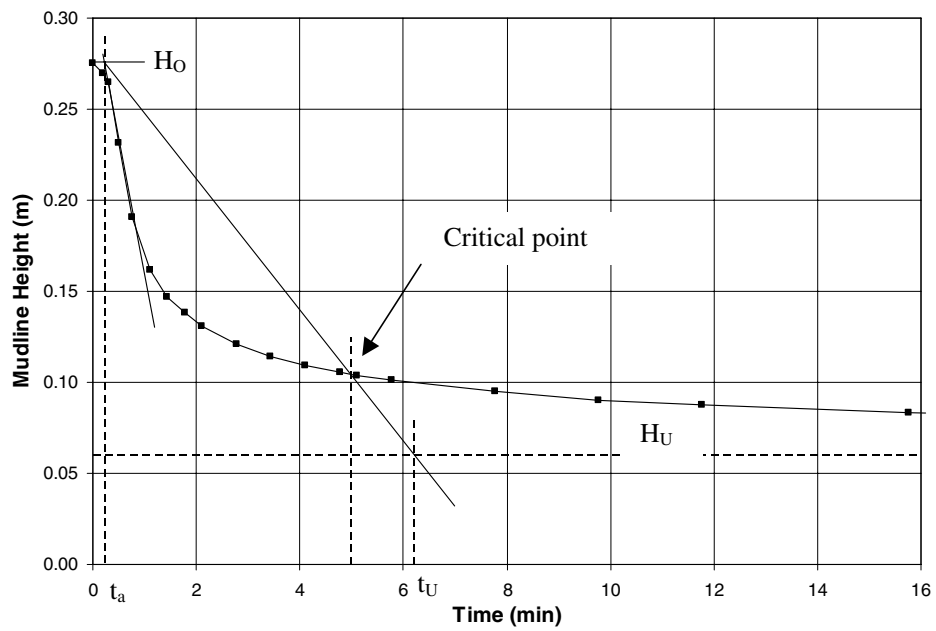
Fig. 13.20. Oltmann construction to determine the critical settling flux.

A line drawn from the point (t_a, H_O) through the critical point on the settling curve to intersect the underflow mudline H_U will determine the time t_U. The detention time is then given by $t_D = (t_U - t_a)$ and the critical flux is given by;

$$\psi_{CRIT} = \frac{C_O H_O}{t_D 1.2}$$

(13.23)

The factor 1.2 is used to give a 20% safety factor. The thickener area is then given by Eq. (13.22).

13.3.4. Long Tube Method for Estimating Thickener Dimensions

Some pulps containing fines or materials of colloidal dimension do not settle with a clear interface. Some do not tend to settle at all. For such suspensions the *long tube method* of determining the dimension of thickeners or clarifiers are useful. The test consists of determining the rate of rise of a fluid with different detention times. The rate of rise is related to the concentration of solids in the overflow.

The test is carried out in a long plastic or glass tube about 3-4 meters in length (height) and about 0.075 m in diameter. Along its length are a number of sampling points. The first sampling point is about 100 mm from the top of the tube with the remaining sampling points every 200-300 mm. The slurry mixed with an appropriate flocculant is charged and the top most level is established at the top most outlet by opening the value to allow any excess slurry to drain off. The pulp is allowed to settle for a time till a visibly clear supernatant liquid level is seen. Pulp samples are then rapidly taken from all the sampling points, starting from the top and the solid concentrations in each sample is determined. The procedure is repeated 4-5 times for different settling times depending on the expected operating conditions of the thickener/clarifier. The results are tabulated for cumulative depth (H) and solid concentration.

The test results indicate that the clarification zone clarity is a function of overflow rate (v_O) and the detention time. The overflow rate is given by:

$$v_O = \frac{H}{t} = \frac{Q_{V(O)}}{A}$$

(13.24)

where H = the cumulative height (or depth),
  t = time,
  $Q_{V(O)}$ = volumetric flowrate in the overflow and
  A = area.

The detention time is related to the feed rate, depth and area as:

$$t_D = \frac{A H}{Q_{V(F)}}$$

(13.25)

where $Q_{V(F)}$ = the volumetric feed rate.

The overflow rate determined by the long tube test is the *ideal* overflow rate, $v_{O(i)}$, that is required for a certain feed concentration and therefore Eq. (13.24) can be rewritten as

$$v_{O(i)} = \frac{H}{t} \tag{13.26}$$

In the operation of a thickener or clarifier, generally a volume overflow rate, $Q_{V(O)}$, is specified (or chosen) for a particular feed solid concentration, C_F. At this overflow a maximum solid concentration C_O is tolerated. From the data it can be seen that:

The pool area, $\quad A = \dfrac{\text{overflow rate required}}{\text{ideal overflow}} = \dfrac{Q_{V(O)}}{v_{O(i)}} \tag{13.27}$

The pool volume $V = $ Overflow rate required x time $= Q_{V(O)} \, t$, and $\tag{13.28}$

The pool depth $\quad H = \dfrac{\text{pool volume}}{\text{pool area}} = \dfrac{V}{A} \tag{13.29}$

The units for $Q_{V(O)}$ is m^3/h, $v_{O(i)}$ is m/h, t is h and the overflow solids concentration tolerable is in ppm.

In practice the overflow concentration is less than that obtained by the long tube experiments. To account for this discrepancy, Perry and Chilton [20] plot suspended solids concentration C against the rise rate and graphically integrate between C=0 and C=C_C. The resulting value is then subtracted from the observed suspended solids concentration at the chosen rise rate.

Osborne [21] however suggests the use of a *suspensoid factor*, $f(s)$, to correct the error. The corrected pool area would be given by:

The pool area $\quad A = \dfrac{Q_{V(O)}}{v_{O(i)}} \cdot \dfrac{1}{f(s)} \tag{13.30}$

where $f(s) = 0.7$.

13.3.5. Estimating Height (depth) of the Compression Layer
The approximate depth of the thickened sludge layer can be readily determined by the method outlined by Osborne [21]. The height, H, of the layer would depend on the total volume of the solids and liquid in the compression zone and inversely as the area of the vessel. That is:

$$H = \frac{V_c}{A} \tag{13.31}$$

where V_C = the total volume of the liquid and the solids in the compression layer.

V_C can be determined if the average concentration of solids in the layer is known. Hence, if the average concentration of solids in the compression zone is C_C (mass solid/volume of the

424

compression zone), then the mass of liquid in the zone per unit volume will be $(\rho_P - C_C)$ and the liquid/solid ratio in the compression zone will be $(\rho_P - C_C)/C_C$. The depth of the compression zone will depend on the amount of sludge deposited and that would depend on the retention time. The retention time is a function of the rate of discharge of the underflow and the underflow concentration. Thus if the feed rate is expressed as $Q_{V(F)}$, the feed concentration as C_F and the retention time in the compression zone as t_D, then the volume of solids plus the volume of liquid in the compression zone would be:

$$V_C = \frac{Q_{V(F)} C_F t_D}{\rho_S} + \frac{Q_{V(F)} C_F t_D}{\rho_L}\left(\frac{\rho_P - C_C}{C_C}\right) \tag{13.32}$$

Thus if A is the cross-sectional area of the thickener, then the height of the compression zone, H_C, will be:

$$H_C = \frac{Q_{V(F)} C_F t_D}{A \rho_S}\left(1 + \frac{\rho_S}{\rho_L}\left(\frac{\rho_P - C_C}{C_C}\right)\right) \tag{13.33}$$

The units are: $Q_{V(F)} = m^3/s$, $t_D = s$, $A = m^2$, $C = kg/m^3$ and $\rho = kg/m^3$.

Dahlstrom Method

Dahlstrom and Fitch [1] obtained the compression zone volume from the settling curve as shown in Fig. 13.21.
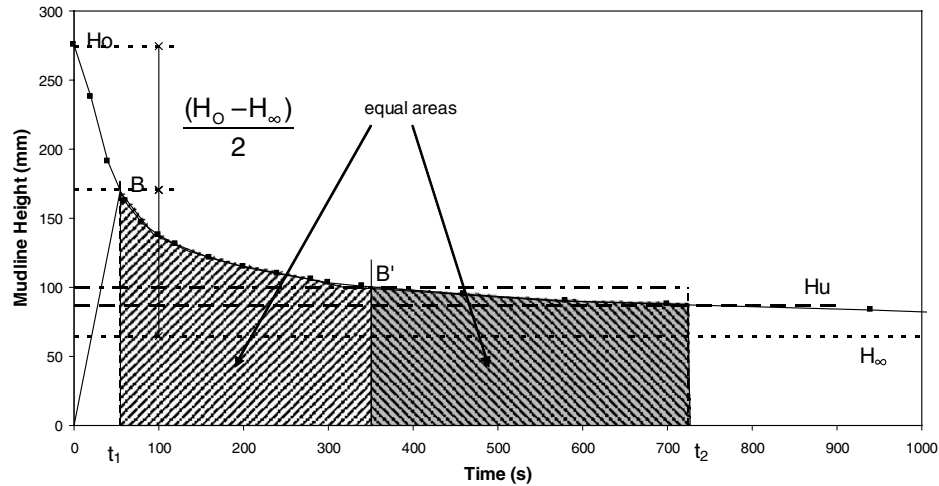
Fig. 13.21. Settling curve showing Dahlstrom's construction for compression zone height [1].

The settling test is carried out in a 2 L cylinder with a picket rake and run for 24 hours to obtain the final sediment height, H_∞. It is assumed that the start of the compression of the sediment occurs at the point B, which is located at the height $(H_O - H_\infty)/2$ and time t_1. The height corresponding to the underflow solids concentration is given by H_U which intersects the sedimentation curve at time t_2. The detention time, t_D, (residence time) in the compression zone required to achieve the desired underflow density is then given by $t_2 - t_1$.

The compression zone volume is calculated from the average solids concentration in the compression zone obtained by integrating the area under the curve from t_1 to t_2. Alternatively, a line bisecting the area under the curve from t_1 to t_2 will intersect the sedimentation curve at B'. The sediment height at this point can be converted to obtain the average concentration, C_C in kg of solid/m^3 of pulp. The compression zone volume is then obtained from:

$$V_C = \frac{Q_{M(F)}}{C_C} t_D SF \qquad (13.34)$$

where   SF   = a scale factor, normally taken as 1.75 and

$Q_{M(F)}$ = the mass flowrate in the thickener feed.

The compression zone height is then obtained by dividing the compression volume by the thickener area. Empirically it is found that if the calculated compression height is greater than 1 meter then the thickener area should be increased or the thickener underflow density reduced to maintain a maximum compression height of 1 meter [1,22].

13.3.6. Estimating the Depth of the Clarifying Zone

For estimating the depth of the clarifying zone, a tall cylinder is again taken and filled with slurry. Sample points are inserted every 200 mm and the clear level recording started immediately and continued at regular intervals. If a clear level is not obtained, a flocculant is added and a height-concentration curve drawn. The overflow rate, v_O, is determined as [11]:

$$v_O = \frac{H_{OF}}{t} = \frac{Q_{V(O)}}{A}$$

That is: $H_{OF} = \dfrac{Q_{V(O)} \, t}{A}$ \qquad (13.35)

where v_O = overflow rate or overflow volume flux expressed as m/s and

H_{OF} = height of the clarification zone.

13.3.7. Estimating the Retention Time

Dahlstrom and Fitch [1] described a procedure for determining the retention time of continuously operating thickeners. The overflow rate was related to the retention time by the relation :

$$t_D = \frac{A \, H_{OF}}{Q_{V(O)} \, A_{EF}} \qquad (13.36)$$

where $Q_{V(O)}$ = overflow rate, m^3/h,
$\quad$ A $\quad$ = cross sectional area of the tank, m^2, and
$\quad$ A_{EF} = areal efficiency factor.

The overflow flow rate can be measuring by determining the overflow velocity, v_O, and using the relationship:

$$v_O = \frac{Q_{V(O)}}{A} A_{EF} \qquad (13.37)$$

Dahlstrom and Fitch reported areal efficiency values between 0.1 and 0.6, depending on the height to diameter of the thickener and feed well, with typical values of 0.20 – 0.25. The overflow velocity must be less than the settling velocity of the smallest particle to be removed. This maximum velocity for thickeners is generally 0.00034 – 0.0020 m/s.

Examples 13.1 – 13.2 illustrate the use of the above concepts.

Example 13.1

The volume rate of flow of slurry from a dust catcher was 3.7 m^3/min. The concentration of slurry (by mass) was 10% and the specific gravity of the solid is 2.75. The slurry is to be thickened to produce a sludge containing 47% minimum solids by mass in a continuous thickener. Settling tests on the sample gave the following data:

Rate of settling, m/min	0.72	0.36	0.24	0.051	0.01
Concentration, % solids by mass	10	15	25	35	45

Estimate the cross-sectional area that will separate 1000 tonnes of solids per hour.

Solution

Take as the basis, 1 kg solid and time in seconds.

Step 1
Solid to be separated/min = 1000 x 1000/60 = 16,667 kg = 277.8 kg/s
The underflow contains 47% solids and 53 % water, hence the underflow water/solids ratio = 53/47 = 1.12.

Step 2
Estimate the water to underflow from the given data as shown in the table below.
The table shows that the maximum flowrate in the overflow stream, per unit sedimentation rate = 858.2 s/m.
According to the given conditions, the sludge contains 277.8 kg/s ($Q_{M(F)}$).
Assuming a density of water = 1000 kg/m^3, the thickener area, from Eq. (13.3) = 858.2 x 277.8/1000 = 238.4 m^2.

Hence the diameter of the thickener = $(238.4/3.14)^{0.5} \times 2 = 17.4$ m.

	Feed rate		Water distribution			Sedimentation rate, v_S		$(F–D)/v_S$
% solids	% water	F (M_W/M_S)	D = U/F (M_W/M_S)	O/F = F–D (M_W/M_S)	m/min		m/s	s/m
(1)	(2)	(3)	(4)	(5)=(3)-(4)	(6)		(7)	(8)=(5)/(7)
10	90	9.00	1.128	7.87	0.72		0.0120	656.0
15	85	5.67	1.128	4.54	0.36		0.0060	756.5
25	75	3.00	1.128	1.87	0.24		0.0040	468.1
35	65	1.86	1.128	0.73	0.051		0.0009	858.2
45	55	1.22	1.128	0.09	0.01		0.0002	567.4

Example 13.2

A slurry containing 300 kg solid per cubic meter of slurry is to be dewatered in a thickener such that the underflow will contain 750 kg/m³. The feed rate to the thickener was expected to be 0.5 m³/min. A batch settling test of the slurry gave the following results:

Solid concentration, C, kg/m³	300.0	362.3	497.4	774.2	960.0	1010.5	1078.7	1128.1
Settling velocity, v_S, mm/min	26.667	15.588	7.148	1.610	0.455	0.271	0.111	0.068

Estimate the maximum area and diameter of the thickener.

Solution

Step 1
Determine ψ from v_s and C values using the expression:

$$\psi = v_S \cdot C \quad (kg/m^2.s)$$

This can be determined for different velocities as illustrated in the table below:
Settling test results from laboratory test

Settling velocity, v_S		Solid concentration, C kg/m³	Settling Flux, $\psi = v_S \cdot C$ kg/m².s
mm/min	m/s x 10^{-6}		
26.667	444.0	300	0.133
15.588	260.0	362.3	0.094
7.148	119.0	497.4	0.059
1.610	26.8	774.2	0.021
0.455	7.58	960.0	0.007
0.271	4.52	1010.5	0.0046
0.111	1.85	1078.7	0.0020
0.068	1.13	1128.1	0.0013

Step 2
Plot settling velocity against solid concentration as in Fig. 13.22. Since the underflow has to be 750 kg/m^3, draw a line, tangent to the curve and passing through 750 kg/m^3 on the x-axis. This line cuts the y-axis at $\psi_{CRIT} = 0.17$ kg/m^2/s.

Step 3
As a first approximation, using Eq. (13.22):

area A $= (Q_{V(F)}\, C_O)/\psi_{CRIT} = 0.5 \times 300/(0.17 \times 60)\, \text{m}^2$

$= 14.7\, \text{m}^2$

and   diameter $= 4.3$ m

Considering a safety factor of 1.5, the practical diameter $= 6.5$ m
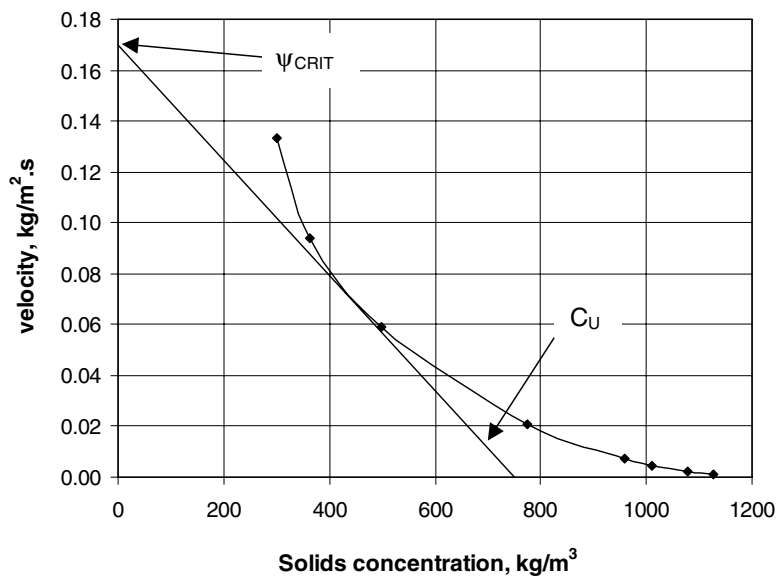
Fig. 13.22. Settling flux vs solids concentration.

In the discussions and computations explored in examples 13.1 and 13.2, the effect of different particles sizes (and possibly density) has not been considered. The velocity of descent of different sized particles will obviously be different. In such a case the sedimentation profile will consist of more than three zones (Fig. 13.23) due to the upward
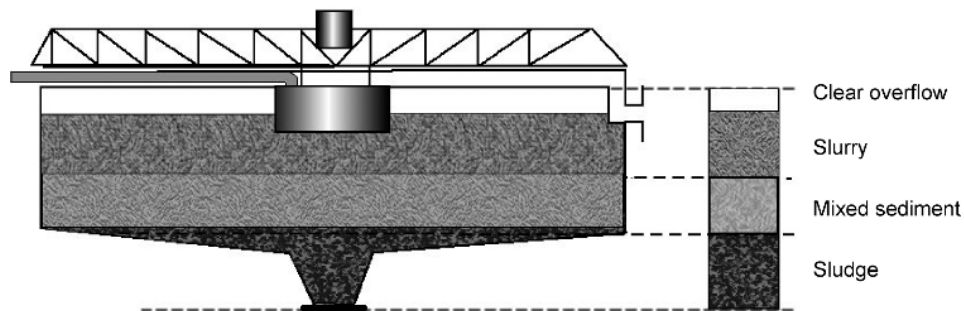
Fig. 13.23. Sedimentation layers resulting from particles of different size and density

flow of the displaced liquid by the movement of the different size of particles. The lines of demarcation between these zones are not well defined and flux determinations are difficult.

Due to such difficulties, adjustments to experimentally computed design parameters have been published from time to time to yield realistic approximations of the different parameters [1,20]. These modifications are summarised in Table 13.2.

Table 13.2
Multiplying factors for different thickener parameters [20].

Parameter	Multiplying factor
Tank size	0.5 – 0.7 to rise rate
Sedimentation time	ratio of static detention time/volume efficiency
Cross-section area of tank	1.2 for diameter > 30 m
	1.5 for diameter < 4.6 m
	1.1-1.25 for safety
Transition zone depth	Add about 2 m
Compression zone depth	1.75

The estimated area of the tank is increased by multiplying by a factor of 1.2 for tank diameters greater than 30 meters and a factor of 1.25 for tanks with estimated diameters less than 5 meters [20].

Often the thickener area and depth are calculated by manufacturers from standard tables established from a large number of field operations. However, no two circumstances are the same and the following method adopted by Eimco [3] is of interest for rapid estimates and may be accepted with reservations. The effective clarification area is obtained from:

$$A_E = \frac{\text{Average daily flow rate}}{\text{Specified overflow rate}}$$

(13.38)
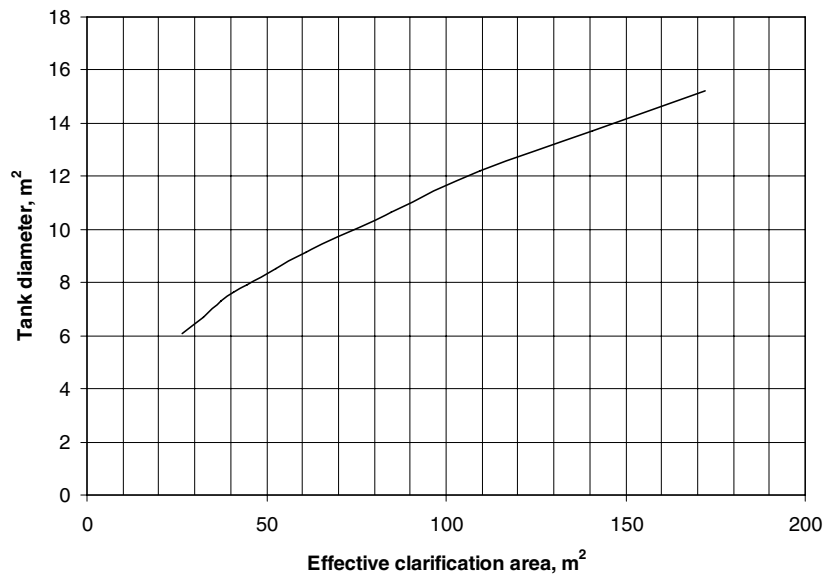
Fig. 13.24. Tank diameter selection [3].

where A_E = the effective clarification area = tank area – feedwell area.

The average daily flow rate is in gallons per day or m^3/h and the specified overflow rate is in gallons per day per ft^2 or $m^3/h.m^2$. The relation between the effective clarification area and the diameter of tank is given in Fig. 13.24.

To calculate the required area for a thickener, the recommended expression is:

$$A = \frac{Daily\, solid\, load\ in\ kilograms}{Floor\, Loading\, Rate} \tag{13.39}$$

where the solid load is in kg/day and the Floor Loading Rate is in $kg/m^2/day$, obtained from Table 13.3.

Table 13.3
Thickener floor loading [3].

% Sludge in feed	Floor Loading $kg/m^2/day$	Typical % Solids in underflow
0	107.51	10
25	73.30	6
35-50	48.87	5
75	29.32	3
100	19.55	2

13.4. Operation of thickeners

The operation of thickeners involves a delicate balance of the feed rate, the overflow rate and the underflow withdrawal rate and is dependant on the concentration of the feed, overflow and underflow streams.

The feed stream generally enters the feed well at a speed of about 15 m/min but this would depend on its characteristics, such as concentration (liquid/solid ratio), particle size, particle shape and viscosity. The characteristics of the overflow and underflow streams depend on the sedimentation time and particle properties like, specific gravity, shape , size and wettability. If the particles are very small, the associated surface charge or zeta-potential is of importance. Flocculants play an important role in affecting the surface charge on particles and help to accelerate or reduce the rate of sedimentation by dispersion or agglomeration.

Rakes help to increase the sedimentation rate and also break up large agglomerates. The rakes are operated between 8-18 m/min. To prevent damage to the rakes and torque meters the recommended operation is to discharge the sludge at regular intervals at predetermined set conditions. It is necessary for the operator to detect the build up on the rakes and operate to avoid the jamming and seizure of the rakes. Usually the built-up mud tends to form islands which grows and develops a moment that could easily damage the rake mechanism. During normal operation the rise rate varies from about $0.01-0.03$ m^3/min/m^2 of cross-sectional area and the detention time is between 2–5 hours.

Some common operating parameters and cross-section of tank sizes for selected metallurgical operations are given in Table 13.4.

Table 13.4.
Thickener and clarifier operating conditions [1,23].

Material	Feed % solids	Underflow % solids	Area m^2/tonne/day	Overflow rate m^3/h/m^2
Copper concentrate	14-50	40-75	0.2-2.0	-
Iron ore (concentrate, coarse)	25-40	60-75	0.02-0.1	-
Iron ore (concentrate, fine)	15-30	60-70	0.15-0.4	-
Lead concentrate	20-25	60-80	0. 5-1.0	-
Nickel carbonate ore (acid leach residue)	15-25	45-60	0.3-0.5	-
Uranium (acid leach residue)	10-30	25-65	0.02-1.0	-
Iron making blast furnace flue dust	0.2-2.0	40-60	-	1.5-3.7
Steel making BOF flue dust	0.2-2.0	30-70	-	1.0-3.7

13.5. Thickeners in Circuits

Thickeners used to produce low solid overflows (eg. about 1% solids), may be referred to as clarifiers. Both thickeners and clarifiers are extensively used in metallurgical operations for dewatering purposes. In processing gold, nickel, iron, copper ores etc. thickeners are used to produce overflows suitable for use as process water in circuits such as flotation. The clear overflow water is used for re-pulping the flue dusts or fine dust from precipitators. Therefore the feed to thickeners vary considerably. A common arrangement is illustrated in Fig. 13.25
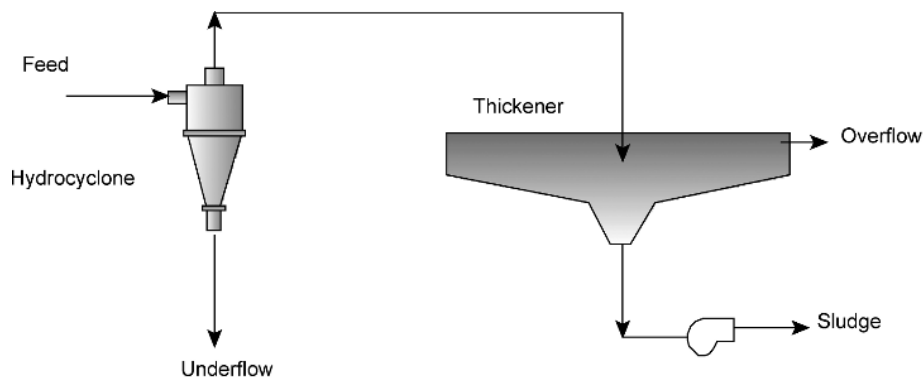
Fig. 13.25. Thickener arrangement.

Thickeners serve as classifiers when a near clear overflow is required. For example clarifiers used in iron blast furnace dust cleaning plant or electrostatic precipitator circuits are required to produce clean overflows as the water is for reuse and the sludge is for secondary use. In such cases the sludge is washed continuously by counter current decantation, where the underflow from a thickener/clarifier is pumped to the next thickener/clarifier (connected in series) forming the feed to the second tank. A typical set up is illustrated in Fig. 13.13 consisting of three units of thickeners/clarifiers.

Such setups are structured so that the overflow from one clarifier/ thickener flows by gravity to the adjacent clarifier. The sludge is usually pumped to the next clarifier. Make up water is added at the third thickener.
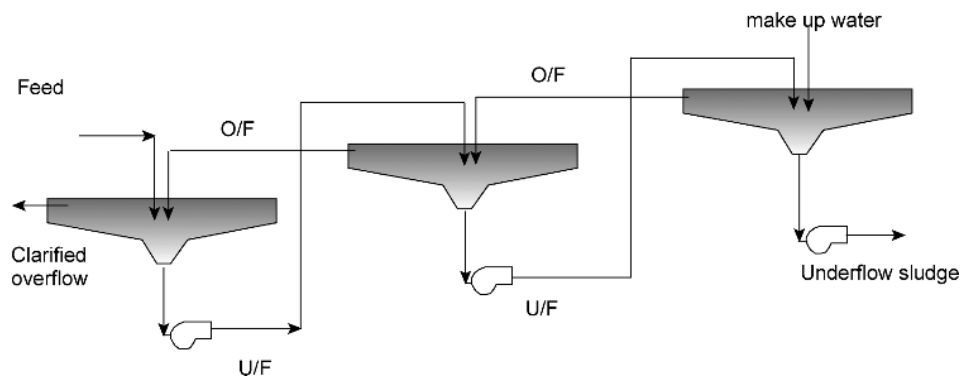
Fig.13.26. Thickeners in a counter-current decantation (CCD) arrangement.

13.6. Problems

13.1.
Settling tests in a cylindrical tube was performed on a slurry containing 300 ppm solids.
After a detention time of 80 minutes, the overflow fluid was found to contain 10 ppm solids
The overflow from the test data was found to be 8.2 m/h. The classifier was required to acieve
an overflow rate of 120 m³/h. Estimate:

1.   The pool volume,
2.   Pool area,
3.   Pool depth,
4.   Pool diameter.

13.2.
Laboratory tests on a sample of slurry showed the heights of the clear interface with time as:

Height, H, mm	600	516	434	285	176	147	128
Time, t, sec	0	100	200	400	650	800	1000

The slurry containing 15% solids (by volume) was required to feed a continuous thickener to
produce an overflow containing no more than 1% solids (by volume). Specific gravity of
solids was 2.65 and water 1.0. If the feed rate is 75 t/h and the desired underflow density is
75% solids by mass, determine:

1.   The settling velocity at each time interval,
2.   The concentration of solids corresponding to each settling velocity,
3.   The flux-concentration curve and
4.   The area of the thickener.

13.3.
Using the data of problem 13.6.2, determine:

1.   The volume of sludge in the underflow and hence the compression zone height
2.   The height of clarification zone.

13.4.
A batch settling test on a flotation tailing gave the following results.

time (min)	mud height (mm)	time (min)	mud height (mm)	time (min)	mud height (mm)
0	340	8	140	25	63
1	290	9	125	30	60
3	236	10	120	40	58
5	189	11	107	50	55
6	175	15	81	60	55
7	150	20	68		

Calculate the thickener area required, in $m^2/t/day$ for the following conditions.

C_o = 50 kg/m^3 pulp
C_u = 340 kg/m^3

13.5.
A settling curve of a 15% solids (by mass) copper concentrate pulp is shown in the graph below. Estimate the thickener diameter required to dewater this material to an underflow of 55 % solids (by mass) at a rate of 1000 t/h. Density of the solid is 4100 kg/m^3 and water is 1000 kg/m^3.
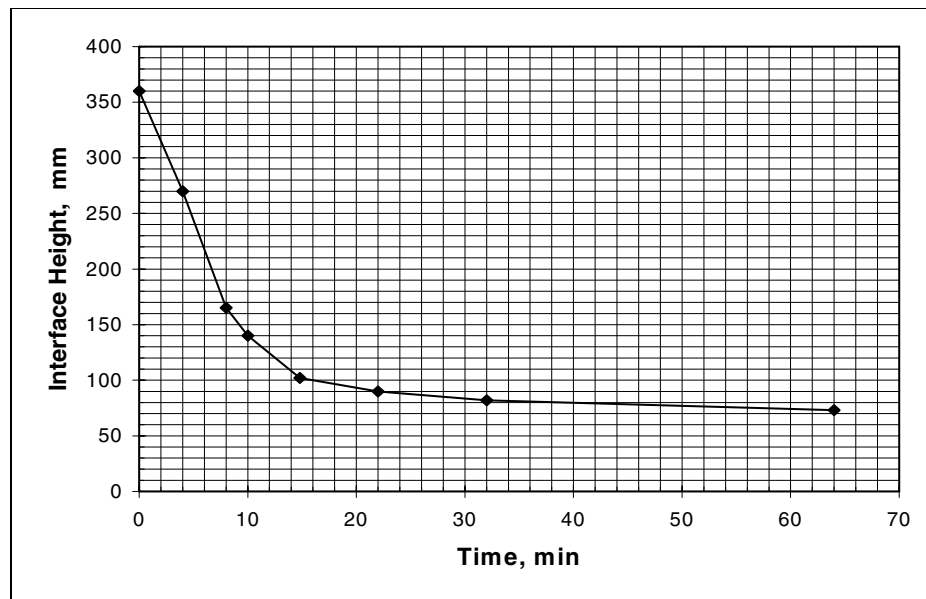
13.6.
A flocculated pulp settles according to the settling curve in the graph below. From these results, and a desired 1000 kL of clarified process water per hour from a feed slurry of 300 tph at 20% solids;

1. locate the critical point on the plot,
2. What is the initial concentration of solids (C_o) and the underflow concentration (C_u) in kg solid/m^3 of pulp,
3. estimate the size of thickener required using the method of Talmage and Fitch.

Data: Solids density = 2800 kg/m^3 water density = 1000 kg/m^3
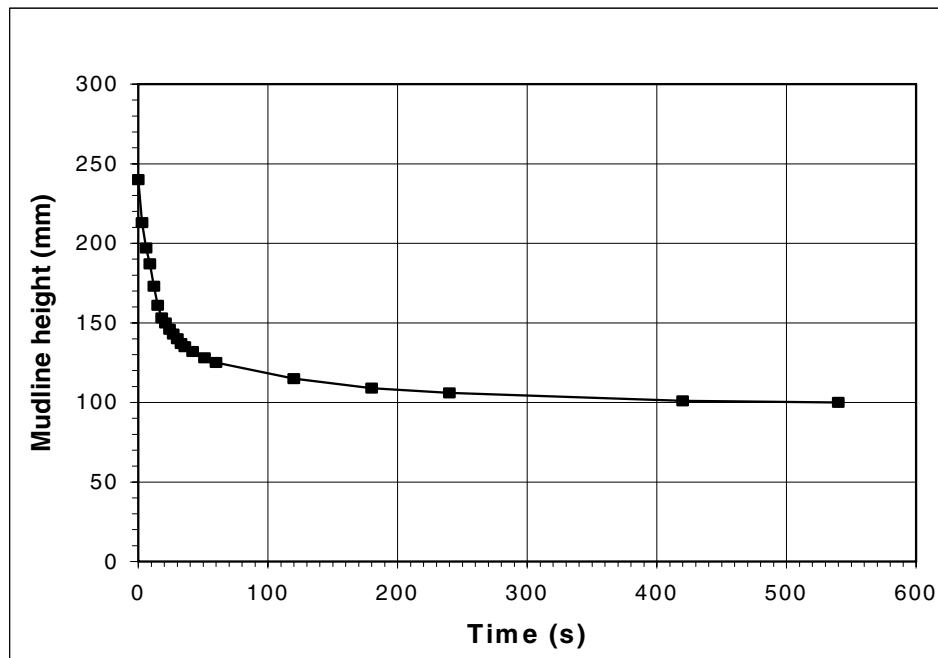
13.7

A slurry of 20% solids (by mass) is to be dewatered to produce a product of 8% moisture at 75 tph. A settling test is carried out on the slurry. The critical point of the settling curve occurs at a mudline height of 80 mm and 250 seconds. The initial mudline height in the test cylinder is 300 mm. Solid density is 2500 kg/m^3 and the water density is 1000 kg/m^3.

1. If the mudline height corresponding to the thickener discharge is 70 mm, what would be the thickener discharge % solids?

2. What method could be used to calculate the thickener area requirement for this slurry? Calculate the thickener diameter using this method.

13.8

A slurry of 20% solids (by mass) is to be dewatered to produce a product of 50% solids (by mass) at 75 tph (solid). A settling test is carried out on the slurry at 20%, 30% and 40% solids. The initial settling rates of the slurries are recorded below. Calculate the thickener diameter requirement for this slurry.

slurry	R (mm/s)
20%	0.7796
30%	0.0780
40%	0.0242

13.9
According to the Kynch theory, the settling velocity of a slurry of a concentration given by the settling interface, is given by the slope of a tangent to the settling curve. If the slope to the settling curve of a flocculated copper flotation tail is 0.4 mm/s at the critical point which occurs at a point (67s,115mm) on the settling curve, calculate the thickener area requirement to treat this slurry if the desired underflow is 65% solids (mass), the feed density is 22% solids (mass) and the initial mudline height in the settling test is 250 mm.

Throughput	=	150 tph
Density of solid	=	2750 kg/m³
Density of water	=	1000 kg/m³

REFERENCES

[1]   D.A. Dahlstrom and E.B. Fitch, in Mineral Processing Handbook, N.L. Wiess (ed), SME/AIME, Chapter 9, 1985, pp. 2-14.

[2]   D.L. King, in Mineral Processing Plant Design, A.L. Mular and R.B Bhappu (eds), AIME, 1980, pp 541-577.

[3]   Eimco 2005, Retrieved September 1, 2005 from http://www.glv.com; http://www.glv.com/docs/product_docs/435/CompClarf50ft%20(pg)LR.pdf

[4]   Eimco 2006, Retrieved January 24, 2006 from http://www.glv.com/ProductList.aspx?secID=2&catID=131

[5]   H.S. Coe and G.H. Clevenger, Transactions AIMME, 55 (1916) 356.

[6]   G.J. Kynch, Trans. Faraday Society, 48 (1952) 166.

[7]   W.P. Talmage and E.B. Fitch, Industrial and Engineering Chemistry, 47 No.1 (1955) 38.

[8]   F. Concha and R. Bürger, *KONA*, No. 20 (2002), 38.

[9]   T. Yalcin, Bulletin of the Canadian Institute of Metallurgy, 81 No. 910 (1988) 69.

[10]   L. Svarovsky, Solid-Liquid Separation, Butterworths, 1977.

[11]   J.J. McKetta, Unit Operations Handbook, vol.2 Mechanical Separations and Materials Handling, Marcel Dekker Inc., 1993.

[12]   P. Mondal and C.B. Majumdar, Journal of the Institution of Engineers (I) - Chemical Engineering, The Institution of Engineers (India), 85 (2004) 17.

[13]   E. Barnea, Chemical Engineer, (1977) 75.

[14]   E.J. Roberts, Transactions, AIME, 184 (1949) 61.

[15]   A. Jernqvist, Svensk Papperstidn., 68 (1965) 506, 545, 578.

[16]   A. Jernqvist, Svensk Papperstidn., 69 (1966) 395.

[17]   E.G. Kelly and D.J. Spottiswood, Introduction to Mineral Processing, Mineral Engineering Services, Denver, 1989.

[18]   N. Yoshioka, Y. Hotta, S. Tanaka, S. Naito and S. Tsugami, Chemical Engineering Japan, 21 (1957) 66.

[19]   H.H. Oltmann, Filtration and Separation, 12 No. 6 (1975) 636.

[20]   R.H. Perry and C.H. Chilton, Chemical Engineering Handbook, R.H. Perry and C.H. Chilton (eds), 5th Edition, McGraw-Hill Book Co., 1973.

[21]   D.G. Osborne, Solid-Liquid Separation, Chapter 5, L. Svarovsky (ed), Butterworth, London, Boston, 1977, pp. 75-99.

[22] B. Fitch, Industrial and Engineering Chemistry, 58 (1966) 18.

[23] R.H. Perry, R.H., Perry's Chemical Engineering Handbook, R.H. Perry, D.W. Green and J.O. Maloney (eds), 6th edition, Chapter 19, McGraw-Hill, 1984, p. 64.

Chapter 14. Solid Liquid Separation - Filtration

14. INTRODUCTION

The separation of solids from liquid by gravity can be easily done by batch or continuous sedimentation processes. The underflow, however still contains appreciable amounts of liquid and the overflow can contains some amount of solids. Further removal of liquid is necessary for some down stream operations. The removal of this liquid is usually possible by passing the suspension through a semi-permeable membrane which is designed to hold the solids and permit the liquid to pass through. In effect the membrane forms a screen. In the early stages of separation across this membrane the solids deposit forming a second semi-permeable medium or cake. These two layers then form the filtering medium for the remainder of the slurry. The structure of the filtering cake changes continuously as more particles deposits with time. The main changes relate to permeability and porosity of the filtering zone. The permeability of the cake depends on the particle size, shape, thickness (depth) of solids and on the liquid properties, such as viscosity. The filtration rate is affected by differential pressure that is applied on the membrane to improve performance. Once a thick cake is formed the permeability decreases to the extent that the process is stopped. Filtration can continue by changing both the membrane and removing the deposited solids. The process of filtration is therefore essentially batch or continuous. Fig. 14.1A shows the function of a typical filtering medium. Fig.14.1B is an enlargement of the semi-permeable medium. The figures show the mechanism of filtration where particles larger than the pore size are held back while the fluid passes through. Particles smaller than the pore space are also liable to pass through, but small particles existing away from the membrane surface may not be separated unless brought in contact with the membrane surface. Once the cake begins to build up, further filtration is continued through the deposited layer of solids as well as the medium. Therefore the permeability of both the filter cake and the medium is of paramount importance.

   Most filter cakes can be compressed to varying degrees by pressure. In some cases, like a siliceous cake, limited packing can be achieved but in others like clayey deposits, compressibility may be high and application of pressure may result in appreciable reduction of permeability of the entire bed. The process of filtration is predominantly carried out at conditions of either constant pressure or constant volume flow rate.

   The filtering process is completed when nearly all the liquid has been removed from the pulp and the filter cake is removed from the filtering medium. Before removing the cake, it can be washed to remove the adhering fluid, the fluid that is retained in the pore spaces in the cake and any solute in the feed that is entrapped within the cake.

   The structure of the supporting base of the filtering medium is a guide to the nomenclature of filters in industry, Thus when the filtering medium is between grooved plates the filter press is known as *plate filters*, when it is in the form of disc they are known as *disc filter*, when in the form of a drum or continuous belt they are known as *drum filters* and *horizontal belt filters*. The method of application of pressure also contributes to the nomenclature, thus industrially they are known as pressure or vacuum filters. Several combinations of these options are practiced including constant rate or constant pressure filtration.
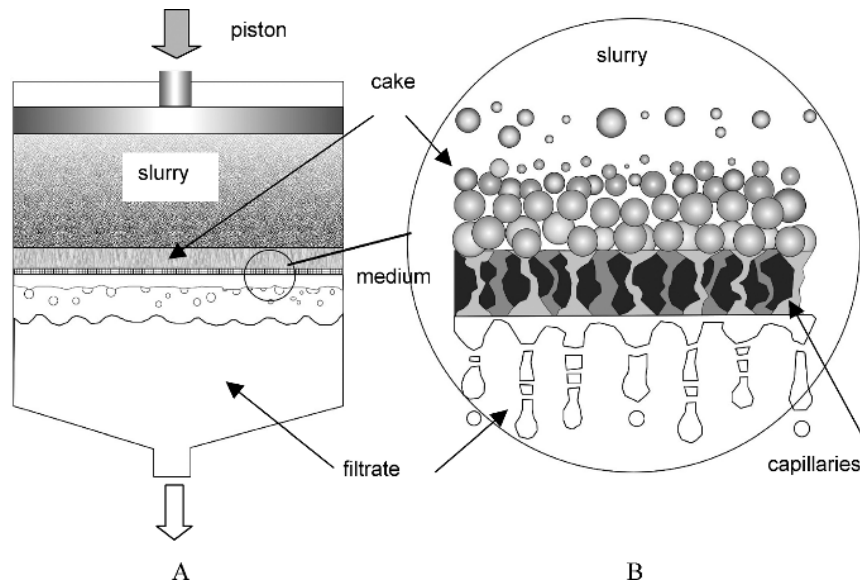
Fig. 14.1. Basic filtration setup

14.1. Design Features of Filters

The semi-permeable membrane that permits the passage of liquids and prevents the solids to permeate is one of the main components of filters. The membrane consists of a large number of capillaries which forms tortuous channels most of which are continuous. With the assumption that the passage of fluid is streamlined, it is reasonable to assume that Poiseuille's law of fluid flow through capillaries is applicable to both the medium and the filter cake. Poiseuille's law states that the rate of filtration per unit area of the filter bed equals the ratio of the driving force to the product of the total resistive forces and the viscosity of the fluid. The total resistive force, R_T, is given by the sum of the resistive forces of the medium, R_M, and of the cake, R_C. That is:

$$R_T = R_C + R_M \tag{14.1}$$

Providing the structure of the cake does not change with pressure, that is, it cannot be compressed, the resistance of the cake will be proportional to the mass of dry cake deposited during filtration. Thus the resistance of the cake is given by:

$$R_C = \frac{\alpha\, M_C}{A} \tag{14.2}$$

where M_C = mass of dry cake, kg,
  A = area, m^2,
  α = specific cake resistance (resistance per unit mass per unit area), m/kg.

If V is the volume of filtrate produced in time t by the application of a differential pressure ΔP, then according to Poiseuille's law:

$$Q_V = \frac{dV}{dt} = \frac{A\,\Delta P}{\mu R_T} = \frac{A\,\Delta P}{\mu[R_C + R_M]} = \frac{A\,\Delta P}{\mu\left[\dfrac{M_C}{A}\alpha + R_M\right]} \qquad (14.3)$$

where Q_V is the volume flow rate.

This is the fundamental equation on which the process of filtration is based. This equation assumes that the flow through the capillaries in the porous medium is streamlined and that R_M is constant, which in practice, may not always be true. Further the resistance of the cake is assumed to be uniform and constant. This also is not always true, particularly for cakes that are compressible. However, R_C is a function of porosity, ε, diameter of the pores d_ε, and the specific surface area of the particles, S, forming the cake.

The specific surface area of the particles is equal to $6/d_P$, where d_P is the diameter of the particles. The porosity, ε, is defined as the ratio of the void volume to the total bed volume. That is:

$$\varepsilon = \frac{\text{Void volume}}{\text{Total volume of bed}} \qquad (14.4)$$

Working with porous media, Darcy [1] established that the pressure drop, ΔP, of a fluid flowing through a porous medium was proportional to the thickness of the bed, L, volume rate of flow, Q, viscosity of the fluid, μ, and inversely proportional to the cross-sectional area, A. That is:

$$\Delta P = \frac{LQ\mu}{K\,A} \qquad (14.5)$$

where K is the proportionality constant and is defined as the permeability of the porous medium.

The permeability is related to the specific cake resistance by the following expression, derived from the comparison of Eqs. (14.3) and (14.5). That is:

$$K = \frac{1}{\alpha(1-\varepsilon)\rho_S} \qquad (14.6)$$

The rate of flow of fluid in time t can be obtained by rearranging Eq. (14.5):

$$Q = \frac{dV}{dt} = \frac{\Delta P\,K\,A}{L\mu} \qquad (14.7)$$

The flow of fluid through the pores is subjected to frictional resistance and therefore cannot be compared directly with flow through the pores in a smooth pipe where the friction is low. Thus the flow rate through a porous medium is considered as a *superficial* velocity.

Eqs. (14.3) and (14.7) are the basis of the mathematical models that describe the filtration process under different operating conditions.

Examination of these equations indicates that they can be integrated in term of constant pressure and constant volume. We shall see later in this chapter how the equations help to understand the filtration processes under different methods of operation.

In industry the entire filtering process consists of a cycle of four main steps:

1. Filtering,
2. Washing of cake,
3. Drying of cake and,
4. Removal of cake.

The designs of filters therefore depend on the filtering process and the cycle adopted. Roughly the different processes used in metallurgical operations may be summarized as shown in Fig. 14.2.
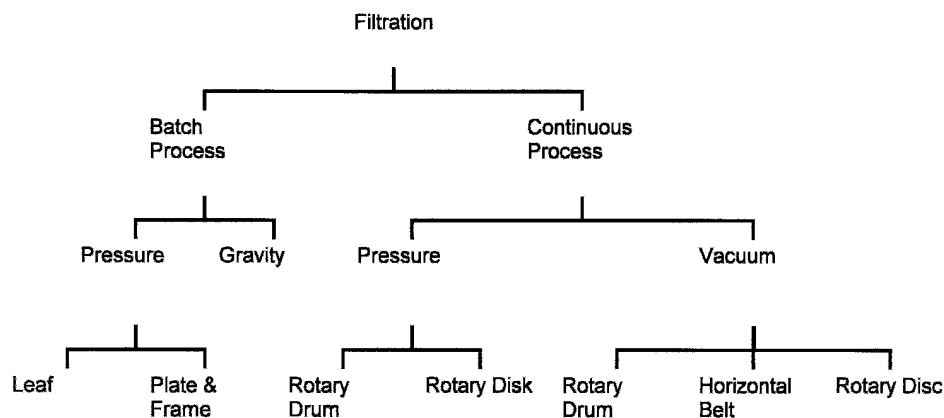
Fig. 14.2. Classification of filtration units.

14.1.1. Batch Processes of Filtration
Two types of batch filters are commonly used in the metallurgical industry. The basis of designs of these filters depend whether gravity forces or external forces are applied to achieve the separation.

Gravity Filters
Gravity filters consists of a circular or rectangular vessels with a semi-permeable membrane forming the base. The membrane is usually laid horizontally. A receptacle is placed below the

membrane to receive the filtrate. The membrane forms the medium of filtration. The feed, in the form of slurry, is charged above the medium and allowed to stand. The liquid component of the slurry is forced to permeate through the membrane by gravitational force and the hydrostatic head of the fluid.

As filtration proceeds the solid deposit builds up with time and the filtrate collected. The filters are operated till the rate of filtration diminishes appreciably. The assembly is then dismantled and the filtrate and deposited cake removed. Usually scrapers are used to dislodge the cake. If the cake is sticky they could be dried before using the scraper. The filtering medium is then replaced, and the operation repeated.

These filters are essentially slow operating and seldom used for metallurgical operation. They are however, used extensively in small scale laboratory work for metallurgical purposes. On an industrial scale, gravity filters are often used for water purification operations.

Plate and Frame Pressure Filter

The simplest batch pressure filter is the plate filter where the slurry is placed between two vertical plates clamped together by an externally operated screw system or hydraulic ram (Fig. 14.3). A series of hollow frames separate the plates which are placed side by side and hung from two parallel rails on either side of the plates. The filtering medium is placed against the sides of the plates and the slurry is pumped between them. The slurry pressure presses the pulp against the medium forcing the liquid through the cloth and leaving the solids as a cake, on both surfaces of the frame.

The plates are usually square shaped with ribbed or studded surfaces. Circular plates are also available in industry. The size of plates varies from about 450 x 450 mm to 2000 x 2000 mm and frames from 10 mm to 202 mm in thickness. They are usually made of steel to withstand pressures in excess of 1800 kPa.

The usual number of plates in commercial practice varies between 25-50 but up to 100 plate filters are reported [2].
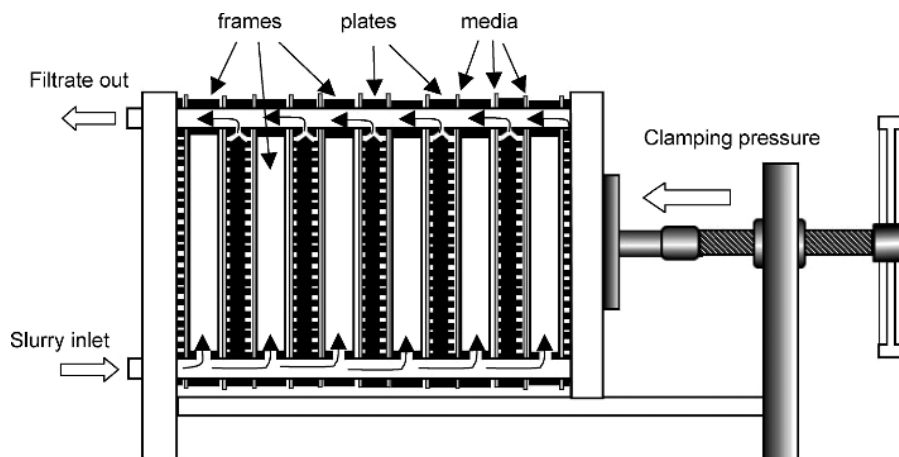
Fig. 14.3. Section of a plate and frame filter press.

In operation, feed in the form of slurry is pumped in through a common channel entering the filters through individual ports. This ensures uniform distribution of feed in each chamber. The feed can be charged either through top or bottom ports in the frame. The filtrate leaves the individual filter beds through ports to a common discharge channel. In some installations the discharge from individual filters can be controlled. This introduces the flexibility of accepting or rejecting the product from a particular plate which can be suspected to be faulty and probably discharging unclear or turbid filtrate into the main product stream. Production of turbid and unclear filtrate often occurs due to a tear or bursting of the filter medium and needs to be isolated.

The normal and often used medium is woven cotton or plastics which permits filtering rates ranging between 0.1 and 0.6 $m^3/h/m^2$. Non-woven plastics with various apertures are also used.

For washing the cake the same hook-up for feed and discharge pipes are used to supply the wash water and to discharge the effluent. The cake is recovered by dismantling the entire unit. Steam is used in some cases to assist in drying the filter cake. The Larox RT Filters have provision for multistage washing, vibration and hot air drying of cakes [3].

Merrill Filters working on these principles have been used in the gold industry for filtering gold cyanide solutions and zinc dust precipitates.

Chamber Filters

The Chamber filters are improved plate and frame filters (Fig. 14.4). These filters use recessed plates which when clamped together form chambers. The recess can be up to 25 mm. By recessing the plate, it forms its own frame and permits a thicker cake than the plate-and-frame filters. The feed usually enters through a central port in the plate. The filtrate escapes through a manifold at the top. The other features of the filter plate are essentially similar to the plate and frame filters.
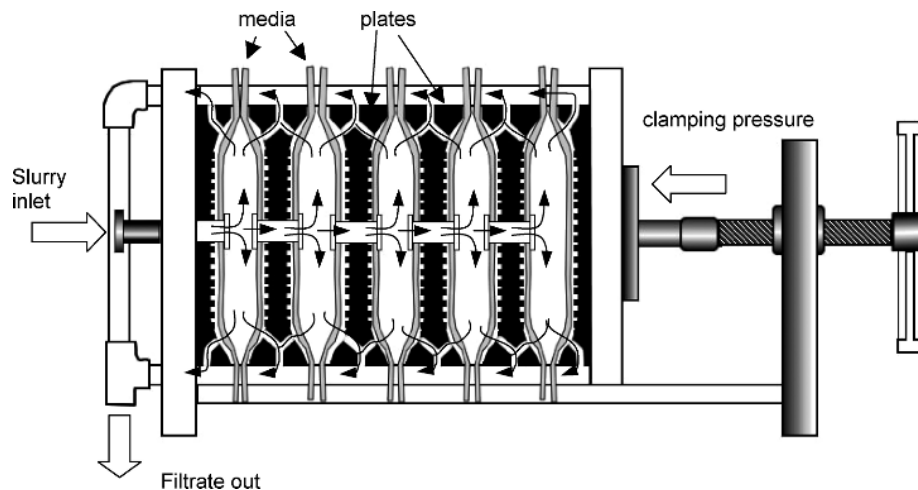
Fig. 14.4. Sketch of a Chamber Press filter.

Chamber filters are usually designed to operate with a maximum of 153 plates with surface areas varying between 0.2 to 2.6 m^2 per chamber [4].

The plates are connected to water lines for washing and to steam line for hot drying of the deposited cake. The cake is released from the medium by reversing the clamping device which is hydraulic or mechanical. Recessed plate filters are preferred where the cake is not very permeable, e.g., cakes produced on filtering slurries with excessive fine clays, or metallurgical slurries like in iron and alumina industries where the hydroxides have to be filtered.

While designing plate filters it is important to remember that the entire filter surface is not effective. For example, the available filtering surface of a filter of size 1450 mm x 1450 mm will be about 12% less than the maximum 2.10 m^2. For smaller filter sizes of say 250 mm x 250 mm, the filtering surface could be less by about 30% [5]. A rough relationship indicating the availability of filtering surface for different sizes of filters is illustrated in Fig. 14.5.

Leaf Filter

These filters, originally known as Dorr-Oliver *Kelly* filters [6], were in use in Australian gold operations but are now seldom used in this industry. The batch pressure leaf filters consists of a number of leafs, mostly rectangular in shape, but they can also be circular. The leaves are grooved plates over which filtering medium made of knitted cloth like, hessian, canvas, woollen sheets or synthetic polymer material is fitted. Both sides of the plate serves as filtering surfaces. A number of such leaves are supported on one or more common rails and placed inside a tank that can be closed (Fig. 14.6). The spacing between leaves usually vary depending on the cake thickness, but 30 mm to 152 mm is common.

Filters are designed to take several leaves. For example, a 914 mm diameter filter can take between 6-13 filters while a 1828 mm diameter filter can take 20 leaves. Filtering areas of 100 - 300 m^2 are common operating at pressures of up to 600 kPa [7].
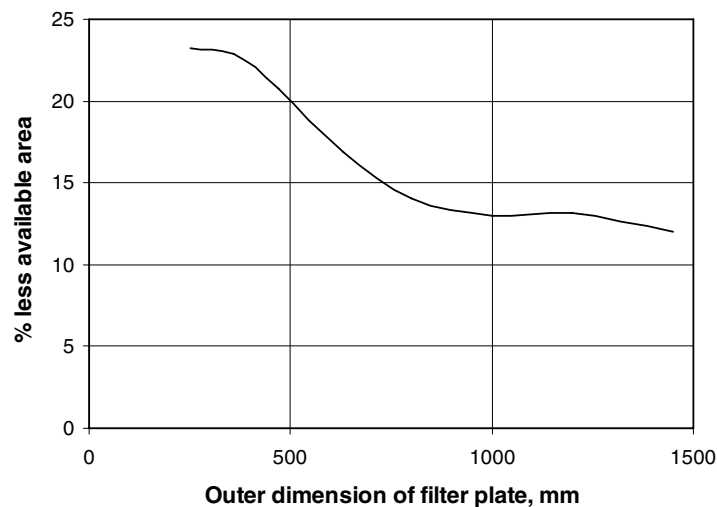
Fig. 14.5. Effective filter area loss for a plate filter; data from Svarovsky [5].
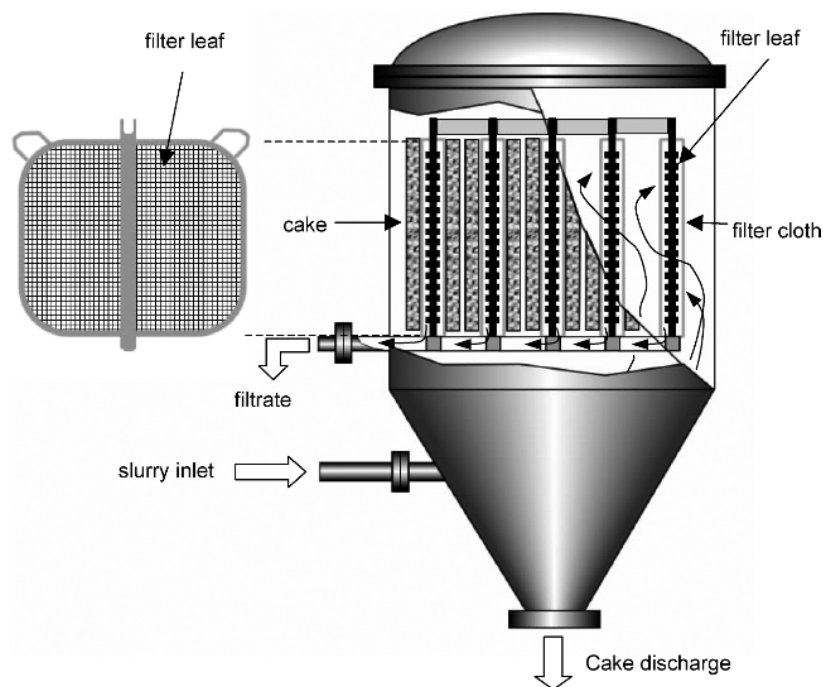
Fig. 14.6. Sketch of a pressure leaf filter.

On locking and sealing the chamber, slurry is pumped in through a common main under the tank and hydrostatic pressure applied. Filters are operated either at constant pressure or constant volume rate. When filtering at constant pressure, filtration is stopped when the filtrate flow is low or negligible. When filtering at constant flow rate, the pressure drops, and the filtration rate falls indicating the end of the operation. When the filtration is carried out under vacuum, it is applied through the discharge manifold. After filtration the leaves are sometimes removed to a second tank for washing and subsequently for drying, if necessary. Several manufacturers have patented methods for removing and washing the cake. For example, Dorr-Oliver (*Sweetland*) filters are designed to open the bottom of the tank and the cake is discharged by blowing compressed air from inside. In *Niagara* filters, the entire nest of leaves, riding on rails, are withdrawn out of the pressure tank, air pressure applied, the cake blown out and dried. Once dried, they are blown off the medium by air. When a wet cake is required, the cake is subjected to a high pressure water hose and scraped off. Most filter leaves in pressure units are stationary, but the circular filter leaves in *Vallez filters* are designed to rotate. The rotation of the leaves yields a more uniform thickness of cake.

Solid-liquid pressure filter are also manufactured with the horizontal plates. In these, the horizontal plates are stacked one below the other. Filtration takes place on one side of the filter plate. These filters are mostly used in chemical and pharmaceutical industries [8,9]. They are not used much in the mineral industry.

14.1.2. Continuous Vacuum Filtration

Types of continuous vacuum filters common in metallurgical operations are the *rotating drum filter*, *rotating disc filter* and *belt filter*.

Rotating Drum Filter

Rotating drum continuous filters consists of a horizontal drum with its bottom one-third section immersed in a tank of slurry that has to be filtered. The drum shell is perforated and covered with shallow compartments which serve as a drainage grid about 22 mm in depth. The grid is covered with metal gauze which in turn is covered with the filtering cloth. The ends of the drum are either open or are closed with a spider through which the trunnion passes (Fig. 14.7). Each sector of the drum is connected from inside to a centrally located complex valve system. The valve has ports connected to vacuum, compressed air and water lines. Two of these rotate with the drum while the others are stationary. The valve acts in a manner such that the one third portion of the drum that is immersed in the slurry is under vacuum. The adjacent half of the drum is also under vacuum, but could be switched to dry air pressure. The remaining portion of the drum is under positive pressure which helps to dislodge the cake from the drum surface.

In the first stage of the filtering cycle the filtrate is drawn into the drum leaving a cake of solids adhering to the medium surface. When the drum continues to rotate, the cake in the first segment emerges from the slurry and is exposed to the atmosphere. It can then be washed under vacuum to rinse the adhering solids. The drum then enters the drying section where the cake is dried by drawing air through it. On further rotation the drum enters the final zone where the cake is blown out using reversed air pressure and discharged.

Several methods of discharging the cake have been adopted. The most common is to place a knife or scraper against the cake along the entire width of the drum. Other devices include:
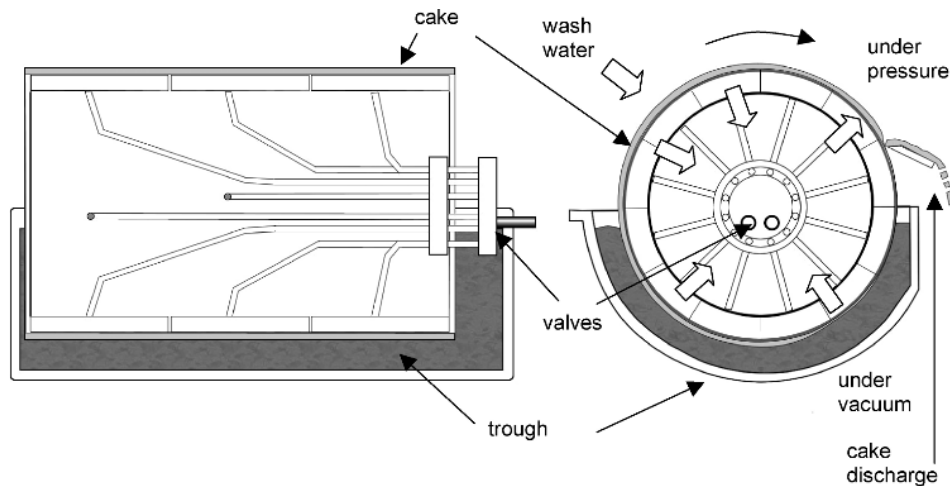
Fig. 14.7. Sketch of a Rotating Drum Filter.

1. Continuous string discharge,
2. Continuous belt discharge,
3. Roller discharge.

The principle of designing and operating the string or belt arrangement to dislodge the cake is the same. Strings are placed parallel to each other 8-10 mm apart and wrapped over the drum surface. Sedimentation of cake takes place on and above the strings during filtration. Fig. 14.8 shows a string or belt passing over two auxiliary rolls at the end of the cycle. When the vacuum is released at the end of the second sector, the strings help to lift the cake off the drum surface which is then discharged. As the drum continues to rotate further, the strings pass between the auxiliary rolls and are washed and returned to the drum. The strings are commonly made of synthetic material like polyester.

In the roller discharge type (Fig. 14.9), the scraper roll rotates in the opposite direction to the drum. The speed of the scraper roll is 5-10% greater than the speed of the rotating drum. The scraper roll is placed against the cake at a suitable distance to slightly compact and peel off the cake from the filtering cloth surface. The surface of the scraper roll is capped with a rubber material. A scraper knife keeps the scraper roll surface clean. This technique of cleaning the drum is particularly suited to sticky clayey cakes, like that of bentonite or kaolinite clay. They are also suitable for highly alkaline red-mud slurry produced in the alumina industry's Bayer process.

A variation of the drum filter design is made for slurries which are unstable and settle rapidly. In such cases, the feed is on the top-end of the drum and as filtration is rapid, arrangements are made to press the filter cake to de-water it. The vacuum system aids the process. The principle is illustrated in Fig. 14.10.

Rotating Disc Filter

The basic design characteristics of the rotating disc filter, like filtering under vacuum, washing the cake under vacuum and removing the cake by blowing the cake off the filter is the same as in the drum filter. Instead of one drum, a number of discs are placed in parallel.
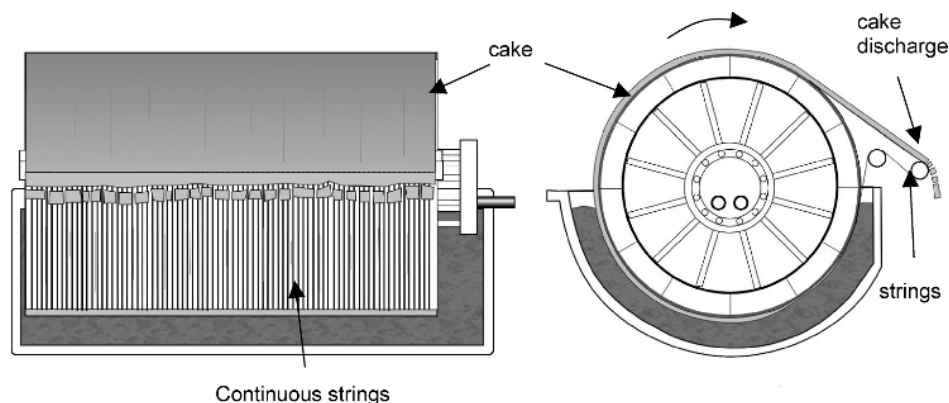
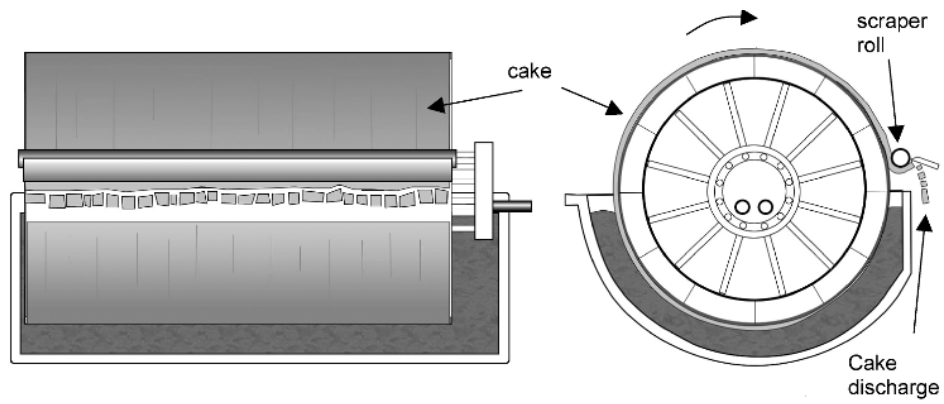Fig. 14.8. Sketch of a continuous string discharge drum filter.

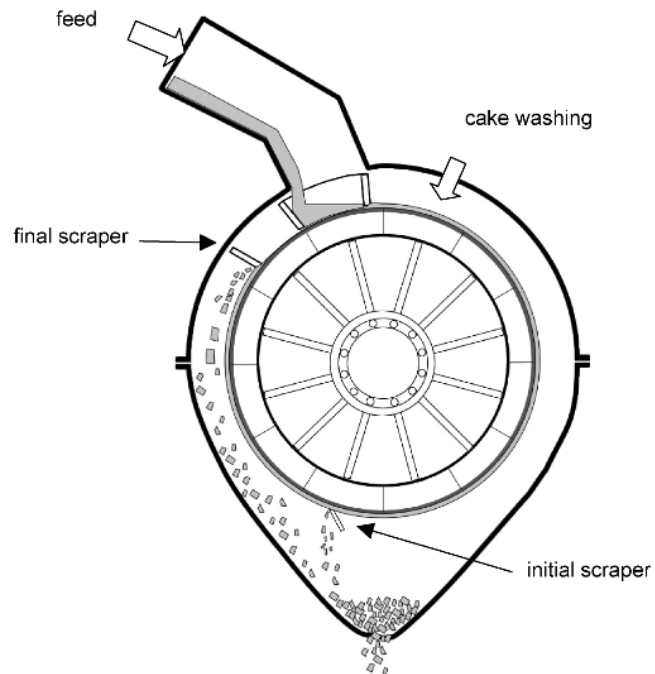Fig.14.9. Sketch of a continuous roller discharge drum filter.

Fig. 14.10. Schematic diagram of top charged drum filter.

The lower end of each disc is attached to a common horizontal pipe which passes through the centre of all the discs in the unit. The central pipe is designed to form the trunnion of the unit and serves as a conduit for the vacuum and pressure lines. The distance between the filters are fixed and this space is used to collect the cake off the filter surface. Each disk is designed to operate separately with its own slurry tank, thus more than one type of pulp can be filtered simultaneously if required. Fig. 14.11 shows a sketch of a disc filter unit.

The largest diameter of discs are about 5.6 m and the smallest available are of laboratory size. The disks have a number of sectors, usually 8–30 [2]. Frames of each sector are covered by a filtering medium in the form of a bag. The bags are made of strong fabric cotton (twill), or plastics to withstand a differential pressures of 0.6–0.8 atmospheres (60–80 kPa). The frames are constructed of either wood, synthetic material (e.g. polypropylene), fibreglass or stainless steel. Between 1–15 discs normally constitute a filtering unit. The filtering medium is chosen to provide porous cakes about 6.5–65 mm thick which translates to a deposition rate of 1.7–12 kg/m^2/min depending on the specific gravity of the mineral. The permeability of the medium normally allows a filtering rate of 0.5–3.5 L/min. For disengaging the cake off the filter surface, the air pressure employed is about 20–250 kPa [10].

Manufacturers of disc filters offer options to the number of discs in a given length of unit. That is, the number of discs in a 1.8 m diameter filter could vary from 1 to 10, offering a filtration area of 4.3 m^2/per disc while for a 3.3 m diameter disc the number of discs could vary between 7 and 13 with a filtering area of 16.7 m^2 per disk (Fig. 14.12).

Ceramic Disc Filters

The Ceramec® filter is a unique rotary disc filter which uses a sintered alumina disc to dewater a slurry under low vacuum. The dewatering occurs by drawing water from the slurry by capillary action. This ensures that no air or particles are drawn into the filter medium to cause blockage. Fig. 14.13 shows a cross-section of the ceramic disc.
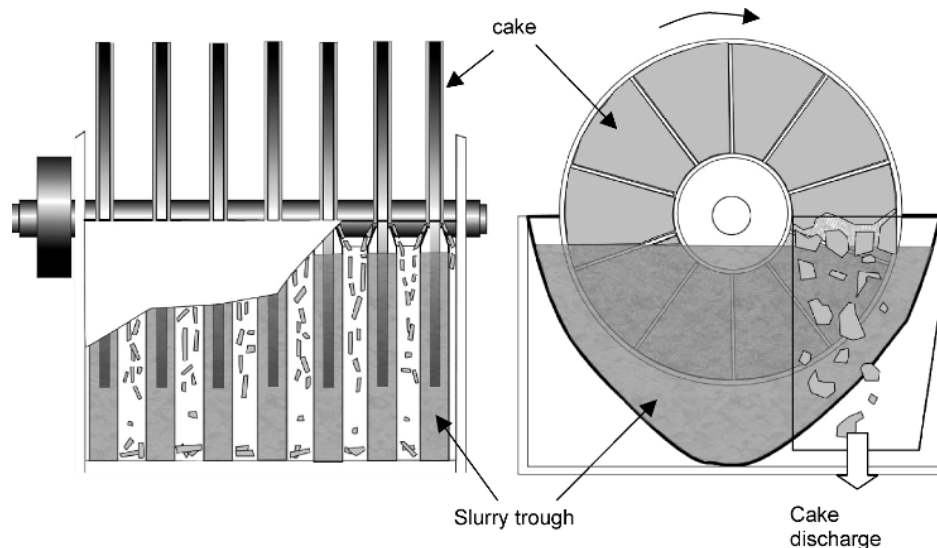

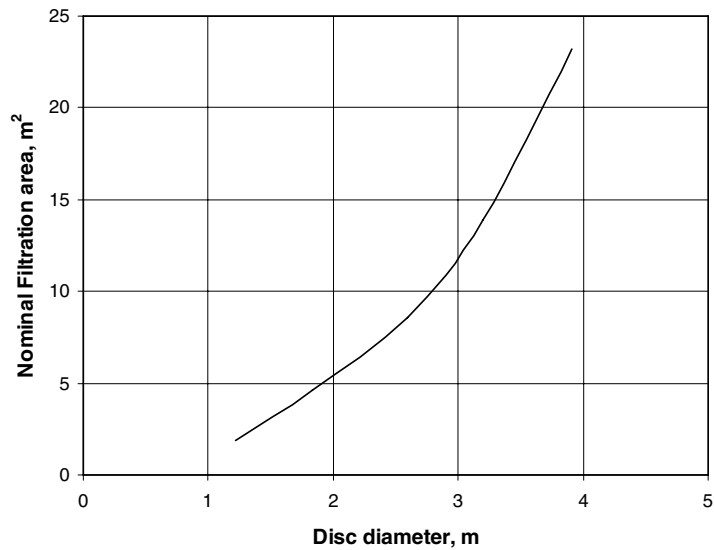Fig. 14.11. Schematic diagram of a disc filter.

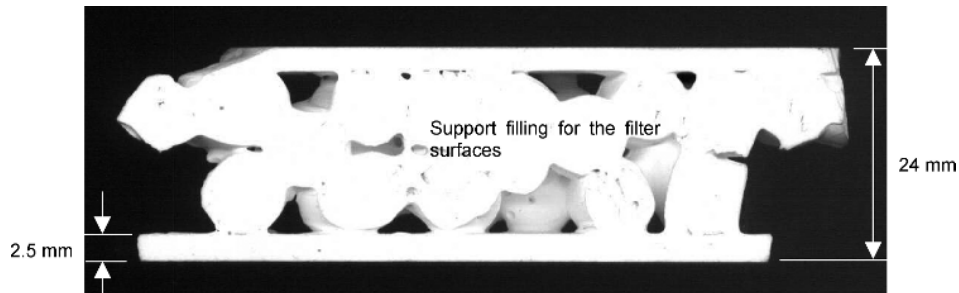Fig. 14.12. Nominal filtration area available per disc [6].

Fig. 14.13. Cross-section of a 24 mm sintered alumina filtration disc.

The low vacuum used in the filter removes the filtrate from the internal passages of the discs while the small pressure differential across the disc causes cake formation. A reduction of up to 90% in energy consumption is possible.

Horizontal Belt Vacuum Filter

Flat horizontal belt and Pan filters have been designed for fast settling and fast filtering slurries like iron ore concentrates. The *Pan tilting* vacuum filters are gradually getting out of use and therefore are not considered here. The horizontal filters are in the form of a

continuous belt made of stainless or alloy steel and a medium in the form of a fabric network. The feed box is at one end of the belt which evenly spreads the slurry across the belt. The steel base of the travelling belt is covered by a rubber lining. The belt is stretched over two pulleys (Fig. 14.14). It is grooved so that the grooves are at right angles to the direction of movement. Between the pulleys the belt is flat and rectangular. The width of the belt of industrial units is usually 1–4 meter with a filtering area of up to 120 m^2 for a 4 m x 30 m belt. Under the belt and between the pulleys is a vacuum box. The vacuum box has compartments that are adjustable along the length. Filtration takes place in the first compartment under vacuum and the filtrate is withdrawn from the bottom. In the second compartment the cake is washed under vacuum by co-current and counter current recycled wash water. Fresh make-up water is added at the last section. The wash waters are withdrawn also from the bottom under vacuum and the washed cake then dewatered and dried. Receivers for filtrate and wash waters are positioned under each section of the vacuum box.

The belt speed is regulated usually between 5–100 mm per second. Cake thickness varies from 6–203 mm depending on the belt speed.

14.1.3. Design Rating of Filters.

Ratings of filters are based on the pore size of the medium. The chosen pore size would have to be smaller than the smallest particles in the pulp. The rating therefore indicates the minimum particle size that can be retained on the filter surface. The rating, R_X, is therefore defined as the ratio of the number of particles larger than the pore size of the medium and is given by:

$$R_X = \frac{\text{No. of particles greater than } d_x \text{ / unit volume of feed}}{\text{No. of particles greater than } d_x \text{ / unit volume of tails}} \qquad (14.8)$$

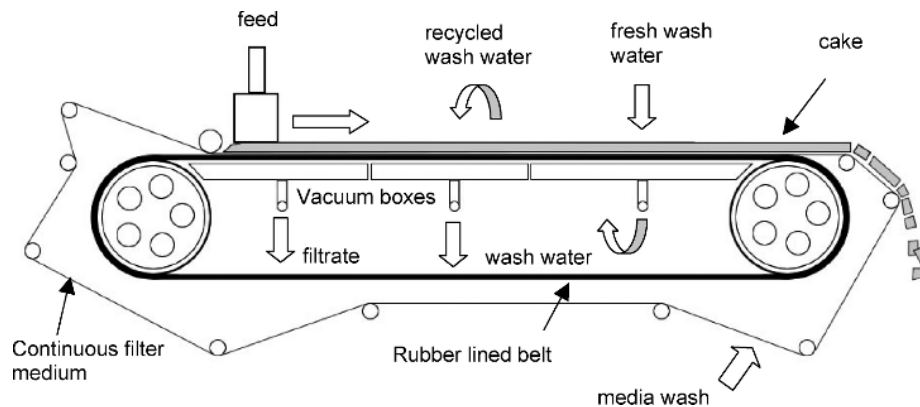where d_X =   the size of the pores.

Fig. 14.14. Sketch of a continuous horizontal belt filter.

Thus an R_{10} value of 100 means that the filter is capable of retaining 99 out of 100 (99%) of all particles greater than 10 μm. Again $R_{200} > 200$ means an efficiency in excess of 199/200 or 99.5% relative to a particle size of 200 μm. The higher the R_X value the greater the amount of coarse particles retained on the filter medium.

In terms of R_X the efficiency E of separation by a filter is given by:

$$E = \left[\frac{(R_X - 1)}{R_X} \right] 100 \qquad\qquad 14.9$$

where E is expressed in terms of per cent. The relation between R_X and E is illustrated in Fig. 14.15 [11].

14.2. Operation of Filters

The filtering process can be divided into two main operations which form a cycle:

1. Solid-liquid separation yielding solid cake and filtrate as products,
2. Treatment of the cake by dewatering, washing and drying.

In a batch process, once a cycle is completed, the assembly is dismantled, cleaned and re-assembled for the next cycle. The cycles are repeated until the entire volume of slurry has been filtered. The time taken for dismantling and re-assembly of the filter affects the total time of a filtering cycle.
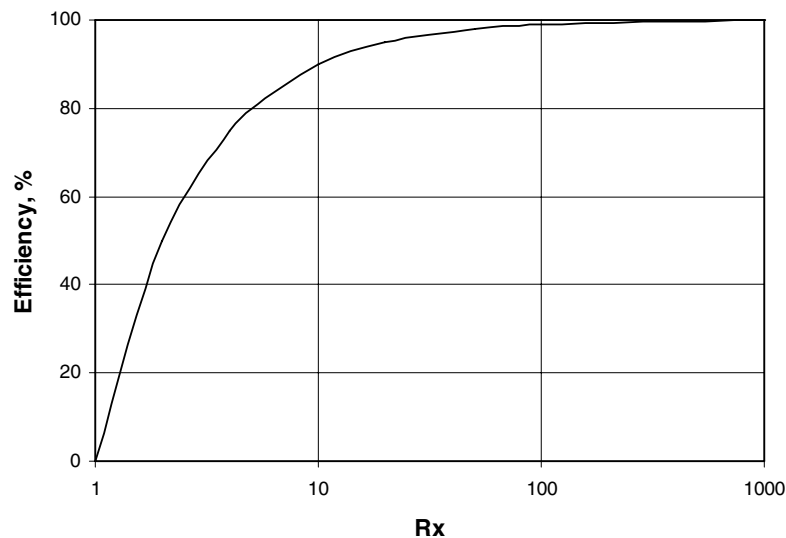
Fig. 14.15. Efficiency of filtration as a function of R_X [11].

In the continuous process, this loss of time is almost minimal. The combined permeability of the medium plus the cake is the rate determining factor of the process. The permeability of the medium can be considered to be constant (unless the pores are clogged by particles smaller than the pores in the medium). The permeability of the cake may not be constant but would depend on the changing structure of the deposited layer which in turn depends on the concentration of particles, particle size, particle shape, particle size distribution in the feed slurry, porosity and thickness of the layer. The permeability of the cake is also affected by the pressure applied. This is specially true for soft compressible cakes.

Once the solid-liquid separation process ceases, the cake can be washed and dried. The final water (moisture) content in the cake is regulated by passing dry (cold or hot) air or gas through the cake. The time taken to wash and de-water the cake affects the time cycle and therefore the economics of the operation.

Experience has shown that dewatering of a cake is a complex phenomenon and there is always a residual water saturation remaining in a cake which cannot be removed easily by the spplication of pressure and prolonged air flow. Dahlstrom [2,12] described the minimum saturation as the *achievable moisture* and ascribed it as a function of:

1. time of de-watering,
2. volume of air/gas through the cake,
3. pressure differential per mass of dry solids per unit area per cycle,
4. area of the filtering surface,
5. particle size distribution in the slurry,
6. shape of particles and
7. slurry density.

The cake moisture, m, is expressed as:

$$m = f(a, m_R, d)$$
(14.10)

where m_R = the equilibrium cake moisture if saturated air is forced through the cake at pressure ΔP,

a = an approach factor indicating the rate of approach to m_R, and

d = a parameter incorporating particle size, shape and size distribution.

The parameter d is related to the specific surface area and a particle size distribution parameter such as the % passing 10 microns. The approach term, a, is the major factor used to determine the optimum achievable cake moisture and can be expressed as:

$$a = \left[\frac{A \Delta P_D}{M_C} \right] Q_{V(D)} \, t_{DW}$$
(14.11)

where ΔP_D = differential pressure during dewatering,

$Q_{V(D)}$ = volume rate of flow of air through the cake as $m^3/s/m^2$ of filter area during the dewatering part of the cycle,

t_{DW} = dewatering time,

M_C = the mass of dry cake per cycle, and

A = filter area.

It is found experimentally that if $Q_{V(D)}$ is less than 0.102 m^3/s/m^2, then Eq. (14.11) can be simplified to:

$$a = \frac{A t_{DW}}{M_C} \qquad (14.12)$$

If the pressure changes then the term ΔP_D must be included. Apart from predicting cake moisture, a is useful in determining vacuum pump energy requirements through ΔP_D and $Q_{V(D)}$.

The mechanism of washing and dewatering cake involves the penetration of the wash liquid in the pores and displacement of liquid from the medium and cake. The process is more effective when the viscosity of the wash water is less than that of the slurry liquid. The time of washing is a function of the flow of wash water and its ability to displace the liquid contained in the cake. That is:

$$t_W = K t_C V_W \qquad (14.13)$$

where t_W = time of cake washing per cycle,
       t_C = time of cake formation per cycle, and
       V_W = volume of wash liquid per unit volume of the water contained in the cake.

Eq. (14.11) holds with the assumption that the radius of particles may be neglected and that the pore size remains unaltered during the filtering process.

14.2.1. Constant Pressure Filtration
When pressure is applied for filtration, it takes some time to build up to the required level. During this period, some filtration takes place. Once the required pressure is attained it can be held constant for filtration to proceed at that pressure (Fig. 14.16). The mathematical expression depicting filtration at constant pressure condition can be obtained by integrating Eq. (14.3), taking ΔP as constant. Eq. (14.3) may be re-written as:

$$dV = \frac{A \Delta P}{\mu \left[\dfrac{\alpha M_C}{A} + R_M \right]} dt \qquad (14.14)$$

But M_C is sometimes written as:

$$M_C = C_F V \qquad (14.15)$$

where V   = the cumulative volume of filtrate, and
       C_F = the feed solid concentration in mass of solid/volume of liquid.

However, since some of the feed water is retained in the cake as residual moisture, this equation will underestimate the mass of deposited cake. By using a mass balance on the moist cake, the true relationship between M_C and V can be derived as:
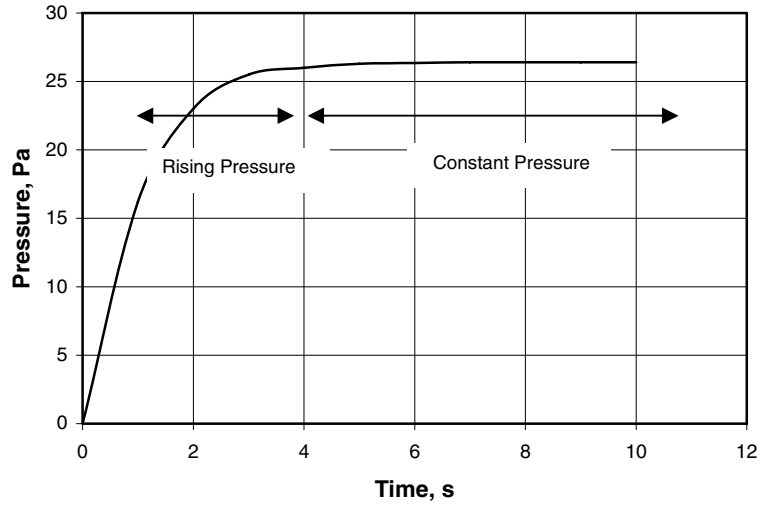
Fig. 14.16. Build up of pressure in a filter press.

$$M_C = \frac{\rho_L \, m_F}{(1 - m \, m_F)} \, V = C_m \, V \tag{14.16}$$

where m_F = mass fraction of solids in the feed,
        m = cake moisture expressed as (mass of wet cake/mass of dry cake),
        ρ_L = density of liquid (filtrate), and
        C_m = solids concentration corrected for cake moisture, kg/m^3

Eq. (14.16) can also be written in the form [5]:

$$M_C = \left[\frac{1}{C_F} - \frac{1}{\rho_S} - \frac{(m-1)}{\rho_L} \right]^{-1} V = C_m \, V \tag{14.17}$$

Substituting the value of M_C from Eq. (14.16) into Eq. (14.14) and rearranging:

$$dV = \frac{A \, \Delta P}{\mu \left[\alpha C_m \left(\dfrac{V}{A} \right) + R_M \right]} \, dt \tag{14.18}$$

For mathematical convenience Eq. (14.18) may be written as:

$$\frac{dt}{dV} = \frac{\mu \, \alpha \, C_m}{A \, \Delta P} \left[\frac{V}{A} \right] + \frac{\mu R_M}{A \, \Delta P} \quad \text{or} \tag{14.19}$$

$$dt = \frac{\mu \alpha C_m}{A^2 \Delta P} V \, dV + \frac{\mu R_M}{A \Delta P} dV \qquad (14.20)$$

Eq. (14.20) can be integrated from V=0 to V=V at constant pressure to give:

$$\frac{t}{V} = \frac{\mu \alpha C_m V}{2 A^2 \Delta P} + \frac{\mu R_M}{A \Delta P} \qquad (14.21)$$

As each of the terms $\dfrac{\mu \alpha C_m}{2 A^2 \Delta P}$ and $\dfrac{\mu R_M}{A \Delta P}$ are constants, Eq. (14.21) can be simplified and expressed as:

$$\frac{t}{V} = \frac{K_1}{\Delta P} V + \frac{K_2}{\Delta P} \qquad (14.22)$$

where $K_1 = \dfrac{\mu \alpha C_m}{2 A^2}$ and $K_2 = \dfrac{\mu R_M}{A}$

Plotting t/V against V should give a straight line with a slope equal to $K_1/\Delta P$ and intercept equal to $K_2/\Delta P$, from which the specific cake resistance and the medium resistance can be determined.

It must be remembered that Eq. (14.22) represents that portion of the pressure–time curve where the pressure is constant (Fig. 14.16). If t_1 is the time at which constant pressure commenced and the operation continued to time t during which time filtrate volumes V_1 and V were obtained, then Eq. (14.20) can be integrated between the limiting values t_1, t and V_1, V to yield Eq. (14.23):

$$(t - t_1) = \frac{K_1}{\Delta P}(V^2 - V_1^2) + \frac{K_2}{\Delta P}(V - V_1)$$

$$= \frac{K_1}{\Delta P}(V - V_1)(V + V_1) + \frac{K_2}{\Delta P}(V - V_1)$$

$$\frac{(t - t_1)}{(V - V_1)} = \frac{K_1}{\Delta P}(V + V_1) + \frac{K_2}{\Delta P} \qquad (14.23)$$

Substituting the values of K_1 and K_2 Eq. (14.23) can be re-written as:

$$\frac{(t - t_1)}{(V - V_1)} = \left[\frac{\mu \alpha C_m}{2 A^2 \Delta P} \right](V + V_1) + \frac{\mu R_M}{A \Delta P} \qquad (14.24)$$

In order to test Eq. (14.24) under industrial conditions it is necessary to ensure that the slurry feed rate, the feed tank levels and the pressure differential are constant.

In practice, it is sometimes observed that Eq. (14.24) breaks down. This has been attributed to possible distortion of the filtering medium, like woven cotton, which has a tendency to stretch.

Example 14.1 illustrates the use of the Eq. (14.24) to determine the cake resistance.

Example 14.1

A nickel mineral of specific gravity 3091 kg/m^3 was pulped using dilute sulphuric acid. The pulp contained 28% solids. After dissolving the soluble salts the pulp was filtered through a thin ceramic medium in the shape of a circular disk of area 0.178 m^2. The initial applied pressure was 10 kPa. The filtrate was collected after a step-wise increase in pressure at known intervals which gave a cake thickness of 12 mm and 12% moisture. The collected data are tabulated below. The temperature of the filtrate was 25°C. Determine the specific resistance of the deposited cake and medium.

data:

No	ΔP (x 10^5 Pa)	Time, s	Filtrate Vol., m^3
1	0.1	72.4	0.072
2	0.4	130.0	0.079
3	0.6	823.0	0.112
4	0.8	1082.4	0.124
5	1.0	1370.0	0.138
6	1.2	1740.9	0.154
7	1.4	2400.0	0.180
8	1.4	3010.0	0.201
9	1.4	3640.0	0.221
10	1.4	4280.0	0.239
11	1.4	4820.0	0.253
12	1.4	5350.0	0.267
13	1.4	5800.0	0.278
14	1.4	6250.0	0.289
15	1.4	6700.0	0.299
16	1.4	7150.0	0.308

Solution

Step 1
From the table it can be seen that after 2400 seconds, constant pressure is reached and that the filtrate volume removed in that time was 0.18 m^3. Thus 2400 s is taken as t_1 and 0.18 m^3 as V_1.

Step 2
We can now determine $t-t_1$ and $V-V_1$ as in the following table:

No.	t–t$_1$	V –V$_1$	(t–t$_1$)/(V–V$_1$)
1	-2327.6	-0.11	21500.0
2	-2270.0	-0.10	22500.0
3	-1577.0	-0.07	23100.0
4	-1317.6	-0.06	23600.0
5	-1030.0	-0.04	24600.0
6	-659.1	-0.03	25200.0
7	0	0.00	-
8	610.0	0.02	28760.0
9	1240.0	0.04	30243.9
10	1880.0	0.06	31864.4
11	2420.0	0.07	32970.0
12	2950.0	0.09	33908.0
13	3400.0	0.10	34700.0
14	3850.0	0.11	35321.1
15	4300.0	0.12	36134.5
16	4750.0	0.13	37010.0

Step 3

Plot (t – t$_1$)/(V–V$_1$) against volume V as shown below. Draw the line of best fit through the points obtained under constant pressure conditions, ie. from V$_1$ onwards.
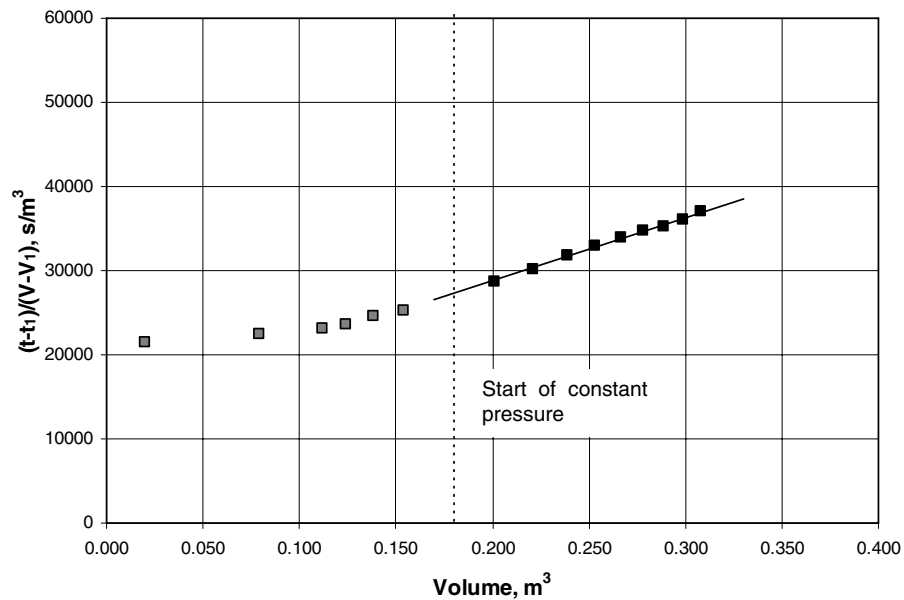
Fig. 14.17. Time-Volume plot for Example 1 data.

In this particular case the equation of the line of best fit is :

$$\frac{(t-t_1)}{(V-V_1)} = 75603.0 \text{ V} + 13644.0$$

That is, the slope of the line is 75603.0 (s/m^6) which is the value of (K$_1$/ΔP) in Eq. (14.23), and the intercept equals 13644.0 (s/m^3) which equals [(K$_2$/ΔP)+(V$_1$K$_1$/ΔP)]. Substituting these values we have:

$$75603.0 = K_1/\Delta P$$

Therefore K$_1$ = 75603.0 x 1.4 x 10^5 = 1.058 x 10^{10} Pa s/m^6

and K$_2$ = [13644.0 − V$_1$ (75603.0)] x ΔP

$$= [13644.0 - 0.18 (75603.0)] \times 1.4 \times 10^5 = 4.964 \times 10^6 \text{ Pa s/m}^3$$

Step 4
From standard tables, the viscosity of sulphuric acid at 25°C is 1.33 mPa s. [13], and the density of 5% sulphuric acid is 1030 kg/m^3 [14].

For a cake moisture of 12%:

$$m = \frac{\text{mass of wet cake}}{\text{mass of dry cake}} = \frac{100}{(100-12)} = \frac{100}{88} = 1.136$$

$$C_m = \frac{\rho m_F}{(1-m m_F)} = \frac{1030 \times 0.28}{1-(1.136 \times 0.28)} = 423.0 \text{ kg/m}^3$$

From Eq. (14.22),

$$\alpha = \frac{2A^2 K_1}{\mu C_m} = \frac{2 \times 0.178^2 \times 1.058 \times 10^{10}}{0.00133 \times 423.0} = 1.19 \times 10^9 \text{ m/kg}$$

and

$$R_M = \frac{K_2 A}{\mu} = \frac{4.964 \times 10^6 \times 0.178}{0.00133} = 6.64 \times 10^8 \text{ m}^{-1}$$

14.2.2. Constant Volume Filtration

In industrial situations a constant volume rate of flow of filtrate is often required to meet the demands of down stream operations, like flotation circuits. To maintain productivity, the filtering pressure has to be increased. It is therefore necessary to establish a relation between volume flow rate and pressure.

Considering Q_V as the volume rate of flow of filtrate, we can write:

$$Q_V = \frac{V}{t} = \frac{dV}{dt} = \text{constant} \tag{14.25}$$

Substituting the value of Q_V for dV/dt in Eq. (14.19) and re-arranging we can write:

$$\Delta P = Q_V \left[\frac{\mu \alpha C_m V}{A^2} + \frac{\mu R_M}{A} \right] \tag{14.26}$$

and from Eq. (14.25):

$$\Delta P = \alpha \mu C_m \left[\frac{Q_V^2}{A^2} \right] t + \frac{\mu R_M Q_V}{A} \tag{14.27}$$

In this case, $\dfrac{\alpha \mu C_m}{A^2}$ and $\dfrac{\mu R_M}{A}$ are constants and can be simplified as $2K_1$ and K_2, and Eq. (14.27) can now be written as:

$$\Delta P = 2K_1 Q_V^2 t + K_2 Q_V \tag{14.28}$$

It can be seen that this equation can be easily evaluated by plotting ΔP against t. The plot should be linear with the slope given by $2K_1 Q_V^2$ and the intercept by $K_2 Q_V$.

Eq. (14.27) is the basic equation for constant volume filtration. It provides the volume rate of filtration, Q_V, and the required change in pressure with time to maintaining the steady flow rate of filtrate.

Example 14.2 illustrates the use of these equations for operating a filter at constant rate of filtration.

Example 14.2

A 20% pulp of a siliceous gold ore had to be filtered at constant rate to recover the gold. The filtering medium was cloth and the filtering surface area 0.09 m^2. Pressure was gradually increased to maintain the filtering rate was at 1.8×10^{-5} m^3/s. Estimate the resistances of the cake and the medium.

Data

Density of solid = 3845 kg/m^3 Density of filtrate = 1000 kg/m^3

Viscosity of filtrate at 25°C = 0.89 mPa s   Cake moisture = 10%

Filtrate recovery time, s	50	100	150	200	250
Differential pressure, (x 10^4 Pa)	1.2	1.52	2.08	2.50	3.0

Solution

Step 1

From the cake moisture of 10%:

$$m = \frac{100}{100 - 10} = 1.11$$

Concentration of feed, $C_m = \dfrac{1000 \times 0.20}{\left(1 - (1.11 \times 0.20)\right)} = 257.1 \quad kg/m^3$

Step 2

Plot the filtrataion data as shown in Fig. 14.18 and determining the line of best fit. The intercept and slope of the line equals 6.86 kPa and 0.0916 kPa/s respectively.

Step 3

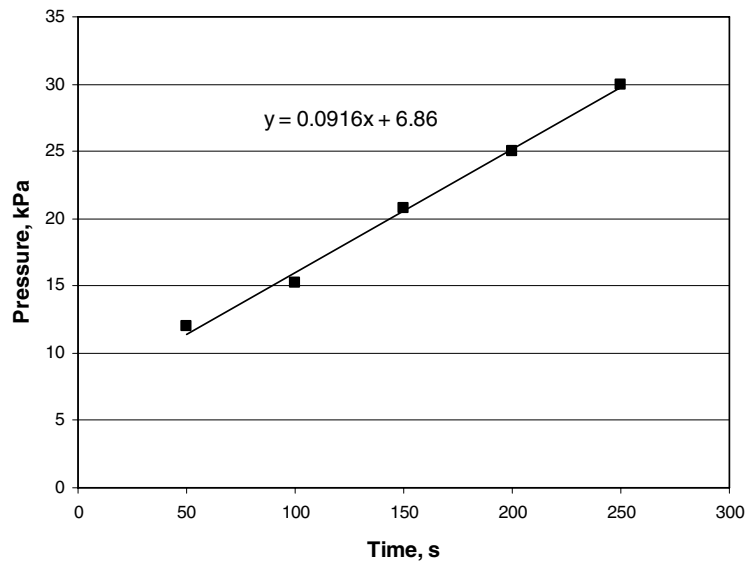From Eq. (14.27) we have:

$$6.86 \times 1000 = \frac{\mu R_M Q_V}{A}$$

Fig. 14.18. Increasing pressure with time for constant rate filtration.

Substituting values we therefore have $R_M = \dfrac{6860 \times 0.09}{1.8 \times 10^{-5} \times 0.00089} = 3.85 \times 10^{10} \ m^{-1}$

Similarly:

$$0.0916 \times 1000 = \frac{\mu \alpha C_m Q_V^2}{A^2}$$

$$\alpha = \frac{91.6 \times 0.09^2}{0.00089 \times 257.1 \times \left(1.8 \times 10^{-5}\right)^2} = 1.00 \times 10^{10} \ \text{m/kg}$$

14.2.3. Variable Pressure and Variable Volume Filtration

Various combinations of constant pressure and variable pressure filtration are practiced eespecially in plate filters. In such cases appropriate combinations of the mathematical models cited in sections 14.2.1 and 14.2.2 are applicable. For example in constant pressure followed by constant volume rate of filtration the two equations are to be applied to determine the cake characteristics and filtering times.

When both the pressure and flow rates are varied the same principle applies. In practice the variable pressures are controlled relatively easily by using centrfugal pumps and less so with diaphram or other pumps.

For such operations, therefore, the time required for a cumulative quantity of filtrate can also be determined using the basic filtration Eq. (14.3) which is re-written as:

$$\Delta P = \frac{Q_V}{A} \left(\frac{\mu \alpha C_m V}{A} + \mu R_M \right) \tag{14.29}$$

Equation (14.29) can be re-written as:

$$V = \frac{A^2}{\mu \alpha C_m} \left(\frac{\Delta P}{Q_V} - \frac{\mu R_M}{A} \right) \tag{14.30}$$

To solve Eq. (14.30), $\dfrac{\Delta P}{Q_V}$ is determined from the characteristics of the pump [5]. For example, the characteristics of a centrifugal pump operating at 1500 rpm is given in Fig. 14.19. In Eq. (14.30), V is the cumulative volume. To determine the time required for filtration it can be seen that:

$$t = \int_0^V \frac{dV}{Q_V} \tag{14.31}$$

In practice the integration is usually recommended by plotting V against $1/Q_V$ and finding the area under the curve between the limits $V = 0$ to $V = V$.

Example 14.3 illustrates the use of the method to determine the time of filtration.

Example 14.3

A slurry containing 900 kg solids per cubic meter of slurry was filtered in a plate and frame press. The total filtering area was 50 m^3. Filtering at constant pressure with a centrifugal pump produced a cake having a resistance of 1.1 x 10^{11} m/kg when a medium of resistance 5 x 10^{10} m^{-1} was against the plates. Determine the cumulative volume of filtrate and time for filtration.

Data: Viscosity of filtrate (water)   = 0.001 Pa.s
        Cake moisture   = 15%
        Filtrate density   = 1000 kg/m^3
        Solid density   = 2800 kg/m^3
        Use Fig. 14.18 for pump characteristics.

Solution

Step 1

Eq. (14.30) may be used to determine V in terms of ($\Delta P/Q_V$).

From a moisture of 15%, $m = \dfrac{100}{(100-15)} = 1.176$
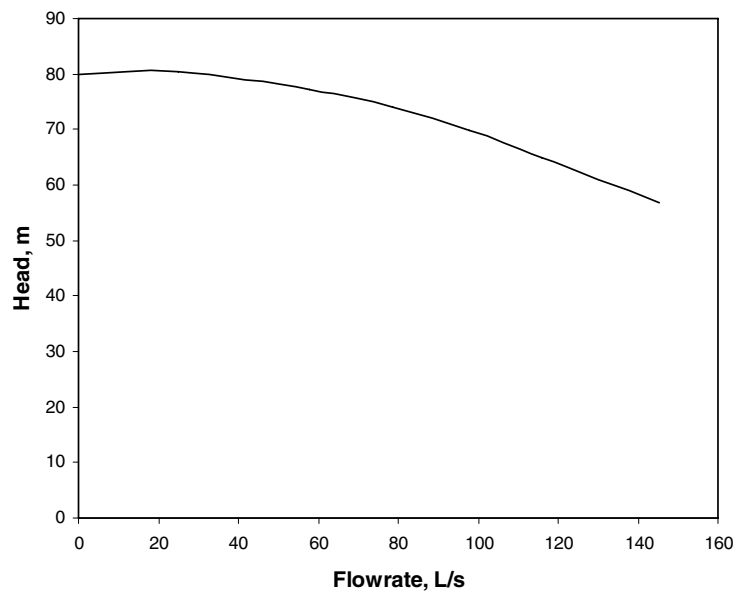
Fig. 14.19. Characteristic curve of centrifugal pump at 1500 rpm.

For a feed concentration of 900 kg of solid in 1 m^3 of slurry:

Volume of solids $= \dfrac{900}{2800} = 0.321 \text{ m}^3$

Volume of water $= 1 - 0.321 = 0.679 \, \text{m}^3$, and

Mass of water in the feed $= 0.679 \times 1000 = 679 \, \text{kg}$

Therefore, the feed fraction of solids, $m_F = 900/(900+679) = 0.570$

Then $C_m = \dfrac{1000 \times 0.57}{\left(1-\left(1.176 \times 0.57\right)\right)} = 1729 \, \text{kg/m}^3$

Step 2.
Substituting the values in the Eq. (14.30):

$$V = \frac{50^2}{0.001 \times 1.1 \times 10^{11} \times 1729} \left[\frac{\Delta P}{Q_v} - \frac{0.001 \times 5.0 \times 10^{10}}{50} \right]$$

$$= 1.31 \times 10^{-8} \left[\frac{\Delta P}{Q_v} - 1.0 \times 10^6 \right]$$

$\dfrac{\Delta P}{Q}$ is determined from the pump characteristics curve and substituted in Eq. (14.30) to determine V.

Step 3
To determine time t, integrate Eq. (14.31) with limits of V = 0 and V= the value from Step 2. The integration may be done graphically by plotting V against 1/Q.

14.2.4. Compressibility of Deposited Cakes

Some filter cakes tend to be soft and compress under the high differential pressures as applied during filtration. Compression involves a decrease in porosity and permeability of the cake.

Where tests are carried out at low pressure and a plant design is required at high pressure, the relationship between ΔP and α is required. The relationship can be obtained experimentally using a compression-permeability cell or obtained from filtration rate data using an empirical expression such as:

$$\alpha = \alpha_0 \Delta P^n \hspace{4cm} 14.32$$

where α_0 = the specific cake resistance at unit pressure and
n = a compressibility index or coefficient.

For incompressible cakes, n = 0 while for most cakes, n = 0.2 – 0.8 but can be greater than 1 for highly compressible cakes.

The constants are determined from plots of t/V versus V at different pressures. The slopes of the plots are given by $K_1/\Delta P$ so that the slope x $\Delta P = K_1$ which is proportional to α. Thus a plot of log(slope x ΔP) versus log(ΔP) will describe the α versus pressure relationship.

Example 14.4

From a set of filtering tests at five constant pressures, the following results were obtained. Determine the compressibility index of the cake. Is the cake compressible?

ΔP=50 kPa		ΔP=100 kPa		ΔP=150 kPa		ΔP=200 kPa		ΔP=300 kPa	
Q_{VL} L/min	V_L L	Q_{VL} L/min	V_L L	Q_{VL} L/min	V_L L	Q_{VL} L/min	V_L L	Q_{VL} L/min	V_L L
0.03	1	0.042	1	0.048	1	0.056	1	0.085	1
0.022	2	0.030	2	0.036	2	0.042	2	0.058	2
0.015	4	0.019	4	0.022	4	0.028	4	0.036	4
0.012	6	0.014	6	0.016	6	0.021	6	0.025	6
0.01	8	0.011	8	0.013	8	0.016	8	0.019	8
-	-	0.009	10	0.011	10	0.014	10	0.015	10

Q_{VL} – Filtration rate; V_L – Filtrate volume.

Solution

Step 1
For convenience Eq. (14.32) may be written as:

$$\frac{\alpha}{\alpha_O} = \Delta P^n \quad \text{and}$$

$$log(\alpha) - log(\alpha_O) = n\,log(\Delta P)$$

Plot reciprocal of filtering rate (t/V) against volume of filtrate collected (V) as shown in Fig. 14.20.

Step 2
The slopes and intercepts of linear regressions of each set of pressure data are given below:

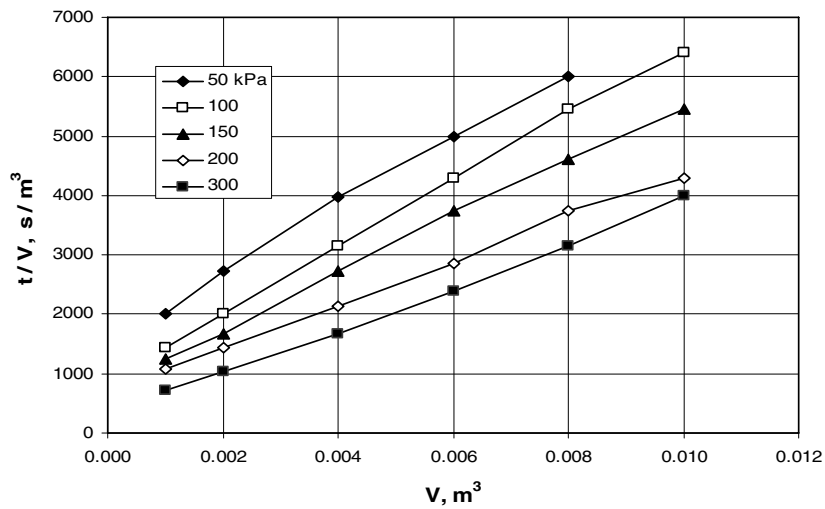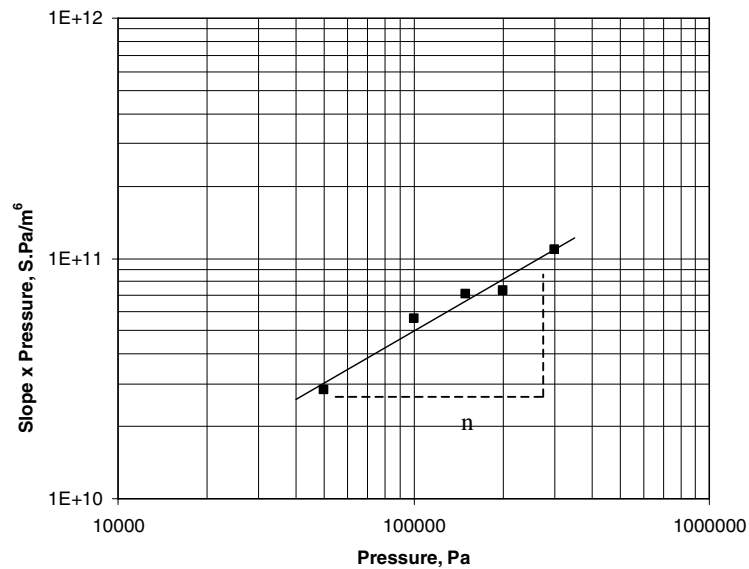| ΔP, kPa	Slope, s/m^6	Intercept, s/m^3	Slope x ΔP
50	567195.1	1559.2	28359756097
100	558729.6	901.0	55872963097
150	475029.5	789.7	71254430501
200	365459.9	701.1	73091976517
300	363321.6	284.3	1.08996E+11

Fig. 14.20. Plot of filtration data at five different pressures.

Fig. 14.21. Plot of slope x ΔP from Fig. 14.20 versus Pressure.

Step 3

Column 4 in the above table is proportional to the specific cake resistance, α.

Plot Column (4) against column (1) on log-log axes. The slope of this line is the value of n. In this case the slope is 0.71, therefore the cake is compressible.

14.2.5. Filtration through Compressible Deposits

We have seen that the flow of fluid through continuous capillaries in a bed is given by Darcy's Law. Re-writing it for convenience we have:

$$v_\varepsilon = \frac{\Delta P d_\varepsilon^2}{K L \mu} \qquad (14.33)$$

where v_ε = interstitial or average pore velocity,
d_ε = the mean diameter of the pores,
L = thickness of the bed,
μ = viscosity of fluid,
ΔP = the applied differential pressure and
K = a proportionality constant.

The average pore velocity, v_ε, is related to the average velocity over the whole cross-sectional area of the bed, v, as:

$$v = \varepsilon v_\varepsilon \qquad (14.34)$$

Thus Eq. (14.33) transposes to:

$$v = \frac{\Delta P \varepsilon d_\varepsilon^2}{K L \mu} \qquad (14.35)$$

The diameter of pores in the cake are never uniform and may even vary within a single capillary. Kozeny [16.17] therefore considered the *hydraulic diameter* being defined as:

$$d_\varepsilon = \frac{\varepsilon}{S(1-\varepsilon)} \qquad (14.36)$$

where S = the wetted perimeter or specific surface of the pore, m^2/m^3.

Substituting the value of d_ε into Eq. (14.35):

$$v = \frac{\varepsilon^3 \Delta P}{K S^2 \mu (1-\varepsilon)^2 L} \qquad (14.37)$$

This is known as the Kozeny-Carman equation and is applicable to compressed cakes as long as the pores are continuous and not blocked by compression due to packing and particle characteristics like flat laminar particles.

Because of frictional losses arising from the flow of filtrate through the cake, there will be a fluid pressure gradient across the cake. The actual compressive pressure will depend on the structure of the cake and the nature of the contacts between the particles, but it can be expressed as a function of the difference between the pressure at the surface of the cake P and that at a depth L in the cake. The packing characteristics of particles in the cake will thus change with depth and the absolute values of L and ε also changes and the method of

computing v becomes complicated. The porosity decreases, and hence the cake resistance increases, from the free surface to the filter medium interface. The simplest method to determine v is to determine the mean or average specific resistance of the bed between pressures 0 to ΔP_C. The mean specific resistance is given by:

$$\frac{\Delta P_C}{\alpha_{AVE}} = \int_0^{\Delta P_C} \frac{d\Delta P}{\alpha} \qquad (14.38)$$

where α_{AVE} = average cake resistance,

ΔP_C = pressure drop across the whole cake = $\Delta P - \Delta P_m$,

$(\Delta P_m$ = pressure drop across the medium),

Further analytical approaches have been made by later workers [18,19] who considered the flow through an element dL of cake at a distance L from the surface of the cake (Fig. 14.22). Other workers [20,21] have attempted incremental analysis of the element dL. The basic steps involved in the analysis of single element is described in the following section. As computer simulation of incremental analyses is more or less an advance on single element analysis, the reader is directed to consult the original papers.

Since the cake resistance varies with depth in the cake, the filtration equation is expressed in differential form as:

$$v = \frac{\varepsilon^3}{K S^2 \mu (1-\varepsilon)^2} \left[\frac{dP_L}{dL} \right] \qquad (14.39)$$

where dV_L = Filtrate volume from the element dL and

dP_L = fluid pressure drop across element dL.

It is assumed that the mass of deposited cake, M_C is an independent parameter, given by:

$$dM_C = A(1-\varepsilon)\rho_s dL \qquad (14.40)$$

Substituting the value of dL from Eq. (14.40) in Eq. (14.39), we get:

$$v = \frac{A\varepsilon^3 \rho_s dP_L}{K S^2 \mu (1-\varepsilon) dM_C} \qquad (14.41)$$

Note: that : 1. K is known as the Kozeny constant and usually taken as equal to 5,

2. the specific resistance of the cake element, $\alpha = \dfrac{K(1-\varepsilon)S^2}{\varepsilon^3 \rho_s}$

Substituting the expression for α, $v = V/At$ and $dM_C = C_m dV$ and re-arranging we have:

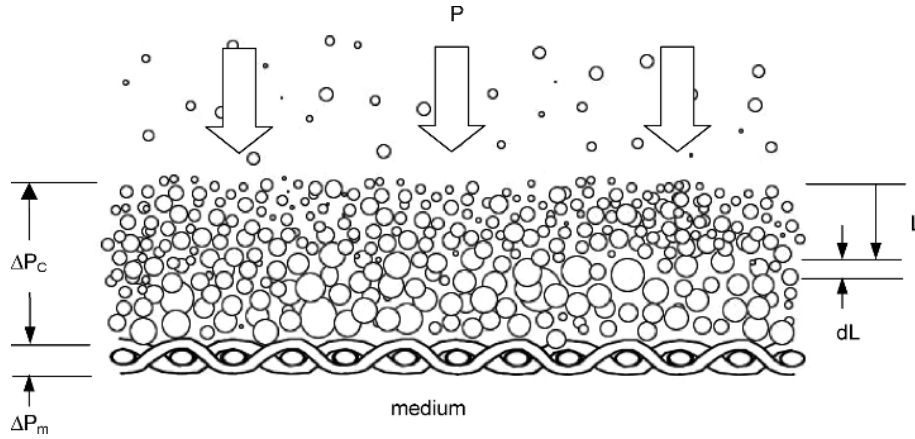$$\frac{dP_L}{\alpha} = \frac{\mu C_m V dV}{A^2 t} \qquad (14.42)$$

Fig. 14.22. Incremential element dL through a compressible cake.

Using the specific cake resistance function in Eq. (14.32) and integrating gives:

$$\int \frac{dP_L}{\alpha_0 \Delta P^n} = \frac{\mu C_m}{A^2} \int \frac{V}{t} dV \qquad (14.43)$$

Assuming a negligible media resistance to simplify the integration gives:

$$V^2 = \frac{2A^2 \Delta P^{(1-n)} t}{\alpha_0 \mu C_m (1-n)} \qquad (14.44)$$

The compressibility factor n is assumed to be reasonably constant over a small range of pressure and has a value between 0.01 to 0.90. Tiller [22] has estimated there is an error of less than 5% in assuming negligible media resistance provided (α M_C/A R_M) is greater than 20.

The average specific cake resistance across the compressible cake is equal to the integral of the change in resistance with pressure across the incremental sections of cake [5,19] as expressed in Eq. (14.38). Using the cake-pressure relationship in Eq. (14.32) and integrating gives:

$$\alpha_{AVE} = \alpha_0 (1-n) \Delta P_C^n \qquad (14.45)$$

14.2.6. Optimum Operation of Filters

The commercial operation of any continuous filter involves:

1.   filtration, for time t_F

2.   washing the cake on the medium, for time t_W
3.   dislodging the cake off the medium, for time t_D.

The time involved in each of these processes, contribute to the filtering cycle. For a rotary filter bed, the time of operation is divided between sectors roughly in the proportion shown in Fig. 14.7. The total cycle time t_C is the sum of the time spent in each section plus any downtime. That is, for a single cycle of operation, if the total time of the filtration operation is t_T and t_D the non–filtering time, then:

$$t_C = (t_F + t_W) + t_D = t_T + t_D \qquad (14.46)$$

The time involved in the filtering operation is given by the standard filtering Eq. (14.22), which may be written as:

$$\frac{K_1}{\Delta P}V^2 + \frac{K_2}{\Delta P}V = t_F \qquad (14.47)$$

where V is the cumulative volume of filtrate.

If cake washing is carried out at the same pressure as filtration, then the washing rate can be estimated as being some function of the filtration rate or a function of the filtrate volume. Thus t_W and t_F will be similar functions of V. The filter production can then be expressed as:

$$Q_M = \frac{C_m V}{\left(t_W + t_F + t_D\right)} = \frac{C_m V}{\left(f_1(V) + f_2(V) + t_D\right)} \qquad (14.48)$$

The optimum filter capacity is then obtained by differentiating Eq. (14.48) with respect to volume and equating to zero. If cake washing is not employed then the filtration capacity is optimum when the filtrate volume is optimum as expressed by the simplified equation:

$$V = \sqrt{\frac{\Delta P\, t_D}{K_1}} \quad \text{or} \quad t_D = \frac{K_1}{\Delta P}V^2 \qquad (14.49)$$

For cases where the filter medium resistance is negligible then from Eq. (14.47) the filtration time is:

$$t_F = \frac{K_1}{\Delta P}V^2 \qquad (14.50)$$

Thus optimum capacity will occur when the down time is equal to the filtration time. In practice, for maximum overall filtration rate, the filtration time must be slightly greater than the down time to allow for the resistance of the filter cloth.

14.3. Capacity of Continuous Vacuum Filters

In metallurgical practice the drum, disc and leaf filters are most commonly used and as the underlying principles of operation are the same, we will consider the capacity of these

continous filter types. The capacity is based on the volume rate of filtrate obtained during the filtering operation.

In a continuous drum, disc or leaf filter only a part of the drum, disc or leaf is immersed in the pulp that has to be filtered. Thus the time of filtration t_F, will depend on the time for which the fraction of the drum is submerged and the time taken for complete rotation, t_C, the cycle time. We have seen that for constant pressure filters:

$$\frac{dt}{dV} = \frac{K_1}{\Delta P}V + \frac{K_2}{\Delta P} \qquad (14.51)$$

The time of filtration can be evaluated by considering the volume of filtrate obtained during the operation. Thus if V is the volume of filtrate obtained then the time of filtration would be given by Eq. (14.47). This is a quadratic equation in V which can be solved for the filtering time t_F during which a section of the drum is immersed in the slurry. If the medium resistance is small, then K_2 may be neglected and the optimum filtrate volume per cycle is given by Eq. (14.50).

This is a rapid method of estimating the volume of filtrate and therefore capacity in a given filtration time. From the filtrate volume, the mass of dry cake deposited in time t_F is calculated from Eq. (14.16) and the solids capacity of the filter calculated as M_C/t_C.

Fig. 14.23 shows that while considering the actual pressure on the filtering surface, the hydrostatic head of the slurry in which the filtering drum, disc or leaf filter is immersed has been neglected. Taking this into account, the total differential pressure, ΔP_T, on the drum surface would be:

$$\Delta P_T = \Delta P_C + H \rho_P g \qquad (14.52)$$

where H = the distance, (m) below the slurry level at any point P,
  ρ_P = the density of the pulp,
  g = the accelaration due to gravity and
  ΔP_C = pressure at the drum surface

Also, if the slurry is not stirred adequately, a density difference will built up with the bottom of the trough having a denser slurry. With a variation of slurry concentration, a variation in slurry thickness would result and the mass deposited per unit area of drum, including possibly the cake characteristics, will not be uniform. Rushton and Hameed [23] suggests that this error can be accounted for by multiplying the total cake resistivity by a factor ranging between 0.9 and 1.0.

The capacity of a rotary drum filter will depend on the time that the drum surface is exposed to the slurry. The deposit time or filtration time will depend on the drum speed and the depth of submergence of the drum in the slurry. Thus if t_F is the time that any point on the drum surface is submerged during a cycle (the filtration time), θ the angle of submergence as indicated in Fig. 14.23 and t_C the time for a complete rotation of the drum, then:

t_F = Fraction of cycle submerged x t_C or

$$t_F = \frac{\theta_D}{360} t_C = \frac{\theta_R}{2\pi} t_C \quad \text{or} \quad \frac{\theta_D}{360\omega} \qquad (14.53)$$
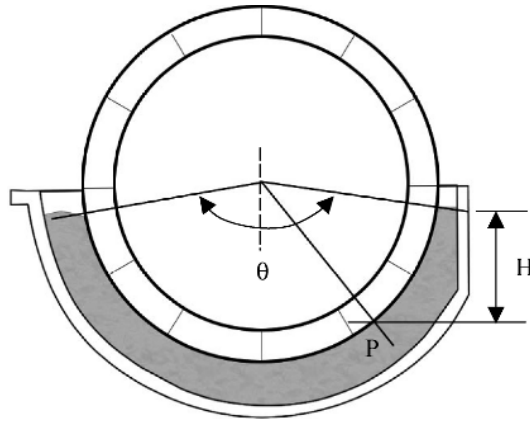
Fig. 14.23. Submergence of drum filter in slurry tank where θ is the angle of submergence.

where θ_D =   angle of submergence in degrees,
         θ_R =   angle of submergence in radians, and
         ω =   rotational speed of the drum in revolutions/s or rpm.

Osborne [24] expressed the mass of dry cake per unit area per unit time, after neglecting the resistance due to the medium, as:

$$\frac{Q_M}{A} = \left[\frac{2\Delta P^{1-n} C_m \phi}{\mu t_c \alpha_o} \right]^{0.5}$$

         14.54

where Q_M =   capacity, $kg/m^2/s$,
         n =   compressibility factor,
         ϕ =   fraction of cycle under filtration
            = $\theta_R/2\pi = t_F/t_C$,
         t_C =   cycle time, one revolution, s,
         μ =   viscosity of fluid,
         C_m =   mass of dry cake per unit volume of filtrate,
         α_o =   specific cake resistance at unit pressure,
         A =   filter area.

Rushton and Hameed [23] included the resistance of the medium and the filter cake and derived the quadratic equation which gave the flow of the filtrate during total filtering time and also the dry solid yield per unit area per filter cycle, as:

$$\frac{Q_M}{A} = \frac{-R_M \pm \sqrt{R_M^2 + \frac{2\alpha C_m \Delta P\, t_F}{\mu}}}{\alpha} \qquad (14.55)$$

The filter capacity is then obtained by dividing Eq. (14.55) by t_C to give $kg/m^2/s$ if the capacity is calculated using the total drum surface area. If the capacity of the filter, Q_M as kg/s, is calculated using the filtration area, ϕA, then Eq. (14.55) should be divided by the filtration time, t_F.

Equation (14.55) serves as a satisfactory model for the performance of rotary vacuum filters.

14.4. Washing of Deposited Cake

The cake formed on the surface of a filtering medium is usually washed to:

1. Removing the adhering fluid from the surface,
2. Removing the entrapped fluid in the pore space between the particles,
3. Removing the solute.

Washing and displacement of retained fluid within a porous cake is a complex phenomenon. The law governing the washing mechanism has been identified as Darcy's law of fluid flow through a porous body, but in dewatering the washing mechanism involves two forms, namely:

1. Displacement of bulk fluid by wash water,
2. Diffusion of fluid held in capillaries within the medium.

In excess of 90% of the contained fluid is usually removed by displacement with water as the wash liquid. The displacement curve tends to be asymptotic with time. In practice, displacement is never complete and a fraction of liquid is retained. Lowering the viscosity of the wash water helps to reduce the residual saturation level. Sqeezing the cake by application of force also helps in reducing the residual water content. The fraction of fluid that remains is often referred to as *connate water*.

The ratio of the volume of wash liquor to the volume of filtrate remaining in the cake in the saturated state is known as the *wash ratio*.

Several early workers [19,25-31] have attempted to establish mathematical models to describe the phenomenon of washing. Of these the displacement model is relatively well established.

14.4.1. Displacement Model of Washing

The process of washing involves the flow of wash water through the cake and the medium, driving the slurry ahead and out of the filtering medium. Thus the same equations as filtration at constant pressure filtration of an incompressible cake in a drum or disc filter applies. In most cases the resistance due to the medium is comparatively very small and may be neglected. For an applied differential pressure, therefore, the volume of wash liquor per unit area of the filter, V_W, would also be given by Eq. (14.21) which is written as:

$$\frac{V_W}{A} = \left[\frac{\Delta P}{2\mu C_m \alpha t_F}\right]^{0.5} t_W \qquad (14.56)$$

The filtrate volume remaining in the saturated cake, V_M, will be

$$\frac{V_M}{A} = \left[\frac{2\Delta P t_F}{\mu C_m \alpha}\right]^{0.5} k \qquad (14.57)$$

Dividing Eq. (14.56) by (14.57) gives:

$$n = \frac{\text{Volume of wash water}}{\text{Volume of filtrate remaining}} = \frac{V_W}{V_M} = \frac{t_W}{2k t_F} \qquad (14.58)$$

where t_F, t_W = times for filtration and washing respectively and
 k = a constant which is generally determined experimentally for specific slurries.

Example 14.5 illustrates the application of the method.

Example 14.5

A rotary drum vacuum operating at constant pressure of 85 kPa was required to wash a cake formed by filtering a slurry containing 5.0% solids by volume. The filtering area was 0.20 m^2 when 0.01 m^3 of feed was filtered. The resistance of the cake and cloth were 1.1 x 10^{12} m/kg and 3.8 x 10^{10} m^{-1} respectively. The cake porosity was determined as 40% . The densities of the solid and water are 2650 and 1000 kg/m^3 respectively, and the viscosity of water 10^{-3} Pa.s. The cake is then washed for 60 seconds at the same pressure. Determine:

1. the washing ratio, and
2. the rate of washing.

Solution

Step 1: Calculate the feed concentration.
Vol. of solids in feed suspension = (5/100) x 0.01 m^3 = 5 x 10^{-4} m^3
Hence water in the feed suspension = (0.01- 0.0005) m^3 = 9.5 x 10^{-3} m^3
Mass of solids in the feed = 5 x 10^{-4} x 2650 = 1.325 kg
Mass of water in the feed = 9.5 x 10^{-3} x 1000 = 9.5 kg

Solids mass fraction in the feed, S = 1.325/(1.325 + 9.5) = 0.1224

Step 2: Calculate the cake properties.
Since porosity of cake = 40%,
Volume of liquid in the pore volume = [0.40/0.60] 5 x 10^{-4} = 3.33 x 10^{-4} m^3,

(assuming a saturated cake)

Mass of water in the cake $= 3.33 \times 10^{-4} \times 1000 = 0.333$ kg

Hence the cake volume $= (5.00 + 3.33) \times 10^{-4} = 8.33 \times 10^{-4}$ m^3

This can also be calculated from $V_{Cake} = V_S/(1-\varepsilon) = 5.0 \times 10^{-4}/(1-0.4) = 8.33 \times 10^{-4}$ m^3

$$\text{Cake thickness} = \frac{\text{Cake volume}}{\text{area}} = \frac{8.33 \times 10^{-4}}{0.2} = 0.004165 \text{ m}$$

Cake moisture, $m = (0.333 + 1.325)/1.325 = 1.2513$

Step 3: Calculate the filtrate volume.
$V = $ water in feed – water in cake $= (95.0 - 3.33) \times 10^{-4} = 9.167 \times 10^{-3}$ m^3

Step 4: Calculate the corrected solids concentration, C_m.

$$C_m = \frac{\rho m_F}{(1 - m m_F)} = \frac{1000 \times 0.1224}{(1 - (1.2513 \times 0.1224))} = 144.537 \text{ kg}/\text{m}^3$$

Step 5: Calculate the wash rate and wash ratio.
Substituting values in Eq. (14.18):

$$Q_V = \frac{dV}{dt} = \frac{85000 \times 0.2}{10^{-3}\left[\dfrac{1.1 \times 10^{12} \times 144.5 \times 9.167 \times 10^{-3}}{0.2} + 3.8 \times 10^{10}\right]} = 2.32 \times 10^{-6} \text{ m}^3/\text{s}$$

Therefore for a wash of 60 seconds, assuming the wash rate is the same as the filtration rate, at the same pressure:
$V_W = 60 \times 2.32 \times 10^{-6} = 1.392 \times 10^{-4}$ m^3

and $V_M = 3.33 \times 10^{-4}$ m^3

$$\text{Hence the wash ratio} = \frac{1.392 \times 10^{-4}}{3.33 \times 10^{-4}} = 0.418$$

14.4.2. Diffusion Model of Washing

The diffusion model of washing is applicable after the displacement of slurry from the cake has been achieved and slurry together with any solute remaining entrapped has to be removed. The phenomenon can be visualised by a simplified conceptual illustration as in Fig. 14.24 where in (A) the filtrate (dark) is located in the capillaries and the pores, in (B) the filtrate has been displaced by the wash fluid, but some remains behind in the capillaries, in (C) further removal of filtrate from capillaries has taken place by diffusion leaving a very small amount

that cannot be displaced even after prolonged washing. The phenomenon is complex especially when removal of solutes are involved, e.g., washing of TiO_2 cake for the removal of ferrous sulphate from the cake [32].
Filtrate removal depends on:

1. pore size, and particle shape and
2. diffusion of the solute from the capillaries into the wash stream.

The diffusion model has difficulties especially in cases of thin cakes where cracking and by-passing of wash liquor is difficult to avoid. To understand the complex phenemenon, the concept of a dispersion parameter was introduced and defined as [33,34]:

$$D_n = \frac{v_I\, L}{D} \qquad\qquad (14.59)$$

where
v_I = average interstitial velocity,
L = depth of bed, and
D = axial dispersion coefficient.

D_n is a function of pore diameter, pore shape factor and molecular diffusion. Using computer simulations, and the concepts of dispersion and molecular diffusion, Purchas and Wakeman [30] worked on the effect of axial distribution and diffusion during washing and corrected the value of the dispersion parameter D_n as:

$$D_{n\,(corrected)} = 0.49 + 1.348\ln [D_n]_{Calculated} \qquad\qquad (14.60)$$
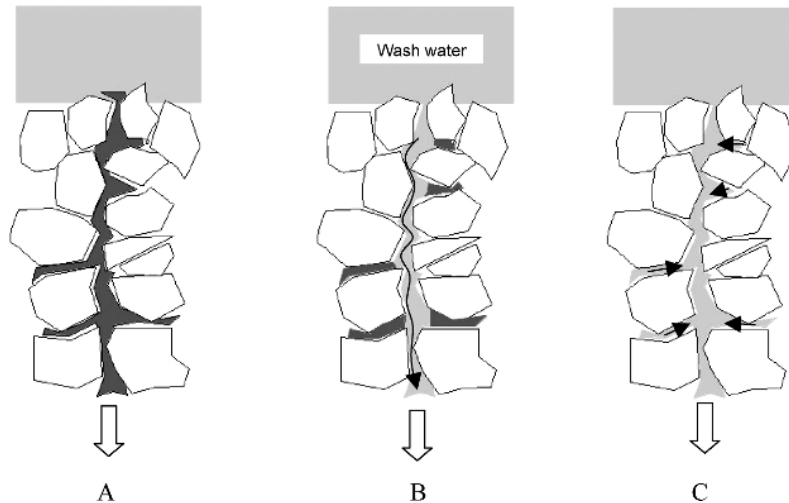

Fig. 14.24. Cake washing by diffusion; A - Filtrate (dark) in capillaries; B - Filtrate displaced by wash water - some filtrate in capillaries; C - Filtrate displaced by diffusion from capillaries.

The corrected values of D_n were recalculated and used to determine the dispersion number.

Wakeman and Attwood [35] published a series of plots relating the ratio of concentration of solute to the initial solute concentration against wash ratios for dispersion coefficients ranging from 0.01 to 100. Typical plots for D equals 0.1, 50 and 100 are illustrated in Fig. 14. 25. Thus, for a desired ratio of filtrate concentration to original concentration of fluid in the pores the wash ratio can be determined directly from the graphs for calculated values of D_n (corrected) using Eq. (14.60).

14.4.3. Washing Efficiency

Choudhury and Dahlstrom [26], using the mass balance at the face of the filtering media, determined the efficiency of filtering in terms of a wash efficiency number, E. Thus the mass fraction, m_C, of the original solute remaining in the cake after filtration was given by the expression:

$$m_C = \left[1 - \frac{E}{100}\right]^n \tag{14.61}$$

where m_C = mass fraction of original solute remaining in the cake,
  E = washing efficiency equal to the % solute removed by a wash ratio on 1.0,
  n = wash ratio.

Eq. (14.61) can be written as:

$$E = \left[1 - m_C^{1/n}\right] 100 \tag{14.62}$$

According to Dahlstrom [2,12], the efficiency of washing is generally of the order of 70% though it ranges from 45% to about 85%.
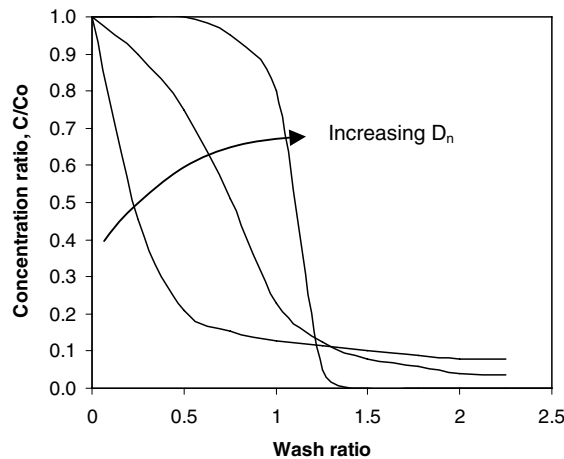

Fig. 14.25, Concentration ratio versus wash ratio [35].

14.5. Drying of Deposited Cake

After the filtration and washing processes, the cake is generally saturated with the washing fluid. To use the cake for subsequent operation it is generally dried. In continuous drum filters the drying process usually commences during the last portion of the filter-cycle. On batch pressure filters a drying period is allowed just prior to the cake being removed from the filter press.

The drying operation is executed by:

1. blowing or drawing hot or cold air, steam or gas through the cake and/or,
2. squeezing the cake.

Blowing air (gas) is the most common method of drying. The immediate effect of air blowing through a cake is to displace a major amount of fluid contained in the pores of the cake. With time, breakthrough occurs. The *breakthrough* or *threshold* pressure is the point where the first drops of the wetting fluid emerge from the cake which corresponds to the point where the first non-wetting fluid enters the inlet face of the cake. The air then passes through without significantly reducing the moisture content. At this stage, the absorbed and adsorbed moisture, (which is the wetting phase), is held on the particles and within the fine pores mainly by capillary forces. The non-wetting phase, that is air or gas, largely permeates through. The moisture removal at this stage is very slow and by diffusion only. In fact a small portion of the moisture is retained in the cake and cannot be removed even at high pressures. If pressure is applied some of the liquid held in the pores will be expelled and removed but with further application of pressure further desaturation does not take place. A typical relation between saturation and applied pressure is illustrated in Fig. 14.26. The figure shows the limiting saturation that could be obtained at the highest pressure applied was about 18%.

The threshold pressure depends precisely on the packing of the particles in the cake and hence is difficult to determine accurately. The modified threshold pressure, as indicated in Fig. 14.26 is less prone to variation.

The permeability of each individual component, that is wash-water and air, while permeating through the porous cake will follow Darcy's law (Eq. (14.7)), which is re-written as:

$$\frac{dV_a}{dt} = K_a A \left[\frac{\Delta P}{\mu_a L} \right] \quad \text{and} \quad \frac{dV_w}{dt} = K_w A \left[\frac{\Delta P}{\mu_w L} \right] \tag{14.63}$$

where the suffixes w (or L) and a represent wash water (or liquid) and air respectively. When both components are simultaneously flowing through the system, as occurs during drying, the effective permeability of each component will depend mostly on the pore size distribution. However, the relative permeability of each component can be assessed by dividing each permeability with a common factor K. The factor, K, is the permeability of a single component completely saturating the cake and the two components fully saturated in the fluid. That is:

Relative permeability of water, $K_{RW} = \dfrac{K_w}{K}$ and $\tag{14.64}$

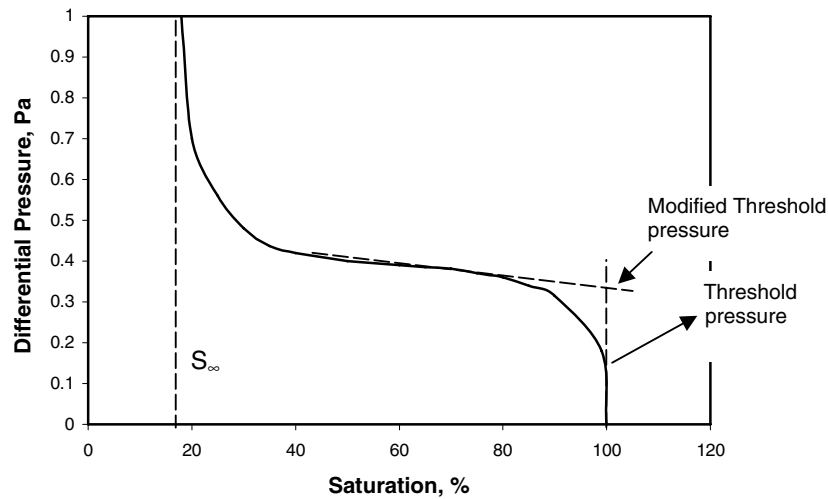Relative permeability of air, $K_{Ra} = \dfrac{K_a}{K}$ $\tag{14.65}$

Fig. 14.26. Pressure-cake saturation curve.

Equations relating the relative permeabilities to a reduced cake saturation was expressed by Lloyd and Dodds [36] and Wyllie and Gardner [37] as the basis of a model for cake drying. Typical relative permeabilities of each component with saturation are illustrated in Fig. 14.27. The curve shows that at about 25% water saturation the air permeability is 100% and the water permeability is nil. That is, the residual saturation of cake is about 25%.

Wakeman [38] attempted a solution of the relative permeability model to predict the residual saturation at a limiting pressure by considering the capillary pressure mainly responsible for holding the wash liquid in the pores. The capillary pressures were related to pore size distribution, the capillary numbers and the reduced saturation of the cake, S_R, expressed as a function of the threshold pressure:

$$S_R = \frac{S-S_\infty}{1-S} = \left(\frac{P_B}{P_{CAP}}\right)^\lambda \tag{14.66}$$

where S = cake saturation, fraction of voids in cake filled with liquid,
  S_∞ = the irreducible saturation, the saturation at high pressure across the cake or the minimum residual saturation,
  P_B = breakthrough or threshold pressure, in absolute pressure,
  P_{CAP} = capillary pressure (absolute pressure) and
  λ = an exponent and an index of the pore size distribution.

Wakeman expressed the relationships between relative permeability and reduced saturation for liquid and gas as:

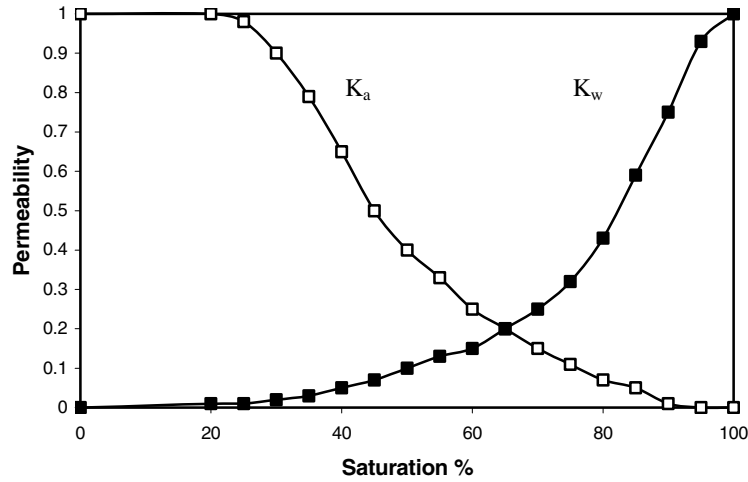$$K_{RL} = S_R^{(2+3\lambda)/\lambda} \quad \text{and} \tag{14.67}$$

Fig. 14.27. Permeabilities of the cake to air and wash water environment.

$$K_{Ra} = \left(1 - S_R\right)^2 \left(1 - S_R^{(2+\lambda)/\lambda}\right) \tag{14.68}$$

To determine the reduced saturation, the modified threshold pressure in Eq. (14.66) has to be determined by drawing a tangent at the point of inflexion in the pressure-saturation curve as illustrated in Fig. 14.26. The breakthrough pressure is expressed by the following relationship for randomly deposited cakes of sand and glass beads.

$$P_B = \frac{4.6(1-\varepsilon)\gamma}{\varepsilon \, \overline{d}} \tag{14.69}$$

where γ = surface tension of the liquid,
  ε = porosity of the cake, and
  $\overline{d}$ = mean particle size.

The correlation for the actual breakthrough pressure by Carman [39] suggested a value of 6.0 for the constant in Eq. (14.69) for packed spheres.

As the residual saturation was assumed to be due to capillaries in the cake Wakeman defined a capillary number, N_C, in terms of the diameter of the pores, porosity of the cake, depth (thickness) of the cake and the pressure differential such that:

$$N_C = \frac{\overline{d}^2 \, \varepsilon^3 \left(\rho_L \, g L + \Delta P\right)}{(1-\varepsilon)^2 L \gamma} \tag{14.70}$$

The capillary number was a function of the reduced saturation and their ratio was constant. That is:

$$\frac{S_R}{(N_C)^\chi} = \text{constant} \tag{14.71}$$

Using Eqs. (14.69)-(14.71) and empirical correlations, the minimum residual saturation was determined for coarse materials such as quartz and fine coal as:

$$S_\infty = 0.155\left(1 + 0.031 N_C^{-0.49}\right) \quad \text{for} \quad N_C \geq 10^{-4} \tag{14.72}$$

Substituting the value of N_C in Eq. (14.71), the residual saturation becomes:

$$S_\infty = \frac{P_B}{d^2 \varepsilon^3}\left[\frac{(1-\varepsilon)^3 L\gamma}{(\rho g L)+\Delta P}\right] \tag{14.73}$$

The following example illustrates the method of calculating the pressure differentials and determining the residual saturation.

Example 14.6

On filtering a slurry in a rotary drum filter a uniform cake of 8 mm thickness was formed. The cake on examination had the following properties:

Mean particle diameter   = 3.03 microns
Density of liquid   = 1000 kg /m^3,
Density of solid   = 2700 kg/m^3,
Cake porosity   = 35%,
Pressure drop across cake   = 86 kPa
Surface tension of filtrate   = 0.072 N/m.

Determine: 1. the threshold pressure,
            2. the Capillary number and
            3. residual saturation.

Solution

Step 1: Calculate the threshold pressure.
Threshold pressure is given by Eq. (14.69). Substituting the values into the equation gives:

$$P_B = \frac{4.6 \times (1 - 0.35) \times 0.072}{0.35 \times 3.03 \times 10^{-6}} = 203.0 \, \text{kPa}$$

Step 2: Calculate the capillary number.
The capillary number is given by Eq. (14.70) as:

$$N_C = \frac{0.35^3 \times (3.03 \times 10^{-6})^2 [(1000 \times 9.81 \times 0.008) + 86 \times 10^3]}{(1 - 0.35)^2 \times 0.008 \times 0.072} = 0.000139$$

Step 3: Calculate the residual saturation.
From Eq. (14.72):

$$S_\infty = 0.155 \left(1 + 0.031 \times (1.39 \times 10^{-4})^{-0.49} \right) = 0.528$$

That is, 52.8% water will be retained after drying.

___

Wakeman [38] suggested a graphical solution for determining the reduced saturation by introducing the concept of *dimensionless time*, t^o, *dimensionless pressure*, ΔP^o, and the average *dimensionless air flow rate*, v^o, defining them as:

$$t^o = \frac{K P_B t}{\mu L^2 \varepsilon (1 - S_\infty)} \tag{14.74}$$

$$\Delta P^o = \frac{P}{P_B} \tag{14.75}$$

$$v^o = \frac{v \mu L}{K P_B} \tag{14.76}$$

where K = permeability of bed, (cake plus medium),
       μ   = viscosity of air or water at the given temperature,
       v   = velocity of air or water (volumetric flux density of fluid relative to solid, $m^3/m^2 s$)

The relationship between t^o and ultimate residual saturation and dimensionless air flow at various differential pressures were determined. Typical plots are illustrated in Figs. 14.28 and 14.29. In order to plot the relationships, the pressure differentials were calculated using the expression:

$$\Delta P_a^o = \left[\frac{P_a}{P_B} \right]_{INLET} - \left[\frac{P_a}{P_B} \right]_{OUTLET} \tag{14.77}$$

By the use of Fig. 14.28 the ultimate residual saturation can be estimated at t^o and at a given operating pressure. Fig. 14.29 indicates the air volume required to achieve the saturation at the calculated dimensionless time. The method of calculating the air flow rate per unit area of filter surface is illustrated in example 14.7.
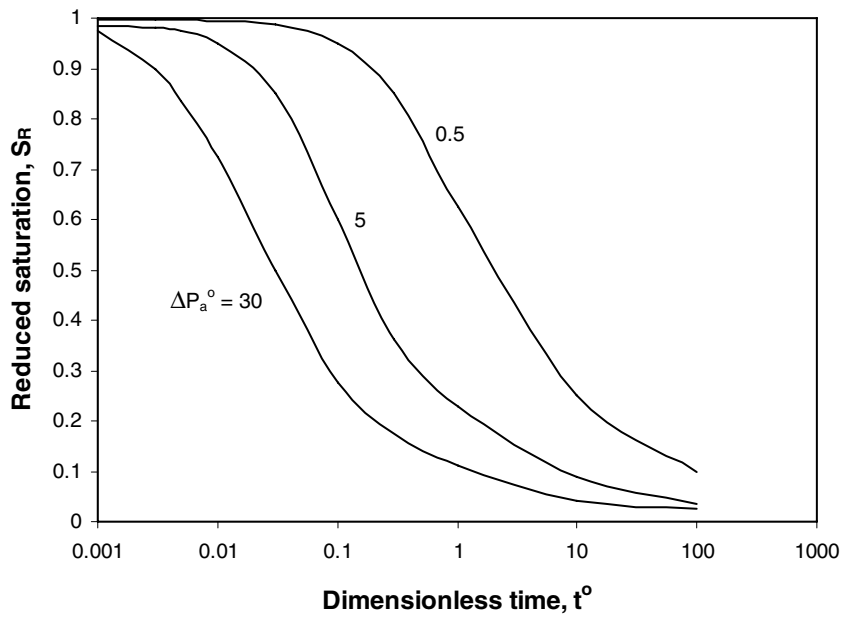
Fig. 14.28. Variation of cake reduced saturation with dimensionless dewatering time and dimensionless pressure [40].

The basis for these charts is for an inlet dimensionless pressure equal to 100. The air flowrate therefore has to be corrected for the actual drying air pressure using the factor [19]:

$$\frac{100 - \Delta P_a}{P_{outlet}^o} \left(\frac{\left(P_{outlet}^o\right)^2 - \left(P_{inlet}^o\right)^2}{\left(100 - \Delta P_a\right)^2 - 10^4} \right) \qquad (14.78)$$

Example 14.7

During the filter cake drying operation described in example 14.6, the inlet air pressure was 5 atmospheres and the air temperature 18° C. The air-pressure below the cake was 1 atmosphere (absolute) or 101.325 kPa. Estimate the flowrate of air per square meter of a drum filter of 2 m in diameter and 4 m in length. A sixth of the drum surface is exposed for drying.
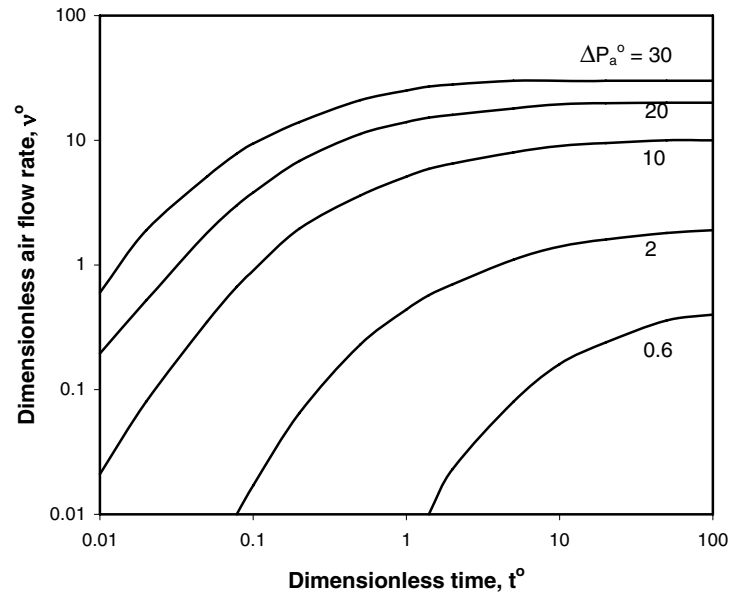
Fig. 14.29. Mean dimensionless air flow rate versus dimensionless dewatering time and dimensionless pressure [30].

Data: Time of air flow = 120 s
  Specific cake resistance = 1.10×10^{11} m/kg
  Depth of cake = 0.008 m
  Porosity of cake = 35%
  Density of solid = 2700 kg/m^3
  Density of water = 1000 kg/m^3
  The viscosity of air at 18°C = 1.82×10^{-5} Pa.s

Solution

Step 1: Calculate the dimensionless differential air pressure.
The threshold pressure determined in example 14.6 is 203.0 kPa. Hence from Eqs. (14.75) and (14.77):

$$P^o_{inlet} = \frac{5 \times 101.325 \times 10^3}{203.0 \times 10^3} = 2.496 \quad \text{and}$$

$$P^o_{outlet} = \frac{1 \times 101.325 \times 10^3}{203.0 \times 10^3} = 0.499$$

$$\Delta P_a^o = P_{inlet}^o - P_{outlet}^o = 2.496 - 0.499 = 2.0$$

From Eq. (14.78) the pressure correction factor is:

$$\frac{100 - \Delta P_a^o}{P_{outlet}^o}\left(\frac{\left(P_{outlet}^o\right)^2 - \left(P_{inlet}^o\right)^2}{\left(100 - \Delta P_a^o\right)^2 - 10^4}\right) = \frac{100 - 2.0}{0.499}\left(\frac{0.499^2 - 2.496^2}{\left(100 - 2.0\right)^2 - 10000}\right) = 2.97$$

Step 2: Calculate the bed permeability.
To determine the permeability, K, of the bed, use Darcy's Eq. (14.6):

$$K = \frac{1}{\alpha(1-\varepsilon)\rho_S}$$

Substituting values:

$$K = \frac{1}{1.1 \times 10^{11} \times (1 - 0.35) \times 2700} = 5.18 \times 10^{-15} \text{ m}^2$$

Step 3: Calculate the dimensionless time.
The dimensionless time is calculated using Eq. (14.74).

$$t^o = \frac{K P_B t}{\mu L^2 \varepsilon(1 - S_\infty)}$$

Substituting values we have:

$$t^o = \frac{5.18 \times 10^{-15} \times 203.0 \times 10^3 \times 120}{0.001 \times 0.008^2 \times (1 - 0.528) \times 0.35} = 11.93$$

Step 4: Calculate the flowrate per unit drum area.
From Fig. 14.29 the corresponding value of v_a^o is 1.5 and applying the pressure correction factor:

$$v_a^o = 1.5 \times 2.97 = 4.455$$

Hence by substituting into Eq. (14.76):

$$v_a = \frac{4.455 \times 5.18 \times 10^{-15} \times 203.0 \times 10^3}{1.82 \times 10^{-5} \times 8 \times 10^{-3}} = 0.03217 \text{ m/s}$$

$$\text{The drum surface area offered for drying} = \frac{2\pi(2/2) \times 4}{6} = 4.1888 \text{ m}^2$$

Therefore the flowrate of air per square meter $= \dfrac{0.03217}{4.1888} = 0.00768 \ \text{m/m}^2 \ \text{s}$

14.6. Optimum Thickness of Cake

The optimum thickness of filter cake, L_{OPT}, depends primarily on its solid bulk density (ρ_B), the concentration of the feed slurry, and the optimum filtrate flow rate, V_{OPT}/t. The optimum thickness is given by:

$$L_{OPT} = \frac{V_{OPT} \ C_m}{\rho_B \ A} \tag{14.79}$$

Shirato and Tiller [31] gives the following operational conditions normally practiced for continuous operation of filters having diameters between 1.8 and 3.7 m that will provide the optimum cake thickness.

Filtration Time   up to 7.5 mins,
Submergence   25% to 75% (normal about 40%),
Rotating speed   0.1-3.0 rpm.

14.7. Filtering Media

Filtering mediums are commercially available with pore size and pore size distributions marked by manufacturers. Thus for the separation of a particular particle size in a slurry, the appropriate medium can be chosen to suit the size distribution of solids in the slurry. The medium should be non-reactive and preferably non-wetting to the slurry.

The media generally used in industrial practice are woven fabric, woven synthetic material and non-woven synthetic material. The woven fabrics are made of plain cloth, twill or satin. Both twill and satin are much stronger than plain cloth. They are woven in different patterns with a variety of weft and warf combinations which offer different permeabilities The pore sizes range between 30 and 5000 μm [19]. The surfaces are sometimes flattened to reduce the pore size.

Satin finish cloths have a polished surface that releases the cake more easily than plain cotton. All cotton material are attacked by alkaline and acidic slurries, hence they are best used under neutral conditions. Cotton and cellolose based weaves shrink or stretch under load and sometimes swell. As a result, the structure of pores and pore sizes are affected which can adversely affect the size of particles in the filtrate.

The woven synthetic material are usually polypropylenes, polyesters and various polyamides. The strength of the synthetic fibres are greater than cotton fibres. Rushton et al [19] quotes 9.0×10^4 N/m for warp and 1.60×10^5 for weft fibres. These materials can withstand acidic and alkaline conditions. Synthetic media of wide ranging permeabilities are available. The manufacturers usually indicate air-permeabiility. The air permeability for nylon cloths is less than for polypropylene.

The non-oven synthetic fibre filter cloths are made from randomly assembled synthetic fibres and pressed together. The fibres are interlocked producing cloth of high permeabilities, and adequate strength for use in batch pressure filters [41,42].

14.8. Filtering Aids

Pulps containing fine kaolinitic or bentonitic clays form cakes that inhitits filtration and soon becomes impermeable as the process proceeds. Filtering such slurries and other gelataneous slurries are therefore difficult to filter. These slurries are therefore "spiked" with material that helps to keep open the porosity and permeability of the cake. It is essental that the added material be non-reactive. These *filter aids* are added in the form of powders of known size distribution.

The normal filtering aids are:

1. Diatomaceous Earth, like Kieslgur, Fuller's Earth, Celite,
2. Cellulose material and asbestos fibre, saw dust,
3. Carbonaceous powder, like activated carbon.

In addition, the hard alumino-silicate minerals like harbolite (perlite) with a SiO_2 content about 75% and 12.5% Al_2O_3, and celite (75-85% SiO_2 and 4-12% Al_2O_3) are also commonly used.

The filtering aids are obtained in the form of crushed and screened powders of the minerals in several grades of pore size, pore size distribution and specific resistances. Sometimes the minerals are calcined when their pore size changes. In celite for instance, the pore size increases by about 40-60% and are uniform and their silica content increases to about 90%.

The natural minerals have a pore size of about 1.5 μm while the calcined mineral pore size is about 2.5 μm.

In batch processes they are added in powder form to slurries as they enter the filtering chamber. The thickness of the layer is regulated so that the medium forms a coat 1-3 mm thick. This roughly translates to about 0.5 to 1.0 kg/m^2 [19]. In the continuous filtering processes, the filtering surface is first coated with the filtering aid material. This is usually achieved by suspending the filter aid in the form of a slurry and pumping to the trough below the filter. The filtering surface is then immersed in the trough. Vacuum is applied and the filter surface thus coated. The quantity of the filter-aid deposited depends on the time of immersion, particle size, shape and viscosity of the pulp. The depth of the layer can be about 15 cm.

Filter aids mixed with the cake are usually discarded after filtration is completed. However, when the cake is also of interest, the filter aid can be chemically treated or the aid material removed physically.

14.9. Filtration in Mineral Processing Circuits

Filters and thickeners are usually integrated in series in the process plant. For example, placed in series with cyclone overflows and underflows and sometime following the filtration circuits, e.g in coal washeries, lead-zinc extraction plants, copper-lead-zinc circuits. A typical layout from a flotation circuit is shown in Fig. 14.30. Several variations are seen in practice. As the filtration rates are relatively slower than most other unit operations constituting a processing plant, several filtering units are placed in parallel to meet the production target.
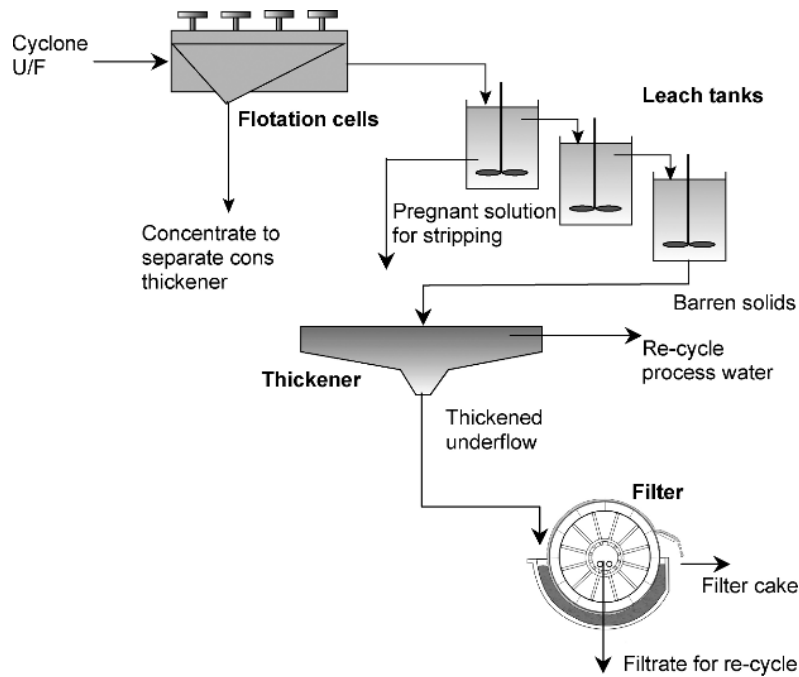
Fig. 14.30. Typical set-up of a filtration circuit.

14.10. Problems

14.1

A siliceous filter feed slurry contained 120 kg solid/m^3. It was filtered in a plate and frame press at a constant pressure of 1.5 x 10^5 Pa through a medium of resistance 2.5 x 10^{10} m^{-1} and cake resistance of 3.62 x 10^{11} m/kg. The press dismantling and reassembly time was 2 minutes. The densities of the liquid and the solids were 1000 kg/m^3 and 2640 kg/m^3

respectively and the filtrate viscosity was 0.001 Pa.s. A filtration test indicated that the ratio of wet to dry filter masses was 1.32. The filter was required to produce 40.5 kg/hour dry solids. Estimate the area of the filter surface required to meet the required yield.

14.2

A rotary drum filter 0.5 m long x 0.45 m diameter was continuously fed with a nickel sulphide slurry containing 0.15 kg of the mineral per kg of water. The filter revolved at the rate of one revolution in 270 seconds. The filtering surface was submerged in the slurry to a level of 18%. A pressure difference of 50 kPa was applied and 350 kg of filtrate obtained per hour. The following laboratory determinations were made:

1. porosity of the deposited dry solids = 33%
2. specific gravity of the mineral   = 4.5
3. cake moisture   = 15%.

Estimate the thickness of the deposit.

14.3

A rectangular pressure filter with a plate size of 0.3 m x 0.25 filtered a mineral suspension at the rate of 2×10^{-4} m^3/s when a pressure differential of 1.5×10^5 Pa was applied.
After filtration, 0.5 minutes were required to dismantle, 1.0 minutes to remove the cake and 0.5 minutes to reassemble the filter . The feed slurry contained 0.4 kg of solids per kg water. Estimate:

1. the number of frames used, and
2. thickness of the frames.

Data: Porosity of cake   = 8 %,
        Density of solid, ρ_S = 4010g/ m^3,
        Cake moisture   = 12%,
        Cake compressibility index = 0.05,
        Viscosity of water   = 0.001 Pa s,
        α_o = 1×10^{10} m/kg

14.4

A drum filter has 33% of its surface (15.7 m^2) submerged in a mineral slurry. The solid content of the slurry was 25% by mass. The densities of the dry mineral and the filtrate were 3020 and 1000 kg/m^3 respectively. The drum filter revolved at 0.35 revs./min with a pressure of 35 kPa applied. The filter cloth resistance was 1.2×10^{10} m^{-1}.
The drum speed was increased and a 4 mm thick cake was formed. The specific resistance of the cake deposit was determined to be 4.8×10^{10} m/kg and the porosity 40%. If the cake saturation is 50% and the filtrate viscosity is 0.001 Pa s determine:

1. the increase in the filtering rate at the increased drum speed,
2. thickness of the deposit at the initial drum speed,
3. the maximum possible increase in filtering rate.

14.5

A Dorr Oliver disc filter has discs of diameter equal to 1.57 m. The filter is fed continuously by a silicious slurry at the rate of 0.4 m^3 of slurry/min. The slurry contained 120 kg of solids/ m^3 water. For 3 mins the filter surface is submerged 33% in the slurry and a pressure of 0.70 $\times 10^5$ Pa is applied for filtration. The average moisture content of the filter cake is 45%. Neglecting resistance of the filter medium, estimate:

1. the filter area required,
2. the number of filtering segments,
3. the flow rate of the filtrate.

Additional Data:

Resistance of deposit	$= 1.88 \times 10^{10}$ m/kg
Compressibility coefficient	$= 0.28$
Density of solids	$= 2.75$ kg/m^3
Density of water	$= 1000$ kg/m^3
Viscosity of water	$= 0.001$ Pa s

14.6

A titania (TiO$_2$) plant produced sludge with a mean particle size was 75 microns. The sludge contained 120 kg of solids/m^3 of slurry. Filtration tests on the slurry showed the following results for the production of 1 litre of filtrate:

Time (mins)	0.5	1.0	1.5	2.0	2.5
Pressure differential (kPa)	17.0	45.0	80.0	128.0	198 0

The filter test area was 0.03 m^2 and the filter cake porosity was 20% on average with a moisture content of 40%. The viscosity of the slurry was 0.00089 Pa s and the density of solid and water were 4300 and 1000 kg/m^3 respectively. Estimate:

1.   the resistance of the cake,
2   the compression coefficient of the cake.

Assume that the media resistance is negligible.

14.7

The porosity of a bed of cake was estimated as 35% and the mean particle size was 75 microns. It had to be washed and dried with a fluid which had a surface tension of 0.052 N/m. Determine the minimum pressure required for the drying process.

14.8

A rotary drum filter was loaded uniformly with 0.035 m thick cake with a 45% porosity and specific resistance of 1.1×10^{10} m/kg. The density of the solid was 2600 kg/m^3 and the mean particle size was 5.0×10^{-6} m. The fluid in the cake had a surface tension of 0.05 N/m and a density of 1000 kg/m^3. If the drying pressure was 103 kPa, estimate:

1.   the capilary number,
2.   the residual saturation.

14.9

Filtration tests were carried out with a plate and frame filter press under the following conditions:

Solid density	$= 2710$ kg/m^3
liquid viscosity at 25°C	$= 0.001$ Pa s

feed concentration   =   10 kg solid/m^3 of **slurry**

Filter dimensions   =   plate and frame press, 10 frames

                                  dimensions 430 x 430 x 30 mm

From the filtration data, calculate the specific cake resistance and the medium resistance for the test.

Pressure (kPa)	time (s)	Filtrate vol. (m^3)	time (s)	Filtrate vol. (m^3)
180	0	0	2736	0.14
180	305	0.02	3229	0.16
180	662	0.04	3719	0.18
180	1017	0.06	4227	0.2
180	1412	0.08	4755	0.22
180	1809	0.1	5299	0.24
180	2271	0.12	5875	0.26

Assume that the cake is incompressible.

14.10

A vacuum filter leaf tests operating at a form pressure (vacuum) of 47 kPa produces a cake resistance and media resistance as given below.

If a horizontal belt vacuum filter uses the same filter cloth and filters the same slurry and has the following dimensions, calculate the filter throughput in dry solids per hour.

Filter leaf test   cake resistance   =   1.29 x 10^{11} m/kg

                         medium resistance   =   0.1645 x 10^{11} m^{-1}

                         solid concentration   =   50% (mass)

                         cake moisture   =   15% (mass)

                         liquid viscosity   =   0.001 Pa s

                         solid density   =   2600 kg/m^3

                         liquid density   =   1000 kg/m^3

Belt filter   feed box dimensions =   900 mm x 1100 mm

                         belt width   =   1 m^2

                         belt speed   =   7.5 m/min

Note: the last filtrate is extracted from the cake just as the cake leaves the feed box.

REFERENCES

[1] H.P.G. Darcy, Les Fontaines Publiques da la Ville de Dijon, Victor Dalmont, Paris, 1856.

[2] D.A. Dahlstrom, in Mineral Processing Handbook, N.L. Weiss (ed), SME/AIME, 1985, pp. 9:14-26.

[3] Larox 2005, Retrieved: November 10, 2005, from http://www.larox.com/MM/index.php

[4] Hoffland Environmental Inc. 2005, Retrieved: 20 September 2005, from http//www.hofflander.com/src/s/0 xml

[5] L. Svarovsky, Solid-Liquid Separation, Butterworths, London, 1977.

[6] GL&V Dorr Oliver 2005, Retrieved: 29 September 2005, from http://www.glv.com/ProductData.aspx?prodID=72&secID=2&catID=132.

[7] J. Halberthal, 2005a, Retrieved: 9 November 2005, from http://www.solidliquid-separation.com/pressurefilters/verticalleaf/verticalleaf.htm.

[8] R. Bosley, Filtration and Separation, 11 (1974) 138.

[9] R. Bosley, in Solid-Liquid Separation Equipment Scale-up, 2nd edition, D.B. Purchas and R.J. Wakeman (eds), Chapter 10, Upland Press, London, 1986.

[10] J. Halberthal, 2005b, Retrieved: 29 September 2005, from http://www.solidliquid-separation.com/VacuumFilters/vacuum.htm.

[11] R.H. Warring, Filters and Filtration Handbook, Gulf Publishing Company, Houston, 1981.

[12] D.A. Dahlstrom, in Mineral Processing Plant Design, A.L. Mular and R.B. Bhappu (eds), 2nd edition, Chapter 28, AIME, 1980, pp. 578-600.

[13] D.R. Lide, CRC Handbook of Chemistry and Physics, H.P.R. Frederikse and D.R. Lide (eds), 1998.

[14] R.H. Perry, D.W. Green and J.O. Maloney, Perry's Chemical Engineers Handbook, 6th edition, McGraw-Hill, 1984.

[15] E. Grist, Cavitation and the Centrifugal Pump:a Guide to Pumps, Chapter 3, Taylor and Francis, 1998.

[16] J. Kozeny, 'Uber kapillare Leitung des Wassers im Boden: Sitzungsberichte, Akademie der Wissenschaften, Wien, 136 (1927), 271.

[17] J. Kozeny, Wasserkroft W. Wasser Wirtschoft, 29 (1933).

[18] J.M. Coulson and J.F. Richardson, Chemical Engineering, Vol.2, 3rd edition, Pergamon Press, 1978.

[19] A. Rushton, A.S. Ward and R.G. Holdich, Solid-liquid Filtration and Separation Technology, 2nd edition, Wiley-VCH, Weinheim, 2000.

[20] K. Stamatakis and C. Tien, Chemical Engineering Science, 46 No.8 (1991), 1917.

[21] R.G. Holdich, Filtration and Separation, 31 No. 8 (1994) 825.

[22] F.M. Tiller, Proc. of Advanced Study Institute, K.J. Ives (ed), Series E, No. 2, Nordhoff International, Leydon, 1975.

[23] A. Rushton and M.S. Hameed, Filtration and Separation, 6 No. 2 (1969), 136.

[24] D.G. Osborne, in Solid–Liquid Separation, L. Svarovsky (ed), Chapter 13, Butterworths, Lond-Boston, 1977, pp.221-242.

[25] F. H. Rhodes, Ind. Eng. Chem., 26 (1934) 1331.

[26] A.P.R. Choudhury and D.A. Dahlstrom, AIChE Journal., 3 (1957) 433.

[27] M.T. Kuo, AIChE Journal, 6 No. 4 (1960) 566.

[28] C.D. Han and H.J. Bixler, AIChE Journal, 13 No. 6 (1967) 1058.

[29] R.J. Wakeman, International Journal of Mineral Processing, 5 (1979) 379.

[30] D.B. Purchas and R.J. Wakeman, in Solid-liquid Equipment Separation Scale-up, 2nd Edition, D.B. Purchas and R.J. Wakeman (eds), Chapter 13, Uplands Press, London, 1986.

[31] M. Shirato and F.M. Tiller, in Filtration Principles and Practice, M.J. Matteson and C. Orr (eds), 2nd edition, Chapter 6, Marcel Dekker, New York, 1987, pp. 299-428.

[32] J. Marecek and P. Novotny, Filtration and Separation, 17 (1980) 34.

[33] R. Aris, Proc. R. Soc. A., 235 (1956) 67.

[34] W.R. Sherman, AIChE Journal, 10 No. 6 (1964) 855.

[35] R.J. Wakeman and G.J. Attwood, Filtration and Separation, 25 No. 4 (1988) 272.

[36] P.J. Lloyd and J.A. Dodds, 64th National Meeting of AIChE, New Orleans, 1969.

[37] M.R.J. Wyllie and G.H.F. Gardner, World Oil Prod. Sect., 1958, 210.

[38] R.J. Wakeman, Filtration and Separation, November/December, 16 No. 6 (1979) 655.

[39] P.C. Carman, Soil Science, 52 (1941) 10.

[40] R.J. Wakeman, Powder Technology, 40 (1984) 53.

[41] D.B. Purchas, Solid-Liquid Separation Technology, Upland Press, London,1981.

[42] D.B. Purchas, Handbook of Filter Media, Elsevier Advanced Technology, Oxford, 1996.

Chapter 15. Gravity Separation

15. INTRODUCTION

Separation by density difference is a process that is as old as recorded history. Separation of gold by density difference dates back to at least 3,000 BC as depicted in writings from ancient Egypt. The principle employed in gravity separation goes back further in time to the formation and weathering of the rocks and the releasing of the minerals they contain and the transport of the mineral grains by heavy rains. It is the driving force for the formation of the alluvial deposits of precious metals and gemstones that have been worked since beyond recorded history as they still are today. Archaeological excavations have discovered mineral concentration activities such as the lead-silver concentrating plant in Attica, Greece, dating from 300-400 BC. So *gravity separation* has a long history as a mineral concentration process.

Not all mineral combinations are amenable to this type of concentration technique. To determine the suitability of gravity separation processes to a particular ore type, a *concentration criterion* is commonly used. A concentration criterion (CC) can be defined as [1]:

$$\text{Concentration Criterion} = \frac{\text{SG of heavy mineral} - \text{SG of fluid}}{\text{SG of light mineral} - \text{SG of fluid}} \qquad (15.1)$$

where   SG   =   specific gravity (or density), and the fluid is typically water or air.

Some concentration criterion ratios for minerals that are treated by gravity separation are given in Table 15.1.

Table 15.1
Concentration criterion for some common minerals separated by gravity separation from a gangue of density 2650 kg/m^3

Mineral	Fluid	CC
Gold	water	10.3
Gold	air	6.8
Cassiterite	water	3.5
Coal	water	3.4
Hematite	water	2.5

A guideline for separability by gravity based on this concentration criterion is given in Table 15.2. Fig. 15.1 shows these limitations graphically over a separation curve described by Burt [2]. Separation is possible above the line and impossible for concentration criteria below the line.
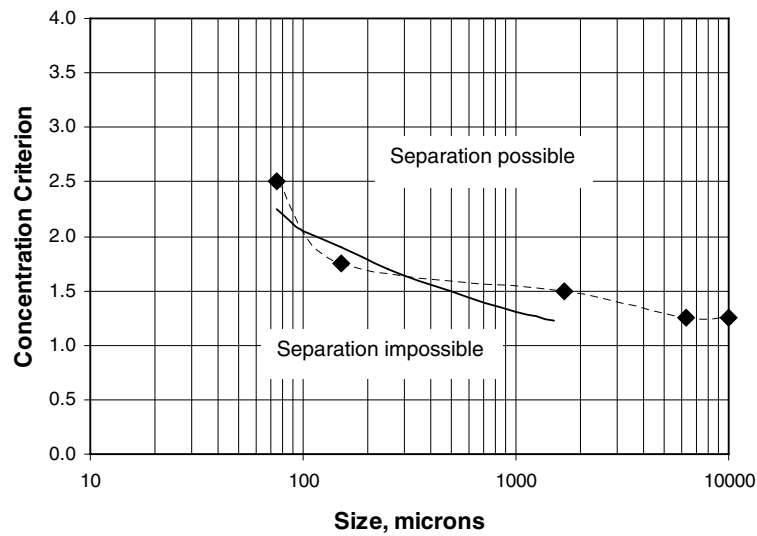
Fig. 15.1. Size limit curve for gravity separation (solid line – Burt [2]) with data from Table 15.2 (points).

Table 15.2
Concentration criterion guide for gravity separation [1].

Concentration criterion	Suitability to gravity separation
CC > 2.5	easy down to 75 μm
1.75 < CC < 2.5	possible down to 150 μm
1.5 < CC < 1.75	possible down to 1.7 mm
1.25 < CC < 1.5	possible down to 6.35 mm
CC < 1.25	impossible at any size

Table 15.1 shows that separation will be easier in a fluid of higher density.

The concentration ratio numbers in Fig. 15.1 and Table 15.2 are a guide only as the ratio is influenced by other factors such as particle shape. Particle shape can be taken into account by including a shape factor defined as the ratio of shape settling factors for the heavy and light minerals. The shape settling factor is the ratio of the terminal velocity of two particles of the same density, same size but different shape. That is:

$$\text{Shape settling factor} = \frac{v_{T(particle)}}{v_{T(sphere)}} \tag{15.2}$$

where v_T = terminal velocity.

15.1. Particle Settling Rates

The separability of minerals by gravity separation relies on a particle's settling rate in a fluid. The terminal velocity of solid spheres settling in a fluid is described by Stokes' Law for fine particles (Eq. (15.3)) or Newton's Law for coarse particles (Eq. (15.4)). Both these equations include particle density as well as particle size.

$$v_T = \frac{g(\rho_S - \rho_F)d^2}{18\mu} \qquad \text{for viscous resistance (Stokes' Law)} \qquad (15.3)$$

$$v_T = \sqrt{\frac{4g(\rho_S - \rho_F)d}{3C_D\rho_F}} \qquad \text{for turbulent resistance (Newton's Law)} \qquad (15.4)$$

where d = particle diameter,
   ρ_S, ρ_F = density of solid and fluid respectively,
   C_D = the drag coefficient,
   μ = fluid viscosity and
   g = gravitational acceleration.

Stokes' equation is said to apply to conditions where the particle Reynolds number is less than 1 and Newton's equation applies for Reynolds numbers > 1000. For particles of quartz in water, this represents an upper size limit of around 110 μm for Stokes' Law and a lower limit of around 3.5 mm for Newton's Law. Thus for particles of quartz between 110 microns and 3.5 mm neither equation accurately describes the settling rate of objects and this size range represents a major size range of interest in gravity separation. A number of researchers have developed empirical correlations to fill this size gap. Dietrich [3] derived a correlation from a data set of 252 values using dimensionless parameters, W^* and D^*, and incorporating shape and angularity factors:

$$W^* = \frac{v_T^3 \rho_F^2}{(\rho_S - \rho_F) g\mu} \qquad (15.5)$$

and

$$D^* = \frac{(\rho_S - \rho_F)g\,d_N^3\,\rho_F}{\mu^2} \qquad (15.6)$$

where d_N = nominal diameter of the largest projected area. An irregular particle will settle in a stable orientation when the largest projected area is perpendicular to the settling direction.

Dietrich's dimensionless parameters are related by the expression:

$$W^* = R_3 10^{R_1 + R_2} \qquad (15.7)$$

where R_1 = a coefficient describing the effect of particle density and given by:

R_1 = $-3.76715 + 1.92944 \,(\log D^*) - 0.09815 \,(\log D^*)^2 - 0.00575 \,(\log D^*)^3 +$
$0.00056 \,(\log D^*)^4$

R_2 = a coefficient describing the effect of particle shape and given by:

$$\log\left(1 - \frac{1 - CSF}{0.85}\right),$$

CSF = Corey shape factor = $\dfrac{d_{MIN}}{\sqrt{d_{MAX} d_{MID}}}$,

d_{MIN}, d_{MAX} and d_{MID} = minimum, maximum and mid-range particle dimension, and

$$R_3 = \left(0.65 - \left(\frac{CSF}{2.83}\tanh\left(\log D^* - 4.6\right)\right)\right)^{\left(1 + \frac{(3.5 - P)}{2.5}\right)}$$

P = a Powers roundness factor, equal to 6 for perfect rounded particles (spheres) and 2-3 for highly angular particles.

Jiménez and Madsen [4] simplified Dietrich's approach defining the dimensionless parameters:

$$V^* = \frac{v_T}{\sqrt{\left(\dfrac{\rho_S - \rho_F}{\rho_F}\right) g d}} \qquad (15.8)$$

and

$$S^* = \frac{d \rho_F}{4\mu}\sqrt{\frac{(\rho_S - \rho_F) g d}{\rho_F}} \qquad (15.9)$$

A linear regression between $(1/V^*)$ and $(1/S^*)$ gave the equation:

$$\frac{1}{V^*} = A + \frac{B}{S^*} \qquad (15.10)$$

The coefficients A and B allowed a solution for the drag coefficient:

$$C_D = \frac{1}{3}\left(A + \sqrt{A^2 + \frac{16B}{Re_P}}\right)^2 \qquad (15.11)$$

where Re_P = particle Reynold's number.

Jiménez and Madsen obtained values of A and B from Dietrich's data for quartz spheres from ~0.06 –1 mm validating the equation for $0.2 < Re_P < 127$. For Reynolds numbers less than 0.2, C_D approached a value of $24.5/Re_P$ in good agreement with Stokes' drag coefficient

but for Reynolds numbers above 1000, C_D approached a constant value of 0.83 compared with a value of 0.44 for Newtonian turbulent resistance.

Table 15.3 shows values of A and B obtained by Jiménez and Madsen for different shaped particles.

Example 15.1 explores the calculation of settling velocities using these equations.

Table 15.3
Coefficients A and B in equation 15.10 for particles of Corey shape factor 0.7 [4].

Parameter P	A	B
2.0 (crushed)	0.995	5.211
3.5 (natural)	0.954	5.121
6.0 (well rounded)	0.890	4.974
Spheres	0.794	4.606

Example 15.1

Determine the settling rates for spherical particles of quartz settling in water for particles of size 38 μm to 16 mm. The density of quartz and water are 2650 and 1000 kg/m³ respectively and the viscosity of water is 0.001 Pa s.

Solution

Step 1: Calculate the terminal velocity for a 38 micron particle of quartz using Stokes' Law:

For a 38 micron particle, using Eq. (15.3),

$$v_T = \frac{(2650-1000) \times 9.81 \times (0.000038)^2}{18 \times 0.001} = 0.001299 \text{ m/s}$$

The Reynolds number for this size particle is:

$$Re_p = \frac{v_T \, d \rho_F}{\mu} = \frac{0.001299 \times 0.000038 \times 1000}{0.001} = 0.0493$$

Step 2: Repeat Step 1 and calculate the terminal velocity of a 38 micron particle using Newton's Law:

For the same particle, using Eq. (15.4):

$$v_T = \sqrt{\frac{4 \times 9.81 \times (2650 - 1000) \times 0.000038}{3 \times 0.44 \times 1000}} = 0.0432 \text{ m/s}$$

and $Re_p = \dfrac{0.0432 \times 0.000038 \times 1000}{0.001} = 1.6406$

Step 3: Repeat Step 1 and calculate the terminal velocity of a 38 micron particle using Dietrich's correlation:

Using Eq. (15.6),

$$D^* = \frac{(2650 - 1000) \times 9.81 \times (0.000038)^3 \times 1000}{0.001^2} = 0.8882$$

and from Eq. (15.7), for CSF = 1.0 for a sphere and P = 6 for a perfect round object,

$$\begin{aligned} R_1 &= -3.76715 + 1.92944(\log 0.8882) - 0.09815(\log 0.8882)^2 - 0.00575(\log 0.8882)^3 \\ &\quad + 0.00056(\log 0.8882)^4 \\ &= -3.8668 \end{aligned}$$

$$R_2 = \log\left(1 - \frac{1 - 1.0}{0.85}\right) = 0$$

$$R_3 = \left(0.65 - \left(\frac{1.0}{2.83}\tanh(\log 0.8882 - 4.6)\right)\right)^{\left(1 + \frac{(3.5 - 6)}{2.5}\right)} = 1.0$$

Then from Eq. (15.7);

$$W^* = 1.0 \times 10^{-3.8668 + 0} = 0.000136$$

and from Eq. (15.5);

$$v_T = \sqrt[3]{\frac{0.000136 \times (2650 - 1000) \times 9.81 \times 0.001}{1000^2}} = 0.0013 \text{ m/s}$$

and $Re_p = \dfrac{0.0013 \times 0.000038 \times 1000}{0.001} = 0.0494$

Step 4: Repeat Step 1 and calculate the terminal velocity of a 38 micron particle using the Jiménez and Madsen correlation:

From Eq. (15.9) and Table 15.3, A = 0.794 and B = 4.606;

$$S^* = \frac{0.000038 \times 1000}{4 \times 0.001} \sqrt{\frac{(2650-1000) \times 9.81 \times 0.000038}{1000}} = 0.2356$$

and substituting into Eq. (15.10)

$$V^* = \frac{S^*}{(AS^*+B)} = \frac{0.2356}{(0.2356 \times 0.794)+4.606} = 0.04916$$

Then from Eq. (15.8);

$$v_T = 0.04916 \times \sqrt{\left(\frac{2650-1000}{1000}\right) \times 9.81 \times 0.000038} = 0.00122 \text{ m/s}$$

and $Re_P = \dfrac{0.00122 \times 0.000038 \times 1000}{0.001} = 0.0463$

Step 5: Repeat calculations in steps 1-4 for other sizes up to 16 mm and compare.
By changing the particle size from 38 microns to 16 mm, the following table is compiled.

d_N (m)	v_T Stokes m/s	v_T Newton m/s	v_T Dietrich m/s	v_T Jiménez m/s	Re
0.000038	0.001	0.0432	0.0013	0.0012	0.05
0.000050	0.002	0.0495	0.0022	0.0021	0.10
0.000075	0.005	0.0607	0.0046	0.0044	0.33
0.000106	0.010	0.0721	0.0082	0.0083	0.87
0.000175	0.028	0.0926	0.0182	0.0192	3
0.00050	0.225	0.1566	0.0740	0.0747	37
0.00075	0.506	0.1918	0.1161	0.1083	81
0.0010	0.899	0.2215	0.1550	0.1355	135
0.0020	3.597	0.3132	0.2829	0.2129	425
0.0040	14.388	0.4429	0.4565	0.3133	1253
0.0060	32.373	0.5425	0.5757	0.3877	2326
0.0080	57.552	0.6264	0.6666	0.4496	3596
0.0100	89.925	0.7004	0.7406	0.5038	5038
0.0160	230.208	0.8859	0.9073	0.6391	10225

The following graphs compares the calculated settling velocities.

In the fine particle range (< 100 microns) the Stokes settling equation and Dietrich and Jiménez correlations are similar. Above 150 microns the Stokes equation starts to deviate from the Dietrich and Jiménez plots. The Newton settling line is significantly different from the other plots at this size range. At the course end of the size range, as seen below, the Jiménez correlation also deviates from the Newton and Dietrich plots.
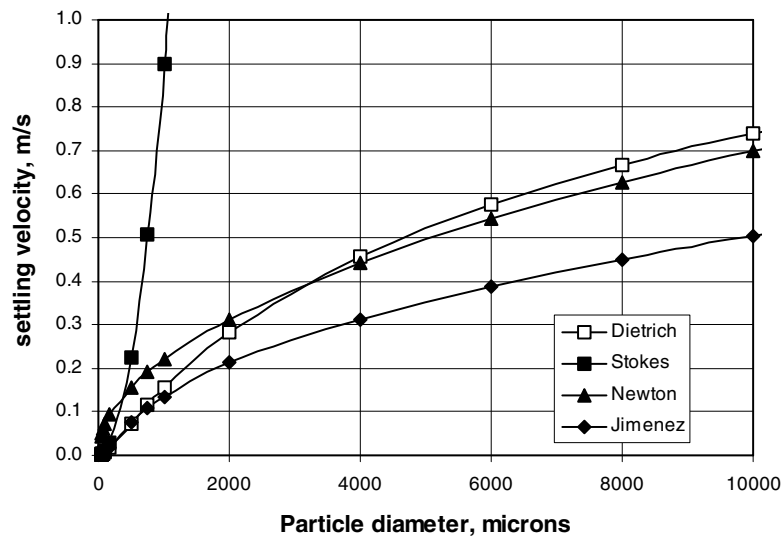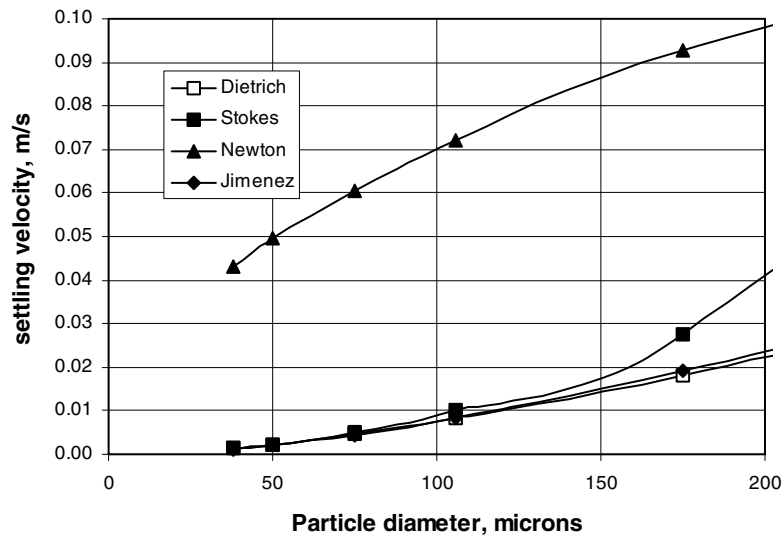
At particle sizes above about 3 mm, the Newton and Dietrich plots are still close. At this point, the Reynolds number is around 1000, the region above which Newton's Law is valid. The Dietrich correlation seems to adequately describe the transition region between the Stokes and Newtonian regimes. The Jiménez correlation deviates from the Dietrich correlation above a size of around 1 mm or a Reynolds number around 135.

The separation by gravity is based on the difference in settling rates or terminal velocities of particles of different density and size. However, with short distances of travel in some separation processes, particles may not have a chance to reach their terminal velocity. How long it takes particles to reach their terminal velocity and what are the displacement distances between particles when they attain their terminal velocity could be a determining factor in the concentration of particles by gravity separation.

The forces acting on a particle settling in a fluid under free settling conditions are gravity, buoyancy in the fluid and drag. Thus:

$$M_S a_P = F_g - F_B - F_D = M_S g - M_S \left(\frac{\rho_F}{\rho_S} \right) g - F_D \qquad (15.12)$$

where $\quad M_S \qquad = \quad$ solid mass,

$\qquad M_S \left(\dfrac{\rho_F}{\rho_S} \right) \quad = \quad$ mass of fluid displaced by the particle,

$\qquad a_P \qquad = \quad$ the particle acceleration, and

$\qquad F_D, F_g, F_B \quad = \quad$ the drag, gravitation and buoyancy forces respectively.

Dividing Eq. (15.12) through by the solid mass gives:

$$a_P = \frac{dv}{dt} = g \left(1 - \frac{\rho_F}{\rho_S} \right) - \frac{F_D}{M_S} \qquad (15.13)$$

The drag force increases with increasing particle velocity and eventually balances the other forces acting on the particle to yield a constant falling velocity, the terminal velocity.
The drag force is given by:

$$\frac{F_D}{M_S} = \frac{C_D v^2 A_C \rho_F}{2 M_S} \qquad (15.14)$$

where $\quad A_C = \quad$ the cross-sectional area of the particle, and
$\qquad v \quad = \quad$ particle velocity.

For a spherical particle:

$$M_S = \frac{\pi d^3 \rho_S}{6} \quad \text{and} \quad A_C = \frac{\pi d^2}{4} \quad \text{thus:}$$

$$\frac{F_D}{M_S} = \frac{3 C_D v^2 \rho_F}{4 d \rho_S} \qquad (15.15)$$

At low particle velocities, for a spherical particle, C_D is given by:

$$C_D = \frac{24}{Re_P} = \frac{24 \mu}{v d \rho_F} \qquad (15.16)$$

where μ = fluid viscosity and
$\quad\quad\quad$ d   = particle diameter.

Thus:

$\dfrac{F_D}{M_S} = \dfrac{18\,\mu v}{d^2\,\rho_S}$ and substituting into Eq. (15.13) gives:

$$\frac{dv}{dt} = \frac{g\left(\rho_S - \rho_F\right)}{\rho_F} - \frac{18\mu v}{d^2\,\rho_S} \quad \text{for} \;\; Re_P < 1 \tag{15.17}$$

At higher velocities, C_D is taken as 0.44 for spherical particles and:

$$\frac{dv}{dt} = \frac{g\left(\rho_S - \rho_F\right)}{\rho_F} - \frac{\left(0.44 \times 3\right) v^2\,\rho_F}{4 d \rho_S} \quad \text{for} \;\; Re_P > 1000 \tag{15.18}$$

Fig. 15.2 is constructed using Eq. (15.17). It shows the increase in particle velocity with time for particles of the same size but different densities. Fig. 15.3 shows a similar plot for larger particles settling as described by Eq. (15.18).
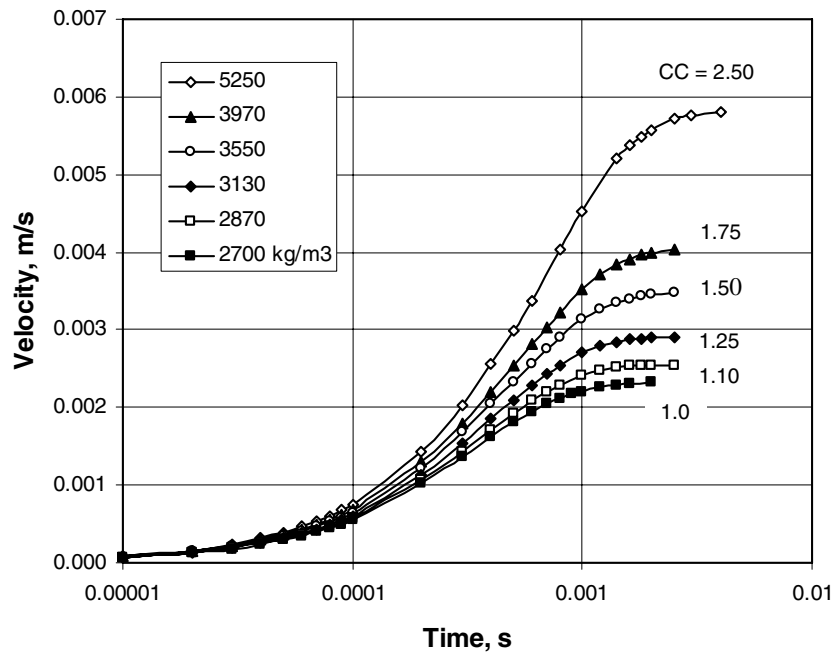

Fig. 15.2. Settling velocity of 50 μm particles of different density in water for different concentration criteria.
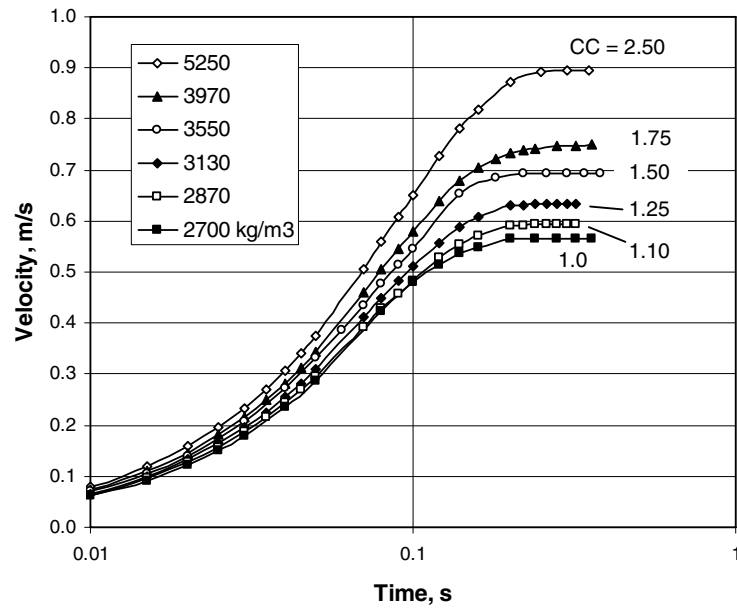
Fig. 15.3. Settling velocity of 6.35 mm particles of different density in water for different concentration criteria.

Table 15.4 summarises the settling velocities and distances travelled for a combination of different concentration criteria and particle sizes corresponding to the size limits shown in Table 15.2. The calculations indicate that the time required for a particle to reach its terminal velocity is quite short, ranging from 0.001 to 0.4 seconds. The lighter particles reach their terminal velocity marginally ahead of the heavier particles.

Table 15.4
Time and distance apart when particles reach their terminal velocity, based on Eqs. (15.17) and (15.18).

Particle size	Concentration criterion	Difference in v_T	Separating distance	Time for heavy particle to reach v_T	Distance apart after 1 second
mm		m/s	mm	seconds	mm
0.050	1.10	0.0002	0.0009	0.0018	0.24
	1.25	0.0006	0.0036	0.0025	0.60
	1.50	0.0012	0.0050	0.0025	1.17
	1.75	0.0018	0.0064	0.0025	1.75
	2.50	0.0035	0.0195	0.0040	3.49
6.35	1.10	0.028	8.80	0.32	27.6
	1.25	0.068	21.60	0.32	67.6
	1.50	0.127	54.60	0.34	127.3
	1.75	0.182	88.20	0.36	182.3
	2.50	0.329	177.00	0.40	329.2

For particles of 6.35 mm size, the terminal velocity is reached after about 0.4 seconds and particles of concentration criterion (CC) 2.5 are separated by several hundred millimetres and separation of particles should be easy. The separation distance between particles decreases as the concentration criterion decrease and thus separation should become more difficult with decreasing concentration criterion.

If the particles don't reach their terminal velocities then the separation distance between particles is reduced. For example, for a particle of CC = 1.25, after 0.1 seconds of settling, the settling velocities are very close and the separation distance between the particles is 3.2 mm which for particles of 6.35 mm diameter is insufficient to segregate into separate layers.

For 50 μm particles, the terminal velocity is reached after a very short time and the distance separating particles at this point is as much as 20 μm for particles with a concentration criterion of 2.5. For 50 μm particles, this is obviously insufficient for separation to occur. As settling time is increases up to 1 second, particle separation, in free settling conditions, will increase to 3.5 mm for particles with a concentration criterion of 2.5. With this separation distance between heavy and light particles, segregation, and ultimately separation, may not be possible for these sized particles. Increasing the settling time further will increase the separation distance and make separation easier. However, the fact that particles of this size are not easily separated even at this value of concentration criterion, indicates that other factors such as particle shape and separator characteristics come into play.

15.1.1. The Effect of Particle Size and Shape

One of the complicating factors is that particles are not a single size. In any feed there is going to be a size variation, even in a closely sized sample. Consider an elutriation column with a prepared feed of −150 +125 μm containing a mixture of pyrite (S.G. 5.0) and arsenopyrite (S.G. 6.1). If a rising column of water is flowing at a velocity between the settling velocity of the two minerals then the heavier mineral will be able to sink and the lighter mineral will be lifted by the water and hence a separation of the two minerals can be made. Fig. 15.4 shows the effect of particle size on the settling velocity and hence the water velocity required to bring about separation. If the water velocity is above the curve, the particle will be lifted and if the water velocity is below the curve, the particle will sink. Thus the region between the curves represents the range of possible water flows that will separate the particles. For the −150 +125 μm size fraction, point D, where the lower size intersects the lower particle density curve represents the water flowrate below which all particles will sink and point C, where the large size intersects the higher particle density curve represents the water flowrate above which all particles will be lifted. Flowrates between C and D will achieve a separation of some sort with some particles being lifted and some particles sinking. Point A at the intersection of the lower size and the higher density curve and point B, the intersection of the higher size and the lower density curve, will be the boundary of the region where a complete separation is possible, but only if point A lies higher than point B. In the case of Fig. 15.4, where the concentration criterion is 1.275, this is not the case and there will always be some contamination of the light mineral and the heavy mineral in each product. For a smaller size fraction such as −106 +90 μm, the window of possible separation flowrates decreases. That is, the separation would become more difficult.

For a higher concentration criterion, such as in the separation of arsenopyrite (S.G. 6.1) from gold (S.G. 18.0), Fig. 15.5 shows the settling curves as a function of particle size. From this plot, for the particle size fraction of −150 +125 μm, point A is above point B and any flowrate within this range should produce a clean separation. But how does it work in practice?
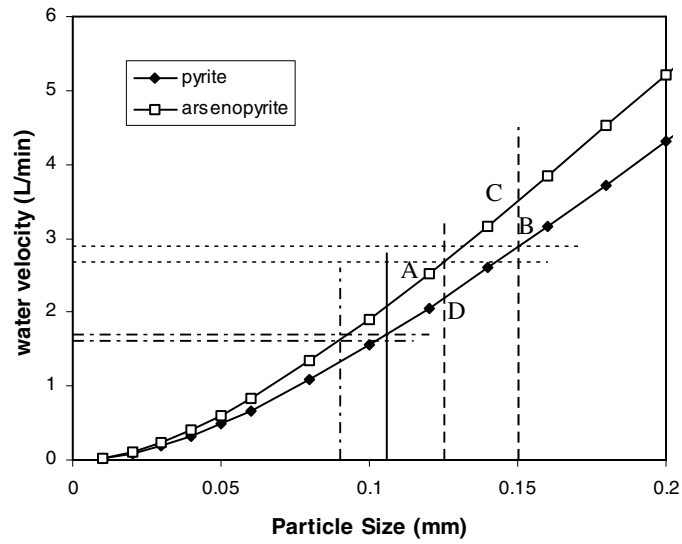
Fig. 15.4. Settling curves for separation of pyrite from arsenopyrite using the Dietrich correlation. The concentration criterion is 1.275.
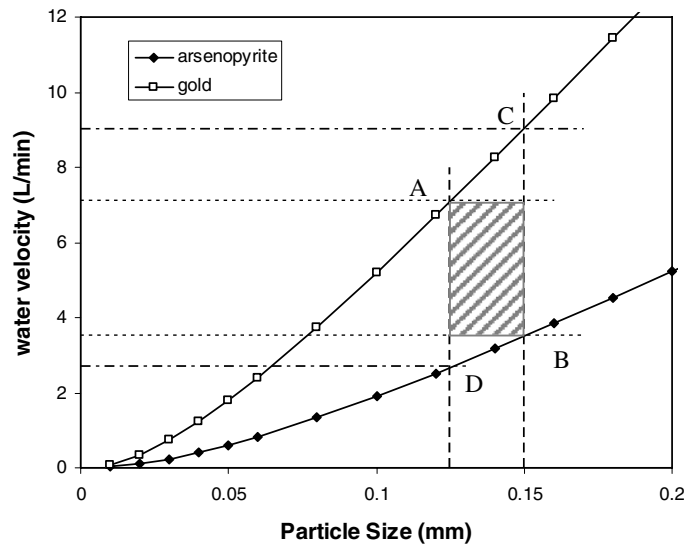

Fig. 15.5. Settling curves for separation of gold from arsenopyrite using the Dietrich correlation. The concentration criterion is 3.33.

A sample of sulphide concentrate, predominantly arsenopyrite and some pyrrhotite and free gold was sized to −150 +125 μm and placed in an elutriation column at a water flowrate of 9 L/min. From Fig. 15.5, this flowrate is at the top limit of the separation zone at which all particles should have risen with the water flow. However a very small number of particles were recovered as a sinks product. If any particles were recovered it would be expected to be predominantly the gold particles. The gold was estimated to have a density of 18000 kg/m³ as some impurities such as silver and copper occur with native gold. However, inspecting the sinks product under a microscope revealed that it contained only about 5% gold with the bulk of the product being sulphides and iron oxides. The size of the particles were towards the top end of the size range.

The float fraction from the elutriation column was re-tested at a water flowrate of 7 L/min which should also have produced a high grade gold product. The mass recovery was also low and contained about 50% gold and 50% sulphides and iron oxides. The gold particles tended to be flatter in shape compared to the sulphides because of the malleability of the gold metal. The flatter shape of the particles would thus give the gold the appearance of similar sized particles but would actually have a lower mass than a more rounded particle of gold of the same size. Thus, the particle shape is allowing a lighter gold particle to fall into the same size fraction as a similarly weighted sulphide particle and the equally settling particles would be extremely difficult to separated by gravity.

Increasing the acceleration on the particles by using some centrifugal device will not change the ease of separation for particles with a low concentration criterion though it will improve the separation for high concentration criteria. For example, for a concentration criterion of 1.275, the difference between point A and point B in Fig. 15.4 is -0.2 L/min for an acceleration of 1G. The minus sign indicating that point A is below point B. By increasing the acceleration to 100G the difference becomes -2.0 L/min, still negative and still a poor separation. By contrast, for a concentration criterion of 3.33, an increase in acceleration from 1 to 100G increases the difference between point A and point B in Fig. 15.5 from +3.6 to +84 L/min indicating a broader range a separating velocities and a greater ease of separation, particularly at finer sizes.

At fine particle sizes, separation by density difference under gravity, becomes less efficient. At this size range flotation is the dominant separation process, though the application of centrifugal acceleration has extended the useful separation size by gravity processes down to 5-10 μm, provided the concentration criterion is favourable.

The advantages of gravity separation are:

1. a lower installed cost per tonne of throughput than flotation,
2. a lower installed power requirement per tonne of throughput,
3. gravity separation does not use expensive reagents and
4. the environmental impact of gravity plant effluent is considerably less than for flotation, due to the absence of organic chemicals.

15.2. Gravity Separation Operations

Gravity concentrating operations are characterised by processes that allow particles to be held slightly apart so that they can move relative to each other and therefore to separate into layers of dense and light minerals. The mechanisms by which this interparticular spacing is accomplished may be used as a convenient means of classifying gravity concentrators.

1. **Jigging** - uses an essentially vertical expansion and contraction of a bed of particles by a pulse of fluid.

2. **Shaking Concentrators** - employ a horizontal motion to the solids-fluid stream to effectively fluidise the particles causing segregation of light and heavy particles.

3. **Flowing Film Concentrators** - initiates particle separation by a layer of slurry flowing down an inclined surface under the influence of gravity. Some of the oldest known concentrators, such as sluices and troughs are flowing film concentrators.

15.3. Jigs

Stratification in a bed of particles results from the repeated pulsation of a current of fluid up through the bed. The particles in the bed are expanded so that when pulsation ceases, the particles are allowed to consolidate under the influence of gravity. Fig. 15.6 illustrates the expansion and contraction of the bed with the heavier, larger particles falling under hindered settling conditions.

The expansion and contraction of the bed is repeated in a cyclic operation until the heavy and light particles have stratified according to their specific gravity. The frequency of pulsations usually varies from 50 - 300 cycles per minute.

bed at rest   pulsation   hindered settling   consolidated trickling
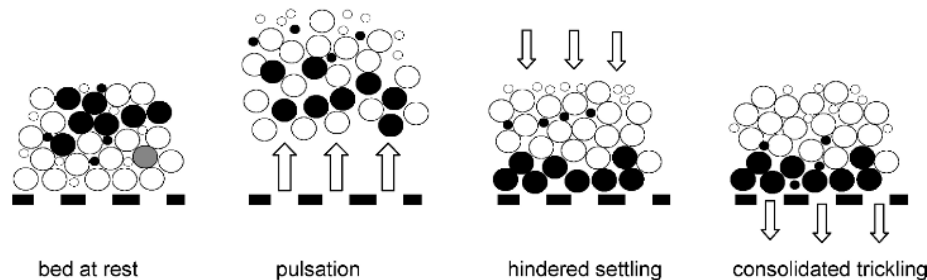
Fig. 15.6. Expansion and contraction of a bed of particles due to jigging action.

A particle settling in a viscous fluid is described by Eq. (15.12). As a particle just starts to move from rest, the particle velocity is small and hence the drag force acting on the particle, F_D, is negligible since the drag force increases with particle velocity relative to the fluid. Thus:

$$a_P = g\left(\frac{\rho_S - \rho_F}{\rho_S}\right) \qquad\qquad 15.19$$

That is, the initial acceleration of the particles depend only on the specific gravity of the solid and fluid and is independent of the particle size. Once the particles reach an appreciable velocity the fluid drag force becomes significant and it opposes the particle's further acceleration to the extent that eventually the particle acceleration drops to zero and a constant terminal velocity is reached which will dependent on the particle diameter as well as density. If the duration of the particle movement under gravity is kept short by having a high cycle frequency then the total distance travelled by the particles will be governed more by the difference in the initial acceleration between particles due to their density difference rather than by their terminal velocities which is also influenced by the particle size. That is, for

particles with a similar terminal velocity, such as would be experienced by small heavy particles and large light minerals, a short jigging cycle would be necessary for separation.

However, for coarser particles, longer strokes with decreased speed is found to give better stratification and hence it may be preferable to split the feed into closely sized fractions and have a jig optimised for each size fraction.

With a long stroke cycle particles will reach their terminal velocities which will dependent on the particle density and size. Hindered settling conditions will prevail. By adjusting the upward flow of fluid the settling velocity of the fine light particles can be overcome and the fine particles will be carried upwards and away from the denser heavier particles. A stronger pulsation stroke will then allow only the large heavy particle to settle against the rising force of fluid. For particles having a similar terminal velocity such as the small heavy particles and the large light particles, separation by this means would not be possible.

Hindered settling is more significant for coarse particle separations where a slower stroke cycle is used, although with coarser feeds, the larger particles may not have time to reach their terminal velocities. The parameters that will effect hindered settling during jigging are particle size, density and shape, the fluid density and viscosity, the percent solids and the separator characteristics.

As the pulsation approaches the top of the stroke the upward velocity of water slows and particles will start to settle again starting with the particles of higher terminal velocity. The particles will then begin to compact down as they settle against the jig screen. The large particles pack together leaving large voids between them into which the smaller particles can continue to settle under gravity. This *consolidation trickling* will help to bring the fine heavy particles down into the heavy layer (Fig. 15.6) and if allowed to go for too long, will also draw the fine light particles down into the heavy layer and thus contaminate the heavy fraction.

Stratification during the dilation stage is controlled by hindered-settling classification with some modification by differential acceleration, and during the stage that the bed is compacted, it is controlled by consolidation trickling. The frequency of the jig cycle and the control of events within each cycle is critical in determining the behaviour of particles within the jig bed. A minimum cycle time is required to allow each phase of the cycle to be optimum for a given feed. Any further increase in cycle time would not be optimum or the bed would be in a compacted state and no further separation would occur during this interval hence affecting the capacity. Cycle speed adjustment is therefore the most important operating variable.

Parameters which determine the cycle frequency include the feed rate, feed size and density and the jig design. A jig pulsation is a case of simple harmonic motion. The period of pulsation can be given by the basic formula for simple harmonic motion based on a compound pendulum [5]:

$$T = 2t = 2\pi \sqrt{\frac{L}{g}} \qquad (15.20)$$

where T = period of pulsation or time for a complete pulsation cycle,
        t = duration of the stroke (half cycle), and
        L = distance between the centre of suspension of the compound pendulum and its centre of oscillation.

510

For a large jig, the tremendous mass of water in oscillating motion (up to 20 tonnes) must be allowed to follow its natural pulsation motion as expressed by Eq. (15.20) which says that the pulsation cycle must vary as the square root of the stroke length as shown in example 15.2.

Example 15.2
If the pulsation frequency is 60 strokes/minute, then:

T = 1 s (= 1/frequency) and from Eq. (15.20):

$$L_1 = \frac{T_1^2 g}{4\pi^2} = \frac{1^2 \times 9.81}{4 \times (3.1415)^2} = 0.248\,m$$

If the pulsation rate is to be halved, then T = 2 s (30 pulsations/minute) and the stroke length should be increased according to:

$$\frac{T_1}{\sqrt{L_1}} = \frac{T_2}{\sqrt{L_2}}$$

$$L_2 = \left(\frac{T_2}{T_1}\right)^2 L_1 = \left(\frac{2}{1}\right)^2 0.248 = 4 \times 0.248 = 1.0\,m$$

If this principle were not followed the result would be excessive stress on the walls of the jig and turbulence within the bed that would disrupt the separation and lower power efficiency.

15.3.1. Length of Pulsation Stroke
The length of the pulsation stroke can be calculated by [5]:

$$v = \frac{N a \pi}{60} \tag{15.21}$$

where v = velocity of water required to suspend the mineral bed,
       a = amplitude of the stroke, and
       N = number of strokes per minute.

Use of this equation is given in example 15.3.

Example 15.3

For a jig treating 5 mm coal and shale of density 1800 and 2500 kg/m³ respectively, calculate the jig stroke amplitude required to expand the bed. The fluid is water at a density of 1000 kg/m³ and viscosity 0.001 Pa s and the Newtonian drag force is 0.44.

Solution

The pulsation must produce a water velocity capable of raising the largest pieces of 5 mm shale. From Eq. (15.4), the terminal velocity of the largest particle is:

$$v_T = \sqrt{\frac{4 \times 9.81 \times (2500 - 1000) \times 0.005}{3 \times 0.44 \times 1000}} = 0.4722 \text{ m/s}$$

If we assume the pulsation rate N = 60 pulses/min, then by rearranging Eq. (15.21):

$$a = \frac{60v}{N\pi} = \frac{60 \times 0.4722}{60 \times 3.1415} = 0.15 \text{ m}$$

Thus a surge of about 150 mm would be required in the jig.

Table 15.5 shows some typical amplitudes and pulsation rates for some jig types.

Table 15.5
Some operating data for various jigs [2].

Jig Type	Particle Size, mm	Amplitude, mm	Frequency, Hz
Baum	5-200	30-40	30-60
Batac	0.5-100	30-60	40-60
Diaphram	0.25-25	20-30	125-150
Diaphram	0.2-10	10-15	150-200

In jigging it is desirable to have a high system density while the bed is fluidised. Lovell and Luckie [6] compared the settling velocities of two particles, to illustrate the effect of relative density with increasing medium density. For two particles of coal having densities of 1650 and 1550 kg/m³ in air (density 1.239 kg/m³), the concentration criterion (ratio of relative densities) is calculated as:

$$CC_{(air)} = \frac{1650 - 1.239}{1550 - 1.239} = 1.065 \tag{15.22}$$

In water it becomes:

$$CC_{(water)} = \frac{1650-1000}{1550-1000} = 1.182 \qquad\qquad \{15.23\}$$

and in a pulp media of density 1540 it is:

$$CC_{(media)} = \frac{1650-1540}{1550-1540} = 11.0 \qquad\qquad \{15.24\}$$

Thus as the medium density approaches the density of the lighter mineral, the settling ratio of these particles will approach infinite. Such high media densities can only be maintained by generating a pseudo heavy liquid from contamination of the water with a build up of small heavy particles from the feed. Though this will benefit the separation, media viscosities will increase under these conditions which will retard particle flow and hinder separation.

15.3.2. Types of Jigs

Jigs are commonly used to clean coal but are also used in heavy mineral separations including alluvial gold. When treating coal, the light fraction is the concentrate and in the mineral industry, the heavy fraction is the concentrate. For this reason, gravity separation products will be referred to as light or heavy rather than the concentrate or tailing.

The jig is commonly an open tank filled with water, with a horizontal screen near the top. Some early jigs were designed where the screen surface, in the form of a basket, moved up and down in a barrel or tank of water hence producing the vertical flow of fluid through the bed of particles. This manual operation is reported in the 16th century work by Agricola [7]. Modern prospectors may still use this simple manual device in water drums or streams. Some movable screen jigs are still designed today, though most modern jigs employ a stationary screen and pulse the water through it. The differences between the various types of jigs available relate to the methods used to generate the pulsation and the manner in which the heavy fraction is removed from the jig. The screen is there to support the bed of particles and the area underneath the screen is called the *hutch*. The tank is usually divided into two main sections; one containing the support screen with the bed of ore and another section which generates the fluid pulse.

Heavy mineral discharge

The heavy discharge from the jig may be either *through the screen* or *over the screen*. In jigging through the screen, all particles in the feed are smaller than the screen aperture and thus have the potential to drop through the screen and collect in the hutch. To stop the light fraction falling through the screen, a false support is provided in the form of a layer of coarse heavy particles called *ragging* which when contacting the screen surface pack down to effectively close off the screen apertures to the feed particles. During the pulsation cycle, the ragging is also dilated and will allow the particles that have formed on top of the ragging, by segregation, to work their way through the ragging and the screen into the hutch. The ragging is usually, but not always, a material of density between the light and heavy fractions of the feed. An example of ragging material is lead shot for gold jigs, steel balls for cassiterite separation and natural materials such as feldspar for coal jigs and hematite for cassiterite and scheelite.

Large jigs are divided into separate compartments with different operating conditions for each compartment, such as roughing and scavenging duties. In large compartments, barriers

are provided on the screen to keep the ragging in place on the screen surface to prevent migration of the ragging to one side of the jig (Fig. 15.7). Up to four successive compartments are placed in series in the hutch. A high-grade heavy fraction may be produced in the first compartment with successive compartments producing higher recoveries but lower grades so that a final light fraction overflowing the final compartment can be discarded.

For feed particles larger than the apertures of the supporting screen, *jigging over the screen* may be practiced, and the heavy product grade is partly controlled by the thickness of the bottom layer which in turn is controlled by the rate of withdrawal through the heavies discharge port. Gates are operated to allow the heavy fraction to drop into a bucket elevator for removal. For coal separation, the light fraction is a *clean coal* product and the heavy fraction is a *reject* or shale product.

Positioning of the gate opening is controlled by the location of the boundary between the light and heavy layers and this is determined by a weighted float positioned in the bed or monitoring the pressure fluctuations in the pulsating water.

Pulsation

The pulsation of water or air through the mineral bed may be generated by rubber diaphragms, pistons or compressed air chambers. Examples of air actuated water pulsation units are the Baum and Batac jigs used extensively for coal separation. Here the settings of air and water are critical for efficient separation with large stroke amplitudes at the feed end for rapid stratification of the coarse shale and short stroke settings at the discharge end for precise stratification of *near gravity* material and fine coal.
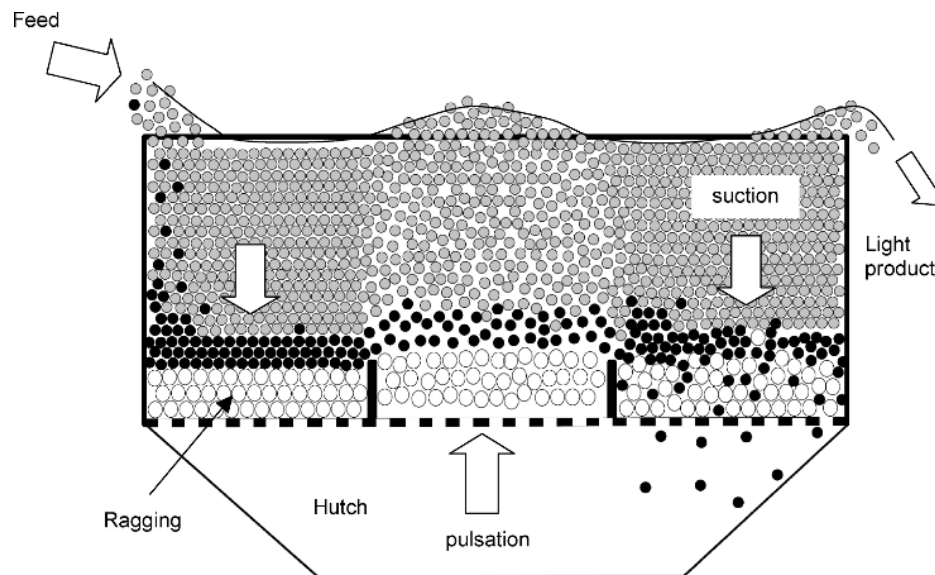

Fig. 15.7. Jigging through the screen.

InLine Pressure Jig

The Inline Pressure Jig (IPJ) is a new application of the jigging principle with a completely enclosed and pressurised jig with a moveable screen action in a circular bed. The pressurisation of the unit, up to 200 kPa, allows the Inline Pressure jig to be completely filled with slurry and water which slows the slurry velocity and eliminates the air-water surface tension for potentially improved recovery. A hydraulic ram pulses the screen in the water with a jigging through the screen operation [8,9].

The advantages of the IPJ are a low water consumption, allowing operation in the recirculating stream of a grinding circuit, a high mass pull of up to 30% to the heavy fraction, feed capacity up to 110 tph, feed sizes up to 30 mm and low power consumption. When used for treating alluvial deposits of precious metals or gemstones, the completely sealed unit offers security.

Centrifugal Jig

In 1990, Kelsey introduced the first commercial unit that incorporated a centrifugal force to jigging. The Kelsey Centrifugal Jig (KCJ) operates at up to 40 times gravitation acceleration in order to extend the separation range of gravity separation down to less than 40 microns.

The Kelsey Centrifugal Jig utilises the Harz design which is divided into two parts, the top section of heavy mineral (ragging) above a screen, and the jig chamber filled with water and pulsed by a diaphragm plunger. The screen and hutch arrangement is turned 90° from the horizontal to the vertical and spun about a vertical axis. Gains achieved with the KCJ include:

1. Operating and maintenance cost savings
2. Improved recovery
3. Improved final concentrate grade, and
4. Simplifying the processing circuit.

15.3.3. Operations

The control of a jig separation is determined by the water addition, stroke frequency and amplitude, the feed rate and the ragging layer. Water is added to the jig as either *top water* (water added above the screen) or *back water* (water added beneath the screen or hutch water). The total water flowing across the top of the jig bed is the *cross water*. This cross water controls the horizontal flow of particles across the top of the bed. The back water reduces the effect of the suction part of the cycle and hence affects the falling water velocity relative to the rising water velocity during the pulsation part of the stroke.

The feed rate must be matched with the discharge rate of the heavy fraction so that a steady state operation can be maintained. If the discharge of the heavy fraction does not keep up with the heavy particles reaching the separated layer then this layer will build up until ultimately some heavy minerals will be lost to the light fraction. Conversely if the discharge rate of heavies through the ragging or through the discharge gate is greater than the rate of segregation of heavy particles into the separation layer then some light particles will eventually be drawn into the heavy fraction, lowering the grade.

The stroke length and frequency are linked according to Eq. (15.21) and the stroke length must be sufficient to produce the amount of bed dilation required for separation.

The size, size distribution, shape and density of the ragging are all important factors that will affect the separation. The deeper and heavier the ragging layer and shorter the pulsation stroke the more difficult it will be for particles to penetrate the ragging and hence the slower will be the heavy fraction discharge. The ragging size is about 3-4 times the maximum

particle size in the feed. Table 15.6 summarises the effect of a number of these variable on the jig operation.

Table 15.6
Effect and operating range of some operational variables on jig separation.

Variable	Value	Effect on Jig operation
Ragging density	increasing	decreases heavy fraction flow
Ragging size	increasing	increases heavy fraction flow
Ragging depth	increasing	decreases heavy fraction flow
Ragging contamination	increasing	decreases heavy fraction flow
Feed size	50 μm – 20 mm	normal range for heavy mineral separation
Feed size	0.5 – 200 mm	normal operation for coal
Capacity	17 – 25 t/h/m²	normal for tin
Capacity	30 – 60 t/h/m²	normal for coal
% solids	30 – 50%	normal operation
Hutch water	increasing	increases recovery to a maximum
Hutch water	increasing	increases enrichment ratio

Taggart [1] gives an estimate of the power consumption of a jig as:

$$P = 7310.16 A \sqrt{d}$$

where P = power in watts,
       A = screen area in m² and
       d = feed size in m.

15.4. Differential Motion Table Separators

Wet concentrating tables developed from continuous belt concentrators which utilised a flowing film of water to effect a separation. The ore moved up an incline slope on an endless belt where the lighter minerals were washed away from the heavy minerals by a film of water flowing down the belt, similar to the *Strake* tables. The *Vanner*, a vibrating continuous belt was developed in the 1860's and bumping tables followed before the modern differential shaking table was developed by Wilfrey in 1896.

A bed of particles which experiences a horizontal shaking motion will undergo segregation on the basis of size and density, for example a gold pan and particles of a conveyor belt. If the particles are of the same density then particles will segregate according to size with the fine particles sinking and the coarse particles rising to the top (Fig. 15.8). If particles of different density exist in the mixture then particles of higher density will sink to a lower level than similar sized but lighter density particles. To achieve this stratification, the shaking motion must be strong enough to expand the bed to the extend that allows particles to penetrate. The shaking motion however must still maintain a particle to particle contact. The fact that small particles of light mineral and large particles of heavy mineral segregate to the same position in the bed suggests that density is not the sole separating force.

15.4.1. Shaking Tables

In the shaking table concentrator, differential motion and a riffled deck with cross flowing water is used to create a particle separation. The shaking motion is asymmetrical, being slow
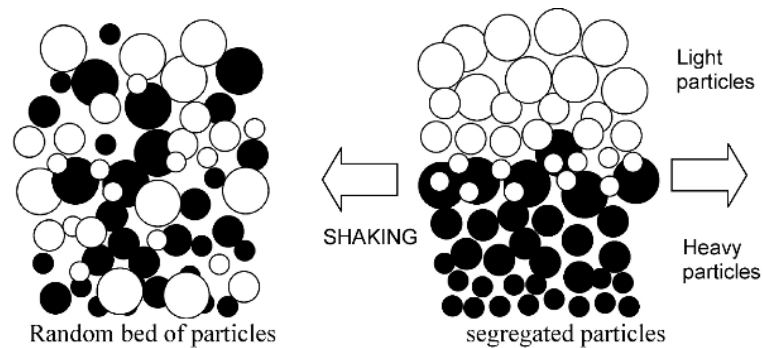
Fig. 15.8. Segregation of particles due to horizontal shaking motion.

in the forward direction and rapid in the reverse direction. This differential motion imparts a conveying action to the table moving those particles which are in contact with the table deck, through friction, in the direction of the motion.

The Wilfley table was designed for ore concentration and since the early days of its development has been used extensively for this purpose. When the table is equipped with decks specially designed for coal washing it was known as a *Massco* table. Since the introduction of the Wilfley table many different makes of tables have been developed for use with minerals and coal.

The table consists of a slightly inclined flat surface or deck with a series of parallel ridges or riffles along the direction of motion (Fig. 15.9). The riffles are tapered towards the opposite end to the reciprocating drive. Feed is introduced at the corner of the table at about 25% solids (by mass) and with the shaking motion, the particles spread out over the table. Wash or dressing water is introduced along the top edge of the deck to assist in segregation and transport of particles on the table. The net effect is that the particles move diagonally across the deck from the feed end.
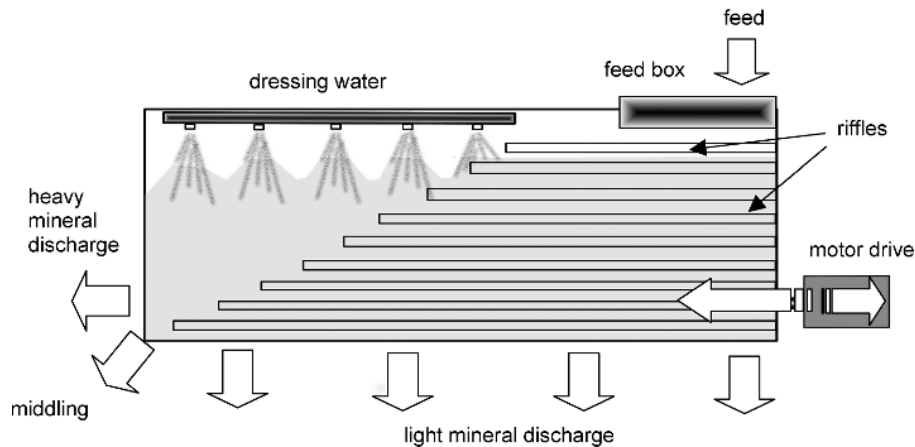

Fig. 15.9. Shaking table arrangement.

As the feed material spreads out over the table the particles stratified in layers behind the riffles. The riffles help to transmit the shaking motion to the particles and prevent the particle washing directly off the table. Successive layers of particles are removed from the top of the riffles by the cross-flowing water as they become exposed by the shortening riffle height as the bed moves away from the feed end of the table. When the remaining particles reach the end of the riffles only a thin layer remains on the table surface. If the table has a smooth unriffled end, then the flowing film of water further cleans the heavy particles before discharging them off the end of the table.

The separating action on a shaking table combines the selective action of the cross-flowing water film (flowing-film) and stratification and hindered settling behind the riffles.

15.4.2. Stratification and Hindered Settling

Stratification due to the nearly horizontal action of the table deck and the flow of water is not the only mechanism at work on the table. There is some suggestion that hindered settling may also assist in the separation in some minor way. The stratification due to the shaking motion of the deck and flow of water is referred to as *table stratification*. Under this process, the small particles will segregate towards the bottom of the bed, behind the riffles, while the large particles collect towards the top. For a mixture of mineral densities in the feed, there will be a mid-layer of particles where the large heavy and small light particles will overlap as indicated in Fig. 15.8. As the cross flowing water flows over the riffles it can cause eddy currents to penetrate the mobile bed before rising to flow over the next riffle. This rising current of water can lift the finer particles to higher positions in the bed by a hindered settling type action and this can assist in the segregation of heavy and light minerals. This effect of hindered settling along any individual riffle is likely to be small but the cumulative effect along the entire series of riffles on the deck might be sufficient to effect the separation of the fine light particles away from the large heavy particles in the bed.

Hindered settling on a table is more effective if the particles in the feed are closely sized. Classification of the table feed improves the performance of the table and increase the capacity.

15.4.3. Operating parameters

Factors which affect the operation of the shaking concentrator are particle size and density, particle shape, the riffle design, deck shape, water and feed flow, stroke and speed of the table and the deck slope. The effect of these variables are summarised in Table 15.7. The correct operation of the table has the middling fraction discharged at the diagonally opposite corner of the table to the feed. For any feed variation, the operating variables are adjusted to maintain this separation point.

The particle shape is not a major factor in the overall tabling process however flat particles do not roll easily across the deck and would tend to be carried along to the heavy mineral discharge end of the table.

Of considerable more importance is the particle size. In both table stratification and hindered settling, the separation of particles becomes more difficult as the range of sizes in the feed increases. If a table feed contains too wide a range of sizes, some size fractions will be separated inefficiently. For efficient table operation, a normal feed size for coal treatment ranges from 0.3 – 9.5 mm [10]. The lower size limit for an effective separation on a table is about 50 μm even if the density difference is high.

For optimum table operation, the feed flow of solids and water onto the table must be uniform and constant. Approximately 90% of the water reports to the light fraction. The

dressing water represents approximately 25% of the total water on the table. The table capacity varies according to the size of the feed particles. Tables can handle up to 2 t/h of 1.5 mm sand and 1 t/h of fine sand. Capacities can be as low as 0.5 t/h for a slimes feed.

Table 15.7
Effect of variables on table performance [2].

Variable	value	Effect
Deck shape	diagonal	increased capacity
		increased grade
		lower middling flow
		finer size separation
Riffling	partial deck	cleaning duty
		treats unsized feed
	full deck	roughing duty
		treats sized feed
Feed rate	2 t/h	for 1.5 mm sand
	0.5 t/h	for -150 μm slimes
	15 t/h	for up to 15 mm coal
Speed & Stroke	260-300 strokes/min	for coarse ore
	12-25 mm	
	280-320 strokes/min	for fine ore
	8-20 mm	
	260-285 strokes/min	for coal
	20-35 mm	
slope (length) &	11-25 mm/m	coarse sand
tilt (cross)	20-25 mm/m	
	9-15 mm/m	medium sand
	15-30 mm/m	
	2-9 mm/m	fine sand
	8-20 mm/m	
	1-7 mm/m	slimes
	4-12 mm/m	
water/solid ratio	20-25% (mass)	mineral separation
	33-40% (mass)	coal separation

The stroke rate for normal operation is between 250-300 strokes per minute. The stroke length required for coal separation can ranges from 10-25 mm. A longer stroke moves the reject (heavy) to the heavy discharge end of the table more rapidly, but requires more water. The amplitude and stroke frequency are interdependent. That is, an increase in stroke length requires a decrease in the stroke frequency to maintain the same transportation speed of the heavy fraction to the discharge point. A fine feed will generally require a higher speed and shorter stroke than a coarse feed. For difficult separations, where the density difference between the two fractions is small of the feed size is small, a short stroke length must be used.

Early tables were generally covered with linoleum with wooden riffles. Modern tables use either rubber riffles cemented to a rubber covered deck or the whole deck is moulded in fibreglass.

Table 15.8 gives a general guide to table operation.

Table 15.8
Table settings for various duties.

Duty	Operating conditions
roughing	increase water flow increase feed rate increase tilt increase stroke use fully riffled deck
cleaning	decrease water flow decrease feed rate decrease tilt decrease stroke use partially riffled deck
fine feed	decrease water flow decrease feed rate increase speed decrease stroke use low profile riffles
coarse feed	increase water flow increase feed rate decrease speed increase stroke use high profile riffles

15.4.4. Types of Tables

A number of different types of tables are available for different applications, and these vary mainly in relation to the type of head motion used.

Sand Tables

A sand table is used for treatment of coarse particles, greater than 100 μm. Some types of sand tables are the *Diester* table used extensively in the coal preparation industry is capable of a longer stroke than a standard *Wilfley* table, which is required for the concentration of the coal particles. The head motion of the *Holman* or *James* table is applied to the corner of the table rather than to the centre as in a normal Wilfley table. In cases where floor space is at a premium, tables can be mounted in vertical stacks of two or three high.

Slimes Tables

The treatment of slime particles (< 100 μm) on any gravity separation device is difficult. The separations achieved are not efficient but before the introduction of flotation or centrifugal devices, slime tables were used. The basic principles of slimes tabling are:

1. the deck area required varies inversely as the feed size,
2. the finer the feed, the gentler and slower the table action must be,
3. the feed size distribution must be even and channelling avoided,
4. the flocculation characteristics of the feed affect its response to gentle flowing action.

The concentration criterion for a mixture of quartz and cassiterite is 3.5 and at less than 50 microns particle size, this is not sufficient to give sharp separation. The concentration criterion for a quartz-gold mixture is nearly 9, and good separation is possible at this size.

Slime tables have a gentler slope and a series of plane surfaces rather than riffles on the deck. The concentrate and/or middlings produced by a slimes table often require further treatment. A number of units have been design to use the principle of a flowing film of water on a flat deck with a shaking motion to concentrate these slimes. Units such as the Bartles-Mozley table and the Bartles Crossbelt concentrator were first introduced for tin processing around 1967. Cassiterite is a friable mineral which readily produces slime size particles.

The Bartles-Mozley separator consists of two stacks of twenty lightweight fibreglass decks. Each deck surface is smooth with dimensions of 1.1 m by 1.5 m long and separated by a gap of 12 mm. The stacks are suspended within a steel framework at an angle of 1-3 degrees. A motor and out of balance weight drives the stack with an orbital motion. The operation is a batch process with feed on for up to 35 minutes then the feed is shut off and the stack assembly is tilted with flushing water to remove the heavy fraction before the cycle starts again. The Bartles-Mozley concentrator is used as a roughing device and the concentrate is cleaned on a Crossbelt concentrator. It is claimed to recover particles down to 5 μm at a rate up to 5 t/h [11].

The heavy fraction from the Bartles-Mozley separator is treated on the Bartles Crossbelt concentrator, introduced in the mid-1970's [12]. The crossbelt is a 2.5 m wide endless belt which is raised along a central ridge to provide a gentle slope towards the two edges of the belt. The belt moves slowly and is also shaken with an orbital motion between two end pulleys approximately 3 m apart. The unit feed is introduced along the central ridge and the light particles which are suspended in the water flow by the orbital motion, flow down the slope and discharge off the edge of the belt. The clean heavy fraction is discharged over the head pulley.
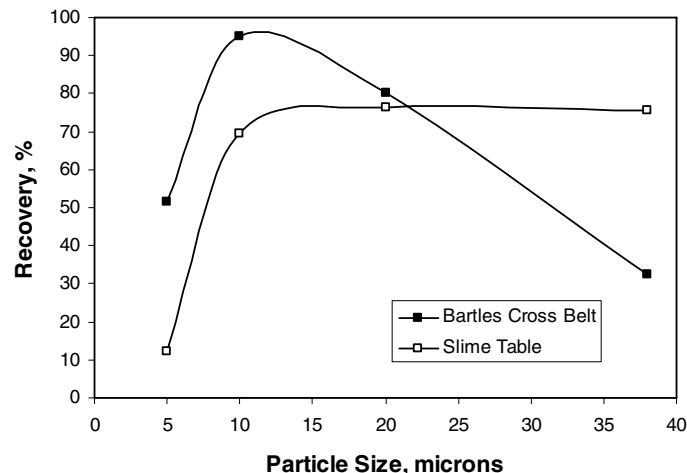

Fig. 15.10. Comparison of the size recovery for a Bartles Crossbelt concentrator and a standard slimes table, treating cassiterite slimes [12].

A comparison of the performance of the Bartles Crossbelt performance with a standard slimes table, treating a feed of 0.7% Sn grade and 97% –40 μm, showed a similar overall recovery of just 55% but the Crossbelt produced a grade of 32% Sn compared with just 13% Sn for the slime table [12]. Fig. 15.10 compares the size by size recovery of the two units and indicates the superior performance of the Bartles Crossbelt in the 5-10 micron range but has a worse performance above 20 microns.

Gemeni Gold Table

The Gemeni table has grooves on the table deck instead of riffles. It thus behaves like a mechanised gold pan in that the heavy gold is trapped in the grooves and the light gangue is washed over the groove and off the table. The gold migrates from groove to groove working its way along the table by the action of the shaking mechanism. The wash water is introduced along the centre of the table, dividing the table into two sloping surfaces. Fig. 15.11 shows the shape of the table and movement of the particles on the deck.

The Gemeni table is a low capacity cleaning device. The table is used in the secure gold room for the upgrading of gold concentrates from other gravity concentration devices. The advantage is that a very high grade at high recovery is achieved and this can be directly smelted to produce gold bullion. The feed size is less than 850 microns for a top feed rate of 0.12 t/h for the Gemeni 250 which is 1.32 m wide by 2.0 m long.

15.5. Flowing Film Concentrators

Settling and separation of particles in a flowing film of fluid form the third classification of gravity separation processes. When a film of water flows down a smooth surface under laminar flow conditions, the velocity gradient across the film thickness is approximately parabolic. That is, the velocity decreases at positions close to the slope surface due to friction with the surface and also decrease at positions close to the air/water interface, also due to friction with the air (Fig. 15.12). For turbulent flow conditions, the velocity profile across the thin film is flatter but still decreases towards the deck surface due to friction or drag.

Particles of different density and size that are dropped into the flowing film will reach the slope surface at different points because of the difference in settling rate. Particles that take longer to settle such as the fine light particles will be carried further down the slope than particles that are faster settling (Fig. 15.13A). For equi-settling particles such as large light particles and small heavy particles, these will contact the slope surface at the same position.

Once the particles start to roll down the slope they will be influenced by their size as smaller particles will be closer to the surface and experience a slower water velocity than large particles which extend further into the water film where the water velocity is greater (Fig. 15.13B). Thus large particles will be pushed down the slope faster than the smaller particles and a new arrangement will eventually form as shown in Fig. 15.13C.

If the particle shape is flat then it will have less tendency to roll and will complicate the separation.

15.5.1. Simple Sluice

The sluice is the simplest implementation of the flowing film principle. This consists of an inclined trough open at both ends. Solid and water are fed in at the top and a flowing film separation occurs on the sloping surface. The completeness of the separation depends on the density and size of the particles and the amount of water and length of the sluice. Tin sluices may be up to 100 m in length. The sluice carries a bed of material many particles thick and
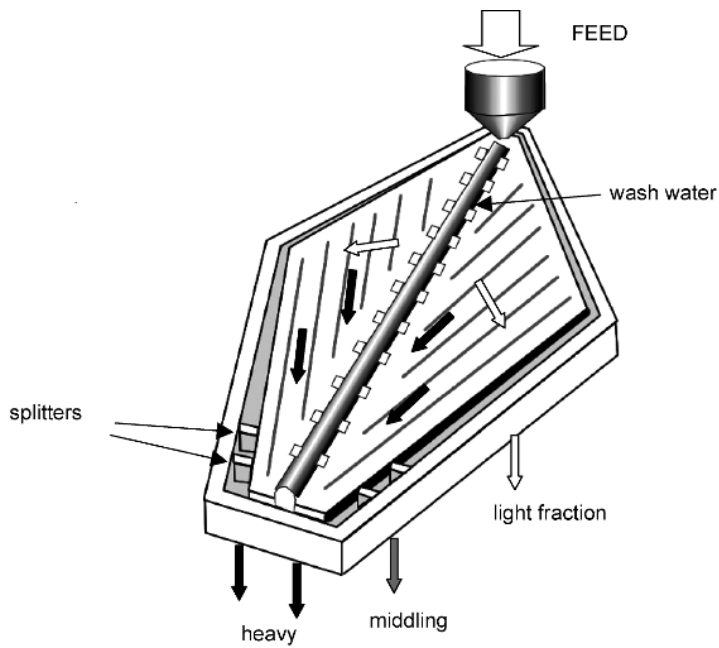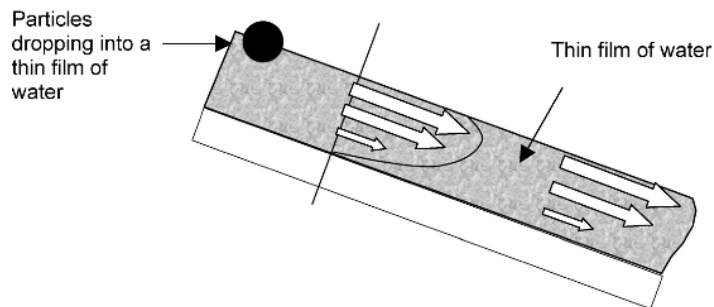
Fig. 15.11. Gemeni gold table.

Fig. 15.12. Velocity profile in a flowing film of water

fluidisation of the bed, which allows segregation of the heavy and light particles in the bed, is produced by the flow of water. This fluidisation is enhanced by having a rough textured surface on the slope such as a layer of pebbles or a cross-riffle section. These obstructions introduce turbulent flow and eddies and provide obstacles against which particles in the bottom layer of the bed can be trapped while the upper layers flow over with the water (Fig. 15.14).
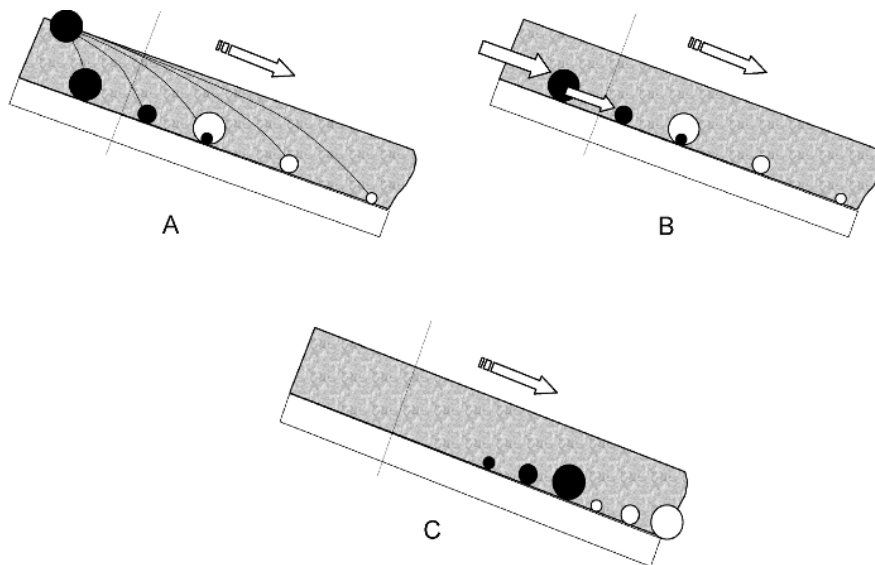
Fig. 15.13. Effect of particle size, density and water velocity on particle segregation in a flowing film of water (● heavy particles, ○ light particles). A – particles of different settling rate; B – different size particles pushed with different force; C – final segregated layers in a flowing film.

Feed sizing is an important pre-treatment to efficient gravity separation by a film flow. When this is satisfied, the smallest and heaviest particles will work their way to the bottom behind any obstruction as the water flowing over the obstruction lifts the lighter particles towards the top and eventually over the obstacle.
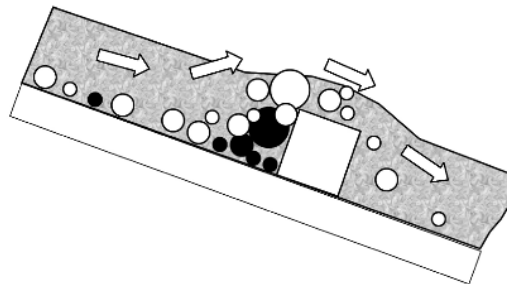

Fig. 15.14. Effect of a riffle on segregation on a sluice.

The main control factors in sluicing are the slope of bed, the water film thickness, the roughness of the surface, the density difference between the valuable mineral and gangue and the pulp density.

The *simple sluice* or *sluice box* is a batch process. After a period of time, some heavy mineral will start to wash over the riffle and be lost in the light tail. Thus, after a certain time the flow is stopped and the heavy minerals collected. The clean-up frequency depends on the feed grade, the feed rate and the size of the sluice and can vary from once a day to once every several weeks.

15.5.2. Strake Table

The gold *strake* consists of a stationary flat sloping surface. The light mineral particles roll down, while the heavier ones are held on a roughened surface such as a removable cloth covering. For example, corduroy cloth was used to cover the strake surface, where the ribs of the corduroy were laid perpendicular to the direction of flow. The variables affecting the separation are the slope, feed size, pulp density and the feed rate.

The cloth covering was subsequently replaced with a rubber belt which had ribs moulded into the surface lying across the flow direction to act as riffles. The rubber belt is continuous and driven at a slow rate up the inclined surface. The water film washed the light particles down the slope and the heavy particles caught behind the ribs on the belt are moved up to discharge off the top of the table. The feed % solids of the pulp is 20-50%.

15.5.3. Spiral Concentrator

The spiral concentrator first appeared as a production unit in 1943 in the form of the Humphrey Spiral, for the separation of chrome-bearing sands in Oregon. By the 1950's, spirals were the standard primary wet gravity separation unit in the Australian mineral sands industry.

In the spiral concentrator the length of the sluicing surface required to bring about segregation of light from heavy minerals is compressed into a smaller floor space by taking a curved trough and forming into a spiral about a vertical axis. The slurry is fed into the trough at the top of the spiral and allowed to flow down under gravity. The spiralling flow of pulp down the unit introduces a mild centrifugal force to the particles and fluid. This creates a flow of pulp from the centre of the spiral outwards to the edge. The heaviest and coarsest particles remain near the centre on the flattest part of the cross-section, while the lightest and finest material is washed outwards and up the sides of the launder (Fig. 15.15). This separation may be assisted by the introduction of additional water flowing out from the centre of the spiral either continuously or at various locations down the length of the spiral. This wash water may be distributed through tubes or by deflection from a water channel that runs down the centre of the spiral. Some present designs have overcome the need for this wash water. Once the particle stream has separated into the various fractions, the heavy fraction can be separated by means of splitters at appropriate positions down the spiral. A concentrate, middlings and tailing fraction can be recovered.

In practice spirals are arranged in stacks or modules of roughers, scavengers and cleaners, where the initial concentrate is retreated to upgrade the fraction to its final grade. Spiral length is usually five or more turns for roughing duty and three turns in some cleaning units. For coal concentration, 6 turns providing a gentler slope with longer residence time for the more difficult separation.

The performance of spirals is dependent on a number of operating parameters, summarised in Table 15.9. Spirals generally a chieve an upgrade ratio of 3:1 (heavy fraction:feed grade)
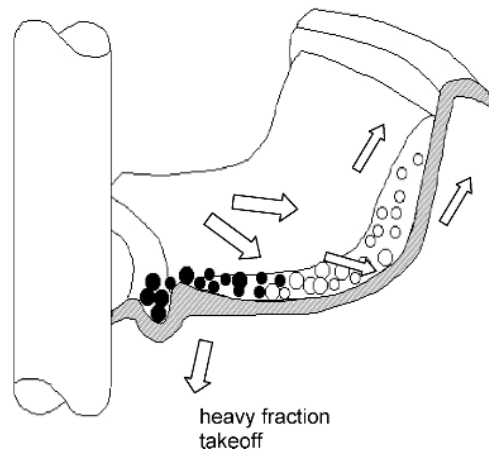
heavy fraction
takeoff

Fig. 15.15. Cross section of a spiral launder.

and hence multiply treatments are required [13]. The presence of slimes adversely affects the spiral performance. More than 5% of -45 μm slimes will affect the separation efficiency.

With the steep pitch of a spiral, two or three spirals can be wound around the same common column and these types of spirals have been used in Australia for more than 20 years. The multistart spirals conserve floor space and launder requirements. These triple-start spirals are built into a twelve spiral module and for these modules, the design of the distributor is critical to ensure that each spiral has a uniform feed.

The splitter blades on these spirals are all adjustable to direct the heavy fraction into pipes or a collecting launder. The current range of spirals available consist of a number of different profiles which have individual separation characteristics. The dimensions of some of the available spirals range from 270 – 406 mm pitch, 590 - 700 mm diameter and 2.1 – 2.4 m high.

The advantages that modern spirals offer are simple construction requiring little maintenance, low capital cost and low operating cost - no reagents required, no dense media losses occur, low operating personnel required.

Table 15.9
Summary of spiral operating parameters.

Variable	Value	Effect
feed size	0.075 – 3 mm	optimum size for coal
	0.045 – 0.85 mm	size range for minerals
feed rate	1 – 5 t/h	design capacity
feed % solids	20 – 30% solids (mass)	less for fine sands
	up to 50%	for coarse feed
	high % solids	high recovery (heavy) low grade
	low % solids	high heavy fraction grade
splitter position	depends on feed properties and required duty	

15.5.4. Cone-Separators or Reichert Cone

The Reichert Cone concentrator was developed in Australia in the 1960's to treat mineral sands. In principle the cone is similar to the sluice in that a slurry stream flows over a sloping surface causing the heavy particles to sink to the bottom of the bed. The separating surface in the Reichert cone is in the form of an upward sloping truncated cone. The heavy minerals, in close contact with the cone surface pass through an annular slot near the bottom of the cone while the light fraction flows over the slot to be treated in another stage or permanently removed. The separation efficiency of the cone is relatively low therefore the fractions (light or heavy fraction or both) are re-treated over several cone sections arranged vertically to allow several stages of cleaning.

The cones are made from fibreglass ranging from 2–3.5 m in diameter. The cones are mounted in frames up to 6 m high. Reichert cones are used in the mineral sand industry, in the treatment of alluvial and placer sands to recover gold, tin or other heavy minerals. The advantages of the cones are:

1. capacity in the range 40–300 t/h with a feed density of 55–70% solids by mass. The cones can handle feed sizes from 30 μm to 3 mm but are most efficient in the range 100-600 μm.
2. low installation cost per unit capacity
3. very low operating cost per tonne treated (cf. spirals and tables)
4. on stream adjustable inserts allow for variations in feed
5. high density streams ensure minimum energy consumption
6. environmentally acceptable, since no reagents used.

15.5.5. Centrifugal Separators

Poor separation of heavy minerals occurs at fine particles sizes. This poor performance can be overcome to some extent by increasing the settling rate of the fine particles by using centrifugal acceleration rather than gravitational acceleration. This lead to the development of the *centrifugal separator*.

The Knelson Concentrator was one of the first of this type of concentrator to find commercial success and is a highly efficient centrifugal separator for free gold or other heavy mineral recovery. The concentrator is a compact high-capacity centrifugal separator with an active fluidised bed to capture heavy minerals. A centrifugal force equal to or exceeding fifty times the gravitational force acts on the particles enhancing the specific gravity difference between the heavy particles and the gangue. The strong centrifugal force traps the heavy mineral in a series of rings located in the spinning drum while the gangue overflows the rings and is flushed out.

The concentrator has the capability to treat 40 t/h of minus 6 mm feed material and will recover in excess of 95% of the precious metal values. Gold particles from 6 mm to minus 30 μm are more efficiently recovered than with other known gravity method at high capacity. Even fine, platy or flour gold particles can be recovered.

The hydraulic section forms a self-cleaning fluidised bed that efficiently entraps high-density minerals while pushing out lighter material. This eliminates problems previously encountered with other centrifugal concentrators, including frequent shutdowns to remove black sands, low throughput and low concentrate ratios in the concentrate. The concentrate grade can be as high as 1,000 times the feed grade.

The original design was a batch operation but the latest designs offer semi-continuous and continuous extraction of the heavy fraction. These concentrators are popular units in the

grinding circuit of gold plants that contain free gold. The cyclone underflow, or a percentage of the cyclone underflow is passed through these concentrators with the concentrate going to the gold room for further upgrading or smelting and the tailings going back to the ball mill. This removes the coarse gold which would remain in the mill circulating load due to the high density of gold. These devices are suitable to capture recirculating gold in the grinding circuit because of their high % solids feed capability allowing a minimum of additional water into the high % solids grinding streams.

Similar devices are the Falcon Concentrator which uses a smooth sided bowl and the Gekko InLine Spinner which uses a riffled bowl and a cutter bar to create turbulence near the bowl surface to enhance the displacement of light particles by heavy particles.

15.5.6. Mozley Multi-Gravity Separator (MGS)

The MGS is designed for fine and ultra fine mineral separation. It is essentially an enhanced gravity separation device using the flowing film and shaking table principle. It can be looked upon as essentially wrapping the horizontal concentrating surface of a conventional shaking table into a cylindrical drum and rotating it. A force of many times greater than normal gravity is exerted on the particles in the flowing film thus greatly increasing the fine particle separation process. An additional shaking action adds shear to the particles increasing the separation process. These actions enable the MGS to recover particles down to 1 μm in diameter with at least 1.0 S.G. difference. The capacities are up to 30 t/h for mineral separation and 50 t/h for coal. Advantages of the Multi-Gravity Separator are quoted as:

1. high recovery: Typically better than 95% of free gold is recovered in a single pass (better than 99% for high grade)
2. high capacity
3. compact size
4. simple design, only one moving part
5. low cost per unit throughput
6. easy cleanup, typically five minutes
7. low maintenance, all wear parts are easily replaced
8. low labour requirement, no specific skills required
9. insensitive to feed variations.

15.6. Dense (or Heavy) Media Separation

15.6.1. Introduction

The previous sections have explored the separation of minerals of different density in a fluid medium where the density of the fluid is less than the density of either mineral. If the density of the medium lies between the densities of the two minerals, then separation becomes much simpler since the lighter mineral will float in the fluid medium and the heavy mineral will sink. Hence separations of this kind are referred to as *sink-float separation*.

The medium used for the separation depends on the specific gravity of the minerals and may be made up of dissolved salts such as calcium chloride in water, where densities around 1350 kg/m^3 may be produced or zinc chloride up to 1800 kg/m^3. This medium density is low but has been used for the separation of coal. Heavy organic liquids have been proposed for industrial use but for reasons of toxicity and cost these are restricted to small scale laboratory use and even here they are becoming less utilised because of the toxic or carcinogenic nature of the organics. Table 15.10 summarises the properties of the heavy liquids used.

The tungstate based inorganic heavy liquids are regenerated by driving off some of the water. In this case the LST is preferred as it is more thermally stable than SPT or LMT and has a lower viscosity. The LST liquid has a pH of around 4 which may have to be considered when treating some minerals such as carbonates and sulphides [14].

Densities up to 12.0 can be achieved for separation of non-magnetic minerals by the use of magnetohydrostatics. This is produced in a paramagnetic salt solution or a ferrofluid by the application of a magnetic field gradient. A ferrofluid is a suspension of a ferromagnetic material, such as magnetite, in a fluid such that the slurry behaves like a magnetic fluid. The particles have an average size of about 10 nm so that they form a stable suspension. The particles are coated with a stabilising dispersing agent or surfactant which helps to prevent particle agglomeration when a strong magnetic field gradient is applied to the fluid.

In a magnetic field the whole fluid responds as a homogeneous magnetic liquid. In magnetohydrostatic separation, the ferrofluid is placed in a non-uniform magnetic field where it experiences an increasing attraction force in the direction of the higher field intensity. If the field strength is in the direction of the gravitational force then the apparent density of the fluid is the sum of the actual density and the magnetic field. This means that the apparent density of the fluid can be adjusted simply by adjusting the magnetic field strength. This type of high density medium is applicable to the separation of non-magnetic particles down to about 50 μm.

15.6.2. Pseudo Heavy Liquids

More commonly where high medium densities are required, pseudo liquids are used which consist of a suspension of finely divided high density particles in water. One of the earliest dense mediums used for the cleaning of coal was -75 μm magnetite in 1922. This was not successful at that time since there was no simple method of keeping the medium clean. In the 1930's the Barvoys process was developed in Holland, which used a mixture of clay (S.G. 2.3) and finely ground (-75 μm) barytes (S.G. 4.2) in a ratio of 2:1 which gave specific gravities up to 1.8. The barytes-clay mixture formed an almost stable pulp which gave an accurate cut between sink and float fractions. Froth flotation was used to regenerate the fouled dense-media by removing fine coal. Another Dutch process, the Tromp process used a finely ground magnetite or specially treated pyrite, to produce a less stable fluid. The settling characteristics of the medium caused the bath density to be lower at the top than at the bottom which tended to aid the separation.

In the treatment of ores other than coal, the lightest mineral is usually quartz or a silicate at a density between 2600 and 3500 kg/m^3. Therefore the substances used to form the dense media must be far denser than used for coal treatment, as the working density of the bath is twice as high as that used for coal cleaning. For example, in coal separation the media fluid needs a density of around 1500 kg/m^3 while separation of galena/sphalerite from gangue silicates requires a fluid density around 2850 kg/m^3, diamonds from kimberlite rock around 2780 kg/m^3 and hematite from silicate gangue around 3000 kg/m^3.

Any substance used for media must have the following characteristics:

1. *Hardness*: It must not easily break down or abrade into a slime under working conditions.
2. *Chemical Stability*: It must not be chemically corrosive or liable to react with the ore minerals undergoing treatment.
3. *Slow settlement at reasonable viscosity*: It must form a fairly stable pulp without having to be ground very fine, otherwise the medium will be too viscous.

4.   *Specific gravity*: It must have high enough specific gravity to give the required bath density at low % solids, again to minimise the viscosity.
5.   *Regeneration*: The dense media must be easy to clean for recycling.
6.   *Price and availability*: The solid should be readily available and cheap. Losses of up to 0.5 kg/t could lead to high operating costs.

Table 15.10
Heavy liquids used for sink-float separations. Group 2A is a probable carcinogen; Group 2B is a possible carcinogen; Group 3 is an unclassifiable carcinogen. [14,15]

Heavy liquid	Formula	S.G.	Dilution	Health
Tri-chloro-ethylene	CCl_2CHCl	1.46	-	group 2A carcinogen
Carbon-tetrachloride	CCl_4	1.5	Most organic liquids	group 2B carcinogen
Bromoform, Tribromomethane	$CHBr_3$	2.87	Alcohol, CCl_4	liver damage, group 3
Tetrabromoethane (TBE)	$C_2H_2Br_4$	2.95	Alcohol, CCl_4 Chloroform	suspected carcinogen
Di-iodo methane (Methylene iodide)	CH_2I_2	3.31	CCl_4, Benzene	moderate toxicity-central nervous system
Clerici solution (thallium malonate/thallium formate)	$(TlCOOH)_2C/$ $TlCOOH$	4.2-5.0	Water	highly toxic, cumulative poison.
lithium heteropolytungstate (LST)	$Li_mX_n(W_{12}O_{40})$	2.95	Water	Low to moderate toxicity
sodium polytungstate (SPT)	$Na_6(H_2W_{12}O_{40})$	3.1	Water	Low to moderate toxicity
lithium metatungstate (LMT)	$Li_6(H_2W_{12}O_{40})$	3.0	Water	Low to moderate toxicity

Material suitable for use as media are listed in Table 15.11.

Table 15.11
Solid materials used to form heavy pseudo liquids.

Material	SG	Regeneration
Galena	7.4–7.6	Froth-flotation
Magnetite	5.0–5.2	Magnetic separation
Mill-scale	~5	Magnetic separation
Ferro-silicon	6.3–7.0	Magnetic separation
Pyrite	5.02	-
Quartz sand	2.65	-

An important consideration in any heavy liquid used for gravity separation is the viscosity. The viscosity must be low enough to allow the particles to separate quickly and not become misplaced. For example, when pure galena is used, a specific gravity of 4.3 is obtainable but the practical limit is about 3.3. Above this S.G. the viscosity became too great to effectively deal with small particle sizes particularly those particles having a density close to that of the medium (near gravity particles). This will place a restriction on the maximum working density of any solid suspension.

Galena has a very high density but is little used in practice because it is soft and brittle and readily breaks down to a slime which is difficult to recover by flotation. In addition, the galena is an expensive commodity and flotation is an expensive process. In recent years the trend is towards the use of magnetic materials to constitute the dense medium because of the ease of recovery by magnetic separation.

Magnetite is low cost and cheap but because of its low density is used only for media densities up to 2.5. This is too low for ore separations but is suitable for coal cleaning.

For treating ores, ferro-silicon is the most widely used material. It is available in a range of silicon compositions but only a certain composition range is suitable for dense medium applications. For example, if the silicon content is greater than 22% it is only weakly magnetic, whereas if the silicon content is less than 15% the corrosion resistance is unsuitable. The specific gravity of ferro-silicon containing 10% Si is 7.0 and decreases to 6.3 at 25% Si. The media densities achievable with different solids is summarised in Table 15.12 As ferro-silicon is expensive some blending with cheaper magnetite is possible for some densities. Coarser ferro-silicon is used for the higher densities as the pseudo liquid will have a lower viscosity at the higher % solids needed to achieve the higher media densities.

The 15% ferro-silicon is non-rusting and has good magnetic properties. Sometimes lime is added to the suspension and a dispersing agent such as tri-sodium phosphate can be used to prevent the slimes from coagulating.

Ferro-silicon media may be prepared by grinding in a ball-mill or by atomisation of the molten material. The atomised variety has a more spherical shape which allows a higher medium density to be obtained (up to 3.4) and a lower apparent viscosity than the more angular particles. The spherical particle are also more chemically stable. The better chemical and physical properties of the atomised variety of ferro-silicon must be balanced against the higher cost.

For efficient separation, the media viscosity should be low. This allows rapid movement of particles and high capacity. Therefore the volume concentration of solids in the medium

Table 15.12
Media densities obtained using various solids.

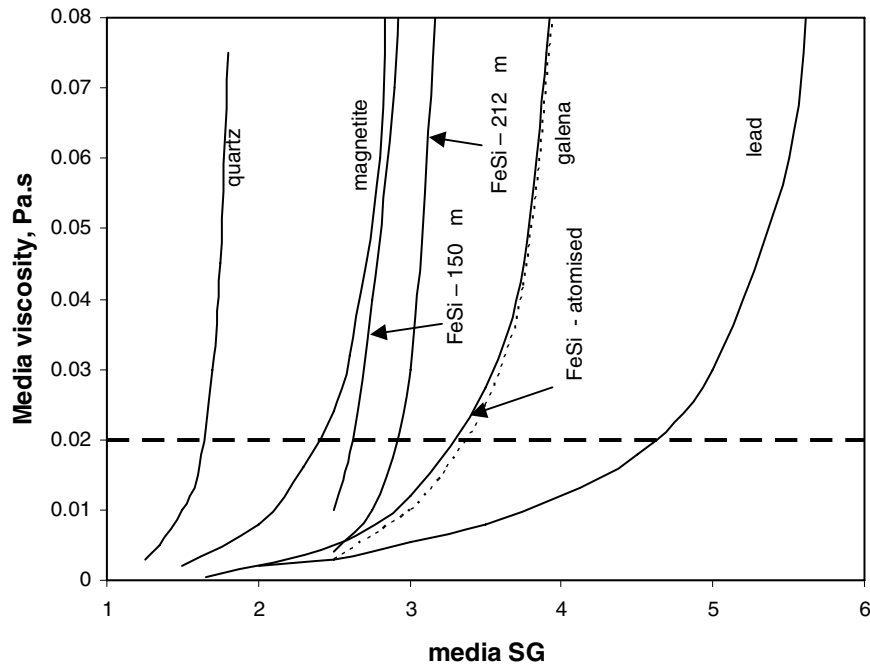| Solid	limiting media S.G.
galena	3.3
magnetite	2.5
15% Si - ferrosilicon	2.5 – 3.5
-150 μm Fe-Si + 10-20% magnetite	2.65 – 2.9
-150 μm Fe-Si only or -212 μm Fe-Si + magnetite	2.8 – 3.0
-212 μm Fe-Si	> 3.0

Fig. 15.16. Viscosity of the heavy media produced from selected solids [16].

should be low since the viscosity of a suspension of solids is dependant on the solids concentration and the particle size. For efficient separation of a feed containing a wide size range, the media volume concentration should be kept to 35-38%. For a narrow size feed, the media can be up to 45-48% solids by volume. Fig. 15.16 shows the viscosity versus medium density for a number of common media solids. The dotted line in Fig. 15.16 represents an approximate critical concentration of solids in water above which the media viscosity is too high for efficient separation.

Example 15.4

How much 10% FeSi needs to be added to 1L of water to make a heavy liquid of S.G. 2.8? What is the maximum media S.G. that can be used with this solid?

Density of FeSi $= 7000 \text{ kg/m}^3$ Density of water $= 1000 \text{ kg/m}^3$

Solution

Step 1: Calculate the mass of solid

Volume of water $= 1\,L = 0.001\,m^3$
Mass of water $= 0.001 \times 1000 = 1.0\,kg$

$$\text{Density of heavy medium} = \frac{\text{mass of medium}}{\text{volume of medium}} = \frac{\text{mass of solid} + \text{mass of water}}{\text{volume of solid} + \text{volume of water}}$$

Let the Mass of solid $= X\,kg$

then volume of solid $= X/7000\,m^3$

Therefore, density of medium $= 2800 = \dfrac{X + 1.0}{\dfrac{X}{7000} + 0.001}$

and solving for X :

$$X = \frac{(2800 \times 0.001) - 1}{1 - \left(\dfrac{2800}{7000}\right)} = 3.0\,kg$$

Step 2: Calculate the maximum medium density.

Assume that the viscosity limit of the medium occurs at a volume % solids of 35%.

Let the volume of the liquid medium $= 100$
then the volume of solid $= 35$
and the volume of water $= 100 - 35 = 65$

The density of the medium then is given by :

$$\text{media density} = \frac{\text{mass of medium}}{\text{volume of medium}} = \frac{(\text{vol.} \times \text{density})_{solid} + (\text{vol.} \times \text{density})_{water}}{100}$$

$$= \frac{(35 \times 7000) + (65 \times 1000)}{100} = \frac{245000 + 65000}{100} = 3100\,\,kg/m^3$$

This calculation assumes that the solid is immiscible in the liquid and hence no volume change will occur. In the case of a soluble solid or two soluble liquids, the volumes will not be additive.

15.6.3. Types of Dense Medium Separators

The aim of the dense medium separation is to produce a float product of lower density and a sink product of higher density than the medium. In some instances a third, middlings product is also produced. A variety of equipment is used to bring about this separation and they are

usually classified into bath or trough separators and centrifugal separators, depending on the separation forces employed.

Gravity Dense Medium Separators

In gravity dense medium separators the minerals and dense medium are fed into a large quiescent pool or tank or trough of the medium. Particles denser the medium will sink and the low specific gravity particles float. The floating material overflows or is removed from the bath by scrapers while the sink material falls to the bottom of the tank and is removed by some means. The many types of static bath separators include those used for coal separation and mineral separation. Since coal separation has a very high floats content in the feed (up to 95%), the separator will need a high floats capacity whereas separators for the mineral industry may require a high sinks capacity depending on the ores being treated (up to 80% for iron ore). Operating requirements therefore differ depending on the type of ore being treated. The types of separators include:

1. *drum separator* consisting of a cylindrical rotating drum, used for mineral and coal separation. The floating product overflows from a weir at the opposite end to the drum feed. The size of the drums range up to about 4.6 m diameter by 7.0 m long, with capacities up to 800 t/h. The drums may consist of a single compartment, producing two products from a single dense medium suspension or consist of two compartments with two baths of different density to produce three or four products. Drum feed size ranges from 6 mm to 30 cm.

2. *Drewboy* bath separator is used widely in the cleaning of coal. The coal is fed into the bath at one end and the floats scraped from the opposite end while the sinks are lifted out from the bottom of the bath by the vanes of a slowly revolving inclined wheel. The Drewboy bath has a high floats capacity and handles a feed from 12.7-600 mm at up to 820 t/h for a 4 m diameter bath.

3. *Cone Separator* is used for ore treatment since it has a relatively high sinks capacity. The feed is dropped into a gently agitated media bath. The floats overflow a weir while the sinks product is removed directly from the bottom of the cone shaped vessel by pump or by an air lift. Cone separators are available in diameters from 0.9 to 6.1 m, with capacities up to 450 t/h. The method of sink discharge limits the maximum feed particle size to about 10 cm. The *Chance cone* is a similarly shaped vessel to the cone separator but differs from the normal dense medium methods in that it uses a rising flow of water to fluidise a bed of sand to simulate a dense fluid. The sand used is sized between 150-600 μm and when fluidised by water rising at 6-12 mm/s the density is in the range 1.4-1.7 and hence is suitable only for coal/shale separation. Gravity control is achieved by varying the water flowrate. Shale or refuse is discharged periodically through a double gate arrangement at the bottom of the cone.

Centrifugal Dense Medium Separators

The buoyant forces acting on the light particles in a dense medium cause them to rise to the surface but the dense particles, being heavier than the liquid they displace, sink to the bottom. The magnitude of the gravitational and buoyant forces that separate the particles is a primary consideration because it governs the velocity with which the particles separate, which it turn determines the capacity of the separating vessel. In a static bath the net gravitational force minus buoyant force may be written as follows:

$$F_g = (M_S - M_F)g \qquad\qquad (15.25)$$

where F_g = gravitational force,
M_S = mass of solid and
M_F = mass of fluid displaced by the particle.

For particles which float, F_g will have a negative value and for sink particles, it will be positive. In a centrifugal separator, specific gravity separations result from application and utilisation of similar forces except that the acceleration of gravity is substituted by a centrifugal acceleration. The equation then becomes:

$$F_C = (M_S - M_F)\frac{v^2}{R} \qquad\qquad (15.26)$$

where F_C = centrifugal force,
v = tangential velocity and
R = radius of the centrifugal separator.

The centrifugal force will be balanced by the resistance of the liquid when the terminal velocity is reached. For small forces, as experienced by particles with a specific gravity near that of the medium, the particles fall in the Stokes range where the fluid resistance is essentially due to viscosity. However, for large forces, the particles will fall in Newton's range where the fluid resistance is primarily inertial and substantially independent of viscosity. It is, therefore, not possible to write an exact equation for the terminal velocity that would be applicable for all particles. Nevertheless, it is apparent that the forces causing the particles to separate in a static bath are proportional to g, whereas in a centrifugal separator they are proportional to v^2/R which is much larger.

Cyclones can be used to develop this centrifugal force. In a typical cyclone the centrifugal force acting on a particle in the inlet region is 20 times greater than the gravitational force in a static bath. In the conical section of the cyclone, v is further increased according to the relationship:

$$v\sqrt{R} = \text{constant} \qquad\qquad (15.27)$$

At the apex of the cyclone where R decreases, the acceleration increases to over 200 times greater than gravity. Thus, the forces tending to separate the light and heavy particles are much greater in a cyclone than in a static bath. This offers two advantages:

1. a relatively high capacity and

2. Because the forces acting on the small particles are also much larger than static separations, the cyclone is much more applicable to the separation of small particles.

The general flow pattern of the medium in the cyclone is similar to that existing in a classifying cyclone. The centrifugal forces within the cyclone not only acts on the fine mineral particles but also acts to some extent on the fine medium particles. The effect is to

progressively increase the specific gravity of the medium as it descends towards the apex since the concentration of medium particles at the apex will be higher than in the feed. Conversely the specific gravity of the medium passing through the overflow orifice is less.

This thickening of the dense medium towards the apex of the cyclone has been postulated as a cause for the observed fact that separations in a cyclone always occurs at a specific gravity higher than the specific gravity of the feed medium. For example a medium made up to a density of 2.6 would produce a separation equivalent to a specific gravity of 2.8 in the cyclone. However it has been observed that a similar increase in separation density is found when heavy organic liquids are used in a cyclone. Therefore it is apparent that there is some other factor contributing to the effect of centrifugal forces on the gravity of separation. Nevertheless the zone near the apex of the cyclone is important when using an unstable suspension as the medium. This is indicated by the influence of the size of the medium particles on cyclone performance. If the medium particle are too coarse, performance is adversely affected. Also, the geometry of the lower part of the cyclone becomes very critical, especially with regard to the underflow diameter. Conversely for medium particles below a limiting size, performance is relatively unaffected and the geometry of the lower part of the cyclone becomes less important.

Dense-medium cyclones are available in several sizes with diameters of 0.5–1.0 m being common in the coal industry. The 0.5 m cyclones have a capacity of about 50 tph of raw coal. A cone angle of about 20° is pretty standard and they are generally mounted with just sufficient angle to the horizontal to allow drainage after a shutdown. For example a 20° cyclone would be mounted with the longitudinal axis about 10° from the horizontal. At very low inlet pressures this gives a superior performance. At normal inlet pressures the cyclone orientation has no influence on performance. Dense medium cyclones will operate with inlet pressures as low as 42–56 kPa, but pressures of 140 kPa and higher are used in practice. At very low pressures the separation is much less effective than at higher pressures, especially for the finer sizes. The pressure can be developed by two methods. The simplest is to simply feed the ore directly into the medium sump and pump the mixture to the cyclone. Alternatively, the medium is pumped to a head tank, which is 5-6 m above the cyclone inlet, where the ore is added. This second method is particularly applicable where the solid feed is friable such as coal, because degradation of the coal in the medium pump is eliminated.

In coal processing, a medium-to-coal ratio of about 5:1 is recommended. A ratio as low as 3:1 can be used, but with some sacrifice in performance.

The Dense Medium Cyclone or DSM cyclone (developed by the Dutch State Mines) is used to treat ores and coal in the size range 0.5 - 40 mm. Other centrifugal dense media devices include the *Swirl Cyclone*, the *Dyna Whirlpool* and the *Vorsyl Separator*. The *hydrocyclone*, *Water-Washing* or *Water-only* cyclone is used in the coal industry for cleaning of the -0.6 mm coal. It does not employ a dense medium and is not generally regarded as a dense medium separation device, although some researchers believe that separation occurs by some autogenous dense medium developed from the coal feed. It was developed by the Dutch State Mines and differs from the conventional dense-medium cyclone by having a much larger cone angle, up to 120° and a longer vortex finder. The hydrocyclone is effective on coal up to 50 mm and down to 150 μm. The essentially unseparated minus 150 μm material is separated from the cleaned coal (overflow) by screening (sieve bend).

Two theories have been put forward to explain the separation in the water only cyclone:

1. *Autogenous dense medium*
This theory proposes that the hydrocyclone behaves as a dense-medium cyclone as particles of intermediate or high specific gravity collect and recirculate in the conical section of the cyclone. These particles then form an autogenous dense-medium through which the sinks have to penetrate to enter the underflow, but the light coal particles cannot penetrate and report to the overflow.

2. *Acceleration theory*
Fontein & Dijksman [17] considered the separation to be occurring in the ascending vortex of the cyclone where both light and heavy particles are subjected to the centrifugal forces. For particles at the same position in the vortex, the initial movement of a particle outwards towards the wall of the cyclone will be dominated by the particle acceleration and the drag force will be low. Eq. (15.26) describes the centrifugal force acting on the particles with negligible drag and thus the acceleration of a particle is given by:

$$a_P = \frac{F}{M} = \frac{(M_S - M_F) v^2}{M_S \quad R} \tag{15.28}$$

For particles occupying the same radial position in the cyclone, having R and v the same and since M_F is the mass of an equal volume of fluid then this simplifies to:

$$a_P = \left(1 - \frac{M_F}{M_S}\right) C = \left(1 - \frac{\rho_F V_S}{\rho_S V_S}\right) C = \left(1 - \frac{1}{SG_S}\right) C \tag{15.29}$$

where C $= v^2/R$ which is constant and equal for all particles and
       SG_S = specific gravity of the particle.

Now for a shale particle of S.G. 2.4 and a coal particle of S.G. 1.3 the initial acceleration of the particle outwards will be given by:

$$a_{shale} = \left(1 - \frac{1}{2.4}\right) C = 0.583 C \quad \text{and} \tag{15.30}$$

$$a_{coal} = \left(1 - \frac{1}{1.3}\right) C = 0.231 C \tag{15.31}$$

    That is, the acceleration on the shale particle is about 2.5 times that on the coal particle. The shale particle is therefore more likely to move out of the ascending vortex to the descending vortex and thus report to the cyclone spigot. The coal particle then is more likely to remain in the ascending vortex and report to the overflow independent of its size.
    As the particle size decreases, the fluid resistance becomes a significant factor. For large particles, the residence time in the cyclone is not long enough for the fluid resistance to become significant. This is not the case for the finer particles and hence the very fine particles tend to report to the light fraction regardless of their density.

The density of separation of a water only cyclone, and hence the grade of the coal product, is determined by the diameters of the discharge orifices (U/F or O/F) or by varying the length of the vortex finder. For example, the washed coal ash content can be reduced by decreasing the diameter of the vortex finder, increasing the diameter of the underflow orifice or decreasing the length of the vortex finder [18].

The separations obtained in a water only cyclone are not as sharp (not as efficient) as those characteristic of the dense-medium cyclone. Therefore the water only cyclone is not applicable to difficult feeds (that is, where the feed contains a large percentage of near-gravity material) or at low separation densities. The hydrocyclone cleaning stage is therefore usually a two-stage recirculation circuit in order to improve the efficiency.

15.6.4. Comparison of Dense Medium Separators and Jigs in Coal Processing

Table 15.13 summarises the performance comparisons between jigs and other gravity and centrifugal separators.

15.7. Gravity Separation Performance

The evaluation of the separation method or performance of a gravity separation device is usually based on a sink-float analysis and *washability curves*. A great many applications of the washability curves are applied to cleaning operations in the coal preparation field (coal washing) so that most reference is made to coal washability curves, however, it must be remembered that the principles will also apply to separations of heavy minerals.

An ideal separation process would be one in which all particles of density lower than the separating density would be recovered in the light or clean product (coal) and all material denser than the separating density would be rejected as the heavy or refuse fraction. This is not achievable in practice. The type of separation between the light and heavy components that might actually occur is illustrated in Fig. 15.17. Material that is much heavier or lighter than the separating density tend to report to their proper fraction but as the density of the particle approaches the density of separation of the unit, the amount of misplaced material increases rapidly. At the density of separation, the amount of misplaced material peaks at 50% as this is how we have defined the density of separation.

The imperfect separation of materials is characteristic of all gravity separation processes. The shape of the curve is determined largely by the inherent difficulty of stratifying materials of only slight density difference and will depend on the feed particles themselves, the feed rate, the media viscosity and separator characteristics. The more efficient the processes the sharper the separation and the narrower the peak. With low efficiency separation processes, the two arms of the peak are more widely separated. The peak will not necessarily be symmetrical.

15.7.1. Sink-Float analysis

The characteristics needed for evaluating a unit performance are normally derived from a float-sink analysis of samples of the clean coal and the reject, followed by ash determinations of the various fractions. Usually a sample of feed is also collected to determine its ash content to determine the yield. No single characteristic describes adequately the efficiency of a separation unit. The most significant is the error curve (Fig. 15.17) and the associated separating gravity, probable error, and imperfection.

A sink-float analysis is akin to a size analysis in that the sample is broken down into its various density fractions rather than size fractions. The sink-float test involves placing the

sample progressively into baths of increasing density and recording the mass of sample within any given density fraction. Normally test work includes determining floats from 5-8 gravity

Table 15.13
Performance comparison of gravity separation units.

Jig	Shaking Table
can adjust to fluctuating feed rates	lower power consumption
can treat feed with high % reject	nominal unit capacity 8 – 12 t/h
can process reasonable capacity in a single unit	nominal size range 0.15 – 12.5 mm
lower operator involvement	Ep 0.10
lower maintenance costs	nominal separation density 1.6 – 1.8
lower floor space	
Jig	**Dense Media cyclone**
lower capital cost	higher sharpness of separation
lower operating cost	suitable for large % of near gravity material (> 10-15%)
can adjust to fluctuating feed rates	nominal unit capacity 10 – 120 t/h
can handle wide size range in feed	Ep 0.04
Jig	**Dense media bath**
minimum water consumption	precise control of separation SG
treat < 5% of near gravity material	easily vary S.G. of separation over large range
lower operating costs – no media	treat > 10% of near gravity material
can treat sizes to 0.5 mm	can separate at S.G. < 1.45
simpler plant control	lower size limit is 5 mm
easier to operate at high cut-points	can treat sizes > 200 mm
	can separate at an accurate cut-point
Jig	**Water only cyclone**
higher feed rate	suitable for feed rates < 200 t/h
change washing gravity easily	Ep 0.25 (single stage), 0.15 (2 stage)
handle new feed size easily	nominal cut-point 1.6 – 2.0
can adjust to wide swings in feed grade	size range 0.1 – 12.5 mm
wash a wide size range	nominal capacity 150 t/h
Ep 0.08	
nominal cut-point, 1.5 – 2.0 SG	
size range 0.15 – 19 mm	
nominal capacity 200-800 t/h	

increments between the density of the light and heavy minerals. The steps may include S.G.'s of 1.30, 1.40, 1.50, 1.60, 1.70, 1.80 up to a S.G. of 2.0. Additional densities between those listed may be required depending on the feed sample. The procedures are described in various standards such as AS 4156.1 [20].

After being rinsed, dried and weighed, all the gravity fractions are analysed for ash. The observed data are presented in table form for each particle size over a range of specific gravities (Table 15.14). Column 1 lists the density fractions with F1.35 representing the material floating at a S.G. of 1.35 and S1.30 representing material that has sunk at a S.G. of
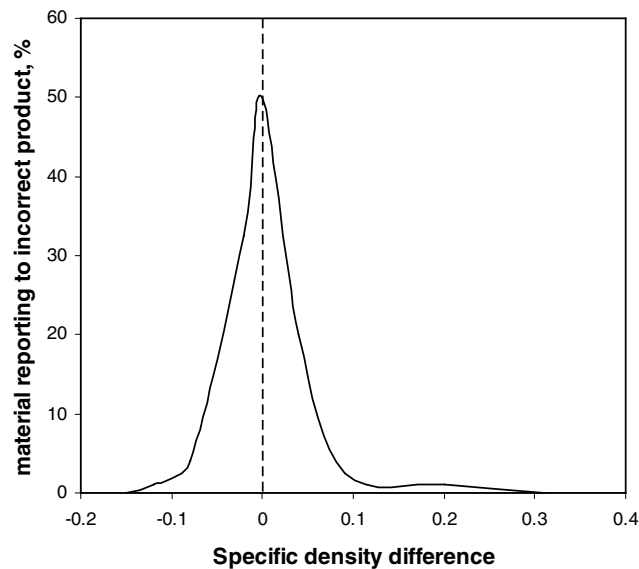
539

Fig. 15.17. Actual gravity separation performance [19].

1.30. Column 2 contains the mass% of the sample that lies within the corresponding density range and column 3 is the grade of the particles in the density fraction as ash%. Column 4 has the amount of ash (mass) in the density fraction obtained by multiplying columns 2 and 3. Column 5 lists the nominal density of the fraction, taken as the floating density. Columns 6 – 11 are the cumulative values of both floats and sinks and the associated ash content summed from the top down for floats and from the bottom of the table up for the sinks. Column 8 is the cumulative grade (weighted average) of the combined floats up to the nominated density and hence the value of 27.5% at 100% cumulative floats corresponds to the total grade of the coal sample being tested. Similarly, column 11 is the cumulative grade of the combined sinks and the value of 27.5% ash at 100% sinks will also equal the sample grade. Columns 12 and 13 calculate the instantaneous ash which represents the highest ash content of any individual particle in the floats at that density. The instantaneous ash is found as follows:

Consider an increase in media density from 1.55 to 1.60. At the higher density, the cumulative floats ash is 15.7 % and the average ash in this new incremental density range (1.55-1.60) is 33.2% (column 3, Table 15.14). Although the average ash in this density increment is 33.2%, there will be some particles which have a higher ash and some which have a lower ash. This average ash content corresponds, for want of a more precise estimate, to a particle having a density half way between 1.55 and 1.60 (Fig. 15.19). The cumulative floats corresponding to this average density is given by the average of the cumulative floats at 1.55 (73.6%, column 6, Table 15.14) and the average cumulative floats at density 1.60 (77.0%). That is:

$$\text{Cumulative floats at 33.2\% ash} = \frac{73.6 + 77.0}{2} = 75.3 \qquad (15.32)$$

Fig. 15.18. Calculation of Instantaneous Ash, column 12, Table 15.14..

Thus if the coal sample was placed in a heavy liquid to float off 75.3% of the mass, then the maximum ash content of any one particle in the floats would have an ash content of 33.2%.

This adjusted cumulative % floats value of 75.3 could also have been obtained by ;

$$\text{Cumulative floats at } 1.55 \ + \ \frac{\text{mass\% in range } 1.55 - 1.60}{2} \quad \text{or}$$

$$\text{Cumulative floats at } 1.60 \ - \ \frac{\text{mass\% in range } 1.55 - 1.60}{2}$$

(15.33)

Column 13 is a repeat of column 3.

15.7.2. Washability Curves
The information from Table 15.14 is presented graphically (Fig. 15.19) in the form of a family of 5 washability curves which indicate the ease or difficulty of the proposed separation.

Cumulative floats curve
This curve is obtained by plotting the cumulative mass percent of floats at each relative density increment against the cumulative ash at that point (columns 6 and 8). Both scales are usually arithmetic although a logarithmic scale may be used for the ash to accentuate

differences in the lower ash ranges. The curve may be used to indicate the yield obtainable for any set ash required. It is plotted on a y-axis with increasing values from top to bottom.

Cumulative sinks curve

This curve is obtained by plotting the cumulative mass percent sinks at each relative density increment against the cumulative ash of the sinks for that separation (column 9 and 11).
The ash point for 100% sinks must equal the ash point for 100% floats. This curve indicates the ash content of the rejects when a certain yield of clean coal is required.

Instantaneous ash curve

This is sometimes referred to as the *elementary ash curve, characteristic ash curve* or *observed curve* and describes the rate of change of ash at different yields (column 12 and 13). It is a derivation of the cumulative percent ash in the floats and shows the rate of change of the ash content at different specific gravities or yields. The instantaneous ash is the highest ash content of any individual particle in the floats at any density.

Relative density curve

This is obtained by plotting the cumulative percent of floats against the relative density for that separation (column 5 and 6). It indicates the yield of clean coal for a perfect separation at a selected relative density.

Distribution or ±0.1 S.G. curve

A density interval, usually ± 0.1 (or 0.05) for specific gravity is specified and then the difference in yield (cumulative floats) between two relative densities, 0.2 apart, is plotted against the mean of those densities. For example, for a S.G. of 1.6, calculate the difference in cumulative floats from a S.G. of 1.50 and 1.70. This represents the percentage of the feed that is close to a separating density of 1.60 (within ± 0.1) or the percentage of near gravity material in the feed. Thus the curve indicates the difficulty of separation. A low value, less than 10%, is satisfactory, whereas a figure in excess of 20% indicates a very difficult separation (see Table 15.15).

The combined curves are shown in Fig. 15.19 and can be used to indicate the parameters of separation. For example, in the washability curves, for a yield of 75%, the clean coal would contain 15.1% ash, rejects 64% ash, separation would be made at 1.575 S.G. and separation would be very difficult (distribution curve reading 24). Table 15.15 is to be used as a guide only and in some cases the distribution curve may have to be extended to ±0.02 or ±0.05 to increase the sensitivity.

In Fig. 15.19 the specific gravity scale increases right to left. This is simply to reduce clutter in the graph as the relative density curve would overlap with the instantaneous and cumulative floats curves. The scale can equally be plotted in ascending order left to right.

15.7.3. Tromp Curves

The data from the float-sink analysis indicates what should be obtained under ideal operating conditions since in the laboratory, time is given for particles to find their correct product. Such conditions do not exist in plant practice and some material will be misplaced by degradation of the coal during processing and the imperfection of the separator unit in that particles of density near that of the medium may not have enough time in the separating vessel to report to the sinks or the floats.

Table 15.14
Sink-Float test Data; Q_{ASH} = Quantity of Ash; Sep SG = separating density; $Dist_{DIST,}$ = Distribution of Ash.

S.G.	Mass%	Ash%	Q_{ASH}	Sep S.G.	Cumulative float			Cumulative Sink			Instantaneous Ash		± 0.1 Dist
					Mass%	Q_{ASH}	$Dist_{ASH}$	Mass%	Q_{ASH}	$Dist_{ASH}$	Mass %	Ash %	
(1)	(2)	(3)	(4)	(5)	(6)	(7)	(8)	(9)	(10)	(11)	(12)	(13)	(14)
			(2)x(3)		Sum(2)	Sum(4)	(7)/(6)	Sum(2)	Sum(4)	(10)/(9)	(6)-(2)/2	(3)	$(6)_{+0.1}-(6)_{-0.1}$
F1.30	9.5	5.0	47.5	1.30	9.5	47.5	5.0	90.5	2699.2	29.8	4.8	5.0	
S1.30-F1.35	9.7	8.1	78.6	1.35	19.2	126.1	6.5	80.8	2620.6	32.4	14.4	8.1	
S1.35-F1.40	13.4	9.9	132.7	1.40	32.6	258.8	8.0	67.4	2487.9	36.9	25.9	9.9	58.1
S1.40-F1.45	17.8	17.2	306.2	1.45	50.4	564.9	11.1	49.6	2181.7	43.9	41.5	17.2	54.4
S1.45-F1.50	17.2	21.9	376.7	1.50	67.6	941.6	14.0	32.4	1805.0	55.7	59.0	21.9	44.4
S1.50-F1.55	6.0	26.0	156.0	1.55	73.6	1097.6	14.8	26.4	1649.0	62.5	70.6	26.0	
S1.55-F1.60	3.4	33.2	112.9	1.60	77.0	1210.5	15.7	23.0	1536.1	66.8	75.3	33.2	12.7
S1.60-F1.70	3.3	40.1	132.3	1.70	80.3	1342.8	16.7	19.7	1403.8	71.3	78.7	40.1	6.1
S1.70-F1.80	2.8	45.9	128.5	1.80	83.1	1471.3	17.7	16.9	1275.3	75.5	81.7	45.9	4.3
S1.80-F1.90	1.5	53.2	79.8	1.90	84.6	1551.1	18.3	15.4	1195.5	77.6	83.9	53.2	3.5
S1.90-F2.00	2.0	65.1	130.2	2.00	86.6	1681.3	19.4	13.4	1065.3	79.5	85.6	65.1	
S2.00	13.4	79.5	1065.3	-	100.0	2746.6	27.5	-	-	-	93.3	79.5	
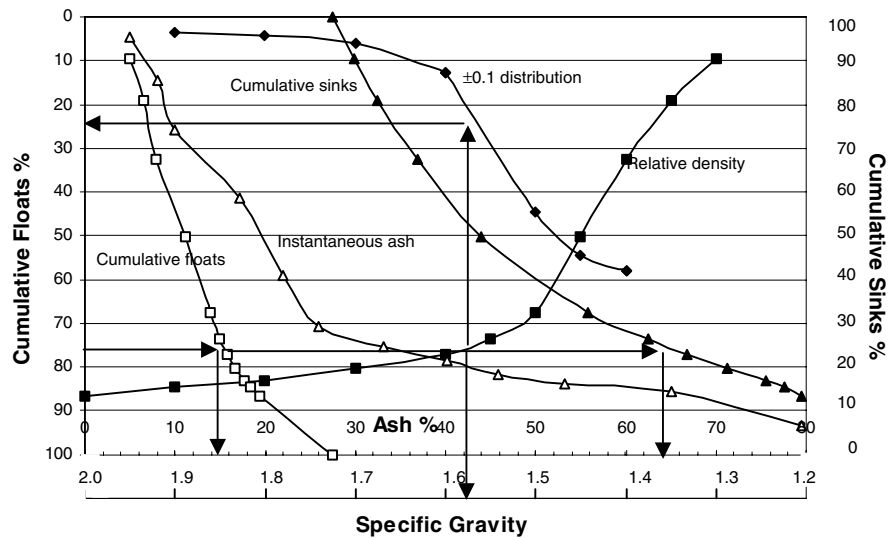
Fig. 15.19. Washability curves based on the sink-float analysis date in Table 15.14.

Table 15.15
Ease of gravity separation based on the % of near gravity material.

mass% within ±0.1 S.G.	Burt [2]; Herbst & Sepulveda [21]	Mills [22], Bird [23]
0 – 7	simple	simple
7 – 10	relatively simple	moderately difficult
10 – 15	moderately difficult	difficult
15 – 20	difficult	very difficult
20 – 25	very difficult	exceedingly difficult
> 25	very difficult	formidable

The partition or distribution curve or Tromp curve is useful in assessing the efficiency or sharpness of the separation, or to predict the performance of a plant treating a particular coal feed. Normally it is relatively independent of the float and sink properties of the coal being dependent upon the particle size distribution and the type of separating unit. Data from float and sink analysis on the raw coal, the clean coal and the reject is used to determine the partition coefficients, which is defined as:

$$\text{Partition Coefficient} = \frac{\text{mass of coal reporting in any SG range}}{\text{mass of feed coal present in that SG range}} \times 100 \qquad (15.34)$$

Table 15.16 shows the sink-float data obtained from a sample of the light fraction and the heavy fraction from a gravity separation process such as a jig or dense medium bath. As in the determination of the Tromp Curve of a classifier, the mass split between the floats (M_{FT}) and sinks (M_{SK}) produced by the separator is required. Thus:

$$M_{FT} = Floats\,yield = \frac{mass\,of\,floats(clean\,coal)}{mass\,of\,raw\,feed} \times 100$$

Table 15.16
Data for determination of a separator efficiency. M_{FT} = floats mass, M_{SK} = sinks mass.

Specific Gravity	Clean Coal analysis (%)	Reject analysis (%)	Floats as % of feed	Sinks as % of feed	Reconstituted feed (%)	Partition coeff
(1)	(2)	(3)	(4)	(5)	(6)	(7)
F1.30	72.75	10.10				
1.30/1.35	19.50	7.03				
1.35/1.40	2.67	5.92				
1.40/1.45	1.83	5.45				
1.45/1.50	0.76	4.19				
1.50/1.55	0.55	4.68				
1.55/1.60	0.43	9.85				
1.60/1.70	0.30	9.06				
1.70/1.80	0.12	8.37				
1.80/1.90	0.09	5.85				
1.90/2.00	0.05	4.67				
S2.00	0.95	24.83				
	100.00	100.00	$100M_{FT}$	$100M_{SK}$		

Column (2) obtained from a sink-float analysis of the process floats

Column (3) obtained from a sink-float analysis of the process sinks

$$M_{SK} = Sinks\,yield = \frac{mass\,of\,sinks(reject\,coal)}{mass\,of\,raw\,feed} \times 100 = 100 - M_{FT}$$

The quantities represented in columns 2 – 7 are given as:

$$column\,2 = \frac{mass\,of\,clean\,coal\,that\,floats\,at\,SG\,range}{total\,mass\,of\,clean\,coal} \times 100 \qquad \{15.35\}$$

$$column\,3 = \frac{mass\,of\,rejects\,that\,float\,at\,SG\,range}{total\,mass\,of\,reject} \times 100 \qquad \{15.36\}$$

$$\text{column}\,4 \;=\; \frac{\text{mass of clean coal} \left(\text{floats}\right) \text{that float at SG}}{\text{total mass of feed}} \; \times 100$$

$$=\; \frac{\text{mass of clean coal that float at SG}}{\left[\text{total mass of clean coal}\right]} \; \times \; \frac{\left[\text{total mass of clean coal}\right]}{\text{total mass of feed}} \times 100$$

$$=\; \text{column}\,2 \; \times \; M_{FT} \qquad\qquad \{15.37)$$

$$\text{column}\,5 \;=\; \frac{\text{mass of reject} \left(\text{sinks}\right) \text{that float at SG}}{\text{total mass of feed}} \; \times 100$$

$$=\; \frac{\text{mass of reject that floats at SG}}{\left[\text{total mass of reject}\right]} \; \times \; \frac{\left[\text{total mass of reject}\right]}{\text{total mass of feed}} \times 100$$

$$=\; \text{column}\,3 \; \times \; M_{SK} \;=\; \text{column}\,3 \times \left(100 - M_{FT}\right) \qquad (15.38)$$

$$\text{column}\,6 \;=\; \frac{\text{mass of feed that floats at SG}}{\text{total mass of feed}} \; \times 100$$

$$=\; \frac{\text{mass of clean coal that floats at SG}}{\text{total mass of feed}} \;+\; \frac{\text{mass of rejects that float at SG}}{\text{total mass of feed}}$$

$$=\; \text{column}\,4 \;+\; \text{column}\,5 \qquad\qquad (15.39)$$

Now since it is only the clean coal fraction that floats in the separator:

$$\text{column}\,7 \;=\; \frac{\text{mass of feed that floats} \left(\text{or sinks}\right) \text{at SG}}{\text{mass of feed at that SG}} \; \times 100$$

$$=\; \frac{\text{mass of clean coal} \left(\text{or reject}\right) \text{that floats at SG}}{\left[\text{mass of feed}\right]} \; \times \; \frac{\left[\text{mass of feed}\right]}{\text{mass of feed at that SG}} \times 100$$

$$=\; \frac{\text{column}\,4}{\text{column}\,6} \; \times 100 \quad \text{or} \quad \frac{\text{column}\,5}{\text{column}\,6} \; \times 100 \qquad (15.40)$$

The partition curve or Tromp curve (introduced by Tromp in 1937) is then obtained by plotting the partition coefficient against the mean of its density range. From the partition curve the separation density or cut point or d_{50} is determined (Fig. 15.20).

The ideal partition curve would indicate that all particles having a density higher than the separating density report to the sinks and particles lighter than the separating gravity report to the floats. The partition curve for the real situation shows that the efficiency is greatest for particles of density furtherest from the separating density and decreases for particles
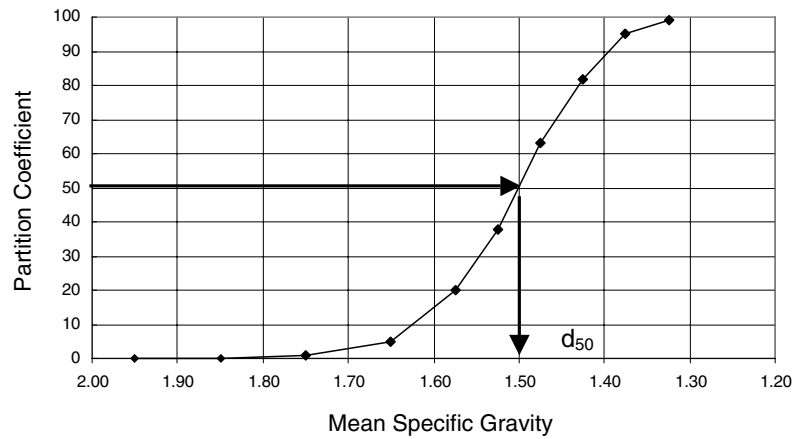
Fig. 15.20. Partition curve for gravity separation of coal indicating the d_{50}.

approaching the separating density. The gradient of the curve is a measure of the sharpness of separation and to indicate the accuracy of the separation, the slope of the partition curve between the 25 and 75 percent partition coefficients is used.

The *probable error of separation* (Ep) is defined as half the difference between the S.G. where 75% is recovered in the sinks and the S.G. at which 25% is recovered in the sinks:

$$E_P = \frac{SG_{25} - SG_{75}}{2} \qquad (15.41)$$

The density at which 50 % of the feed reports to the floats or to the sinks is known as the effective density of separation, which may not be exactly the same as the operating density.

The probable error is relatively characteristic of a process and units which have a low Ep, such as heavy medium processes (Ep = 0.02 to 0.03) are considered efficient separators. Table 15.16 indicates the probable error for different gravity separation processes. The higher the difficulty of separation as indicated in Table 15.15 the greater is the need to use a separator with a low probable error. The value of the probable error depends on the specific gravity of separation, the d_{50}. The probable error will increase as the specific gravity of separation increases, unjustifiably indicating a less sharp separation. Therefore the Imperfection is used as a further method of comparing separating processes independent of the separating density. The Imperfection is defined as:

$$I = \frac{probable\, error}{partition\, density - 1} = \frac{E_P}{d_{50} - 1} \qquad (15.42)$$

Table 15.17
Probable errors for some gravity separation processes.

Process	E_P
Table	0.03-0.11
DM Bath	0.01-0.02
DM Cyclone	0.01-0.04
Hydrocyclone	0.08-0.14
Baum Jig	0.03-0.12

However, these refer to only a portion of the partition curve and to assess the overall operation it is preferable to consider the full series of partition coefficients. In the case of a new coal deposit, if the float-sink analysis data is available and the partition curve for the separation process is known, then it is possible to calculate the potential percentage recovery and product grade for the processing of the coal by the preparation method selected.

Table 15.18 shows the sink-float analysis of a ROM coal sample with the partition coefficient of a jig separator. In this table, column 6 is the actual mass of floats to be expected from the separator and column 7 is the mass of ash expected at that density. These are expressed as:

$$column\,6 \;=\; column\,2 \times column\,5$$

$$= \frac{[total\,mass\,of\,floats\,at\,SG]\times100}{mass\,of\,feed} \times \frac{mass\,that\,actually\,floats\,at\,SG\times100}{[total\,mass\,of\,floats\,at\,SG]}$$

$$= \frac{mass\,that\,actually\,floats\,at\,SG}{mass\,of\,feed} \times 10000 \tag{15.43}$$

$$column\,7 \;=\; column\,6 \times \frac{mass\,of\,floats\,ash}{mass\,of\,floats\,at\,SG} \times 100$$

$$= \frac{[mass\,of\,actual\,floats\,at\,SG]}{mass\,of\,feed} \times 10000 \times \frac{mass\,of\,floats\,ash}{[mass\,of\,floats\,at\,SG]} \times 100$$

$$= \frac{mass\,of\,floats\,ash\,at\,SG}{mass\,of\,feed} \times 10^6 \tag{15.44}$$

From Table 15.18, the yield and grade of the floats and sinks can be estimated.

The predicted yield is given by:

Table 15.18
Sink-float analysis of a raw coal sample with the partition coefficient of a gravity separator.

Specific Gravity	Mass %	Ash %	Mass x Ash	Partition Coeffic.	Floats Mass	Mass of Ash
(1)	(2)	(3)	(4)	(5)	(6)	(7)
					(2)x(5)	(3)x(6)
F1.30	2.2	3.5	7.7	100	220	770
S1.30/F1.35	8.2	5.8	47.6	99	812	4712
S1.35/F1.40	14.3	8.2	117.3	95	1358	11144
S1.40/F1.45	15.6	10.4	162.2	82	1279	13300
S1.45/F1.50	9.6	21.3	204.5	63	605	12884
S1.50/F1.55	6.4	28.2	180.5	38	243	6859
S1.55/F1.60	3.8	38.9	147.8	20	76	2956
S1.60/F1.70	3.1	43.1	133.6	5	16	668
S1.70/F1.80	2.3	55.8	128.3	1	2	128
S1.80/F1.90	2.6	56.6	147.2	0	0	0
S1.90/F2.00	3.0	68.8	206.4	0	0	0
S2.00	28.9	83.6	2416.0	0	0	0
				Σ	4611	53421

$$\text{predicted yield} = \frac{\text{total mass of floats}}{\text{mass of feed}} \times 100 \tag{15.45}$$

and since the sum of column 6 $= \dfrac{\text{total mass of floats}}{\text{mass of feed}} \times 10000$

$$\text{then Predicted yield} = \frac{\Sigma(6)}{100} = 46.11\% \tag{15.46}$$

and $\text{Predicted ash} = \dfrac{\text{total mass of floats ash}}{\text{total mass of floats}} \times 100$

$$= \frac{\Sigma(7)}{\Sigma(6)} = \frac{53421}{4611} = 11.6\% \tag{15.47}$$

The theoretical yield is given by the cumulative sum of the floats up to the specific gravity of separation. In the above example, this is at 1.50 S.G. Therefore:
Theoretical Yield = Σ(2) to S.G. 1.50 = 49.9 % $\tag{15.48}$

The Theoretical Ash is given by the sum of the floats mass x ash up to the specific gravity of separation. In the above example:

$$\text{Theoretical Ash} = \frac{\Sigma(4)\text{to SG}1.50}{\Sigma(2)\text{to SG}1.50} = \frac{539.3}{49.9} = 10.8\% \tag{15.49}$$

The actual yield, M_{FT}, is found from the expression:

$$M_{FT} = \frac{A_R - A_F}{A_R - A_C} \times 100 \tag{15.50}$$

where A_R = ash of total refuse,
A_F = ash of total feed and
A_C = ash of clean coal.

15.7.4. Sink-Float Alternatives

Because of the importance of washability and sink-float analysis to the coal industry and the health hazards associated with organic liquids, considerable effort is being aimed at alternatives to the organic liquid method. To determine the partition curve of a gravity separation unit, density tracers may be used. These are plastic particles manufactured to precise density such as 0.005 SG units [24]. These tracers are available in cubic shape from 1 to 64 mm or as crusher particles to simulate real ore with sizes from 0.125 to 32 mm or more. Density ranges are from 1.24 to 4.5 S.G. and can be colour coded or made magnetic or fluorescent for ease of recovery. A range of tracers of different density and size are added to the unit feed and retrieved from the floats and sinks fractions. The ratio of numbers in the floats and feed will give the partition coefficient.

For an alternative to the sink-float analysis, the Julius Kruttschnitt Mineral Research Centre (JKMRC) have developed an automatic gas pycnometer in which the dry density of individual particles is determined by separate mass and volume measurements [25]. The instrument is capable of analysing 30 particles a minute. A sink-float data analysis requiring about 3000 particles can be obtained in 100 minutes.

15.8. Problems

15.1

Calculate the terminal velocity difference between hematite and quartz particles at a particle size of 150 microns and 50 microns. Comment on the differences and hence discuss the limitations of normal gravity separation devices and how these might be overcome.

Density of hematite = 5000 kg.m^3
Density of quartz = 2600 kg/m^3
Density of water = 1000 kg/m^3

15.2

Plastic tracers of 2 mm size were added to the feed of a dense medium cyclone. The number and density of each tracer added and retrieved in the underflow are given below. Determine the separating density of the cyclone by plotting the Tromp curve.

Tracer density	number of tracers in the feed	number of tracers in the sinks
2.7	10	0
2.8	10	0
2.9	50	1
3.0	100	16
3.1	300	241
3.2	100	98
3.3	100	99
3.53	300	299

15.3

Cost studies have shown a favourable financial return from using dense media separation to pre-concentrate gold ore waste dumps comprising + 1mm material. The following laboratory results have been obtained.

Head Grade	S.G.	Cum. mass % Sinks	Cum. Au (g/t)
1.15	2.875	21.99	5.04
	2.900	16.33	6.63
	2.925	11.66	9.15
	2.950	9.11	11.51

1. What would be the separation density required to obtain a gold recovery of at least 95%.
2. What type of medium could be used to achieve this density.
3. What is the percentage of near gravity material at the cut density and hence the difficulty of separation.

15.4

Specific gravity analysis of size fractions of the feed to a dense medium cyclone are presented in the table below.

Discuss the separation of the size fractions by the cyclone with particular reference to:

1. Sharpness of separation
2. Specific gravity of separation and
3. Ash of clean coal

Comment on the variation of floats ash with separating density and the variation of sharpness of separation with the amount of near gravity material (% of material within ± 0.10 S.G. units of the S.G. of separation).

12 x 9.5 mm: 15.2 %

Specific gravity	Percent		Cumulative percent	
	Mass	Ash	Mass	Ash
Float-1.28	5.9	1.8	5.9	1.8
1.28-1.30	30.8	3.5	36.7	3.2
1.30-1.35	32.1	7.6	68.8	5.3
1.35-1.40	8.5	13.5	77.3	6.2
1.40-1.45	3.3	18.9	80.6	6.7
1.45-1.50	1.4	24.1	82.0	7.0
1.50-1.60	1.6	30.4	83.6	7.4
1.60-1.70	0.9	38.9	84.5	7.8
1.70-1.80	0.8	45.1	85.3	8.1
1.80-Sink	14.7	84.9	100.0	19.4

6.3 x 2.3 mm: 41.3 %

Specific gravity	Percent		Cumulative percent	
	Mass	Ash	Mass	Ash
Float-1.28	11.1	1.3	11.1	1.3
1.28-1.30	33.0	2.8	44.1	2.4
1.30-1.35	27.6	6.8	71.7	4.1
1.35-1.40	9.0	12.2	80.7	5.0
1.40-1.45	3.6	17.3	84.3	5.5
1.45-1.50	1.2	22.0	85.5	5.8
1.50-1.60	1.5	28.3	87.0	6.2
1.60-1.70	0.8	37.1	87.8	6.4
1.70-1.80	0.6	42.0	88.4	6.7
1.80-Sink	11.6	83.7	100.0	15.6

1.18 x 0.6 mm: 1.2 %

Specific gravity	Percent		Cumulative percent	
	Mass	Ash	Mass	Ash
Float-1.28	3.3	1.2	3.3	1.2
1.28-1.30	40.1	1.7	43.4	1.7
1.30-1.35	24.3	5.7	67.7	3.1
1.35-1.40	8.3	11.3	76.0	4.0
1.40-1.45	4.2	15.7	80.2	4.6
1.45-1.50	1.8	19.5	82.0	4.9
1.50-1.60	1.9	25.2	83.9	5.4
1.60-1.70	0.9	34.3	84.8	5.7
1.70-1.80	0.5	39.1	85.3	5.9
1.80-Sink	14.7	82.3	100.0	17.1

Distribution, percent to washed coal
(specific gravity fraction):

	12 x 9.5 mm	6.3 x 2.3 mm	1.18 x 0.6 mm
Float-1.28	99.8	99.4	98.8
1.28-1.30	99.5	99.4	99.4
1.30-1.35	98.1	98.5	98.7
1.35-1.40	79.8	92.1	96.9
1.40-1.45	12.8	57.1	92.7
1.45-1.50	2.2	16.6	81.7
1.50-1.60	0	3.2	49.1
1.60-1.70	0	2.1	12.9
1.70-1.80	0	0	4.7
1 .80-Sink.	0	0	2.9

15.5

Calculate the mass ratio of solid to liquid to make up a dense media of 3.1 S.G. using galena
(S.G. 7.4) as the solid and bore water (S.G. 1.1) as the liquid.

15.6

What material could be used, from the following list (material/SG), to achieve a medium
density of 2800 kg/m^3 ? (and avoiding viscosity problems)

magnetite (5.2)	ferrosilicon (7.1)	lead shot (11.4)
galena (7.5)	quartz (2.6)	pyrite (5.0)
mill scale (4.95)	barites (4.5)	

15.7

A sink-float analysis is performed on a sample of drill core from a coal deposit. The results
are given below.
What is the best possible yield and grade that could be expected from this deposit using a jig
washer? Compare this with the theoretical yield and grade

SG	Mass %	Assay %	SG	Partition coefficient
1.30	6.9	5.0	1.30	99.2
1.35	9.7	7.1	1.35	97.7
1.40	10.4	8.2	1.40	89.3
1.45	15.7	9.6	1.45	79.6
1.50	17.2	10.8	1.50	32.1
1.55	14.1	18.7	1.55	18.5
1.60	9.8	33.2	1.60	10.9
1.70	5.1	40.1	1.70	8.5
1.80	2.1	45.9	1.80	3.9
1.90	1.5	53.2	1.9	2.3
2.0	2.0	65.1	2.0	0.9
+2.0	5.5	79.5		

15.8

A number of plastic tracers of different density are added to the feed to a JIG separator. The FLOATS and SINKS are sampled and as many of the tracers as possible are recovered. From the data below determine the partition coefficient for the jig and then determine the density of separation for the jig by plotting a Tromp Curve.

S.G. of tracer	Number of tracers		
	in feed	in heavy fraction	in light fraction
1.5	10	0	10
2.0	10	1	7
2.5	10	2	6
3.0	10	4	5
3.5	10	7	3
4.5	10	9	0
5.0	10	10	0
6.0	10	10	0

15.9

A representative sample of a crushed hard rock cassiterite (SnO_2) deposit is subjected to a sink-float analysis using magnetohydrostatics. The results are given below. From this information and the partition coefficients of the Jig from problem 15.8, determine the actual yield of concentrate (SINKS) and the grade (% SnO_2) expected for this ore and a jig concentrator.

Compare this ACTUAL yield with the THEORETICAL yield (obtained with a perfect separator).

SG	Mass %	Assay % SnO_2
F2.00	9.5	0.001
S2.00-F2.50	9.7	0.01
S2.50-F3.00	13.4	0.01
S3.00-F3.50	17.8	18.8
S3.50-F4.00	18.8	39.1
S4.00-F4.50	9.8	54.3
S4.50-F5.00	6.4	66.2
S5.00-F5.50	3.3	75.6
S5.50-F6.00	2.8	83.4
S6.00-F6.50	1.5	86.9
S6.50-F7.00	2.0	95.3
S7.00	5.0	99.5

5.10

If an ore contains a valuable mineral of density 4500 kg/m³ and a gangue of density 2800 kg/m³ discuss the likely success of separation using gravity separation in potable water (density 998 kg/m³) and bore water (density 1290 kg/m³)? The mean particle size is 100 microns.

REFERENCES

[1]   A.F. Taggart, Handbook of Mineral Dressing, John Wiley and Sons, New York, 1945.
[2]   R.O. Burt, Gravity Concentration Technology, Developments in Mineral Processing, volume 5, Elsevier, Amsterdam, 1984.
[3]   W.E. Dietrich, Water Resources Research, 18 No.6 (1982) 1615.
[4]   J.A. Jiménez and O.S. Madsen, J. Waterways, Port, Coastal and Ocean Engineering, 2003, pp. 70-78.
[5]   G.A. Vissac, Transactions AIME, Mining Engineering, (1955) 655.
[6]   H.L. Lovell and P.T. Luckie, in Coal Preparation, J.W. Leonard (ed), AIMME, New York, 1979, pp. 9.92-9.99.
[7]   G. Agricola, De Re Metallic, H.C.Hoover and L.H. Hoover (trans.), Dover, New York, 1556.
[8]   A.H. Gray, Proceedings, The AusIMM Annual Conference, Ballarat, 1997, pp. 259-265.
[9]   N. Moony, and S. Gray, SME Annual Meeting, Orlando Florida, Pre-print 98-184, 1998, pp. 1-7.
[10] A.W. Deurbrouck and E.R. Palowitch, in Coal Preparation, J.W. Leonard (ed), AIMME, New York, 1979, p. 10.48.
[11] R.O. Burt and D.J. Ottley, International Journal of Mineral Processing, 1 (1974) 347.
[12] R.O. Burt, International Journal of Mineral Processing, 2 (1975) 219.
[13] Outokumpu 2005, Retrieved:December 19, 2005 from http://www.outokumputechnology.com/19147.epibrw.
[14] Heavy Liquids 2005(a), Retrieved:December 20, 2005 from http://www.heavyliquids.com/product_LST/hl.htm, http://www.heavyliquids.com/product_LST/faq.htm#1
[15] Chem Alert II, Chemical Safety Management Services software, Risk Management Technologies, 2005.
[16] J.M. Currie, Unit Operations in Mineral Processing, Colarado School of Mines, 1973.
[17] F.J. Fontein and C. Dijksman, in Recent Developments in Minerals Dressing, Institute of Mining and Metallurgy, London, 1952, p. 229.
[18] M. Sokaski, M.R. Geer and W.L. McMorris, in Coal Preparation, J.W. Leonard (ed), AIMME, New York, 1979, pp. 10.3-10.39.
[19] H.F. Yancey, and M.R. Geer, Trans. AIMME, Mining Eng., (1951) 507.
[20] AS 4156.1 1994, Coal Preparation – Higher Rank Coal – Float and Sink Testing, Standards Australia, 1994.
[21] J.A. Herbst and J.L. Sepulveda, in Mineral Processing Handbook, N.L. Weiss (Ed), SME/AIME, 1985, pp. 30-48.
[22] C. Mills, in Mineral Processing Plant Design, A.L. Mular and R.B. Bhappu (eds), Chapter 18, SME/AIME, 1980, pp. 404-426.
[23] Bird, Proceedings of the Third International Conference on Bituminous Coal, Pittsburgh: Carnegie Institute of Technology, 1931.
[24] Partition Enterprises 2005, Retrieved:December 23, 2005 from http://www.partitionenterprises.com.au/density.html
[25] JKTech 2005, Retrieved: December 23, 2005 from http://www.jktech.com.au/products/products/pycnometer/jk_pycnometer.htm

Chapter 16. Flotation

16. INTRODUCTION

In 2005 flotation celebrated its 100th anniversary since the first commercial introduction in Broken Hill in 1905. Since then flotation has grown to be the prime mineral processing operation for both hard rock and coal separations. Flotation is a separation process that has found prominence because of the need to treat complex or low grade ores where the average particle size for liberation is too small for efficient gravity separation or where the gravity difference between minerals is too small. Flotation relies on the surface of the valuable mineral being hydrophobic while the surface of the gangue minerals is hydrophilic. When the three phases, solid, liquid and gas are in contact, an equilibrium is established between the solid-air, solid-liquid and liquid-air interfacial tensions, γ_{SA}, γ_{SL}, and γ_{LA} as shown in Fig. 16.1.

The angle between the tangent to the curve at the three phase contact and the solid surface, at equilibrium, is the contact angle θ, and is taken as the angle through the fluid phase of higher density. In a flotation system this will be the water phase.

At equilibrium, the balance of the surface forces is given by the Young equation:

$$\gamma_{SA} = \gamma_{SL} + \gamma_{LA} \cos \theta \tag{16.1}$$

The balance of forces can be altered by any factor which changes any of the interfacial tensions. A new equilibrium position is established and a new contact angle formed. The contact angle is a measure of how well the air bubble spreads or wets the solid surface. A low contact angle (nominally less than 90°) indicates a hydrophilic surface while an angle greater than 90° represents a hydrophobic surface. A hydrophobic surface is one which will favour
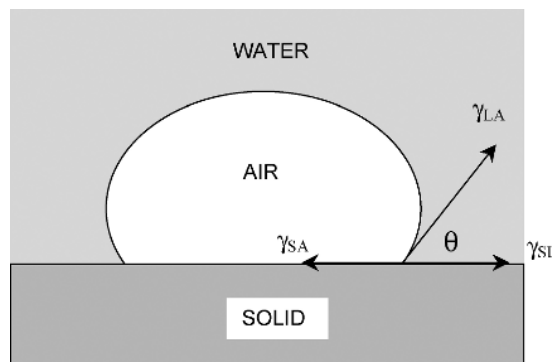
Fig. 16.1. Three phase contact between solid, liquid and air.

contact with air over water due to a lower free energy and hence will readily *stick* to an air interface if one is available. However in the flotation of mineral particles, a contact angle much less than 90° is still capable of sticking to an air bubble and hence floating.

The interfacial tension, γ_{LA}, is the surface tension of the liquid and is readily measured. The solid interfacial tensions or surface energies is mainly determined by the chemical bonds within the solid and are not easily measured. For example, the two forms of carbon, graphite and diamond, although having the same composition, have vastly different surface energies as a result of their different lattice structure (graphite 110 and diamond 5600 mNm^{-1}). For high surface energy solids (i.e. high γ_{SA}) such as metals and ionic solids such as sulphides and oxides, according to Eq. (16.1), the contact angle will tend to be small and the contact area between solid and air will be small and the liquid will wet the solid (hydrophilic or aerophobic).

If the solid surface energy is low, for example graphite, hydrocarbon solids such as coal, kerogen (hydrocarbon component of oil shale) or sulphur then the contact angle and contact area can be large and the solid will be hydrophobic or aerophilic. (In addition a hydrophobic surface needs to be non-polar or at least not capable of producing a polar surface by association with water molecules).

Since the measurement of the solid surface energy in air or water is difficult, the usefulness of Eq. (16.1) to make any prediction as to the floatability of a mineral is limited. If we consider a three phase contact as shown in Fig. 16.1 where the air bubble detaches from the solid surface then the solid/air interface is replaced by a solid/water and an air/water interface. The change in free energy accompanying this replacement of a unit area of the solid/air interface by a solid/liquid interface is given as:

$$\Delta G = (\gamma_{SL} + \gamma_{LA}) - \gamma_{SA} \tag{16.2}$$

Combining with Eq. (16.1) gives:

$$\Delta G = \gamma_{LA}(1 - \cos \theta) \tag{16.3}$$

where ΔG = the free energy change.

This equation contains the terms γ_{LA} and θ which are both easily measured. If the free energy change is negative then the separation of bubble and solid will occur and if the free energy change is positive then conditions are not favourable for separation to occur.

The free energy is often referred to as the *work of adhesion* between a bubble and the solid surface. An increase in contact angle would then indicate an increase in ΔG and hence the forces tending to hold the bubble and solid together is greater. But it must be remembered that this is a thermodynamic function expressing the maximum possible increase in free energy of the system resulting from the bubble-particle detachment, which is realised only when there are no other energy consuming effects such as deformation of the bubble surface, and where all gravitation effects are absent and the system is at equilibrium.

This hydrophobic characteristic occurs naturally on a small number of common minerals including graphite, sulphur, talc, molybdenite and coal. For solids which are naturally hydrophilic (which covers most minerals) the contact angle can be modified by changing the surface energy of one or more of the phases. If able to do so, surfaces will tend to contract to reduce surface area and hence reduce the surface energy. Alternatively if another component

is introduced into the system it will adsorb or concentrate at an interface if it reduces the surface energy of that interface.

The term *adsorption* refers to the existence of a higher concentration of any particular component at the surface of a liquid or solid phase than is present in the bulk. Adsorption is important in relation to the chemical reagents in flocculation and frothers and collectors in flotation. For flotation to be successful, the adsorption of chemicals onto the mineral surface must be performed selectively so that only the valuable mineral surface becomes hydrophobic while the gangue mineral surfaces become or remain hydrophilic.

16.1. Flotation Reagents

The chemicals used in flotation are divided into three classes:

1. *Collectors*: organic chemicals which make the surface hydrophobic and hence the mineral is capable of being collected in the process.
2. *Frothers*: organic chemicals which reduce the surface tension of the water to stabilize the bubbles into a froth layer at the top of the flotation cell to make concentrate removal easier.
3. *Modifiers*: organic or inorganic chemicals used to modify the slurry conditions to enhance the difference in surface chemistry between the valuable and gangue minerals.

16.1.1. Collectors

Collectors are generally heteropolar organics with a charged polar group and an uncharged non-polar group. The non-polar group is typically a hydrocarbon chain and in the beginning of the flotation process this hydrocarbon chain was provided in the form of oil. This oil flotation was phased out in the early 1920's by the development of more selective organics such as the xanthates and dithiophosphates. Oil in the form of kerosene or diesel is still used as the principal collecting agent in the coal and other industries. The process of collection can be illustrated by taking a clean glass plate and placing a few drops of water onto the surface as shown in Fig. 16.2

The water spreads out over the plate because glass is hydrophilic. In Fig. 16.3, a thin film of oil or grease is smeared over the plate surface and a few drops of water are again placed on the plate. In this case the water shrinks up into droplets as the oil film is hydrophobic. The thin film of oil has converted the hydrophilic glass surface to an hydrophobic surface.

Minimisation of the system free energy is the driving force for the reduction of the amount of high energy oil/water interface. Thus the water will shrink to minimize the contact area between the water and oil. When an air interface is available as shown in Fig. 16.4, the oil molecule, represented by a stick figure will concentrate at the air interface and extend into

Clean glass surface
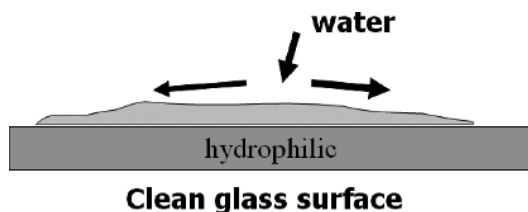
Fig. 16.2. Spreading of water over a hydrophilic clean glass surface.
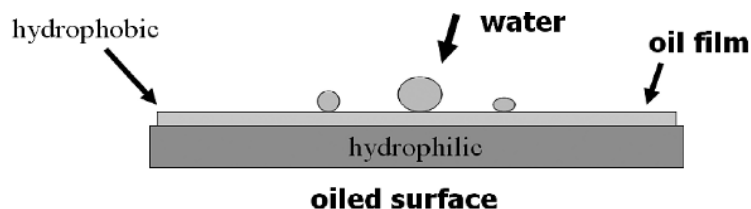
Fig. 16.3. Beading of water on an oiled hydrophilic surface.

the air phase as much as possible. The molecule is represented as aligning perpendicular to the air/water interface. The collectors used in flotation contain a non-polar hydrocarbon chair with a polar group on the chain. The polar group may be ionised and hydrophilic so that the organic may be water soluble. The polar group is also modified to be specifically attracted to certain minerals. At an air/water interface the hydrocarbon chain of the collector will stick out into the air phase at right angles to the interface while the hydrophilic polar group remains in the water phase (Fig. 16.3). If a suitable mineral surface is present and the polar group is attracted to the solid surface, a raft of collector ions will be adsorbed onto the mineral surface, effectively forming a thin film of oil on the mineral surface and hence making the surface hydrophobic, through adsorption rather than a physical smearing (Fig. 16.4B). If an air interface is now provided, in the form of an air bubble, the hydrocarbon chain will extend into the air phase and if the bond strength between the polar group and the mineral surface is strong enough, the particle will be lifted to the surface by the buoyancy of the air bubble (Fig. 16.4C).

Collectors may be non-ionic (hydrocarbon oils) or ionised. The ionised collectors are either cationic, (amines) or anionic (fatty acids or sulphydril compounds such as xanthates or dithiophosphates).
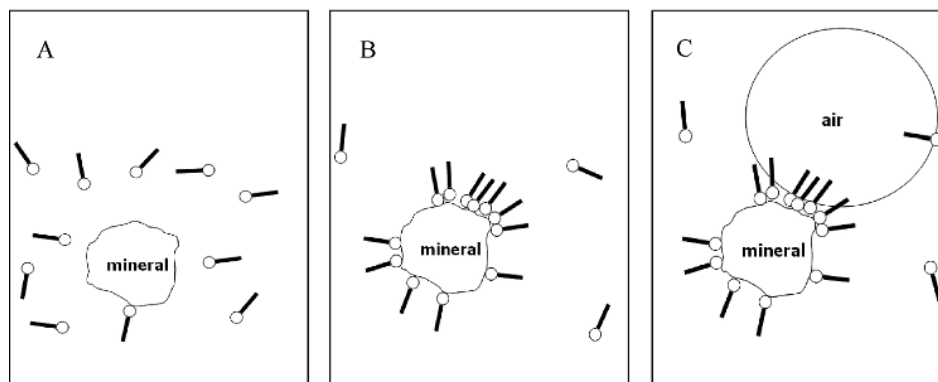
Fig. 16.4. A: Collector dissolved in the aqueous phase, B: Adsorption onto a mineral surface and C: attachment of an air bubble onto the hydrophobic surface.

16.1.2. Frothers

Frothers are surfactants, usually organic heteropolar compounds such as alcohols or polyglycol ethers. Due to the heteropolar nature, the frother adsorbs at the air/water interface and as a result, lowers the water surface tension. This has the effect of producing smaller bubbles and more importantly it stabilises the froth when it reaches the top of the slurry. If the bubbles burst when they reach the air/water surface then any minerals they carry will drop back into the slurry forming a scum at the surface. The prime role of the frother is to stabilise the froth formed at the interface long enough for the concentrate to be removed from the flotation cell. Once removed from the cell, the froth must break to allow the mineral particles to be re-pulped for further processing.

The effect of frother concentration on the surface tension of water is an initial rapid drop in surface tension before leveling out to a constant minimum value. The optimum frother concentration is not the amount which gives the minimum surface tension but in the region where the surface tension is capable of rapid change with concentration. This is the region of greatest froth stability.

When the thin liquid film at the bubble wall experiences an external stress and stretches locally, the increase in surface area produces a local decrease in surfactant concentration. This in turn increases the surface tension momentarily to allow the thin film to recover without rupturing. If there is no change in surface tension with local film thinning, for example if the liquid is pure or the frother concentration is in excess then the froth will be unstable. For excess frother concentration, all that will happen is the formation of very small bubbles which burst on reaching the pulp surface.

Frothers commonly used include natural chemicals like *pine oil, cresylic acid* and synthetic reagents such as *methyl isobutyl carbinol* (MIBC) and *polyglycol ethers*. Ideally frothers should possess little or no collecting properties and vice versa so that both functions can be controlled separately.

16.1.3. Modifiers

This class of reagents covers all chemicals whose principal function is neither collecting nor frothing. These may be further divided into *depressants, activators* and *pH regulators*.

A depressant is any chemical which inhibits or prevents the adsorption of a collector by a mineral particle and thereby prevents its flotation. An activator prepares the mineral surface to enhance the adsorption of the collector. pH regulators adjust the pulp pH to give optimum performance for a particular reagent and mineral ore. The common pH regulators are lime, soda ash and sulphuric acid.

Other reagents that may be used in specific cases include *dispersants* for removing clay slimes from mineral surfaces and *precipitants* for removing interfering ions from solution.

The main use of these modifying agents is in the differential flotation of a mixed ore. That is the successive removal of two or more valuable minerals from each other by flotation. For example the separation of each copper, lead, zinc and iron sulphides from a single ore is *selective flotation* whereas the flotation of the combined sulphides from the gangue is referred to as *bulk flotation*.

16.2. Flotation Equipment

The equipment used in flotation must provide an air interface for hydrophobic particles to become attach. The air interface is provided in the form of air bubbles introduced into a tank of slurry with agitation to provide an environment for maximum contact between particles and

bubbles. The flotation equipment can be divided into several categories according to the method of introducing the air into the cell. These include:

1. Mechanical (Sub Aeration)
2. Pneumatic
3. Vacuum
4. Electroflotation
5. Dissolved air flotation

The first two types of flotation machines are by far the most widely used in industry. Vacuum and dissolved air flotation relies on the precipitation of air dissolved in the water onto the hydrophobic particles. Electroflotation involves the electrolysis of water into fine bubbles of hydrogen and oxygen.

16.2.1. Mechanical Flotation Cells

These types of machines or cells consist of a highly turbulent region produced by an impeller, to provide the necessary agitation to keep the particles in suspension, disperse the air bubbles and bring about particle-bubble contact. In addition to this, the cell must contain a quiescent zone where the mineral-ladened bubbles can rise to the surface of the cell without loss of particles due to disruptive turbulence. A number of different cell designs have been developed to meet these needs. Removal of froth from the cell can either be by unassisted overflow or mechanical scraping by the use of paddles.

Continuous flotation cannot be performed in a single cell because of losses due to short circuiting of pulp between feed inlet and pulp outlet. It is therefore usual to use 4 to 12 cells in series. This also increases the residence time of the particles in the cells, giving the slow floating particles a chance to report to the froth layer. Cells in series can be interconnected with an overflow weir between cells, a partial baffle or no baffle at all. When no baffle is present it is known as a *hog trough* or *open flow* machine.

In the case of the partial baffle and no baffle cells, short circuiting of the cells can occur. These open flow machines were developed to handle larger tonnages in bulk flotation circuits.

16.2.2. Pneumatic Flotation Cells

In these types of cells, pulp and air are injected into the cell through a nozzle to produce intimate contact between air and particles. The air jet is used not only to provide aeration but also to suspend the particles and provide circulation. This usually means that an excessive amount of air must be used, and as a result these types of machines are not as common as mechanical cells in plants. Examples of pneumatic cells is the *Davcra* cell, the *Column* cell and the *Jameson* cell.

Column flotation is a pneumatic cell that uses a tall column of pulp rather than a traditional cell. Air is introduced at the bottom of the column and feed is introduced countercurrently near the top of the column. In column flotation air bubble agitation is not sufficient to keep large particles in suspension so that residence times are short in comparison to a bank of mechanical flotation cells. Originally developed in Canada in the 1960's as cleaning cells, this type of cell has become common in the flotation circuit of new plants, both as roughing and cleaning cells with diameters up to 4 or 5 m.

The majority of float cells in use are the mechanical type. The choice of which flotation cell to use is governed by both metallurgical performance and personal liking.

16.2.3. Laboratory Flotation Machines
The two most important requirements of laboratory flotation machines are reproducibility and performance similar to commercial operations. These two criteria are not always satisfied. The basic laboratory machines are scaled down replicas of commercial machines such as Denver, Wemco and Agitair. In the scale down, there are inevitable compromises between simplification of manufacture and attempts to simulate full scale performance. There are scaling errors for example in the number of impeller and stator blades and various geometric ratios. Reproducibility in semi-batch testing requires close control of impeller speed, air flow rate, pulp level and concentrate removal.

16.2.4. Flotation Cell Requirements
Regardless of which type of flotation cell is used to achieve mineral or coal flotation, a machine has two main requirements:

1. Suspension
2. Aeration

In suspension, it is essential that the impeller or air jet of the machine is capable of keeping the solids in the pulp in suspension. If the degree of agitation is inadequate then solids, particularly the largest particles will tend to settle out. Some settling out, for example in the corners of the cell, is not serious but significant sanding of the cell floor will upset pulp flow patterns within the cell and prevent proper contact between suspended particles and air bubbles. Particles not in suspension cannot make effective contact with air bubbles.

Effective aeration requires that the bubbles be finely disseminated, and that the air rate is sufficiently high, not only to provide sufficient bubbles to make contact with the particles but also to provide a stable froth of reasonable depth. Usually the type and amount of frother will be able to influence the froth layer, but the frother and air rate can both be used as variables.

The difficulty facing the flotation designer is that the cell performance is a strong function of the size of the particles to be floated, and that flotation feeds contain a wide range of particle sizes. For any given particle size, the effects of impeller speed and bubble diameter can be summarised as follows [1]:

1. If the impeller speed is too low, the particles are not maintained in suspension, but settle in significant quantities at the base of the cell.
2. If the impeller speed is too high, the turbulence in the cell is sufficient to rupture the bond between the particle and bubble, and so the recovery drops.
3. If the bubble size is too low, the bubble are too small to give sufficient buoyancy to the particles to lift them to the top of the pulp.
4. If the bubble size is too large, the fewer will be the number of bubbles created for a constant air flowrate. Since the overall rate of flotation depends on the number as well as the size of the bubbles, the recovery will drop.

This sets the boundaries for the optimum conditions of impeller speed and bubble size for flotation of any feed. If the feed size range is broad, then the optimum conditions for flotation of the coarse particles may be considerable different to the optimum conditions for the flotation recovery of the fine particles.

The pressure near the centre of the rotating impeller is lower than the ambient pressure at the same point if the rotating impeller were not present. This is due to the centrifugal pressure

gradients induced by the rotation. The pressure near the impeller may be so low as to be less than the hydrostatic pressure in the pulp so that a pipe placed near the impeller and open to the atmosphere may suck air into the impeller region. This is known as *induced air* and the practice of introducing air into the impeller region is called *sub-aeration*. Common practice in coal flotation is to use this induced air as the only aeration mechanism. In mineral flotation it is common to *supercharge* the air to provide a slight excess pressure to give a greater amount of air per unit volume of pulp.

The amount of air specified by cell manufacturers is usually in the range $0.5 - 2$ m^3 air per minute/m^3 pulp, and for use in coal flotation, the figure is towards the bottom end of this range.

The impeller behaves as a pump and circulates the slurry around the cell. The volumetric flowrate, Q_{VL}, for simple flat-bladed impellers is given approximately by [1]:

$$Q_{VL} = 0.75 \, \omega \, D^3 \quad \text{m}^3/\text{min} \tag{15.4}$$

where ω = the speed of rotation (revolutions/min) and
        D = the impeller diameter (m).

Flotation impellers would be expected to follow a similar equation, although a slightly different constant may be found. The circulation rates are very high. For example, a 14.2 m^3 cell with an impeller of diameter 0.84 m, rotating at 114 rpm, would have an internal circulation of 51 m^3 per minute, thus circulating the cell contents between three and four times a minute. The interaction of the liquid circulating in the cell due to the impeller and the air introduced into the impeller generates the size and distribution of bubbles found in the cell. The effect of air flowrate, Q_{VA}, on the formation of bubbles in the cell is described below. The ratio $Q_{VA}/\omega D^3$ is called the air-flow number. In general, for a fixed impeller diameter and speed:

1. At very low rates ($Q_{VA}/\omega D^3 < 0.02$), the air enters the core of the vortices formed behind the tips of the blades, with a strong outwards velocity component due to the pumping action. The bubble size and number is small.
2. At higher rates ($0.02 < Q_{VA}/\omega D^3 < 0.05$), cavities form behind the impeller blades, becoming increasingly large as the air rate increases. Bubbles form from the breakup of the trailing edges of the cavities. The bubble size and number increases.
3. Larger gas rates ($Q_{VA}/\omega D^3 > 0.05$) the impeller FLOODS. The gaps between the blades are blinded by large slugs of air which form very large bubbles.

As the air rate continually increases, the power consumption decreases, because an increasing proportion of the space in the impeller is occupied by air. Increasing the air rate leads to a lower liquid circulation rate, to the extent that the suspended particles may settle out. The general behaviour of the power ratio (the ratio of power consumed in the cell to the power consumed with no air flow) versus the air-flow number is shown in Fig. 16.5.

The onset of flooding coincides with a sudden drop in the power consumption, and is influenced somewhat by impeller design. For best operation a cell should operate well below the flooding gas velocity. Flooding results in very large bubbles, which are of little value for flotation. For example it is found that a reduction in air flow to an induced air flotation cell by closing off part of the air intake can substantially improve the recovery.
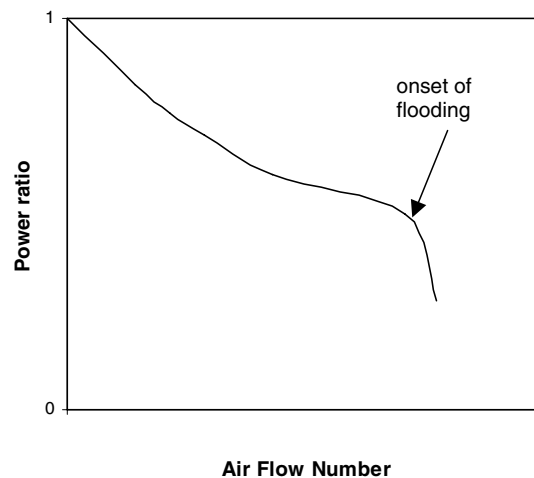
Fig. 16.5. Variation of power ratio with air flow rate.

16.3. Flotation Circuits

Flotation is carried out as a continuous operation in a series or bank of cells. This increases the floating time, allowing ample opportunity for particle-bubble attachment to occur. The residence time of particles in the bank of cells range from 5 to 15 minutes. The rate at which the particles float will depend on particle composition, pulp density, particle size and degree of turbulence in the cell. The arrangement of a number of cells in series allows the collection of different products from the various cells. For example, liberated particles in general float more rapidly than composite particles so that a high grade concentrate can be collected from the first few cells in a bank and froth from the remaining cells can be collected as a middling concentrate.

Quite often the grade of concentrate recovered from a single stage of flotation is not high enough and requires re-floating in one or more stages of flotation referred to as *cleaner* or *recleaner* stages. The series of cells that produce the initial concentrate is called the *rougher* stage and any subsequent retreatment of the rougher tailings is referred to as *scavenging*. The scavenger section of the flotation circuit is given higher reagent dosages and long flotation time to float as much valuable mineral as possible and maximise recovery. On the other hand the cleaner stage experiences milder flotation conditions of lower pulp density and lower reagent concentrations to reduce entrainment in the froth and to ensure only the high grade particles will float. To maximise the grade from the cleaner cells, the residence times is generally shorter. For example, rougher and scavenger flotation might take 10 minutes and cleaner flotation, 3 minutes.

The concentrate product from the scavenger cells and/or the tailings from the cleaner or recleaner cells are usually low grade because of locked or composite particles and physically entrained gangue minerals. Also it may contain free valuable mineral particles, present due to physical entrainment, odd shape or size or surface contamination. These low grade products maybe retreated by a re-grind stage and further flotation. The details of the regrinding practice depend largely on the ore characteristics. For example the presence of composites in

any concentrate (such as the rougher concentrate) in any great number would dictate that the concentrate be sent for re-grinding.

An example of some flotation circuits arrangements are shown in Fig. 16.6. A flotation circuit usually contains some provision for handling fluctuations in the flowrate of ore to the plant, either minor or major. Any minor fluctuations can be smoothed out by incorporating an agitator/conditioning tank between the grinding section and the flotation circuit. This is used to maintain a constant rate of feed to the flotation cells and to condition the feed with initial reagent prior to entering the cell. In addition, recovery is often improved by some degree of staged addition of reagents down the bank of cells. In some cases, additional conditioning time is provided by adding reagents to the grinding mill feed and/or discharge.

To accommodate large fluctuations of flow rate, for example if part of the grinding circuit is shut down for maintenance, the flotation circuit can be run in a number of identical modules operating in parallel. If the flow rate drops dramatically then this can be handled by shutting down one or more banks of cells. The more parallel modules built in, the more flexible the plant, but the greater are the control problems involved.

The number and size of cells required in a plant is determined by a number of factors, primarily the tonnage flow rate of material through the circuit. A large number of small cells gives greater flexibility and metallurgical performance whereas a small number of large cells of the same total capacity have a smaller capital cost, less floor area per unit volume and lower power consumption and lower operating costs. With the higher tonnages of lower grade ore now being treated by the minerals industry, the trend is towards large volume flotation cells. The choice of flotation cell size best suited to any specific application must consider the pulp flow rate, the number of parallel modules in the flotation section, the minimum number of cells in each row required to eliminate pulp short-circuiting and the required pulp residence time. Economic considerations favour large cells in rougher-scavenger operations since it is this part of the flotation circuit that handles the largest tonnages. Some of the largest cells available are the Outokumpu TankCells having a volume of 300 m^3 and Wemco's 250 m^3 Smartcell™.

Flotation feed is generally the ball mill cyclone overflow but in cases where some of the valuable minerals are liberated at coarse sizes and are recirculated in the cyclone underflow, these can be recovered before overgrinding by treating the cyclone underflow by flotation. A flotation cell designed to treat the coarse cyclone underflow is the Skimair® or Flash flotation cell. This is designed to handle a coarse feed at a relatively high % solids as experienced in the cyclone overflow. Since the fine particles have been removed in the cyclone overflow entrainment of non-floating fines is minimised and the flash flotation concentrate generally is suitable for the final concentrate.

16.4. Flotation Kinetics

16.4.1. Batch Flotation

The concentrate obtained from a batch flotation cell changes in character with time as the particles floating change in size, grade and quantity. In the same way, the concentrate from the last few cells in a continuous bank is different from that removed from the earlier cells. Particles of the same mineral float at different rates due to different particle characteristics and cell conditions.

The recovery-time curve of a batch test is generally of the form shown in Fig. 16.7. The recovery of any particular mineral rises to an asymptotic value R_∞ which is generally less than 100%. The rate of recovery at time t is given by the slope of the tangent to the curve at t, and
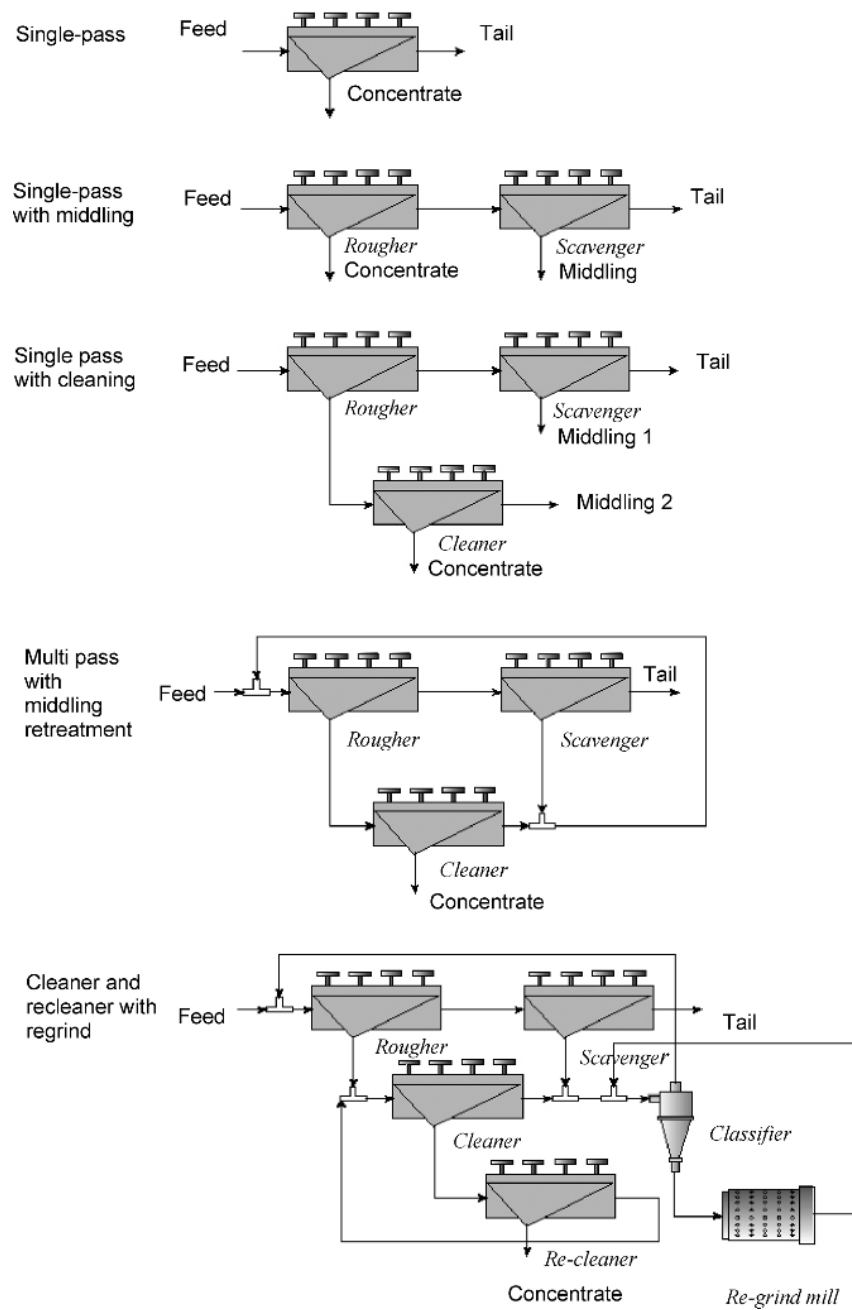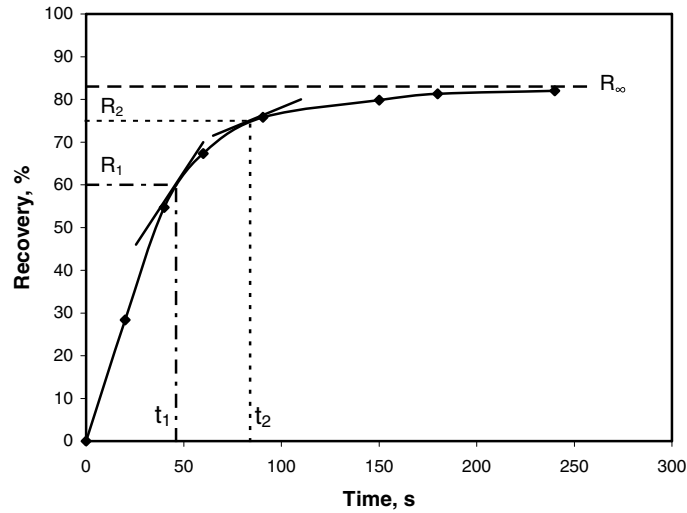
Fig. 16.6. Flotation cell arrangements.

Fig. 16.7. Time-recovery plot from batch flotation test.

the rate of recovery at time t_1 is clearly greater than the rate at time t_2. There is a direct relationship between the rate of flotation and the amount of floatable material remaining in the cell, that is:

$$\frac{\text{slope at } t_1}{\left(R_\infty - R_1\right)^n} = \frac{\text{slope at } t_2}{\left(R_\infty - R_2\right)^n} = k \tag{16.5}$$

or   Flotation rate $= k \times$ (concentration in the cell)^n (16.6)

The flotation rate is equal to the rate of change of concentration of floatable material in the cell, and Eq. (16.6) may be re-written as the differential Eq. (16.7).

$$-\frac{dC}{dt} = k C^n \tag{16.7}$$

This is the basic rate equation, in which the value of n denotes the order of the equation and k is the flotation rate constant.

16.4.2. First Order Rate Equation
Integration of Eq. (16.7) with n = 1 (first order), gives:

$$C = C_0 e^{-kt} \tag{16.8}$$

where C_0 = the concentration of valuable material in the cell at zero time, and
         C = the concentration of valuable material remaining in the cell at time t.

Taking the logs of Eq. (16.8):

$$\ln\left(\frac{C_0}{C}\right) = kt \qquad (16.9)$$

and if the experimental values of ln (C_0/C) are plotted against t, the graph should be a straight line of slope k if n = 1.

As the maximum recovery is seldom 100%, if the concentration of valuable material remaining unfloated in the cell after infinite flotation time is C_∞, then Eq. (16.9) is more accurately expressed as:

$$\ln\left(\frac{C_0 - C_\infty}{C - C_\infty}\right) = kt \qquad (16.10)$$

In terms of recovery, R, by definition is given by:

$$R = \left(\frac{C_0 - C}{C_0}\right) \qquad (16.11)$$

and after prolonged flotation times:

$$R_\infty = \left(\frac{C_0 - C_\infty}{C_0}\right) \qquad (16.12)$$

therefore dividing Eq. (16.11) by Eq. (16.12) gives:

$$\frac{R}{R_\infty} = \left(\frac{C_0 - C}{C_0 - C_\infty}\right) \qquad (16.13)$$

$$\text{or} \quad R = R_\infty\left(\frac{C_0 - C}{C_0 - C_\infty}\right) \qquad (16.14)$$

From Eq. (16.10):

$$\left(\frac{C_0 - C_\infty}{C - C_\infty}\right) = e^{kt} \qquad (16.15)$$

Inverting and subtracting from one gives:

$$1 - \left(\frac{C - C_\infty}{C_0 - C_\infty}\right) = 1 - e^{-kt} \qquad (16.16)$$

then: $\left(\dfrac{C_0 - C_\infty - C + C_\infty}{C_0 - C_\infty}\right) = \left(\dfrac{C_0 - C}{C_0 - C_\infty}\right) = 1 - e^{-kt}$ (16.17)

and substituting into Eq. (16.14) gives:

$$R = R_\infty \left(1 - e^{-kt}\right)$$ (16.18)

In the derivation of these equations, it has been assumed that the only independent variable has been the concentration of *floatable* material, and that everything else has remained constant such as the bubble concentration, size and size distribution, reagent concentrations, cell operation etcetera. If the operator were to alter the air setting, for example, half way through the test, the time-recovery plot would not be a smooth curve, and the same value of k would not apply before and after the air had been altered.

When other variables are not held constant, the rate equation may be written in general the form:

$$-\frac{dC}{dt} = k \prod C_i^{n_i}$$ (16.19)

where $\prod$ = the general product,

C_i = the concentration of any species which might affect the rate of flotation of the particular species in question, and

n_i = the order of the equation with respect to C_i.

For example, C_i might denote the concentration of floatable species, air, gangue and reagents. For any given flotation test, we may assume that the reagent concentrations etc. remain constant, and the equation simplifies to:

$$-\frac{dC}{dt} = k C_S^m C_A^n$$ (16.20)

where C_S and C_A are the concentrations of floatable particles and air bubbles, respectively.

k is thus a complex function involving reagent concentrations, particle and bubble sizes, induction times, flotation cell design, rate of froth removal, power input and previous treatments and will only be constant as long as these conditions remain constant. In a well-controlled laboratory experiment these may all be maintained reasonably constant, then by varying C_S and C_A in turn, the exponents m and n can be determined. Since the rate of aeration is usually also kept constant, Eqs. (16.19) and (16.20) simplify to Eq. (16.7).

For any given conditions, k is a quantitative measure of the probability of the particles of a species being recovered in the concentrate. It can be used to compare different reagent conditions in the same cell, or different flotation cells treating the same pulp. Each particle type in an ore (for example, chalcopyrite, pyrite, pyrrhotite and quartz) will have its own value of k in any test, and the ratios of these values are a quantitative measure of the selectivity of the operation.

k is not a measure of the recovery of a mineral in an operation. The recovery is a function of k and the time of flotation. But the rate constant, k, is the basic concept of the kinetic

approach to the flotation process, and is the factor whose accurate determination is necessary for all of the following developments in flotation.

16.4.3. Second Order Rate Equation

The flotation rate equation is given by Eq. (16.7). For second order flotation, n = 2, and integration over the limits $t = 0$, $C = C_0$ and $t = t$, $C = C$:

$$-\int \frac{dC}{C^2} = k \int dt \tag{16.21}$$

$$\left[\frac{1}{C}\right]_{C_0}^{C} = k\,t \tag{16.22}$$

$$\frac{1}{C} - \frac{1}{C_0} = \frac{C_0 - C}{C C_0} = k\,t \tag{16.23}$$

$$C_0 - C = C C_0 k\,t \tag{16.24}$$

$$C_0 = C(1 + C_0 k\,t) \tag{16.25}$$

$$\text{or } C = \frac{C_0}{(1 + C_0 k\,t)} \tag{16.26}$$

and to plot graphically this can be written as:

$$\frac{C_0}{C} = 1 + C_0 k\,t \tag{16.27}$$

For a maximum recovery of R_∞ less than 100%, then:

$$\frac{dC}{dt} = -k(C - C_\infty)^n \tag{16.28}$$

and on integration:

$$C = \frac{C_0 + C_\infty(C_0 - C_\infty)k\,t}{1 + (C_0 - C_\infty)k\,t} \tag{16.29}$$

It is important to always work in terms of floatable material rather than total material. That is, always take into account the value of C_∞ or R_∞ (see example 16.1). For graphical plotting, Eq. (16.27) becomes:

$$\frac{C_0 - C_\infty}{C - C_\infty} = 1 + (C_0 - C_\infty)k\,t \tag{16.30}$$

Therefore a plot of $(C_O - C_\infty)/(C - C_\infty)$ vs. t will yield a straight line if the flotation rate is second order (n = 2). An analogous equation can be written for recovery (from Eq. (16.5)):

$$\frac{dR}{dt} = k(R_\infty - R)^2 \qquad (16.31)$$

which on integration gives:

$$R = \frac{R_\infty^2 k t}{1 + R_\infty k t} \qquad (16.32)$$

from which:

$$\frac{t}{R} = \frac{1}{R_\infty^2 k} + \frac{t}{R_\infty} \qquad (16.33)$$

or $\quad \dfrac{1}{t} = \dfrac{k R_\infty^2}{R} - k R_\infty \qquad (16.34)$

is the form for graphical representation. Data for very short periods of flotation are required to be able to distinguish second order kinetics by this graphical method.

Example 16.1

A sample of coal is floated in a small laboratory cell using a kerosene collector (H1) and a dithiophosphate promoter (DP) in combination with H1. Concentrates were collected at 0.5 minute intervals up to 3 minutes then a final concetrate at 7 minutes. The concentrates were dried, weighed and then assayed by ashing. From the data given below, calculate the flotation rate constant of the coal for the two reagents conditions.

Collector H1			Collector DP + H1		
Time, min	Mass, g	Ash %	Time, min	Mass. g	Ash %
0	461.8	58.5	0	456.4	58.7
0.5	43.6	13.2	0.5	56.5	21.2
1.0	18.3	15.1	1.0	30.9	26.0
1.5	11.9	16.1	1.5	30.3	25.7
2.0	10.3	14.7	2.0	23.6	26.8
2.5	5.4	15.0	2.5	17.3	28.6
3.0	4.7	13.7	3.0	13.3	27.3
7.0	17.5	12.8	7.0	21.1	31.0
tail	350.1	72.6	tail	263.3	83.1

Volume of cell = 250 mL

Solution

Step1: Calculate the concentration of coal in the cell (test H1).

The percentage of coal in the cell is calculated from the ash content by assuming the % coal = 100 - % ash. This is not strictly correct but for this example it will be accurate enough. The initial concentration for the collector H1is then given as:

$$C_o = \frac{\text{mass of coal in the feed}}{\text{volume of cell}} = \frac{461.8 \times (100-58.5)}{250 \times 100} = 0.767 \text{ g/mL}$$

For the concentration remaining in the cell after the first half minute:

$$C = \frac{\text{mass of coal remaining in the cell}}{\text{volume of cell}} = \frac{\text{mass of coal initially} - \text{sum of coal floated up to time t}}{\text{volume of cell}}$$

$$C = \frac{[461.8 \times (100-58.5)] - [43.6 \times (100-13.2)]}{250 \times 100} = 0.615 \text{ g/mL}$$

similarly for float concentrates at 1.0 – 7.0 minutes:

Repeating the above calculations for the remaining H1 and DP/H1 tests gives:

Time mins	(H1) C g/mL	(DP/H1) C g/mL
0	0.767	0.753
0.5	0.615	0.575
1.0	0.554	0.484
1.5	0.514	0.394
2.0	0.479	0.325
2.5	0.461	0.275
3.0	0.444	0.236
7.0	0.383	0.178

Step 2: Estimate the infinite concentrations in each test.

Plotting the concentration versus flotation time gives the following graph:

From this plot, the values of C_∞ are estimated at 0.36 and 0.14 for the H1 and DP/H1 test respectively.

Step 3: Determine the order of the kinetics and determine the rate constants.

The concentration ratios are calculated as follows:

For float test H1:

At time t = 0.5 minutes,
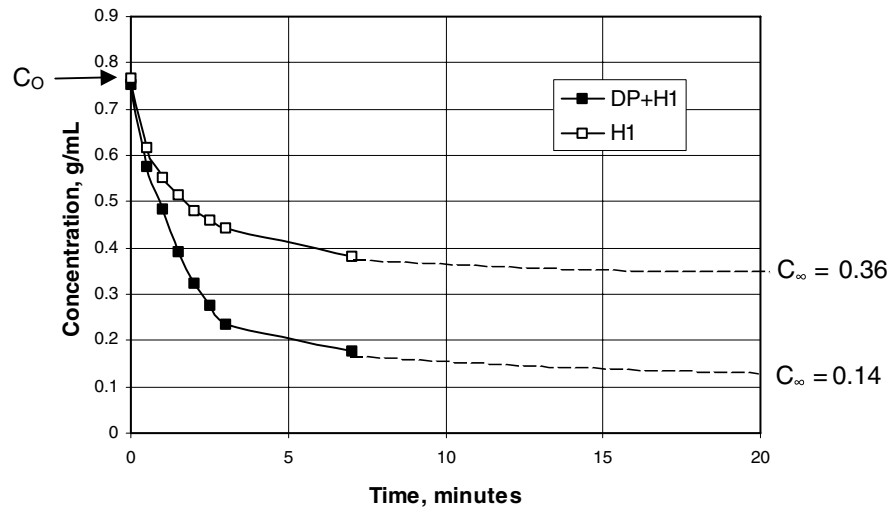
Decrease in cell concentration during the flotation tests

$$\frac{C_0 - C_\infty}{C - C_\infty} = \frac{0.767 - 0.36}{0.615 - 0.36} = 1.60 \quad \text{and}$$

$$\ln\left[\frac{C_0 - C_\infty}{C - C_\infty}\right] = \ln(1.60) = 0.47$$

Repeating the above calculations for the remaining H1 and DP/H1 tests gives the following table. The last two columns in this table are calculated on the basis of total coal in the cell rather than *floatable* coal.

Time mins	$\dfrac{C_0-C_\infty}{C-C_\infty}$	$\ln\left(\dfrac{C_0-C_\infty}{C-C_\infty}\right)$	C_0/C	$\ln(C_0/C)$
0	1	0	1	0
0.5	1.60	0.47	1.25	0.22
1	2.10	0.74	1.39	0.33
1.5	2.64	0.97	1.49	0.40
2	3.42	1.23	1.60	0.47
2.5	4.05	1.40	1.67	0.51
3	4.84	1.58	1.73	0.55
7	17.64	2.87	2.00	0.69

For first order, plot columns 1 and 3 according to Eq. (16.10) which will give a straight line of slope k. For second order, plot columns 1 and 2 according to Eq. (16.30) will give a straight line of slope $(C_0 - C_\infty)k$.
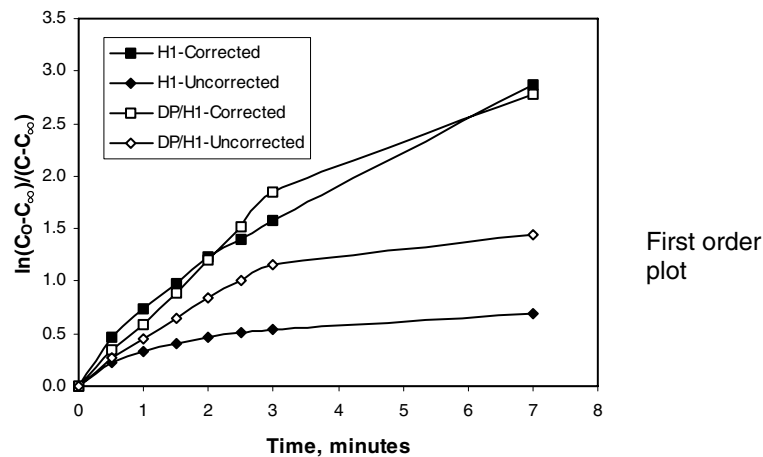
First order plot

The first order plot shows that when plotting the data according to Eq. (16.9) (uncorrected concentration) the DP/H1 combined reagent has a rate constant of approximately twice that of the H1 test. When applying the correction for unfloatable coal (cell contents at infinite time) the two reagents give a similar rate constant. Thus it is important in calculating the flotation rate constant to always consider the floatable material. The difference between the two reagents in this instance is not the effect on the rate of flotation of the coal but rather the effect on the infinite recovery which is 80% and 53% for the DP/H1 and H1 reagents respectively. The same effect of corrected and uncorrected concentrations is shown in the second order plot.

Neither the first order or second order plots show a perfect straight line over the whole timed concentrates. The coefficient of determination, r^2, is similar for both plots at 0.87-0.94 for the corrected data.
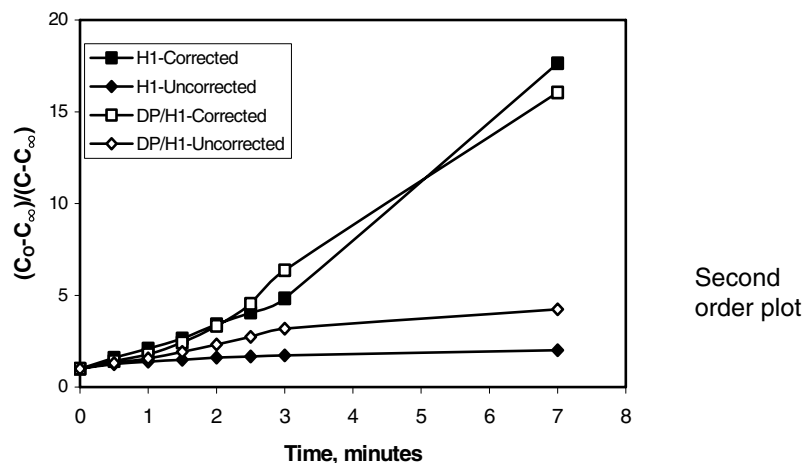
Second order plot

Using the first order plot, linear regression on the data gives:

k_{H1} = slope = 0.4628 min^{-1} for reagent H1 and
k_{DP} = slope = 0.4632 min^{-1} for reagent DP/H1

Using the second order plot, a linear regression on the data gives:

$$k_{H1} = \frac{slope}{(C_O - C_\infty)} = \frac{2.011}{(0.767 - 0.36)} = 4.94 \, min^{-1} \text{ and}$$

$$k_{DP} = \frac{slope}{(C_O - C_\infty)} = \frac{1.9237}{(0.753 - 0.14)} = 3.14 \, min^{-1}$$

16.4.4. Non-Integral Order

The rate equation can be considered, in general, to be somewhere between first order and second order, approaching first order for flotation of single minerals or in very dilute pulps, and approaching second order for low-grade ores or more concentrated pulps. This is represented by the equation:

$$k^i t = \frac{\dfrac{R^i}{R_\infty^i}}{1 - \left(\dfrac{R^i}{R_\infty^i}\right)} \left[1 - \frac{R_\infty^i}{R_\infty} \right] - \left(\frac{R_\infty^i}{R_\infty} \right) \ln \left[1 - \frac{R^i}{R_\infty^i} \right] \tag{16.35}$$

where R_∞ is the total mineral present of all species 'i'.

When only one mineral is involved or if the solid to liquid ratio is very low ($R_\infty^i = R_\infty$) then this equation simplifies to the first-order equation and if $R^i \ll R$, Eq. (16.35) reduces to a form of the second order equation. Thus Eq. (16.35) is the general equation describing the flotation process, based on the kinetic model of flotation.

16.4.5. Experimental Results

The confirmation of the order of the rate equation is usually obtained graphically as has been done by many investigators for both first and second order kinetics. It has been suggested [2] that a more sensitive test would be to investigate the effect of variation in floatable mineral concentration (that is, pulp density variation) on the time required for a 50% change in recovery. If the *half time* remains constant with different pulp densities then the rate equation would be first order, if the half time was not constant then higher order kinetics would be involved.

However, in the graphical determination of the order of the rate equation there is sufficient difference between the first and second order curves that provided the experiments are carried out accurately, it is not difficult to distinguish between first and second order or if in fact neither rate law holds.

These rate equations assume that the rate coefficient for each mineral species is constant. However, by considering different functions for the distribution of rate coefficients for the mineral species, the first order rate equation can by applied to most cases of experimental

batch data. Dowling et al [3] evaluated a number of first order batch flotation models available in the literature. Some of the models considered were:

1. The classical first order kinetic model described by Eq. (16.8) which assumes a monodisperse feed with particles of constant floatability. If the plot of ln (C_O/C) is not linear then either the rate is not first order or the floatability of particles is not constant. If the rate is first order but the floating particles in the pulp do not have identical properties, i.e., there is a continuous range of rate constants for the mineral being recovered, the integrated form of the rate equation for a semi-batch process becomes:

$$C = C_O \int_0^\infty \exp(-k\,t)\,f(k,0)\,dk \qquad (16.36)$$

where $f(k,o)$ represents a continuous distribution of rate constants.

The distribution of rate constants may arise from intergrowths of minerals or a distribution of particle sizes. The problem then is related to the accurate estimation of the distribution of rate constants. Different interpretations of this distribution of rate constants give rise to a number of first order rate models:

2. The Klimpel form of the first order equation is given by [4]:

$$R = R_\infty \left[1 - \frac{1}{k\,t}\left(1 - \exp(-k\,t)\right) \right] \qquad (16.37)$$

where k = rate constant representing the largest allowable value of a rectangular distribution.

The difference between the classical model and the Klimpel model is in the representation of the rate constant distribution as uniform or rectangular. A rectangular distribution is one in which the quantity is constant over a fixed interval. For example, the rate constant has a fixed or constant value over a limited property range. For low and high values of the property, the rate constant is zero. Compare this with the classical first order model where the rate constant is assumed to have a constant value for all property values.

3. Kelsall [5] proposed a flotation model incorporating two rate constants, describing a fast floating component and a slow floating component. The use of two rate constants was considered to give a better approximation to the distribution of particle floatabilities than could be obtained with a single rate constant. The mathematical description of the model as modified by Jowett [6], is given by:

$$R = (R_\infty - \phi)\left(1 - \exp(-k_F t)\right) + \phi\left(1 - \exp(-k_S t)\right) \qquad (16.38)$$

where ϕ = fraction of flotation components with the slow rate constant,
$\quad k_F$ = fast rate constant (min-1) and
$\quad k_S$ = slow rate constant (min^{-1}).

This model attempts to describe non linear rate data (log[C/Co] vs time) by the sum of two straight lines.

4. Another form of the distribution of rate constants is a modified gamma function proposed by Loveday [7] and Inoue and Imaizumi [8].
In terms of recovery, the model becomes;

$$R = R_\infty \left(1 - \left(\frac{k}{k+t} \right)^P \right)$$

(16.39)

The model has three parameters. The gamma distribution can be simplistically described as being made up of the sum of P exponential distributions.

5. Flotation results may be represented by an expression analogous to an equation describing the time concentration for a series of fully mixed reactors [9]. In recovery terms this may be expressed in a mathematical form, similar to the Gamma model:

$$R = R_\infty \left(1 - \left(\frac{1}{1 + \frac{t}{k}} \right) \right)$$

(16.40)

This model describes the first order time-recovery of a component from a monodisperse feed with an exponential distribution of floatabilities.

A spreadsheet fitting experimental kinetic batch data to the above first order models is available for downloading from http://wasm.curtin.edu.au/yand/downloads.html.

16.4.6. Continuous Flotation

If we consider a continuous, single-cell operation under steady state conditions then dC/dt = 0 and the batch rate equation breaks down. From a feed of constant quantity and quality the cell produces a concentrate and a tailing whose characteristics also do not change with time. For such a cell the rate constant (or specific flotation rate) is defined by Eq. (16.41), where $M_{S(C)}$ is the mass of solid concentrate, and $M_{S(T)}$ is the mass of solid tailing.

In terms of the fractional recovery in the single cell, assuming all of the mineral is floatable, (that is $R_\infty = 1$), then Eq. (16.42) is obtained.

$$k = \frac{\text{flotation rate (mass / unit time)}}{\text{mass of floatable material remaining in the cell}} = \frac{M_{S(C)} / t}{M_{S(T)}}$$

(16.41)

$$k \lambda = \frac{M_{S(C)}}{M_{S(T)}}$$

(16.42)

where λ = the nominal residence time of the pulp in the cell (cell volume/volume flow rate of tailings),
$M_{S(C)}$ = mass of solid in the concentrate, and
$M_{S(T)}$ = mass of solid in the tailing.

then $\quad 1+k\lambda \;=\; 1+\dfrac{M_{S(C)}}{M_{S(T)}} \;=\; \dfrac{M_{S(T)}+M_{S(C)}}{M_{S(T)}} \;=\; \dfrac{M_{S(F)}}{M_{S(T)}}$ $\qquad$ (16.43)

where $\;M_{S(F)} \;=\;$ mass of solid feed.

then the fractional recovery in the cell, R' (the recovery from the feed to that cell), is given by:

$$R^{'} \;=\; \dfrac{M_{S(C)}}{M_{S(F)}} \;=\; \dfrac{M_{S(C)}}{M_{S(T)}} \cdot \dfrac{M_{S(T)}}{M_{S(F)}} \;=\; \dfrac{k\lambda}{1+k\lambda} \qquad (16.44)$$

For several such cells in series, where the volume of concentrate recovered from each cell is small compared with the total flow, the fractional recovery in the first cell, from the feed to the first cell, will be:

$$R^{'}_{1} \;=\; R_{1} \;=\; \dfrac{M_{S(C)1}}{M_{S(F)}} \;=\; \dfrac{k\lambda}{(1+k\lambda)} \qquad (16.45)$$

The fractional recovery in the second cell from the feed to that cell (that is, from the tailings of cell 1) is also given as:

$$R^{'}_{2} \;=\; \dfrac{k\lambda}{(1+k\lambda)} \;=\; \dfrac{M_{S(C)2}}{M_{S(T)1}} \qquad (16.46)$$

The recovery from the cell 2 in terms of the original feed to cell 1 will be:

$$R_{2} \;=\; \dfrac{M_{S(C)2}}{M_{S(F)}} \;=\; \dfrac{M_{S(C)2}}{M_{S(T)1}} \cdot \dfrac{M_{S(T)1}}{M_{S(F)}} \;=\; \dfrac{k\lambda}{(1+k\lambda)} \cdot \left(1-R_{1}\right) \;=\; R_{1}\left(1-R_{1}\right) \qquad (16.47)$$

and the total recovery from N cells will be:

$$R \;=\; R_{1} + R_{1}(1-R_{1}) + R_{1}(1-R_{1})^{2} + \ldots + R_{1}(1-R_{1})^{N-1} \;=\; 1-\left(1-R_{1}\right)^{N} \qquad (16.48)$$

Substituting Eq. (16.45) into Eq. (16.48) we obtain:

$$R \;=\; 1-\left(1+k\lambda\right)^{-N} \qquad (16.49)$$

Eq. (16.49) is also obtained by substituting $t = N\, t_{R}$ into Eq. (16.18) where t_{R} is the effective residence time, given by:

$$t_{R} \;=\; \dfrac{\ln\left(1+k\lambda\right)}{k} \qquad (16.50)$$

This shows that under semi-batch conditions, the residence time for the same recovery as in a bank of N cells is N t_R. For a single continuous cell where N = 1, Eq. (16.49) can be written as:

$$\frac{R}{(1-R)} = k\lambda \qquad (16.51)$$

so that if the residence time is varied and the recovery measured, a plot of R/(1-R) vs time will give a straight line of slope k. The use of Eqs. (16.45) and (16.49) is illustrated in example 16.2.

Example 16.2

Consider the treatment of a very simple ore that contains 5 t/h of pyrite and 95 t/h of mineral quartz, and that the ore is fed to a bank of cells so that the retention time in each cell is two minutes. If we sample the feed, concentrate and tailings from any cell we may calculate the recovery of the two minerals in the cell from the feed to that cell. If the recoveries are calculated as:

R_{Pyrite} = 37.5% and
R_{quartz} = 3.8%

Substituting in Eq. (16.45) the rate constant is calculated as:

$$\frac{37.5}{100} = \frac{k\lambda}{1+k\lambda}$$

$$0.375(1+k\lambda) = k\lambda$$

$$0.375 + 0.375k\lambda = k\lambda$$

$$0.375 = k\lambda(1-0.375)$$

$$k_{pyrite} = \frac{0.375}{\lambda(1-0.375)} = \frac{0.375}{2 \times 0.625} = 0.30\,\text{min}^{-1}$$

and similarly, k_{quartz} = 0.02 min^{-1}

Using Eq. (16.49) the products of a bank of any number of cells can be calculated. For example, from six cells in series the recoveries from the feed will be:

$$R_{pyrite} = 1-(1+0.30 \times 2)^{-6} = 0.9404 \text{ or } 94.0\% \text{ and}$$

$$R_{quartz} = 1-(1+0.02 \times 2)^{-6} = 0.2097 \text{ or } 21.0\%$$

The tonnages of the two minerals in the concentrate will be:

$$Q_{pyrite} = Q_{feed(pyrite)} \times R_{pyrite} = 5.0 \times 94.0\% = 4.70 \, t/h$$

$$Q_{quartz} = Q_{feed(quartz)} \times R_{quartz} = 95.0 \times 21.0\% = 19.92 \, t/h$$

and the total concentrate mass $= 4.70 + 19.92 = 24.62 \, t/h$

and the grade of the concentrate will be:

$$grade = \frac{M_{pyrite}}{M_{feed}} \times 100 = \frac{4.70}{24.62} \times 100 = 19.1\% \, pyrite \, by \, mass$$

Similarly, the recovery of each mineral, and hence the total tonnage of concentrate and its grade, can be calculated for any change in feed rate (change in the value of λ in Eq. (16.49)).

Kinetic equations therefore appear to be suitable for at least some useful estimations in the plant. The model developed so far is based upon a rate equation of any order but, for their application, the value of n must be known. We must also know whether the value of n remains constant for all conditions of flotation, or whether we have to apply rate equations of different order in different circumstances.

Similarly, not only will different minerals have different values of k, but the same mineral will have different values of k under different conditions of reagent addition and cell operation. In fact k is used to determine the optimum conditions of reagent addition and cell operation. If simulations are to be developed for the purposes of prediction and control, it will be necessary to be able to predict the various values of k under different circumstances.

16.4.7. Laboratory Testing of Kinetic Relationships

Batch Testing

The technique involved in batch flotation testing to verify the kinetic model of flotation involves the collection of the concentrate over carefully timed intervals, drying, weighing, assaying each concentrate and the final tailing, calculating the values of C_0, C_∞ and several values of C at different flotation times, and plotting:

$$\ln\left(\frac{C_0 - C_\infty}{C - C_\infty}\right) \quad versus \, t \quad for \, first - order \quad or$$

$$\left(\frac{C_0 - C_\infty}{C - C_\infty}\right) \quad versus \, t \quad for \, second - order$$

The batch flotation technique, however has many disadvantages which can be summarised as follows:

1. The concentration of floatable material in the cell at any time t, is obtained only from the difference between the mass in the feed and the mass floated up to time t. This implies that material must be removed immediately it appears in the froth, otherwise it will appear as non-floated. This immediate removal is physically impossible in the early stages of the test when rapid flotation is occurring and when the most accurate data should be obtained. Towards the conclusion of the test, when C is approaching C_∞ the term $\ln (C_O - C_\infty)/(C - C_\infty)$ is subject to considerable error.

2. Rapid changing of concentrate trays in the early stages of the test is subject to high relative errors in timing.

3. The concentrate contains fluid from the cell, so that the pulp level in the cell is continually falling. Even if the pulp level, and hence the volume of pulp in the cell, can be measured the aeration and agitation characteristics of the cell may change with decreasing pulp volume. Thus the level of the pulp should be maintained constant by the addition of fluid to the cell.

4. The fluid removed with the concentrate contains a higher concentration of any surface active agent, particularly frother, than the pulp. The concentration of any such reagent in the pulp must therefore decrease with time. This can be made up by adding make-up water containing reagents dissolved in the appropriate amounts, but the determination of what these amounts should be is virtually impossible.

5. A further criticism of the batch procedure is the difficulty of denoting zero time. There is a time lag between turning the air on in a batch cell and the formation and removal of concentrate. Any time in a batch test, however, may be denoted as zero time, and it is far better to let the test proceed until froth removal is under control before taking experimental samples.

Better reproducibility of flotation results from batch cells has centred on improvements to the subjective process of froth removal. For serious kinetic studies, laboratory cells have been designed or modified to improve or eliminate the manual scraping of froth from the top of the cell. For example, the Australian Standard 2579.1 [10] for hard coal froth flotation testing specifies a modified Denver laboratory cell comprising a Perspex deflector block for pushing the froth around the impeller shaft to the front of the cell for easier, more convenient and more reproducible froth removal. In a similar manner, the Leeds flotation cell was developed to give accurate control over impeller speed, air-flow rate, pulp level and froth removal [11]. This cell design involves a stationary, slightly inclined froth deflector plate placed above the cell so that it just touches the top of the froth and deflects it forward over the cell lip. Automatic pulp level control is also incorporated into the designs.
Froth removal by the use of mechanical paddles are also used in laboratory flotation cells in an attempt to eliminate human bias in concentrate removal.

Steady-State Testing

For improved scale-up between laboratory measured rate constants and plant values, the laboratory test should be carried out in a continuous cell and ideally in a minimum of 2 cells in series. If the feed pulp to a continuous flotation cell is maintained constant in all respects, the cell will attain steady-state conditions rapidly (after the passage of 2-3 cell volumes). Thereafter the quantity and quality of the concentrate and tailing will not change with time, and they can be sampled accurately. Two methods of varying the solids concentration in the cell may be used:

1. Changing the feed pulp density or
2. Changing the feed rate.

Changing the feed pulp density immediately poses the problem of how reagent additions should be varied to provide an identical chemical environment from test to test. It seems inherently more reliable to start each test with an identical feed pulp, and to vary the feed rate to the cell.

The success of the steady-state method depends upon obtaining a representative sample of the pulp in the cell. If the cell acts as an ideal mixer, the new feed entering the cell is rapidly distributed, the pulp in the cell is uniformly mixed, and the tailing stream emerging is an accurate sample of the pulp in the cell in all respects. The mixing characteristics of flotation cells can be obtained using tracer techniques. These tests showed that the behaviour of water in a continuous cell indicated ideal mixing in some but not all cases. The mixing behaviour of the solids should be tested separately as water will tend to pass through a cell faster than the solids.

Once a continuous cell has settled down to steady-state conditions the product streams will not vary with time unless and until the feed changes in some respect. In a laboratory test, with limited amounts of feed pulp and agitation volume, a change if feed is inevitable.

If all of the requirements of the continuous technique can be met (constant feed, steady state separation, ideal mixing in the cell), it is far superior to the batch technique. The investigation of the steady-state condition can be carried out by analysing samples of the concentrate and tailing over consecutive time intervals. If they remain unchanged, the system may be considered to be in steady-state. The tailing, however, is to be taken as a sample of the pulp in the cell, and this can only hold if the cell is acting as an ideal mixer.

If an impulse of tracer is introduced into an ideal mixer and its concentration at time $t_0 = y_0$, it can be shown that its concentration at time t is given by:

$$y = y_0 \exp\left(\frac{-t}{\lambda}\right)$$

(16.52)

If the logarithm of the concentration y is plotted against t, a straight line will indicate ideal mixing and the slope of the line will be the reciprocal of the nominal residence time (Fig. 16.8).

For more than one cell in series, the residence time of particles in the bank will change. The residence time for a series on N cells is given by:

$$P(t) = \left(\frac{N}{t}\right)^N \frac{t^{N-1} e^{-\frac{Nt}{\lambda}}}{(N-1)!}$$

(16.53)

where $P(t)$ = the probability that particles will have a residence time t,
        N = number of tanks or cells in series,
        λ = the mean residence time.

The residence time distribution is shown in Fig. 16.9 where the mean residence time is 2 minutes. The curve for N = 1 corresponds to an ideally mixed cell as shown in Fig. 16.8.
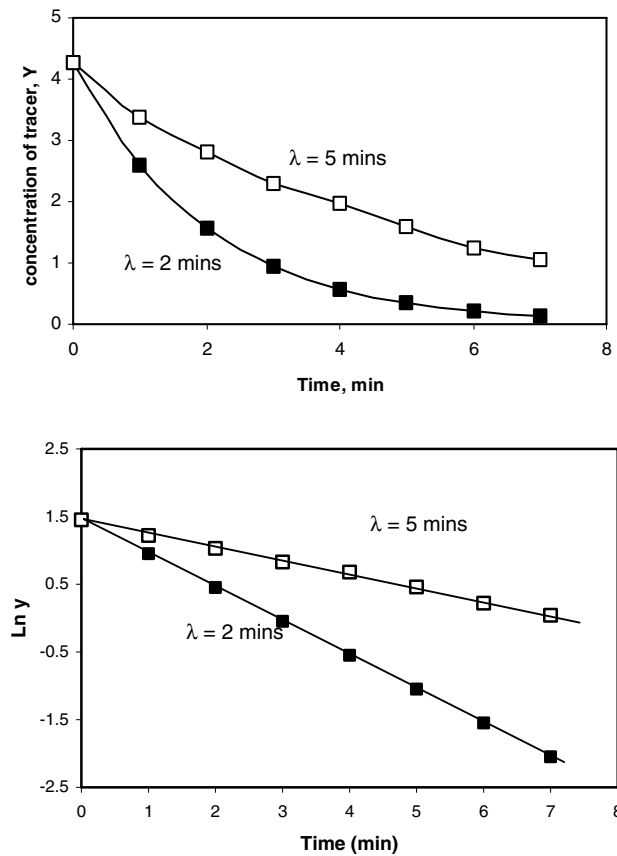
Fig. 16.8. Exponential decay in concentration of a pulse of tracer for an ideally mixed cell.

For a single cell of volume, V, most of the particles exit the cell straight away, though at extended times, beyond 5 minutes, there are still some particles exiting the cell. Increasing the number of cells to 2 and decreasing each cell volume to V/2 to maintain the same total volume shows that it takes a bit longer before particles of the tracer start to exit the last cell and more come out at about the same time. If the number of cells is increased to 50, and the cell size decreased to V/50, it takes even longer for particles to exit the last cell and the peak of residence times becomes sharper and approaches plug flow behaviour with the mean residence time of 2 minutes. Most particles have the same longer residence time and hence will have a greater chance to float in a large number of small cells compared to a small number of large volume cells.

Fig. 16.10 shows the results of a series of tests where the retention time is varied and recovery is plotted according to Eq. (16.51).
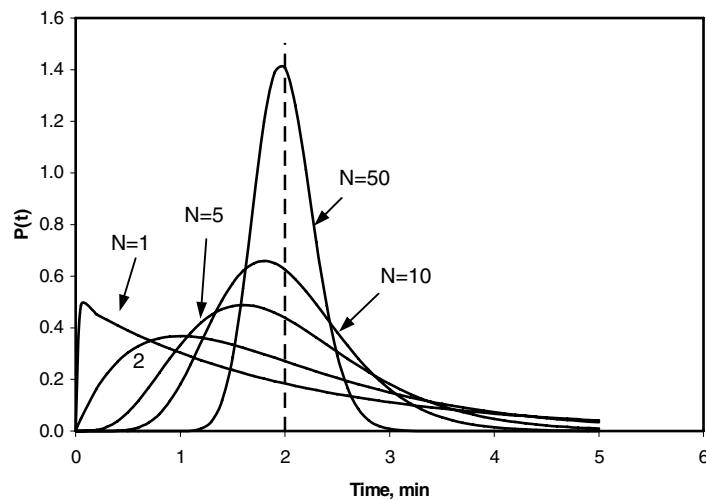
Fig. 16.9. Residence time distribution for a bank of n cells in series.

One graph shows the results corrected for the unrecoverable portion of the mineral and the other graph uncorrected. Both are good straight lines, indicating the suitability of a first order rate equation to describe the recovery of a mineral species in the flotation process. The slope of the graph is equal to the flotation rate constant and illustrates the importance of correcting for unfloatable material in determination of the true rate constant.
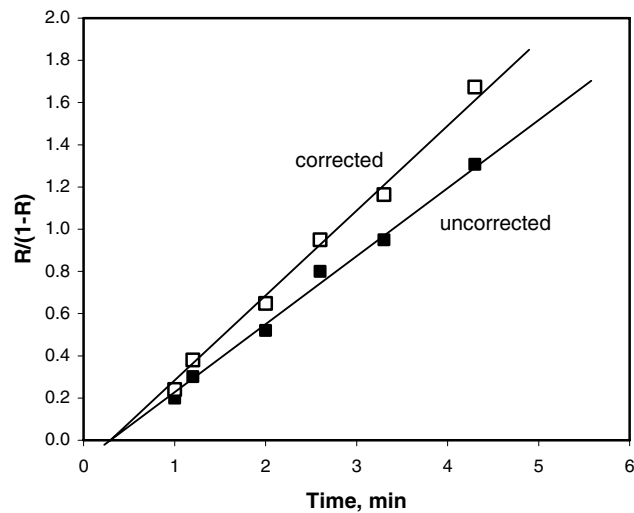
Fig. 16.10. Relationship between recovery and retention time.

The majority of researchers who have used the more accurate, steady-state method of testing have produced evidence supporting a first order equation. If, however, the micro-mechanisms of the flotation process and those factors that affect the flotation rates of particles are considered, the use of a first order equation to describe the flotation of all of the particles of a species is likely to be an oversimplification of the problem.

16.5. Factors Affecting the Rate of Flotation

In the kinetic model we have been considering the flotation process as analogous to a chemical reaction in which instead of colliding and reacting ions or molecules we have interaction between mineral particles and air bubbles. The flotation rate constant can be used to quantify the effect of numerous variables on the flotation process. This can be carried out in laboratory flotation machines with the knowledge that the scale-up of the laboratory batch rate constant may not be accurate though, in general, the trends in rate constant variation with changing flotation variables will be followed.

16.5.1. Impeller Speed

There are several factors of cell operation that are important in the determination of the flotation rates. If it is assumed that the collision of particles with freely moving bubbles is the dominant mechanism, and that bubble precipitation provides a favourable preliminary step to collision and adhesion, then for a given flow rate of air to a cell, an increase in impeller speed should cause more air solution and precipitation, and should break up the undissolved air into finer bubbles. This increases the rate constants of all of the mineral particles up to the point where the agitation is so intense that bubble-particle combinations are disrupted by the severe turbulence, and flotation rates fall again. This is illustrated in Fig. 16.11.

16.5.2. Air Flowrate

For a given impeller speed, an increase in the amount of air to a cell may be expected to increase the value of the rate constant for a species. Fig. 16.12 shows the effect of increasing
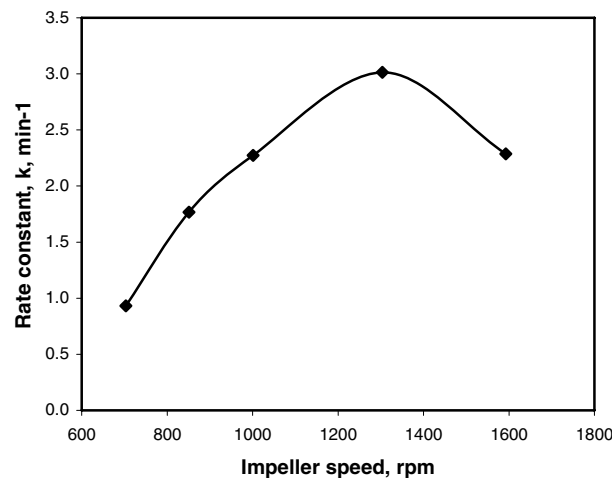
Fig. 16.11. Relationship between flotation rate constant k and impeller speed.
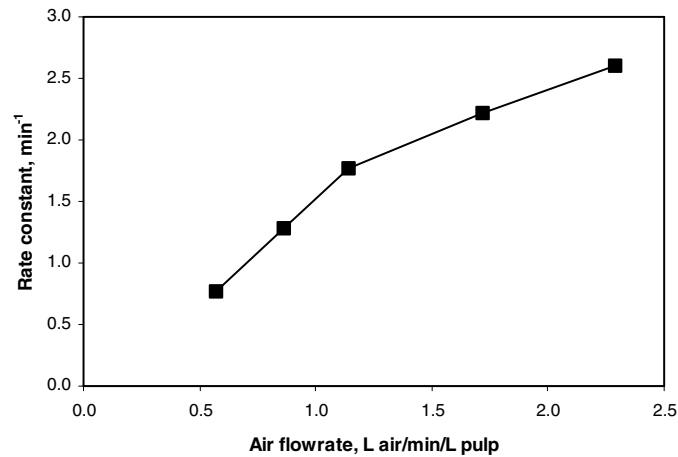
Fig.16.12. Relationship between flotation rate of quartz and air flow rate.

air concentration on the rate constant. As the volume of air increases the rate constant at first increases but at a particular air flowrate the slope of the graph decreases. When more air is forced through the impeller, its residence time in the shear zone is decreased, so that, although the concentration of air in the cell increases, this air is in the form of larger bubbles and the value of the rate constant remains almost unaffected.

16.5.3. Particle Size

The probability of collision and adhesion of a particle with a freely moving bubble must vary with the size of the particle because of:

1. its projected area
2. its inertia which will govern whether or not a particle may cut across flow lines around the bubbles
3. the possibility of its being thrown off the bubble even after adhesion has taken place due to disruptive turbulence
4. the extent to which collision may distort the bubble and alter the time of contact, and
5. the effect of particle size upon the induction time.

These factors all assume that the particles are homogeneously mixed in the cell. In cells treating coarse and dense particles, such as in flash flotation cells, the coarsest may be concentrated in the lower part of the cell, where their chances of collision with air bubbles are greatly reduced. In any given cell, considering the size of the bubbles produced and the disruptive forces present due to the turbulence of the pulp, there is a maximum size beyond which particles cannot be floated in mechanical cells. This maximum is about 420 microns with sulphide ores and is correspondingly coarser for a lighter material like coal. Once any particle becomes attached, its chances of being pulled off the bubble again decreases with decreasing size.

In practice, these physical effects mean that different sized particles of the same mineral, under the same chemical conditions, must be expected to have different rate constants. Fig. 16.13 and 16.14 shows the variation of flotation recovery and rate constant with particle size for the flotation of a coal sample.

For a sulphide float, the maximum rate constant relates to an intermediate size of about 35 microns, whereas for the less dense coal, the optimum size for maximum flotation recovery is 100–200 microns.
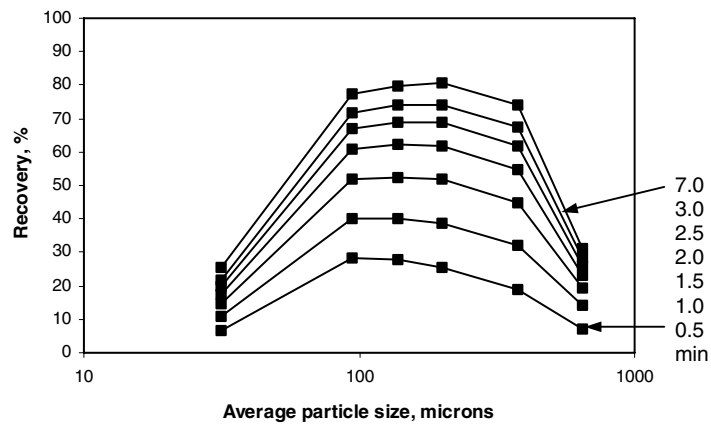
Fig. 16.13. Relationship between recovery and particle size for coal for increasing flotation time (data from [12]).
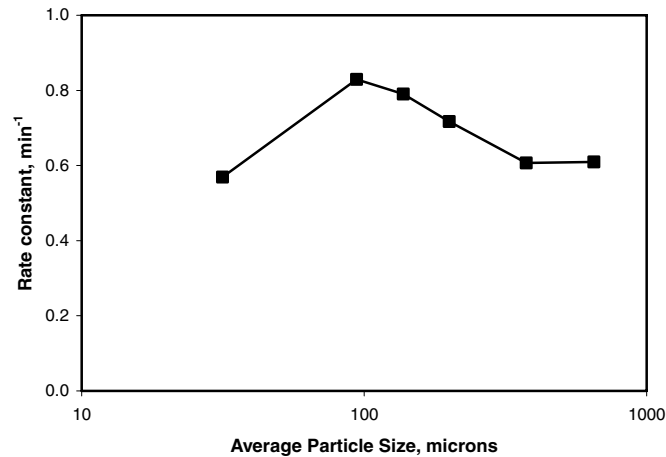
Fig. 16.14 Relationship between flotation rate constant k and particle size for coal (data from [12]).

16.5.4. Reagents

Collectors

The functions of a collector is to transform the hydrophilic surface of the freshly broken mineral particles to the hydrophobic state. The effectiveness of a collector may be measured by either:

1. contact angle between an adhering air bubble and the mineral surface, or
2. the induction time required for adhesion to take place.

Both of these parameters give a good indication of the probability of adhesion taking place upon contact. In any series of tests, the contact angle formed between an air bubble and a particle surface increases with collector concentration up to a maximum value, θ_{MAX}, which is characteristic of the collector, and to some extent, independent of the mineral. For example. ethyl xanthate gives a characteristic contact angle of 60° with several different minerals.

Other xanthates give a θ_{MAX} value which increase with the length of the hydrocarbon chain in the xanthate ion, varying from about 50° for methyl xanthate to about 95° for a 16-carbon chain xanthate. The iso-xanthates, those in which the hydrocarbon chain is branched rather than having all the carbon atoms in a straight line, have slightly higher maximum contact angle values for the same number of carbon atoms.

If collectors other than xanthates are used, the value of θ_{MAX} depends again on the length of the hydrocarbon chain, and not on the nature of the polar group in the collector ion. Therefore, other things being equal, θ_{MAX} for the ethyl mercaptan C_2H_5-SH is the same as θ_{MAX} for sodium ethyl xanthate.

In the laboratory it has been shown that the flotation rate constant increased with collector concentration up to a maximum, and this maximum rate constant varies with the type of collector; that is, the length of the hydrocarbon chain. Under laboratory conditions, the maximum contact angle requires a certain collector concentration and takes time for the adsorption of the collector to take place. In some systems, the maximum contact angle may not be achieved for an hour or more. In a continuous plant, this would mean that the longer the pulp remained in the circuit, the larger the contact angle would become and the higher would be the rate constant.

In a freshly ground ore, it has been shown that the surfaces of the particles of any one mineral differ from place to place. The exposed surfaces may be those of different crystallographic planes, or impurities may be present in very small amounts. The outcome is that the collector is not adsorbed evenly over the whole surface, but in patches. If more collector is added, it tends to be adsorbed on the same sites, rather than on clean areas, so that the equilibrium condition is has xanthate adsorbed in these areas, with bare patches in between. This can only result in the contact angle being smaller, or the induction time being greater, than that observed in the laboratory.

Although the actual values of the contact angles and induction times obtained in the laboratory are not generally applicable to plant conditions, the trends demonstrated will almost certainly be followed in the plant and it can be expected that the rate constants of the particles in a plant will vary according to these trends. In practice, the amount of xanthate added is considered to be sufficient to establish an equilibrium contact angle after only a very brief conditioning time and that xanthate addition is unlikely to be rate-controlling. If, however, starvation amounts of reagent are used to obtain selectivity, small changes in this quantity may have profound effects. The addition of xanthate to a copper ore for example

will not only affect the chalcopyrite but also the pyrite and pyrrhotite that may be present. If the amount of xanthate added is sufficient that the chalcopyrite is in the plateau region of response, we may expect that the extra xanthate may have little effect upon the rate constant for the chalcopyrite. The gangue sulphides, however, may not have been in their plateau regions, and the same increase in xanthate may have a great effect on the rate constants of these sulphides.

Any given xanthate addition produces its own values of k and C_∞ for any given mineral, and an increase in xanthate may alter both k and C_∞, resulting in very different recoveries and grades. Stage addition of reagents may have these same effects.

Frothers

The main function of the frother is to permit the formation of a froth that is sufficiently stable to hold the floated minerals so that they may be removed as a concentrate. It has other important effects on the flotation process that may be interpreted in terms of the flotation rate constants of the minerals.

The ideal froth is one in which the entrapped gangue particles drain but the valuable minerals are held for long enough to be removed into the concentrate launder. Frother type and frother concentration both affect the quality of the froth. Too little froth gives an unstable froth which tends to collapse; a little too much frother may cause the froth to be too tight, allowing very little drainage; more frother causes the froth again to become unstable. All these effects will alter the rates of recovery of the various mineral types and hence their effective flotation rate constants. Fig. 16.15 shows the effect of frother concentration on the flotation rate constant.

The concentration of frother also affects the physical conditions in the pulp. Increase in frother concentration causes the air to form finer and more numerous bubbles, increasing the rate constants of all the minerals. Bubbles in the presence of any surface-active agent tend to maintain their spherical shape, and are distorted by collision to a lesser extent. A high concentration of frother, if it is given sufficient time to be adsorbed and oriented at the liquid-gas interface, tends to prevent the adhesion of bubbles to hydrophobic mineral particles.

All of these factors affect the flotation rate constants of the mineral particles in a given flotation cell. Within the general operating limits, an increase in frother concentration will cause an increase in the rate constants of all the particles.

Modifying agents

Generally a collector and a frother is not sufficient in a flotation system. Even in an operation producing only one concentrate, the separation is not only one of a sulphide from a non-sulphide, for example, but also a sulphide from other sulphides. By the use of xanthate alone, the rate constants for the gangue sulphides will generally be of the same order as that of the chalcopyrite, and high grade concentrates can only be obtained by the addition of depressants, which greatly reduce the values of the rate constants of the gangue sulphides.

16.6. Application of Kinetic Equations

16.6.1. Practical Considerations

A simple case of the application of the kinetic rate equation for continuous flotation to the prediction of the products of a bank of cells was given in example 16.1. The use of this equation, however, depended on four simplifying assumptions, namely:
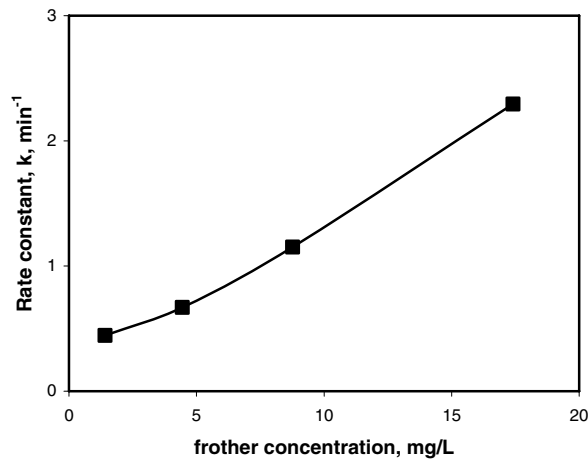
Fig. 16.15. Relationship between flotation rate constant k and frother concentration.

1.   the cells in the bank are identical in all physical respects. That is, no change in physical environment occurs which might have an effect on the values of the rate constants,

2.   the effective chemical environment of the particles remains constant throughout its flow through the bank. That is, no chemical change takes place which would affect the various values of the rate constant,

3.   the volume flow rates of the various concentrates from the cells are negligibly small, and

4.   the cells are all ideal mixers and are baffled so that no pulp from any cell may flow into the preceding cell.

Physical Differences from Cell to Cell

Individual cell volumes in a bank are usually equal, although in fully baffled cells, the heights of overflow weirs may be varied and may affect the volumes. In normal, steady-state operation, these volumes may be equalised by physical adjustment. Most of the other operating variables will differ to some degree from cell to cell, in particular cell impeller speeds, due to belt slippage, etc., impeller-stator clearances (in some types of cells), due to wear, and air flow rates, due to partial blockage of air passages. In addition, the rate of arrival of air bubbles at the pulp-froth interface can be expected to be a first order function of the concentration of air bubbles in the cell. For an ideally mixed cell, the pulp flowing out of the cell will contain air bubbles at a concentration equal to that in the cell. When flowing from one cell to the next, if the air does not escape from the pulp (in an ordinary overflow weir it probably will; in a cell baffled so that flow from cell to cell takes place below the pulp surface, it should not), the concentration of air bubbles must be expected to rise from cell to cell. The concentration of air in the Nth cell of a bank is given by:

$$C_{AN} = C_{A1}\frac{r^{N-1}}{(1-r)} \qquad\qquad (16.54)$$

where $r = \dfrac{k_A^{'}}{k_A + k_A^{'}}$

k_A = rate constant for air removal via froth (dependent on interfacial area/volume ratio)

$k_A^{'}$ = rate constant for air removal via tailings (dependent on pulp flow rate)

Chemical Differences from Cell to Cell

As the pulp flows down the bank of cells, surface active agents, particularly the frother, will be removed preferentially in the concentrate. This would be expected to reduce the values of the rate constant of all the particle types, although not necessarily by the same amount. The adsorption of xanthate on sulphides is practically irreversible so that a decrease in xanthate concentration would be expected to have little effect after adsorption has taken place. Inorganic reagents show little, or even negative adsorption at gas-liquid interfaces.

It is probable, therefore, that the only important change in chemical environment would be that of frother concentration, except in those cases when chemical reactions are incomplete when the pulp enters the first cell. This may be true of pH adjustment using lime and some depressing and activating reactions.

Variation in Residence Time

In most cases of flotation the volume flowrates of concentrate, at least from the first few cells in a bank of roughers, cleaners or recleaners are not negligible and the residence time of the remaining pulp must increase from cell to cell. In this case, if the residence time in the various cells are t_1, t_2, ... t_N, then:

$$R_1 = \frac{kt_1}{1+kt_1} \qquad\qquad (16.55)$$

$$R_2 = \frac{kt_2}{1+kt_2}(1-R_1) \qquad\qquad (16.56)$$

$$R_N = \frac{kt_N}{1+kt_N}\left(1-\sum_{i=1}^{N-1}R_i\right) \qquad\qquad (16.57)$$

The total recovery from the bank of N cells $= \displaystyle\sum_{i=1}^{N}R_i$

There is no algebraic simplification in this case and the expression must be solved numerically.

Mixing in the Cells

In a continuous cell, an ideal mixer can be indicated by a straight line. Fig. 16.16 shows the results of tracer tests carried out on fully-baffled rougher cells, using a KBr tracer, and is further evidence of ideal mixing in certain cells. Note, the use of a water soluble ion such as Br⁻ will only measure the mixing behaviour and retention time for the water in the cell.
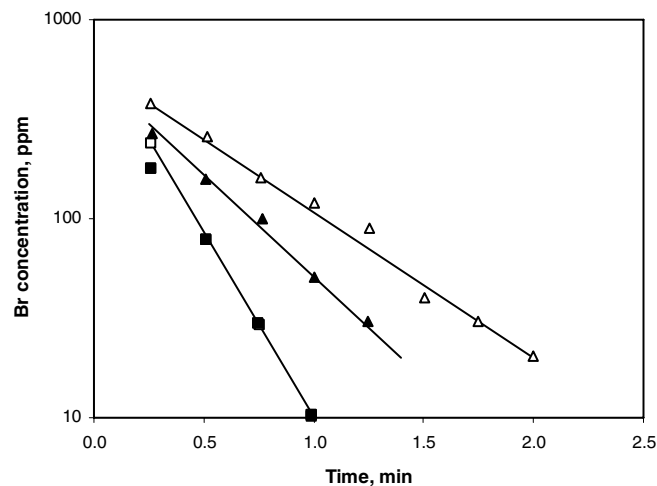
Fig. 16.16. Concentration of Br⁻ ion tracer as a function of time for a number of cells in a flotation
bank.

A pulse tracer test on an open flow machine indicated a nominal residence time in the bank
of less than half that expected from the ratio of the machine volume to the feed volume flow
rate. Since a heavy concentrate was removed, the retention time of the pulp would have been
expected to be even greater than this calculated figure. The most likely explanation is that a
major portion of the pulp is swept rapidly along the back of the trough (or the front,
depending on the direction of impeller rotation), and that the remainder of the available
volume is occupied by *back-mixed* pulp and possibly dead space. This test indicated that the
open flow machine does not behave as a series of discrete ideal mixers, and that the absence
of effective baffling causes the volume available for pulp treatment to be used inefficiently.

16.6.2. Basic Data for Process Simulation
In this section, we will consider only cells which are fully baffled, and in which ideal mixing
takes place and we also assume that a first order rate equation describes the flotation of any
particle species, and that the value of the rate constant, k, for any given species remains
constant from cell to cell, but not necessarily that retention times remain constant from cell to
cell. A value of k, the rate constant may be determined in the laboratory and this value may
be expected to vary with changes in some physical and chemical conditions, and the k values
obtained are not directly applicable to the plant because the value of k is characteristic of the
cell in which the process is carried out. Similarly, we have seen how the retention time in
continuous cells may be measured by the use of tracers but we are unable to predict how the
retention time varies in a cell with change of feed rate or flotation rate, except in the very
simple case where the concentrate volume flow rate is negligible.

There are several methods of determining the values of the rate constants of the various
mineral species in a bank of continuous cells, but most of them involve the analysis of a large
number of samples (two per cell).

In an *ideal* batch test or in a continuous cell under plug flow conditions, Eq. (16.10) applies if flotation is a first order rate process. This equation does not apply to banks of cells comprising a series of ideal mixers. For such a bank of cells the expression:

$$\ln\left(\frac{C_0 - C_\infty}{C - C_\infty}\right) = N\ln(1 + k\lambda)$$

(16.58)

describes the decay in the concentration of the species in the pulp, where N is the cell number, and λ is the nominal retention time of the pulp in the cell. This equation is valid only for cases where λ is constant from cell to cell, that is when the volume of concentrate removed is negligible.

In the case of plug-flow, a graph of ln $(C_O - C_\infty)/(C - C_\infty)$ versus time will be a straight line of slope k. In the case of a series of ideal mixers, a graph of ln $(C_O - C_\infty)/(C - C_\infty)$ versus N (which is proportional to time t if λ is constant) will be a straight line of slope ln $(1 + k\ \lambda)$, from which k may be derived if λ is known.

On the basis of the equation for a bank of ideal mixers, the value of k may be obtained from the analysis of one sample ofower accuracy achieved. pulp taken from within each cell, providing that concentrate volumes are negligible.

The results of a series of tests based on this method is shown in the Fig. 16.17 and Fig. 16.18.

The method involves the analysis of one sample per cell in the bank, although alternate cells could have been omitted and a l If the values of k of several mineral species are to be determined, then every sample would have to be analysed for every species. It is desirable, therefore that the number of samples to be analysed should be as small as possible. It would also be better if all of the samples on which the analysis is based were taken by automatic samplers, over relatively long periods of time. This is only feasible when sampling the bank feed, concentrate and tailing.
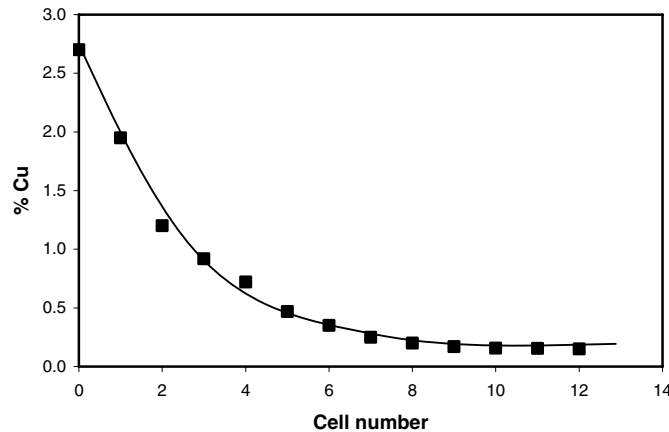
Fig. 16.17. Variation of copper concentrations within a bank of 12 cells.
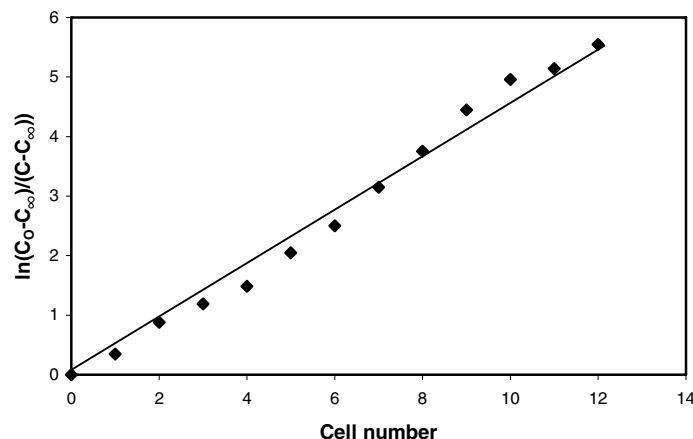
Fig. 16.18. Relationship between concentration in cell pulp and cell number.

The retention time may be measured relatively easily by a tracer, such as KBr and using a bromine selective electrode to determine concentration in solution, so that if the retention times are measured in some of the cells and samples of the bank feed, concentrate and tailings are taken, the values of k of the different species may be calculated by an iterative technique as follows:

1. Using an estimated value of the rate constant of any particle type, and the values of the retention times measured experimentally, calculate the recovery that would be obtained at this rate constant, using Eq. (16.45) etc..
2. Compare this calculated recovery with the actual recovery obtained from the plant samples.
3. If the recoveries are not sufficiently close, adjust the estimated value of k and repeat the calculations.
4. Repeat steps 1 – 3 until the required accuracy is obtained.
5. Repeat steps 1 – 4 for the other particle types in the feed.

The advantages of this method are:

1. Only three samples are comprehensively analysed.
2. Full allowance is made for variation in retention times.
3. Carrying out the actual retention time experiments in the plant is physically simple and rapid and requires no special equipment.
4. Not all cells in a long bank would have to be subjected to retention time tests. The retention times in consecutive identical cells would be expected to increase according to a reasonably *smooth curve* relationship.
5. It does not involve the application of any formulae that are algebraic approximations and it may be used on a bank of any number of cells.

16.7. Other Flotation Models

There have been a number of models developed to describe the flotation process, of which the Kinetic Model of flotation is one. A brief description of some of the other mathematical approaches to the flotation phenomenon follows.

16.7.1. Probability Models

The specific flotation rate, rate constant or flotation rate coefficient may be defined as the rate of flotation (mass per unit time) of a pulp constituent divided by the mass of that constituent in the pulp body of the flotation cell. That is:

$$k = \frac{Q_{MS(C)}}{M_{SP}} \qquad (16.59)$$

where k = specific flotation rate,
  $Q_{MS(C)}$ = mass flow rate of a pulp constituent into the concentrate, and
  M_{SP} = mass of that constituent in the pulp.

From the hypothesis of Gaudin et al [13], this can be written in terms of the probability of success of a sequence of events such that:

$$k = P_C.P_A.F \qquad (16.60)$$

where P_C = probability of collision of a given particle with an air bubble, during a given time interval,
  P_A = probability that the particle will adhere to the bubble after collision, and
  F = froth stability factor which takes into account occurrences in the froth which may cause the particle to become detached from the bubble and drop back into the pulp.

The froth stability factor is sometimes expressed in terms of further probability terms:

$$F = P_E.P_F \qquad (16.61)$$

where P_E = probability of levitation of the bubble-particle aggregate to the froth/pulp interface without detachment and
  P_F = probability that particles in the froth will survive the drainage of liquid from the froth and be carried into the concentrate.

The probability of collision, P_C, is a function of the radii of particle and bubble, their relative velocity, the density of the particle and the viscosity of the fluid. The probability of adhesion, P_A, corresponds to the likelihood of a particle successfully thinning and rupturing the wetting film and forming an angle of contact that will ensure stable attachment to the bubble surface. In addition, for adherence of the particle to the bubble, the attachment forces must withstand the dislodging forces including gravitational pull, fluid drag and the crowding of adjacent particles at the bubble surface. The probability of attachment will be a function of the equilibrium contact angle, the surface tension between the air and liquid, the particle and bubble radius and the particle density. The probability of emergence, P_E, is a function of

contact angle and particle and bubble size, and the probability of froth drainage, P_F, is also a function of the liquid/air surface tension, the contact angle and particle size and density.

In the simple form of the probability model, the mass, $M_{S(T)}$, of a component in the tailing from a single continuous cell at steady state is related to the mass $M_{S(F)}$ of the component in the feed by:

$$M_{S(T)} = M_{S(F)}(1-P) \qquad (16.62)$$

If the probability of recovery, P, is constant and independent of the cell number, N, then for a bank of cells:

$$M_{S(T)} = M_{S(F)}(1-P)^N \qquad (16.63)$$

This simple form of the probability approach is similar to the simplest form of the kinetic model.

16.7.2. Two-Phase Model

This model of the flotation process is based on the flow into and out of a cell and the two-directional transfer of material between two distinct phases, the pulp and the froth as shown in Fig. 16.19.

The mass flow rate balance relationships for Fig. 16.19 are:

Froth phase: $\quad \dfrac{dM_{S(f)}}{dt} = -\dfrac{M_{S(f)}Q_{V(C)}}{V_f} + a f_P(M_{S(P)}) - b f_f(M_{S(f)}) \qquad (16.64)$

Pulp phase: $\quad \dfrac{dM_{S(P)}}{dt} = Q_{V(F)}C_{S(F)} - \dfrac{M_{S(P)}Q_{V(T)}}{V_P} + b f_f(M_{S(f)}) - a f_P(M_{S(P)}) \qquad (16.65)$
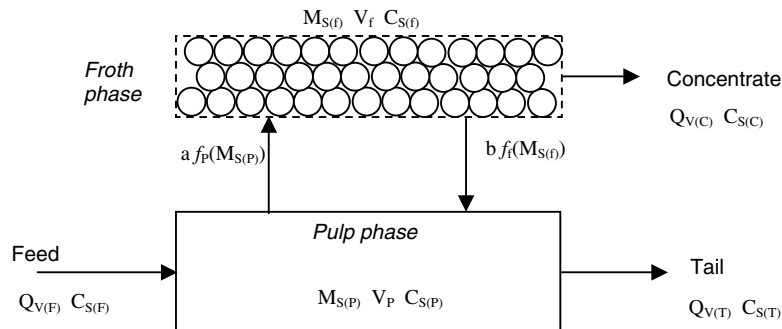
Fig. 16.19. The two-phase model [14].

where M_S = mass of floatable solid,
Q_V = volumetric flow rate,
V = volume,
f = function relating to the order of kinetics,
a = rate coefficient for mass transfer from pulp to froth,
b = rate coefficient for mass transfer from froth to pulp.

Subscripts F, C, f, P and T refer to feed, concentrate, froth, pulp and tailing phases respectively.

Assuming mass transfer in both directions is first order kinetics, $f_f(M_{S(f)}) = M_{S(f)}$, and $f_P(M_{S(P)}) = M_{S(P)}$, and for constant volume:

$$Q_{V(F)} = Q_{V(T)} + Q_{V(C)} \tag{16.66}$$

These three equations may be solved for various cases such as the semi-batch or continuous flotation case. The specific flotation rate coefficient, k, in the classical flotation model at steady state may be defined as:

$$k = \frac{a}{\left(1 + \frac{bV_f}{Q_{V(c)}}\right)} \tag{16.67}$$

Although there is considerable evidence that the kinetics of the flotation process interpreted in terms of a one-phase model is first order, it does not follow that when the pulp and froth phases are considered separately each behaves according to first-order kinetics. For example, experiments with sized fractions of iron oxides concluded that the kinetics of forward pulp to froth transfer and the return drainage from froth to pulp were mainly second order. In summary:

1. Multiphase models postulate ideal mixing in each phase and two-way mass transfer between the several phases according to simple kinetics.
2. The two-phase (pulp-froth) model describes the steady- state satisfactorily but it is only marginally successful in describing the transient state. The model does not scale up well.
3. The model does not take account of water flow between the phases, or air flow, although flow in and out of the system is described.
4. Two-phased models can be developed into multiphase models with several layered phases in the froth to account for concentration gradients, and two phases in the pulp to handle residence time effects. Modelling the froth in layers also provides for a degree of plug-flow effect with axial dispersion.
5. Many of the parameters of the two-phase model are difficult to measure and it has not been widely used.

16.7.3. Bubble Surface Area Flux

The Julius Kruttschnitt Mineral Research Centre (JKMRC) investigated the problem of a changing feed floatability as flotation proceeds down a bank of cells and considered the flotation rate of particles according to the following general equation:

Flotation response = particle characteristic x cell characteristic (16.68)

where the cell characteristics can be considered in terms of the two phases, froth and pulp.

The form of the model is [15]:

$$k = P S_B R_F \qquad (16.69)$$

where   P   = a parameter related to ore floatability,
         S_B = the bubble surface area flux and
         R_F = a froth recovery factor.

The bubble surface area flux is defined as the total surface area of bubbles available in the cell per unit cross-sectional area of cell per unit time and hence will depend on the bubble size and velocity.

$$S_B = \frac{6 J_G}{d_{32}} \qquad (16.70)$$

where J_G = the superficial gas velocity, m/s and
         d_{32} = the Sauter mean bubble diameter, m.

The Sauter mean diameter is the diameter of a bubble having the same specific surface (volume per unit surface area) as the whole bubble size distribution. That is:

$$d_{32} = \frac{\sum n_i d_i^3}{\sum n_i d_i^2} \qquad (16.71)$$

where n_i = number of bubble of diameter d_i.

The Sauter diameter is measured by a bubble size analyser such as the University of Cape Town Bubble Size Analyser [16] or from digital images such as the McGill Bubble Size Analyser [17]. The superficial gas velocity is measured by capturing a volume of bubbles for a set time in a tube of fixed cross-sectional area.

Factors that affect the bubble size and velocity will determine the bubble surface area flux. These include the cell and impeller design, impeller speed, air flow rate and the frother type and concentration.

The froth recovery factor, R_F, is defined as the efficiency with which the particles arriving at the froth/pulp interface reach the concentrate. This is dependant on the residence time of air in the froth, which is determined by froth depth. For a zero froth depth, R_F is 100% while an exceptionally deep froth will have a R_F, and k, of zero. R_F will thus be the ratio of the overall rate constant and the collection zone rate constant and lies between 0 and 100%. Other factors affecting the froth recovery factor are the air flow rate, impeller design, cell design, impeller speed and frother type and concentration.

The ore floatability, P, is affected by the ore mineralogy, particle liberation and particle size, reagent coverage of the particle surface and the pulp chemistry. For a given froth

recovery factor, a plot of rate constant versus bubble surface area flux has been shown to give a straight line, the slope of which, from Eq. (16.69), will be equal to P [15].

Substituting Eq. (16.69) into Eq. (16.44) gives:

$$R = \frac{PS_BR_F\lambda}{1+PS_BR_F\lambda} = \sum_{i=1}^{n} M_i \frac{P_iS_BR_F\lambda}{1+P_iS_BR_F\lambda} \tag{16.72}$$

16.8. Problems

16.1

An ore consisting of a valuable component A and a gangue, component B, is floated in a rougher/scavenger/cleaner circuit. The rougher/scavenger part of the circuit is shown below:
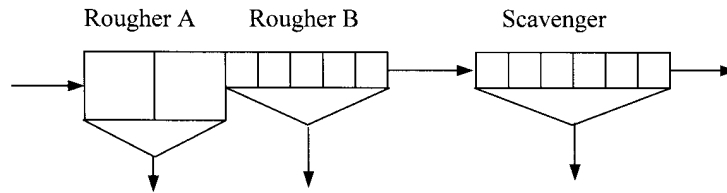
Rougher bank A consists of 2×50 m^3 cells
Rougher bank B consists of 10×10 m^3 cells, and
Scavenger bank consists of 12×10 m^3 cells

Feed grade   =   1.48 % A, 98.52 % B
feed rate to rougher bank A =   350 tph
solid density   =   2800 kg/m3
water density   =   1000 kg/m3
feed density in Rougher A   =   30 % solids (by mass)
feed density in Rougher B   =   30 % solids
feed density in Scavenger   =   25 % solids

Samples are taken of the concentrates and tailings from each bank of cells at steady state, and analysed for component A and B. The results are as follows:

Rougher bank A   Feed   =   1.48% A, 98.52% B
                   Concentrate =   14.2% A, 85.8% B
                   Tailing   =   0.72% A, 99.28% B
Rougher bank B   Concentrate =   5.7% A, 94.3% B
                   Tailing   =   0.35% A, 99.65% B
Scavenger bank   Concentrate =   2.5% A, 97.5% B
                   Tailing   =   0.19% A, 99.81% B

Assume that the concentrate flow rates are negligible compared to the feed rate.

a.   From the assays, calculate the recovery achieved in each bank and from the rougher/scavenger circuit as a whole.
b.   calculate the flotation rate constant of components A and B in each bank

16.2

From the values of rate constants obtained in question 16.1, estimate the difference in overall recovery from the rougher/scavenger circuit if the cells were re-arranged to a rougher bank A of 14 x 10 m^3 cells, a rougher bank B of 8 x 10 m^3 cells and a scavenger bank of 2 x 50 m^3 cells. Assuming the rate constants in each bank remain the same in the new configuration.

16.3

A batch flotation test of a copper ore of grade 0.24 % Cu is given below:

Time, t s	Conc. Mass, g	Assay %
20	24.9	2.47
40	15.0	1.93
60	13.2	1.80
120	35.2	1.34
300	63.3	0.16

Feed mass = 1036.8 g
Cell volume = 3 litres

Calculate the flotation rate constant, assuming first order kinetics.

16.4

The flotation of magnesite with sodium oleate in a batch flotation cell gave the following results:

Time (min)	Recovery (%)	Time (min)	Recovery (%)
1	11.0	10	50
2	20.0	11	52
3	28.0	13	54
4	34.5	15	53
5	40.0	18	55
7.5	45.0	22	55

Determine the order of the flotation kinetics and hence calculate the rate constant.

16.5

A nickel flotation bank of 12 cells is surveyed and the flotation recovery and residence time in each cell is given below.

1. Calculate the flotation rate constant of the nickel mineral in the individual cells 1, 6 and 12.
2. Calculate the flotation rate constant of the nickel mineral in the first cell, the first 6 cells (cumulative) and the whole 12 cells in the bank.
3. Comment on the results of parts 1 and 2.

Cell No.	Ni Recovery (cumulative)	Residence time min.	Cell No.	Ni Recovery (cumulative)	Residence time min.
1	16.31	0.39	7	74.81	2.9
2	33.51	0.8	8	78.31	3.3
3	46.71	1.2	9	81.01	3.8
4	56.71	1.6	10	83.11	4.2
5	64.41	2.0	11	84.81	4.7
6	70.31	2.5	12	86.11	5.1

16.6

The following laboratory flotation results were achieved on a lead ore. Calculate and compare the flotation rate constants for galena in the rougher and scavenger cells.

Test	Cumulative Time, min.	Cum. Recovery Galena (%)	Test	Cumulative Time, min.	Cum. Recovery Galena (%)
Pb	0.5	19.5	Pb	0.5	1.2
rougher	1.5	38.8	scavenger	1.5	4.4
feed	4	51.1	tail	4	11.3
	8	56.9		8	20.9
	12	59.6		11	26.8
	20	62.7		20	40.3

16.7

A laboratory flotation test on a copper sulphide ore gave the following results:

Time, s	Mass, g	Assay, % Cu
20	30.8	2.98
40	33.7	1.69
60	26.0	0.98
120	50.0	0.83
200	22.6	0.45
Tail	768.2	0.08

1. Calculate the concentration, C_t, remaining in the 3 litre cell after time t.
2. Determine the rate constant
3. If a bank of continuous cells has the same rate constant, how many cells would be required to achieve a recovery of 85% if the cell size is 16 m^3 and the feed is 1344 m^3/h.

16.8

An ore contains 5% of copper sulphides and 95% of gangue silicates. If the sulphides float at a rate of 0.2 min^{-1} and the gangue floats at a rate of 0.01 min^{-1}, what grade of concentrate

would be achieved in a bank of 10 cells treating 100 t/h if the total residence time for the bank is 20 minutes?

What would be the grade after 5 cells?

16.9
A laboratory batch flotation test gave the following results.

Starting mass = 1000 g
Cell volume   = 3 L
Feed grade   = 3% pyrite

Time, s	Mass floated	Assay % pyrite	Time, s	Mass floated	Assay % pyrite
0					
20	96.2	9.24	120	205.2	10.81
40	148.4	9.72	150	208.5	10.97
60	176.7	10.11	180	209.9	11.06
90	197.0	10.53	210	210.5	11.11

1. Determine the rate constant and infinite recovery of sulphide and quartz if the sample only contains these two minerals

2. Calculate the grade and recovery for a bank of 4 cells (32 m^3 each) if the feed rate is 430 m^3/h. Assume the same rate constant and infinite recovery as in the batch cell.

16.10
A pyrite/quartz ore (2 components) was subjected to a series of batch float tests. The concentrate from the first test was refloated in a second cell, the concentrate from this cell was refloated in a third cell etc. The tests, conditions and results were as follows:

Test 1:
Feed assay   = 4% pyrite/96% quartz
Feed % solids = 30% (mass)
Feed Mass   = 1000 g
air flow   = 9 L/min
Float Time   = 5 minutes

	Pyrite	*Quartz*
Rate constant, k	0.044 s^{-1}	0.047 s^{-1}
Infinite recovery, R_∞ (as fraction)	0.705	0.27

Test 2:
Feed % solids = 20 % (mass)
Float Time   = 3 minutes

	Pyrite	*Quartz*
Rate constant, k	0.064 s^{-1}	0.040 s^{-1}
Infinite recovery, R_∞ (as fraction)	0.591	0.181

Test 3:

Feed % solids   =   15 % (mass)
Float Time   =   2 minutes

	Pyrite	*Quartz*
Rate constant, k	0.0815 s^{-1}	0.032 s^{-1}
Infinite recovery, R_∞ (as fraction)	0.52	0.136

Test 4:

Feed % solids   =   12 % (mass)
Float Time   =   2 minutes

	Pyrite	*Quartz*
Rate constant, k	0.0942s^{-1}	0.052 s^{-1}
Infinite recovery, R_∞ (as fraction)	0.483	0.109

A flotation circuit is available consisting of a rougher bank of 5 cells, cleaner banks of 3 cells, 2 cells and 2 cells (4 banks in total), each cell having a nominal residence time of 1 minute.

1.   Assuming the rate data obtained in the laboratory test is appropriate for industrial size continuous cells, calculate the minimum number of cleaning stages required to obtain a concentrate grade of at least 60% pyrite. The flotation feed contains 4% pyrite at a treatment rate of 500 t/h.
2.   Calculate the overall pyrite recovery achieved at a concentrate grade of 90% pyrite.

16.11
For a bank of 5 cells having a nominal residence time of 1 minute per cell, the calculated recovery is not the same as a single cell having a nominal residence time of 5 minutes. Why?

16.12
A survey of a copper rougher bank allowed evaluation of the ore floatability, P, as 8.3×10^{-5} and the superficial gas velocity was 6.5 mm/s and the Sauter mean bubble diameter was 0.78 mm. The copper recovery in the rougher bank was calculated at 60.1% and the mean residence time was 6.1 minutes. If the bubble surface area flux is increased to 88.1 s^{-1} calculate the change in copper recovery.

REFERENCES
[1]   G.J. Jameson, G.J., Proceedings, Improving Froth Flotation of Coal, ACIRL, (1983) 1.
[2]   N. Arbiter, Transactions of AIME, 190 (1951) 791.
[3]   E.C. Dowling, R.R. Klimpel and F.F. Aplan, Minerals and Metallurgical Processing, 2 (2) (1985) 87.
[4]   R.R. Klimpel, in Mineral Processing Plant Design, A.L. Mular and R.B. Bhappu (eds), SME/AIME, (1980) 907.
[5]   D.F. Kelsall, Transactions of the IMM, 70 (1961) C191.
[6]   A. Jowett, Transactions of the IMM, 83 (1974) C266.

[7] B.K. Loveday, Transactions of the IMM, 75 (1966) C219.

[8] T. Inoue and T. Imaizumi, 8th International Mineral Process. Congress, Leningrad, S-15 (1968) 13.

[9] T. Imaizumi and T. Inoue, Proceedings 6th International Mineral Processing Congress, Cannes, A. Roberts (ed), Pergamon Oxford, (1965) 581.

[10] Australian Standard 2579.1 – 1983, (1983).

[11] C.C. Dell. and M.J. Bunyard, Transactions of the IMM, 81 (1972) C246.

[12] R.G. Burdon and D.S. Yan, Final Report, NERDDP Project No. 613 (82/2193) (1984).

[13] A.M. Gaudin, R. Schuhmann and A.W. Schlechten, Journal of Physical Chemistry, 64 (1942) 902.

[14] C.C. Harris and H.W. Rimmer, Transactions of the IMM, 75 (1966) C153.

[15] B.K. Gorain, T.J. Napier-Munn, J.-P. Franzidis anf E.V. Manlapig, Minerals Engineering, 11 (7) (1998) 615.

[16] J.P. Tucker, D.A Deglon, J.-P. Franzidis, M.C. Harris and C.T. O'Connor, Minerals Engineering, 7 (5/6) (1994) 667.

[17] J.R. Hernandez and J.A. Finch, Centenary of Flotation Symposium, Brisbane, (2005) Retrieved: January 11th 2006 from
http://www.ausimm.com/flot2005/html/presentations/snapshot_hernandez-aguilar.pdf.

Chapter 17. Metallurgical Process Assessment

17. INTRODUCTION

The objective of all mineral processing operations is to concentrate the minerals of interest and reject the unwanted material associated with the ores. The process is often complex as seen in the previous chapters since minerals exist both physically and chemically combined with each other. Ideal clean separation of the mineral from the unwanted fraction, known as *gangue* or *tailings*, is therefore almost impossible. In the process of separation therefore a third fraction appears which is a mixture of the gangue constituents and the minerals of interest. This fraction is known as the *middlings* and is retreated to recover as much of the valuable mineral as possible to increase recovery but at the same time maintain a high product grade.

On repeated treatment, some of the middlings finds their way to the concentrates and some report to the tailings. Thus both the concentrate and the tailings are diluted resulting in a loss of grade of the concentrate. To what extent this loss of grade can be accepted would depend on the economics of the process. The scheme of operation usually followed is represented by Fig. 17.1 where it can be seen that the middlings fraction could be repeatedly treated to recover some mineral of interest that is relatively less contaminated with the gangue minerals.

Each stream has therefore to be assessed to determine the mass and the concentration of the mineral of interest.

This chapter deals with the method of assessing the distribution of minerals in the concentrate, middlings and tailings streams and their recovery.

17.1. Analyses of Constituents

The first step in analyzing the constituents of each stream is to obtain representative samples of the streams. The methods of sampling, the sample size and the errors involved
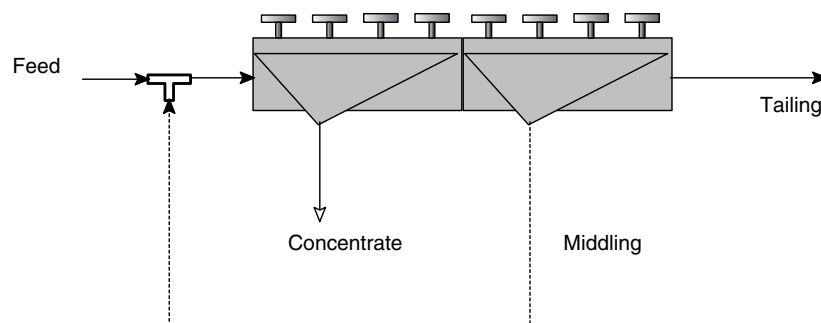
Fig. 17.1 Production of concentrate, middling and tailing streams.

have been discussed in Chapter 1. Correct representative sampling is a challenge. In industrial large scale continuous operations, where the streams are ever changing, sampling is even more difficult. At best a large number of samples provide data for an average value.

Initial qualitative assessment of the raw material that forms the feed stream to a separating process is done by identifying the minerals present under an optical microscope. To get a better idea, X-Ray diffraction (XRD) and X-Ray Fluorescence (XRF) analysers are employed. These provide quantitative analysis of elements in the rock sample. The nature of interlocking of minerals in rocks and grains is normally assessed by examining polished sections of the rock particles under an optical and/or electron microscopes which can be operated at large magnifications (from 5,000 to more than 10,000 times magnification is common). For observing, the distribution of elements within a grain, polished sections are examined by Scanning Electron Microscope. The Electron Probe Micro-analyser helps to quantify the distributions of different elements within a grain. Recently Scanning Tunnelling Microscopes have been tried to examine individual atoms on the surface while Time of Flight - Secondary Ion Mass Spectrometers (ToF-SIMS) can analyse surface atoms from either mineral surfaces or adsorbed species. These instruments provide a means of understanding the complexities of separation of minerals and also indicate the possibility of liberation or otherwise. These assessments are essentially in the dry state and on small samples.

For estimating quantitatively the presence of elements in continuous operating stream, wet analytical chemical methods are most reliable. However, this is a slow process. To speed up the determinations and to get an equally reliable result Atomic Adsorption Spectro-photometers or Inductively Coupled Plasma atomic emission spectrometers are used where a solution containing the metal ion of interested is aspirated in a flame (AAS) or a plasma (ICP) in which the metal ion is converted into a free atom vapour. A monochromatic light beam is directed through the flame and the amount of radiation of a specific energy level is detected. This electron energy level is specific for an element which helps to identify it. A calibration curve with known amounts of the element and flame intensity helps in quantifying the presence of each element.

In operating plants where analytical results are required with least delay, attempts have been made to analyse the composition in situ while the process is in progress. Both dry and wet methods have been attempted with varying degrees of success. For example, in the iron ore industry, the iron (Fe) content of the ore is examined as it travels on the conveyor belt. The Fe- content is determined by using a *neutron-capture, γ-ray transmission and pair production technique*. In this method, the ore is irradiated by Ra^{226} γ-radical placed at the bottom of a conveyor belt. This produces electron-positron pairs. The intensity of the pair production is related to the iron content. Tests by Aylmer, Holmes and Rutherford [1] indicate reliable results are possible with iron ore streams.

In wet streams, as in grinding circuits, continuous quantitative analysis of more than one element in a stream is obtained by the use of On-Stream or In-Stream analysers. Here a radio-active source is used to irradiate elements present in a stream (or slurry). Several elements can be detected and quantified simultaneously. For details, any text book on instrumental analysis can be consulted.

In some operations the feed stream is from a single supply of ore from one mine when sampling and assaying is relatively easy, but in most cases ores from several sources form the feed to a process. In such circumstances either each source is separately sampled and blended at pre-arranged proportion (according to grade and availability) or a composite sample is analysed.

It is a general experience that in industry a sampling error of ± 2% is acceptable.

17.2. Definition of Terms

We need to be clear about the definition of terms used in assessing the different streams in a process.

17.2.1. Mass or Weight

The weight of an object is the effect of gravity acting on the mass of the object and is equal to the mass x gravitational acceleration = M g. Therefore the weight of an object will change depending on the value of g which will change depending on the geological location of the object. In outer space for example, objects are *weightless*. The object in outer space will however still have mass and though weightless, a heavy object will require a larger force to move it than a lighter object. Back on earth, the object on a spring balance will record the weight of the object. A larger gravitational acceleration as experienced at sea level compared to a mountain top for example, will extend the spring more recording a larger weight for the same object mass. The same object on a knife edge or double pan balance will record the mass of the object as the influence of gravity is negated by the equal force acting on the second pan of standard masses. On a single pan electronic balance, the object's mass is also recorded as the influence of gravity is compensated for electronically. Since mass is the absolute measurement and weight is variable and mass is the usual quantity measured on most balances, unless using a spring balance, this text will refer to mass exclusively.

In a mineral processing operation, the throughputs and capacities of units are expressed as tonnes/h or tonnes/day. These tonnages invariably refer to the dry tonnes passing through a process even if the process is treating a slurry of solid and water. This is principally due to the fact that it is the solid that contains the valuable mineral and hence the mass of this component is of the most concern.

17.2.2. Slurry

A slurry is a suspension of solids in a liquid. It is also referred to as *pulp*. In the metallurgical industry, the liquid is almost always water. The concentration of solids in a slurry, C, is expressed as:

$$C = \frac{\text{Mass of solids in slurry}}{\text{Mass of solids in slurry} + \text{Mass of liquid}} \times 100 \qquad (17.1)$$

It can also be expressed on a volumetric basis (mass = volume x density) and is often referred to as percent solids usually by mass by also by volume. Thus the % solids of the slurry can be written as:

$$C = \%S = \frac{M_S}{M_S + M_L} \times 100 \qquad (17.2)$$

Thus a 30% solids slurry by mass means 30 g (or kg or tonnes) of solids in 70 g (or kg or tonnes) of water.

The concentration may also be expressed as per cent solids in the slurry, that is, if %S is the percent solids by mass in the slurry and ρ_{SL} and ρ_S the densities of the slurry and solids, it follows that in a slurry:

1. volume fraction of solids $= \dfrac{\%S\ \rho_{SL}}{100\ \rho_S}$ (17.3)

2. volume fraction of water $= \dfrac{\left(100\ \rho_S - \%S\ \rho_{SL}\right)}{100\ \rho_S}$ (17.4)

That is, $\dfrac{\%S\ \rho_{SL}}{100\ \rho_S} + \dfrac{\left(100\ \rho_S - \%S\ \rho_{SL}\right)}{100\ \rho_S} = 1.0$

and

$\%S = \dfrac{100\ \rho_S\left(\rho_{SL} - \rho_L\right)}{\rho_{SL}\left(\rho_S - \rho_L\right)}$

and $\rho_{SL} = \dfrac{100\rho_S\ \rho_L}{\rho_L\ \%S + \left(100 - \%S\right)\rho_S} = \dfrac{M_S + M_L}{V_S + V_L}$ (17.5)

The mass of 1 litre of slurry $= \rho_{SL} \times 10^{-3}$ kg for density in units of kg/m^3. (17.6)

The percent solids in a slurry will most often be quoted as mass % rather than volume % since mass is the property of main concern. Percent solids in some plants is also referred to as *pulp density*, though in reality the two terms mean different things as shown in Eqs. (17.2) and (17.5). The reader should be careful to make the distinction.

The specific gravity of common solids, at different solid-water ratios are given in Appendix A-1 and the pulp properties given in Appendix A-6.

17.2.3. Grade
Grade refers to the concentration of a mineral in a stream and is expressed as a percentage. It is determined by chemical assaying and may be expressed as:

$$\text{Grade} = \frac{\text{Mass of Mineral constituent in a stream}}{\left(\text{Mass of Mineral} + \text{Mass of gangue}\right)\text{in the stream}} \times 100 \quad (17.7)$$

For a number of ores, such as base metal ores, grade is quoted in terms of the contained metal rather than the mineral.

17.2.4. Recovery
Recovery describes the amount of mineral or metal of interest that is present in the concentrate in relation to that present in the feed stream. This is usually expressed as a percentage and written as:

$$\text{Recovery} = \frac{\text{Mass of mineral or metal in the concentrate stream}}{\text{Mass of mineral or metal in the feed stream}} \times 100 \quad (17.8)$$

Thus if we take 100 kg of a feed stream containing 2.5% nickel and if 20% by mass of the feed stream forms the concentrate, then the mass of concentrate is 20 kg. If the grade of

nickel in the concentrate equals 10%, then 20 kg of concentrate will contain 0.1 x 20 = 2 kg nickel. Hence Ni recovered is 2/2.5 x 100 = 80% by mass.

17.2.5. Distribution

The concept of distribution can be seen from the following illustration. In the above example only 80% of the mineral present has been accounted for in the concentrate, the rest of the mineral must be in the tailings, neglecting the existence of a middling product. Since the mass of the concentrate is 20 kg, then the mass of the tailings must be 80 kg. Let us assume that chemical analysis indicated that the nickel in the tailings was 0.6%. The nickel distribution between the concentrate and tailing product streams is then calculated as illustrated in Table 17.1.

Table 17.1
Metallurgical statement of the distribution of nickel between the streams

Stream	Mass of stream, kg M	Ni Assay, % A	Mass of Ni M x A	Distribution MA/Σ(MA)
Feed	100	2.5	2.5	100
Concentrate	20	10.0	2.0	2.0/2.5 = 80%
Tailings	80	0.6	0.48	0.48/2.5 = 19.2%

Thus 80% of nickel has been recovered into the concentrate and 19.2% lost in the tailings.

Table 17.1 is almost an ideal case as such clear separation is never possible in mineral processing operations. A fraction invariably appears as *middling*. The distribution in the middlings fraction is determined in the same manner as described above. That is, the analysis of metal in all the streams is ascertained and the distribution calculated. Provided the assays of the streams are accurate then the distribution or recovery in each of the streams will balance or add up to 100%. In Table 17.1 the total distribution of nickel adds up to 99.2% as a result of sampling or assay errors.

17.3. Material Balance

Material balance estimations is one of the most useful and powerful methods of assessing unit and integrated operations. It is used to calculate recoveries and distributions of valuable components at the end of the monthly accounting period or for estimating quantities in streams (mass or assay) that can't be easily measured. The results from a mass balance is strongly influenced by the accuracy of stream sampling and assaying. Where difficulties arise in the balancing of a circuit the it is usually one or both of these factors that should be suspect. Streams that are difficult to sample (e.g. cyclone underflow) or difficult to assay (e.g. low value streams such as tailing streams) need special attention. Mass balancing described here in only basic as the complexity in balancing increases with more complex circuits and recycle streams and with less information from sampled streams. The modern spreadsheet programmes are idea for these calculations and specialised mass balancing programs such as JKMetAccount, JKSimMet, Limn and USBC are available for complex calculations.

The basic principle involved is the conservation of mass. For a process at equilibrium or *steady state*, it can be expressed as:

mass input in all streams to a unit or circuit =

$\qquad$ mass output in all streams from a unit or circuit $\qquad\qquad$ (17.9)

However, in actual practice, during a continuous operation, a steady state is difficult to maintain with feed variations and process hiccups. Therefore it will be more correct to rewrite Eq. (17.9) as:

mass input in all streams to a unit or circuit = mass output in all streams
from a unit or circuit ± holdup within a process   (17.10)

The units are in mass or mass rates, either of the total material or of the constituent of interest, that is:

mass input in all streams of component i = mass output in all streams of
component i ± holdup of component i within a process   (17.11)

Water can be one of the constituents used in a mass balance for a wet process. In a size separation unit such as a screen or classifier the mass in specific size fractions can be used as *components* in a mass balance.

For a material balance to provide meaningful data, several samples need to be taken and the variance of errors to be established. Errors originate not only in the procedure of sampling but also in the method of measuring. Napier-Munn et al [2] suggests that:

1.   Error = 1% for > 9% (by mass) in a $\sqrt{2}$ size fraction.
2.   Error = [0.1+ actual %] x 10^{-1} for < 9% (by mass) in a $\sqrt{2}$ size fraction.

Where the mass balance of multi-component system is concerned, the error of each component is more difficult to establish. For an acceptable representative stream, the sum of the squares of errors in each size fraction should be minimum. This would give the best fit of mass split.

Consider the two product process in Fig. 17.2 at steady state. In the metallurgical operation a feed, F, containing a size i is split into two products with the underflow (classifier) containing the mass fraction C and (1-C) going to the overflow. C is the mass split to the underflow (underflow mass/feed mass) and (1-C) the mass split to the overflow (overflow mass/feed mass). Also let the mass fraction of size i in the feed, underflow and overflow streams be $m_{i\,(F)}$, $m_{i\,(U)}$ and $m_{i\,(O)}$ respectively, then according to Napier-Munn et al. [2] the mass-balance error (Δ_i) of each size fraction, (here size i), will be given by:
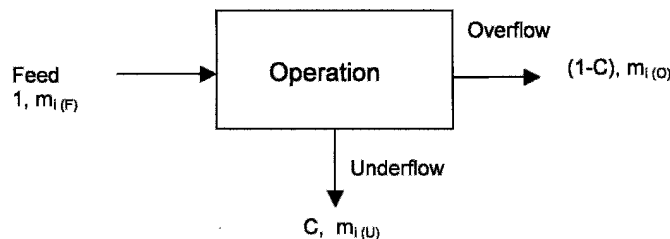
Fig. 17.2. A two product separation process

$$\Delta_i = m_{i(F)} - C\, m_{i(U)} - (1-C)\, m_{i(O)} \tag{17.12}$$

The errors in each stream will not be the same but will have to be determined against the variance of each size fraction. The best fit, C, to the underflow is:

$$C = -\frac{\displaystyle\sum_i \frac{\left(m_{i(O)} - m_{i(U)}\right)\left(m_{i(F)} - m_{i(O)}\right)}{\sigma_i^2}}{\displaystyle\sum_1 \frac{\left(m_{i(O)} - m_{i(U)}\right)^2}{\sigma_i^2}} \tag{17.13}$$

where σ_i is the standard deviation for the particle size i over a number of samples from the feed. Eq. (17.13) accounts for errors in each input stream, after which estimates of recovery can be made reasonably accurately.

17.3.1. Two Product Formula

In an operation where the interest is to recover a mineral in a single concentrate, the set up is usually called a two product system, producing one concentrate and one tailing stream. To calculate the recovery of the metal or mineral, the material balance method is applied. The resulting formula is known as the *Two Product Formula* [3].

To derive the formula let us assume that in an operation, samples are taken simultaneously from feed, concentrate and tailing streams and that the weighted average corrected analysis of each stream is:

1.   Feed stream

Feed mass $= M_{(F)}$, and
mineral assay in the feed $= A_{(F)}$

2.   Concentrate stream

Concentrate mass $= M_{(C)}$, and
mineral assay in the concentrate $= A_{(C)}$

3.   Tailings stream

Tailings mass $= M_{(T)}$, and
mineral assay in the tails $= A_{(T)}$

For a two product process, the material balance will be:

Input mass of feed $=$ Output mass of concentrate $+$ Output mass of tailings.

That is: $M_{(F)} = M_{(C)} + M_{(T)}$ \hfill (17.14)

Similarly for the component metal:

$$M_{(F)}A_{(F)} = M_{(C)}A_{(C)} + M_{(T)}A_{(T)} \qquad (17.15)$$

From Eqs. (17.14) and (17.15), $M_{(T)}$ can be eliminated by multiplying Eq. (17.14) by A_T and subtracting the result from Eq. (17.15), thus:

$$M_{(F)}A_{(F)} - M_{(F)}A_{(T)} = M_{(C)}A_{(C)} - M_{(C)}A_{(T)} \quad \text{and}$$

$$M_{(F)}(A_{(F)} - A_{(T)}) = M_{(C)}(A_{(C)} - A_{(T)}), \text{ and hence} \qquad (17.16)$$

$$\frac{M_{(C)}}{M_{(F)}} = \frac{\left(A_{(F)} - A_{(T)}\right)}{\left(A_{(C)} - A_{(T)}\right)} \qquad (17.17)$$

Eq. (17.17) can also be written in terms of tailing mass by eliminating the concentrate mass from Eqs. (17.14) and (17.15).

By definition, Eq. (17.8), recovery $R = \dfrac{M_{(C)}A_{(C)}}{M_{(F)}A_{(F)}} \times 100$

and from Eq. (17.17), $R = \dfrac{\left(A_{(F)} - A_{(T)}\right)A_{(C)}}{\left(A_{(C)} - A_{(T)}\right)A_{(F)}} \times 100 \qquad (17.18)$

Eq. (17.18) is applicable in any plant or laboratory situation where two products are involved in an operation. This is illustrated by the Example 17.1

Example 17.1

A gold ore containing 20 ppm gold was fed to a ball mill in a concentrator at the rate of 200 t/h. The concentrate analyzed 400 ppm and the tailings 0.15 ppm Au. Calculate the recovery and distribution of gold.

Solution

Step 1
The given data indicates: $A_{(F)} = 20$ ppm, $A_{(C)} = 400$ ppm and $A_{(T)} = 0.15$ ppm and $M_{(F)} = 200$ t/h. The concentrate mass, $M_{(C)}$ is unknown but can be determined using Eq. (17.17),

$$\frac{M_{(C)}}{M_{(F)}} = \frac{(A_{(F)} - A_{(T)})}{\left(A_{(C)} - A_{(T)}\right)} = \frac{20 - 0.15}{400 - 0.15} = 0.0496$$

$$M_{(C)} = 0.0496 \times 200 = 9.9 \text{ t/h}$$

Step 2

$$\text{Recovery, R} = \frac{M_{(C)}A_{(C)}}{M_{(F)}A_{(F)}} \times 100 = \frac{9.9 \times 400}{200 \times 20} \times 100 = 99.3\%$$

Step 3

The distribution of gold in the streams is best illustrated in the following table:

Stream	Mass, M t/h	Gold assay, A, ppm	M x A	Recovery or Distribution,%
Feed	200	20	4000	100
Concentrate	99.94	40	3997.6	99.9
Tailings	100.06	0.02	2.00	0.1

The units of assay can be any mass based concentration unit as long as the same unit is used throughout, e.g. ppm, g/t or mass%.

17.3.2. Three Product Formula

When a process produces three output streams such as an additional middling or second concentrate stream, then the mineral or metal distribution can be calculated using the same principle as that of the two product formula. Such situations frequently occur in metallurgical plants. The recovery formula is generally known as the *Three product formula* [3].

To illustrate the method, the presence of only two metals, (A and B) is considered here for a metallurgical circuit involving crushing, grinding, classification and flotation. In each unit process, the feed is considered as the concentrate from the previous process. Let us assume that the masses and concentrations of the minerals (metals) in the three streams are as given in Table 17.2

Table 17.2
Nomenclature for a three product process

Stream	Mass t/h	Metal A Assay, %	Metal B Assay, %
Feed	$M_{(F)}$	$A_{A(F)}$	$A_{B(F)}$
Concentrate 1	$M_{(C1)}$	$A_{A(C1)}$	$A_{B(C1)}$
Concentrate 2	$M_{(C2)}$	$A_{A(C2)}$	$A_{B(C2)}$
Tails	$M_{(T)}$	$A_{A(T)}$	$A_{B(T)}$

Considering the overall material and metal balances of the system the following equations apply:

$$M_{(F)} = M_{(C1)} + M_{(C2)} + M_{(T)} \quad \text{for the overall mass balance} \qquad (17.19)$$

$$M_{(F)} A_{A(F)} = M_{(C1)}A_{A(C1)} + M_{(C2)} A_{A(C2)} + M_{(T)} A_{A(T)} \quad \text{for component A} \qquad (17.20)$$

$$M_{(F)} A_{B(F)} = M_{(C1)}A_{B(C1)} + M_{(C2)} A_{B(C2)} + M_{(T)} A_{B(T)} \quad \text{for component B} \qquad (17.21)$$

As before eliminating T from the Eqs. (17.20) and (17.21) the value of $M_{(C1)}$ will be given by:

$$\frac{M_{(C1)}}{M_{(F)}} = \frac{\left(A_{A(F)} - A_{A(T)}\right)\left(A_{B(C2)} - A_{B(T)}\right) - \left(A_{B(F)} - A_{B(T)}\right)\left(A_{A(C2)} - A_{A(T)}\right)}{\left(A_{A(C1)} - A_{A(T)}\right)\left(A_{B(C2)} - A_{B(T)}\right) - \left(A_{B(C1)} - A_{B(T)}\right)\left(A_{A(C2)} - A_{A(T)}\right)} \quad (17.22)$$

and similarly:

$$\frac{M_{(C2)}}{M_{(F)}} = \frac{\left(A_{A(F)} - A_{A(T)}\right)\left(A_{B(C1)} - A_{B(T)}\right) - \left(A_{B(F)} - A_{B(T)}\right)\left(A_{A(C1)} - A_{A(T)}\right)}{\left(A_{A(C2)} - A_{A(T)}\right)\left(A_{B(C1)} - A_{B(T)}\right) - \left(A_{B(C2)} - A_{B(T)}\right)\left(A_{A(C1)} - A_{A(T)}\right)} \quad (17.23)$$

The recovery of metal A in concentrate 1 will be $= \dfrac{A_{A(C1)}M_{(C1)}}{A_{A(F)}M_{(F)}} \times 100$ $\qquad$ (17.24)

and the recovery of metal B in concentrate 2 will be $= \dfrac{A_{B(C2)}M_{(C2)}}{A_{B(F)}M_{(F)}} \times 100$ $\qquad$ (17.25)

The application of the method is best understood by Example 17.2

Example 17.2

A copper-zinc ore was fed to an integrated mineral processing system at the rate of 250 t/h. The final products were a copper concentrate and a zinc concentrate and tailing. Analysis of each stream were:

Stream	Assay	
	%Cu	%Zn
Feed	25.0	3.1
Copper concentrate	78.2	6.3
Zinc concentrate	2.1	55.4
Tailings	0.7	0.8

Determine the mass flows in the two concentrate streams and the recovery of metal in each product stream.

Solution

Step1
To determine the masses of copper and zinc concentrate streams, Eqs. (17.22) and (17.23) can be directly applied. Thus:

Mass of copper concentrate $= 250 \times \dfrac{(25 - 0.7)(55.4 - 0.8) - (3.1 - 0.8)(2.1 - 0.7)}{(78.2 - 0.7)(55.4 - 0.8) - (6.3 - 0.8)(2.1 - 0.7)}$

$= 78.4$ t/h

$$\text{Mass of zinc concentrate} \quad = \quad 250 \times \frac{(25.0 - 0.7)(6.3 - 0.8) - (3.1 - 0.8)(78.2 - 0.7)}{(2.1 - 0.7)(6.3 - 0.8) - (55.4 - 0.8)(78.2 - 0.7)} = 2.64 \text{ t/h}$$

Step 2

$$\text{Recovery of copper} = \frac{78.2 \times 78.4}{25.0 \times 250} \times 100 \quad = \quad 98.0\%$$

$$\text{and Recovery of zinc} = \frac{2.64 \times 55.4}{250 \times 3.1} \times 100 \quad = \quad 18.9\%$$

A spreadsheet such as *MS Excel* can be used to calculate the distributions in each streams and *Solver* can be used to estimate the concentrate masses without using the three product formulae above. A simple spreadsheet to do this is shown below.

	A	B	C	D	E	F	G	H	I	J	K
1											
2											
3			Stream	Mass	Cu Assay	Zn Assay	MxA (Cu)	MxA (Zn)	Recovery	Recovery	
4									Cu	Zn	
5			Feed	250.0	25.0	3.1	6250.0	775.0	100.0	100.0	
6			Cu Con	78.3	78.2	6.3	6126.1	493.5	98.0	63.7	
7			Zn Con	2.6	2.1	55.4	5.5	146.2	0.1	18.9	
8			Tail	169.0	0.7	0.8	118.3	135.2	1.9	17.4	
9											
10			Fitted using Solver								
11										Sum of recoveries	
12								square of			
13								difference			
14					2.76E-06	7.63E-12					
15					-8.7E-06	7.64E-11					
16						8.4E-11		Sum of square of difference			
17											
18					difference in total recovery and 100%						
19											

Cells D6, D7 are the unknown concentrate masses
Cell D8 is the feed minus the concentrate masses

Recoveries in cells I6:J8 are calculated in the same manner as in Table 17.1. The sum of the recoveries in the concentrates and tailing should add up to 100% as in cells I5, J5. If the system is not balanced, the sum of the recoveries will be different from 100% and the difference is calculated in cell E14 for copper and cell E15 for zinc. These differences are squared in cells F14:F15 to remove negative numbers and the sum of the squares in cell F16 is minimised using Solver and cells D6 and D7 as variables. The Solver solution is shown in the above spreadsheet and the recoveries or distribution of copper and zinc calculated in cells I6:J8.

Example 17.3

A lead-zinc ore was treated at the rate of 100 t/h to an integrated system to produce concentrates of lead and zinc minerals. A closed circuit was chosen so that the middling produced was re-treated. The average lead and zinc concentrations in each stream were:

Stream	Assay, Pb. Stream,%	Assay Zn stream ,%
Feed	1.8	23.5
Pb. Concentrate	82.0	2.0
Pb tail (head of zinc)	0.5	24.0
Zn concentrate	29.5	77.1
Tails	0.3	1.2

Determine the mass flowrates of the product stream and the distribution of lead and zinc.

Solution

Step 1
Using the two product formula:

$$\text{Mass of Pb Concentrate} = 100 \times \frac{(1.8 - 0.5)}{(82.0 - 0.5)} = 1.60 \text{ t/h, using the lead assays}$$

$$\text{and} \qquad = 100 \times \frac{(23.5 - 24.0)}{(2.0 - 24.0)} = 2.27 \text{ t/h, using the zinc assays}$$

$$\text{Mass of Zn concentrate} = (100 - 1.6) \times \frac{(24.0 - 1.2)}{(77.1 - 1.2)} = 29.55 \text{ t/h, using the zinc assays}$$

$$\text{or} \qquad (100 - 1.6) \times \frac{(0.5 - 0.3)}{(1.0 - 0.3)} = 25.56 \text{ t/h, using the lead assays}$$

A judgement will need to be made as to the reliability of the analytical techniques and/or the sampling procedures before deciding on the accuracy of the calculated values.

Step 2
The distribution of the metals is calculated in a similar manner to Table 17.1 and Example 17.2. The results is shown in the following table. The calculated feed or head assay is a good means of checking the balance if a measured head assay is available.

Stream	Mass t/h	Pb Assay %	Zn Assay %	MxA (Pb) t/h	MxA (Zn) t/h	Recovery Cu, %	Recovery Zn, %
Feed	100.0	1.8	23.5	180.0	2350.0	100.6	100.6
Pb Con	1.60	82.0	2.0	130.8	3.2	72.7	0.14
Zn Con	29.56	1.0	77.1	29.6	2279.1	16.4	97.0
Tail	68.8	0.3	1.2	20.7	82.6	11.5	3.5
**	1.81	23.6	181.0	2364.9			

** Calculated head

17.4. Circulating Load

The premise in the methods of assessing the streams so far has been that the circuits were open, that is, maximum product was obtained at reasonable rates in the concentrate. In actual practice it is found that all concentrate do not satisfy the required specifications of size and concentration. Hence the concentrate has to be treated to separate the unwanted fraction. The out of specification fraction is submitted for further separation by passing on to downstream processes or by adding it to the original feed. In the latter case, a continuous circulating load is set up in the system as illustrated in Fig 17.3. The recirculation operation results in improved recovery and grade. Fig. 17.3 illustrates such a situation for a simple grinding circuit where the coarse underflow fraction from the classifier is circulated for retreatment while the overflow fine fraction is the product. The *circulation ratio* C_R is defined as the ratio of the flowrates of the circulating stream to the flowrate of the new feed to the mill, which at steady state is equal to the fine product leaving the circuit.

$$C_R = \text{Circulation Ratio}, \quad C_R = \frac{T}{Q} \times 100 \tag{17.26}$$

When a classifier returns the coarse fraction of its feed material to the mill, then the total load to the mill is increased and is the sum of the new feed stream plus the coarse returns. Thus in a closed circuit system the circulating load C_L according to Austin et al [4] is defined as:

$$C_L = \frac{\text{Rate of new feed} + \text{Amount recycled}}{\text{Rate of new feed}} \times 100$$

$$= 100 + \frac{\text{Amount recycled}}{\text{Rate of new feed}} \times 100 \tag{17.27}$$
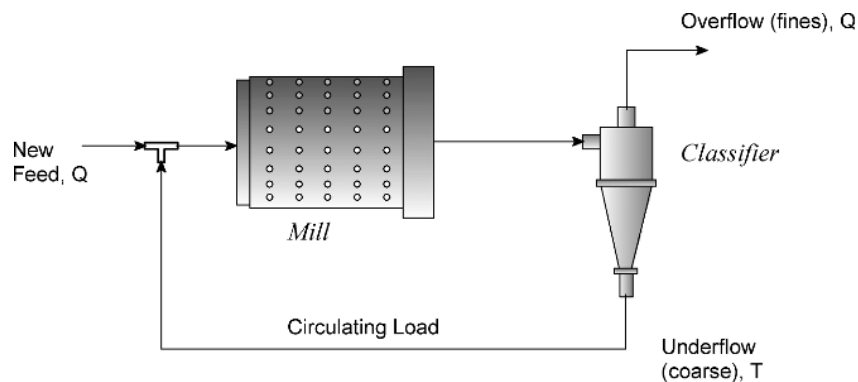
Fig. 17.3. Circulating stream in a closed circuit grinding/classification circuit.

This can be written as:

$$C_L = 100 + C_R \qquad (17.28)$$

The circulating load C_L and the circulation ratio C_R are both expressed as a percent. There is some confusion by different authors between the circulation ratio and the circulating load. The circulating load in slurry streams is not easily measured without instrumentation such as density gauges and flowmeters and hence is usually calculated by mass balancing. For a comminution circuit closed with a screen or classifier, a mass balance can be performed on the masses in individual size intervals around the size separator or on the cumulative masses passing or retained at a given size. If individual size intervals are used then a weighted average should be performed on a number of size intervals.

Bond [4] considered the circulating load associated with two general circuit configurations. In the first (Fig. 17.3) the stream returning from the classifier is to the mill feed. In the second (Fig. 17.4) the new feed is classified first and the oversize material sent to the grinding mill.

In both cases the same general formula applies. By a balance of the mass in size interval i, the circulating ratio in the classifier circuit shown in Fig. 17.4 is given by:

$$\text{Circulating load } (C_L) = \frac{(\text{Classifier under size} - \text{New feed to circuit})}{(\text{Feed to classifier} - \text{Classifier over size})} \times 100 \qquad (17.29)$$

Thus if $m_{i\,(F)}$ = mass fraction of size i in the feed to the circuit,

$m_{i\,(CF)}$ = mass fraction of size i in the feed to the classifier,

$m_{i\,(U)}$ = mass fraction of size i in the classifier undersize,

$m_{i\,(O)}$ = mass fraction of size i in the classifier oversize and

$m_{i\,(D)}$ = mass fraction of size i in the mill discharge,

then the circulating load for the circuit in Fig. 17.4 can be written as [4]:
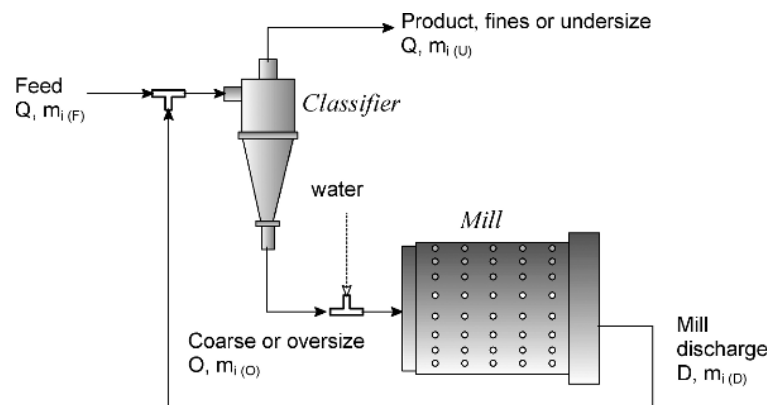
Fig. 17.4. Grinding/classification circuit with recirculating stream.

$$C_L = \frac{\sum \left| m_{i(CF)} - m_{i(U)} \right|}{\sum \left| m_{i(O)} - m_{i(CF)} \right|} = \frac{\sum \left| m_{i(F)} - m_{i(U)} \right|}{\sum \left| m_{i(O)} - m_{i(D)} \right|} = \frac{\sum \left| m_{i(F)} - m_{i(CF)} \right|}{\sum \left| m_{i(CF)} - m_{i(D)} \right|} \qquad (17.30)$$

In the case of the circuit in Fig. 17.4, the mass passing through the mill and the mass recirculating in the cyclone underflow are the same, hence the circulation ratio and circulating load will be the same.

For the circuit in Fig. 17.3, the circulating ratio, by a similar mass balance of size fractions will be:

$$C_R = \frac{\sum \left| m_{i(U)} - m_{i(D)} \right|}{\sum \left| m_{i(D)} - m_{i(O)} \right|} \times 100 \qquad (17.31)$$

To determine the circulation ratio C_R, it is usual to determine the water to solid ratios of the streams (masses can also be taken), by taking simultaneous samples for the same duration. Considering the water/solid ratio, R, for the different streams as in Fig. 17.4 and:

R_F = New feed,
R_D = Mill discharge,
R_{CF} = Feed to classifier,
R_O = Classifier oversize, course stream,
R_U = Classifier undersize, fines stream.

Then applying Bond's concept, the circulation load would be:

$$C_R = \frac{\left(R_D - R_F \right)}{\left(R_O - R_D \right)} \times 100 = \frac{\left(R_U - R_{CF} \right)}{\left(R_{CF} - R_O \right)} \times 100 \qquad (17.32)$$

When more than one circulating load is operating in an integrated circuit, the mass balances have to be established for each circuit.

Example 17.4 and 17.5 illustrates the methods of determining circulating load with and without the knowledge of the size distribution of solids in each stream.

Example 17.4

An integrated circuit consisted of a crusher, grinding mill and a classifier. The circuit produced 4800 t of ground ore per day. The underflow from the classifier was returned to the mill for re-grinding. The classifier feed contained 45% solids (by mass) and the classifier underflow and overflow streams contained 80% and 20% solids respectively. Calculate the circulation ratio and the circulating load.

Solution

Step 1
Determine the liquid/solid ratios in each stream.

Solid-liquid ratios of:

1. Classifier feed stream $= \dfrac{100-45}{45} = 1.22$

2. Classifier underflow (oversize) stream $= \dfrac{100-80}{80} = 0.25$

3. Classifier overflow (undersize) stream $= \dfrac{100-20}{20} = 4.0$

Step 2

Eq. (17.32) may be used to determine circulation ratio C_R:

$$\text{Circulating ratio} = \dfrac{(4.0-1.22)}{(1.22-0.25)} = 2.33 \times 100 = 233\%$$

Circulating load $= 100 + C_R = 100 + 233 = 333\%$

Example 17.5

A rod mill was integrated with a hydrocyclone and produced a grind at the rate of 250 t/h. Samples taken simultaneously from the discharge of the rod mill and the overflow and underflow streams from the hydrocyclone gave the following results. Calculate the circulating ratio and circulating load.

Screen Size	Rod Mill		Hydrocyclone O/F		Hydrocyclone U/F	
	Mass %	Cum %	Mass %	Cum %	Mass %	Cum %
-4.0 mm	2.0	2.0	0.0	0.0	36.0	36.0
-4 +2 mm	40.4	42.4	0.2	0.2	15.2	51.2
-2 +1mm	6.3	48.7	1.8	2.0	8.1	59.3
-100+420µm	5.1	53.8	15.6	17.6	5.1	64.4
-420+210 µm	16.6	70.4	21.2	38.8	13.8	78.2
-210+105 µm	19.0	89.4	20.4	59.2	18.5	96.7
-105+74 µm	5.5	94.9	25.0	84.2	2.8	99.6
-74 µm	5.1	100.0	15.8	100.0	0.5	100.0

Solution

Step 1

Let us choose arbitrarily the following three sizes: -4 +2.0 mm, -1000 +420 µm, -210 +105 µm instead all the eight sizes. to illustrate the principle of calculations.

Step 2

Calculate the circulation ratio for each screen interval chosen. Thus

For size -4.0+2.0 mm $\qquad C_R = \dfrac{42.4-0.2}{51.2-42.4} = 4.79$

For size -1000+420 μm $\qquad$ $C_R = \dfrac{53.8 - 17.6}{64.4 - 53.8} = 3.41$

For size -210+105 μm $\qquad$ $C_R = \dfrac{89.4 - 59.2}{97.6 - 89.4} = 4.13$

Average C_R for the sizes = 4.11 = 411%

The circulation load is then = 100 + 411 = 511%

A practical but rapid and approximate method to determine the circulating load in a grinding mill and classifying circuit is suggested by Barber-Greene[5]. The procedure is to determine the percent (by mass) of -200 mesh in the classifier feed (mill discharge) and classifier overflow and classifier underflow streams. Then for feed mass flowrate, Q_F, the classifier underflow (Fig. 17.3) will be given by:

$$Q_{(O)} = Q_{(F)} \left[\frac{m_{(U)} - m_{(D)}}{m_{(D)} - m_{(O)}} \right]$$ (17.33)

where $\quad Q_{(O)}$ = Mass flowrate of the classifier oversize (underflow)

$\qquad Q_{(F)}$ = Mass flowrate of the new feed

$\qquad m_{(U)}$ = % -200 mesh in classifier undersize (overflow),

$\qquad m_{(O)}$ = % -200 mesh in classifier oversize (underflow),

$\qquad m_{(D)}$ = % -200 mesh mill discharge (i.e. classifier feed),

Then the circulation ratio is given by:

$$C_R = \frac{Q_{(O)}}{Q_{(F)}} \times 100$$

Other screen sizes could be chosen for the calculation as shown in Example 17.5. A similar rapid method can be applied by taking the solid/liquid ratios of the streams as given in Eq. (17.32) and individual size fractions as given in Eqs. (17.30) and (17.31).

17.5. Problems

17.1
A calcite sample is ground in a mill in close circuit with a hydrocyclone. Samples were taken from the feed, overflow and underflow streams and their solid to water ratios determined as 2.5, 7 and 0.3 respectively. Calculate the circulating load of the circuit.

17.2

An iron ore company milled ore at the rate of 150 t/h in a ball mill in closed circuit with a classifier. The underflow (course) stream was re-circulated to the mill till a steady value was obtained in the cyclone overflow stream. The specific gravities of each stream were measured as:

1. Mill discharge stream to classifier = $SG_{(MD)}$
2. Product overflow from classifier = $SG_{(OF)}$
3. Product underflow from classifier = $SG_{(UF)}$

Establish a mass balance and derive an expression for the circulating load.

17.3

A copper sulphide ore was crushed and milled in close circuit with a classifier. The overflow from the classifier fed a rougher cleaner flotation circuit at the rate of 500 t/h. The ore assayed 2.75% Cu. The re-circulating load in flotation circuit was 270%. The overall recovery was 76% at a grade of 92%. Calculate:

1. Mass flowrates of the cleaner concentrate and rougher tailings,
2. Grade of copper in the rougher tailings.

17.4

The screen analysis of feed, product and tailings from a classifier were:

Size, (microns)	Feed %	Overflow %	Underflow %
850	15.2	0	18.3
500	8.5	0	10.2
250	33.6	2.9	39.9
125	34.2	65.4	27.8
75	8.5	31.8	3.7
	100.0	100.0	100.0

The classifier was fed with ground silica at the rate of 50t/h. Estimate:

1. Mass (tonnes) of dry ore per day in classifier underflow,
2. Mass (tonnes) of dry ore per day from classifier overflow.

REFERENCES

[1] J.A. Aylmer, R.J. Holmes, L. Rutherford, International J. of Nuclear Geo Physics, Pre-print. Private Communication.
[2] T.J. Napier-Munn, S. Morrell, R.D. Morrison and T. Kojovic, Mineral Comminution Circuits, JKMRC, 1999.
[3] B.A. Wills, Mineral Processing Technology, Pergamon Press, Oxford, 1981.
[4] L.G. Austin, R.R. Klimpel, and P.T. Luckie, Process Engineering of Size Reduction, SME/AIME, New York, 1984.
[5] F.C. Bond, Mineral Processing Handbook, N.L. Weiss (ed), 1985, p. 3A 23.
[6] Barber-Greene, Mine and Smelter Application Guide, Bulletin 820-979, 1979.

Chapter 18. Process Control

18. INTRODUCTION

The mathematical models described in previous chapters serve adequately for successful configuration and implementation of unit processes as well as distributed and complex processes. The basic premise in the applications of these models has been that the operation was under steady state conditions. In actual practice however, the steady state condition is easily disturbed by changes in operation variables when the mathematical models are affected. If an ideal steady state condition was taken as the mean of the variations and the deviation from the mean determined, then with proper instrumentation it may be possible to return to steady state operation. Over the years, suitable instruments have been devised for the purpose. They are activated by electric signals generated by individual variables. These signals are programmed to recognize the deviation from the mean. They then suitably operate to restore normal conditions. The main objective for process control therefore is to establish a dynamic mathematical model, monitor the deviation from the model and finally restore the original conditions of operation.

The process of controlling a dynamic system is complicated especially in mineral processing systems where a number of variables are involved simultaneously. Developments towards automatic control of plant operations have been commensurate with the development of computer science and instrument technology. Its implementation has resulted in consistent plant performance with improved yield and grade of the product with less manpower.

The term "process control" therefore refers to an engineering practice that is directed to the collection of devices and equipment to control processes and systems. Computers find application in simple systems, such as single loop controllers and also in large systems as the Direct Digital Controller (DDC), Supervisory control systems, Hybrid Control Systems and Supervisory Control and Data Acquisition (SCADA) systems. Further developments in process control are supported by many secondary concepts such as computer aided Engineering (CAE).

The commonly used present system is the Distributed Control System (DCS). It is made up of three main components, the data highway, the operator station and the microprocessor based controllers. The data highway handles information flow between components ensuring effective communication. The microprocessor controllers are responsible for effective control of the processes and are configured to handle as single or multi-loop controllers. The operator station allows the control command to be given, maintain the system data base and display the process information. The displays normally used are the group and detail displays, trend displays and alarm annunciated displays.

In this chapter we will primarily discuss how mathematical models with appropriate instrumentation are used for controlling the quality and quantity of yield of a mineral processing operation.

18.1. Controller Modes

Process control systems can be divided into two major groups:

1. Continuous control that involve monitoring and controlling of events continuously,
2 Digital controls that involve the use of computers and microprocessors.

In this book the continuous control system is dealt with more as it forms the basis of the present digital system.

Controlling, say the level of a flotation tank which is being filled continuously and from which the pulp is withdrawn continuously, can be done crudely by observing the rise (or fall) of level and restoring it manually by manipulating valves and increasing or decreasing the input flow rate to the tank. Such an on-off method would result in an unsteady profile of level (Fig. 18.1). This situation is unacceptable in most mineral processing circuits. To solve the problem instruments have been devised and strategies developed to minimize the fluctuations in level. Automatic controllers have therefore being devised which serve to control flow rates, density of slurries, tank and bin levels, pump operations and almost all unit operations like crushers, mills, screens, classifiers, thickeners, flotation vessels and material handling systems.

The two basic control strategies or modes of these controllers are known as:

1. feed back control system, and
2. feed forward control system.

In the feed back control system the output from a process is monitored continuously by a sensor. When the output changes the sensor detects the change and sends signals to a *comparator* which compares the signal with the set point for normal steady state operation. It then estimates the *error* or the deviation from the mean. The error signal is passed on to the controller which compares the signal with the true set point and sends a signal to an operating device to reduce the error to zero. The signals are electrical, mechanical or pneumatic devices. Fig. 18.2 is a typical block diagram illustrating the feed back system
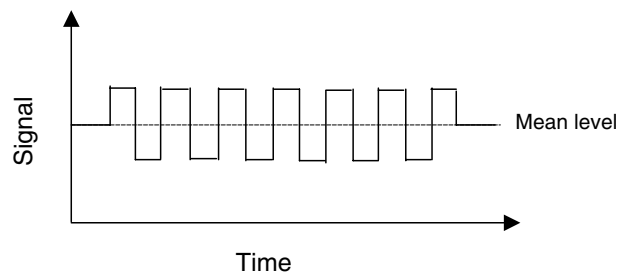
Fig. 18.1. Manual on-off control of flotation cell level.
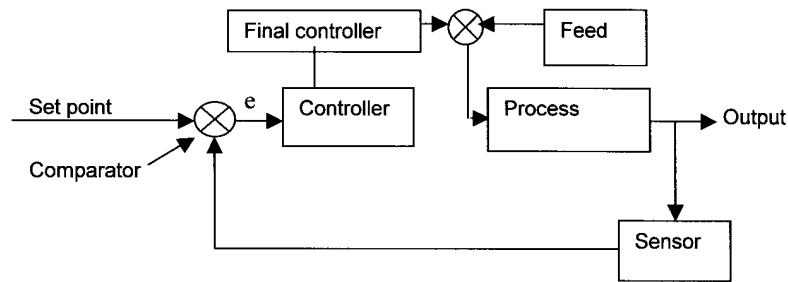
Fig.18.2. Block diagram of Feed Back control system.

It can be seen that the comparator has three functions. Its first function is to correctly receive signals of measured value from the signal monitor. Its second function is to compare the signal with the set point and then compute the deviation against the norm (set point) and its third function is to activate the final controller to correct the error.

There are two process factors that make the feed back control unsatisfactory. These are the occurrence of frequent disturbances, often of large magnitude, and the lag time within the process between occurrence of an event and delay in recognizing the signal. As shown later, these disturbances and lag times can be measured and corrective steps applied.

In the feed forward set up, the input signal, say of the feed, is monitored and controlled prior to the feed entering the process. In so doing it is expected that the feed to the process is unaltered and therefore the process performance remains unaffected. A block diagram of the feed forward system (Fig. 18.3) illustrates the principle of its operation.

In this set up the indicator in the input stream indicates the deviation in the input stream characteristics, (like feed flow rate) to the controller. The controller confines its activity to the incoming stream (and not on the process), computes the magnitude of the error and signals to the controller to provide appropriate action to restore the input stream characteristics to its original level.
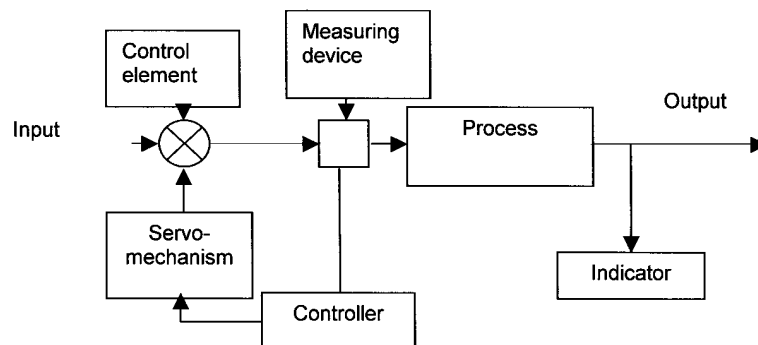
Fig.18.3. Block diagram of Feed Forward system of control.

Controllers are designed so that the output signal is:

1. proportional to the error
2. proportional to the integral of the error,
3. proportional to the derivative of the error,
4. proportional to a combination of the modes.

When the output signal O, is proportional to the error e, it is known as *proportional controller*. Mathematically the control action is expressed as:

$$O = G_P \ e \tag{18.1}$$

where G_P is the proportionality constant and e the error. G_P is usually known as the *gain*.

It can be seen that the gain is the ratio of the fractional change in the ratio of the output to input signals. When e = 0, the output signal is also equal to 0. That is, no signal is emitted from the monitor. In this situation Eq. (18.1) is written as:

$$O = O_O \ + \ G_P \, e \tag{18.2}$$

The proportional operation is expressed as *proportional band*. The band width is the error to cause 100% change on the metering gauge or chart.

The *integral controllers* are known as *reset controllers*. They are so designed that the output is proportional to the time integral of the error. Thus the output signal, O, is given by:

$$O \ = \ G_I \ \int_0^t e.dt \tag{18.3}$$

where G_I is a constant. For integral mode the reset action is more gradual than the proportional controllers.

The *derivative mode* of controllers stabilizes a process and the controller occupies an intermediate position. An example would be the monitoring of bubbling fluid level where only the average fluid level is measured and monitored, like the level in a flotation cell. The output signal in the derivative mode is expressed as:

$$O \ = \ G_D \frac{de}{dt} \tag{18.4}$$

where G_D is the constant.

In practice, the proportional mode is usually combined with integral or derivative modes but most of the time all the three modes are combined. In each combination the output is an additive function, that is for:

1. For proportional and integral (P+I) mode:

$$O = O_O + G_P \ e \ + G_I \ \int_0^t e.dt \tag{18.5}$$

2   For proportional +derivative (P+D) mode:

$$O = O_0 + G_P e + G_D \left(\frac{de}{dt} \right)$$ (18.6)

3.   For proportional +integral +derivative (P+I+D) mode:

$$O = O_O + G_P e + G_I \int_0^t e.dt + G_D \left(\frac{de}{dt} \right)$$ (18.7)

When any controller receives a signal from a sensor, the response time depends on the mode of the controller. Of the three modes, the response of the P+I+D (PID) controllers is the fastest. The P+I (PI) controllers takes slightly more time, while the P+D (PD) and P controllers never return to the original situation but remains at a level. The difference between the original level and the new steady level of proportional controllers is known as *off-set*. or the *droop*. The off-set value is therefore the difference between the steady state and the required control level or set point. In the P+I or P+I+D control systems no off-set is necessary Fig. 18.4 illustrate the relative control time taken by controllers operating on different modes.

In the operation of a P+I+D controller the derivative term signifies the rate of control action on a process affected by a disturbance.

18.2. Signals and Responses

Any signal resulting from a disturbance during an operation is known as a *forcing function*. The common types of forcing functions are:

1.   step function,
2.   pulse function,
3.   decaying exponential function, and
4.   sinusoidal function.
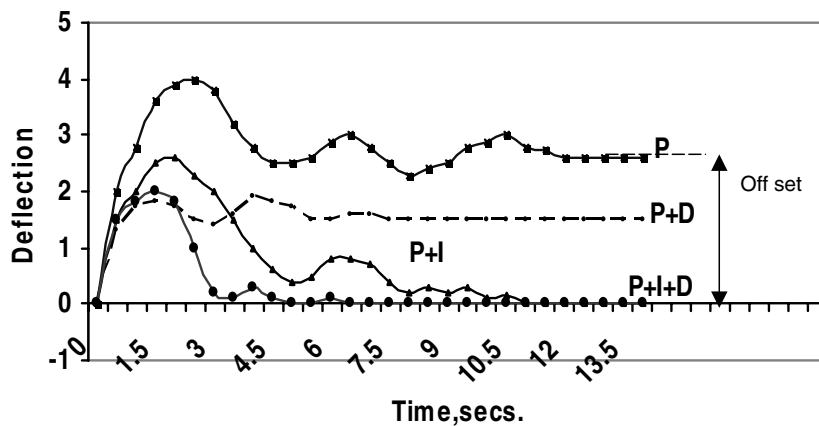
Fig. 18.4. Responses by controllers subjected to unit step disturbance.

The step function is instantaneous It involves no time as illustrated in Fig. 18.4. The magnitude of the signal is given by the height X and u(t) is unit step at time, t = 0. The condition can be mathematically expressed as:

$$f(t) = \begin{cases} 0, & t < 0 \\ 1, & t > 0 \end{cases}$$

(18.8)

When a disturbance is repeated at regular intervals it is described as a *pulse function*. It may be described as two equal functions of magnitude X operating in opposite directions. Fig. 18.6 illustrates a pulse function, where the pulse duration 0 - 1 is repeated. As can be seen in Fig. 18.6, the pulse function is time based and may be defined as:

$$f(t) = \begin{cases} 0, & t < 0 \\ x, & 0 \le t \le t_0 \\ 0, & t > t_0 \end{cases}$$

(18.9)

where   x   =   the height of the function and t the width.
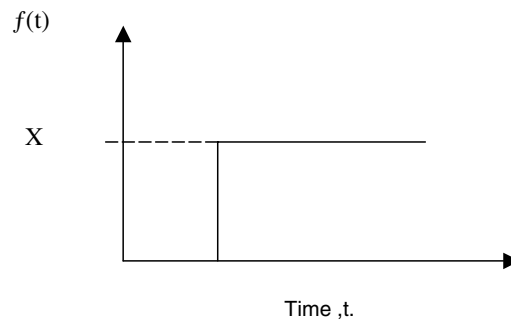
Fig. 18.5. Step Function.
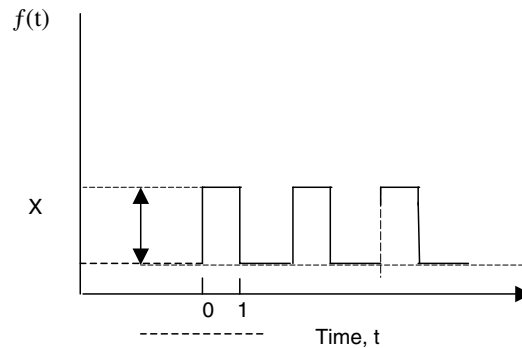
Fig. 18.6. Pulse Function.

The impulse function is a special case of a pulse function in which x = k/t₀, where k is a constant. It means that the area (x t₀) is a constant. A decaying exponential function shown in Fig. 18.7 may be written as:

$$f(t) = x(t) \, e^{-st} \tag{18.10}$$

Here: $f(t)$ = 0 at t < 1 and equal to e^{-st} at t > 0 where x(t) is the unit step.

A sinusoidal time function is described by the equation:

$$f(t) = \sin \omega t \tag{18.11}$$
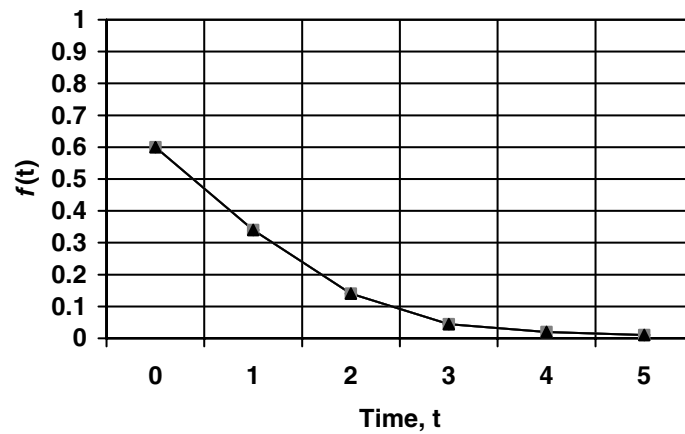
Fig. 18.7. Exponentially decaying curve.
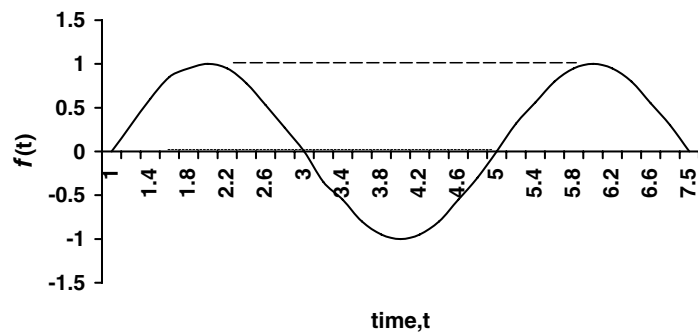
Fig. 18.8. Sinusoidal function.

and its properties are:

$$f(t) = \begin{cases} 0, & t < 0, \\ x \sin \omega t, & t \geq 0 \end{cases} \tag{18.12}$$

A sinusoidal time function is illustrated in Fig. 18.8. Forcing functions are generally represented by first or second order differential equations. That is:

$$A_o y = X(t) \qquad\qquad \text{Zero Order} \tag{18.13}$$

$$A_1 \frac{dy}{dx} + A_o y = X(t) \qquad\qquad \text{First order} \tag{18.14}$$

$$A_2 \frac{d^2 y}{dx^2} + A_1 \frac{dy}{dx} + A_o y = X(t) \qquad\qquad \text{Second order} \tag{18.15}$$

where   X   = input variable or input function and
        Y   = output variable, A_0, A_1 and A_2 are the constants.

For convenience of mathematical manipulations in control systems, Eqs. (18.13) - (18.15) are written in the form of Laplace transforms. On integration the time domain is obviously eliminated and a dummy operator is introduced. Thus, sequentially, the three equations transforms to:

$$\frac{Y(s)}{X(s)} = 1 \tag{18.16}$$

$$\frac{Y(s)}{X(s)} = \frac{1}{(\tau s + 1)} \tag{18.17}$$

$$\frac{Y(s)}{X(s)} = \frac{1}{\tau_1 s + \tau_1 s \tau_2 s + \tau_2 s} = \frac{1}{(\tau_1 s + 1)(\tau_{2s} + 1)} \tag{18.18}$$

where s is the Laplace dummy operator and τ the time constant.

The advantage of using such a technique is that the transforms can be added and subtracted by simple algebraic rules. After the operation the result may be inverted back to time domain (like taking logs and anti-logs of numbers). Derivation of the equations are explained in Appendix C.

18.3. Input and Output Signals of Controllers
The relation between the output and input signals of controllers is conveniently expressed by the ratio of the output and inputs transforms. The ratio of the transforms is known as the *transfer function*. In this book this is referred as T_F. The transfer functions of different modes of control systems can be easily determined. Where the error is e and G_P, the gain and τ the time, the transfer functions of different control modes are given in Table 18.1.

Table 18.1
Transfer function of controllers

Controller	Transfer function
Proportional (P)	G_{Px}
Proportional+Integral (P+I)	$G_P = [(\tau_I s + 1 / \tau_I s]$
Proportional+Differential (P+D)	$G_P = [1 + \tau_D s]$
Proportional+Integral+Differential (PID)	$G_P [(\tau_{Is} + \tau s * \tau_2 s + 2) / \tau_I s]$

The use of Laplace transforms to determine the response of a function of first and second order differential equations are illustrated in Examples 18.1 and 18.2.

Example 18.1

Let us assume that it is required to solve the following first order differential equation by the use of Laplace transforms.

$$\frac{dx}{dt} + 2x = 1 \tag{18.19}$$

Based on the condition $x(0) = 0$

Solution

Step 1
Using Laplace transform table in Appendix C-1, Eq. (18.19) transforms to:

$$sx(s) + 2x(s) = \frac{1}{s} \quad \text{or} \quad x(s) [s+2] = \frac{1}{s} \tag{18.20}$$

Using the theory of partial fractions, Eq. (18.20) may be split as:

$$x(s) = \frac{1}{s(s+2)} = \frac{A}{s} + \frac{B}{(s+2)} \tag{18.21}$$

where A and B are constants.

Step 2
The problem now resolves to determining A and B. To determine A, multiply both sides of Eq. (18.3) by s to give:

$$\frac{1}{(s+2)} = A + \frac{sB}{(s+2)} \tag{18.22}$$

Eq. (18.22) holds for all values of s. Setting $s = 0$, $A = \frac{1}{2}$
To determine B, multiply both sides of Eq. (18.21) by (s+2) giving:

$$\frac{1}{s} = \frac{A(s+2)}{s} + B \tag{18.23}$$

Eq. (18.23) is true for all values of s, Setting s = -2, B = -½. Thus Eq. (18.21) converts to:

$$x(s) = \frac{1}{2s} - \frac{1}{2} \tag{18.24}$$

This inverted to time domain gives:

$$x(t) = 0.5e^{-0.5\,t} \tag{18.25}$$

Example 18.2

Determine the response to a unit step function applied to a process defined by the second order differential equation:

$$\left[\frac{d^2y}{dx^2} + 5\frac{dy}{dx} + 6\right]y(t) = \left(\frac{dy}{dx} + 1\right)f(t) \tag{18.26}$$

Initial condition is x=0

Solution
Step1

Putting $\frac{dy}{dx} = s$, y(t)) =Y(s), and f(t) = F(s)
we get,

$$(s^2 + 5s + 6)Y(s) = (s+1)F(s) \tag{18.27}$$

Since a unit function is involved F(s) $= \frac{1}{s}$ (Appendix C-1)

That is $Y(s) = \dfrac{(s+1)}{s(s+2)(s+3)}$ \hfill (18.28)

Expanding Eq. (18.28) by the partial fraction method:

$$Y(s) = \frac{(s+2)}{s(s+2)(s+3)} = \frac{A}{s} + \frac{B}{(s+2)} + \frac{C}{(S+3)} \tag{18.29}$$

For estimating A, take Lt s → 0, next putting s = 0 as in Example 18.1 and substituting in Eq. (18.29):

$$A = Lt_{s\to 0}\frac{(s+1)}{s(s+2)(s+3)} = \frac{1}{2\times3} = \frac{1}{6} \tag{18.30}$$

Similarly for estimating B take Lt s → -2, next putting s = - 2 in Eq. (18.29):

$$B = Lt_{s \to -2} \frac{(s+1)}{s(s+3)} = \frac{-2+1}{-2(-2+3)} = \frac{1}{2} \qquad (18.31)$$

And similarly for estimating C, take Lt s → - 3, next putting s = - 3 in (18.29)

$$C = Lt_{s \to -3} \frac{(s+1)}{s(s+2)} = \frac{-3+1}{-3(-3+2)} = -\frac{2}{3} \qquad (18.32)$$

Thus Eq. (18.29) can now be written as:

$$Y(s) = \frac{1}{6s} + \left(\frac{1}{2} \times \frac{1}{s+2} \right) - \left(\frac{2}{3} \times \frac{1}{s+3} \right) \qquad (18.33)$$

Eq. (18.33) can now be inverted to time domain, t, using table in Appendix C-2 getting:

$$Y(t) = \frac{1}{6} + \frac{1}{2} e^{-2t} - \frac{2}{3} e^{-3t} \qquad (18.34)$$

18.4. Integration of Processes and Block Diagram

Laplace transforms and the transfer functions are conveniently used to study the input and output of processes in series or parallel. For example, for two identical unit processes operating in series, if the transfer function of each of the process is T(p) then the input and output of each process can be illustrated in Fig. 18.9 and Fig. 18.10. According to definition, the transform T(p) is given by:

$$T(P) = \frac{O_1}{I_1} \qquad (18.35)$$

and the transfer function for process 2 shown in Fig. 18.10 will be:

$$T(p) = \frac{O_2}{I_2} \qquad (18.36)$$

If the processes were combined in series then the transform of the inputs would be the sum of $I_1 + I_2$, and the transform of the combined output will be:

$$O_1 + O_2 = T(p) I_1 + T(p) I_2 = T(p) [I_1 + I_2] \qquad (18.37)$$

If however, three processes were in series (Fig. 18.11) and the transfer function of each were $T_1(p)$, $T_2(p)$ and $T_3(p)$, for inputs I_1, I_2, I_3, then for each process the transforms will be:
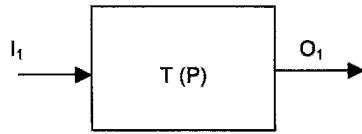
Fig. 18.9. Block diagram for process 1.   Fig. 18.10. Block diagram for process 2.
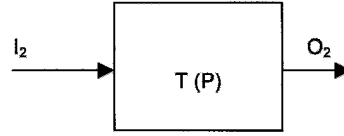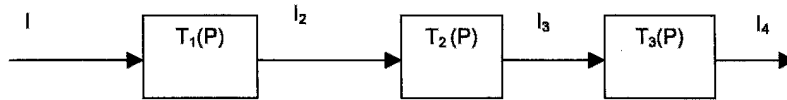
Fig. 18.11. Processes operating in series.

$$T_1(p) = \frac{I_2}{I_1}, T_2(p) = \frac{I_3}{I_2} \text{ and } T_3(p) = \frac{I_4}{I_3} \qquad (18.38)$$

According to definition the transfer function T(p), for the three processes combined in series would be:

$$T(p) = \frac{I_4}{I_1}$$

It can be seen that the product $T_1(p)\, T_2(p)\, T_3(p) = \frac{I_2}{I_4} \cdot \frac{I_3}{I_2} \cdot \frac{I_4}{I_3} = \frac{I_4}{I_1}$ \qquad (18.39)

Thus Eq. (18.39) shows that the overall transform of a process consisting of a number of processes in series is a product of transforms of individual processes.

However, when the processes are operating in parallel, as in Fig. 18.12 with a common input I and output O_4 and if the individual outputs were O_1, O_2, and O_3 respectively, then again by definition, the transforms for individual unit process will be:

$$T_1(p) = \frac{O_1}{I}, T_2(p) = \frac{O_2}{I}, T_3(p) = \frac{O_3}{I} \qquad (18.40)$$

Again according to definition the combined transfer function will be $= \dfrac{O_4}{I}$

It can be seen that :

$$\frac{O_4}{I} = [O_1 + O_2 + O_3 \ ] = \frac{1}{I}\left[T_1(P) + T_2(P) + T_3(P)\right] \qquad (18.41)$$
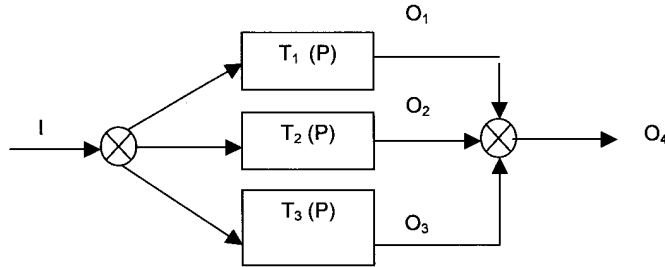
Fig.18.12. Processes operating in parallel.

Thus for processes in parallel the overall transform can be obtained by adding the individual transforms. With the help of Laplace transforms it is possible to estimate the output transforms of processes in series or parallel.

18.5. Setting and Tuning Controls

The responses of controllers are not immediate but take a finite time to attain the final value. A rule of thumb for setting is to study the response curve and to arbitrarily (trial and error) set the tuner such that the decay ratio is 4:1 between the first two successive peaks. The decay ratio being defined as the ratio of the heights of succeeding peaks in the decay curve. However, for setting and tuning two well established methods have been practiced, namely Ziegler and Nichol [1] method and Cohen and Coon [2] method. Both methods are empirical. Both methods yield similar results. In the following therefore the method by Cohen and Coon only is described.

In Cohen and Coon's approach, a feed-back system is set up and the loop is opened. A small step function (load) is injected. The response is recorded against time. A block diagram of the set up is illustrated in Fig. 18.13 and a typical response curve is shown in Fig. 18.14. The ultimate response, U_R is the steady state value and is given by the asymptote to the curve (Fig. 18.14). In order to determine the parameters for tuning a tangent is drawn through the point of inflection and its intersection with the x-axis (D_{Ti} in Fig. 18.14) determined. This is the "apparent" dead time. The slope S_L of the tangent is [U_R / t_A]. where t_A is the apparent time constant. That is:

$$S_L = \frac{U_R}{t} \tag{18.42}$$

The steady state gain G_C between pulse P and ultimate response U_R is:

$$U_R = P\,G_C \tag{18.43}$$

Cohen and Coon assumed that an open-loop system of a process behaves as a first order system described by the first order transfer function:
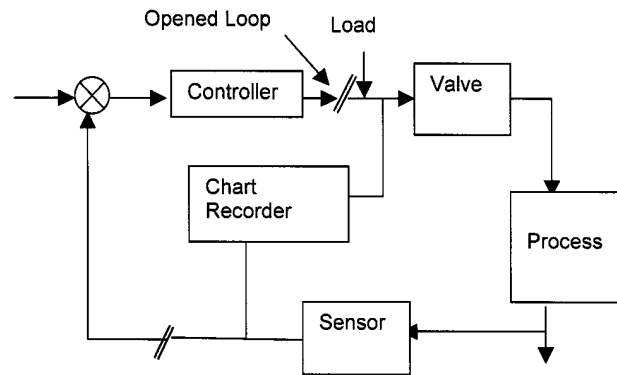
Fig. 18.13. Block diagram indicating Cohen and Coon's set up [3].
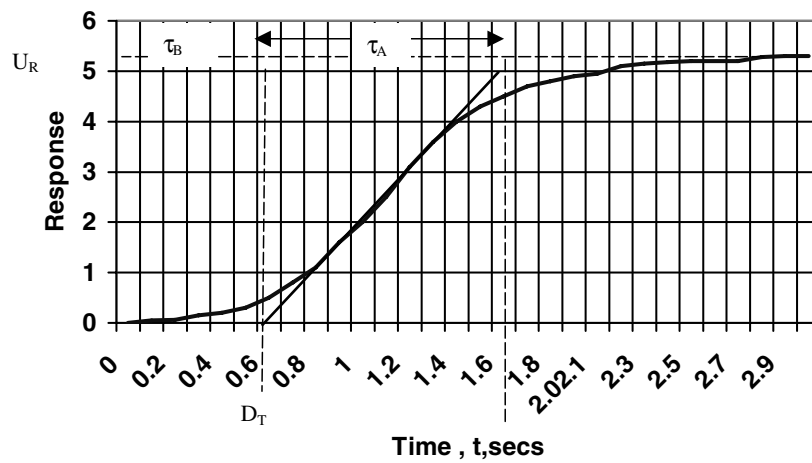
Fig. 18.14. Response curve to unit step change in Cohen and Coon's setup.

$$T_p(s) = \frac{K_C\, e^{\tau_B \cdot P}}{1 + \tau_A P} \qquad (18.44)$$

Using the data from Fig. 18.14, and from Eqs. (18.42) and (18.43) Cohen and Coon [2] empirically established rules for determining the settings for different modes of control.

The empirical method designed by Cohen and Coon (and also Ziegler and Nichols), are being increasingly replaced by the "model methods" of tuning [4,5,7]. Two such model methods presently used are:

1. ITAE (Integral Time weight absolute error),
2. IMC (Internal model control).

The ITAE method arises from the fact that the decay ratio of 4:1 for the first two peaks is not necessarily the same for the subsequent peaks. Thus an error is introduced. To minimizing this error, the process is considered as first order with a time delay. The output-input ratio is given by the transfer function:

$$\frac{O_S}{I_S} = \frac{G_P\, e^{\tau_D s}}{\tau_P s + 1} \qquad\qquad (18.45)$$

where O_S = Output of process,
$\quad\quad\ I_s$ = Input to process,
$\quad\quad G_P$ = Process gain,
$\quad\quad\ \tau_D$ = Process time delay,
$\quad\quad\ \tau_P$ = Process time constant
$\quad\quad\ \tau_C$ = Closed loop time constant
$\quad\quad\ I_S$ = Input to process (Controller output)

The controller settings for P+I and P+I+D controllers as derived by the ITAE method are given in Tables 18.2 and 18.3. The nomenclature used in the tables refer to Fig. 18.14. The ratio of $\tau A\,/\,\tau_B = T_R$ is taken and the closed loop time constant is taken as τ_C The ITAE method minimizes the integral of the time weighted absolute error. The IMC method uses a closed loop with a time constant τ_C and for:

$$\frac{\tau_C}{\tau_B} > 0 \ \text{ and that } \tau_c > 0.1\ \tau_A$$

The settings of P+1 and P+I+D controllers for the IMC method is also included in Tables 18.2 and 18.3.

Table 18.2
PI Controller Settings [6].

Setting	ITAE	IMC
G_c	$\dfrac{0.586}{G_P}[\tau_R]^{-916}$	$\dfrac{\tau_A}{G_P(\tau_C + \tau_B)}$
τ_i	$\dfrac{\tau_A}{1.03 - 0.165[\tau_R]}$	τ_A

Table 18.3
PID Controller Settings [6].

Setting	ITAE	IMC
G_C	$\dfrac{0.965}{G_P}[\tau_R]^{-0.85}$	$\dfrac{(2\tau_A + \tau_B)}{G_P(2\tau_C + \tau_B)}$
τ_i	$\dfrac{\tau_A}{0.796 - 0.1465(\tau_R)}$	$\dfrac{\tau_B}{2} + \tau_A$
τ_D	$\tau_A \times 0.308 \times [\tau_R]^{-0.929}$	$\dfrac{\tau_A \tau_B}{2\tau_A + \tau_B}$

In a particular situation the choice of selecting one or other method of setting depends on the acceptance of the nature of the oscillatory response which most suits the situation. In practice, preliminary controller settings are set according to recommendation given in Tables 18.2 and 18.3, but the final fine tuning is done visually. However more sophisticated numerical methods of quantifying controller responses have been introduced like IAE (Integral of Absolute Error) and ISE (Integral of Squared Error). Flintoff [8] has mentioned the use of software. Software like MATLAB is increasingly being used.

18.6. Complex Advanced Controllers

With the increasing complexities of processes, additional control set ups have been introduced. The basic principles of operation of these complex controllers are the same as those already mentioned. Of these, three are of direct use to mineral processors:

1. Error squared controllers,
2. Ratio Controllers,
3. Cascade controllers.

18.6.1. Error squared controller

Some process systems require little control action when the process variable is very near the set point. In such cases, control action can be achieved satisfactorily by using the error squared in the PI and PID algorithm instead of simple error terms. Controllers using this technique permit the use of low gain setting when the error is small and does not hold the controlled variable at a particular set point but operate as an 'average control'. When the disturbance is large the gain is increased to avoid large deviations. According to Gault [9] a "dead band" effect is produced. The dead band effect around the set point can be removed by using $(\varepsilon + \varepsilon^2)$ term as the error. It should be noted that $\varepsilon^2 = \varepsilon^* |\varepsilon|$ which retains the sign of the error.

18.6.2. Ratio Controller

When two loads in a process have to be controlled simultaneously such that the ratio between them remains constant, the controllers used are *ratio controllers*. As an example, say in grinding mill circuits where the feed is set at a definite ore/water ratio, the water flow controller set point has to be set at a definite ratio with the tonnage rate to ensure the pulp density to the mill remains constant.

The functional module that implements the ratio, is essentially a multiplier, thus if P_{V1} and P_{V2} are two process variables then:

$$Pv_1 = R\ Pv_2 \quad or\ R = \frac{Pv_1}{Pv_2} \qquad\qquad (18.46)$$

R is known as the settable ratio. The ratio station has similar features to the PID system [10].

The prime role of the ratio station is to provide a way of generating the set point. The ratio itself becomes a set point controlled by higher level control in a structured system.

The ratio controllers can be used both in open and closed loops. Such controllers are often used in practice in flotation circuits where the water additions is related to the target feed rate and in circuits where pH control is required, say lime additions, in gold cyanidation process.

18.6.3. Cascade Controller

By using a single controller it is difficult to control a process that involves say, two or more stages of different dynamic characteristics. The problem is aggravated when the response time of the first or main controller is longer than the second. In such cases the introduction of a second controller is necessary. The second controller operates in conjunction with the first controller but only at a particular stage of the process where the disturbance can be detected with minimum dead time and short response time. Such a control system is known as *Cascade Control*. It can be described as a multi-loop control system. A typical example is illustrated in Fig. 18.15 where the objective is to maintain a constant level of a tank.

Fig. 18.15 shows that the main loop controls the tank level. The loop operates slowly compared to the fluctuations of the feed stream. The feed stream in its part is controlled by a faster inner loop that controls the flow. The second controller has an external set point which changes with the level controller and operates at a much slower rate.

Cascading slightly improves the compensation of disturbances entering the outer loop, but the compensation of the inner loop is greatly improved. The set point of the inner flow
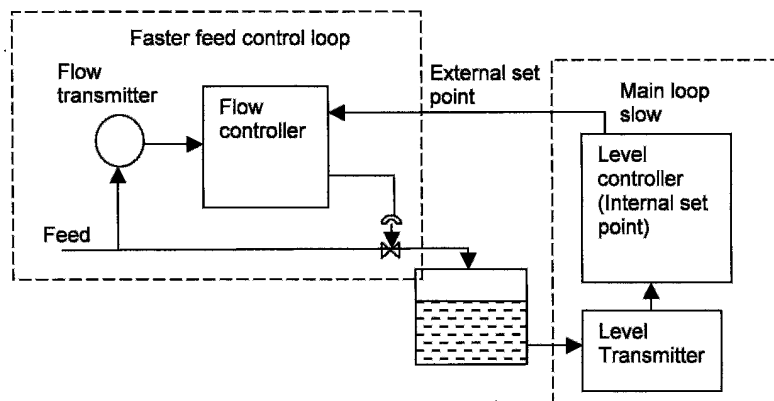
Fig. 18.15. Cascade Controller system.

controller is obtained from the output of the level controller. The cascade control system provides a high degree of stabilization to the overall control.

18.6.4. Adaptive Controller

An adaptive control system automatically compensates for variations in system dynamics by adjusting the controller characteristics so that the overall system performance remains the same, or rather maintained at optimum level. This control system takes into account any degradation in plant performance with time. The adaptive control system includes elements to measure (or estimate) the process dynamics and other elements to alter the controller characteristics accordingly. The controller adjusts the controller characteristics in a manner to maintain the overall system performance. The basic essentials of the adaptive system are:

1. Identification of system dynamics,
2. Decision, and
3. Modification.

Once the system is identified, (which is a difficult process) the decision function operates. This in turn activates the modification function to alter the particular process parameter and to maintain optimum performance.

The common ways of evaluating performance are by model comparison and performance criteria. In the model comparison system, a model is selected that bears resemblance to the desired system characteristics. In it, all effects of the system characters and effects of disturbances are known. According to Gault [9] the response characteristics of the control system variable parameters are "slaved" to the response characteristics of the reference model. The error between the model and the control system is acted on. This action is accomplished by an adaptive operation which produces the required system gains. The path of adaptation is the minimization of the integral of the error square.

In the performance criterion, a general performance index such as the integral of the error squared is chosen and continuously computed. The system is adjusted to keep the value of the index at a minimum level. A development of this is the Kalmin Filter [7]. This is a complicated process. Interested readers are referred to the work of Stephanopoulos [11], Flintoff and Mular [12],

18.7. Dead Time Compensation

So far we have assumed that a variation in the feed and process will be monitored immediately and corrective action to any disturbance taken immediately. But in practice a time is elapsed between the change and the time at which the change is detected. For example, an apron feeder discharging ore is set to feed a travelling belt conveyor. A short section of the conveyor is mounted on load cells which measure the mass rate of ore travelling. Time elapses before any change in the feed mass rate occurs on the feeder and the time it is detected by the load cells of the conveyor as the load cells are located at a distance (Fig. 18.16). This is the dead time of the controller loop and is often referred to as *transportation-lag or distance-velocity-lag.*

To design a control loop therefore the transform for the dead time has to be considered. Suppose a plant is constructed by some means so that the plant transfer function Gs is the transfer function without the dead time and let $\tau_D(s)$ is the dead time. A typical feed back block diagram of such a plant would be as illustrated by Fig. 18.17. In this typical setup, unfortunately, the signals cannot be measured directly as the dead-time occurs as a distinct

element. Hence a dead time compensation devise is sought. Compensation is introduced by taking the output signal and passing it through a model to cancel the original signal. The method is further explained below with an example.

Suppose a model is constructed by some means so that it is composed of a dead time τ_M. In a typical feed back system (Fig. 18.17) if an output signal from the controller is passed through the model then it can be measured, as seen in Fig. 18.18.

In Fig. 18.18 the cancelling model is added to the normal feed back model. This arrangement is known as *Smith predictor* or *dead time compensator*. A successful use of this concept was made by Anderson et al [13] while designing four SAG mill feeder controls in Freeport, Indonesia.

18.8. Instrumentation and Hardware

18.8.1. Instrumentation

The function of the instruments is to measure the steady state and transient behaviours of processes in a physical world. Usually the design of instruments involves multi-disciplinary activities all of which a mineral processor need not be involved, but he should be aware of the reliability, including correct operation of the instrument and also their sensitivities.
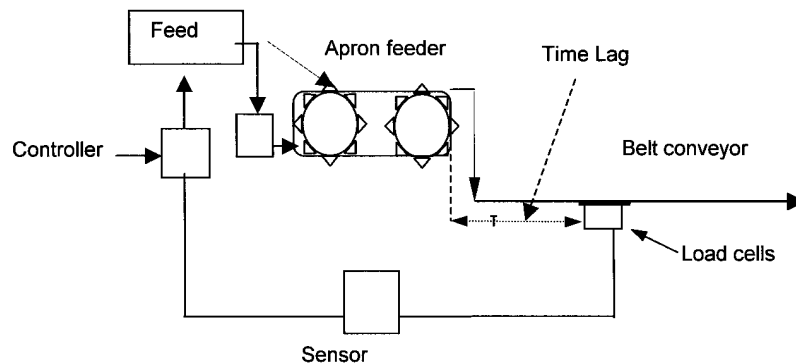
Fig. 18.16. Dead Time Lag.
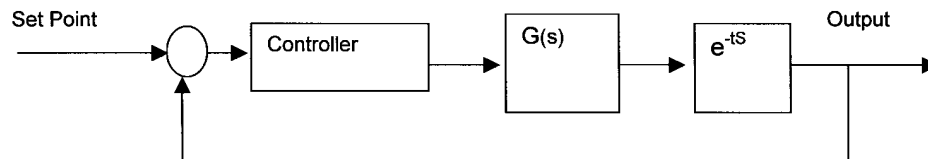
Fig. 18.17. Typical Feed Back loop.
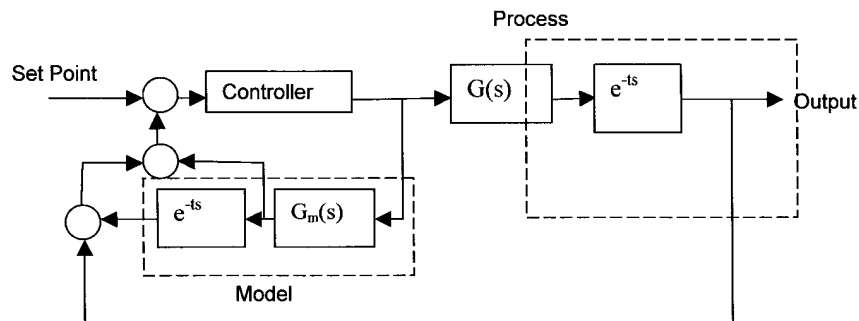
Fig. 18.18. Dead Time Compensator to feed back loop.

Further, it is necessary to ensure that their loading effects are minimal and that the signal is passed without attenuation, loss of magnitude or phase change. For most instruments such operation software is available from instrument manufacturers.

Instrumental errors are inherent within an instrument arising from its mechanical structure and electronic components. This important limitation must be recognized when selecting and using instruments.

Most loops are operated by PID controllers which are implemented by DCS (distributed control systems) operating software. This means that the control system is not centralised but is composed of interconnected multiple units. In most other cases, ratio or cascade loops are employed. According to Flintoff and Mular [10] an average grinding mill has about 2000 loops of which 97% use PID. All systems operate on 4-20 mA output signals. Multi transmitter signal input is available so that different control loops can be rapidly configured. Microprocessors provide a range of control functions.

The present day instrumentation takes care of the DCS system and therefore the control mechanism is complicated and is more in the domain of the instrument engineer. However, the metallurgist and process engineers needs to know the basics in order to best utilize control mechanisms.

Instrumentation and control of mineral processing operations is usually visualized as involving connected building blocks. Process control and instrumentation consider these blocks divided into three or four levels: These are:

1. Basic block   Level - 1
2. Supervision block   Level - 2
3. High level block   Level - 3
4. "Watch dog"   Level - 4

A general description and function of these levels follow.

Level 1 control

This is the regulatory level where basic controls loops like, P+I control loops include control of feed tonnages from bins, conveyors, manipulating of bins, water addition loop (in milling circuit) pump speed and sump level controls, thickener overflow density control etc are involved (depending on the process circuit).

Level 2

This is a supervisory control stage that includes process stabilization and optimizing, usually using cascade loop and ratio loops. For example, in a ball mill circuit the ratio loop controls the ball mill water while the cascade loop controls the particle size of product by manipulating the tonnage set point.

Level 3

Controls at this level include maximizing circuit throughput, limiting circulating load (where applicable).

Level 4

This is a higher degree of supervisory controls of various operations including plant shut downs for maintenance or emergency. Austin [14] has referred to level 4 controls as "watch-dog" control.

The usual instruments covering the regulatory levels in mineral processing plants are shown in Table 18.4:

Table 18.4
Instruments and their uses in mineral processing plants

Instrument	Property measured and use
Weightometer	Measures mass flow rate of material. Usually a small length of conveyor belt rests on load cells
Level indicator	Measures level by, ultrasonic, pressure differential or simply by a float-ball
Flow meters	Measures mass rate of flow generally by non-invasive methods. like Magnetic flow meters, Ultrasonic flow meters.(Doppler effect) The invasive types include orifice flow meters.
Density gauges	Measures fluid and pulp densities either on stream with Gamma ray density gauges, or by taking samples and using Marcy density gauge.
Pressure gauges / Thermo-couples	Measures pressure or pressure differentials pneumatic,/hydraulic systems and temperatures
Particle size analyzer	Measures particle size passing a particular sieve size, e.g., 75 microns on stream (OSA) by generating ultrasonic signals
pH indicator	For measuring acidity and alkalinity of solutions
D/A-A/D converter	For converting digital to analog signals and analog to digital signals
Attenuators	Converting amplitude of input/output signals.

18.8.2. Hardware

Pneumatic Valves

In mineral processing operations where flow of fluids and slurries are frequently measured, a valve at the inlet and outlet of operation is common. In effect the valve serves as a part of the operation as distinct from instruments which indicate the status of a particular operating condition. In several circuits it forms the final control of the system. Therefore its transform has to be included in block diagram algebra.

Fig. 18.19 is a schematic diagram indicating the principles of operation of a typical pneumatic valve. The flow through the valve is governed by the design of its shape and space allowed between the valve and the valve seat. The extent of flow is generally given by the stem position.

Valves are shaped so that the flow through could have a linear, square root or hyperbolic relation to opening. Mathematically these can be expressed as:

Linear	$F(x) = x$
Square root	$F(x) = \sqrt{x}$
Hyperbolic	$F(x) = 1/\alpha - (\alpha-1)x$

where x is the opening distance.

In Fig. 18.19 it can be seen that the pneumatic pressure actuates the diaphragm which in turn affects the stem which operates the position of the opening manipulated by a plug.

To determine the transform of the valve operation, let us assume that the area of the diaphragm is A, and that it is displaced by a distance δ when a force (H δ) is exerted via a spring, H being the Hook's constant. A frictional force, μ, is active in the opposite direction due to the tight packing to stop leaks between the stem and the body of the valve. The frictional force μ, acting, say upwards, for a short time t, would be $\mu \, d\delta/dt$.
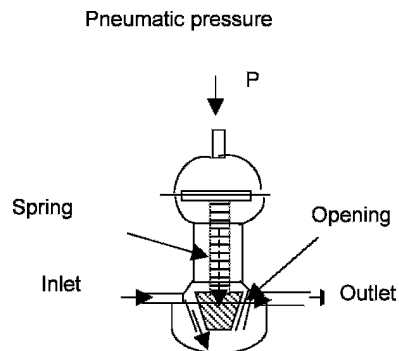
Fig. 18.19. Schematic diagram of a valve for control fluid flow.

644

Let P be the signal representing the force that opens and closes the valve. The displacement δ of the valve (diaphragm) is equal to the opposing pressure of the spring.

$$PA = \frac{M}{g}\frac{d^2\delta}{dt^2} + \mu\frac{d\delta}{dt} + H\delta \qquad (18.47)$$

Dividing by H and transposing,

$$\frac{M}{g}\frac{1}{H}\frac{d^2\delta}{dt^2} + \frac{\mu}{H}\frac{d\delta}{dt} + \delta = \frac{PA}{H} \qquad (18.48)$$

This is a second order differential equation and as we can put:

$$\tau^2 = \frac{M}{g}\frac{1}{H} \text{ , also } 2\xi\tau = \frac{\mu}{H} \text{ and } G_P = \frac{A}{\delta} \qquad (18.49)$$

The standard transform of this second order system is:

$$\frac{\overline{\delta}s}{\overline{P}(s)} = \frac{A/H}{[M/Hg]}\left[s^2 + \frac{\mu}{H}\ s + 1\right]1 \qquad (18.50)$$

The present trend is to invariably use electronically operated actuators instead of pneumatically operated valves. In either case the transform will remain unaltered [15].

18.8.3. Other Hardware
Other hardware relates to electrical functions (capacitance, resistance, and inductance) mechanical systems like springs, frictional systems, rotational systems and mechanisms to suit particular setups. Transfer functions of some common selected hardware are given in Appendix C-2.

18.9. Controls of Selected Mineral Processing Circuits
Mineral processing operations are dynamic systems. Disturbances arise primarily due to variations in process inputs and also due to the process machinery both of which combine to affect the smooth operation of processes. To understand the strategy of process optimization and control for steady operation let us consider a simple unit operation like the control of the solid level in bins and hoppers or the fluid level in a tank. The principle underlying the control strategy is the same in both systems while the hardware and operation methods differ. Level control of bins, bunkers and solids storages, are more complicated as the solids in these vessels are almost never level. For smooth liquid level in tanks, this problem obviously does not arise. In the following section the simpler situation of controlling the fluid level in tanks or similar vessel is examined.

18.9.1. Controlling Liquid Level in Tanks
Let us consider a tank fed by a liquid at the rate of F_I. The tank level has to be maintained by an output F_0. Let us assume that a level L (Fig. 18.20) has to be maintained in the dynamic state using a sensor to measure the hydrostatic pressure difference between the top and the
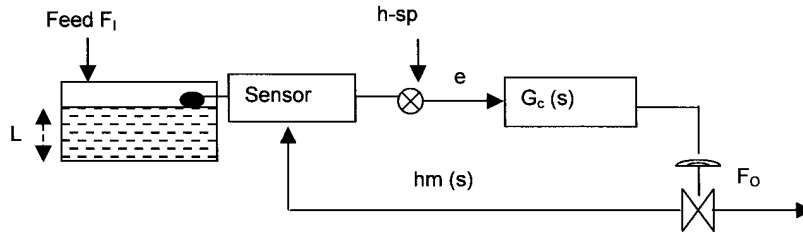
Fig. 18.20. Liquid level control [11].

bottom level of the tank. Let us also assume that a disturbance is applied to the feed system and the output F_0 is the manipulative variable which is irreversible. A block diagram describing the process is given in Fig. 18.20.

The operation involves a change in level L in time t. If A be the cross-sectional area of the tank which is continuously fed and emptied, the process may be expressed mathematically as:

$$A\frac{dL}{dt} = F_1 - F_0 \qquad (18.51)$$

where F_1 = load, and F_0 = manipulative variable, (output). The transfer function of this first order differential equation is:

$$\overline{L}(s) = \frac{1}{As}F_1(s) - \frac{1}{As}F_0(s) \qquad (18.52)$$

To examine the steady state condition the transfer function of each of the component is required. For determining the transfer function of sensor its operation has to be examined. We have already considered the sensor as a differential pressure transducer, where the differential pressure is generated by the pressures at the top and bottom levels of the fluid in the tank.

As the height of the liquid level changes it is obvious that ΔP also changes by an amount proportional to L, that is: $\Delta P = \kappa L$ where κ is a constant. If the change is brought about by the displacement of the sensing diaphragm by an actuating pressure ΔP, then a force balance around the sensing diaphragm can be established. Let Lm be the displacement of the diaphragm of the sensing device due to a change in level affected by a pressure differential ΔP and τ_1 ,ξ and k_P are constants that are functions of the instruments. Then according to Stephanopoulas [11] the sensor operation may be described by a second order differential equation as:

$$\tau^2\frac{dLm}{dt^2} + 2\xi\tau\frac{dLm}{dt} + Lm = K_p\Delta P \qquad (18.53)$$

And the transfer function of this second order equation is:

$$\overline{Lm}(s) = \frac{G_p K}{\tau^{2s} s^2 + 2\xi\tau s + 1} \overline{L}(s)$$ (18.54)

Eq. (18.54) therefore is the transfer function of the sensor.

Let us assume that a P+I controller is used and a set point Lsp is set, Then the transfer function of the error, e will be:

$$\overline{e} = [\overline{Lsp}(s) - \overline{L}_m(s)]$$ (18.55)

We have seen (Table 18.2) that for a P+I controller whose output is $\overline{O}$, the transfer function is given by:

$$\overline{O}(s) = G_c \left[1 + \frac{1}{\tau_I s} \right] \overline{e}(s)$$ (18.56)

For the final control element, that is a control valve, the transfer function of the response is a first order system and therefore can be written as:

$$\overline{F}_o(s) = \frac{Ge}{\tau_2 + 1} \overline{e}(s)$$ (18.57)

From the block diagram it can be seen that the components operate in series. Thus Eq. (18 39) applies. In the general case, if $G_C(s)$ is the transfer function of the controller, $G_F(s)$, that of final element, $G_P(s)$, of the process, G_m that of the sensor (measuring device), then according to block diagram algebra the response of the output to the change of set point will be:

$$\overline{O}_1(s) = \frac{G_P(s) G_F(s) G_C(s)}{1 + G_p(s) G_F(s) G_C(s) G_m(s)} \times \overline{O}_{SP}$$ (18.58)

And the effect on output due to a disturbance (change in load) will be:

$$\overline{O}_2(s) = \frac{G_d(s)}{1 + G_p(s) G_F(s) G_C(s) G_m(s)} \times \vec{d}(s)$$ (18.59)

The closed loop response will be the sum of Eqs. (18.58) and (18.59), that is:

$$\overline{O}(s) = \frac{G_P(s) G_F(s) G_c(s)}{1 + G_P(s) G_F(s) G_c(s)} + \frac{G_d}{1 + G_p(s) G_F(s) G_c(s) G_m(s)} \times \overline{d}(s)$$ (18.60)

The response in time domain to a change in the level due to a change in load will be given by the inverse of Eq. (18.60) which would contribute to the control the level of tank.

The principles explained in this simple control system are applicable to all controlling operations. In integrated unit processes encountered in normal mineral processing operations, the applications become more complicated and would depending on the circuit diagram.

In the following, principle considerations which go to control selected mineral processing operations are described.

18.9.2. Crushing Plant Control

The control of any crushing operations starts with the control of the feed system. Lynch [16] has summarized the disturbances in a crusher as:

1. ore properties (size and hardness),
2. ore feed rate,
3. crusher settings (close and open settings) – alterations due to wear and tear ,
4. surge in feed load and plant power draw.

The control loops of a gold crushing plant are shown in Fig. 18.21 [14]. Two regulatory control loops and a supervisory control loop are shown. The function of one regulatory loop (shown within dotted lines) is to control the feed tonnage on the feeder conveyor and the other to regulate the crusher power which in turn regulates the feed. The supervisory loop is a cascade loop which deals with any imbalance between the two regulatory loops through level changes in the feed hopper.

The basic instrumentation involved would include a transducer to monitor the closed side setting (and or open side setting), an A/D connection to the controller and a D/A connection to the level indicator [16].

18.9.3. Grinding Mill Control in Closed Circuit

The principle objective for controlling grinding mill operation is to produce a product having an acceptable and constant size distribution at optimum cost. To achieve this objective an attempt is made to stabilize the operation by principally controlling the process variables. The main disturbances in a grinding circuit are:
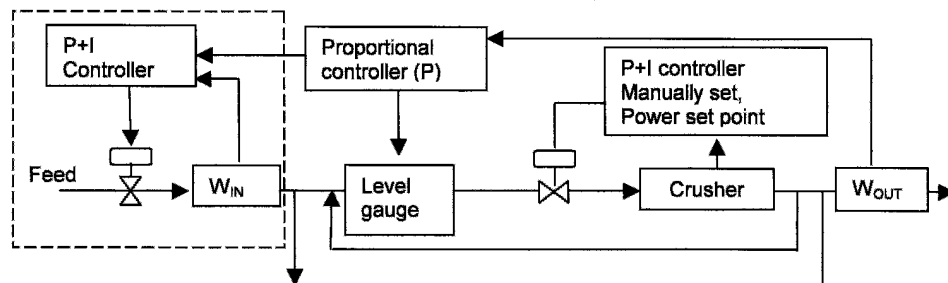
Fig. 18.21. Control of gold crushing plant [14].

1. change in ore characteristics (ore feed rate, grindability, feed particle size distribution, mineral composition and mineral characteristics like abrasiveness, hardness),
2. changes in mill operating parameters like variation of input flow rate of material like surging of feed caused by pumps and level of mill discharge sump.

The mill control strategy has to compensate for these variations and minimize any disturbances to the hydrocyclone that is usually in closed circuit. The simplest arrangement is to setup several control loops starting from the control of water/solid ratio in the feed slurry, sump level control, density control of pulp streams at various stages and control of circulating load. Presently most mills use centrifugal pumps for discharging from the sump. This helps to counter surges and other problems related to pumping. For feed control the most likely option is to use a feed forward control while for controlling the hopper level and mill speed and other loops the PI or PID controller is used. The control action should be fast enough to prevent the sump from overflowing or drying out. This can be attained by a cascade control system. The set point of the controller is determined from the level control loop. This type of control promotes stability.

As an example, for completely controlling a grinding mill circuit the operation of a SAG mill is considered here as these mills seem to be slowly displacing the normal ball mill operations.

The SAG mill characteristics have already been mentioned earlier in Chapter 9. The main variables are:

1. solid mass transported through the mill (solid feed plus the circulation load),
2. the mill discharge solids, and
3. the overflow solid flow.

From the control point of view, the additional interests are:

1. overfilling of the mill,
2. grate restrictions and,
3. power draft.

Each of these is controlled by specific controlled inputs, i.e., feed rate, feed water and discharge water flows. The overflow solids fraction is controlled by monitoring the ratio of total water addition (W_{TOT}) to the solid feed rate. The ratio being fixed by the target set point of the overflow solid fraction.

Usually the charge volume of SAG mills occupy between 30-40% of its internal volume at which the grinding rate is maximized. When the charge volume is more, then the throughput suffers. The fill level is monitored by mill weight measurement as most modern mills are invariably mounted on load-cells.

During the operation of SAG mills, it is sometimes observed that the sump levels fall sharply and so does the power draft. This phenomenon is attributed to flow restrictions against the grate. When this occurs it is necessary to control, (or in extreme circumstances), stop the incoming feed.

The power draft is the result of the torque produced by the mill charge density, lift angle of the charge within the mill and fill level. The relationship between these parameters is complex and difficult. Therefore to control mill operation by power draft alone is difficult.

For the purpose of stabilization of the circuit, the basis is to counteract the disturbances. Also the set points must be held. The set points are attributed by dynamic mass balances at each stage of the circuit.

In modern practice the structure and instrumentation of the control systems of tubular grinding mills are designed to operate in three levels or in some cases four levels. The control loops and sensors for a SAG-mill and the levels of control are illustrated in Fig. 18.22. According to Elber [10,17], the levels are:

Level 1

The operation at Level 1 mainly consists of controlling the feed rate and the water inputs. In addition to this the SAG mill revolving speed and secondary circulating load also forms ancillary loops.

There are four main control loops in Level 1 (Table 18.4).

Table 18.4
Control loop of SAG mill

Control Loop	Control Variables
Feed Flow rate	Feeder Speed (Feed motor speed)
Sump water flow	Valve position
Sump level (Discharge feed regulator)	Level indicator

The main sensors are:

1. load cell for mill weight,
2. power measurement (ammeters, voltmeters), and
3. density gauges (γ-ray density gauge) for on line, non-invasive, measurement of slurry densities.

Level 2

The function of Level 2 is to stabilize the circuit and to provide the basis of optimizing function in Level 3. Three cascade loops operating in level 2 controls that function in conjunction with level 1 controllers. The cascade loops are:

1. mill load feed rate (controlled by feeder speed),
2. mill discharge, (% solids), and
3. mill product, (% solids).

The set points are supplied by level 3 controllers for all the cascade loops. The mill load and percent solids in the two streams are calculated from signals received by sensors in the water flow stream, the sump discharge flow rate and the density readings from density meters in the pulp streams. The mill load cells supply the charge mass. The load cell signals are compensated for pinion up thrusts [10].

The set points for the mill load and the two pulp densities are given by level 3 controls. The points may also be set by neural method of analysis or fuzzy logic expert systems.
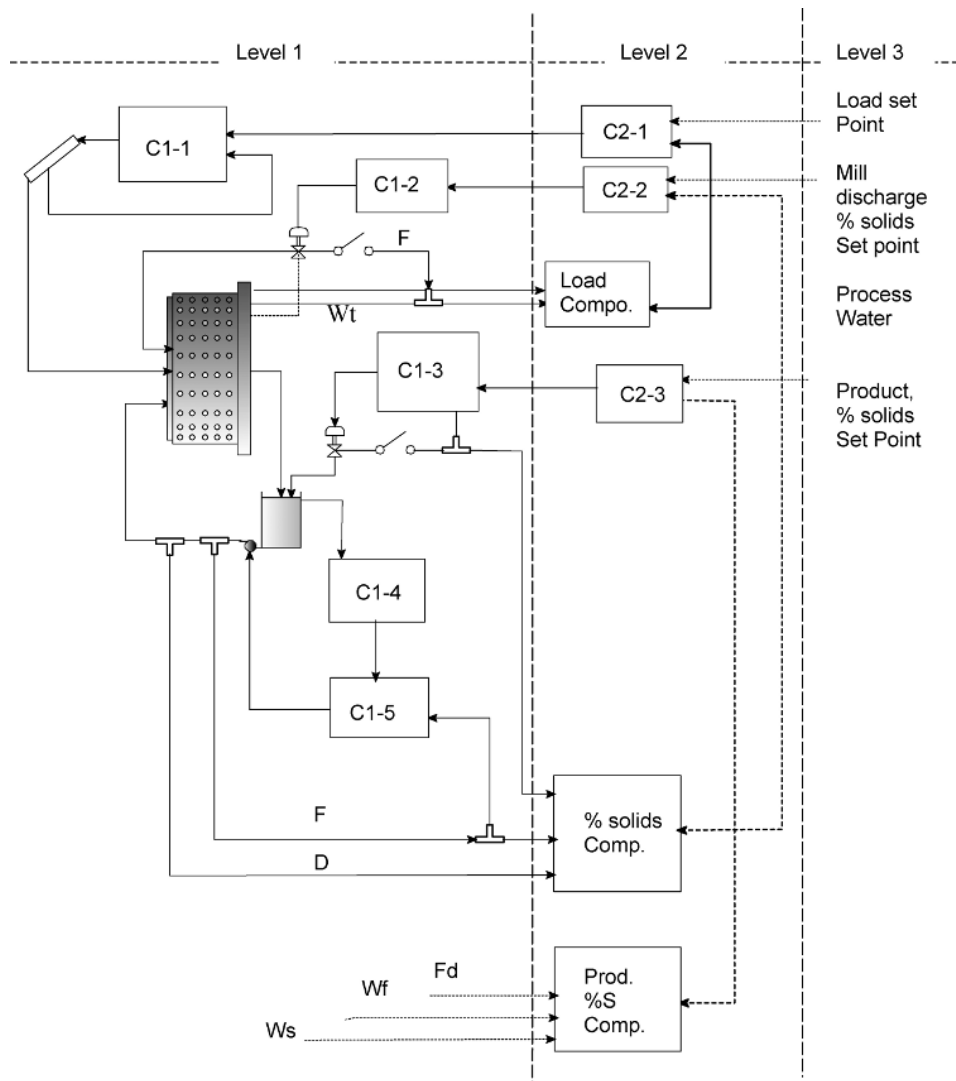
Fig. 18.22. Three levels of control of a AG/SAG mill.

To determine the set point for the optimum mill load, a relation between load, consisting of different feed blends and performance (the maximum achievable throughput) is established. Similar observations are made for mill discharge density and mill discharge flow.

For some routine standard situations ready made supervisory work station computer programs, especially for Levels 1 and 2, are available.

Level 3

The primary function at Level 3 is optimisation of the SAG mill operation. That is, control of the product at optimum level. In an integrated situation where ball mill and cyclone is in the circuit, the optimisation must take place keeping in mind the restraints imposed by down stream requirements. This optimisation can best be achieved by developing a software for computer use. Usually a large database is required to cover infrequent control actions.

18.9.4. Thickener Control

The control of thickener operation is directed to obtaining a clear overflow as rapidly as possible. The sedimentation rate is usually accelerated by additions of flocculants. Flocculants are added in the feed pipe (or feed launder) and maximum dispersion attempted by appropriate design of its entry to the thickener tank. The object is to entirely cover all the surface of mineral particles. The choice of flocculent and its concentration vary. It depends on the minerals present in the slurry, their composition and their surface characteristics. It is necessary not to have too much turbulence at the entry point of the tank.. For this purpose, the overflow level is kept sufficiently high above the feed level to ensure acceptable solid concentration in the overflow.

Fig.18.23 is a schematic diagram of a thickener showing the different parameters. From a process control point of view the design parameters and major variables are:

1. height of the overflow clear fluid, H,
2. height of the bed level from discharge end, H_B,
3. solids inventory, S,
4. sold mass inflow, S_I,
5. solids mass outflow, S_0,
6. average bed solid volumetric fraction, v_S

It can be seen that the solid inventory $S = A\ H_B\ v_S\ \rho_S$, where ρ_S is the solids density.
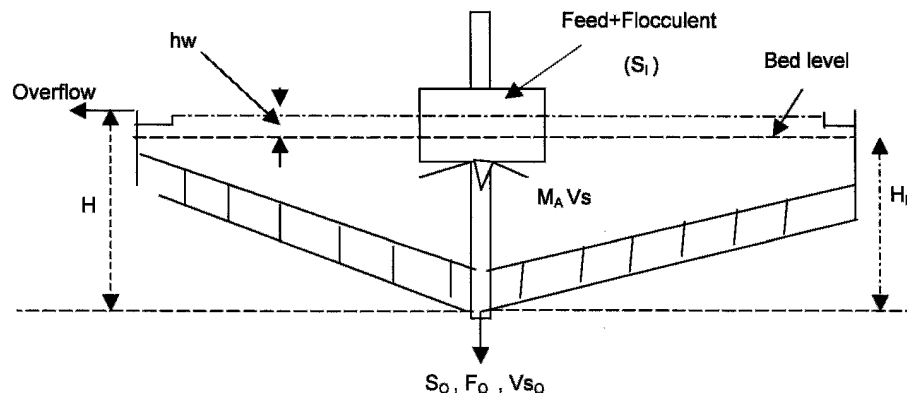
Fig. 18.23. Schematic diagram of thickener.

At the bed level the solids residence time, t_R will be:

$$t_R = \frac{S}{S_I} \tag{18.61}$$

The dynamic solids mass balance is:

$$\frac{dS}{dt} = (S_1 - S_0) \tag{18.62}$$

During operation, if the feed flow changes, i.e., increases or decreases, the flocculent input changes proportionately. A control loop in the flocculent charging device involving a pump is required to follow these changes at an appropriate level of control.

The power, P, required by the pump, which is assumed to be connected to a horizontal pipe with no bends, is given by:

$$P = k \ \mu \ (F_D)^2 \ kW/h \tag{18.63}$$

where
k = constant (proportional to pipe length),
μ = viscosity,
F_D = underflow discharge flow rate.

The pump pressure obviously varies as the solids mass outflow (kg/m^3) and according to Elber [10], is given by:

$$P = \frac{k}{\rho^2} \frac{\mu}{B_s^2} S^2 \, 0.96 \quad Pa \tag{18.64}$$

Control Strategy

The control of the solid contents in the overflow and underflow streams is the basis of thickener control. The average bed density (solids inventory) has to be controlled by the underflow flow rate and the flocculent additions to the slurry. To attain target overflow solids concentration the underflow density should be sufficiently high. This is obtained by longer residence time of treated slurry in thickener.

The underflow flow rate is measured by magnetic or ultrasonic flow meters.
The control scheme can now be summarized:

Level 1: Control loops
Two main loops are placed in Level 1. The first main loop (# 1) is for underflow control. The second main loop (#2) is for the control of flocculent flow.
At level #1, the essential process measurements for underflow control are:

1. rake torque with a torque meter fixed to the rakes,
2. bed level by using a simple float or vertical position sensor,
3. thickener bed pressure, by measuring the pulp pressure on the floor by a sensor.

At level #2 for flocculent loop control, measurements are chiefly flow rates of fluids by standard flow meters and power draft measurements for variable speed positive displacement pump. Other measurements at this level include:

1.   pump speed,
2.   underflow density measurement (γ-ray density gauge),
3.   pump discharge pressure by standard pressure gauge.

Level 2: Control loops

The aim of Level 2 is to keep the underflow bed level close to target. The set point of the bed level is therefore controlled by the bed level controller. In practice it is found that the bed level can be disturbed by high bed density which could result in high torque on the rakes. To avoid such situations the basic flow control is designed to be over-ridden. This is achieved by providing a high-selector that outputs the flow set point [10]. Such an arrangement is shown in Fig. 18.24 where it can be seen that the bed density and rake torque with maximum limiting values are connected to the high selector. The output from high selector or the flow controller set point has a set low limit. A safe flow is therefore maintained from the underflow. The pump that pumps the underflow is set to high and low speed limits taking signals from the output of the flow controller The advantage of this system is that in the event the thickener operation ceases due to say, stoppage of mill operation, and therefore feed to the thickener, the underflow pump continues to operate till the thickener is empty and chances of clogging is remote.

The pump speed controller incorporates limiting power draft so that the pump does not trip at high power

For controlling the flocculent flow signals are taken from the bed density controller. Controlling the flocculent flow is difficult by this method as it takes time for the flocculent to properly mix with the rest of the inventory. The speed of response varies with the rate of change of bed density. Elber [10] suggests using underflow flow to "control inventory in conjunction with bed level-flocculent dosage cascade."
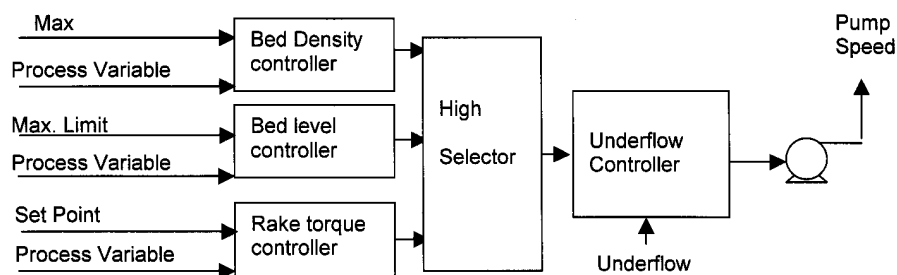
Fig.18.24. Underflow control setup [10].

Level 3: Control loops
Level 3 control involves optimisation of thickener operation (and pipe lines). This includes cost function based on:

1.   flocculent consumption,
2.   pump power,
3.   discharges to tailings.

All these factors depend on the underflow density set point. Optimum conditions are usually ascertained by trial and error method by taking signals from the underflow density, pump discharge pressures and pump power drafts and estimating the corresponding cost functions.

18.9.5.   Control of Hydrocyclone Operation

During steady operation the products from a hydrocyclone has a definite cut point. However due to variations in the feed slurry characteristics and changes in the hydrocyclone geometry, especially the diameter of the apex due to abrasion, the cut point changes during operation. It is necessary to hold the performance at the desired d_{50C} value for down stream operations. The control strategy could be to monitor the deviation of the cut point. The alteration in cut point was obviously due to change in feed characteristics and additionally to changes in cyclone geometry due to abrasion. Working with a D6B Krebs hydrocyclone and quartz suspension of known particle size distribution Gupta and Eren [18] indicated that for a constant pressure differential, the relative effect on d_{50C} was:

$$D_U > \varphi_i > Q > H > T$$

where D_U =   Diameter of apex, cm.,
          φ_i =   Volumetric fraction of solids in the feed slurry,
          Q =   Rate of flow , m^3/min,
          H =   Height of the cyclone, cm,
          T =   Temperature, $^\circ$C.

The logic of the control program adopted was to calculate the d_{50C} value during a steady state condition using a mathematical model. When the cut-point was altered due to any change in the variables the computer sequentially searched for the offending variable and restored it to the original value. The restoration was done by iteration using perturbance technique. The advantage of the technique was to predict changes using the previous reading as the initial value. Thus a variable (D_u, φ, Q or T) was chosen by the computer and the established model was considered as $f(x)$ and the step changes in d_{50C} calculated using the expression:

$$\Delta d_{50C} = \left. \frac{df(x)}{dx} \right|_{x=0\Delta}^{x=\Delta x} . \tag{18.65}$$

where x expressed the variables. After repeated iteration when the set value of d_{50C} was achieved, or tended to zero, the iterations ceased. A PID controller was adequate.

An important factor in designing control loops is the instrumental and programmable time delays. In the case of hydrocyclone automation, the sources of time delays is given in Table 18.5.

Each instrument has to have a separate time delay factor which could be up to 3 seconds Programmable time delays introduced during iteration could be greater than instrumental time delays

Table 18.5
Source of time delays in a hydrocyclone circuit.

Equipment	Time delay source
Motor pump set	Frequency controller, Inertia in motor load.
Vortex finder positioner	V/I and I/P conversions, Pressure transmission, Mechanical movements, Servo- Mechanism operations
Spigot diameter	V/I and I/P conversions.
Density gauges and Flow meters	Electronic, Adjustable response time
Computer	Conversions

Fig. 18.25 shows the set up and instrumentation for automatic control of a Krebs D6B-hydrocyclones. The apex of the cyclone was fitted with a rubber sleeve which could be pneumatically squeezed to alter its diameter. The vortex finder was specially designed to travel up and down. The centrifugal pump was fitted with a frequency controller. The control strategy is illustrated in Fig. 18.26.

Laboratory trials suggested that when a hydrocyclone variable was subjected to a step change and the d_{50C} value deviated, the operation of the hydrocyclone could be restored such that the d_{50C} could be maintained to within ± 5 % of the calculated value. The mathematical model used for calculations was derived to suit specific slurry conditions. The conclusion was that such techniques could be developed for automatic control of the cut point of hydrocyclones.

18.10. Advances in Process Control Systems

Mineral processing operations involve a number of process variables that change randomly with uncertain frequencies. The control strategies developed with the use of PID controllers have been found to be inadequate especially in non-linear systems and systems with large lag times. The present development to solve these problems fall under two categories:

1. development of algorithms for dynamic models involving complex statistical approach,
2. adoption of "Expert Systems" where mathematical modelling appear to be inadequate.
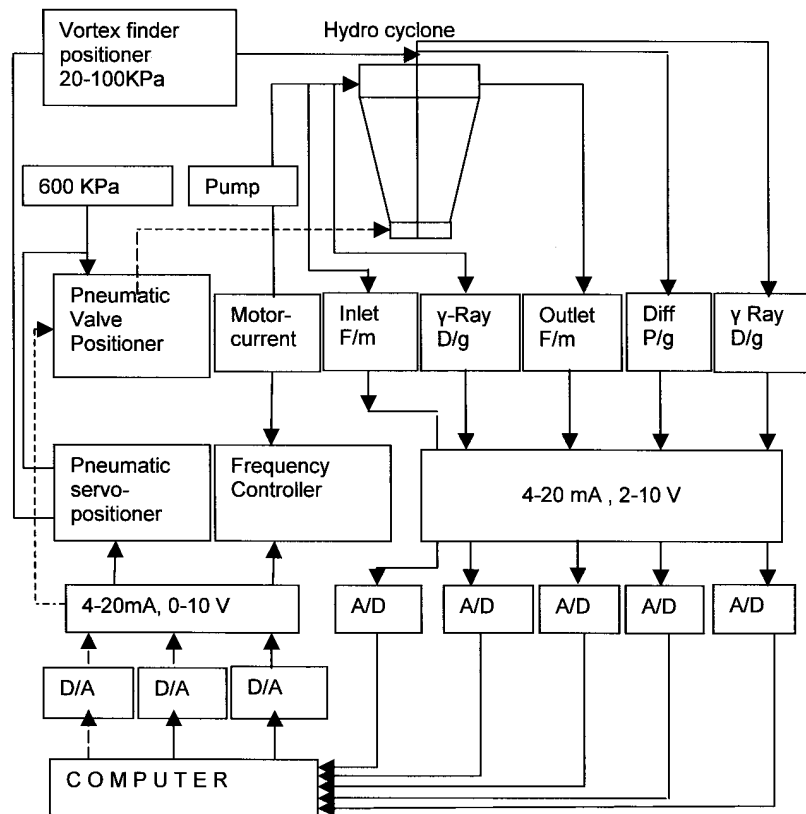
F/m = Magnetic Flow meter, D/g= γ-Ray Density gauge, P/G= Pressure gauge,
D/A = Digital to analog transducer, A/D =Analog to digital transducer

Fig. 18.25. Basic instrumentation for automatic control of hydrocyclone [18].

The algorithms developed and used in practice for non-linear systems are:

1.   self tuning control (STC),
2.   extended horizontal control.

In some cases new filtering strategies have been introduced, like Kalman filter [19-21]. These filters take care of variables that cannot be measured easily (like noise).

18.10.1. Self Tuning Control (STC)
The self tuning control algorithm has been developed and applied on crusher circuits and flotation circuits [22-24] where PID controllers seem to be less effective due to immeasurable

Fig. 18.26. Strategy for automatic control of d_{50C} in a hydrocyclone.

change in parameters like the hardness of the ore and wear in crusher linings. STC is applicable to non-linear time varying systems. It however permits the inclusion of feed forward compensation when a disturbance can be measured at different times. The STC control system is therefore attractive. The basis of the system is:

1. on-line identification of process model,
2. use of the control model in the process design.

The mathematical basis of the process is the least square model. When the time delay, t, is greater than zero, the process model is described in the predictive form [7].

The disadvantage of the set up is that it is not very stable and therefore in the control model a balance has to be selected between stability and performance. A control law is adopted. It includes a cost function C_F and penalty on control action. The *control law* has been defined as:

$$C_F = [O_{PR}(t + t_d + 1) - O_{SP}]^2 + \Pi O_c(t)^2 \qquad (18.66)$$

where O_{SP} = output set point,
Π = penalty on control action.

To obtain maximum stability and therefore minimum variance of the output, a suitable form of equation has been derived as:

$$O_C(t) = \frac{\beta}{(\beta^2 + \Pi)} [\{ \alpha_1 O_{PR}(t) + .. + \alpha_n O_{PR}(t-n+1) + O_{Sp} \} -$$

$$\beta [\beta_1 O_C(t-1) + .. + \beta_P O_C(t-P)] \frac{1}{(\beta_0^2 + \pi)} \qquad (18.67)$$

where $O_C(t$ = output Controller at time t,
O_{SP} = output ser point
$O_{PR}(t)$ = output (Process) at time t,
$\varepsilon(t)$ = error at time t,
t = time,
n = order of system,
k = constant,
α, β = parameters
π = n + t − 1

The parameters α and β are estimated by setting up a suitable algorithm and calculated for different times. When $\pi = 0$, then n + t = 1. Eq. (18.67) acts as a self tuning regulator [6].

In some cases, like the control of a crusher operation, a constant term has to be introduced in Eq. (18.67) as at zero control action and the crusher operates at steady state.

A block diagram showing the self tuning set-up is illustrated in Fig. 18.27. The disadvantage of STC controllers is that they are less stable and therefore in its application a balance has to be derived between stability and performance.

18.10.2. Horizontal Control (Extended)
This is also a model based process. In this case the control action is based on:

1. empirical model of the process,
2. specified cost function of the process.

The empirical model predicts the process output for a certain predicted time. The error is not fixed as in a PID system, but extends over a time period and minimized. The concept is therefore time based and known as *an extended horizontal control system*. The algorithm is known as Multivariable, Optimal Control Action or MOCCA [25]. The MOCCA system can be considered as an improvement on the level concept described earlier. It is based on the fact that the prediction of output equals the sum of the future actions plus past control action. It is developed around a step response under steady state conditions by combining:

1. extended horizontal control,
2. multivariable control,
3. feed forward control,
4. control constraints.

To derive the model, Sripada and Fisher [25] considered a steady state condition. Also for a single input-single output system (SISO), the predicted output for horizon 1 to P is obtained in N number of step responses. The future and past control actions were written as:

$$\text{Future control actions} = \Sigma^i_{j=1} \ Sr \ \Delta u \ (k+i-j) \tag{18.68}$$

$$\text{Past control actions} = \Sigma^N_{j=i+1} \ Sr \ \Delta u \ (k+i-j) + G_S \ u_{N+1} \tag{18.69}$$

where   Sr   = Discrete step response coefficient,
        Δu = Incremental control action,
        i   = 1 to P where P= the prediction horizon,
        G_S = Gain (steady state),
        N   = Number of step response coefficients required to describe the past control action.
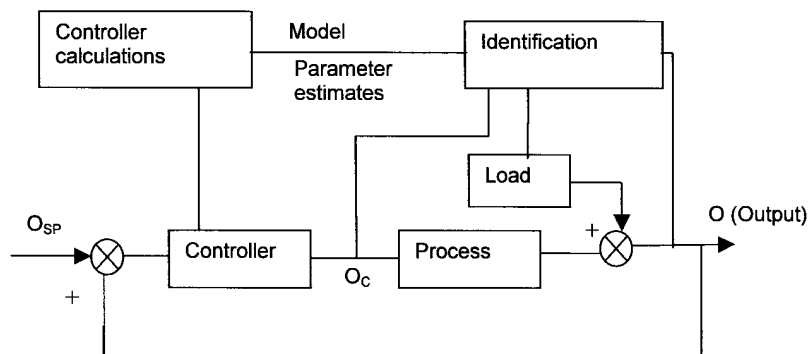
Fig. 18.27. Block diagram of Self Tuning Control (STC) [6].

The predicted output, O (k+1) is the sum of Eqs. (18.68) and (18.69), that is:

$$O (k+i) = \Sigma^i_{j=1} \; Sr_j \; \Delta u \; (k+i-j) + \Sigma^N_{j=i+1} \; Sr_j \; \Delta u \; (k+i-j) + G \; u_{N+} 1 \qquad (18.70)$$

We can see that Eq. (18.70) is applicable for prediction of horizon P where i = 1 to P and for control horizon H where i - j >H.

The predicted horizon P, is the number of predicted outputs that the control objective has been optimized The control horizon H is the number of future control actions which minimize the cost function against the predicted horizon.

Optimization of the control system is achieved from performance criteria including any constraints. It is necessary to know the set point and predicted output trajectories for future control effort. The errors and control efforts have to be minimized. For the error trajectory the square of the difference of set point trajectory and the predicted output trajectory is taken. Taking these into consideration Vien et al [6] describes the cost function, Cf, in terms of minimizing the error trajectory plus control effort. Taking the weighted least square performance, the cost function Cf is given as:

$$Cf = \frac{1}{2} \; [\; (Sp_T - O_{PT}])T_W \; (Sp_T - O_{PT}) + [(\Delta.u_F)T_M \; (\Delta.u_F) \;] \qquad (18.71)$$

where Sp_T = set point trajectory,
O_{PT} = predicted output trajectory,
$\Delta \, u_F$ = future control effort, and
T_M = input weighting matrices,
T_W = output weighting.

The first term in Eq. (18.71) is for minimizing error trajectory and the second term is for minimizing control effort.

A block diagram for a MOCCA setup is shown in Fig. 18.28. The diagram can be considered as a:

1. control block,
2. supervisory block,
3. feedback loop with filter and predictor, and
4. process model.

Based on the process model, the control block calculates the predictions for future control actions, the supervisory block generates the desired set point trajectory. The feedback loop with filter and disturbance predictor corrects incongruity between the model and unaccounted, therefore unmeasured, disturbances. It also reduces the noise levels. The predictor in the feed back control loop intimates the future effects of disturbances. Combination of the feed back corrections and the predictions from the model provide the necessary estimate of output.

MOCCA can be tuned for stability which is attained with small values of H/P ratio. To improve performance the ratio (H/P) needs to be about zero.

MOCCA has been found to be far superior to the conventional PID or PI controllers and is being increasingly used. It is particularly useful where long time delays are involved. Its advantage is that it uses discrete step response data and can be used to model processes with
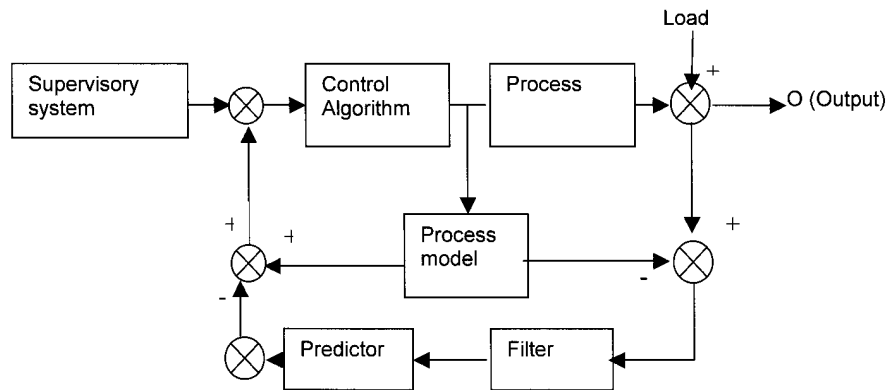
Fig. 18.28. Block diagram of MOCCA control system [6].

unusual dynamic behaviour. Its added advantage over the PID system of control is that it rises faster and has no overshoot. This system has been used successfully in control of grinding circuits.

18.11. Expert Systems

18.11.1. Fuzzy System of Control

So far we have assumed that the numerical solutions are possible in the control of process operations. There are however many instances when numerical methods cannot be applied, such as the gradual effect of wear and tear on the mill liners, spigot diameter change in a hydrocyclone operation or the effect of such energy consuming phenomenon like noise. Difficulties are compounded by the large number of variables in an operation and non-linear relationships. In such cases, heuristic search for answers have been sought. Naturally heuristic approach results in, some answers that are correct, others are not. Or some answers may be satisfactory and acceptable while others are not. In mineral processing operations, operators generally use their common sense to arrive at an answer some of which are satisfactory and produce required grades and recoveries. That is, with their acquired knowledge and skills they are able to control systems satisfactorily. Knowledge is an intellectual property gained by experience, but it can be quantified, say from 0-1 where, 0 is the least and 1 represent maximum knowledge. The numbers in between may be referred to as different degrees otherwise shades of knowledge. Linguistic forms of knowledge thus expressed in numeric form has been characterized and known as *Fuzzy thinking* according to *fuzzy rules* [27,28].

The symbolic language developed by experience can be put in expert system shells in the usual programming languages. The knowledge may be stored in *frames* or *production rules* or in the form of combined frame and production rules. The frame is a technique which for an object allows the specification of object and allotment of slots associated with that object.

Thus in the mineral industry, a flotation cell or a tumbling mill will be the object and the slots are attributes. In a flotation system the attributes are items like froth depth, cell capacity, air and so on. Zadeh [26] considered the above concepts and applied it to control strategy. According to this theory, an element x is either a member of a set $\mu_A(x)$, or not a member of a set. That is, it is based on a binary system which can be expressed as:

$$\text{Membership of set A, } \mu_A(x) = \begin{vmatrix} 1 & \text{if } x \text{ is a member of } A, \\ 0 & \text{if } x \text{ is not a member of } A \end{vmatrix}$$

Thus a fuzzy set A is characterized by a membership function represented as $\mu_A(x)$ where x is the membership number of x in A and x an assigned number (say) between 0 and 1. The fuzzy sets can be combined to form fuzzy subsets. Thus the union of sets A and B may be written as $A \cup B$. They can also intersect ($A \cap B$). The basic operations may be written as [36]:

Union (OR) $\qquad \mu_A(x) \cup \mu_B(x) = \max \{\mu_A(x), \mu_B(x)$

Complement (NOT) $\qquad \mu_{-A}(x) = 1 - \mu_A(x)$

Intersection (AND) $\qquad \mu_A(x) \cap \mu_B(y) = \min[\mu_A(x), \mu_B(x)$

where x and y are the two variables defined for sets A and B. Set A may be considered as the input variable while set B is the output variable.

From the process control aspect the relation between A and B may be written using fuzzy relationship in the form of IF and THEN. That is:

IF error is large THEN control action is large

Thus in the case of a closed circuit crushing operation involving a bin at the discharge end of crusher, IF the bin level is *low* THEN the crusher power has to be increased for rapid crushing. Other relations between bin level and crusher power may be similarly logged using the terms *High, Low, No Change* etc. The relations between power draw, bin level and feed rate can be drawn as in Table 18.6. As various levels of bin and power draw are possible, these can be assigned values 0-10; 10 being the maximum and 0 the minimum Thus inputs can be quantified by Fuzzy language. Similarly the output may also be described by Fuzzy language. Thus a set of rules in fuzzy language is set up for a fuzzy controller which provides an approximate description of control action.

Table 18.6
Relations between power draw, bin level and feed rate.

IF		THEN
Power Draw	Bin level	Feed Rate
Low	Fine	No change
Low	Not fine	Positive change
High	High	Negative change

Table 18.6 shows that the basic operations are simple though there is an element of vagueness. The vagueness can be quantified and a fuzzy algorithm developed to convert fuzzy input to fuzzy output using available software. The association of rules governing the fuzzy controller is the fuzzy decision algorithm for process control. Harris and Meech [29] lists the following actions to develop fuzzy rules:

1. observe and interview operator,
2. identify and standardize the linguistic process variables,(high low, bad not-bad etc)
3. define membership functions of fuzzy sets that represent linguistic variable, and
4. assemble fuzzy rule strategy.

The output of a fuzzy system is also fuzzy expressed in membership values of each variable in a process. It is therefore necessary to defuzzify using an inference process to a discrete value. The inferencing process can be a data driven search to obtain a goal or conclusion. This is known as *forward chaining*. It can also be a goal driven search where the goal is assumed and available data examined to support or reject it. This is known as *backward chaining*. The inferencing process is generally known as an *Inference Engine*. A fuzzy logic control system of a process is illustrated in Fig. 18.29.

The implementation of fuzzy logic control is presently done by using software that are commercially available. In complicated process control systems, like the control of flotation, fuzzy logic has been integrated with conventional PID systems.

A survey of literature indicates that Fuzzy system of control has been used mostly in milling and flotation circuits [30-34]. Freeman et al [32] has indicated an increase in productivity in the gold milling circuit at Kalgoorlie Consolidated Gold Mines, Fimiston Plant and increased stability in alumina grinding at the Comalco Bell Bay plant.

The greatest advantage of the use of Fuzzy logic is that it can tackle non-linear systems and such systems that are difficult to use mathematically. It may be mentioned that even though the Fuzzy control system may appear simple and has obvious advantages as it takes into account non-measurable variables in a process, in practice considerable effort is required to control the tuner.
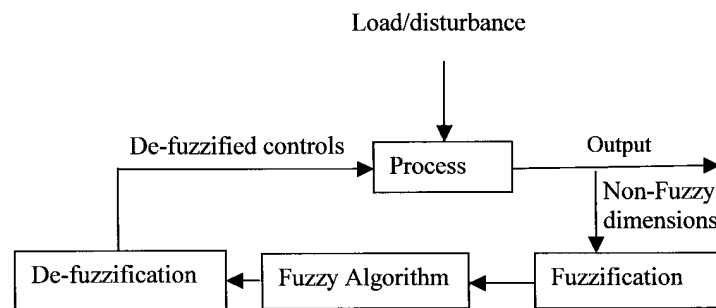
Fig. 18.29. Fuzzy Control System.

18.11.2. Neural and Artificial Network Methods (ANN) of Control

The alternate methods of control where conventional methods are unsatisfactory and processes that are non-linear are:

1.   neural and Artificial Neural Network method, (ANN), and
2.   non-Monotonic Logic method.

We shall only deal with the ANN method. This method helps to stabilize and control a process. Its set up is easier and it does not require elaborate statistical work or phenomological data collection. Eren and Fung [36] describe the method as "a mapping from measurement history to commands". Mapping involves machine learning which is usually referred to as artificial intelligence. The ANN is a branch of artificial intelligence and is being increasingly applied to complex mineral processing operations like flotation [37].

A neural network consists of a box containing single computational elements known as neurons. The neurons exist in layers and are dynamically interconnected by *synapses*. The arrangement of interconnections of the neurons or *topology* is fixed by the designer. Each neuron has an internal parameter called *weight*. Each neuron is a processing elemen*t* or *node* and forms an input-output field. The information contained in the nodes is the weight and link-field. Each neuron output is a single numerical activity. The function of the elements (node) is to add the weighted inputs and pass the results to the next layer using a non-linear sigmoidal function of the type:

$$\alpha_j = \frac{1}{1 + e^{(\beta \; \varphi \; j)}} \tag{18.72}$$

where α_j =   activation of neuron j,
        β =   steepness of activation function,
        φ =   applied input potential.

The input potential, φ, to each neuron is defined in terms of the synapses and weights between the neurons i and j and the threshold of neuron j, thus:

$$\varphi = \Sigma \; S_{ij} \; \alpha_j + \tau_j \tag{18.73}$$

where S_{ij} =   Synapses weight between neurons i and j,
        τ_j =   Threshold of neuron j

Neurons get activated when the value of the sigmoidal function is greater than the threshold value (τ_j).

A simplified three layer arrangement of neurons is illustrated in Fig. 18.30 where it can be seen that each neuron in the first layer receives weighted inputs I_1, I_2, I_3 and I_4. Output from each neuron in a layer is then passed on to each neuron in the following (right) layer and the outputs from each neuron in the second layer activate neurons in the subsequent layer, this ultimately results in an output. Each neuron undergoes a non-linear transfer function which is sigmoidal in character.

According to Cortez and Durau [36] three layers of neurons are generally sufficient to solve non-linear situations. The number of hidden neurons in a net-work is estimated from the number of input and output neurons. Thus if a vector of n number of neurons is in a input
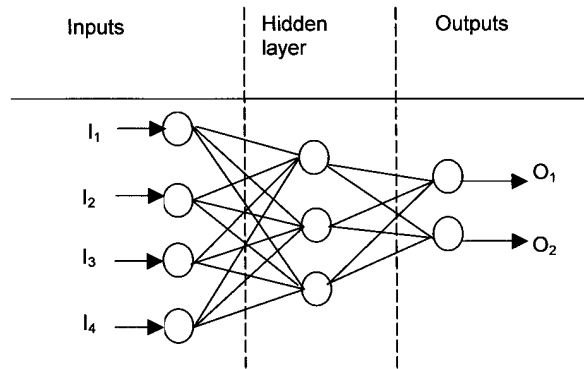
Fig. 18.30. Artificial neural network conceptual view.

layer and m neurons in the output layer, then the intermediate hidden middle layer would have 2m + 1 neurons.

Neurons are trained by the input of values required by the operating system. When the values produce a sigmoidal function greater than the preset (or threshold value), then the element is activated and sets to the trained value.

Two variations of ANN arrangements are used to control processes. They are the *Back propagation method* and the *Feed forward back-propagation* (EBP) method. Of these, EBP is the preferred method. Fig. 18.31 illustrates the EBP setup.

Training technique of EBP involves estimation of error which is the difference in output pattern (produced by forward pass) and the target value. Starting from the output, the error is worked back progressively to the input layer of neurons. In so doing, a gradient of error is established between neurons. The gradient is summated for each weights associated with each neuron for all input – outputs. Due to establishment of the gradient, the weights W_{ij} have to be revised and updated. For neurons i and j the updated weight would be:

$$W_{ij}^{N} = L_R \Sigma \frac{\delta e}{\delta W_{ij}}$$

(18.74)

where L_R = learning rate,
       N   = Nth. Iteration,
       E   = summated error.

The learning rate L_R is a discrete step size. Care must be taken regarding the step size, as a high value of L_R will give a large value of W which will make the system unstable, again if a low value of L_R is adopted then convergence will take a long time.

Updating is achieved by iteration till error for outputs are reduced to acceptable limits. Application of Eq. (18.74) is tricky due to difficulty of choosing the appropriate step size. To ease the problem a momentum term $[M(\Delta W_{ij})^{n-1}$ is added to Eq. (18.74) where M is the momentum term and has a value 0 to 1.
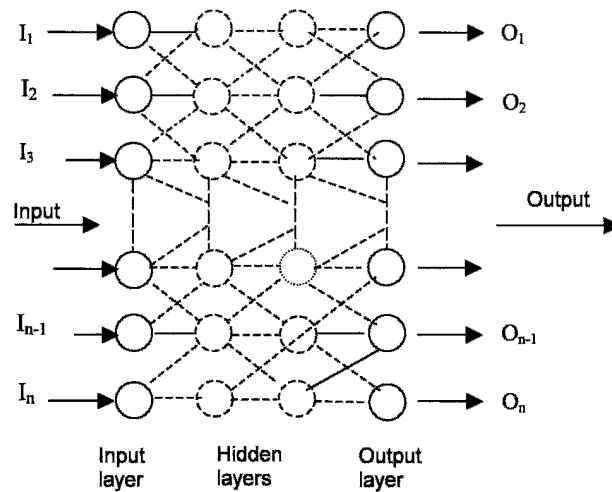
Fig. 18.31. EBP Artificial neural network [37].

Once trained, the ANN can accept linear and non-linear discrete or continuous functions. The operator can then take the help of established mathematical software, like MATLAB or similar package to control the system. The software must be supported by appropriate hardware.

18.12. Mechanics of Digital Process Control Systems

The modern process plants are increasingly controlled by computers and digital devices. But the signals generated by the processes are in analogue, therefore the analogue information acquired are converted to digital form. The analogue to digital (A/D) converter is used for signal conversion (Fig. 18.26). Usually multiplexers and sample-and-hold together devices are included. The multiplexer enables connection to several transducers to same sensors and transducers to the same signal processing media if required.

Digital systems are particularly useful in performing mathematical operations, numeric displays when required, also for storing and transmitting information. It is particularly useful for the application of specific software.

Microprocessors and microcontrollers constitute the heart of almost all types of digital process control systems. They play an important role in data handling data processing and control. Application of micro-processors are in the field of data handling which includes data acquisition, data processing, interpretation, storage and communication. It is also used for instrumentation control of sensors and actuators. Microprocessors provide a meaningful human-machine interface. Micro-controllers and digital signal processors are special micro-processors, the difference is in the degree of specialization.

18.12.1. Inputs and Outputs

The inputs and outputs of a process controlling system is usually performed through *a data acquisition board* with 8-16 number of analogue inputs. These boards are the key elements to

connect a computer to a process in order to measure or control its operation. The data acquisition board is made up of an analog multiplexer, an amplifier (with programmable gain) a sample and hold circuit and A/D set up. The data acquisition board also offer analogue outputs to carry control operation and also supply I/O lines and counters. The counters are used for applications such as counting the number of times an event offers (see Fig. 18.26)

18.12.2. Process Communications and Network

In process control instruments are often networked by computers to measure variables of a process. The arrangement for performing the overall measurement is called a *measuring system.*

In measuring, the information generated by each device is communicated between the instruments themselves or between other devices like recorders and display units. Transmission of data are done easily by digital control systems, however as the measurement system becomes large as a result of inclusion of many instruments, the communication to computers can become complex. In such cases, the devices are networked either in groups or as a whole by a central computer. The standard networking topologies like star, ring field bus are used.

Digital network is applied to Direct Digital Control (DDC) and Supervisory control. Of more interest to mineral processing systems are:

1. programmable Logic Controllers (PLC), and
2. supervisory Control Data Acquisition (SCADA).

The Programmable logic controllers are industrial computers in which the hardware and software has been specially adapted to a particular environment. They are therefore dedicated computers.

The PLC works by continually scanning a program, for example, see Fig.18.26, where the reiteration and data have been scanned 360 times, the average taken and computation progressed as per mathematical model established for the process. The scanning cycle consists of 3 main steps as seen in Fig. 18.32.
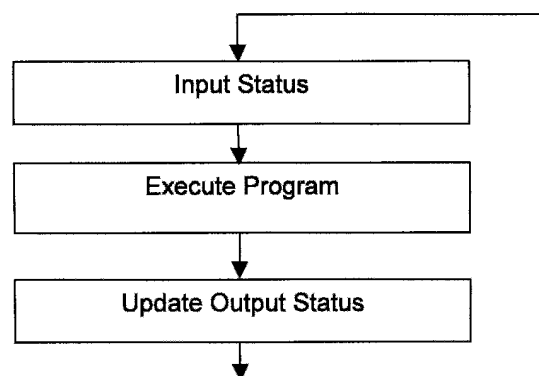
Fig.18.32. PLC Operation Cycle.

The input modules take AC or DC 240V and converts to logic level 0-5V signals. The output AC modules are Triac driven and are arranged in sink configuration. The DC output modules are controlled by transistor circuits.

The Supervisory Control Data Acquisition (SCADA) is used to monitor and control distributed systems from a master location. It serves as an umbrella for the control of production (including tailings), stockpiling and shipments. It finds application for controlling, scanning, monitoring data and data acquisition. It has three main components:

1   multiple remote terminal units,
2   central control room with host computers, and
3   software support.

While the remote terminal units are used to acquire data from physical devices like sensors, pumps, actuators, the central control units acting as host computers allows for supervisory level control of remote sites. It also provides the human-process interface that is, it permits operators to view and if necessary control any part of the plant equipment. SCADA softwares are written in terms of pre-defined variables suitable for a particular operation.

18.13. Problems

18.1
A decaying metallurgical process is expressed by the differential equation:
$$\frac{dx}{dt} + 5x = 0$$
The initial condition is x(0) =0 Trace the decay curve for 5 seconds.

18.2
The response function of a process is given by:

$$\frac{dx}{dt} + x = 5$$

The initial condition is x(0) = 0. Draw the curve for t = 1-5 seconds.

18.3
A process is defined by the equation:

$$\frac{d^2x}{dt^2} + 4x\frac{dx}{dt} + 4x = 1$$

The base conditions are: x(0) =x'(0) =0
Determine the nature of the curve and the limiting value.

18.4
The output and input transfer functions ratio of a process is given by:
$$\frac{Y(S)}{X(S)} = \frac{\tau_1 + 1}{\tau_2 + 2}$$

If in an unit step function x(t) is applied, determine:

1. Y(t)

2. Draw the curve Y(t) against $\dfrac{\tau_1}{\tau_2}$ when $\dfrac{\tau_1}{\tau_2} = 3$

18.5
A lime mixing tank having cross-section $1m^2$ is operated at a steady level of 0.6 m. The lime suspension is removed for a gold treating plant at a constant rate of 0.3 m^3 per min. irrespective of head. The resistance at the outlet valve R equals 1.7 m/m^3. If the input rate is Q m^3/m and h(t) the height of the liquid level, determine the transfer function h(s)/Q(s).

18.6
A proportional controller is used to control the level of a sludge tank between 3.0 and 3.1 m. The controller is operated pneumatically such that it goes from 1-5 when in fully open and fully shut positions and the level from 3.05 to 3.75 m with the set point held constant. Determine:

1.   the proportional band,
2.   gain,
3.   if the proportional band was doubled what will be the level change.

18.7
The level of a CIP tank was controlled by a controller as in Fig. 18.30 that was operated pneumatically. It was found that the control output pressure changed by 2000 N/m^2 for 1.0 m variation in level. If the pressure changed by 4000 N/m^2 resulted in a change from fully open to fully closed position of the controller valve. Determine:

1.   the gain,
2.   the proportional band.

18.8
An open loop system performs in the same manner as its transfer function. A unit step was applied as shown in the diagram and from the trace of response recorded below, determine the settings of a PID controller.
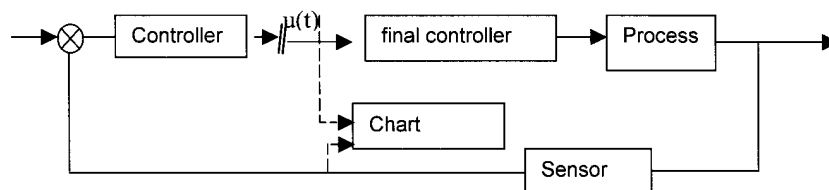
Time, secs	Response	Time, secs	Response	Time, secs	Response
0.0	0.000	1.0	2.050	2.0	4.950
0.1	0.050	1.1	2.600	2.1	5.100
0.2	0.053	1.2	3.150	2.2	5.150
0.3	0.150	1.3	3.550	2.3	5.150
0.4	0.200	1.4	3.940	2.4	5.200
0.5	0.300	1.5	4.300	2.5	5.200
0.6	0.450	1.6	4.500	2.6	5.210
0.70	0.800	1.7	4.700	2.7	5.280
0.8	1.100	1.8	4.800	2.8	5.350
0.9	1.500	1.9	4.900	2.9	5.300

REFERENCES

[1]   J.G. Ziegler and N.B. Nichols, *ASM,* 64 (1942) 759.

[2]   G.H. Cohen and G.A. Coon, , Theoretical considerations of activated control Trans ASME, 75 (1953) 827.

[3]   J.M. Coulson and J.F. Richardson, Chemical Engineering, Vol.3, 2nd (ed)., Pergamon Press.

[4]   A.M. Lopez, C.L. Smith and P.W. Murill, British Chem. Eng., 14 (1969) 1533.

[5]   D.L. Rivera, M. Morari and S. Skogestad, Industrial Eng. Progress Design Dev., 25 (1986) *252.*

[6]   A. Vien, R.P. Edwards and B.C. Flintoff, International Conference on Process Control, Jan. 1998, pp. 337-352.

[7]   A. Vien, B.C. Flintoff and R.P. Edwards, 24th Canadian Mineral Processors Conference, Ottawa, 1992, paper 6, pp. 1-8.

[8]   B.C. Flintoff, Control of Mineral Processing Systems, Preprint.

[9]   G.A. Gault, Process Control Lecture Series, WA. School of Mines, Kalgoorlie, Private Communication. 1984.

[10]   L. Elber, Process Control for Mineral Processing and Metallurgists and Engineers, Lecture Series, WA School of Mines, Private Communication, 1990.

[11]   G. Stephanopoulos, Chemical Process Control, Prentice Hall International, 1984.

[12]   B. Flintoff and A. Mular, A practical guide to process controls in Mineral Industry, Gastown printers, 1992.

[13]   L. Anderson, R. Perry, A. Neale, International Conference on Process Control, Paper No. 24, 1998, pp. 359 –379.

[14]   J.W. Austin, Vancouver CMP presentation, Dec 4., Pre-print, 1987.

[15]   N.P. Cheremisinoff , Process Level instrumentation and Control, Marcel Dekker, New York and Basel, 1981.

[16]   A. Lynch, Mineral Crushing and Grinding Circuits, Elsevier Amsterdam, 1977.

[17]   L. Elber, Proceedings SAG/SEM 1989 Aus.I.M.M., Australia Nov., 1989.

[18]   A. Gupta and H. Eren, Proceedings, Aus.I.M.M., 295 No. 2 (1990) 31.

[19]   P.M.Barnham and D.E. Humphreys, Theory and Applications of Kalman Filtering, C. Leondes (ed), AGARD Monograph, 139 (1970) 45.

[20]   B.W.Leach, Report NRC-NAE-MWC-57, National Research Council, 1984.

[21]   O.A. Bascur and J.A. Herbst, in Design and Installation of Concentration Circuits, A.L. Mular and M.A. Anderson (eds), 1986, p. 835.

[22] U. Borrison, and R. Syding, Automatica,12 (1976).

[23] E.V. Manlapig, A.J. Thorton and G. Gongalez, Copper 87, Vol 3, A.Mular, G. Gonzalez and C. Barahona (eds), CIM Chile, 1987, p. 387.

[24] M. Frankin, in Process Control and Automation in Extractive Metallurgy, E.Partelpoeg and D. Hammestoete (eds), AUME, 1989.

[25] N.R. Sripada and D.G. Fisher, Multivariable, Optima, Constrained Control Algorithm (MOCCA) Part 1, Formulation and application, Department of Chemical Engineering, University of Alberta, 1984.

[26] L.A. Zadeh, Fuzzy Sets Information and Control, Vol.3, 1965, pp. 338-353.

[27] L.A. Zadeh, IEEE Transon System Mon. and Cyb., SMC-3, No. 1, 1973, pp. 28-34.

[28] L.A. Zadeh, IEEE, Spectrum, Aug, 1984, pp. 26-32.

[29] C.A. Harris and J.A. Meech, Fuzzy Logic: A potential control technique for mineral processing, 24th Annual Met Conference, Vancouver, 1985.

[30] L.C. Hales, Proceedings of the Engineering Foundation Conference, Dec. 1989, pp. 289-302.

[31] C.A. Harris and G.A. Kosick, 20th Annual Meeting of Canadian Mineral Processors, Ottawa Ontario, 1988, p.149.

[32] N. Freeman, W. Keenan, S. Hancock and G. Lepage, 5th Mill Operators Conference,, Aus. I.M.M., Roxby Downs, 1994, pp. 193- 199.

[33] M.J. Burrows, J.D. Carriere, J. Leung and D. Laguitton, 21st. Annual Meeting of Canadian Processors, Ottawa, 1989.

[34] J.A. Herbst, W.T. Pate and A.E. Oblad, Advances in Autogenous and Semi-Autogenous Grinding Technology, A.L. Mular and G.E. Agar (eds), University of British Columbia, 1989, p. 669.

[35] L. Cortez and F. Durao, APCOM XXV 1995 Conference, Brisbane 9-14 July, 1995, pp. 39-43.

[36] H. Eren and C.C. Fung, Automation and Control Equipment, private communication.

[37] H. Eren, C.C. Fung and A. Gupta, Aus.IMM Annual Conference, Perth, 1996, pp. 225-229.

APPENDIX A-1

AVERAGE WORK INDEX OF SELECTED MINERALS
(Source. Chem Eng. Handbook, R.O.Perry & C.H.Chilton, Int Student's ed, McGraw Hill, p 8-11, and
SME Mineral Processing Handbook, Weiss (ed), 1985 p 3A-27)

MINERAL	Sp. Gr	Bond Work Index	MINERAL	Sp.Gr	Bond Work Index
Barite	4.28	6.24	Phosphate Rock	2.66	10.13
Basalt	2.89	20.41	Pyrite Ore	3.48	8.9
Bauxite	2.38	9.45	Pyrrhotite Ore	4.04	9.57
Cement Clinker	3.09	13.49	Quartzite	2.71	12.18
Chrome Ore	4.06	9.6	Rutile	2.84	12.12
Coal	1.63	11.37	Sandstone`	2.68	11.53
Coke	1.51	20.70	Silica	2.71	13.53
Copper Ore	3.02	13.13	Silicon Carbide	2.73	26.17
Diorite	2.78	19.4	Silver Ore	2.72	17.30
Dolomite	2.82	11.31	Spodumene	2.75	13.70
Feldspar	2.59	11.67	Tin Ore	3.94	10.81
Flint	2.65	26.16	Titanium Ore	4.23	11.88
Fluorspar	2.98	9.76	Uranium Ore	2.70	17.93
Galena	5.39	10.19	Zinc Ore	3.68	12.42
Garnet	3.30	12.37			
Gold Ore	2.86	14.83			
Granite	2.68	14.39			
Graphite	1.75	45.03			
Gypsum Rock	2.69	8.16			
Ilmenite	4.27	13.11			
Iron Ore (Hematite)	3.76	12.68			
Iron Ore(Specular Hematite)	3.29	15.4			
Iron Ore(Magnetite)	3.88	10.21			
Iron Ore (Tachonite)	3.52	14.87			
Kyanite	3.23	18.87			
Lead Ore	3.44	11.40			
Lead-Zinc Ore`	3.37	11.35			
Limestone	2.69	11.61			
Manganese Ore	3.74	12.46			
Mica	2.89	134.5			
Nickel Ore	3.32	11.88			

APPENDIX A-2

ABRASIVE INDEX OF SELECTED MINERALS
(Averaged over 200 determinations)

(Source: Marshal, V.C. (1975) Comminution, Institute of Chemical Engineers)*

MATERIAL	ABRASIVE INDEX
Alumina	0.891
copper ore	0.147
chrome ore	0.120*
dolomite	0.016
diorite	0.230*
gold ore	0.200*
hematite	0.165 (0.0952)*
limestone	0.032 (0.026)*
lead-zinc ore	0.152*
magnesite	0.075
Magnetite	0.165(0.252)*
manganese ore	0.113*
Nickel Ore	0.122*
Quartz	0.183*
Quartzite	0.775(0.691)*
Taconite	0.624(0683)*

APPENDIX A-3

CONVERSION OF MATERIAL SIZE TO 80% PASSING EQUIVALENT

Based on Gates- Gaudin-Schuman Equation : $Size_2 = \left[\dfrac{\% \, Passing \, Size \, 2}{\% \, Passing \, Size \, 1} \right]^2 \times Size_1$

MATERIAL SIZE mm.		80% Passing Equivalent F or P
99 % -38.1	99 % -38.1 mm	25,000
99 % - 25.4	99 % - 25.4	18,00
99 % - 19.1	99 % - 19.1	12,00
99 % - 2.7	99 % - 2.7	8,500
99 % - 9.5	99 % - 9.5	6,000
99 % - 6.73	3 mesh	4,200
99 % - 4.76	4 mesh	3,000
99 % - 3.36	6 mesh	2,100
99 % - 2.38	8 mesh	1,500
99 % - 1.68	10 mesh	1,000
99 % - 1.19	14 mesh	800
99 % - 841 μm	20 mesh	550
99 % - 595 μm	28 mesh	440
99 % - 420 μm	35 mesh	270
99 % - 297 μm	48 mesh	150
99 % - 210 μm	65 mesh	105
99 % - 149 μm	100 mesh	72
99 % - 105 μm	150 mesh	55
99 % - 74 μm	200 mesh	36
99 % - 88 μm	325 mesh	20

* Source: Chemical Engineers Handbook (1950), J.H. Perry & C.H. Chilton (eds), p 8-10.

APPENDIX A-4

BULK DENSITY OF STEEL RODS CHARGED IN TUMBLING MILLS
Source: C.A.Rowlands & D.M.Kjos, Mineral Processing and Plant Design, Mullar & Bhappu (eds),
Chapter 12, Rod & Ball Mills.

Rod Mill diameter, m	Rod mill length, m	Rod length (L)	L/D	Bulk density rod charged, t/m^3
0.91	1.22	1.07	1.40	5.847
1.22	1.83	1.68	1.57	5.847
1.52	2.44	2.29	1.67	5.847
1.83	3.05	2.90	1.73	5.847
2.13	3.35	3.20	1.62	5.766
2.44	3.66	3.51	1.53	5.766
2.59	3.66	3.51	1.44	5.766
2.74	3.66	3.51	1.38	5.766
2.89	3.96	3.81	1.41	5.606
3.05	4.27	4.11	1.44	5.606
3.20	4.57	4.42	1.47	5.606
3.35	4.88	4.72	1.50	5.606
3.51	4.88	4.72	1.43	5.606
3.65	4.88	4.72	1.37	5.606
3.81	5.49	5.34	1.48	5.446
3.96	5.79	5.64	1.50	5.446
4.12	5.79	5.64	1.44	5.446
4.27	6.10	5.94	1.46	5.446
4.42	6.10	5.94	1.41	5.446
4.57	6.10	5.94	1.36	5.446

APPENDIX A-5

SPECIFICATIONS OF NEW GRINDING STEEL RODS
(Source : Marcy Rod/ Ball Mills Bulletin 820 – 979 Application Guide)

Size		Volume	Mass of each rod	Approx. No / m^3	Approx. No/ per mt
Length m	Dia. mm	m^3	kg		
25.4	30.5	0.0015	12.23	515	68.2
31.75	30.5	0.0024	19.03	329	43.6
38.1	30.5	0.0035	27.18	230	30.0
50.8	30.5	0.0062	48.50	131	17.3
6305	30.5	0.0096	75.65	81.2	10.9
7602	30.5	0.0139	108.72	56.5	7.30
88.9	30.5	0.019	148.13	42.4	5.45
101.6	30.5	0.025	193.4	31.8	4.54
127	30.5	0.0415	302.601	21.2	2.73

APPENDIX A-6   PULP PROPERTIES

| %S | Mass Ratio of solid/pulp | S.G. and Vol. (m³) of one tonne of pulp containing solids of different S.G. | | | | | | | |
| | | 2.50 | | 2.70 | | 2.90 | | 3.10 | |
		S.G.	Vol.	S.G.	Vol.	S.G.	Vol.	S.G.	Vol.
5	1:19.000	1.031	0.970	1.033	0.969	1.034	0.967	1.035	0.966
6	1:15.667	1.037	0.964	1.039	0.962	1.041	0.961	1.042	0.959
7	1:13.826	1.044	0.958	1.046	0.956	1.048	0.954	1.050	0.953
8	1:11.500	1.050	0.952	1.053	0.950	1.055	0.948	1.057	0.946
9	1:10.111	1.057	0.946	1.060	0.943	1.063	0.941	1.065	0.939
10	1:9.000	1.064	0.940	1.067	0.937	1.070	0.934	1.073	0.932
11	1:8.091	1.071	0.934	1.074	0.931	1.078	0.928	1.081	0.925
12	1:7.333	1.078	0.928	1.082	0.924	1.085	0.921	1.088	0.919
13	1:6.692	1.085	0.922	1.089	0.918	1.093	0.915	1.097	0.912
14	1:6.144	1.092	0.916	1.097	0.912	1.101	0.908	1.105	0.905
15	1:5.667	1.099	0.910	1.104	0.906	1.109	0.902	1.113	0.898
16	1:5.250	1.106	0.904	1.112	0.899	1.117	0.895	1.122	0.892
17	1:4.882	1.114	0.898	1.120	0.893	1.125	0.889	1.130	0.885
18	1:4.556	1.121	0.892	1.128	0.887	1.134	0.882	1.139	0.878
19	1:4.263	1.129	0.886	1.136	0.880	1.142	0.876	1.148	0.871
20	1:4.000	1.136	0.880	1.144	0.874	1.151	0.869	1.157	0.865
21	1:3.762	1.144	0.874	1.152	0.868	1.160	0.862	1.166	0.858
22	1:3.545	1.152	0.868	1.161	0.861	1.168	0.856	1.175	0.851
23	1:3.348	1.160	0.862	1.169	0.855	1.177	0.849	1.185	0.844
24	1:3.167	1.168	0.856	1.178	0.849	1.187	0.843	1.194	0.837
25	1:3.000	1.176	0.850	1.187	0.843	1.196	0.836	1.204	0.831
26	1:2.846	1.185	0.844	1.196	0.836	1.205	0.830	1.214	0.824
27	1:2.704	1.193	0.838	1.205	0.830	1.215	0.823	1.224	0.817
28	1:2.571	1.202	0.832	1.214	0.824	1.225	0.817	1.234	0.810
29	1:2.448	1.211	0.826	1.223	0.817	1.235	0.810	1.244	0.804
30	1:2.333	1.220	0.820	1.233	0.811	1.245	0.803	1.255	0.797
31	1:2.226	1.229	0.814	1.243	0.805	1.255	0.797	1.266	0.790
32	1:2.125	1.238	0.808	1.252	0.799	1.265	0.790	1.277	0.783
33	1:2.030	1.247	0.802	1.262	0.792	1.276	0.784	1.288	0.776
34	1:1.910	1.256	0.796	1.272	0.786	1.287	0.777	1.299	0.770
35	1:1.857	1.266	0.790	1.283	0.780	1.298	0.771	1.311	0.763
36	1:1.778	1.276	0.784	1.293	0.773	1.309	0.764	1.323	0.756
37	1:1.703	1.285	0.778	1.304	0.767	1.320	0.758	1.334	0.749
38	1:1.632	1.295	0.772	1.315	0.761	1.331	0.751	1.347	0.743
39	1:1.564	1.305	0.766	1.325	0.754	1.343	0.744	1.359	0.736
40	1:1.500	1.316	0.760	1.337	0.748	1.355	0.738	1.372	0.729
41	1:1.439	1.326	0.754	1.348	0.742	1.367	0.731	1.385	0.722
42	1:1.381	1.337	0.748	1.360	0.736	1.380	0.725	1.398	0.715
43	1:1.326	1.348	0.742	1.371	0.729	1.392	0.718	1.411	0.709
44	1:1.273	1.359	0.736	1.383	0.723	1.405	0.712	1.425	0.702
45	1:1.222	1.370	0.730	1.395	0.717	1.418	0.705	1.439	0.695
46	1:1.174	1.381	0.724	1.408	0.710	1.431	0.699	1.453	0.688
47	1:1.128	1.393	0.718	1.420	0.704	1.445	0.692	1.467	0.682
48	1:1.083	1.404	0.712	1.433	0.698	1.459	0.686	1.482	0.675
49	1:1.041	1.416	0.706	1.446	0.691	1.473	0.679	1.497	0.668

%S	Mass Ratio of solids to pulp	S.G. and Vol. (m³) of one tonne of pulp containing solids of different S.G.							
		2.50		2.70		2.90		3.10	
		S.G.	Vol.	S.G.	Vol.	S.G.	Vol.	S.G.	Vol.
50	1:1.000	1.429	0.700	1.459	0.685	1.487	0.672	1.512	0.661
51	1:0.961	1.441	0.694	1.473	0.679	1.502	0.666	1.528	0.655
52	1:0.923	1.453	0.688	1.487	0.673	1.517	0.659	1.544	0.648
53	1:0.887	1.466	0.682	1.501	0.666	1.532	0.653	1.560	0.641
54	1:0.852	1.479	0.676	1.515	0.660	1.547	0.646	1.577	0.634
55	1:0.809	1.493	0.670	1.530	0.654	1.563	0.640	1.594	0.627
56	1:0.786	1.506	0.664	1.545	0.647	1.580	0.633	1.611	0.621
57	1:0.754	1.520	0.658	1.560	0.641	1.596	0.627	1.629	0.614
58	1:0.724	1.534	0.652	1.575	0.635	1.613	0.620	1.647	0.607
59	1:0.695	1.548	0.646	1.591	0.629	1.630	0.613	1.666	0.600
60	1:0.667	1.563	0.640	1.607	0.622	1.648	0.607	1.685	0.594
61	1:0.639	1.577	0.634	1.624	0.616	1.666	0.600	1.704	0.587
62	1:0.613	1.592	0.628	1.640	0.610	1.684	0.594	1.724	0.580
63	1:0.580	1.608	0.622	1.657	0.603	1.703	0.587	1.745	0.573
64	1:0.563	1.623	0.616	1.675	0.597	1.722	0.581	1.765	0.566
65	1:0.538	1.639	0.610	1.693	0.591	1.742	0.574	1.787	0.560
66	1:0.515	1.656	0.604	1.711	0.584	1.762	0.568	1.809	0.553
67	1:0.493	1.672	0.598	1.730	0.578	1.782	0.561	1.831	0.546
68	1:0.471	1.689	0.592	1.749	0.572	1.803	0.554	1.854	0.539
69	1:0.449	1.706	0.586	1.768	0.566	1.825	0.548	1.878	0.533
70	1:0.429	1.724	0.580	1.788	0.559	1.847	0.541	1.902	0.526

The SG of the liquid is taken as 1.0 for these calculations.

For solid densities other than the ones given in the table, the slurry properties can be calculated as follows:

$$\text{Mass ratio of solid to pulp} = \frac{100 - \%S}{\%S}$$

$$\text{S.G. of pulp} = \frac{100}{\dfrac{\%S}{SG_S} + \dfrac{(100 - \%S)}{SG_L}}$$

$$\text{Volume of 1 tonne of pulp} = \frac{1}{SG_P \times \rho_W} \ m^3$$

where %S = mass % solids,
  SG_S = specific gravity of the solid,
  SG_L = specific gravity of the liquid (solution) = density of liquid/density of water,
  SG_P = specific gravity of the pulp, and
  ρ_W = density of water in t/m³.

APPENDIX A-7

STANDARD SIEVE SIZES

Standard Size	Tyler mesh	Standard Size	Tyler Mesh
125 mm		710 µm	24
106		600	28
100		500	32
90			
75			
63		425	35
53		355	42
50		300	48
45			
37.5			
31.5		250	60
26.5		212	65
25.0		180	80
22.4			
19.0			
16.0		150	100
13.2		125	115
12.5		106	150
11.2		90	170
9.5		75	200
8.0	2.5	63	250
6.7	3.0		
6.3			
5.6	3.5	53	270
4.75	4	45	325
4.00	5	38	400
3.35	6		
2.80	7		
2.36	8		
2.00	9		
1.70	10		
1.40	12		
1.18	14		
1.00	16		
850 microns*	20		

* 1.0 mm = 1000 microns (µm)

A more complete list of sieve sizes and different international standards are available in the spreadsheet conversion.xls available for download from
http://wasm.curtin.edu.au/yand/downloads

APPENDIX B-1

BOND WORK INDEX TEST PROCEDURE FOR DETERMINATION
OF THE BOND BALL MILL WORK INDEX

The procedure described by Bond (1960) is as follows. The Bond Ball Mill Work Index determination is carried out in a standard test mill and under standard conditions. The test mill has an internal diameter of 305 mm and is 305 mm long. It has a smooth lining with rounded corners, and no lifters.

The ball charge consists of a specified number of balls, weighing approximately 20.1 kg, and ranging in diameter from 15.2 to 44.4 mm (0.6 to 1.75 in.) diameter (43 of 1.75, 67 of 1.17, 10 of 1, 71 of 0.75, 94 of 0.61 in.). Mill speed is set at a standard 70 rpm.

The circuit being simulated is shown below;
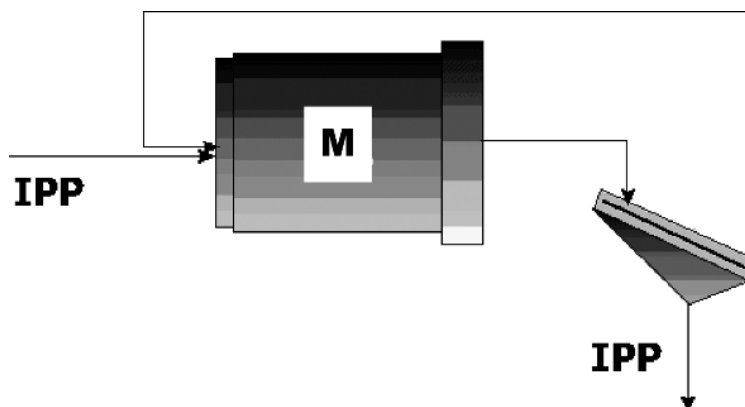
A detailed description of the test procedure follows:

1. The dry feed is crushed to -3360 μm (-6 mesh), using staged crushing.
2. Add the crushed ore, -3.36 mm, to a 1000 mL measuring cylinder to the 700 mL mark, lightly packed and not overly consolidated. Weigh the resulting mass of ore, M. The mass M represents the mill charge for each grind.
3. Calculate the Ideal Period Product (IPP) assuming a 250% circulating load (the mass of circulating material is 2.5 times the new feed to the closed circuit or the screen undersize, at steady state. If the mass of the new feed is 1 and the mass of the circulating load is 2.5 then the mass being ground in the mill is 3.5)

   IPP = M / 3.5

4. Determine the sieve analysis of the feed. Ensure that the test screen size is one of the screens used in the size analysis.

5. If the feed sieve analysis shows that more than 28% is finer than the test screen size, take the number of revolutions for the first period as zero and pass the feed charge directly over the test screen to remove the undersize then bring the total feed charge mass for the next period up to the desired mass by the addition of a representative amount of new feed.

6. Place the feed charge, M_o, in the mill.

7. Run the mill for N revolutions where N is between 50 (coarse test screen sizes) and 100 or more (fine test screen sizes) for material of average hardness.

8. At the end of the grind, dump the charge onto a heavy duty screen to separate the balls from the ore. Inspect the mill and ball coatings and remove any if present. Return the balls to the mill.

9. Screen the mill discharge at the test screen size.

10. Weigh and record the total screen oversize, R.

11. Calculate and record the mass of test screen undersize (product), m. Weigh the actual undersize as a check.

$$m = M_o - R$$

12. Calculate the amount of product size material in the feed using the feed sieve analysis and the amount of new feed present in the mill charge at the beginning of the period.

amount of product size material in the feed $= (1 - r_o)$ IPP

where r_o is the fraction of feed material coarser than the test screen.

13. Calculate the net grams of product which is the mass of product minus the mass of product size material in the feed.

net grams of product $= m - (1 - r_o)$ IPP

14. Calculate the net grams produced per revolution, G, by dividing the net grams of product by the number of revolutions in the period.

$$G = [m - (1 - r_o) \text{ IPP}]/N$$

15. Add a representative amount of new feed to the test screen oversize to bring the combined mass up to the mill charge, M.

16. Calculate the mass which should be ground in the next period in order to obtain the desired circulating load. This amount is the ideal period product (step 3) minus the amount of product size material in the mill feed (step 12).

mass which should be ground in the next period $=$ IPP $- (1 - r_o)$ IPP $= r_o$ IPP

17. Calculate the number of revolutions, N, for the next period. This is the amount of material which should be ground (step 16) divided by the net grams per revolution of the preceding period (step 14).

$$N = r_o \text{ IPP}/G$$

18. Return the combined circulating load and new feed to the mill and repeat steps 6 to 17. At least five periods of grinding should be completed.

19. The net grams per revolution should approach an equilibrium value, where the net grams per revolution becomes constant for at least three periods, or the net grams per revolution shows a reversal in trend.

20. Take an average of the net grams per revolution of the last two or three periods, G_{bp}.

21. Determine the size distribution of the test screen undersize (product).

22. Determine the 80% passing sizes of the product, P_{80}, (from step 21) and the representative feed, F_{80}, (from step 4).

23. Calculate the laboratory Work Index from the following equation:

$$W_{i,TEST} = \frac{48.95}{A^{0.23} G_{bp}^{0.82} \left(\frac{10}{\sqrt{P_{80}}} - \frac{10}{\sqrt{F_{80}}} \right)} \text{ kWh/t}$$

where A = test-sieve size in µm,
G_{bp} = mass of the undersize per mill revolution (g/rev), and
P_{80} = 80% passing size of circuit product.
F_{80} = 80% passing size of the new feed.

The Bond formula applies specifically to wet, closed-circuit grinding in a ball mill with an internal diameter of 2.44 m and a feed of minus 3350 µm.

To relate the calculations to other mills requires the use of a number of empirical efficiency factors.

A spreadsheet, *Bondcalc.xls*, is available for download from http://wasm.curtin.edu.au/yand/downloads.

APPENDIX B-2

BOND WORK INDEX TEST PROCEDURE FOR DETERMINATION
OF THE BOND ROD MILL WORK INDEX

The procedure described by Bond (1960) is as follows. The Bond Rod Mill Work Index determination is carried out in a standard test mill and under standard conditions. The test mill has an internal diameter of 305 mm and is 610 mm long. It has a wave lining.

The rod charge consists of a eight rods, weighing approximately 33.38 kg, and are 533 mm in length. Six rods are 38.1 mm diameter and the remaining two rods are 44.5 mm diameter. The mill is operated at a speed of 46 rpm in a horizontal position for most of the test but is periodically tilted to even out any segregation that occurs at the mill ends.

The circuit being simulated is shown below;
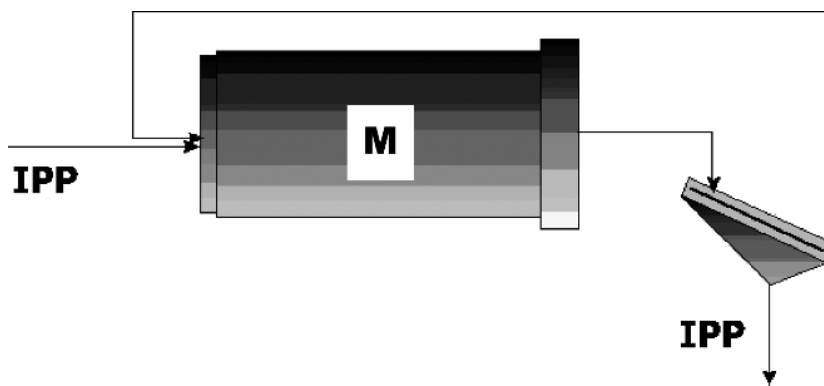
A detailed description of the test procedure follows:

1.   The dry feed is crushed to –13.2 mm, using staged crushing.
2.   Add the crushed ore, -3.36 mm to a 2000 mL measuring cylinder to the 1250 mL mark, lightly packed and not overly consolidated. Weigh the resulting mass of ore, M or calculate the mass from the ore bulk density;

        The mass M represents the mill charge for each grind.

3.   Calculate the Ideal Period Product (IPP) assuming a 100% circulating load (the mass of circulating material is equal to the new feed to the closed circuit or the screen undersize, at steady state. If the mass of the new feed is 1 and the mass of the circulating load is 1 then the mass being ground in the mill is 2.0)

        IPP   =   M/2.0

4.   Determine the sieve analysis of the feed. Ensure that the test screen size is one of the screens used in the size analysis.

5.   If the feed sieve analysis shows that more than 50% is finer than the test screen size, take the number of revolutions for the first period as zero and pass the feed charge directly over the test screen to remove the undersize then bring the total feed charge mass for the next period up to the desired mass by the addition of a representative amount of new feed.

6.   Place the feed charge, M, in the mill.

7.   Run the mill for N revolutions where N is initially around 30. The mill is operated horizontally for 8 revolutions, tilted downwards 5 degrees for 1 revolution, tilted up 5 degrees for 1 revolution and the cycle repeated.

8.   At the end of the grind, dump the charge by removing the feed and cover plate, tilt the mill 45 degrees downwards and run the mill for 30 revolutions. The rods are retained inside the mill by a grid.

9.   Screen the mill discharge at the test screen size.

10.   Weigh and record the total screen oversize, R.

11.   Calculate and record the mass of test screen undersize (product), m. Weigh the actual undersize as a check.

$$m = M - R$$

12.   Calculate the amount of product size material in the feed using the feed sieve analysis and the amount of new feed present in the mill charge at the beginning of the period.

$$\text{amount of product size material in the feed} = (1 - r_o)\, IPP$$

where r_o is the fraction of feed material coarser than the test screen.

13.   Calculate the net grams of product which is the mass of product minus the mass of product size material in the feed.

$$\text{net grams of product} = m - (1 - r_o)\, IPP$$

14.   Calculate the net grams produced per revolution, G, by dividing the net grams of product by the number of revolutions in the period.

$$G = [m - (1 - r_o)\, IPP]/N$$

15.   Add a representative amount of new feed to the test screen oversize to bring the combined mass up to the mill charge, M.

16.   Calculate the mass which should be ground in the next period in order to obtain the desired circulating load. This amount is the ideal period product (step 3) minus the amount of product size material in the mill feed (step 12).

$$\text{mass which should be ground in the next period} = IPP - (1 - r_o)\, IPP = r_o\, IPP$$

17.   Calculate the number of revolutions, N, for the next period. This is the amount of material which should be ground (step 16) divided by the net grams per revolution of the preceding period (step 14).

$N = r_o \, IPP/G$

18. Return the combined circulating load and new feed to the mill and repeat steps 6 to 17. At least five periods of grinding should be completed.

19. The net grams per revolution should approach an equilibrium value, where the net grams per revolution becomes constant for at least three periods, or the net grams per revolution shows a reversal in trend.

20. Take an average of the net grams per revolution of the last two or three periods, G_{rp}.

21. Determine the size distribution of the test screen undersize (product).

22. Determine the 80% passing sizes of the product, P_{80}, (from step 21) and the representative feed, F_{80}, (from step 4).

23. Calculate the laboratory Work Index from the following equation:

$$W_{i,TEST} = \frac{68.2}{A^{0.23} G_{rp}^{0.625} \left(\dfrac{10}{\sqrt{P_{80}}} - \dfrac{10}{\sqrt{F_{80}}} \right)} \quad kWh/t$$

where
A = test-sieve size in μm,
G_{rp} = mass of the under-size per mill revolution (g/rev), and
P_{80} = 80% passing size of circuit product.
F_{80} = 80% passing size of the new feed.

APPENDIX B-3

ROD MILL POWER AT MILL PINIONSHAFT (HORSEPOWER)

(Souce: C.A. Rowlands, Jr. and D.M. Kjos, SME/AIME Mineral Processing Plant Design, A.L.Mular and R.B. Bhappu (eds), 1980)

Rod Mill Diameter (m)	Rod Mill Length (m)	Rod Length (l,m)	L/D	Mill Speed		Bulk Density Rod Charge (kg/m3)	Rod Charge Weight (mt) % Volumetric Loading			Mill Power % Volumetric Loading		
				rpm	%Cs		35	40	45	35	40	45
0.91	1.22	1.07	1.40	36.1	74.5	5847	1.00	1.13	1.27	7	8	8
1.22	1.83	1.68	1.57	30.6	74.7	5847	2.25	2.58	2.90	23	25	26
1.52	2.44	2.29	1.67	25.7	71.2	5847	6.91	7.95	8.89	57	61	64
1.83	3.05	2.90	1.73	23.1	70.7	5847	13.10	15.00	16.80	114	122	128
2.13	3.35	3.20	1.62	21.0	69.9	5766	20.00	22.80	25.60	181	194	204
2.44	3.66	3.51	1.53	19.4	69.3	5766	29.00	33.20	37.40	275	295	310
2.59	3.66	3.51	1.44	18.7	69.0	5766	33.00	37.70	42.50	318	341	359
2.74	3.66	3.51	1.38	17.9	67.5	5766	36.00	41.10	45.50	344	369	388
2.89	3.96	3.81	1.41	17.4	67.6	5606	42.70	48.80	54.90	416	446	470
3.05	4.27	4.11	1.44	16.8	67.0	5606	51.50	59.00	63.80	507	544	572
3.20	4.57	4.42	1.47	16.2	66.4	5606	61.40	70.10	78.90	609	653	687
3.35	4.88	4.72	1.50	15.9	66.8	5606	72.50	82.80	93.50	735	788	829
3.51	4.88	4.72	1.43	15.5	66.6	5606	79.70	90.70	103.00	819	878	924
3.66	4.88	4.72	1.37	15.1	66.4	5606	82.70	99.80	112.00	906	972	1023
3.81	5.49	5.34	1.48	14.7	66.0	5446	104.00	119.00	134.00	1093	1173	1234
3.96	5.79	5.64	1.50	14.3	65.6	5446	120.00	137.00	154.00	1264	1356	1426
4.12	5.79	5.64	1.44	14.0	65.5	5446	130.00	148.00	166.00	1385	1486	1562
4.27	6.10	5.94	1.46	13.6	64.9	5446	147.00	169.00	190.00	1580	1695	1783
4.42	6.10	5.94	1.41	13.3	64.6	5446	159.00	181.00	204.00	1715	1840	1935
4.57	6.10	5.94	1.36	13.0	64.3	5446	171.00	194.00	219.00	1853	1988	2091

APPENDIX C-1

LAPLACE TRANSFORMATION

The Laplace transformation is a mathematical operation which helps to solve linear, ordinary differential equations with constant coefficients. The Laplace transforms F(s) of a function involving time f(t) is defined as f(s) according to the equation:

$$F(s) = L[f(t)] = \int_0^\infty f(t).e^{-ST} dt$$

"L" is the symbol for Laplace transform and read as "transform of", that is, transform of f(t). to s domain. Integration of the right hand side of the equation does not involve the variable function of time t, but transforms to the variable s. For example, the Laplace transform of function f(t) = 1 can be written as:

$$F(s) = \int_0^\infty (1).e^{-St} dt = 1/s$$

Hence L[t] = 1/s

That is, variable t is replaced by variable s. Selected transforms normally required is given in the table below.

LAPLACE TRANSFORMS OF COMMON DIFFERENTIAL EQUATIONS FROM TIME DOMAIN τ TO s DOMAIN

f(t)	F(s)
u(t)	1/ s
U_1(t)	1
ee^{-st}	1/s+1
$\sin\omega t$	$w / s + \omega^2$
$\cos\omega t$	$\omega / s^2 + \omega^2$
$t^n / n!$	$1 / s^{N+1}$
$t^n e^{at/n!}$	$1 / (S-A)^{N+1}$
Kf(t)	KF(s)
f_1(t) $\pm f_2$(t)	F_1(S) $\pm F_2$(s)
f'(tt)	sF(S)-f(s)
f''(t)	$s^2 F(s) - sf(0) - f('(0)$
f^N(t)	$s^N F(s) - s^{n-1} f(0) - .... - f^{n-1}$(0)
$f^{(-1)}$(t)	$[F(s)//s] + [f^{(-1)}(0)] / s$
$f^{(-N)}$(t)	$[F(s)/ s^N] + [f^{((-1)'}(t) / s^n] + ...+ [f^{(-n)}(t) /s]$
$e^{-st} \sin kt$	$K / [(s+a)^2 + k^2]$
$E^{-ST} \cos kt$	$[s+A] / (s+a)^2 + k^2$

Source:Automatic Control Engineering , Francic H.Raven, 1968 McGraw-Hill Kogakusha Int.
Students edition

LAPLACE TRANSFORMS OF COMMON HARDWARE*

1. MECHANICAL NETWORK

Spring

f(t) $f(t)=K\int_0^t u(t).dt$ $f(t)=Kx(t)$ $\dfrac{f(x)}{s(s)}=K$

Friction

$f(t)=f(K_uU(t))$ $f(t)=K_u\dfrac{dx(t)}{dt}$ $\dfrac{f(s)}{x(s)}=k_u$

Mass

$f(t)=M\dfrac{du(t)}{dt}$ $f(t)=M\dfrac{d^2x(t)}{dt}$ $-\dfrac{f(s)}{x(s)}=M$
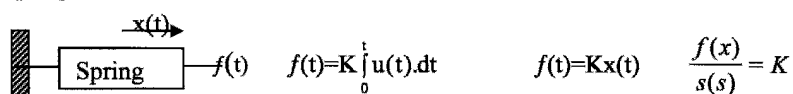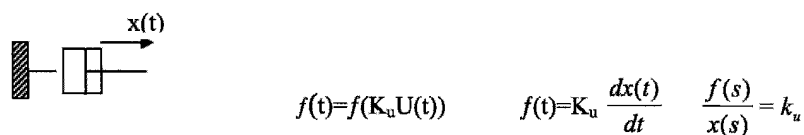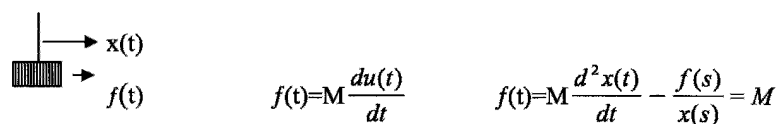
2. ELECTRICAL NETWORK

Capacitance

$u(t)=\dfrac{1}{C}\int_0^t i(t)dt$ $u(t)=\dfrac{1}{C}q(t)$ $\dfrac{u(s)}{i(s)}=\dfrac{1}{Cs}$

Resistance

$u(t)=Ri(t)$ $u(t)=R\dfrac{dq(t)}{dt}$ $\dfrac{u(s)}{i(s)}=R$

Inductance

$u(t)=L\dfrac{di(t)}{d(t)}$ $u(t)=L\dfrac{d^2q(t)}{dt^2}$ $\dfrac{u(s)}{i(s)}=Ls$
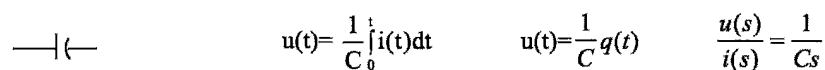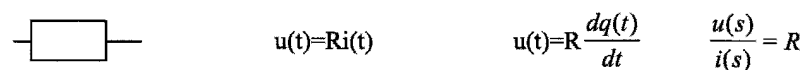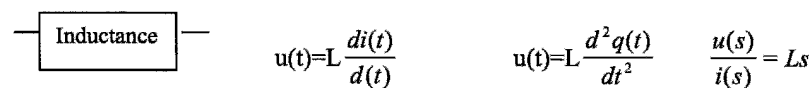
SOURCE: H.Eren and C.C.Fung "Automation and control equipment"
See complete list by W.S.Levine "The Control Handbook", Boca Raton FL, CRC Press

APPENDIX D-1

COMMON CONVERSION FACTORS

			Equals	(SI unit)
AREA	1	ft^2	0.09290304	m^2
	1	in^2	0.00064516	m^2
DENSITY	1	g/cm^3	1000	kg/m^3
	1	lb/in^3	27679.9	kg/m^3
ENERGY	1	Joule	1	Nm
	1	BTU (Aus)	1055.06	Joules
$J = kg\ m^2/s^2 = Nm$	1	cal (Int)	4.1868	Joules
	1	kW h	3600000	Joules
FORCE	1	dyne	0.00001	N
	1	erg/cm^2	0.001	Nm-1
$N = kg\ m/s^2 = J/m$	1	kg f	9.80665	N
	1	lb f	4.448222	N
LENGTH	1	ft	0.3048	m
	1	in	0.0254	m
MASS	1	oz (troy)	0.031103477	kg
	1	lb (avoirdupois)	0.45359237	kg
	1	ton (2240 lb)	1016.047	kg
	1	ton (2000 lb)	907.1847	kg
POWER	1	ft lbf/s	1.355818	W
W = J/s	1	hp	745.6999	W
PRESSURE	1	atm	101325	Pa
	1	bar	100000	Pa
$Pa = N/m^2 = J/m^3$	1	mm Hg (0^oC)	133.3224	Pa
	1	psi	7030.7	Pa
TEMPERATURE	0	^oC	273.15	K
	32	^oF	0	^oC
VISCOSITY	1	cp	0.001	Pa s
	1	cSt	0.000001	m^2/s
VOLUME	1	ft^3	0.02831685	m^3
	1	gal (Aus)	0.00454609	m^3
	1	gal (USA)	0.003785412	m^3
	1	L	0.001	m^3
WORK	1	kWh/ton (imp)	0.984206439	kWh/t
	1	kWh/s.ton	1.10231136	kWh/t

An extended list of conversion factors, physical constants, composition of chemical compounds, mineral data, screen size equivalents and general geometry formulae are available for download as a spreadsheet from: http://wasm.curtin.edu.au/yand/downloads.

APPENDIX D-2

VISCOSITY OF PURE WATER 0-100^0

TEMP ^{0} C	Viscosity, Pa s	TEMP ^{0} C	Viscosity, Pa s	TEMP ^{0} C	Viscosity, Pa s
0.0	0.001798	34.0	0.0007340	68.0	0.0004155
1.0	0.001728	35.0	0.0007194	69.0	0.0004098
2.0	0.001671	36.0	0.0007052	70.0	0.0004042
3.0	0.001618	37.0	0.0006915	71.0	0.0003987
4.0	0.001597	38.0	0.0006783	72.0	0.0003934
5.0	0.001519	39.0	0.0006654	73.0	0.0003882
6.0	0.001472	40.0	0.0006529	74.0	0.0003831
7.0	0.001428	41.0	0.0006408	75.0	0.0003781
8.0	0.001386	42.0	0.0006291	76.0	0.0003732
9.0	0.001340	43.0	0.0006178	77.0	0.0003684
10.0	0.001307	44.0	0.0006067	78.0	0.0003638
11.0	0.001271	45.0	0.0005964	79.0	0.0003592
12.0	0.001235	46.0	0.0005856	80.0	0.0003547
13.0	0.001202	47.0	0.0005755	81.0	0.0003503
14.0	0.001169	48.0	0.0005650	82.0	0.0003460
15.0	0.001139	49.0	0.0005561	83.0	0.0003418
16.0	0.001109	50.0	0.0005468	84.0	0.00033747
17.0	0.001081	51.0	0.0005378	85.0	0.0003337
18.0	0.001053	52.0	0.0005290	86.0	0.0003297
19.0	0.001027	53.0	0.0005204	87.0	0.0003259
20.0	0.001002*	54.0	0.0005121	88.0	0.0003221
21.0	0.0009779	55.0	0.0005040	89.0	0.0003184
22.0	0.0009548	56.0	0.0004961	90.0	0.0003147
23.0	0.0009325	57.0	0.0004884	91.0	0.0003111
24.0	0.0009111	58.0	0.0004800	92.0	0.0003076
25.0	0.0008904	59.0	0.0004736	93.0	0.0003042
26.0	0.0008705	60.0	0.0004665	94.0	0.0003008
27.0	0.0008513	61.0	0.0004596	95.0	0.0002975
28.0	0.0008327	62.0	0.0004528	96.0	0.0002942
29.0	0.0008148	63.0	0.0004462	97.0	0.0002911
30.0	0.0007975	64.0	0.0004398	98.0	0.0002879
31.0	0.0007808	65.0	0.0004335	99.0	0.0002948
32.0	0.0007647	66.0	0.0004273	100.0	0.0002818
33.0	0.0007491	67.0	0.0004213		

* The value of 1.0019±0.0000003 mPa s is considered as the absolute value of viscosity of water at 20^0 C

(contribution National Bureau of Standards)

INDEX